

Wednesday

104th Scientific Assembly and Annual Meeting November 25–30 | McCormick Place, Chicago





SPDL40

Keeping Radiology Weird: Spot Diagnoses from the Pacific Northwest (Case-based Competition)

Wednesday, Nov. 28 7:15AM - 8:15AM Room: E451B



AMA PRA Category 1 Credit ™: 1.00 ARRT Category A+ Credit: 1.00

FDA Discussions may include off-label uses.

Participants

Barry G. Hansford, MD, Chicago, IL (*Presenter*) Nothing to Disclose Kyle K. Jensen, MD, Portland, OR (*Presenter*) Nothing to Disclose Alice W. Fung, MD, Portland, OR (*Presenter*) Nothing to Disclose

For information about this presentation, contact:

funga@ohsu.edu

LEARNING OBJECTIVES

1) The participant will be introduced to a series of musculoskeletal and abdominal radiology case studies via an interactive game approach designed to encourage 'active' consumption of education material. 2) The participant will be able to use their mobile wireless device (tablet, phone, laptop) to electronically respond to various imaging case challenges; participants will be able to monitor their individual and team performance in real time. 3) The attendee will receive a personalized self-assessment report via email that will review the case material presented during the session, along with individual and team performance. This interactive session will use RSNA Diagnosis Live. Please bring your charged wireless device (phone, tablet, laptop) to participate.



SPSH40

Hot Topic Session: Fast MSK MR Imaging

Wednesday, Nov. 28 7:15AM - 8:15AM Room: E450A



AMA PRA Category 1 Credit ™: 1.00 ARRT Category A+ Credit: 1.00

FDA Discussions may include off-label uses.

Participants

Soterios Gyftopoulos, MD, Scarsdale, NY (Moderator) Nothing to Disclose

For information about this presentation, contact:

Soterios.Gyftopoulos@nyumc.org

LEARNING OBJECTIVES

1) Describe the evolution of MRI and the reasons for and against the implementation of fast MR imaging. 2) Describe the advantages and disadvantages of current and emerging techniques for fast MR imaging. 3) Describe how machine learning can be used to accelerate MR imaging.

Sub-Events

SPSH40A Fast MR Imaging: What, How, and Why

Participants Soterios Gyftopoulos, MD, Scarsdale, NY (*Presenter*) Nothing to Disclose

For information about this presentation, contact:

Soterios.Gyftopoulos@nyumc.org

LEARNING OBJECTIVES

1) Review the evolution of MR imaging from its inception to its current state. 2) Discuss the reasons for and against fast MR imaging.

SPSH40B Current Techniques for Fast MR Imaging

Participants

Naveen Subhas, MD, Shaker Heights, OH (Presenter) Research support, Siemens AG

LEARNING OBJECTIVES

1) Review current techniques that are available to obtain faster MRI scans including abbreviated MRI, single sequence 3D MRI and parallel imaging. 2) Discuss advantages and limitations of these techniques.

SPSH40C Emerging Techniques for Fast MR Imaging

Participants

Jan Fritz, MD, Baltimore, MD (*Presenter*) Research Grant, Siemens AG; Scientific Advisor, Siemens AG; Scientific Advisor, Alexion Pharmaceuticals, Inc; Speaker, Siemens AG

For information about this presentation, contact:

jfritz9@jhmi.edu

LEARNING OBJECTIVES

1) To review new and emerging acceleration techniques for 2D and 3D MRI. 2) To identify advantages and limitations of the different acceleration techniques. 3) To apply the most appropriate acceleration techniques for various clinical scenarios of musculoskeletal MRI.

SPSH40D Machine Learning for Fast MR Imaging

Participants Michael P. Recht, MD, New York, NY (*Presenter*) Nothing to Disclose

For information about this presentation, contact:

michael.recht@nyumc.org

LEARNING OBJECTIVES

1) Explain the basic concepts behind using machine learning for MR image reconstruction. 2) Understand the advantages provided

by machine learning image reconstruction.



MSRT41

ASRT@RSNA 2018: Ultrasound versus MRI for Imaging of the Female Pelvis

Wednesday, Nov. 28 8:00AM - 9:00AM Room: N230B



AMA PRA Category 1 Credit ™: 1.00 ARRT Category A+ Credit: 1.00

Participants

Deborah Levine, MD, Boston, MA (Presenter) Editor with royalties, Taylor & Francis Group; Editor with royalties, Reed Elsevier;

For information about this presentation, contact:

dlevine@bidmc.harvard.edu

LEARNING OBJECTIVES

1) Understand the various adnexal masses that can be confused with neoplasms, and when MR might be useful in differentiating various types of adnexal masses. 2) Recognize features of endometriosis and when MR can add additional information that might alter patient care. 3) Understand the role of MR in triage of patients potentially under uterine artery embolization for fibroids.



RCA41

Prostate MRI (Hands-on)

Wednesday, Nov. 28 8:00AM - 10:00AM Room: S401AB

GU MR

AMA PRA Category 1 Credits ™: 2.00 ARRT Category A+ Credits: 2.25

Participants

Jelle O. Barentsz, MD, PhD, Nijmegen, Netherlands (*Presenter*) Advisor, SPL Medical BV Daniel J. Margolis, MD, Los Angeles, CA (*Presenter*) Consultant, Blue Earth Diagnostics Ltd Roel D. Mus, MD, Groesbeek, Netherlands (*Presenter*) Nothing to Disclose Joyce G. Bomers, Arnhem, Netherlands (*Presenter*) Nothing to Disclose Jurgen J. Futterer, MD, PhD, Nijmegen, Netherlands (*Presenter*) Research Grant, Siemens AG Rianne R. Engels, Nijmegen, Netherlands (*Presenter*) Nothing to Disclose Michiel Sedelaar, MD, PhD, Nijmegen, Netherlands (*Presenter*) Nothing to Disclose Antonio C. Westphalen, MD, Mill Valley, CA (*Presenter*) Nothing to Disclose Leonardo K. Bittencourt, MD, PhD, Rio De Janeiro, Brazil (*Presenter*) Nothing to Disclose Vibeke B. Logager, MD, Herlev, Denmark (*Presenter*) Nothing to Disclose Baris Turkbey, MD, Bethesda, MD (*Presenter*) Nothing to Disclose Joseph J. Busch, MD, Chattanooga, TN (*Presenter*) Nothing to Disclose

For information about this presentation, contact:

Renske.vandelft@radboudumc.nl

LEARNING OBJECTIVES

1) Understand the Pi-RADS v2 Category assessment to detect and localize significant cancer for both peripheral zone and transitional zone lesions. 2) Recognize benign pathology like inflammation and BPH and to differentiate these from significant prostate cancers.

ABSTRACT

In this Hands-on Workshop, the participants will able to review up to 47 multi-parametric MRI cases with various prostatic pathology using a dedicated workstation. Focus will be on the overall assessment of PI-RADS v2 category, which enables them to score the probability of the presence of a significant cancer in patients with elevated PSA and/or clinical suspicion. All cases are from daily non-academic practice, and have various levels of difficulty. The cases include: easy and difficult significant peripheral-transition- and central zone cancers, inflammation, BPH, and the most common pitfalls. Internationally renowned teachers will guide the participants during their PI-RADS v2 scoring. The coursebook can be found at: http://bit.ly/rsna2018 . Please note: To guarantee the best learning experience, we can only allow 100 people in the room (2 per computer). First come first serve.

Active Handout:Renske Lian van Delft

http://abstract.rsna.org/uploads/2018/16002005/Workshop RSNA 2018 Coursebook small RCA.pdf



MSCP41

Case-based Review of Pediatric Radiology (Interactive Session)

Wednesday, Nov. 28 8:30AM - 10:00AM Room: E450B



AMA PRA Category 1 Credits ™: 1.50 ARRT Category A+ Credit: 1.75

Participants

Ricardo Restrepo, MD, Miami, FL (Director) Nothing to Disclose

For information about this presentation, contact:

ricardo.restrepo@nicklaushealth.org

Sub-Events

MSCP41A Pediatric Brain Disorders

Participants Korgun Koral, MD,MBA, Dallas, TX (*Presenter*) Nothing to Disclose

MSCP41B Pediatric Vascular Disorders

Participants Josee Dubois, MD, Montreal, QC (*Presenter*) Nothing to Disclose

For information about this presentation, contact:

josee.dubois.hsj@ssss.gouv.qc.ca

LEARNING OBJECTIVES

1) Define the classification of the vascular anomalies. 2) Describe the imaging findings of the most common vascular anomalies. 3) Identify the mimickers of the vascular tumors.

ABSTRACT

During this interactive session, vascular anomalies cases will be presented allowing the learners to recognize the imaging findings and to understand the importance of performing US and MR for diagnosis. Key points will be discussed to avoid misdiagnosis.

MSCP41C Pediatric Abdominal Disorders

Participants

Patricia T. Acharya, MD, Loma Linda, CA (Presenter) Nothing to Disclose

LEARNING OBJECTIVES

1) Identify a wide range of pediatric abdominal disorders. 2) Describe imaging features of various pediatric abdominal disorders.

ABSTRACT

During this interactive session, pediatric abdominal disorder cases will be presented allowing the learners to recognize and describe the imaging features of various diagnostic entities. Key points will be discussed to avoid misdiagnosis.

MSCP41D Pediatric Pelvic Disorders

Participants

Jennifer K. Son, MD, Baltimore, MD (Presenter) Nothing to Disclose

LEARNING OBJECTIVES

1) Identify a wide range of pediatric pelvic disorders. 2) Describe imaging features of various pediatric pelvic disorders.

ABSTRACT

During this case-driven, interactive session, pediatric pelvic disorders will be presented allowing the participants to recognize and describe the imaging features of various diagnostic entities.



MSES41

Essentials of Cardiac Imaging

Wednesday, Nov. 28 8:30AM - 10:00AM Room: S100AB

САСТ

AMA PRA Category 1 Credits ™: 1.50 ARRT Category A+ Credit: 1.75

Sub-Events

MSES41A Aortic Valvular Disease

Participants

John P. Lichtenberger III, MD, Bethesda, MD (Presenter) Nothing to Disclose

For information about this presentation, contact:

jlichtenberger@mfa.gwu.edu

LEARNING OBJECTIVES

1) Describe the detailed imaging anatomy of the aortic valve, including congenital variants and malformations. 2) List incidental and known aortic valvular diseases detectable on radiography, CT, and MRI and organize that list based on epidemiology. 3) Select the best imaging modality to evaluate a given aortic valvular disease. 4) Adjust imaging protocols to optimize the evaluation of common aortic valvular diseases.

ABSTRACT

The increasing temporal and spatial resolution of imaging technology, the advancing functional data obtainable by imaging modalities, and the ever-broadening knowledge of aortic valvular disease present a challenge to both general and subspecialized imagers. This lecture will focus on the most common and most important diseases of the aortic valve encountered in clinical practice, whether those diseases are discovered incidentally or are known and must be comprehensively characterized. Emphasis will be placed on avoiding pitfalls and on obtaining and providing clinically useful information.

MSES41B Cardiac Devices: Appearance on Imaging

Participants

Karin E. Dill, MD, Worcester, MA (Presenter) Nothing to Disclose

MSES41C Imaging Complications of Myocardial Infarction and CABG

Participants Seth J. Kligerman, MD, Denver, CO (*Presenter*) Nothing to Disclose

For information about this presentation, contact:

skligerman@ucsd.edu

LEARNING OBJECTIVES

1) Learn about the early and late complications of myocardial infarction. 2) Understand how each of these manifestations appear on cross-sectional imaging. 3) Discuss medical and surgical treatment options.

ABSTRACT

Acute myocardial infarction is a leading cause of mortality in the United States. However, even if a patient survives the initial insult, myocardilal damage can lead to both early and late complications including left ventricular free wall rupture, ventricualr septal rupture, papillary muscle rupture, pericardits, and aneurysm formation. Some of these are life-threatening complications that require immediate diagnosis. The purpose of this talk is the review the various patholgies that involve the myocardium and pericardium, review their imaging findings, and dicuss treatment options.

MSES41D Cardiac CT in Acute Chest Pain

Participants

Christian Loewe, MD, Vienna, Austria (Presenter) Speaker, Bracco Group; Speaker, General Electric Company; Speaker, Siemens AG

For information about this presentation, contact:

Christian.loewe@meduniwien.ac.at

LEARNING OBJECTIVES

1) To learn about the current and possible future role of Cardiac CT in the management of patients suffering from acute chest pain. 2) To become familiar with the most important imaging biomarkers in acute coronary syndromes. 3) To discuss possible algorithms for the management of patients with acute chest pain. Three potentially life-threatening disorders can become clinically evident by the unspecific symptom of "acute chest pain", and in two out of them including pulmonary embolism and acute aortic syndrome CT angiography was established as the first diagnostic modality of choice. Given the high evidence for the value of Cardiac CT in ruling out relevant coronary artery disease in stable patients and facing still existing challenges to safely triage patients in chest pain units, the possible role of Cardiac CT in this clinical scenario is under evaluation and discussion. It is proven that CT can be used to safely rule out acute coronary syndromes with a very high negative predictive value and that CT can help to early discharge patients from the chest pain unit. However, the possible role in the positive diagnosis of an acute coronary syndrome is not as clear. Within this presentation, an overview about the technical possibilities of using CT in the management of acute chest pain patients will be provided. Furthermore, the most important differential diagnoses will be addressed with the most relevant imaging findings in the acute setting. The main focus of the presentation, however, will be on the existing challenges and possible solutions of using Cardiac CT in patients with acute coronary syndromes. New CT techniques, including CT derived FFR as well as CT perfusion will be introduced and their potential in the emergency setting should be outlined.

 $\ddot{\imath}_{\mathcal{C}}^{1/2}\ddot{\imath}_{\mathcal{C}}^{1/2}\&p\ddot{\imath}_{\mathcal{C}}^{1/2}V$



MSSR41

RSNA/ESR Sports Imaging Symposium: Upper Extremity Sports Injuries (Interactive Session)

Wednesday, Nov. 28 8:30AM - 10:00AM Room: E352



AMA PRA Category 1 Credits ™: 1.50 ARRT Category A+ Credit: 1.75

Participants

Laura W. Bancroft, MD, Orlando, FL (*Moderator*) Author with royalties, Wolters Kluwer nv; Speaker, World Class CME; Editor, Thieme Medical Publishers, Inc; Travel support, Thieme Medical Publishers, Inc; ; Andrew J. Grainger, MRCP, FRCR, Leeds, United Kingdom (*Moderator*) Consultant, Levicept Ltd; Director, The LivingCare Group;

For information about this presentation, contact:

andrewgrainger@nhs.net

Sub-Events

MSSR41A Shoulder Injuries in the Throwing Athlete

Participants

Lynne S. Steinbach, MD, Tiburon, CA (Presenter) Nothing to Disclose

LEARNING OBJECTIVES

1) To understand the biomechanics of throwing forces as they relate to the shoulder. 2) To become familiar with rotator cuff, labroligamentous, and osseous abnormalities caused by overhead sports.

ABSTRACT

Overhead throwing athletes develop significant abnormalities as a result of acquired adaptations to the extremes of motion in the dominant shoulder. These abnormalities may eventually result in an inability to throw with the same velocity, the so-called "dead arm" syndrome. These abnormalities involve tendons, ligaments, labrum, muscles, nerves, vessels, and bones. This presentation will review the biomechanics of throwing forces as they relate to the shoulder. The MR imaging characteristics of the resultant abnormalities in the labroligamentous structures and the rotator cuff will also be highlighted. As a prototype, the throwing motion in baseball occurs over a period of approximately 2 seconds and is divided into six stages: wind up, cocking, early and late acceleration, deceleration, and follow through. The late cocking, acceleration, and deceleration phases produce the greatest stress on the glenohumeral joint structures. As with other throwing sports, the superior labrum and rotator cuff are often affected by these extreme forces.

MSSR41B Soft Tissue Wrist Injury in the Athlete

Participants

Christian W. Pfirrmann, MD, MBA, Forch, Switzerland (Presenter) Nothing to Disclose

LEARNING OBJECTIVES

1) To learn about the patterns of injury seen at the wrist in athletes. 2) To understand the advantages and disadvantages of different modalities for imaging the athlete's wrist. 3) To recognize the imaging appearances of cartilage and ligamentous injury at the wrist.

MSSR41C Interactive Case Discussion

Participants Lynne S. Steinbach, MD, Tiburon, CA (*Presenter*) Nothing to Disclose Christian W. Pfirrmann, MD, MBA, Forch, Switzerland (*Presenter*) Nothing to Disclose

LEARNING OBJECTIVES

1) To appreciate pathologic and normal developmental changes in skeletally immature throwing athletes, especially around the physis. 2) To consolidate the knowledge gained from the session with interactive cases of upper limb athletic injury as it relates to the skeletally immature throwing athlete.

ABSTRACT

The first part of this interactive session will show some cases of pathologic and normal developmental changes around the physis of shoulders of skeletally immature throwing athletes. The second part of this intercactive sessions will show and diuscuss cases with athletic unjuries about the wrist.



Lung Cancer Screening Diagnosis Live (Interactive Session)

Wednesday, Nov. 28 8:30AM - 10:00AM Room: E353C



AMA PRA Category 1 Credits ™: 1.50 ARRT Category A+ Credit: 1.75

Participants

Caroline Chiles, MD, Winston-Salem, NC (Moderator) Advisory Board, ImBio, LLC

For information about this presentation, contact:

cchiles@wakehealth.edu

LEARNING OBJECTIVES

 Confirm compliance with screening guidelines, including patient eligibility, scanning protocols, radiation dose, CMS requirements and National Lung Screening Registry. 2) Incorporate shared decision making and smoking cessation in the lung screening visit. 3) Assign Lung-RADS categories to nodules encountered at baseline and annual screening CT. 4) Evaluate atypical screening findings.
 Manage incidental findings, including COPD, coronary artery calcification, and potential extrapulmonary malignancies.

GENERAL INFORMATION

This interactive session will use RSNA Diagnosis Live[™]. Please bring your charged mobile wireless device (phone, tablet or laptop) to participate.

Sub-Events

RC501A Logistics of Screening

Participants

Jared D. Christensen, MD, Durham, NC (Presenter) Advisory Board, Riverain Technologies, LLC

For information about this presentation, contact:

jared.christensen@duke.edu

LEARNING OBJECTIVES

1) Confirm compliance with screening guidelines, including patient eligibility, scanning protocols, radiation dose, CMS requirements, and National Lung Screening Registry.

RC501B Shared Decision Making and Smoking Cessation

Participants Robert Volk, PhD, Houston, TX (*Presenter*) Nothing to Disclose

RC501C Nodule Assessment and Lung-RADS Categories

Participants

Mylene T. Truong, MD, Houston, TX (Presenter) Nothing to Disclose

Honored Educators

Presenters or authors on this event have been recognized as RSNA Honored Educators for participating in multiple qualifying educational activities. Honored Educators are invested in furthering the profession of radiology by delivering high-quality educational content in their field of study. Learn how you can become an honored educator by visiting the website at: https://www.rsna.org/Honored-Educator-Award/ Mylene T. Truong, MD - 2015 Honored EducatorMylene T. Truong, MD - 2018 Honored Educator

RC501D Interesting Cases Encountered in a Screening Program

Participants

Brett M. Elicker, MD, San Francisco, CA (Presenter) Nothing to Disclose

For information about this presentation, contact:

brett.elicker@ucsf.edu

LEARNING OBJECTIVES

1) Describe the role of imaging in the multi-disciplinary approach to suspected lung cancer. 2) Compare the different management options in suspected lung nodules detected on lung cancer screening CT. 3) Summarize how to appropriately use Lung-RADS when interpreting lung cancer screening CTs.

RC501E Participants Findings on the Low-Dose CT

Carol C. Wu, MD, Bellaire, TX (Presenter) Author, Reed Elsevier

For information about this presentation, contact:

carolcwu@gmail.com

LEARNING OBJECTIVES

1) To discuss the prevalence and significance of incidental findings on LDCT. 2) To review the latest evidence-based management recommendations for various incidental findings on LDCT.



International Radiology Outreach

Wednesday, Nov. 28 8:30AM - 10:00AM Room: S502AB

ED

AMA PRA Category 1 Credits ™: 1.50 ARRT Category A+ Credit: 1.75

Participants

Donald P. Frush, MD, Durham, NC (Moderator) Nothing to Disclose

For information about this presentation, contact:

donald.frush@duke.edu

LEARNING OBJECTIVES

1) Learn about opportunities for international educational outreach. 2) Understand challenges with developing, implementing and maintaining outreach programs. 3) Be familiar with tactics to develop, implement and maintain outreach programs. 4) Be able to describe the RAD-AID as a model for international educational outreach. 5) Benefit from the opportunity to discuss with panel members issues related to efforts at international educational outreach.

Sub-Events

RC502A Contemporary Strategies and Tactics for Global Radiology Education Outreach

Participants

David A. Rosman, MD, Boston, MA (Presenter) Nothing to Disclose

For information about this presentation, contact:

drosman@mgh.harvard.edu

LEARNING OBJECTIVES

1) To learn about concepts behind sustainable involvement in low and middle resource countries. 2) Discuss the starting of a residency that is designed for low resource settings in order to create long term radiology sustainability and partnership that is bilateral rather than one designed for volunteerism.

RC502B Connecting the World: Opportunities and Obstacles for Radiology Education Outreach

Participants

Eric J. Stern, MD, Seattle, WA (Presenter) Nothing to Disclose

LEARNING OBJECTIVES

1) To gain a greater understanding of the many opportunities for international radiology educational outreach, with a focus on webbased activities. 2) To appreciate the multifaceted efforts aimed at providing and expanding the awareness and ready access to the many radiology educational resources currently available for under resourced radiology communities.

RC502C RAD-AID: Looking Ahead and a Vision for the Future

Participants Daniel J. Mollura, MD, Bethesda, MD (*Presenter*) Nothing to Disclose



Read with the Experts (Cardiac Radiology) (Interactive Session)

Wednesday, Nov. 28 8:30AM - 10:00AM Room: N228



AMA PRA Category 1 Credits ™: 1.50 ARRT Category A+ Credit: 0

FDA Discussions may include off-label uses.

Participants

Jill E. Jacobs, MD, New York, NY (*Moderator*) Nothing to Disclose Cylen Javidan-Nejad, MD, Saint Louis, MO (*Presenter*) Nothing to Disclose Smita Patel, FRCR, MBBS, Ann Arbor, MI (*Presenter*) Nothing to Disclose Sanjeev Bhalla, MD, Saint Louis, MO (*Presenter*) Nothing to Disclose Amar B. Shah, MD, New York, NY (*Presenter*) Nothing to Disclose

For information about this presentation, contact:

ashah27@northwell.edu

jill.jacobs@nyumc.org

LEARNING OBJECTIVES

1) Use cardiac CTA cases to allow participants to generate an appropriate differential diagnosis using Cardiac CTA and Cardiac MRI when reviewing cases. 2) Develop a better understanding of when Cardiac CTA and Cardiac MRI can be used for diagnosis.

Honored Educators

Presenters or authors on this event have been recognized as RSNA Honored Educators for participating in multiple qualifying educational activities. Honored Educators are invested in furthering the profession of radiology by delivering high-quality educational content in their field of study. Learn how you can become an honored educator by visiting the website at: https://www.rsna.org/Honored-Educator-Award/ Sanjeev Bhalla, MD - 2014 Honored EducatorSanjeev Bhalla, MD - 2016 Honored EducatorSanjeev Bhalla, MD - 2017 Honored EducatorSanjeev Bhalla, MD - 2018 Honored Educator



Musculoskeletal Series: Shoulder MRI

Wednesday, Nov. 28 8:30AM - 12:00PM Room: S406A



AMA PRA Category 1 Credits ™: 3.50 ARRT Category A+ Credits: 4.00

FDA Discussions may include off-label uses.

Participants

Adam C. Zoga, MD, Philadelphia, PA (*Moderator*) Nothing to Disclose Lawrence M. White, MD, FRCPC, Toronto, ON (*Moderator*) Nothing to Disclose Erin F. Alaia, MD, New York, NY (*Moderator*) Nothing to Disclose Lynne S. Steinbach, MD, Tiburon, CA (*Moderator*) Nothing to Disclose

For information about this presentation, contact:

lawrence.white@uhn.ca

llenchik@wakehealth.edu

Erin.Fitzgerald@nyumc.org

Sub-Events

RC504-01 Rotator Cuff

Wednesday, Nov. 28 8:30AM - 8:55AM Room: S406A

Participants Douglas W. Goodwin, MD, Lebanon, NH (*Presenter*) Nothing to Disclose

LEARNING OBJECTIVES

1) To describe the spectrum of normal and pathologic imaging features of the rotator cuff.

RC504-02 Labrum/Cartilage

Wednesday, Nov. 28 8:55AM - 9:20AM Room: S406A

Participants Lawrence M. White, MD, FRCPC, Toronto, ON (*Presenter*) Nothing to Disclose

For information about this presentation, contact:

Lawrence.White@sinaihealthsystem.ca

LEARNING OBJECTIVES

1) Describe the normal anatomy and function of the labrum and articular cartilage of the glenohumeral joint. 2) Identify appropriate imaging techniques and protocols for assessment of the labrum and articular cartilage of the glenohumeral joint 3) Describe the spectrum of normal and pathologic MR imaging features of the labrum and articular cartilage of the glenohumeral joint.

RC504-03 Isolated Teres Minor Oedema and/or Atrophy: A Manifestation of Adhesive Capsulitis with Involvement of the Primary Motor Branch of the Teres Minor Muscle at the Stout Fascial Sling

Wednesday, Nov. 28 9:20AM - 9:30AM Room: S406A

Participants

Aamer F. Iqbal, MBChB, Newport, United Kingdom (*Presenter*) Nothing to Disclose Suresh Dalavaye, FRCR, MBBS, Swansea, United Kingdom (*Abstract Co-Author*) Nothing to Disclose Ayesha Z. Khatib, MBBS, Cardiff, United Kingdom (*Abstract Co-Author*) Nothing to Disclose

For information about this presentation, contact:

ai5720@doctors.net.uk

PURPOSE

Isolated teres minor denervation in the absence of a structural lesion involving the axillary nerve is not an uncommon finding on shoulder MRI. Pathologies such as rotator cuff injuries and axillary nerve traction injury have been mentioned. In our centre, we have identified a number of cases of teres minor oedema in patients with adhesive capsulitis. A study by Chafik et al (2013) described the complex anatomy of the teres minor muscle and found a combined fascia of the infraspinatous, teres minor, long head of triceps and deltoid muscle which forms a stout fascial sling attaching just medial to the inferior glenoid articular cartilage. They discovered that the primary motor branch of the teres minor runs inferior to this prior to entering the muscle. We believe that

posterior inferior joint capsule involvement in adhesive capsulitis results in teres minor oedema and/or atrophy secondary to denervation of this primary motor branch.

METHOD AND MATERIALS

This retrospective study analysed all MRI shoulders with a radiolological diagnosis of adhesive capsulitis between 2014-17. Each study was re-reviewed to assess the posterior joint capsule for thickening and its proximity to the described location of the stout fascial sling, the axillary neurovascular bundle and the teres muscle for oedema and/or atrophy.

RESULTS

There were a total of 59 cases with 'adhesive capsulitis' between 2014-2017. There were 38 males and 21 females. The age range was 23-74yrs with a mean age of 47.7yrs. 48(81%) patients had thickening of the posterior inferior joint capsule in close proximity to the described location of the fascial sling. Of these, 36(75%) patients had oedema and/or atrophy. 24(50%) patients had isolated teres minor oedema and 14(29%) patients had isolated muscle atrophy. No axillary bundle lesion were identified.

CONCLUSION

The primary motor branch of the teres minor muscle courses just inferior to the stout fascial sling insertion onto the glenoid neck before it becomes sub-fascial. Adhesive capsulitis with thickening of the posterior inferior joint capsule in close proximity to the stout fascial sling may result in denervation of the primary motor branch of the teres minor resulting in isolated oedema and/or atrophy.

CLINICAL RELEVANCE/APPLICATION

Adhesive capsulitis should be excluded in symptomatic patients thought to have idiopathic isolated muscle oedema/atrophy undergoing surgical decompression of the Teres minor nerve.

RC504-04 Magnetic Resonance Arthrogram Features That Can Be Used to Distinguish Between Iatrogenic Extravasation and True Inferior Glenohumeral Ligament Complex Tears

Wednesday, Nov. 28 9:30AM - 9:40AM Room: S406A

Participants

Lidi Wan, MD, MD, San Diego, CA (*Presenter*) Nothing to Disclose Wilbur Wang, MD, San Diego, CA (*Abstract Co-Author*) Nothing to Disclose Brady K. Huang, MD, San Diego, CA (*Abstract Co-Author*) Nothing to Disclose Matthew Sharp, San Diego, CA (*Abstract Co-Author*) Nothing to Disclose Niloofar Shojaeiadib, San Diego, CA (*Abstract Co-Author*) Nothing to Disclose Eric Y. Chang, MD, San Diego, CA (*Abstract Co-Author*) Nothing to Disclose

For information about this presentation, contact:

liw142@ucsd.edu

PURPOSE

To identify MR imaging features on shoulder arthrography which can distinguish between iatrogenic-induced extravasation and real IGHL complex lesions and to determine the diagnostic performance of these imaging features.

METHOD AND MATERIALS

This was an IRB-approved, retrospective multi-institution study. 1,740 MR arthrograms were screened for extravasation through the IGHL complex. Exams were independently scored by 3 MSK fellowship-trained radiologists. The IGHL complex was assessed along the anterior-posterior and medial-lateral locations. Morphology of the disrupted margin was evaluated: maximum thickness of the portion floating in contrast (thin, <1mm; medium, 1-3mm; thick, >3mm), caliber change at the torn margin (tapering or reverse tapering), and regularity of the torn margin (single thin fascicle, mop-head, scarred). T-tests, chi-squared tests, and sensitivity/specificity were calculated.

RESULTS

35 exams fulfilled the strict inclusion criteria. Of those with true tears, 8/16 (50%) had a torn anterior band whereas 0/19 cases of iatrogenic induced extravasation demonstrated anterior band disruption (p<0.001). In those with iatrogenic induced extravasation, 12/19 (63.2%) had solitary extravasation through the posterior half of the axillary pouch, compared to none in true IGHL complex lesions (p<0.001). Thick ends were present in 10/16 (62.5%) of the true IGHL complex lesion group whereas 0/19 (0%) demonstrated this finding in the iatrogenic induced extravasation group (p < 0.001). Scarred margins were seen in 8/16 (50%) with true IGHL complex lesions and none of the iatrogenic induced extravasation cases (p<0.001). Presence of a torn anterior band, thick ligament, reverse tapered caliber, and scarred appearance of the torn margin were shown to be 100% specific and a torn posterior band demonstrated 84.2% specificity for true IGHL complex tears. The presence of solitary involvement of the posterior portion of axillary pouch demonstrated 63.2% sensitivity for iatrogenic induced contrast extravasation, but was 100% specific.

CONCLUSION

We have identified MR arthrogram features that can aid the radiologist in distinguishing between iatrogenic-induced extravasation and real IGHL complex lesions.

CLINICAL RELEVANCE/APPLICATION

Discriminating between a true IGHL complex tear from iatrogenic extravasation can be difficult on shoulder MR arthrography, however we have identified features that may aid the radiologist.

RC504-05 Cost-Effectiveness of MR Arthrography versus MRI for Slap Tears

Wednesday, Nov. 28 9:40AM - 9:50AM Room: S406A

Jordan Conroy, Cleveland, OH (*Abstract Co-Author*) Nothing to Disclose James Koo, New York, NY (*Abstract Co-Author*) Nothing to Disclose Morgan Jones, MD, Cleveland, OH (*Abstract Co-Author*) Nothing to Disclose Anthony Miniaci, MD, Cleveland, OH (*Abstract Co-Author*) Nothing to Disclose Soterios Gyftopoulos, MD, Scarsdale, NY (*Abstract Co-Author*) Nothing to Disclose

PURPOSE

To determine if direct magnetic resonance arthrography (MRA) is more cost-effective than a non-contrast magnetic resonance imaging (MRI) in the diagnososis and management of superior labral anterior to posterior (SLAP) tears.

METHOD AND MATERIALS

Our base case was a 25-year-old with clinical findings of a SLAP tear in whom an imaging test is being ordered for further management. Decision analysis software (TreeAge Pro) was used to create a model from the healthcare perspective to evaluate the cost-effectiveness of 4 imaging strategies: 3-Tesla (T) MRA, 3T MRI, 1.5T MRA and 1.5T MRI. Probability and utility estimates were obtained from published literature. Commercial insurance and Medicaid reimbursements were derived from 2017 Medicare rates. Effectiveness was measured in quality-adjusted life years (QALY) over a 2-year period and costs were calculated in 2017 U.S. dollars.

RESULTS

3T MRI is the least expensive (\$6126) and most effective (1.62165 QALY) strategy for our base case and is dominant to 3T MRA (\$6799, 1.6165 QALY), 1.5T MRA (\$7036, 1.60407 QALY) and 1.5T MRI (\$6965, 1.58446 QALY). 3T MRA becomes the most costeffective option if the specificity of 3T MRI drops below 90.4% with a willingness-to-pay (WTP) threshold of \$100,000. If 3T is excluded from the analysis, 1.5T MRA is dominant for our base case but 1.5T MRI becomes the most cost effective option if its specificity is higher than 80.3%. The results remained robust and did not change over a reasonable range of costs, utilities, probabilities and WTP thresholds in 1-way, 2-way and probabilistic sensitivity analyses.

CONCLUSION

3T MRI is the most cost-effective option for management of SLAP tears. If a 3T magnet is not available, 1.5T MRA is the most cost effective option. In both circumstances, the most cost effective option is the test with highest specificity.

CLINICAL RELEVANCE/APPLICATION

MRA has been traditionally considered the test of choice when evaluating labral tears, including SLAP tears. This study, however, shows that if imaging is performed at 3T, MRI is the most cost effective option and may obviate the need for patients to undergo a more invasive test.

RC504-06 Post-arthroscopy Shoulder

Wednesday, Nov. 28 9:50AM - 10:10AM Room: S406A

Participants

Adam C. Zoga, MD, Philadelphia, PA (Presenter) Nothing to Disclose

For information about this presentation, contact:

adam.zoga@jefferson.edu

Active Handout:Adam C. Zoga

http://abstract.rsna.org/uploads/2018/18000806/Zoga- post arthroscopy shoulder - handout RC504-06.pdf

LEARNING OBJECTIVES

1) To be comfortable evaluating radiographs of the shoulder after arthroscopic intervention. 2) To be prepared to select and prescribe an optimal MRI protocol. 3) To be able to identify common glenoid labrum repairs and glenoid augmentations.

RC504-07 Acromioclavicular and Sternoclavicular Joints

Wednesday, Nov. 28 10:20AM - 10:40AM Room: S406A

Participants

Bruce B. Forster, MD, Vancouver, BC (Presenter) Stockholder, Canada Diagnostic Centres

For information about this presentation, contact:

bruce.forster@vch.ca

LEARNING OBJECTIVES

1) Identify imaging findings in AC and SC joint trauma and be able to indicate how imaging changes management.

RC504-08 Multilevel Glenoid Morphology and Retroversion Assessment in Walch B2 and B3 Types

Wednesday, Nov. 28 10:40AM - 10:50AM Room: S406A

Awards

Student Travel Stipend Award

Participants

Kamran Munawar, MD, New York, NY (*Presenter*) Nothing to Disclose Soterios Gyftopoulos, MD, Scarsdale, NY (*Abstract Co-Author*) Nothing to Disclose Joseph D. Zuckerman, MD, New York, NY (*Abstract Co-Author*) Nothing to Disclose Mandeep S. Virk, MD, New York, NY (*Abstract Co-Author*) Nothing to Disclose

Mohammad M. Samim, MD, MRCS, New York, NY (Abstract Co-Author) Nothing to Disclose

For information about this presentation, contact:

kamran.munawar@nyumc.org

PURPOSE

A major factor that impacts the long-term outcome and complication rates of total shoulder arthroplasty (TSA) is the preoperative posterior glenoid bone loss quantified by glenoid retroversion. The purpose of this study was to assess if glenoid retroversion angles vary significantly at different glenoid heights in patients with Walch B2 and B3 glenoid types. Glenoid version measurements were also compared between 'conventional' CT slices and 'true' axial slices.

METHOD AND MATERIALS

386 consecutive CT shoulder studies performed for shoulder arthroplasty preoperative planning were retrospectively reviewed. Patients with B2 and B3 glenoid types were included. 'True axial' CT reconstructions were created using a validated technique. Two readers independently measured glenoid retroversion angles according to the Friedman method on true axial CT images using the 'intermediate' glenoid line at three glenoid heights: 75% (upper), 50% (equator) and 25% (lower). The 'clinical' glenoid version was measured on the conventional axial images and compared with the version measurement on the true axial images.

RESULTS

29 B2 and 8 B3 glenoid types were included. There was no statistically significant difference between the retroversion measurements performed by each reader at the three glenoid levels on the B2 or B3 glenoid types. Inter-reader correlation was substantial. There was a statistically significant difference in the mean glenoid retroversion measured on conventional versus true axial images for both B2 and B3 glenoid types, with 2° overestimation on conventional compared to true axial images (p=0.01).

CONCLUSION

We demonstrated that glenoid version can accurately be measured at any level between 25% to 75% of the glenoid height for Walch B2 and B3 types and that the conventional axial CT overestimates the degree of retroversion when compared with the true axial.

CLINICAL RELEVANCE/APPLICATION

Glenoid retroversion measurement is a crucial component of the pre-operative evaluation of patients with advanced glenohumeral osteoarthritis and can be measured accurately on true axial images at the glenoid equator.

RC504-09 Adhesive Capsulitis: MRI Correlation with Clinical Stages and Proposal of MRI Staging

Wednesday, Nov. 28 10:50AM - 11:00AM Room: S406A

Participants

Amarnath Chellathurai, MD, FRCR, Chennai, India (*Presenter*) Nothing to Disclose Kanimozhi Damu JR, MBBS, MD, Coimbatore, India (*Abstract Co-Author*) Nothing to Disclose Anand N. Parimalai, MD, Chennai, India (*Abstract Co-Author*) Nothing to Disclose Amritha Asokan, MBBS, Chennai, India (*Abstract Co-Author*) Nothing to Disclose Vijay Karthik Jagan, MBBS, Coimbatore, India (*Abstract Co-Author*) Nothing to Disclose Rajasekaran Sivaprakasam, DMRD, PhD, Chennai, India (*Abstract Co-Author*) Nothing to Disclose

For information about this presentation, contact:

amarrd02@yahoo.co.in

PURPOSE

The purpose of this study was to correlate the MR findings of adhesive capsulitis with clinical stages and thereby propose a MR staging system.

METHOD AND MATERIALS

This study consisted of 74 patients with clinically diagnosed adhesive capsulitis. The edema of the inferior glenohumeral ligament, pericapsular edema , thickness of anterior band of IGHL and axillary pouch, thickness of coracohumeral ligament, obliteration of fat in the subcoracoid triangle were evaluated by MRI.

RESULTS

Thickening of the anterior band of IGHL showed most significant correlation with the clinical stages. The distribution of edema of IGHL and pericapsular edema also showed significant correlation with the clinical stages of adhesive capsulitis. Pericapsular edema and IGHL edema was not observed in stage IV. Based on the correlation between MR findings and clinical staging , we propose a MR staging of adhesive capsulitis. The thickness of anterior band of IGHL on humeral side in range of 4.5 + 0.9 mm with no obliteration of fat in the subcoracoid triangle seen in stage I and thickness of anterior band of IGHL on humeral side in range of 7.6 + 1.9 mm with no obliteration of fat in subcoracoid triangle seen in stage II. Obliteration of fat in subcoracoid triangle with mild edema of IGHL is seen in stage III and Obliteration of fat in subcoracoid triangle with no edema of IGHL is seen in stage IV.

CONCLUSION

MR is an useful tool for evaluation and prediction of clinical stage of adhesive capsulitis.

CLINICAL RELEVANCE/APPLICATION

Imaging based grading system of adhesive capsulitis can aid in the identification of the stage of the disease even when the clinical manifestations are subtle. This helps in initiation of appropriate treatment to halt the disease progression , prevent the complications and avoid invasive treatment procedures.

RC504-10 Evaluation of On-Track/Off-Track Lesions in Anterior Shoulder Instability Using 3D Isotropic MR Arthrography and ABER (Abduction-External Rotation) Position

Participants

Federico Bruno, MD, L'Aquila, Italy (*Presenter*) Nothing to Disclose Simone Quarchioni, Laquila, Italy (*Abstract Co-Author*) Nothing to Disclose Pierpaolo Palumbo, MD, L'Aquila, Italy (*Abstract Co-Author*) Nothing to Disclose Ester Cannizzaro, MD, L'Aquila, Italy (*Abstract Co-Author*) Nothing to Disclose Camilla Gianneramo, LAquila, Italy (*Abstract Co-Author*) Nothing to Disclose Silvia Mariani, MD, L'Aquila, Italy (*Abstract Co-Author*) Nothing to Disclose Antonio Barile, MD, L'Aquila, Italy (*Abstract Co-Author*) Nothing to Disclose Carlo Masciocchi, MD, L'Aquila, Italy (*Abstract Co-Author*) Nothing to Disclose

For information about this presentation, contact:

federico.bruno.1988@gmail.com

PURPOSE

To assess the ability of shoulder 3D MRA and additional ABER scans to quantify bipolar bone loss and detect on-track/off-track lesions in traumatic shoulder instability, using MPR CT images as a reference standard

METHOD AND MATERIALS

We evaluated 23 consecutive patients (15 men, 8 women, mean age 27.6 years, range 19-46) with anterior shoulder instability. All patients were submitted to 3D-CT of the shoulder and direct shoulder MR Arthrography using three-dimensional (3D) isotropic PD sequences in standard and ABER position. Two observers evaluated the images twice in a randomized and blinded way to calculate the glenoid track, the Hill-Sachs interval and to predict engagement using the 'on-track/off-track' method. The intra- and inter-observer agreement were calculated

RESULTS

Of the 23 defect combinations, 14 were classified as non-engaging and 9 as engaging, using the 'on-track/off-track' method. The intra-observer reliability was 0.921 for 3D-CT and 0.786 for MR Arthrography . The inter-observer agreement ranged from 'substantial' to 'almost perfect' for both glenoid track and Hill-Sachs interval measurement (p<0.005). ABER MR Arthrography predicted engagement accurately in 21 cases (91.3%).

CONCLUSION

MR Arthrography using 3D isotropic PD sequences is a feasible approach for measuring bony defects in patients with anterior shoulder instability and bipolar bone loss using the 'on-track/off-track' method. The same sequence in ABER position showed and added value in direct prediction of the presence of engaging lesions

CLINICAL RELEVANCE/APPLICATION

Prediction of engaging lesions using the glenoid track method represents a valuable tool for the surgeon, that can be used preoperatively to plan the type of stabilization procedure to be performed in patients with anterior shoulder instability

RC504-11 Extra-articular Shoulder

Wednesday, Nov. 28 11:10AM - 11:35AM Room: S406A

Participants

Erin F. Alaia, MD, New York, NY (Presenter) Nothing to Disclose

For information about this presentation, contact:

Erin.Fitzgerald@nyumc.org

LEARNING OBJECTIVES

1) Apply a systematic approach to evaluating extra-articular pathology about the shoulder. 2) Review commonly encountered osseous and soft tissue extra-articular shoulder pathology.

RC504-12 Biceps

Wednesday, Nov. 28 11:35AM - 12:00PM Room: S406A

Participants Lynne S. Steinbach, MD, Tiburon, CA (*Presenter*) Nothing to Disclose

LEARNING OBJECTIVES

1) Review the MR imaging characteristics of normal anatomy, congenital variants and abnormalities of the long head of the biceps at the shoulder.

ABSTRACT

The long head of the biceps tendon originates at the supraglenoid tubercle and attaches to the superior labrum at the anchor. It courses through the glenohumeral joint where it is anchored by a pulley comprised of the superior glenohumeral ligament and coracohumeral ligament before it extends into the bicipital groove and down to the corresponding muscle of the upper arm. There can be anomalies of the biceps tendon ranging from absence to origin from the supraspinatus tendon. The supraspinatus aponeurosis is present in some individuals and lies in front of the biceps in the groove. This should not be mistaken for a tear. The tendon can become degenerated with tendinosis and can tear in the glenohumeral joint at any location. It often tears near the labral attachment and in younger patients this is associated with a SLAP lesion. In the region of the pulley proximal to the groove it can undergo tendinosis and the enlargement of the tendon prevents its excursion into the groove, producing pain upon motion of the biceps for everyday tasks. This is called the hourglass biceps. The biceps pulley may tear. The biceps is intimately associated

with the subscapularis and supraspinatus tendons when it enters the bicipital groove. Tears of these tendons can be associated with biceps subluxation or dislocation. This has been classified by Habermayer. The biceps sheath is continuous with the glenohumeral joint, so fluid surrounding the biceps can be normal. Fluid in the sheath can also be associated with tenosynovitis in the groove. The tendon may tear at any location along its length. Treatment for biceps problems is usually resection of the proximal biceps (tenotomy) or resection of the proximal biceps with anchoring of the proximal portion in the humerus (tenodesis).



Neuroradiology Series: Stroke

Wednesday, Nov. 28 8:30AM - 12:00PM Room: E450A



AMA PRA Category 1 Credits ™: 3.50 ARRT Category A+ Credits: 4.00

FDA Discussions may include off-label uses.

Participants

Max Wintermark, MD, Lausanne, Switzerland (*Moderator*) Advisory Board, General Electric Company; Consultant, More Health; Consultant, Magnetic Insight; Consultant, Icometrix; Consultant, Nines;

Achala S. Vagal, MD, Mason, OH (*Moderator*) Research Consultant, Nervive; Research Grant, Imaging Core Lab; Research Grant, ENDOLOW; Grant, Johnson & Johnson

For information about this presentation, contact:

max.wintermark@gmail.com

Sub-Events

RC505-01 Update on Stroke Management in the Era of DAWN and DEFUSE-3

Wednesday, Nov. 28 8:30AM - 9:00AM Room: E450A

Participants

Raul G. Nogueira, MD, Boston, MA (*Presenter*) Investigator, Steering Committee, Stryker Corporation; Steering Committee, Medtronic plc; Executive Committee, Penumbra, Inc; Investigator, Advisory Board, Neuravi Ltd; Advisory Board, phenox GmbH; Advisory Board, Anaconda; Advisory Board, F. Hoffmann-La Roche Ltd; Advisory Board, Biogen Idec Inc; Advisory Board, Prolong Pharmaceuticals; Advisory Board, Allm, Inc; Advisory Board, Stockholder, Viz-Al; Advisory Board, Stockholder, Vesalio; Advisory Board, Stockholder, Ceretrieve; Editor, Interventional Neurology Journal; ;

RC505-02 Lifetime Benefit and Cost Consequences of the Achieved Grade of Reperfusion After Thrombectomy for Stroke Based on HERMES Collaboration Data

Wednesday, Nov. 28 9:00AM - 9:10AM Room: E450A

Participants

Wolfgang G. Kunz, MD, Munich, Germany (Presenter) Grant, Medtronic plc Mohammed A. Almekhlafi, MD, MSc, Calgary, AB (Abstract Co-Author) Grant, Medtronic plc Bijoy Menon, MBBS, MD, Calgary, AB (Abstract Co-Author) Grant, Medtronic plc Jeffrey Saver, MD, Los Angeles, CA (Abstract Co-Author) Grant, Medtronic plc Diederik Dippel, Rotterdam, Netherlands (*Abstract Co-Author*) Research Grant, Stryker Corporation; Grant, Medtronic plc Mayank Goyal, MD, FRCPC, Calgary, AB (*Abstract Co-Author*) Grant, Medtronic plc; Consultant, Medtronic plc; Consultant, Stryker Corporation; Consultant, Terumo Corporation; Consultant, Cerenovus David S. Liebeskind, Los Angeles, CA (Abstract Co-Author) Nothing to Disclose Tudor G. Jovin, MD, Pittsburgh, PA (Abstract Co-Author) Grant, Medtronic plc Antoni Davalos, MD, Barcelona, Spain (Abstract Co-Author) Grant, Medtronic plc Serge Bracard, Nancy, France (Abstract Co-Author) Grant, Medtronic plc Francis Guillemin Sr, MD, Nancy, France (Abstract Co-Author) Grant, Medtronic plc Bruce Campbell, Melbourne, Australia (Abstract Co-Author) Grant, Medtronic plc Peter Mitchell, Melbourne, Australia (Abstract Co-Author) Grant, Medtronic plc Phil White, MSc, MD, Newcastle-upon-Tyne, United Kingdom (Abstract Co-Author) Research Consultant, Terumo Corporation; Institutional Research funded, Terumo Corporation; Grant, Medtronic plc Keith Muir, MD, Glasgow, United Kingdom (Abstract Co-Author) Grant, Medtronic plc Scott Brown, PhD, St Louis, MN (Abstract Co-Author) Grant, Medtronic plc Andrew Demchuk, MD, Calgary, AB (Abstract Co-Author) Grant, Medtronic plc Michael D. Hill, MD, Calgary, AB (Abstract Co-Author) Grant, Medtronic plc Charles B. Majoie, MD, PhD, Amsterdam, Netherlands (Abstract Co-Author) Institutional Research Grant, Stryker Corporation

For information about this presentation, contact:

wolfgang.kunz@med.lmu.de

PURPOSE

The benefit that endovascular thrombectomy (EVT) offers to stroke patients with large vessel occlusions depends strongly on reperfusion grade as defined by the eTICI (extended Thrombolysis in Cerebral Infarction) scale. Our aim was to determine the lifetime quality of life and cost consequences of reperfusion for patients, healthcare systems, and society.

METHOD AND MATERIALS

A Markov model estimated lifetime quality-adjusted life years (QALY) of EVT-treated patients and associated costs based on eTICI

grades (model structure in Figure 1). The analysis was performed from a United States perspective with two cost frameworks: 1) healthcare costs and 2) societal costs, which include productivity losses and costs of informal care given by family members. Input parameters were based on best available evidence (Table 1), including patient data from the 7-trial HERMES collaboration (ESCAPE, EXTEND-IA, MR CLEAN, REVASCAT, SWIFT PRIME, PISTE, THRACE; Figure 2). The lead analysis was conducted for stroke onset at 65 years. Probabilistic sensitivity analysis was performed using Monte Carlo simulations.

RESULTS

Lifetime QALYs increased for every grade of improved reperfusion (Figure 3A). On average, eTICI 3 resulted in 6.50 QALYs over the patients' lifetimes, eTICI 2c (90-99%) in 5.89 QALYs, eTICI 2b (67-89%) in 5.79 QALYs, eTICI 2b (50-66%) in 4.80 QALYs, eTICI 2a in 3.55 QALYs, and eTICI 1 or 0 in 2.57 QALYs. In contrast, the healthcare and societal costs of each QALY yielded by EVT decreased for every grade of improved reperfusion (Figure 3B). The advantage of achieving eTICI 3 over eTICI 2b (50-66%) reperfusion results in average cost-savings of about \$15,000/QALY per patient incurred by the healthcare system and \$20,000/QALY per patient incurred by the society.

CONCLUSION

Every grade of improved reperfusion grants stroke patients additional QALYs and substantially reduces healthcare and societal costs per QALY.

CLINICAL RELEVANCE/APPLICATION

Procedural strategies to achieve complete reperfusion (eTICI 3) should be assessed for safety and feasibility, even when initial reperfusion seems to be adequate (eTICI 2b).

RC505-03 Preliminary Study of Hypoxic Exposure Effect on Cerebral Blood Perfusion of Pilots Using 3D ASL

Wednesday, Nov. 28 9:10AM - 9:20AM Room: E450A

Participants

Liu Jie, Zheng Zhou, China (*Presenter*) Nothing to Disclose Wanshi Zhang, MD, Beijing, China (*Abstract Co-Author*) Nothing to Disclose Cheng Jing liang, Henan, China (*Abstract Co-Author*) Nothing to Disclose Long Qian, Beijing, China (*Abstract Co-Author*) Nothing to Disclose

For information about this presentation, contact:

tongnuo@yeah.neet

PURPOSE

To investigate how the cerebral blood perfusion changed in pilots with hypoxic exposure through the measurement of resting cerebral blood flow (CBF) using a 3D pcASL technique

METHOD AND MATERIALS

35 healthy male pilots (mean age 30 years, mean total flight time 1328 h) were included in this study. In order to investigate the change of CBF of the brain in the condition of hypoxic exposure, the low oxygen mixed gas inhaled by participants through a breathing mask was approximate to the air composition at the altitude of 3000 m with the oxygen concentration of 14.5%. Pulse oximetry was applied to monitor in real-time the immediate pulse and oxygenation saturation of each subject pre- and post-hypoxic exposure. Then, 3D pcASL images were acquired at both pre- (pre-OI) and post-low oxygen mixed gas inhalation (post-OI) using 3D-FSPGR BRAVO sequence on a 3.0T scanner (GE MR750, WI, US) with the scanning parameters: TR/TE= 4632ms/10.5ms; FOV=24cm2; slice thickness = 4.0mm; bandwidth=62.5KHz; flip angle=111°. Thereafter, CBF maps could be calculated from the acquired 3D pcASL images using an automatic software in the AW workstation of GE. To enhance the spatial normalization, T1 axial plane anatomical image were also acquired. CBF maps were preprocessed and analyzed by FSL and SPM8

RESULTS

After hypoxic exposure, the pulse was (63.97 ± 10.43) beats/min, the oxygen saturation was (92.46 ± 3.64) %, it's significant lower than initiate examination ((71.46±10.63) beats/min, (96.31±1.23) %). 3D pcASL scan for pilots after hypoxic exposure showed lower CBF values in various regions, including bilateral superior temporal gyrus (STG), middle temporal gyrus (MTG), lingual gyrus, left inferior temporal gyrus (ITG), right middle occipital gyrus (MOG), inferior occipital gyrus (IOG), fusiform gyrus, cuneus and cerebellum (P<0.05), as shown in Tab.1 and Fig. 1

CONCLUSION

3D pseudo-continuous arterial spin-labeling technique could monitor CBF changes in pilots with hypoxic exposure, and the cerebral blood perfusion after hypoxic exposure was decreased mainly in the temporal and right occipital lobes.

CLINICAL RELEVANCE/APPLICATION

For the first time, in this study we mimicked hypoxic environment equal to 3000m altitude and obtained the CBF of the subjects before and after hypoxic exposure using 3D pcASL, and then fixed the corresponding brain areas.

RC505-04 Clinical and Imaging Parameters Associated With Pre-Hospital Infarction Growth in Patients with Large Vessel Occlusion Stroke Undergoing Endovascular Thrombectomy

Wednesday, Nov. 28 9:20AM - 9:30AM Room: E450A

Participants

Daniel Puhr-Westerheide, MD, Munich, Germany (*Presenter*) Nothing to Disclose Steffen Tiedt, Munich, Germany (*Abstract Co-Author*) Nothing to Disclose Lukas Rotkopf, Munich, Germany (*Abstract Co-Author*) Nothing to Disclose Moriz Herzberg, Munich, Germany (*Abstract Co-Author*) Nothing to Disclose Paul Reidler, MD, Munich, Germany (*Abstract Co-Author*) Nothing to Disclose Wolfgang G. Kunz, MD, Munich, Germany (*Abstract Co-Author*) Grant, Medtronic plc Felix Schuler, Munich, Germany (*Abstract Co-Author*) Nothing to Disclose Lars Kellert, Munich, Germany (*Abstract Co-Author*) Nothing to Disclose Kolja M. Thierfelder, MD,MSc, Rostock, Germany (*Abstract Co-Author*) Nothing to Disclose Franziska Dorn, Munich, Germany (*Abstract Co-Author*) Nothing to Disclose Frank Wollenweber, Munich, Germany (*Abstract Co-Author*) Nothing to Disclose

For information about this presentation, contact:

daniel.puhr-westerheide@med.uni-muenchen.de

PURPOSE

Large vessel occlusion (LVO) stroke leads to highly variable infarction growth before hospital admission as demonstrated by DAWN and DEFUSE 3. Our aim was to identify the clinical and imaging parameters affecting pre-hospital infarction growth in patients undergoing subsequent thrombectomy.

METHOD AND MATERIALS

We selected patients with documented times from symptom onset (TFSO) and CT perfusion (CTP) imaging on admission out of 226 consecutive patients treated with thrombectomy for anterior circulation LVO stroke. Two independent, blinded readers evaluated imaging. Ischemic core volume (ICV) was determined based on CTP using automated thresholds. Pre-hospital infarction growth was defined as ICV divided by TFSO, assuming linear progression during the time from symptom onset to admission. For collateral assessment, the regional leptomeningeal collateral score (rLMC) was assessed. Clinical data including the National Institutes of Health Stroke Scale (NIHSS) score on admission were obtained. Regression analysis was performed to adjust for confounders.

RESULTS

In the total 94 patients included in this study, the median pre-hospital infarction growth was 0.34 mL/min. In regression analysis including age, sex, stroke side, NIHSS, clot burden score, Alberta Stroke Program Early CT Score, rLMC scores and systemic blood pressure on admission, only rLMC scores showed an independent association with pre-hospital infarction growth (b=-0.31, p=0.042). Trichotomizing patients by rLMC score yielded 31 patients with good (rLMC >16; 33%), 28 with intermediate (rLMC 13-16; 30%) and 35 with poor collaterals (rLMC <13; 37%). The pre-hospital infarction growth was 0.22 mL/min in patients with good, 0.35 mL/min in patients with intermediate and 0.58 mL/min in patients with poor collateral scores. The unadjusted data of ICV and TFSO are plotted by collateral grade in Figure 1.

CONCLUSION

Pre-hospital infarction growth strongly depends on collateral flow and may be a useful parameter to triage slow and fast stroke progressors. In contrast, clinical or other imaging parameters contained no relevant information on the individual stroke dynamics.

CLINICAL RELEVANCE/APPLICATION

In primary stroke centers, pre-hospital infarction growth may be interpolated to estimate the stroke progression during transfer times to thrombectomy centers and provide decision support on which patients to transfer.

RC505-05 Volumetric Segmentation of Acute Brain Infarcts on Diffusion-Weighted Imaging using Deep Learning

Wednesday, Nov. 28 9:30AM - 9:40AM Room: E450A

Awards Student Travel Stipend Award

Participants Ken Chang, Boston, MA (*Presenter*) Nothing to Disclose James M. Brown, PhD, Charlestown, MA (*Abstract Co-Author*) Nothing to Disclose Andrew Beers, Charlestown, MA (*Abstract Co-Author*) Nothing to Disclose Bruce R. Rosen, MD, PhD, Charlestown, MA (*Abstract Co-Author*) Nothing to Disclose Hakan Ay, Boston, MA (*Abstract Co-Author*) Nothing to Disclose Jayashree Kalpathy-Cramer, MS, PhD, Charlestown, MA (*Abstract Co-Author*) Consultant, Infotech Software Solution

For information about this presentation, contact:

kalpathy@nmr.mgh.harvard.edu

PURPOSE

Important decisions in stroke management currently rely on accurate estimation of the volume of acute ischemic brain injury. However, manual delineation of stroke regions is time-consuming and subject to inter-rater variability. In this study, we evaluate the ability of a deep learning approach for ischemic stroke volumetric segmentation in a large clinical dataset of 1,247 patients.

METHOD AND MATERIALS

Our patient cohort included 1,247 patients from the NIH-funded Heart-Brain Interactions in Human Acute Ischemic Stroke Study, recruited between June 2009 and December 2011. Expert manual annotations of acute infarcts were generated using an image outlining software (MRICron). The patients were randomly divided into training (n = 998) and testing (n=247) set in a 4:1 ratio. Only the training set was used to train our deep-learning algorithm. We utilized the 3D U-Net architecture, a network designed for fast and precise segmentation, with Nestorov Adaptive Moment Estimation optimizer and a soft dice loss function. 20 patches of size 64x64x8 were extracted for each patient in the training set and augmented by sagittal flipping. The network was trained for 30 iterations through all extracted patches on a NVIDIA Tesla P100 graphics processing unit.

RESULTS

Within the training set, the mean dice similarity coefficient was 0.679 (95% Confidence Interval, CI, 0.018-0.931) with a mean sensitivity of 0.703 (95% CI 0.026-0.979) and specificity of 1.000 (95% CI 0.977-1.000). Within the testing set, the mean dice was 0.626 (95% Confidence Interval, CI, 0.009-0.912) with a mean sensitivity of 0.648 (95% CI 0.018-0.990) and specificity of 0.999 (95% CI 0.995-1.000). In comparing manually and automatically derived infarct volumes, the Intraclass Correlation Coefficient was 0.938 (p<.0001) in the training set and 0.964 (p<.0001) in the testing set.

CONCLUSION

Our fully-automatic pipeline for stroke segmentation demonstrate the potential for deep learning-based tools to automate ischemic stroke volumetrics.

CLINICAL RELEVANCE/APPLICATION

Automatic localization and calculation of volume of ischemic stroke on diffusion-weighted imaging may bypass the need for manual segmentation, assist with timely decision making for clinical management, and hence, reduce the risk of adverse patient outcomes.

RC505-06 Fast Stroke Triage: CT and MR Protocols

Wednesday, Nov. 28 9:40AM - 10:10AM Room: E450A

Participants

Howard A. Rowley, MD, Madison, WI (*Presenter*) Research Consultant, Bracco Group; Research Consultant, Guerbet SA; Research Consultant, General Electric Company; Consultant, W.L. Gore & Associates, Inc; ;; ;; ;;

For information about this presentation, contact:

hrowley@uwhealth.org

LEARNING OBJECTIVES

1) List the key goals of imaging triage in acute ischemic stroke. 2) Streamline workflow in CT and MRI to facilitate rapid and accurate treatment selection. 3) Describe the practice and pitfalls of perfusion methods in acute stroke triage. 4) Build fast and effective CT and MR protocols for stroke triage in your practice.

Honored Educators

Presenters or authors on this event have been recognized as RSNA Honored Educators for participating in multiple qualifying educational activities. Honored Educators are invested in furthering the profession of radiology by delivering high-quality educational content in their field of study. Learn how you can become an honored educator by visiting the website at: https://www.rsna.org/Honored-Educator-Award/ Howard A. Rowley, MD - 2016 Honored Educator

RC505-07 When to Swing at the Curveball: Treating Stroke Patients Who Don't Quite Match the Clinical Trials

Wednesday, Nov. 28 10:20AM - 10:50AM Room: E450A

Participants

Steven W. Hetts, MD, San Francisco, CA (*Presenter*) Royalties, Penumbra, Inc; Stockholder, ThrombX Inc; Researcher, Stryker Corporation; Researcher, Terumo Corporation; Researcher, Siemens AG

For information about this presentation, contact:

steven.hetts@ucsf.edu

LEARNING OBJECTIVES

1) Describe groups of patients suffering acute ischemic strokes who fall outside the inclusion criteria for recent randomized controlled trials who, nevertheless, may benefit from acute endovascular therapy. 2) Develop an approach to trauma patients at risk for ischemic stroke. 3) Evaluate the treatment of patients outside the age ranges subjected to clinical trials to date.

RC505-08 Texture Analysis to Identify Early Thrombus in Stroke Patients with Cerebral Artery Occlusion: A High-resolution MRI Study

Wednesday, Nov. 28 10:50AM - 11:00AM Room: E450A

Participants

Jinhao Lyu, Beijing, China (*Presenter*) Nothing to Disclose Yanqun Yao, Taiyuan, China (*Abstract Co-Author*) Nothing to Disclose Ruifeng Zhao, Jincheng, China (*Abstract Co-Author*) Nothing to Disclose Huabing Li, Jincheng, China (*Abstract Co-Author*) Nothing to Disclose Jilong Jin, Jincheng, China (*Abstract Co-Author*) Nothing to Disclose Xiaoxiao Ma, Beijing, China (*Abstract Co-Author*) Nothing to Disclose Lan Lin, Beijing, China (*Abstract Co-Author*) Nothing to Disclose Yina Lan, Beijing, China (*Abstract Co-Author*) Nothing to Disclose Jianfeng He, Beijing, China (*Abstract Co-Author*) Nothing to Disclose Lin Ma, MD, Beijing, China (*Abstract Co-Author*) Nothing to Disclose Xin Lou, MD, PhD, Beijing, China (*Abstract Co-Author*) Nothing to Disclose

PURPOSE

In the present study, we aimed to identify the features of early thrombus by qualitative evaluation and by quantitatively texture analysis based on thrombus imaging from High-resolution vessel wall imaging (HRVWI).

METHOD AND MATERIALS

The prospective study recruited patients with cerebrovascular occlusion from January 2017 to January 2018. Three-dimensional black blood T1WI HRVWI was performed in a 3.0T scanner (Skyra, Siemens) with a voxel size of 0.6mm. Thrombus was identified when visible embolization of intraluminal material downstream was present. Early thrombus was defined as symptomatic culprit thrombus within 24 hours after symptom onset. Late to chronic thrombus was defined as symptomatic culprit thrombus >24 hours after symptom onset, previous confirmed thrombus and asymptomatic thrombus. Signal intensity patterns and vascular involvement patterns of thrombus on black blood T1WI HRVWI were categorized into patterns as illustrated in Figure. Regions of interest (ROIs) were manually outlined on the optimal 2D multiple planar reconstructions of the thrombus. Each ROI was decimated to 64 gray-levels. A gray-level co-occurrence matrix was calculated for each ROI. Comparisons between patients with early thrombus and with

late to chronic thrombus were performed. ROC was performed to measure the area under the curve (AUC) for the diagnostic efficiency estimation.

RESULTS

Totally 19 patients with 23 occlusive vessels were recruited in the current study. Four occlusive vessels were confirmed to have early thrombus and 19 occlusive vessels were confirmed to have late to chronic thrombus. For thrombus qualitative analysis, the proportion of each signal intensity pattern and vascular involvement pattern of early thrombus and late to chronic thrombus on black blood T1WI HRVWI showed no significant differences. In texture analysis, 'correlate' was significantly different between early thrombus and late to chronic thrombus. AUC of 'correlate' to differentiate early thrombus from late to chronic thrombus was 0.908(P<0.001). A threshold of <= 0.330 was with a sensitivity of 100% and specificity of 78.95%.

CONCLUSION

Textural feature may be an effective imaging marker to identify early thrombus. Further studies are warranted to verify the finding.

CLINICAL RELEVANCE/APPLICATION

The textural analysis is helpful to identify early thrombus in patients with ischemic stroke and thus to support the therapy decision making.

RC505-09 Detection of the Ischemic Core in Multiphase-CT Angiography: Validation of Patients with Acute Ischemic Stroke

Wednesday, Nov. 28 11:00AM - 11:10AM Room: E450A

Participants

Tomomi Omura, Akita, Japan (*Presenter*) Nothing to Disclose Yongbum Lee, PhD, Niigata, Japan (*Abstract Co-Author*) Nothing to Disclose Noriyuki Takahashi, Akita, Japan (*Abstract Co-Author*) Nothing to Disclose Toshibumi Kinoshita, MD, PhD, Akita, Japan (*Abstract Co-Author*) Nothing to Disclose Mamoru Kato, PhD, Akita, Japan (*Abstract Co-Author*) Nothing to Disclose Yuki Shinohara, MD,PhD, Akita, Japan (*Abstract Co-Author*) Nothing to Disclose Hideto Toyoshima, BSc, Akita, Japan (*Abstract Co-Author*) Nothing to Disclose

For information about this presentation, contact:

t-omu@akita-noken.jp

PURPOSE

Multiphase CT angiography (MP-CTA) is a quick and easy-to-use imaging tool for assessing collateral circulation in patients with acute ischemic stroke (AIS). Pial arterial filling in the ischemic territory of the AIS patients is assessment by comparing it to similar arteries in the unaffected hemisphere. However, no method has been established for identifying the ischemic core territory which is an indication of mechanical thrombectomy. We developed a novel method to assess ischemic core of brain tissue using MP-CTA images. The purpose of this study is to verify the usefulness of a novel method (phase ratio map; PR map) compared with MP-CTA images in assess of AIS patients.

METHOD AND MATERIALS

The AIS patients was scanned using an area detector CT scanner (Aquilion ONE Groval Standard Edition; Toshiba Medical). CT images were acquired at 80 kV and 80 mA. CTP source images (CTP-SI) were obtained at 1-s intervals using dynamic multiphase imaging. PR map was constructed using CTP-SI. An early-phase image (EPI) was generated by computing the average of CTP-SI for 5 s in the vicinity of the peak enhancement curve of the normal hemisphere. Similarly, a late-phase image (LPI) was generated by computing the average of CTP-SI for 5 s immediately after the early phase. Subsequently EPI and LPI were denoised of images and was subtracted by mask image. Finally, The PR map was created by dividing the EPI by the LPI. The pixel value of the PR map is determined by the filling degree of the contrast medium. The ischemic core without filling shows 0, the ischemic region with a slow filling shows 1 or less. MP-CTA produced slab MIP images with a thickness of 24 mm using EPI and LPI. Pial arterial filling of MP-CTA was scored from the best 5 points to the worst 0 point ordinal scale. Twenty three patients (14 men, 9 women; mean age: 66.8 years) with AIS underwent CTP. To investigate the validity of the PR map, the ischemic core territory and the MP-CTA scoring were compared.

RESULTS

The ischemic core size of PR map was consistent with the score of MP-CTA (score 4: 0 ml, score 3: 2.7 ± 2.2 ml, score 2: 8.6 ± 5.4 ml). In addition, PR map visually showed clear ischemic core territory.

CONCLUSION

The results suggested that the PR map would provide more robust information than MP-CTA in the diagnosis of AIS patients.

CLINICAL RELEVANCE/APPLICATION

Acute ischemic stroke, Large vessel occlusion, Multi phase CT-Angiography, Mechanical thrombectomy

RC505-10 Stroke Outcome Prediction from Meta Information Available at Patient Admission

Wednesday, Nov. 28 11:10AM - 11:20AM Room: E450A

Participants

Yuan Xie, Stanford, CA (*Presenter*) Nothing to Disclose Bin Jiang, Beijing, China (*Abstract Co-Author*) Nothing to Disclose Enhao Gong, PhD, Stanford, CA (*Abstract Co-Author*) Stockholder, Subtle Medical Ying N. Li, Stanford, CA (*Abstract Co-Author*) Nothing to Disclose Guangming Zhu, Beijing, China (*Abstract Co-Author*) Nothing to Disclose Bo Zhou, Stanford, CA (*Abstract Co-Author*) Nothing to Disclose Patrik Michel, Lausanne, Switzerland (*Abstract Co-Author*) Nothing to Disclose Max Wintermark, MD, Lausanne, Switzerland (*Abstract Co-Author*) Advisory Board, General Electric Company; Consultant, More Health; Consultant, Magnetic Insight; Consultant, Icometrix; Consultant, Nines; Greg Zaharchuk, MD, PhD, Stanford, CA (*Abstract Co-Author*) Research Grant, General Electric Company; Stockholder, Subtle Medical;

PURPOSE

Acute stroke patients' recovery are usually evaluated using mRS, ranging from 0 for no symptoms to 6 for deceased. Early estimation of future mRS has high clinical utility as it represents recovery outcome, with mRS <=2 considered as a good recovery. We demonstrate that by applying machine learning techniques to a mix of clinical and imaging-derived data, we can accurately predict 3-month outcome in acute stroke patients.

METHOD AND MATERIALS

520 internal carotid artery (ICA) and middle cerebral artery (MCA) stroke patients were included in the study, with 3-month mRS as the goal of prediction. 24 initial features such as age, gender, Alberta stroke program early CT score (ASPECTS), and infarct volume from CTP and CT angiograms at patient's admission were used for prediction. Gradient Boosting Tree model (GBT) and Extreme Gradient Boosting Machine (xgboost) were constructed for binary prediction of mRS ('good' : 0~2, 'bad': 3~6) and full multiclass prediction (mRS 0~6). Final features were curated from the 24 initial features through a stochastic feature selection algorithm. Hyperparameters were optimized for minimized mean square error (MSE) of regression task. 5-fold cross validation was applied to estimate model performance.

RESULTS

Feature curation shows that xgboost can accurately predict the mRS using only 5 features: ASPECTS, age, hyperdense middle cerebral artery sign, NIH stroke score at 24 hours, and left-sided North American Symptomatic Carotid Endarterectomy Trial score. Binary xgboost produced an Area-under-curve (AUC) of 0.884 with selected features and an AUC of 0.873 without feature selection. Binary GBT achieved a slightly lower AUC of 0.876 with selected features, and 0.849 without feature selection. For multiclass prediction, xgboost achieved Mean Squared Error (MSE) of 1.6 and 85.2% predictions are within +/- 1 categories. GBT achieved also a MSE of 1.6 while only 68.2% predictions are within +/- 1 categories.

CONCLUSION

Using information available at diagnosis, machine learning models can accurately predict the recovery outcome at 3 months. An xgboost algorithm using curated clinical and imaging-based features achieves the best performance.

CLINICAL RELEVANCE/APPLICATION

Using machine learning, an acute stroke patient's 3-month outcome can be accurately predicted with data available at admission, improving treatment planning and recovery evaluation.

Honored Educators

Presenters or authors on this event have been recognized as RSNA Honored Educators for participating in multiple qualifying educational activities. Honored Educators are invested in furthering the profession of radiology by delivering high-quality educational content in their field of study. Learn how you can become an honored educator by visiting the website at: https://www.rsna.org/Honored-Educator-Award/ Max Wintermark, MD - 2018 Honored Educator

RC505-11 Stroke Aphasia Treatment Strengthens Functional Network Activity

Wednesday, Nov. 28 11:20AM - 11:30AM Room: E450A

Participants Michael Iorga, Chicago, IL (*Presenter*) Nothing to Disclose James Higgins, BA, Chicago, IL (*Abstract Co-Author*) Nothing to Disclose Todd Parrish, PhD, Chicago, IL (*Abstract Co-Author*) Nothing to Disclose

For information about this presentation, contact:

michael.iorga@northwestern.edu

PURPOSE

Aphasia is a common and debilitating complication of stroke, for which treatment is unrefined and responses are highly variable. However, functional magnetic resonance imaging (fMRI) is not used in the assessment of stroke aphasia. By monitoring changes in resting networks which occur with deficits and treatment, treatment-responsive patterns may be identified. Once the relationship of aphasia therapy and functional imaging is better defined, there is potential to predict which therapy a given patient will benefit most from, and how to modify existing treatments to maximize outcomes.

METHOD AND MATERIALS

We followed 60 right-handed subjects with past left hemisphere strokes from three institutions who participated in one of three aphasia therapies (sentence comprehension & production, naming, spelling). Each subject had a resting-state fMRI at baseline, and following three months of treatment. Group independent component analysis (GICA) was used to decompose all scans into 20 primary networks. The fractional amplitude of low-frequency fluctuations (fALFF) was measured for each network's time series, and compared in subjects before and after treatment.

RESULTS

Of twenty networks, three were observed to increase in activity across sentence comprehension and production treatment, four increased in spelling treatment, and five increased in naming treatment (p < 0.05, Wilcoxon Signed Rank Test). Four networks were found to differentiate between initial aphasia deficits (p < 0.05, Kruskal-Wallis Analysis of Variance). A naive bayesian classifier was constructed, using these four networks as features, which classified aphasia deficits with 75% accuracy (leave-one-out cross-validation).

CONCLUSION

Stroke aphasia treatment for sentence comprehension & production, naming, and spelling each alter patterns of activity in restingstate functional networks. Networks are typically treatment-specific, with the exception of one component which was elevated across treatments. Most components were more pronounced in the right hemisphere. Component specificity was observed at baseline across deficits, suggesting potential utility for fMRI in aphasia assessment.

CLINICAL RELEVANCE/APPLICATION

Treatment outcomes for stroke aphasia have high variability, suggesting treatment requires further optimization. Changes in resting fMRI networks may provide insight to treatment effects.

RC505-12 Carotid Plaque Imaging

Wednesday, Nov. 28 11:30AM - 12:00PM Room: E450A

Participants

J. Kevin Demarco, MD, Bethesda, MD (Presenter) Nothing to Disclose

LEARNING OBJECTIVES

1) Define the CT and MR appearance of three vulnerable carotid plaque features. 2) Describe how these three vulnerable plaque features are associated with improved risk assessment compared with simple carotid stenosis measurements. 3) Assess the ability of MR to depict the individual patient's response to new medical therapy by measuring the change in these three vulnerable carotid plaque features.



Essentials of Temporal Bone Imaging

Wednesday, Nov. 28 8:30AM - 10:00AM Room: E451A

CT HN MR NR

AMA PRA Category 1 Credits ™: 1.50 ARRT Category A+ Credit: 1.75

FDA Discussions may include off-label uses.

For information about this presentation, contact:

shatzkes@hotmail.com

Sub-Events

RC506A Optimizing Temporal Bone CT and MR Imaging

Participants

Joseph M. Hoxworth, MD, Scottsdale, AZ (Presenter) Nothing to Disclose

LEARNING OBJECTIVES

1) Appraise the adequacy of CT and MR protocols for temporal bone imaging. 2) Modify temporal bone CT and MR protocols based on specific clinical indications.

RC506B Cholesteatoma and Non-cholesteatomatous Inflammatory Disease

Participants Amy F. Juliano, MD, BOSTON, MA (*Presenter*) Nothing to Disclose

For information about this presentation, contact:

amy_juliano@meei.harvard.edu

LEARNING OBJECTIVES

1) Be familiar with the inflammatory disease entities that occur in the temporal bone. 2) Understand the pathophysiology of cholesteatoma and other inflammatory processes. 3) Recognize the imaging appearance of these diseases on CT and MR imaging. 4) Know the differential diagnoses, versus when certain imaging characteristics may be pathognomonic for one particular entity.

RC506C Temporal Bone Tumors

Participants Nikdokht Farid, MD, San Diego, CA (*Presenter*) Nothing to Disclose

For information about this presentation, contact:

nfarid@ucsd.edu

LEARNING OBJECTIVES

1) To become familiar with the different types of tumors which arise in the temporal bone by considering the differential for masses in specific regions of the temporal bone-i.e. internal auditory canal, jugular fossa region, middle ear, and petrous apex. 2) To recognize key imaging features of the various types of tumors arising in the temporal bone in order to provide accurate and useful differential diagnoses to our clinical colleagues.

RC506D Imaging of the Post-operative Temporal Bone

Participants Gul Moonis, MD, New York, NY (*Presenter*) Nothing to Disclose

For information about this presentation, contact:

gm2640@cumc.columbia.edu

LEARNING OBJECTIVES

1) Review surgical options for otomastoiditis and cholesteatoma. 2) Learn to differentiate between canal wall up and down mastoidecotomy. 3) Discuss the complications pertaining to temporal bone surgeries. 4) Illustrate imaging findings of cochlear implants.



Urolithiasis: Urologist Perspective, Recent Imaging Advances, and Relevance to Practice (Interactive Session)

Wednesday, Nov. 28 8:30AM - 10:00AM Room: S404CD

GU

AMA PRA Category 1 Credits ™: 1.50 ARRT Category A+ Credit: 1.75

Participants

Avinash R. Kambadakone, MD, Boston, MA (Moderator) Nothing to Disclose

For information about this presentation, contact:

akambadakone@mgh.harvard.edu

LEARNING OBJECTIVES

1) Understand the urologist's perspective on stone disease and the value of imaging in the decision-making process. 2) Learn the imaging advances in diagnosis of urolithiasis including Dual energy CT techniques. 3) Discuss the multi-modality imaging techniques in diagnosis of stone disease including re-emergence of ultrasound. 4) Review the management updates in stone disease and its relevance to radiology practice.

Sub-Events

RC507A Urologist Perspective on Urolithiasis

Participants

Brian H. Eisner, MD, Boston, MA (Presenter) Advisory Board, Sonomotion

RC507B Imaging Approach for Right Flank Pain in the Emergency Department (Basics and What's New in ED)

Participants

Jennifer W. Uyeda, MD, Boston, MA (Presenter) Consultant, Allena Pharmaceuticals, Inc; Invited Speaker, Siemens AG

LEARNING OBJECTIVES

1) List the various imaging modalities used to evaluate right flank pain. 2) Compare the various available types of imaging modalities to assess right flank pain. 3) Identify CT appearances of nephroureterolithiasis and associated complications. 4) Apply structured reporting of nephroureterolithiasis on CT.

RC507C Advances in CT and Radiation Dose

Participants Avinash R. Kambadakone, MD, Boston, MA (*Presenter*) Nothing to Disclose

For information about this presentation, contact:

akambadakone@mgh.harvard.edu

LEARNING OBJECTIVES

1) Describe the advances in the imaging diagnosis of urolithiasis with focus on DECT. 2) Learn about CT radiation dose concerns and apply strategies to diminish the risk.

RC507D Interesting Case Presentations

Participants Nicole M. Hindman, MD, New York, NY (*Presenter*) Nothing to Disclose

For information about this presentation, contact:

nicole.hindman@nyumc.org

LEARNING OBJECTIVES

1) Learn the most common chemical stone compositions, risk factors for developing, ways to image and appropriate treatment for each type. 2) Learn imaging techniques for stone diagnosis, including Dual Energy Techniques. 3) Learn information Urologists need to know for diagnosis, monitoring and management of renal stones. 4) Review updated surgical and medical management of renal stones.



Emergency Radiology Series: Contemporary Topics in Imaging of Trauma

Wednesday, Nov. 28 8:30AM - 12:00PM Room: S406B



AMA PRA Category 1 Credits [™]: 3.50 ARRT Category A+ Credits: 4.00

Participants

Kathirkamanathan Shanmuganathan, MD, Baltimore, MD (*Moderator*) Nothing to Disclose Clint W. Sliker, MD, Baltimore, MD (*Moderator*) Nothing to Disclose Ludo F. Beenen, MD, Amsterdam, Netherlands (*Moderator*) Nothing to Disclose Michael N. Patlas, MD, FRCPC, Hamilton, ON (*Moderator*) Nothing to Disclose

For information about this presentation, contact:

kshanmuganathan@umm.edu

patlas@HHSC.CA

Sub-Events

RC508-01 AAST and Other Trauma Grading Systems

Wednesday, Nov. 28 8:30AM - 9:00AM Room: S406B

Participants

Kathirkamanathan Shanmuganathan, MD, Baltimore, MD (Presenter) Nothing to Disclose

For information about this presentation, contact:

kshanmuganathan@umm.edu

Active Handout:Kathirkamanathan Shanmuganathan

http://abstract.rsna.org/uploads/2018/18000578/RSNA - handout RC508-01.pdf

RC508-02 CT Imaging of Hepatic Trauma: Predictors of Arterial Injury and Need for Intervention

Wednesday, Nov. 28 9:00AM - 9:10AM Room: S406B

Participants

Ken Zhao, MD, New York, NY (*Presenter*) Nothing to Disclose Bedros Taslakian, MD, New York, NY (*Abstract Co-Author*) Nothing to Disclose Meredith McDermott, MD, New York, NY (*Abstract Co-Author*) Nothing to Disclose Eric T. Aaltonen, MD, MPH, New York, NY (*Abstract Co-Author*) Nothing to Disclose

For information about this presentation, contact:

ken.zhao@nyumc.org

PURPOSE

Determine which CT findings are predictive of arterial injury and need for intervention in the setting of hepatic trauma.

METHOD AND MATERIALS

From June 2011 to April 2017, 42 trauma patients (30 male, 12 female; mean age 36.1; age range 16-82) underwent contrastenhanced CT angiography (CTA) and subsequent conventional hepatic angiography within 24 hours at two level 1 trauma centers. Hepatic injuries on CTA were graded based on the American Association for the Surgery of Trauma (AAST) liver injury scale. Scans were assessed for the presence and extent of contrast extravasation, hemoperitoneum, and lacerations. Hepatic angiograms were reviewed for evidence of arterial injury, including contrast extravasation and pseudoaneurysm. The chi-squared test was used to evaluate the univariate association between the tested parameters. A p value of less than 0.05 was considered to be statistically significant.

RESULTS

There were 3 (7%) AAST grade 1, 9 (21%) grade 2, 15 (36%) grade 3, 14 (34%) grade 4, and 1 (2%) grade 5 injuries. Twenty one (50%) patients had arterial extravasation, 41 (98%) had parenchymal laceration, and 39 (93%) had hemoperitoneum on CT. The AAST liver injury scale was significantly associated with angiographic evidence of arterial injury (x^2 10.8, p=0.029); 46.7% (7/15) of grade 3 injuries and 57.1% (8/14) of grade 4 injuries demonstrated this finding. High AAST grade liver injuries (3-5) were also significantly associated with angiographic evidence of arterial injury when compared with low grade injuries (1-2); 0% (0/12) of low grade and 50% (15/30) of high grade injuries demonstrated arterial injury on angiography (x^2 9.3, p=0.002). In addition, extravasation > 1 cm on CTA demonstrated a significant association with arterial injury on angiography; 57.1% (8/14) versus 25% (7/28) when CTA extravasation > 1 cm was not present (x^2 4.2, p=0.040).

CONCLUSION

High grade injuries per the AAST liver injury scale and presence of contrast extravasation > 1 cm on CTA are associated with positive angiographic findings in the setting of hepatic trauma. This study also suggests that low grade injuries (1-2) have a very low likelihood of arterial injury on angiography.

CLINICAL RELEVANCE/APPLICATION

CT based predictors of arterial injury in the setting of hepatic trauma would help clinicians manage patients and diagnostic radiologists make appropriate recommendations.

RC508-03 The Role of CEUS in the Detection and Grading of Renal Injuries in Blunt Abdominal Trauma

Wednesday, Nov. 28 9:10AM - 9:20AM Room: S406B

Participants

Deepak Ravichandran, MD, New Delhi, India (*Presenter*) Nothing to Disclose Atin Kumar, MD, New Delhi, India (*Abstract Co-Author*) Nothing to Disclose Raju Sharma, MD, New Delhi, India (*Abstract Co-Author*) Nothing to Disclose Ashu S. Bhalla, MD, New Delhi, India (*Abstract Co-Author*) Nothing to Disclose Shivanand R. Gamanagatti, MBBS, MD, New Delhi, India (*Abstract Co-Author*) Nothing to Disclose

For information about this presentation, contact:

deepakindy2@gmail.com

PURPOSE

Contrast Enhanced CT (CECT) is the gold standard for the detection of renal injuries in blunt abdominal trauma (BAT). However its disadvantages include radiation exposure and the risks associated with iodinated contrast media. Contrast enhanced ultrasound (CEUS) provides an alternative tool for the detection and grading of renal injuries. This study was done to find the sensitivity of detection of renal injuries and to compare the AAST grading on CECT and CEUS

METHOD AND MATERIALS

Consecutive hemodynamically stable patients with BAT with CECT showing solid abdominal organ injuries were recruited in this ethically approved study. These patients underwent CEUS by a radiologist blinded to the findings of CECT and the injuries were identified and graded on both CECT and CEUS using the American Association for the Surgery of Trauma(AAST) scales. The sensitivity and specificity of detection on CEUS was obtained with CECT as the gold standard and the agreement between the grading on CECT and CEUS was analysed using kappa statistics. The injuries were further classified as high grade (AAST grades IV & above) and low grade (AAST grades I to III) and agreement between grading on CECT and CEUS was analysed

RESULTS

Among the 105 patients included as a part of a larger study, there were 22 renal injuries in the 210 kidneys assessed. CEUS detected 19 out of the 22 injuries and these injuries were graded on AAST scales and compared. The sensitivity, specificity, PPV and NPV of detection of renal injuries on CEUS using CECT as the gold standard was 86.4%, 100%, 100% and 98.4% respectively. On comparing the grading on CEUS and CECT, there was no significant agreement with a kappa value of 0.46 (>0.75 significant). On combining the grades as low grade and high grade injuries on both modalities, there is poor agreement between the grading with a kappa value of 0.46. The reason for the discrepancy is because US contrast agents are purely intravascular and do not get excreted through the renal pelvicalyceal system. Hence, the patients with PCS injuries were downgraded as grade III on CEUS

CONCLUSION

Though CEUS has a reasonable accuracy for detection of renal injuries but is poor for grading them and hence cannot be used to triage management.

CLINICAL RELEVANCE/APPLICATION

While CEUS is accurate in detecting renal injuries, it is unreliable as an alternative modality to CECT in grading renal injuries and in suggesting further management.

RC508-04 Liver Trauma: Vascular Injury on Computed Tomography as a Predictor of Patient Outcome

Wednesday, Nov. 28 9:20AM - 9:30AM Room: S406B

Awards

Student Travel Stipend Award

Participants Nicholas Wilson, MD, Boston, MA (*Presenter*) Nothing to Disclose Avneesh Gupta, MD, Boston, MA (*Abstract Co-Author*) Nothing to Disclose Stephan W. Anderson, MD, Cambridge, MA (*Abstract Co-Author*) Nothing to Disclose Diana Dinh, MD, Boston, MA (*Abstract Co-Author*) Nothing to Disclose John M. Campbell, Brookline, MA (*Abstract Co-Author*) Nothing to Disclose Daniel Adran, Boston, MA (*Abstract Co-Author*) Nothing to Disclose Daniel Adran, Boston, MA (*Abstract Co-Author*) Nothing to Disclose Alec Maggi, Rossmoor, CA (*Abstract Co-Author*) Nothing to Disclose Jasmine Gandhi, Boston, MA (*Abstract Co-Author*) Nothing to Disclose Muhammad M. Qureshi, MBBS, MPH, Boston, MA (*Abstract Co-Author*) Nothing to Disclose Robert W. Schulze, MD, MBA, Boston Ma, MA (*Abstract Co-Author*) Nothing to Disclose Christina A. LeBedis, MD, Boston, MA (*Abstract Co-Author*) Nothing to Disclose

For information about this presentation, contact:

PURPOSE

To assess the utility of MDCT findings in predicting patient outcomes after liver injury.

METHOD AND MATERIALS

This retrospective study was IRB approved and HIPAA compliant. Informed consent was waived. Patients >= 16 years old who sustained blunt or penetrating trauma and found to have liver laceration from 5/1/2005 - 2/28/2017 were included. During this interval, 169 patients met inclusion criteria (123 male, 46 female; mean age of 34; age range 16-80 years old; 61 blunt trauma, 108 penetrating trauma). Liver injury was graded in blinded, consensus fashion by two abdominal fellowship trained radiologists (9 and 13 years-experience) using the AAST liver injury scale. Additional CT variables recorded in blinded fashion were contained vascular injury and active extravasation. Length of stay, treatment (interventional radiology or operative), and peri-operative transfusion were recorded from the electronic medical record. Multivariate linear regression was performed to determine crude and adjusted parameter estimate for length of stay. Logistic regression models were run and crude and adjusted odds ratio were calculated to estimate association between categorical variables.

RESULTS

41/128 (24.3%) patients who sustained hepatic injury have concomitant hepatic vascular injury; 23/61 (38%) in the setting of penetrating trauma and 18/108 (17%) in the setting of blunt trauma. Hospital length of stay was increased by 9.0 days for hepatic vascular injury regardless of mechanism, and by 6.0 days for those with high AAST grade (grades 4-6) as compared to referents. Patients with high grade AAST liver lacerations (grades 4-6) and patients with hepatic vascular injuries were more likely to require treatment (interventional radiology or operative) compared to referents, OR 4.74, 95% CI 2.21-10.16, p<0.0001 and OR 7.0, 95% CI 2.96-16.54, p<0.0001, respectively.

CONCLUSION

There is a high incidence of hepatic vascular injury in patients with liver laceration (24.3%). High grade hepatic laceration and the presence of hepatic vascular injury is predictive of longer lengths of stay and need for treatment.

CLINICAL RELEVANCE/APPLICATION

Hepatic vascular injury in patients who sustained blunt or penetrating liver trauma is predictive of patient outcomes.

Honored Educators

Presenters or authors on this event have been recognized as RSNA Honored Educators for participating in multiple qualifying educational activities. Honored Educators are invested in furthering the profession of radiology by delivering high-quality educational content in their field of study. Learn how you can become an honored educator by visiting the website at: https://www.rsna.org/Honored-Educator-Award/ Stephan W. Anderson, MD - 2018 Honored Educator

RC508-05 Pitfalls in Abdominal Trauma CT

Wednesday, Nov. 28 9:30AM - 10:00AM Room: S406B

Participants

Michael N. Patlas, MD, FRCPC, Hamilton, ON (Presenter) Nothing to Disclose

For information about this presentation, contact:

patlas@hhsc.ca

LEARNING OBJECTIVES

1) To discuss the impact of suboptimal trauma MDCT protocols. 2) To review common and uncommon pitfalls in interpretation of abdominal trauma MDCT examinations. 3) To suggest strategies to improve detection of easily missed injuries.

RC508-06 Correlation between CT-Based Liver Injury Severity Scoring, Contrast Extravasation and Subsequent Management

Wednesday, Nov. 28 10:00AM - 10:10AM Room: S406B

Awards

Student Travel Stipend Award

Participants

Martin Reim, MD, Tartu, Estonia (*Presenter*) Nothing to Disclose Pilvi Ilves, Tartu, Estonia (*Abstract Co-Author*) Nothing to Disclose Andrus Lomp, BA,MSc, Tartu, Estonia (*Abstract Co-Author*) Nothing to Disclose Vladislav Mihnovits, MD, Tartu, Estonia (*Abstract Co-Author*) Nothing to Disclose Urmas Lepner, PhD, Tartu, Estonia (*Abstract Co-Author*) Nothing to Disclose Peep Talving, PhD, Tartu, Estonia (*Abstract Co-Author*) Nothing to Disclose

For information about this presentation, contact:

reimmartin@gmail.com

PURPOSE

The liver is the second most commonly injured abdominal solid organ. The aim of the study was to elucidate the correlation between CT-based liver injury severity scoring, contrast extravasation and subsequent management.

METHOD AND MATERIALS

Data on consecutive trauma admissions to two major national trauma facilities with liver injuries between 1/2009 and 12/2013 were retrospectively reviewed using ICD-10 codes (S36.10). The images were accrued from the population-based Picture Archive (PACS). CT scoring per American Association for the Surgery of Trauma organ injury scale was utilized to stratify liver injuries into

minor/moderate (grades I-III) vs. severe (grades IV-V) injuries. The primary outcomes were operative management and in-hospital mortality.

RESULTS

A total of 81 cases were included. The mean age of the cohort was 31.5 ± 12.2 years and 26.9% were female. Overall, grade I-III injuries in 86.4% (n=70) and grade IV-V injuries in 13.6% (n=11) were observed. The most common associated injuries involved chest wall (n=44; 54.4%), lung (n=42; 51.8%), lower ribs (n=32; 39.5%). Overall, 17.3% (n=14) and 82.7% (n=67) were subjected to operative and non-operative management, respectively. There was no correlation between CT scoring of liver injuries and surgical management (p=0.196). CT signs of active bleeding was noted in 20 patients (25%) and 30% (n=6) of these patients underwent operative treatment. The remaining 10% (n=2) of patients with active bleeding were embolized per interventional radiology (IR). One patient had IR intervention for a concomitant abdominal injury and one was treated surgically for a splenic injury. A total of 8 cases (13%) without CT-verified active bleeding (n=60) required surgery. There was no statistically relevant correlation between CT-based active liver hemorrhage and subsequent operative treatment (p=0,102). The overall mortality of the study population was 2.5% (n=2).

CONCLUSION

The majority of the population-based liver injuries were minor or moderate and CT-scoring of liver injuries did not determine subsequent surgical management. There was no correlation between CT signs of active bleeding and operative treatment decision. Further prospective studies are warranted.

CLINICAL RELEVANCE/APPLICATION

To improve our clinical practices we need to analyze our previous performance using existing injury scoring criteria and imaging characteristics regarding clinical outcome and decision making.

RC508-07 Treatment Decisions in Blunt Splenic Trauma: Insights from a UK Trauma Centre

Wednesday, Nov. 28 10:10AM - 10:20AM Room: S406B

Awards

Student Travel Stipend Award

Participants

Jim Zhong, Leeds, United Kingdom (*Presenter*) Nothing to Disclose Fathallah Islim, Leeds, United Kingdom (*Abstract Co-Author*) Nothing to Disclose James Lenton, Wakefield, United Kingdom (*Abstract Co-Author*) Nothing to Disclose Simon J. McPherson, MBBS, North Yorkshire, United Kingdom (*Abstract Co-Author*) Nothing to Disclose Jai Patel, MD, FRCR, Leeds, United Kingdom (*Abstract Co-Author*) Nothing to Disclose Tim Stansfield, Leeds, United Kingdom (*Abstract Co-Author*) Nothing to Disclose Jonathan Jones, Leeds, United Kingdom (*Abstract Co-Author*) Nothing to Disclose Karen Flood, BMedSc, MBBS, Leeds, United Kingdom (*Abstract Co-Author*) Nothing to Disclose

PURPOSE

To review the imaging findings and clinical outcomes in blunt splenic trauma (BST) and identify common themes that help stratify management and determine the role of interventional radiology (IR), specifically splenic embolization (SE).

METHOD AND MATERIALS

Retrospective study. All patients admitted with BST from 01/01/2010 to 01/01/2018 included. Data collected included demographics, injury severity, haemodynamic stability, treatment type (Non-operative, IR or surgery), complications and follow-up. 4 Attending IRs reviewed the admission CT imaging whilst blinded to the original report or outcomes. Based on the CT findings and haemodynamic stability of the patient they were asked to recommend non-operative, SE (proximal or distal) or surgery for each case. The inter-observer agreement was calculated using Fleiss Kappa on SPSS for the CT findings and management plan.

RESULTS

257 patients included. Median age 27(3-90). 178 were male and 49 female. 15 patients had isolated splenic injuries and 212 had >2 organ system injuries. 220 had a CT scan on presentation. CT findings included splenic contrast extravasation(n=44), pseudoaneurysms(n=24), splenic lacerations(n=196, 30 full thickness and 23 involved the splenic hilum), perisplenic haematoma(n=105) and haemoperitoneum(n=65). For initial treatment, 17 had splenectomy, 32 had SE and 178 were managed conservatively. 5 had delayed SE following failure of conservative management. A total of 12 patients had proximal SE and 25 had distal SE. The 4 Attendings were in most agreement on the presence of active bleeding on CT (89%), Fleiss' Kappa 0.696. For chosen method of treatment, the overall inter-observer agreement was 84% (range 83-93%) and Fleiss' Kappa was 0.614. For haemodynamically stable patients with active bleeding on CT with either perisplenic haematoma or haemoperitoneum, all Attending IRs opted for SE with a view to distal embolization for splenic preservation.

CONCLUSION

Both clinical and imaging findings are invaluable in guiding management of blunt splenic trauma. In the presence of splenic injury and active bleeding on CT imaging even with a stable patient, splenic artery angiogram with a view to embolization is recommended.

CLINICAL RELEVANCE/APPLICATION

In the presence of splenic injury and active bleeding on CT imaging even with a stable patient, splenic artery angiogram with a view to embolization is recommended.

RC508-08 Uncommon Sites of Abdominal Trauma

Wednesday, Nov. 28 10:30AM - 11:00AM Room: S406B

fmunera@med.miami.edu

LEARNING OBJECTIVES

1) Describe MDCT findings of unusual sites of injury in patients with blunt abdominopelvic trauma. 2) Describe management implications.

ABSTRACT

Uncommon sites of injury can be overlooked. This lecture will use cases to highlight MDCT findings of unusual sites of injury in abdominoplevic trauma such as the pancreas, adrenal, colon, uterus/fetus, gallbladder, abdominal aorta, IVC, renal veins, etc.

RC508-09 Segmented Pelvic Hematoma Volumes, Intravenous Contrast Extravasation Volumes, and Extravasation Rate Are All Independently Predictive of Major Arterial Injury After Pelvic Fracture: Analysis of a Prospective Cohort

Wednesday, Nov. 28 11:00AM - 11:10AM Room: S406B

Participants

David Dreizin, MD, Baltimore, MD (*Presenter*) Research Grant, Siemens AG ; Matthew P. Dattwyler, MD, Baltimore, MD (*Abstract Co-Author*) Nothing to Disclose Alexis R. Boscak, MD, Baltimore, MD (*Abstract Co-Author*) Nothing to Disclose Christina A. LeBedis, MD, Boston, MA (*Abstract Co-Author*) Nothing to Disclose Nikki Tirada, MD, Baltimore, MD (*Abstract Co-Author*) Spouse, Research Grant, Siemens AG Stephan W. Anderson, MD, Cambridge, MA (*Abstract Co-Author*) Nothing to Disclose Nemil Shah, MD, Boston, MA (*Abstract Co-Author*) Nothing to Disclose Oam Bhate, Cary, NC (*Abstract Co-Author*) Nothing to Disclose Uttam Bodanapally, MD, Baltimore, MD (*Abstract Co-Author*) Speakers Bureau, Siemens AG; Travel Support, Siemens AG;

For information about this presentation, contact:

ddreizin@umm.edu

PURPOSE

The predictive value of hematoma volumes for major arterial injury after pelvic fractures is known. Area measurements of contrast extravasation (CE) and area rate of change between phases are also important. A model using hematoma volume and contrast extravasation volume on multiphasic CT is derived.

METHOD AND MATERIALS

Patients with CT in the trauma bay were screened prospectively for pelvic ring disruptions between July 2016-Oct 2017. Patients were excluded if CT was performed: after a) laparotomy or angiography, b) at another institution, or c) without IV contrast. Hematoma volumes (HMVs) were measured in all remaining patients. Patients with HMV < 50 mL were not considered at risk for arterial injury requiring intervention and were excluded a priori. Included patients were additionally assessed for: binder, Tile grade, comminution, fracture gap (> 5 mm), obturator/greater sciatic fracture, atherosclerosis, multiple/bilateral foci of arterial blush, art and PVP CE volume, and difference in CE volume between phases (bleeding rate). Variables with p<0.05 on univariate analysis (tests for proportions, Chi squared test for trend, comparison of means) were included in logistic regression with backward elimination to determine independent predictors and derive a parsimonious predictive model.

RESULTS

241 patients had pelvic ring disruptions on CT. 121 had non-negligible hematoma volumes (>50 mL). 19 patients underwent catheter embolization for pelvic arterial bleeding. In univariate analysis, predictor variables included hematoma vol (p < 0.0001), Tile grade (p = 0.002), multiple/bilateral foci of extravasation (p = 0.049), arterial blush vol (p < 0.0001), PVP blush vol (p = 0.004), and bleeding rate: PVP-art (p = 0.001). In logistic regression, hematoma vol (OR 1.007 Δ per mL), arterial CE vol (OR 194.3 Δ per mL), PV CE vol (OR 0.015 Δ per mL), bleeding rate (OR 61.7 Δ per mL), and Tile C vertical instability (OR 6.2) remained as independent predictors.

CONCLUSION

Hematoma vol, CE vol on art and PV phase, and bleeding rate between phases are independent predictors of major arterial hemorrhage after pelvic fracture. The generalizability of the model is under evaluation using a dataset from a second high-volume level I trauma center.

CLINICAL RELEVANCE/APPLICATION

Volumetric measurements of hematoma, arterial and PV CE, and rate of change of CE between phases can potentially improve prediction of major arterial injury after pelvic fractures.

Honored Educators

Presenters or authors on this event have been recognized as RSNA Honored Educators for participating in multiple qualifying educational activities. Honored Educators are invested in furthering the profession of radiology by delivering high-quality educational content in their field of study. Learn how you can become an honored educator by visiting the website at: https://www.rsna.org/Honored-Educator-Award/ Stephan W. Anderson, MD - 2018 Honored Educator

RC508-10 Non-Vascular Thoracic Trauma

Wednesday, Nov. 28 11:10AM - 11:40AM Room: S406B

Participants Krystal Archer-Arroyo, MD, Atlanta, GA (*Presenter*) Nothing to Disclose

karche2@emory.edu

Active Handout:Krystal Archer-Arroyo

http://abstract.rsna.org/uploads/2018/18000580/RSNA 2018 Non-Vascular Chest Trauma RC508-10.pdf

LEARNING OBJECTIVES

1) Describe common imaging findings of tracheobronchial injury. 2) Classify parenchymal injuries of the lung. 3) Discuss rib fracture patterns and pre-operative planning for chest reconstructive surgery.

RC508-11 A 2018 International Survey to Assess Use of Intraluminal Contrast in CT Protocols for Penetrating Torso Trauma

Wednesday, Nov. 28 11:40AM - 11:50AM Room: S406B

Awards

Student Travel Stipend Award

Participants

Cory J. Ozimok, BSC, MD, Ottawa, ON (*Presenter*) Nothing to Disclose Vincent M. Mellnick, MD, Saint Louis, MO (*Abstract Co-Author*) Nothing to Disclose Michael N. Patlas, MD, FRCPC, Hamilton, ON (*Abstract Co-Author*) Nothing to Disclose

For information about this presentation, contact:

patlas@hhsc.ca

PURPOSE

There is controversy regarding the administration of oral and rectal contrast in CT protocols to detect bowel injury in the context of penetrating torso trauma. Given the lack of published societal guidelines, our goal was to survey trauma radiologists across North America and abroad to determine consensus on CT protocols for penetrating trauma.

METHOD AND MATERIALS

With IRB approval, an anonymous 10-question online survey was distributed via email to 589 radiologists in the American Society of Emergency Radiology (ASER) member database. The survey was open for a 4-week period in February 2018. A commercially available website that allows subscribers to create and analyze survey results was used for analysis.

RESULTS

We received 124 responses (21% response rate) with majority from U.S. institutions (82%), followed by Europe (7%), Canada (6%), Asia (3%) and Australia/New Zealand (2%). Seventy-four percent of respondents indicated they do not routinely administer oral contrast in penetrating trauma and 68% do not administer rectal contrast. The decision to administer intraluminal contrast is made by the referring physician at 52% of institutions, the attending radiologist at 18% and a resident or fellow at 20%. Most centers do not use software to assess trajectory of penetrating trauma (90%). There is in-house attending level coverage at 54% of institutions. When asked if trauma scans are reviewed before removing the patient from the table, 41% of respondents answered 'No' and of those who answered 'Yes,' 12% said they are reviewed by an attending, 33% by a resident, and 4% by a fellow.

CONCLUSION

The majority of major trauma centers do not routinely administer oral or rectal contrast in cases of penetrating torso trauma and the decision is often made by the referring physician.

CLINICAL RELEVANCE/APPLICATION

There is international consensus that the added benefit of intraluminal contrast to detect bowel injury in CT protocols for penetrating trauma is outweighed by the delay in patient management.

Honored Educators

Presenters or authors on this event have been recognized as RSNA Honored Educators for participating in multiple qualifying educational activities. Honored Educators are invested in furthering the profession of radiology by delivering high-quality educational content in their field of study. Learn how you can become an honored educator by visiting the website at: https://www.rsna.org/Honored-Educator-Award/ Vincent M. Mellnick, MD - 2016 Honored EducatorVincent M. Mellnick, MD - 2018 Honored Educator

RC508-12 Imaging and Clinical Predictors of Outcomes in Torso Trauma

Wednesday, Nov. 28 11:50AM - 12:00PM Room: S406B

Awards

Student Travel Stipend Award

Participants

Pedro V. Staziaki, MD, Boston, MA (*Presenter*) Nothing to Disclose Aaron Maybury, Jamaica Plain, MA (*Abstract Co-Author*) Nothing to Disclose Neha Gangasani, Boston, MA (*Abstract Co-Author*) Nothing to Disclose Michael J. Hsu, MD, Boston, MA (*Abstract Co-Author*) Nothing to Disclose Mustafa Qureshi, Boston, MA (*Abstract Co-Author*) Nothing to Disclose Christina A. LeBedis, MD, Boston, MA (*Abstract Co-Author*) Nothing to Disclose Jorge A. Soto, MD, Boston, MA (*Abstract Co-Author*) Nothing to Disclose Stephan W. Anderson, MD, Cambridge, MA (*Abstract Co-Author*) Nothing to Disclose

PURPOSE

To access the utility of CT findings with clinical parameters to predict clinical outcomes in trauma

TO assess the utility of CT finalitys with clinical parameters to predict clinical outcomes in trauma.

METHOD AND MATERIALS

IRB-approved retrospective study of all adults who sustained blunt/penetrating trauma in a Level 1 trauma center in 2015.Clinical parameters: admission blood pressure (SBP), heart rate, Glasgow Coma Scale (GCS), hemoglobin, hematocrit (HCT) and lactate. A blinded radiologist assessed CT for colon, kidney, liver, spleen, bony pelvic ring, lung parenchyma, and/or rib injuries.Outcomes: admission to ICU, length of stay (LOS) in the ICU, life-saving procedures (conventional angiography/intervention, surgery) and total LOS in the hospital.Multivariate linear and logistic regression models were employed and covariate-adjusted parameter estimates and odds ratios (OR) with 95% confidence intervals (CI) were computed.

RESULTS

Among 723 patients, 162 were excluded due to missing lab data, resulting in 561 patients (72% males, age 39 ± 18 years).168 patients were admitted to the ICU. Liver (OR 15.9 [4.8-52.5]), spleen (OR 15.9 [4-62.8]), pelvis (OR 3.4 [1.5-7.5]), lung (OR 3.3 [1.5-7.1]) and rib (OR 4.1 [2.4-7.3]) injuries in addition to age, GCS and lactate predicted admission to the ICU. Among these, the LOS in the ICU was 6 (3-11) days. Only pelvic injury (2.4, p < 0.05) was associated with longer LOS in the ICU.31 patients had life-saving procedure. Colon (OR 37.3 [7.4-189.3]), liver (OR 3.9 [1.2-12.3]), spleen (OR 8.5 [2.3-31.0]) and pelvis (OR 4.8 [1.7-13.7]) injuries, in addition to lactate, predicted undergoing procedures.Total LOS in the hospital was 2 (1-5) days. Kidney (3.6, p = 0.02), liver (2.9, p = 0.03), spleen (3.5, p = 0.02), pelvis (7.2, p < 0.01), lung (3.8, p < 0.01) and rib (2.2, p < 0.01) injuries in addition to age, GCS, HCT and lactate were associated with longer LOS.

CONCLUSION

Liver, spleen, pelvis, lung and rib injuries are predictive of ICU admission, among which only pelvic injury predicts longer LOS in the ICU. Colon, liver, spleen and pelvis injuries are predictive of life-saving procedure. Kidney, liver, spleen, pelvis, lung and rib are predictive of increased LOS in the hospital. These are independent of age, SBP, GCS, HCT or lactate.

CLINICAL RELEVANCE/APPLICATION

Radiologists can demonstrate value by developing strong predictive models of interest to clinicians and administrators alike.

Honored Educators

Presenters or authors on this event have been recognized as RSNA Honored Educators for participating in multiple qualifying educational activities. Honored Educators are invested in furthering the profession of radiology by delivering high-quality educational content in their field of study. Learn how you can become an honored educator by visiting the website at: https://www.rsna.org/Honored-Educator-Award/ Jorge A. Soto, MD - 2013 Honored EducatorJorge A. Soto, MD - 2014 Honored EducatorJorge A. Soto, MD - 2015 Honored EducatorJorge A. Soto, MD - 2017 Honored EducatorJorge A. Soto, MD - 2018 Honored Educator Educator K. Soto, MD - 2018 Honored Educator



Challenging Abdominal Imaging Cases (Interactive Session)

Wednesday, Nov. 28 8:30AM - 10:00AM Room: E353B

GI

AMA PRA Category 1 Credits ™: 1.50 ARRT Category A+ Credit: 1.75

Participants

Judy Yee, MD, Bronx, NY (Moderator) Research Grant, EchoPixel, Inc; Research Grant, Koninklijke Philips NV;

GENERAL INFORMATION

This interactive session will use RSNA Diagnosis Live[™]. Please bring your charged mobile wireless device (phone, tablet or laptop) to participate.

Sub-Events

RC509A Challenging Cases: Pancreas/Biliary

Participants Jorge A. Soto, MD, Boston, MA (*Presenter*) Royalties, Reed Elsevier

LEARNING OBJECTIVES

1) Through the use of illustrative cases, this presentation will help develop a strategy to provide logical differential diagnoses for solid and cystic pancreatic lesions. 2) Recognize common imaging pitfalls that can lead to errors in diagnosis of pancreatic and biliary lesions. 3) Understand how the various imaging modalities play a complementary role in imaging of the pancreas and biliary tract.

Honored Educators

Presenters or authors on this event have been recognized as RSNA Honored Educators for participating in multiple qualifying educational activities. Honored Educators are invested in furthering the profession of radiology by delivering high-quality educational content in their field of study. Learn how you can become an honored educator by visiting the website at: https://www.rsna.org/Honored-Educator-Award/ Jorge A. Soto, MD - 2013 Honored EducatorJorge A. Soto, MD - 2014 Honored EducatorJorge A. Soto, MD - 2015 Honored EducatorJorge A. Soto, MD - 2017 Honored EducatorJorge A. Soto, MD - 2018 Honored Educator

RC509B Challenging Cases: Mesentery

Participants Milana Flusberg, MD, Bronx, NY (*Presenter*) Nothing to Disclose

LEARNING OBJECTIVES

1) Review various common and uncommon mesenteric and peritoneal processes. 2) Use clinical and imaging features to narrow the differential diagnosis of a mesenteric or peritoneal abnormality. 3) Develop a search pattern for often overlooked mesenteric and peritoneal findings.

RC509C Challenging Cases: Liver

Participants Zhen J. Wang, MD, Hillsborough, CA (*Presenter*) Stockholder, Nextrast, Inc

For information about this presentation, contact:

Jane.Wang@ucsf.edu

LEARNING OBJECTIVES

1) Describe key imaging features of various liver masses. 2) Apply the most appropriate imaging exams for the characterization of liver masses.

RC509D Challenging Cases: Bowel

Participants

David H. Kim, MD, Middleton, WI (Presenter) Shareholder, Cellectar Biosciences, Inc; Shareholder, Elucent Medical;

LEARNING OBJECTIVES

1) Be able to apply a logic-based approach to difficult abdominal cases. 2) Be aware of typical pitfalls that may mimic disease. 3) See some unusual abdominal diagnoses or unusual presentations of more common disease.



Renal and Scrotal Ultrasound with Renal Contrast and Elastography

Wednesday, Nov. 28 8:30AM - 10:00AM Room: E350



AMA PRA Category 1 Credits ™: 1.50 ARRT Category A+ Credit: 1.75

FDA Discussions may include off-label uses.

LEARNING OBJECTIVES

1) Identify the imaging features of a variety of etiologies of renal masses and understand the potential overlap between malignant, non-malignant mass-like lesions and pseudomasses. 2) Recognize the potential limitations of ultrasound in the identification of renal masses and learn to maximize technique. 3) Demonstrate the wide range of appearances of parenchymal diseases on ultrasound and develop an approach to evaluation of parenchymal disease with ultrasound. 4) To learn the basic technical principles of contrast-enhanced ultrasound. 5) To apply these principles in everyday practice. 6) To learn the indications for CEUS in the evaluation of cystic renal lesions. 6) To explain the principles and limitations of elastographic techniques applied to the kidney. 7) To learn about the impact of the renal structure on elasticity values. 8) To identify the significant structural changes responsible for variations of renal elasticity. 9) Describe the normal anatomy of the scrotum. 10) Describe common mass-like pathologic conditions of the scrotum. 11) Describe the significance and management of testicular microlithiasis.

Sub-Events

RC510A Ultrasound Evaluation of Renal Masses and Parenchymal Disease

Participants

Michael D. Beland, MD, Providence, RI (*Presenter*) Research Grant, Canon Medical Systems Corporation; Consultant, General Electric Company

For information about this presentation, contact:

mbeland@lifespan.org

LEARNING OBJECTIVES

1) Identify the imaging features of a variety of etiologies of renal masses and understand the potential overlap between malignant, non-malignant mass-like lesions and pseudomasses. 2) Recognize the potential limitations of ultrasound in the identification of renal masses and learn to maximize technique. 3) Demonstrate the wide range of appearances of parenchymal diseases on ultrasound and develop an approach to evaluation of parenchymal disease with ultrasound.

RC510B Contrast Evaluation of Renal Masses

Participants

Dirk-Andre Clevert, MD, Muenchen, Germany (*Presenter*) Speaker, Siemens AG; Speaker, Koninklijke Philips NV; Speaker, Bracco Group; Speaker, Samsung Electronics Co, Ltd;

For information about this presentation, contact:

dirk.clevert@med.uni-muenchen.de

LEARNING OBJECTIVES

1) To learn the basic technical principles of contrast-enhanced ultrasound. 2) To apply these principles in everyday practice. 3) To learn the indications for CEUS in the evaluation of cystic renal lesions.

ABSTRACT

Never before has a new technique changed the field of ultrasound in such a revolutionary way as the use of ultrasound contrast media. With the introduction of second-generation ultrasound contrast agents, contrast-enhanced ultrasound (CEUS) has become widely available as an adjunct to the conventional B-mode sonography in suspect or oncologic imaging. This course will focus on the use of contrast-enhanced ultrasound in the characterisation of cystic renal lesions its impact on clinical decision-making.

RC510C Renal Elastography: Where Are We?

Participants

Nicolas Grenier, MD, Bordeaux CEDEX, France (*Presenter*) Advisory Board, Supersonic Imagine; Travel support, Guerbet SA; Travel support, Bracco Group; Travel support, General Electric Company;

For information about this presentation, contact:

nicolas.grenier@chu-bordeaux.fr

LEARNING OBJECTIVES

1) To explain the principles and limitations of elastographic techniques applied to the kidney. 2) To learn about the impact of the renal structure on elasticity values. 3) To identify the significant structural changes responsible for variations of renal elasticity.

ABSTRACT

Ultrasound elastography is a new imaging technique under development that provides information about renal stiffness. Kidney elasticity quantification with ultrasound should be better performed with a quantitative technique, based on shear wave velocity measurements (ARFI or SSI methods). Kidney stiffness changes can be affected by mechanical factors such as external pressure induced by the probe and intrarenal characteristics such as tissue anisotropy, which is high in renal medulla, vascularization, which is high within the cortex, and hydronephrosis. Chronic kidney disease (CKD) incidence and prevalence are increasing in Western countries, due particularly to diabetes mellitus and hypertension-related nephropathies. During progression of such renal parenchymal diseases, cellular density may increase, mainly during acute inflammatory phases, and the interstitial matrix may be invaded by fibrosis. All components of these tissue changes may induce an increase of renal elasticity which is not specifically related to fibrosis. Tubular, glomerular, interstitial and vascular changes may also be responsible for an increase of stiffness. This is why, further studies are now necessary before to understand the real impact of elastography measurement in clinical nephrology.Considering characterization of renal tumors with elastography, clinical experience is still limited. Preliminary results show that benign tumors seem to have lower values of elasticity than malignant ones, but, here too, more experience is also necessary.

RC510D There is a Mass in the Scrotum: What Does it Mean?

Participants

Thomas C. Winter III, MD, Salt Lake City, UT (*Presenter*) Speakers Bureau, General Electric Company; Research support, Siemens AG;;;

LEARNING OBJECTIVES

1) Describe the normal anatomy of the scrotum. 2) Describe common mass-like pathologic conditions of the scrotum. 3) Describe the significance and management of testicular microlithiasis.

ABSTRACT

This didactic lecture will review proper sonographic technique for scrotal examination, review normal anatomy of the scrotum as demonstrated by ultrasound, and will then progress to a description of the common pathologic and normal conditions that may present as a scrotal mass.



Head and Neck PET/CT: Clinical Approach

Wednesday, Nov. 28 8:30AM - 10:00AM Room: S504CD



AMA PRA Category 1 Credits [™]: 1.50 ARRT Category A+ Credit: 1.75

Sub-Events

RC511A Oropharyngeal Cancer: Evolving Challenges-Clinician's Perspective

Participants

Bhishamjit Chera, MD, Chapel Hill, NC (Presenter) Nothing to Disclose

LEARNING OBJECTIVES

1) To understand how radiological interpretation of pre-treatment and post-treatment imaging studies influences the management of patients with head and neck cancer.

RC511B CT and MRI Anatomy and Interpretation

Participants Valerie L. Jewells, DO, Chapel Hill, NC (*Presenter*) Nothing to Disclose

For information about this presentation, contact:

jewells@med.unc.edu

LEARNING OBJECTIVES

1) Provide radiologists with the tools to access CT and MRI imaging for head and neck cancer. 2) Teach attendees how to address the images in a manner that will assist the ENT surgeon for staging and surgical planning. 3) Address the principles for critical thinking and analysis as well as preparation and skill development for a head and neck tumor board.

ABSTRACT

A successful multidisciplinary head and neck tumor board requires coordination and imaging review on the part of radiology to assist the surgeon, radiation oncolcogist and medical oncologist. The goal is to reach the best option for each individual patient depending upon tumor type, staging and underlying medical conditions. Appropriate imaging and interpretation is key to this endeavor. These topics will be addressed through discussion of selective CT and MRI cases from our weekly tumor board. References: 1. Heineman T, St John MA, Wein RO and Weber RS. It takes a village: The importance of multidisciplinary care. Otoloaryngol Clin North Am 2017 Aug;50(4):679-687. 2. Liao CT, Kang CJ, Lee LY et al. Association between multidisciplinary team care approach and survival rates in patients with oral cavity squamous cell carcinoma. Head Neck 2016 Apr;38 Suppl 1:E5444-53. 3. Shah BA, Qureshi MM, Jalisi et al. Analysis of decision making at a multidisciplinary head and neck tumor board incorporating evidence-based National Cancer Comprehensive Network (NCCN) guidelines. Pract Radiat Oncol 2016 Jul-Aug;6(4):248-54.

RC511C FDG-PET/CT: Applications and Interpretation

Participants

Terence Z. Wong, MD, PhD, Chapel Hill, NC (Presenter) Consultant, Lucerno Dynamics, LLC;

LEARNING OBJECTIVES

1) Describe applications for FDG-PET/CT for initial evaluation and follow up of patients with head and neck cancer. 2) Learn the value of combining metabolic findings on FDG-PET findings with morphology on CT and endoscopic appearance. 3) Understand potential etiologies of false positive and false negative studies.

ABSTRACT

Optimal evaluation of patients with head and neck malignancies requires a multidisciplinary approach. Correlation of FDG-PET, CT, direct visualization, and clinical examination is important to provide the best management of these patients.

RC511D Panel Discussion: Q&A

Participants Bhishamjit Chera, MD, Chapel Hill, NC (*Presenter*) Nothing to Disclose Valerie L. Jewells, DO, Chapel Hill, NC (*Presenter*) Nothing to Disclose Terence Z. Wong, MD, PhD, Chapel Hill, NC (*Presenter*) Consultant, Lucerno Dynamics, LLC;

LEARNING OBJECTIVES

Case examples which highlight the value of multidisciplinary approaches for managing patients with head and neck cancer.



Vascular Series: MR Angiography: New Techniques and Their Application

Wednesday, Nov. 28 8:30AM - 12:00PM Room: S503AB



AMA PRA Category 1 Credits ™: 3.50 ARRT Category A+ Credits: 4.00

FDA Discussions may include off-label uses.

Participants

Thomas K. Foo, PhD, Niskayuna, NY (*Moderator*) Employee, General Electric Company

Martin R. Prince, MD, PhD, New York, NY (*Moderator*) Patent agreement, General Electric Company; Patent agreement, Hitachi, Ltd; Patent agreement, Siemens AG; Patent agreement, Canon Medical Systems Corporation; Patent agreement, Koninklijke Philips NV; Patent agreement, Nemoto Kyorindo Co, Ltd; Patent agreement, Bayer AG; Patent agreement, Lantheus Medical Imaging, Inc; Patent agreement, Bracco Group; Patent agreement, Mallinckrodt plc; Patent agreement, Guerbet SA;

LEARNING OBJECTIVES

1) To review the latest MR techniques for vascular imaging. 2) Learn how to optimize MR Angiography pulse sequences. 3) Review a spectrum of Vascular Disease on MRI/MRA.

Sub-Events

RC512-01 K-Space Options for Improving MRA

Wednesday, Nov. 28 8:30AM - 9:05AM Room: S503AB

Participants

Walter F. Block, PhD, Madison, WI (*Presenter*) Stockholder and Co-founder, TherVoyant; Research support, General Electric Company;

Active Handout:Walter F. Block

http://abstract.rsna.org/uploads/2018/18002602/RSNA kspace mra improved Block RC512-01.pdf

LEARNING OBJECTIVES

View learning objectives under main course title.

RC512-02 Sub-Millimetric 4D Flow MR in Small Intracerebral Aneurysms at 7 Tesla with Experimental Verification in Upscaled 3D Printed Replica

Wednesday, Nov. 28 9:05AM - 9:15AM Room: S503AB

Participants

Pierre-Francois Van de Moortele, Minneapolis, MN (*Presenter*) Nothing to Disclose Mostafa Toloui, PhD, Minneapolis, MN (*Abstract Co-Author*) Nothing to Disclose Omid Amili, PhD, Minneapolis, MN (*Abstract Co-Author*) Nothing to Disclose Sean Moen, BS, Minneapolis, MN (*Abstract Co-Author*) Nothing to Disclose Ang Zhou, PhD, Minneapolis, MN (*Abstract Co-Author*) Nothing to Disclose Sebastian Schmitter, Braunschweig, Germany (*Abstract Co-Author*) Nothing to Disclose Susanne Schnell, Chicago, IL (*Abstract Co-Author*) Nothing to Disclose Ruoyun Ma, Minneapolis, MN (*Abstract Co-Author*) Nothing to Disclose Michael Markl, PhD, Chicago, IL (*Abstract Co-Author*) Institutional research support, Siemens AG; Consultant, Circle Cardiovascular Imaging Inc; Kamil Ugurbil, Minneapolis, MN (*Abstract Co-Author*) Nothing to Disclose Bharathidasan Jagadeesan, MD, Minneapolis, MN (*Abstract Co-Author*) Nothing to Disclose

For information about this presentation, contact:

vande094@umn.edu

PURPOSE

To demonstrate the reproducibility of hemodynamic parameters in small intracranial aneurysms measured with 7 T MRI in an upscaled 3 D Printed model of the same aneurysms at 3 T.

METHOD AND MATERIALS

<u>Scan:</u> Five patients with silent aneurysm(s) were scanned at 7T. TOF was obtained for lesion localization and mask generation. ECG-gated, 4-points 3-directional 4D Flow was used in an axial 3D slab centered on the aneurysm with 15 cardiac phases, 2 k-space lines per cardiac phase, voxel size 0.76x0.76x0.8mm3, TR/TE=50.4ms/3.38ms, VENC=0.8m/s, Images were processed in

Matlab (noise filtering, correction for maxwell term and eddy current, velocity computation); vessel masks segmented in MimicsTM (based on TOF and/or PC-MRA from 4D Flow data); 3D streamlines and vorticity visualized using TecplotTMs; WSS was computed in matlab. <u>Replica:</u> Based on TOF, PC-MRA or CT-Scan, 3 aneurysms were numerically modelled, upscaled, 3D printed and assembled in an MR-compatible, dynamic fiow circuit filled with a fiuid chosen for its Reynolds and Womersley numbers4. Time re-scaled patient specific cardiac input functions from in-vivo measurements fed a programmable pump. 4D Flow MR data were acquired at 3T with this setting (see Fig.1).

RESULTS

A few studies failed because because of ECG issues, motion, or too small aneurysm size. When successful, 4D Flow revealed sharply defined velocity vectors and derived parameters. Velocity streamlines showed a tendency to form circular patterns rotating inside the aneurysm. It appears that at some cardiac cycle phases stronger local WSS develop on part of the aneurysm wall, despite a low velocity. 3T measures of 4D Flow in the upscaled 3D printed replica of the same aneurysm (Fig.1) demonstrated fairly similar velocity patterns when compared to in-vivo data.

CONCLUSION

We successfully obtained sub-millimetric in-vivo 4D Flow scans in small IAs at 7T. 4D Flow at 3T of aneurysm-specific 3D printed replicas yielded flow patterns comparable to those obtained in-vivo. We believe that the very promising results of this pilot study pave the way for us to study a larger cohort of patients. 3D models of ruptured IAs could provide relevant information when in-vivo scanning is impossible.

CLINICAL RELEVANCE/APPLICATION

Our results show good agreement between invivo measurements at 7 T and invitro measurements at 3 T in an unruptured 6 mm internal carotid artery aneurysm .

RC512-03 Focused, Ferumoxytol Enhanced MR Angiography (f-FEMRA) in Five Minutes Table Time for Patients With Claustrophobia: A Comparative Study

Wednesday, Nov. 28 9:15AM - 9:25AM Room: S503AB

Participants

Puja Shahrouki, Los Angeles, CA (Abstract Co-Author) Nothing to Disclose

Kim-Lien Nguyen, MD, Los Angeles, CA (Abstract Co-Author) Nothing to Disclose

John M. Moriarty, MD, Los Angeles, CA (*Abstract Co-Author*) Speaker, AngioDynamics, Inc Consultant, AngioDynamics, Inc Speaker, Sequent Medical, Inc Consultant, Sequent Medical, Inc Speaker, Argon Medical Devices, Inc Consultant, Argon Medical Devices, Inc Adam N. Plotnik, MBBS, FRANZCR, Los Angeles, CA (*Abstract Co-Author*) Nothing to Disclose Takegawa Yoshida, MD, Los Angeles, CA (*Abstract Co-Author*) Nothing to Disclose

J. Paul Finn, MD, Los Angeles, CA (*Presenter*) Speakers Bureau, Bayer AG; Scientific Advisory Board, AMAG Pharmaceuticals, Inc.

For information about this presentation, contact:

pfinn@mednet.ucla.edu

PURPOSE

To demonstrate the diagnostic performance of focused ferumoxytol-enhanced MR angiography (f-FEMRA) for evaluation of thoracic, abdominal and pelvic vasculature in <5 minutes in patients with claustrophobia.

METHOD AND MATERIALS

In this IRB-approved study, 13 patients (age 61.425.2 years, 6 F) with claustrophobia underwent *f*-FEMRA between December 2014 and August 2017 with an abbreviated acquisition protocol. Ferumoxytol 4mg/kg was administered as a slow infusion outside the scanner bore and steady state FEMRA was completed using default tuning and shim parameters to minimize adjustment time on a 3.0T MRI system. We retrospectively identified a matching cohort of 13 patients who had multi-phase, gadolinium-enhanced (GE) MRA with gadobenate dimeglumine, 0.15 mmol /kg. Two radiologists independently scored the images for arterial and venous image quality, motion artifacts, and diagnostic confidence using a 5-point scale where a score of 5 indicated the highest image quality and confidence and lowest level of artifact. Readers indicated whether they felt additional imaging was required for diagnostic assessment. Signal-to-noise ratio (SNR) and contrast-to-noise ratio (CNR) of the aorta and inferior vena cava (IVC) were measured All assessments were compared between groups and P-values <0.05 were considered statistically significant.

RESULTS

All scans were fully diagnostic and assessed with high confidence (scores >=4). Both reviewers indicated additional imaging was not required in all 26 (100%) studies. There was no significant difference between *f*-FEMRA and GEMRA for diagnostic confidence (4.86 \pm 0.24 vs 4.69 \pm 0.25, P = 0.125), arterial image quality (4.62 \pm 0.57 vs 4.65 \pm 0.49, P = 0.775) and motion artifact score (4.58 \pm 0.49 vs 4.58 \pm 0.28, P > 0.99). *f*-FEMRA had a significantly higher score for venous image quality than GEMRA (4.62 \pm 0.42 vs 4.19 \pm 0.56, P = 0.039). The CNR of the IVC was significantly higher for steady-state *f*-FEMRA than GEMRA regardless of the enhancement phase (P < 0.05).

CONCLUSION

Comprehensive and fully diagnostic vascular imaging of the thorax, abdomen and pelvis can be completed in less than 5 minutes of scan time with *f*-FEMRA.

CLINICAL RELEVANCE/APPLICATION

In patients with claustrophobia, comprehensive vascular imaging was completed successfully in as little as five minutes using *f*-FEMRA with noninferior diagnostic performance to conventional GEMRA.

RC512-04 Accuracy of ECG-Gated Time-Of-Flight Magnetic Resonance Angiography (TOF-MRA) versus Contrast Enhanced Magnetic Resonance Angiography (CE-MRA) at 3T for the diagnosis Peripheral Arterial Disease (PAD) of the Lower Limb

Awards Trainee Research Prize - Medical Student

Participants Saanchi A. Malhotra, MBBS, Mumbai, India (*Presenter*) Nothing to Disclose

For information about this presentation, contact:

saanchim20@gmail.com

PURPOSE

To evaluate the sensitivity, specificity, PPV, NPV and diagnostic accuracy of ECG-gated TOF-MRA at 3T for the diagnosis of PAD of the lower limb.

METHOD AND MATERIALS

A prospective study was conducted with 50 patients(age:mean=64y)with clinically diagnosed PAD. On a 3T MRI machine, TOF-MRA was performed using 16 channel body coil (with ecg gating and presaturation), from the level of the infrarenal aorta to the dorsalis pedis artery. CE-MRA was performed with 15ml Gd Dimeglumine injected at a flow rate of 0.4ml/sec followed by normal saline flush. All the images were viewed on a 3D workstation using standard 3D reconstruction software. The degree of stenoses was graded for 27 anatomic segments in each patient. The subjective image quality (5-point Likert scale) and degree of stenoses in each vascular segment (5-point likert scale) were evaluated by 2 observers and compared using the Mann-Whitney U and nonparametric Wilcoxon signed-rank test, respectively. Sensitivity, specificity, PPV and NPV of the TOF-MRA for the detection of significant (>50%) stenoses were assessed relative to the CE-MRA as the reference standard.

RESULTS

For TOF-MRA, 394/1326 segments(29.71%) were rated as significantly stenosed. For CE-MRA, 393/1326 segments(29.6%) were rated as significantly stenosed. DSA results were available for 324 segments. The sensitivity of TOF-MRA for detecting significant stenosis was 100% as compared to CE-MRA, the specificity was 99.89%, the PPV was 99.75%, the NPV was 100% and accuracy was 99.92%. In the pairwise comparison, TOF-MRA and CE-MRA techniques yielded significantly similar stenoses grades in all but 5 of 27 segments. These segments were right proximal ATA, right proximal PTA, right distal PTA, right proximal peroneal, left proximal ATA (p value <0.05)

CONCLUSION

ECG-gated TOF-MRA at 3T showed a high sensitivity, specificity, PPV, NPV and diagnostic accuracy, as compared to CE-MRA in the evaluation of significant stenoses in the lower limb arteries at a reasonable imaging time.

CLINICAL RELEVANCE/APPLICATION

Previous studies have shown the superiority of CE-MRA over TOF-MRA at 1.5T magnetic strength. ECG-gated TOF-MRA at 3T has comparable diagnostic accuracy to CE-MRA for the diagnosis of PAD of the lower limb and thus offers an alternative to the currently used imaging tests for PAD, especially in patients in whom the administration of iodinated or gadolinium-based contrast agents is contraindicated.

RC512-05 4D Flow MRA

Wednesday, Nov. 28 9:35AM - 10:10AM Room: S503AB

Participants

Shreyas S. Vasanawala, MD, PhD, Palo Alto, CA (*Presenter*) Research collaboration, General Electric Company Consultant, Arterys Inc Research Grant, Bayer AG

LEARNING OBJECTIVES

1) To know components required to implement clinically 4D flow. 2) To know types of clinically relevant data that can be extracted from 4D flow. 3) Become familiar with approaches to integrating 4D flow into clinical protocols.

ABSTRACT

4D flow is a time resolved volumetric phase contrast MRI technique. This presentation will cover essential components required to implement 4D flow in a clinical setting, review types of clinically relevant data that can be extracted from 4D flow, and present several approaches to integrating 4D flow into clinical MRI protocols. Essential components include a pulse sequence and postprocessing software. Data that can be extracted includes blood flow, cardiovascular function, and anatomy. Protocols can be greatly simplified with 4D flow, enabling a decoupling of image acquisition and interpretation, thereby enhancing efficiency of patient, technologist, and radiologist time.

RC512-06 Comprehensive MRA: Morphology and Function

Wednesday, Nov. 28 10:20AM - 10:55AM Room: S503AB

Participants

Tim Leiner, MD, PhD, Utrecht, Netherlands (Presenter) Speakers Bureau, Koninklijke Philips NV Research Grant, Bayer AG

For information about this presentation, contact:

t.leiner@umcutrecht.nl

LEARNING OBJECTIVES

To review state of the art and investigational methods for evalation of vascular morphology and function

LEARNING OBJECTIVES

View learning objectives under main course title.

RC512-07 4D Flow MRI Improves Dissection Flap Fenestration Detection and Characterization in Type B Aortic Dissection

Wednesday, Nov. 28 10:55AM - 11:05AM Room: S503AB

Participants

Bradley D. Allen, MD, Chicago, IL (Presenter) Nothing to Disclose

Pascale Aouad, MD, Creteil, France (Abstract Co-Author) Nothing to Disclose

Amir Ali Rahsepar, MD, Bridgeport, CT (Abstract Co-Author) Nothing to Disclose

Nicholas S. Burris, MD, San Francisco, CA (*Abstract Co-Author*) Entitled to royalties from liscensure of intellectual property to Imbio LLC

Christopher J. Francois, MD, Madison, WI (*Abstract Co-Author*) Departmental research support, General Electric Company; Alex Barker, Chicago, IL (*Abstract Co-Author*) Nothing to Disclose

Chris Malaisrie, Chicago, IL (*Abstract Co-Author*) Consultant, Edwards Lifesciences Corporation Proctor, Edwards Lifesciences Corporation Speaker, Edwards Lifesciences Corporation Consultant, Baxter International Inc Speaker, ABIOMED, Inc Speaker, Werfen Life Group SAU

James C. Carr, MD, Chicago, IL (*Abstract Co-Author*) Research Grant, Astellas Group; Research support, Siemens AG; Speaker, Siemens AG; Advisory Board, Guerbet SA

Jeremy D. Collins, MD, Chicago, IL (*Abstract Co-Author*) Consultant, Guerbet SA Grant, Siemens AG Grant, C. R. Bard, Inc Michael Markl, PhD, Chicago, IL (*Abstract Co-Author*) Institutional research support, Siemens AG; Consultant, Circle Cardiovascular Imaging Inc;

For information about this presentation, contact:

bdallen@northwestern.edu

PURPOSE

Flap fenestrations are key determinants of false lumen hemodynamics in type B aortic dissection. The purpose of this study was to compare dissection flap fenestration visualization between 4D flow MRI, conventional MRI/MRA, and CTA and qualitatively describe fenestration flow using 4D flow MRI.

METHOD AND MATERIALS

Nineteen patients with residual or chronic type B dissections (age: 59±12 years, M/F: 11/8) who had undergone MRI/MRA of the thoracic aorta including 4D flow MRI were retrospectively identified. Fourteen of the 19 patients had CTA performed within 2 years of MRI/MRA with no interval surgery. 4D flow images were post-processed and visualized on dedicated software (cvi42, Circle, Canada). Blinded image review was performed independently by two radiologists (rev 1 and rev 2). Cine 4D flow velocity maximum intensity projection (MIP) images were qualitatively evaluated for flow jets between true and false lumens, and MRI/MRA and CTA images were reviewed using a standard clinical approach. The number of fenestrations (including entry and exit tears) were reported. Frequency of fenestration detection was compared between all three techniques using a χ^2 -test and assuming alpha of 0.05.

RESULTS

4D flow MRI detected more fenestrations relative to MRI/MRA (rev 1: +3 (33/30), rev 2: +5 (30/25)) and similar numbers relative to CTA (rev 1: +1 (26/25), rev 2: -3 (23/26)). MRI/MRA detected fewer fenestration relative to CTA (rev 1: -6 (19/25), rev 2: -5 (21/26)). These differences were not statistically significant (p > 0.05), although we were underpowered to detect small differences in detection rate. Only fenestrations with associated flow jets were identified using 4D flow. Both observers report that diastolic flow from false to true lumen (retrograde) was the easiest hemodynamic feature to identify. Many fenestrations demonstrated biphasic flow between lumens (rev 1: 18/33, rev 2: 16/30).

CONCLUSION

4D flow MRI in type B dissection patients has the potential to better detect and hemodynamically characterize fenestrations. Future work will correlate these hemodynamic characteristics with thrombosis and aneurysmal enlargement of the false lumen to better direct medical or surgical management.

CLINICAL RELEVANCE/APPLICATION

4D flow MRI may improve detection and hemodynamic characterization of type B aorta dissection flap fenestrations with the potential to better inform patient risk-stratification and surgical planning.

RC512-08 Safe Follow-up after EndoVascular Aortic Repair (EVAR) with Non-contrast Magnetic Resonance Imaging (NCMRI): the SAFEVAR Study (Preliminary Data)

Wednesday, Nov. 28 11:05AM - 11:15AM Room: S503AB

Participants

Giulia Lastella, MD, Milan, Italy (*Presenter*) Nothing to Disclose Paola M. Cannao, MD, Milano, Italy (*Abstract Co-Author*) Nothing to Disclose Marco Ali, Milan, Italy (*Abstract Co-Author*) Nothing to Disclose Massimiliano Marrocco-Trischitta, San Donato Milanese, Italy (*Abstract Co-Author*) Nothing to Disclose Francesco Secchi, MD,PhD, Milano, Italy (*Abstract Co-Author*) Nothing to Disclose Francesco Sardanelli, MD, San Donato Milanese, Italy (*Abstract Co-Author*) Speakers Bureau, Bracco Group; Advisory Board, Bracco Group; Research Grant, Bayer AG; Advisory Board, General Electric Company; Reserach Grant, General Electric Company; Speakers Bureau, Siemens AG; Reserach Grant, Real Imaging Ltd;

For information about this presentation, contact:

francesco.secchi@grupposandonato.it

PURPOSE

Endovascular aortic repair (EVAR) is become a standard tecnique for the treatment of aortic and/or iliac aneurysm. A common short and long time complication is endoleak, which is well-known identified with arterious phase CT images. Magnetic resonance imaging

(MRI) could be useful, without use of contrast, in its early identification and during the follow-up of these patients. The presence of hyperintensity in MRI in the area closed to the EVAR is related to the presence of endoleak. Our aim was to evaluate the correlation between hyperintensity in MRI and endoleak and its appearance in CT.

METHOD AND MATERIALS

Forty-two patients after EVAR for aortic and/or iliac arterial aneurysms were enrolled and underwent MRI and contrast-enhanced CT in the same day between 0,01 and 1,55 years after the implantation. MRI was focused on true fast imaging with steady-state free precession (TRUFI) and half-Fourier-acquisition single-shot turbo spin-echo (HASTE) sequences at the precise level of the vessel were EVAR was implanted. CT was performed before and after iodate contract injection with basal and arterious phase contrast images. Two independent observers reviewed MRI to evaluate the presence of hyperintensity near the EVAR. Then, they evaluated in CT images the presence of endoleak and classified them according to the classification of Stanford in type I and II.

RESULTS

MRI revealed that 11 patients had no hyperintensity, and no one of these had endoleak in CT images. 31 patients presented hyperintensity in MRI, and 19 of these reveled a presence of endoleak (6 type I, 13 type II). Sensitivity, specificity, positive predictive value and negative predictive value of both observers were 100% (19/19), 48% (11/23), 61% (19/31) and 100% (11/11) respectively.

CONCLUSION

The absence of hyperintensity near the EVAR in MRI images can exclude the eventual presence of endoleak; nonetheless the hyperintensity can correlate with the presence of endoleak and require CT with iodate contrast to confirm it.

CLINICAL RELEVANCE/APPLICATION

Endoleaks can be previously excluded if there is no hyperintensity in MRI images without contrast injection. Data are still insufficient, but evidence revealed that CT can be considered as a second level exam only in the presence of hyperintensity after MRI without contrast.

RC512-09 Prone Position Scan Reduces B1 Inhomogeneity Effect in Non-Contrast-Enhanced MR Angiography of Lower Extremities

Wednesday, Nov. 28 11:10AM - 11:25AM Room: S503AB

Participants

Katsumi Nakamura, MD, Kitakyushu, Japan (*Presenter*) Nothing to Disclose Akiyoshi Yamamoto, RT, Kitakyushu, Japan (*Abstract Co-Author*) Nothing to Disclose Hiroki Matoba, Kitakyushu, Japan (*Abstract Co-Author*) Nothing to Disclose Yuji Shintani, RT, Kitakyushu, Japan (*Abstract Co-Author*) Nothing to Disclose Mitsue Miyazaki, PhD, La Jolla, CA (*Abstract Co-Author*) Nothing to Disclose

For information about this presentation, contact:

nakamura.katsumi@gmail.com

PURPOSE

To compare image quality on non-contrast MR angiography (MRA) acquired in prone position (prone-MRA) and that in supine position (supine-MRA) for the visualization of lower extremity arteries, and evaluate an effect of prone-MRA for improvement in B1 inhomogeneity

METHOD AND MATERIALS

Ten relatively thin volunteers (8 males, 2 females, mean age: 26.3 y.o.) underwent both supine- and prone-MRA examinations. The body mass index (BMI) range was from 17.3 to 24.0 (mean 20.2 ± 2.1). The arterial visualization was evaluated using a five-point scale. Overall successful rate was also calculated. Artifacts were compared in both prone- and supine-MRA images. Non-contrast MRA (Fresh blood imaging) was performed on a 3T-clinical imager using ECG-gated 3D half-Fourier FSE. After acquisition, the system subtracts the systolic triggered from diastolic triggered data. Systolic and diastolic delay times were automatically determined using a DelayTracker software. B1 map was obtained at a pelvic-femoral level in order to evaluate B1 inhomogeneity, and a B1 value ratio index (BRI) was calculated; BRI = (B1 value of right thigh) - (B1 value of left thigh) / B1 value of right thighx100.

RESULTS

The visualization of the left superficial femoral artery in the supine-MRA was significantly decreased due to B1 inhomogeneity compared to that in prone-MRA (average score = 3.7, 4.5, respectively, p<0.05). In B1 map analysis, B1 inhomogeneity in an anterior region of the left femoral indicated superb improvement in the prone position than in the supine position (BRI were 5.3, 12.0, respectively, p<0.05). The overall successful rate was increased from 50% in the supine-MRA to 90% in the prone-MRA. Misregistration artifacts were slightly greater in supine-MRA; however, appearances of other artifacts were considerably small and almost similar between the two methods.

CONCLUSION

Prone-MRA alleviates B1 inhomogeneity effect, causing an arterial signal loss of the pelvic-femoral region in supine-MRA, especially in thin volunteers. Proximal portion of superficial femoral artery must be insensitive to B1 inhomogeneity in the prone position. However, comfortless of prone-MRA scan is required to consider in elder patients.

CLINICAL RELEVANCE/APPLICATION

Non-contrast MR angiography (MRA) acquired in prone position alleviates B1 inhomogeneity effect, causing an arterial signal loss of the pelvic-femoral region in supine-MRA, especially in thin volunteers.

RC512-10 MRA and 3T or Higher Field Strength

Participants Winfried A. Willinek, MD, Bonn, Germany (*Presenter*) Speakers Bureau, Bayer AG Speakers Bureau, Bracco Group Speakers Bureau, General Electric Company Speakers Bureau, Koninklijke Philips NV Speakers Bureau, Sirtex Medical Ltd

LEARNING OBJECTIVES

View learning objectives under main course title.



Pediatric Series: Pediatric Radiology

Wednesday, Nov. 28 8:30AM - 12:00PM Room: S405AB



AMA PRA Category 1 Credits ™: 3.00 ARRT Category A+ Credits: 3.75

FDA Discussions may include off-label uses.

Participants

Brian D. Coley, MD, Cincinnati, OH (*Moderator*) Royalties, Reed Elsevier; Travel support, Canon Medical Systems Corporation; Travel support, Koninklijke Philips NV; Board of Directors, NeoView Ltd; Departmental Research support, Canon Medical Systems Corporation; Departmental Research support, Koninklijke Philips NV Geetika Khanna, MD, MS, Iowa City, IA (*Moderator*) Nothing to Disclose Mary-Louise C. Greer, FRANZCR, MBBS, Toronto, ON (*Moderator*) Research Grant, AbbVie Inc; Christopher I. Cassady, MD, Houston, TX (*Moderator*) Nothing to Disclose

For information about this presentation, contact:

mary-louise.greer@sickkids.ca

brian.coley@cchmc.org

Sub-Events

RC513-01 Pediatric Lung Sonography

Wednesday, Nov. 28 8:30AM - 8:50AM Room: S405AB

Participants

Brian D. Coley, MD, Cincinnati, OH (*Presenter*) Royalties, Reed Elsevier; Travel support, Canon Medical Systems Corporation; Travel support, Koninklijke Philips NV; Board of Directors, NeoView Ltd; Departmental Research support, Canon Medical Systems Corporation; Departmental Research support, Koninklijke Philips NV

For information about this presentation, contact:

brian.coley@cchmc.org

LEARNING OBJECTIVES

1) To describe the basic findings of normal pediatric lung ultrasound. 2) Differentiate normal from abnormal, and determine when the application of lung ultrasound may provide benefit on patient diagnosis and management.

RC513-02 Convolutional Neural Networks Accurately Determine Bone Age Utilizing Radiographs of the Second Digit Alone

Wednesday, Nov. 28 8:50AM - 9:00AM Room: S405AB

Awards

Student Travel Stipend Award

Participants

Nakul Reddy, MD, Houston, TX (*Presenter*) Nothing to Disclose Jesse C. Rayan, MD, Houston, TX (*Abstract Co-Author*) Nothing to Disclose J. H. Kan, MD, Houston, TX (*Abstract Co-Author*) Nothing to Disclose Ananth Annapragada, PhD, Houston, TX (*Abstract Co-Author*) Stockholder, Alzeca Biosciences, LLC Stockholder, Sensulin, LLC Stockholder, Abbott Laboratories Stockholder, Johnson & Johnson Wei Zhang, PhD, Houston, TX (*Abstract Co-Author*) Nothing to Disclose

PURPOSE

Convolutional neural networks (CNN) have shown remarkable success in evaluating bone age, achieving accuracy beyond conventional evaluation by a radiologist in the RSNA Pediatric Bone Age Challenge in 2017. The primary purpose of our study was to determine if bone age can be estimated by a CNN using radiographs of the second digit alone. A secondary purpose was to evaluate the effect of reduced radiation dose on the accuracy of bone age determination.

METHOD AND MATERIALS

Data was obtained from the RSNA pediatric bone age challenge training data set (Larson et al), which included 12606 hand radiographs and 200 test radiographs. Bone ages ranged from 1 month to 19 years of age. An object detector network (RetinaNet) by Lin et al, was used to extract the second digit terminal and middle phalanx. A grayscale convolutional neural network based on Inception v3 architecture was used to output a scalar value. Training was performed over 400 epochs, with randomized weights, on a desktop system equipped with a GTX 1070 Ti graphics card. Three subsets of the data were evaluated by the CNN: the whole hand/wrist, the second digit, and second digit with addition of Gaussian noise to simulate radiation reduction (25% standard

deviation of the pixel intensity distribution).

RESULTS

The average difference in assessed bone age of the entire hand/wrist by the CNN compared to the reviewers' consensus age was 4.8 months (standard deviation of 4.35). Comparing reviewers to second digit only with standard radiation differed by 7.3 months (standard deviation of 6.30), and comparing with second digit only with radiation reduction simulation differed by 6.8 months (standard deviation of 6.16).

CONCLUSION

A CNN can extract a clinically useful bone age from the second phalanx, similar to whole hand/wrist evaluation by both CNNs and pediatric radiologists. Adding noise to the images to simulate the effect of reduced radiation dose results in no change in bone age estimates.

CLINICAL RELEVANCE/APPLICATION

These results suggest a potential for reduced radiation burden as well as convenience in evaluating for bone age in pediatric patients when compared to the current state of the art.

RC513-03 Improving the Accuracy of Deep Learning Networks for Bone-Age Estimation by Incorporating Radiological Insight Guided Feature Analysis

Wednesday, Nov. 28 9:00AM - 9:10AM Room: S405AB

Participants

Vasanthakumar Venugopal, MD, New Delhi, India (*Presenter*) Nothing to Disclose Shyam Sundar Krishna Murthy, BEng, BEng, Bangalore, India (*Abstract Co-Author*) Employee, Koninklijke Philips NV Vidur Mahajan, MBBS, New Delhi, India (*Abstract Co-Author*) Nothing to Disclose Vijayananda Jagannatha, MS, Bangalore, India (*Abstract Co-Author*) Employee, Koninklijke Philips NV Harsh Mahajan, MD, MBBS, New Delhi, India (*Abstract Co-Author*) Nothing to Disclose

For information about this presentation, contact:

drvasanth@mahajanimaging.com

PURPOSE

The Greulich-Pyle (GP) method of bone age determination primarily involves estimation of ossification of the epiphyseal centers around the radiocarpal, carpometacarpal and the proximal interphalangeal joints and the carpal bones. This radiological insight was applied to devise a novel sequential approach, involving segmentation of relevant wrist anatomy from hand X-Rays followed by deep learning, and compared it against a standard deep learning technique to assess bone age in pediatric population between 7 years to 18 years.

METHOD AND MATERIALS

Dataset containing 12,600 radiographs provided by RSNA for Bone Age Challenge is used for this work. Out of the 12,600 we used ~10,000 radiographs of children between 7 years to 18 years of age. The intensity values of the hand radiographs are standardized across dataset by histogram matching image pre-processing techniques. A pre-processing algorithm was created to crop relevant regions, i.e. proximal phalanges, metacarpals, carpals and distal ends of radius and ulna, from the hand radiographs. Finally, ~9,000 cropped images were used to train a convolutional neural network implemented in the research version of HealthSuite Insights (Philips HealthTech) to predict the bone age from the image. The remaining images (~1,000) were used for validation purposes. Additional datasets of 200 test images released by RSNA and 50 test images obtained as part of routine clinical practice (extracted from PACS and anonymised using HIPAA compliant methods) were used to calculate Mean Absolute Error (MAE). Similar MAE was calculated for the same convolutional neural network implemented in the research version of HealthSuite Insights (Philips HealthTech) trained on the images without cropping the images.

RESULTS

The performance of deep learning model trained using cropped images was found to be superior with MAE of 5.08 months compared to the model trained using the full radiographs, which had MAE of 5.51 months.

CONCLUSION

The accuracy of machine learning models for specific tasks on radiographs can be improved by training using cropped/segmented radiographs containing areas of anatomy relevant to the task.

CLINICAL RELEVANCE/APPLICATION

Automated and accurate bone age estimation has wide-ranging clinical and medicolegal applications. Our novel method combines radiologist guided feature-based analysis with deep learning to improve the accuracy.

RC513-04 Diagnostic Accuracy of Post-Mortem Computed Tomography (PMCT) in Children

Wednesday, Nov. 28 9:10AM - 9:20AM Room: S405AB

Participants

Susan C. Shelmerdine, MBBS, FRCR, London, United Kingdom (*Presenter*) Nothing to Disclose Natasha Davendralingam, MBBS, London, United Kingdom (*Abstract Co-Author*) Nothing to Disclose Liina Palm, London, United Kingdom (*Abstract Co-Author*) Nothing to Disclose Nat Cary, Wantage, United Kingdom (*Abstract Co-Author*) Nothing to Disclose Neil J. Sebire, London, United Kingdom (*Abstract Co-Author*) Nothing to Disclose Owen Arthurs, MBBChir, PhD, Cambridge, United Kingdom (*Abstract Co-Author*) Nothing to Disclose

PURPOSE

To determine the diagnostic accuracy of PMCT compared to standard autopsy (gold standard) in children

METHOD AND MATERIALS

This single centre, retrospective study reviewed whole body non-contrast PMCTs over 6 years (2012-18) in children <16 years with corresponding full autopsy reports, irrespective of clinical indication for referral. Perinatal deaths (i.e. death *in utero* or within 24 hours of delivery) were excluded. PMCT was reported by radiologists with at least 2 years of paediatric post-mortem radiology experience. Autopsy was performed by experienced paediatric pathologists according to routine clinical practice. All imaging was reported blinded to autopsy findings. Overall diagnoses and findings by body systems at PMCT were compared to autopsy findings to evaluate diagnostic accuracy statistics.

RESULTS

136 cases were included (74(54.4%) male). The mean age was 2.1 years (median: 7 months, range: 2 days - 14.7 years). All cases and imaging were diagnostic. A cause of death at autopsy was found for 77/136 (56.6%) cases. PMCT gave a correct cause of death in 55/77 (71%) cases i.e. 55/136 overall (40.4%), with the majority attributable to traumatic brain and/or body injuries. For overall cause of death, diagnostic accuracy rates of PMCT with 95% confidence intervals were sensitivity of 71.4% (60.5%, 80.3%), specificity of 81.4% (69.6%, 89.3%), PPV of 83.3% (72.6%, 90.4%), NPV of 68.6% (57%, 78.2%) and concordance rate of 75.7% (67.9%, 82.2%). By body systems the sensitivity for PMCT was highest for intracranial (75.6%; 60.7-86.2%) and musculoskeletal pathologies (98.4%; 91.4-99.7%) and lowest for cardiac (31.3%; 14.2-55.6%), and abdominal findings (46.2%; 23.2-70.9%).

CONCLUSION

PMCT gives acceptable diagnostic accuracy rates of up to 75% in a paediatric population. Highest accuracy rates were found for intracranial and musculoskeletal pathologies.

CLINICAL RELEVANCE/APPLICATION

This is the largest paediatric PMCT accuracy study to date showing good concordance with autopsy, particularly for intracranial and musculoskeletal pathologies.

RC513-05 Impact of Adaptive Statistical Iterative Reconstruction-V on Radiation Dose and Image Quality in Children with Chest CT Scan

Wednesday, Nov. 28 9:20AM - 9:30AM Room: S405AB

Participants

Xiufeng Song II, PhD,PhD, QINGDAO, China (*Abstract Co-Author*) Nothing to Disclose Chunhong Yin, MD, Qingdao, China (*Presenter*) Nothing to Disclose Qinghua Song III, MD, Qing Dao, China (*Abstract Co-Author*) Nothing to Disclose Yang Li IV, MD,MD, Qingdao, China (*Abstract Co-Author*) Nothing to Disclose Hua Geng V, PhD,PhD, Shanghai, China (*Abstract Co-Author*) Nothing to Disclose

For information about this presentation, contact:

song-sxf@163.com

PURPOSE

To investigate the impact of adaptive statistical iterative reconstruction-V (ASIR-V) on radiation dose and image quality in children with chest CT scan

METHOD AND MATERIALS

280 patients underwent chest CT scan using a 256-row multi-detector CT (MDCT). The patients and divided into 4 groups (A, B, C and D) of 70 each. Conventional FBP reconstruction algorithm was used in group A. 80kV tube voltage, automated tube current modulation (Smart mA 10-720) and noise index (NI) 13 was used in image acquisition. Subjective image quality were assessed independently by three radiologists. A five-point scale (from 1=poor to 5=excellent) system was used. The Mann-Whitney U test and Kruskal-Wallis H test was used to test whether measurements between groups were different.

RESULTS

Radiation dose in the study group was reduced as compared with the control group. Effective dose in the group B (0.68 ± 0.38), C(0.37 ± 0.06), and D (0.15 ± 0.03) were lower than group A(1.3 ± 0.22). On the image quality evaluation, the 70%ASIR-V image has better image quality on the lung window and the mediastinum window. The the SD value of the fat and muscle (12.09 ± 3.44 , 12.37 ± 3.58) is obviously lower than the SD value of 0%, 80% and 90% ASIR-V (p<0.05), The SNR (4.83 ± 0.62 , 2.93 ± 0.54) was significantly higher than the SNR value (p<0.05) of the 0%, 80% and 90% ASIR-V images, and the subjective score of the 70%ASIR-V image in the lung and medial window (4.15 ± 0.51 , 4.09 ± 0.53) was also better than the score of 0%, 80% and 90%ASIR-V (p<0.05). Post ASIR-V can improve the image quality.

CONCLUSION

The ASIR-V technique of GE Revolution-CT with 70% pre-ASIR-V and 90% post-ASIR-V technique can reduce radiation dose while maintain good overall image quality.

CLINICAL RELEVANCE/APPLICATION

Adaptive statistical iterative reconstruction technology can significantly improve the children's chest radiation dose and CT image quality under low voltage scan conditions. The best new multi-model iterative reconstruction algorithm (ASIR-V) obtained in this study has certain guiding significance for low-tube voltage chest CT scan in children.

RC513-06 Comparative Evaluation of a Novel Portable Bedside Fluoroscopy System That Uses a Cassette-Sized Detector to the Standard of Care for ICU Pediatric Imaging

Wednesday, Nov. 28 9:30AM - 9:40AM Room: S405AB

Participants

Mark C. Liszewski, MD, Bronx, NY (Presenter) Grant, Carestream Health, Inc; Advisory Board, Carestream Health, Inc

Samuel Richard, PhD, Rochester, NY (*Abstract Co-Author*) Employee, Carestream Health, Inc Jordana Gross, Bronx, NY (*Abstract Co-Author*) Nothing to Disclose Terry L. Levin, MD, Mamaroneck, NY (*Abstract Co-Author*) Nothing to Disclose Einat Blumfield, MD, Scarsdale, NY (*Abstract Co-Author*) Co-founder and President, Radnostics LLC Spouse, Co-founder, Radnostics LLC Spouse, CEO, Radnostics LLC Benjamin Taragin, MD, Beit Shemesh, Israel (*Abstract Co-Author*) Medical Advisory Board, Carestream Health, Inc

For information about this presentation, contact:

mliszews@montefiore.org

PURPOSE

To evaluate the imaging performance of a portable bedside fluoroscopy unit in pediatric patients and compare it to a standard of care (SOC) in-room fluoroscopy unit in preparation for a pre-clinical study in the intensive care unit (ICU).

METHOD AND MATERIALS

Nineteen patients (< 3 years of age) scheduled to undergo upper gastrointestinal series (UGI) or voiding cystourethrograms (VCUG) were recruited under an IRB-approved protocol designed to evaluate the non-FDA approved portable fluoroscopic unit. Informed consent was obtained from the patients' guardians. The unit, a modified portable radiographic system with a cassette-sized detector (Carestream Health Revolution, USA) was positioned adjacent to the in-room fluoroscopy system (Philips Healthcare Optimus 80, Netherlands). Images were captured on both units; each study began on the portable unit and ended on the SOC unit. All diagnoses were based on SOC images. The SOC system was operated under a low-dose pediatric protocol and the portable unit used a comparable technique (i.e., 2.5 fps and no grid). Study dose was recorded on both units. To evaluate image quality, four pediatric radiologists (blinded to the system used to obtain the image) were asked to score 20 images from each system based on spatial resolution (SR), image contrast (IC), uniformity (UY), noise appearance (NA) and overall quality (OQ) using the Radlex score (1-4). The same attributes were evaluated using a preference test, by displaying side-by-side images of the same exam acquired on each system.

RESULTS

Average dose rates for the SOC and portable systems were 0.32mGy/min and 0.31mGy/min, respectively (p= 0.38). The Radlex scores for SOC and portable systems for the single stimulus study were 2.9 and 3.0 (IC) (p=.08), 3.1 and 2.8 (UY) (p<0.05), 2.7 and 2.9 (SR) (p<0.05), 2.4 and 2.6 (NA) (p<0.05), 2.8 and 3.0 (OQ) (p<0.05), respectively. While most attributes scored slightly higher for the portable system, the side-by-side comparative study found no significant system preference for any of the image quality attributes.

CONCLUSION

The portable fluoroscopy prototype is capable of providing comparable image quality at equivalent dose levels to an in-room system for young children.

CLINICAL RELEVANCE/APPLICATION

The ability to provide fluoroscopy at the bedside is expected to improve patient outcomes in neonatal and pediatric ICUs by reducing the need to transport critically ill patients.

RC513-07 Neonatal Imaging Pearls

Wednesday, Nov. 28 9:40AM - 10:00AM Room: S405AB

Participants

Christopher I. Cassady, MD, Houston, TX (Presenter) Nothing to Disclose

LEARNING OBJECTIVES

1) Recommend an appropriate strategy for the work up of common neonatal imaging problems. 2) Assess practically, based on outcomes data where available, the utility of imaging in the management of the ill neonate.

RC513-08 Whole Body Imaging in Cancer Predisposition Syndromes

Wednesday, Nov. 28 10:20AM - 10:40AM Room: S405AB

Participants

Mary-Louise C. Greer, FRANZCR, MBBS, Toronto, ON (Presenter) Research Grant, AbbVie Inc;

For information about this presentation, contact:

mary-louise.greer@sickkids.ca

LEARNING OBJECTIVES

1) To specify cancer predisposition syndromes where whole body MRI plays a role in surveillance. 2) Apply a systematic approach to analysis of whole body imaging. 3) Identify related tumors.

RC513-09 Utility of Follow-up Head Ultrasound in Premature Infants Less than 32 Weeks Gestational Age When the Initial Head Ultrasound is Normal

Wednesday, Nov. 28 10:40AM - 10:50AM Room: S405AB

Participants

Matthew A. Zapala, MD,PhD, San Francisco, CA (*Presenter*) Nothing to Disclose Mithun Diwakar, MD, PhD, San Mateo, CA (*Abstract Co-Author*) Nothing to Disclose Dawn Gano, MD, San Francisco, CA (*Abstract Co-Author*) Nothing to Disclose Jesse L. Courtier, MD, San Francisco, CA (*Abstract Co-Author*) Founder, HoloSurg3D, Inc; Consultant, HoloSurg3D, Inc Andrew S. Phelps, MD, San Francisco, CA (*Abstract Co-Author*) Nothing to Disclose

For information about this presentation, contact:

Matthew.Zapala@ucsf.edu

PURPOSE

To determine the incidence of abnormal findings on follow up routine head ultrasounds (US) performed on premature infants less than 32 weeks gestation at 4 weeks post-natally when the initial head US performed in the first week of life is normal.

METHOD AND MATERIALS

An IRB-approved HIPAA-compliant retrospective study was performed on premature infants imaged at a tertiary care academic pediatric hospital from January 2012 to December 2015. Inclusion criteria included premature infants less than 32 weeks gestational age with a head US in the first week of life read as normal and a routine head US performed at 4 weeks of age. Infants with severe congenital defects were excluded. Follow up reports were then classified as normal or abnormal and abnormal reports were reviewed for findings.

RESULTS

Of the 194 premature infants that met inclusion criteria, none had Papile grade II, III, or IV germinal matrix hemorrhage. Fourteen patients (7%) had new grade I germinal matrix hemorrhage. At outpatient clinic follow-up (range 6 months to 3 years), all of the 14 patients with grade I germinal matrix hemorrhage were meeting appropriate developmental milestones, and none had significant neurological deficit.

CONCLUSION

When initial head ultrasounds in premature infants are found to be normal, follow up routine head ultrasounds at 4 weeks of age are typically found to be normal. Those rare abnormal cases are restricted to grade 1 germinal matrix hemorrhages. The clinical significance of isolated grade 1 germinal matrix hemorrhages in premature infants on long-term neurocognitive development is unclear. However, several large cohort studies have found no difference in rates of cerebral palsy among premature infants with grade 1 germinal matrix hemorrhages and those without.

CLINICAL RELEVANCE/APPLICATION

In premature infants less than 32 weeks gestational age, with no severe congenital defects, screening routine follow up head ultrasound at 4 weeks of age is of limited clinical utility if the initial postnatal head ultrasound is normal.

RC513-10 Game Plan for a Double-Play or Extra-Point: Can Dual-Source, Dual-Energy CT Help Reduce Radiation Dose and Contrast Volume in Children?

Wednesday, Nov. 28 10:50AM - 11:00AM Room: S405AB

Participants

Azadeh Tabari, Boston, MA (*Presenter*) Nothing to Disclose Michael S. Gee, MD, PhD, Boston, MA (*Abstract Co-Author*) Nothing to Disclose Cristy Savage, RT, Boston, MA (*Abstract Co-Author*) Nothing to Disclose Andrew Primak, PhD, Malvern, PA (*Abstract Co-Author*) Employee, Siemens AG Bernhard Schmidt, PhD, Forchheim, Germany (*Abstract Co-Author*) Employee, Siemens AG Mannudeep K. Kalra, MD, Boston, MA (*Abstract Co-Author*) Research Grant, Siemens AG; Research Grant, Canon Medical Systems Corporation

For information about this presentation, contact:

atabari@mgh.harvard.edu

PURPOSE

We hypothesized that dual-source, dual energy CT (DS-DECT) can reduce radiation dose and contrast volume compared to single energy CT (SECT) scanning in children.

METHOD AND MATERIALS

Our ongoing, institutional review board approved study included 64 children who underwent contrast enhanced CT of the chest (n=38) or abdomen (n=26) on 2nd or 3rd generation dual source CT (Siemens Flash or Force) for clinically justified reasons. Equal number of patients were scanned with SECT (with automatic kV selection, CARE kV & AEC, CARE Dose4D) and DS-DECT (each with 19 chest CT, 13 abdomen CT). Clinical indications, radiologic findings, and any study limitations (noise or artifacts) were assessed. Patient demographics (age, gender, weight), scan parameters (kV, mAs, section thickness) CT dose descriptors (size specific dose estimates [SSDE], dose length product [DLP]), and contrast volume (370 mg% Isovue, Bracco) were recorded. Descriptive statistics were performed for data analysis.

RESULTS

Patient ages and weights in DS-DECT (11±6 years; 47±32 kg) and SECT (10±6 years; 44±27 kg) groups were not different (p>0.05). Most DS-DECT and SECT were performed for oncologic staging, abnormal prior imaging, and trauma. Chest SECT exams were performed at 80-100kV, and abdominal SECT at 80-120kV. Respective SSDE and DLP were: chest DS-DECT 3.3±2.0mGy, 187±75mGy.cm; chest SECT 5.2±3.0mGy, 129±118mGy.cm; abdominal DS-DECT 3.7±2.0mGy, 161±89mGy.cm; abdominal SECT 6.1±3.0mGy, 179±70mGy.cm (SSDE, DS-DECT < SECT, p<0.01). Chest and abdomen DS-DECT were performed with 9-18% lower contrast volume compared to weight and region matched children scanned with SECT. All DS-DECT and SECT studies were deemed acceptable for evaluation of chest and abdominal findings.

CONCLUSION

In children, dual-source DECT enables substantial radiation dose and contrast volume reductions compared to single energy CT performed with automatic exposure control & automatic kV selection techniques.

CLINICAL RELEVANCE/APPLICATION

Dual-source, dual energy CT help reduce radiation dose and contrast volume in children undergoing contrast enhanced chest and abdominal CT.

RC513-11 Comparison of the Diagnostic Performance of the 2017 ACR TI-RADS Guideline to the 2015 Guideline in Children with Thyroid Nodules

Wednesday, Nov. 28 11:00AM - 11:10AM Room: S405AB

Participants

Gali Shapira Zaltsberg, MD, Ottawa, ON (*Presenter*) Nothing to Disclose Elka Miller, MD, Ottawa, ON (*Abstract Co-Author*) Nothing to Disclose Claudia M. Martinez Rios Arellano, MD, Ottawa, ON (*Abstract Co-Author*) Nothing to Disclose Juan Bass, Ottawa, ON (*Abstract Co-Author*) Nothing to Disclose Ellen Goldbloom, Ottawa, ON (*Abstract Co-Author*) Nothing to Disclose Ken Tang, Ottawa, ON (*Abstract Co-Author*) Nothing to Disclose Kerri A. Highmore, MD, Ottawa, ON (*Abstract Co-Author*) Nothing to Disclose

PURPOSE

To investigate the inter-rater reliability and diagnostic performance of the 2017 Thyroid Image Reporting and Data System (TI-RADS) guideline in the pediatric population and compare it to the previous 2015 TI-RADS guideline.

METHOD AND MATERIALS

This retrospective study comprised 77 children with thyroid nodules noted on US at a tertiary-level pediatric hospital. Three pediatric radiologists and one pediatric radiology fellow graded the US findings using both 2017 and 2015 TI-RADS guidelines. Reliability of radiologists' ratings was assessed two ways: % inter-rater agreement among all pairwise combinations of within-patient ratings, and intra-class correlation coefficients based on a two-way random model (ICC2,1). Area under the receiver operating characteristic curve (AUROCC) was assessed to compare the discriminative ability of the various TI-RADS categories of scoring system against histopathology/cytology or stability on US over a 2-year follow-up period for cases without tissue diagnosis.

RESULTS

Percent pairwise agreement for 2017 TI-RADS points, levels, recommendations, and the 2015 TI-RADS levels was 33.3 % (95% CI-29.2-37.8%), 50.9% (46.3-55.4%), 64.9% (60.5-69.1%), and 35.7% (31.5-40.2%) respectively. Estimated ICC2,1 for the same four scoring system was 0.48 (95%CI: 0.36 -0.59), 0.5 (0.39-0.62), 0.55 (0.44-0.66), and 0.42 (0.29-0.55) respectively. AUROCC for the 2017 TI-RADS points, levels, recommendations, and the 2015 TI-RADS levels was 0.73 (95% CI- 0.62-0.84), 0.72 (0.61-0.83), 0.78 (0.69-0.87), and 0.74 (-0.66-0.82) respectively. Difference in AUROCCs between the TI-RADS 17 levels and TI-RADS 15 levels was estimated to be -0.02 (95% CI: -0.05 -0.09).

CONCLUSION

Inter-rater reliability and diagnostic performance was moderate across scoring systems derived from both the 2015 and 2017 TI-RADS when applied to a pediatric population. No one scoring system was shown to be clearly superior in terms of diagnostic performance. Further work to adjust the recommendations for pediatric patients needs to be considered.

CLINICAL RELEVANCE/APPLICATION

The 2015 and 2017 TI-RADS scoring systems show similar moderate inter-rater reliability and diagnostic performance when applied to a pediatric population.

RC513-12 Diagnostic Yield of Renal Ultrasound with Doppler Studies in Children with Hypertension

Wednesday, Nov. 28 11:10AM - 11:20AM Room: S405AB

Participants Shaun Hinen, MD, Charleston, SC (*Presenter*) Nothing to Disclose Scott P. Landreth, MD, Charleston, SC (*Abstract Co-Author*) Nothing to Disclose Heather R. Collins, PhD, Charleston, SC (*Abstract Co-Author*) Nothing to Disclose Jeanne G. Hill, MD, Charleston, SC (*Abstract Co-Author*) Nothing to Disclose Anil G. Rao, MD, Charleston, SC (*Abstract Co-Author*) Speaker, Siemens AG

PURPOSE

Renal Doppler study is a commonly performed exam in the pediatric population. In our experience, the majority of these are normal. The aim of this study is to assess the diagnostic yield of this test in children who have hypertension.

METHOD AND MATERIALS

A retrospective analysis of 1000 consecutive pediatric renal Doppler studies was done. Study indications, renal lengths, renal arterial and venous Doppler findings, and incidental findings were noted. Demographic data, blood pressure, blood pressure percentile, height, weight percentile, BMI, kidney size, and lab values were collected. A Wilcoxon signed-rank test was performed on relevant variables to evaluate differences in the RAS absent group with the medians from RAS positive patients.

RESULTS

Of 1000 studies, 638 renal Doppler studies were done for the evaluation of hypertension. There were 7 diagnoses of renal artery stenosis (RAS) with left-sided disease in 3 patients, right-sided involvement in 1 patient, and both renal arteries affected in 3 patients (1 had bilateral compression from neuroblastoma, 1 had bilateral narrowing in association with coarcation of the abdominal aorta and 1 had bilateral stenosis in association with Takayasu's arteritis with worse narrowing on the right). Two of the left-sided patients had a kidney size discrepancy greater than 1 cm and the remaining RAS patients had no significant renal size discrepancy. Only 1 of the 7 patients had an indication other than hypertension, and this patient had a known history of Wilms tumor with left nephrectomy. The remaining 631 studies were negative for RAS although one patient had non-diagnostic results with discordant findings on U/S, CT and MRI. There was no correlation between weight %/blood pressure % (sys/dia) as measured by Pearson

Correlation [.07 and .008].

CONCLUSION

Renovascular cause for hypertension in children is extremely low. Selective referral of pediatric patients with hypertension for renal Doppler studies can improve the diagnostic yield of this test. In the absence of renal size discrepancy, Doppler study may not be indicated. A renal ultrasound study without Doppler could be considered for initial evaluation of pediatric patients with hypertension.

CLINICAL RELEVANCE/APPLICATION

Selective referral and/or stricter adherence to guidelines for hypertensive pediatric patients can improve the diagnostic utility of Renal Doppler studies, as the majority of these studies are normal.

RC513-13 Novel Quantitative Contrast-Enhanced Ultrasound Detection of Hypoxic Ischemic Injury in Neonates and Infants: Pilot Study I

Wednesday, Nov. 28 11:20AM - 11:30AM Room: S405AB

Participants

Misun Hwang, MD, Philadelphia, PA (*Presenter*) Nothing to Disclose Anush Sridharan, PhD, Philadelphia, PA (*Abstract Co-Author*) Nothing to Disclose Kassa Darge, MD,PhD, Philadelphia, PA (*Abstract Co-Author*) Nothing to Disclose Becky Riggs, Baltimore, MD (*Abstract Co-Author*) Nothing to Disclose Chandra Sehgal, PhD, Philadelphia, PA (*Abstract Co-Author*) Nothing to Disclose John Flibotte, Philadelphia, PA (*Abstract Co-Author*) Nothing to Disclose Thierry Huisman, MD, Baltimore, MD (*Abstract Co-Author*) Nothing to Disclose

For information about this presentation, contact:

Hwangm@email.chop.edu

PURPOSE

To investigate whether quantitative contrast-enhanced ultrasound (CEUS) can accurately identify neonates and infants with hypoxic ischemic brain injury and monitor associated perfusion abnormalities.

METHOD AND MATERIALS

In this prospective cohort study, 8 neonates and infants with suspicion for hypoxic ischemic injury were evaluated with CEUS between August 2017 and December 2017. CEUS brain scans of the 8 neonates and infants were acquired for assessment of brain perfusion. Main outcomes and measures included comparison of quantitative CEUS parameters between normal and affected patients. CEUS perfusion maps were compared to cerebral magnetic resonance imaging (MRI) for those with available MRI data.

RESULTS

An interesting trend was observed in the central gray nuclei-to-cortex perfusion ratios. The ratios at peak enhancement, wash-in area under the curve, perfusion index and maximum wash-in slopes were lower in all the affected cases as compared to the normal group. Statistically, all these comparisons were approaching significance (p=0.0571), but not currently significant given the small sample size. Additionally, when the central gray nuclei-to-cortex perfusion ratio was plotted for all time points along the time intensity curve (TIC), it was observed that the affected cases exhibited a trend that was qualitatively different from the normal cases. In the affected cases, the ratio TICs either stayed under 1.0 for the entire enhancement period or reached 1.0 close to peak wash-in before falling just under 1.0 for the remaining period of enhancement. However, in the unaffected subjects, there was a steep wash-in that crossed the 1.0 threshold and remained above 1.0 for most of the enhancement period.

CONCLUSION

Bedside CEUS is an easily obtainable brain imaging technique that has the potential to reliably identify infants and neonates with evolving hypoxic brain injury. A larger prospective study evaluating the correlation between CEUS findings and the gold-standard of MRI diffusion-weighted and perfusion-weighted imaging is needed to establish this as a diagnostic tool.

CLINICAL RELEVANCE/APPLICATION

Our preliminary data also suggests that hypoxic ischemic injury can be detected via both qualitative and quantitative contrastenhanced ultrasound evaluation.

Honored Educators

Presenters or authors on this event have been recognized as RSNA Honored Educators for participating in multiple qualifying educational activities. Honored Educators are invested in furthering the profession of radiology by delivering high-quality educational content in their field of study. Learn how you can become an honored educator by visiting the website at: https://www.rsna.org/Honored-Educator-Award/ Kassa Darge, MD,PhD - 2016 Honored Educator

RC513-14 The Use of MRI in an Acute Abdomen as an Alternative to CT in Young Patients

Wednesday, Nov. 28 11:30AM - 11:40AM Room: S405AB

Participants

Rukhtam Saqib, MBChB, Manchester, United Kingdom (*Presenter*) Nothing to Disclose Velauthan Rudralingam, MBBCh, Cheshire, United Kingdom (*Abstract Co-Author*) Nothing to Disclose Sathi A. Sukumar, MD, Wythenshawe, United Kingdom (*Abstract Co-Author*) Nothing to Disclose

For information about this presentation, contact:

rukhtamsaqib@doctors.org.uk

PURPOSE

In acute abdominal pain. ultrasound is the preferred imaging modality in vounger patients, particularly females, often followed by CT

if negative and ongoing clinical concern. However, this comes with a radiation cost. MRI offers no ionizing radiation, excellent tissue contrast and can be used without nephrogenic iodinated contrast. It has been shown to be effective in diagnosis acute appendicitis, diverticulitis and cholecystitis. Nevertheless, there are disadvantages such as higher cost, limited availability, claustrophobia and a relative contra-indication in early pregnancy. Furthermore, MRI abdomens in the acute setting are likely to need interpretation by experienced GI radiologists. Our aim was to assess the role of MRI in the acute abdomen as an alternative to CT.

RESULTS

A total of 47 patients, 36 female and 11 males. The most common indication for imaging was right iliac fossa pain (66%). 39/47 patients had a prior ultrasound of which 20/39 were abnormal and 19 reported as normal. 30/39 of these patients had a MRI within 48 hours of the ultrasound. Of the 19 normal ultrasounds, 5 had abnormal MRI findings and included appendicitis, ovarian cyst haemorrhage (two cases), ileitis and acute epiploic appendagitis. Patients went onto have MRI as there was ongoing clinical suspicion of an acute abdomen. All abnormal ultrasounds were abnormal on subsequent MRI and were performed to increase the diagnostic confidence of the ultrasound findings. 17/20 of these had similar findings on MRI, but 3 cases showed minor differences but MRI was organised by the Consultant performing the ultrasound. In the 1st case, the history was right iliac fossa pain and to rule out intra-abdominal abscess. The ultrasound showed an incidental gallstone but was not able to assess the abdomen/retroperitoneum adequately therefore a MRI was organised by the Consultant Radiologist which showed acute right septic hip arthritis with extension into the adjacent adductor muscles. In the 2nd case, the history was of lower abdominal pain with a raised white cell count. The ultrasound showed gross pelvic and abdominal ascites but was unable to identify the cause so a MRI was arranged, demonstrating a ruptured corpus luteal cyst. In the 3rd case, the history was right upper quadrant pain and the ultrasound was non-specific with sluggish bowel so MRI was arranged, showing haemorrhagic ovarian cyst. Overall, 32/47 of the MRIs demonstrated acute pathology, with the most common diagnosis acute appendicitis. 8/47 went to MRI directly of which 5 were normal and the remaining 3 showed appendicitis (two cases) and small volume non-specific free fluid in a male patient.

CONCLUSION

Ultrasound is a good primary imaging modality with excellent correlation between the abnormal ultrasounds and MRI (86%). These results have given confidence to the ultrasound diagnosis which may lead to reduced cross-sectional imaging in the future. We suggest an ultrasound as first line, but recommend MRI when ultrasound is normal but clinically suspicious of an acute abdomen, or when abnormal ultrasound findings needed further confirmation to increase the level of diagnostic accuracy and avoid negative laparoscopies/laparotomies. MRI has potential to fast track discharge patients, reducing the burden on the hospital and should ideally be performed within 24 hours.

METHODS

A 12 month retrospective review between 1.4.16 and 31.3.17 was performed and all inpatients undergoing a MRI abdomen were included. Prior ultrasound findings were noted and compared to the MRI.

PDF UPLOAD

http://abstract.rsna.org/uploads/2018/18015075/18015075_e9hl.pdf

RC513-15 Pediatric Abdominal MRI: Understanding Signal Intensity Patterns

Wednesday, Nov. 28 11:40AM - 12:00PM Room: S405AB

Participants

Geetika Khanna, MD, MS, Iowa City, IA (Presenter) Nothing to Disclose

LEARNING OBJECTIVES

1) To describe the normal signal intensity patterns of abdominal visceral organs. 2) Learn to recognize disease/diagnosis based on MR signal intensity pattern alteration.



Interventional Series: Peripheral and Visceral Occlusive Disease

Wednesday, Nov. 28 8:30AM - 12:00PM Room: S105AB



AMA PRA Category 1 Credits ™: 3.50 ARRT Category A+ Credits: 4.00

FDA Discussions may include off-label uses.

Participants

Bulent Arslan, MD, Chicago, IL (*Moderator*) Advisory Board, Medtronic plc; Advisory Board, Guerbet SA; Speakers Bureau, Biocompatibles International plc; Speakers Bureau, C. R. Bard, Inc; Advisory Board and Speakers Bureau, Boston Scientific Corporation; Speakers Bureau, Penumbra, Inc

Laura K. Findeiss, MD, Atlanta, GA (Moderator) Nothing to Disclose

For information about this presentation, contact:

bulent_arslan@rush.edu

LEARNING OBJECTIVES

1) Describe pros and cons of intervention for median arcuate ligament compression on the celiac axis. 2) Review clinical presentation and endovascular treatment options for acute and subacute portal vein thrombus. 3) Outline three recommendations for endovascular treatment of peripheral vascular disease. 4) Describe how and when to intervene in patients with mesenteric ischemia. 5) Describe two vascular compression syndromes.

Sub-Events

RC514-01 Compressive Arterial Syndromes

Wednesday, Nov. 28 8:30AM - 8:50AM Room: S105AB

Participants

Minhaj S. Khaja, MD, MBA, Ann Arbor, MI (Presenter) Consultant, Penumbra, Inc; Speaker, Penumbra, Inc

For information about this presentation, contact:

mkhaja@umich.edu

LEARNING OBJECTIVES

1) Review the role of cross-sectional imaging and IR in the diagnosis and potential treatment of compressive arterial syndromes. 2) Illustrate case based examples of compressive arterial syndromes.

RC514-02 Acute Portal Venous Thrombosis

Wednesday, Nov. 28 8:50AM - 9:10AM Room: S105AB

Participants

Wael E. Saad, MBBCh, Ann Arbor, MI (Presenter) Speaker, W. L. Gore & Associates, Inc; Consultant, Siemens AG

LEARNING OBJECTIVES

View Learning Objectives under main course title.

RC514-03 Mid-Term Result of Thoracic Endovascular Aortic Repair in Octogenarians and Nonagenarians

Wednesday, Nov. 28 9:10AM - 9:20AM Room: S105AB

Participants

Takashi Hashimoto, Tsu, Japan (*Presenter*) Nothing to Disclose Noriyuki Kato, Tsu, Japan (*Abstract Co-Author*) Nothing to Disclose Takafumi Ouchi, Tsu, Japan (*Abstract Co-Author*) Nothing to Disclose Ken Nakajima, Tsu, Japan (*Abstract Co-Author*) Nothing to Disclose Takatoshi Higashigawa, MD, Tsu, Japan (*Abstract Co-Author*) Nothing to Disclose Shuji Chino, MD, Matsusaka, Japan (*Abstract Co-Author*) Nothing to Disclose Hajime Sakuma, MD, Tsu, Japan (*Abstract Co-Author*) Nothing to Disclose Hajime Sakuma, MD, Tsu, Japan (*Abstract Co-Author*) Nothing to Disclose Hajime Sakuma, MD, Tsu, Japan (*Abstract Co-Author*) Research Grant, Fuji Pharma Co, Ltd; Research Grant, DAIICHI SANKYO Group; Research Grant, FUJIFILM Holdings Corporation; Research Grant, Siemens AG; Research Grant, Nihon Medi-Physics Co, Ltd; Speakers Bureau, Bayer AG

PURPOSE

Thoracic endovascular aortic repair (TEVAR) is expected to benefit old patients with high operative risk. We investigated the outcome of TEVAR in octogenarians and nonagenarians.

METHOD AND MATERIALS

From May 1997 through December 2017, 638 patients had undergone TEVAR for TAA or AD in our hospitals. We retrospectively reviewed the medical records of 113 patients aged 80 years or older (17.7%) among them.

RESULTS

There were 78 men and 35 women. The mean age was 83.4±3.1 years (mean±standard deviation). Emergent TEVAR was performed in 28 patients (25.7%). Thirty-day mortality rate and the rate of 30-day mortality plus major adverse events calculated using Japan score were 24.0±22.5% and 40.7%±20.2%, respectively. Mortality rate and the rate of mortality plus morbidity calculated using STS score were 6.6±5.1% and 25.8±13.9%, respectively. Operative mortality rate calculated using euroSCORE was 11.7±10.9%. To preserve aortic arch branches, bypass surgery was added to 1 aortic branch in 6 patients, 2 branches in 11 patients, 3 branches in 1 patient. In 5 patients, chimney technique was used to preserve the left subclavian artery. To preserve a celiac artery, periscope technique was used in 1 patient, and bypass surgery was added in 1 patient. The mean follow-up term was 23.5±21.1 months. Overall survival rate was 96.4% at 1 month, 94.5% at 3 months, 88.1% at 1 year, and 83.7% at 3 years. Cause of early death was aortic rupture in 2 patients, sepsis in 1, and cancer in 1. Aorta-related adverse event free rate was 88.5% at 1 month, 85.6% at 3 months, 81.3% at 1 year, and 71.3% at 3 years. Regarding patients undergoing elective TEVAR, overall survival rate was 98.8% in 1 month and 3 months, 91.9% at 1 year, and 88.4% at 3 years. Aorta-related adverse event free rate was 89.4% at 1 month and 3 months, 85.3% at 1 year, and 76.7% at 3 years. Excluded 6 patients whose discharge to unknown, 107 patients were analyzed about discharge to home or not. After logistic regression, emergency and combined procedure were the negative predictors of home discharge.

CONCLUSION

TEVAR in octogenarians and nonagenarians seems to be acceptable in terms of life prognosis. Emergency and combined procedure were the negative predictors of home discharge.

CLINICAL RELEVANCE/APPLICATION

TEVAR in octogenarians and nonagenarians seems to be acceptable in terms of life prognosis or high operative risk.

RC514-04 Frequency and CTA-based Volumetric Analysis of Endoleaks after Fenestrated Endovascular Aortic Aneurysm Repair (FEVAR) using Custom and Off-the-Shelf Devices

Wednesday, Nov. 28 9:20AM - 9:30AM Room: S105AB

Participants

David E. Timaran Montenegro, MD, Mexico City, Mexico (*Presenter*) Nothing to Disclose Marilisa Soto Gonzalez, MD, Dallas, TX (*Abstract Co-Author*) Nothing to Disclose Angie Garcia, MD, Dallas, TX (*Abstract Co-Author*) Nothing to Disclose Carlos Timaran, Dallas, TX (*Abstract Co-Author*) Consultant, Cook Group Incorporated Consultant, Getinge AB Consultant, W. L. Gore & Associates, Inc

For information about this presentation, contact:

david_timaranQyahoo.com

PURPOSE

The aim of the study was to assess the type, frequency, morphologic characteristics and outcomes of endoleaks after FEVAR/BEVAR using custom-made- devices (CMDs) and off-the-shelf branched devices.

METHOD AND MATERIALS

A single institutional study was performed to assess the frequency and volume of endoleaks after FEVAR using fenestrated/branched CMDs and off-the-shelf devices. All fenestrated procedures were performed using investigational CMDs under a physician-sponsored investigational device exemption. Endoleaks were detected and characterized on duplex and CT angiography. CTA-based volumetric analysis was performed using Terarecon software. Kruskal-Wallis and Mann-Whitney U tests were used for univariate analysis.

RESULTS

Over a 25-month period, 70 patients (52 men [74%] and 18 women [26%]) with a median age of 68 years (interquartile range [IQR], 63.5-73 years) underwent FEVAR using Fenestrated/Branched Custom-Made-Devices (CMDs) (64[91%]) and Zenith T-Branch (6[9%]). The median number of fenestrations/branches was 4 (IQR, 3-4). Endoleaks were detected in 11 patients (7.7%) accounting for a total of 15 endoleaks during follow-up. Endoleaks were found at a median time of 1 month (Interquartile range [IQR], 1-8 months). Type IB endolaks were found in 1 patient (7%), type IC in 8 (53%), type II in 3 (20%), and type III in 3 patients (20%). Overall median endoleak volume was 10 cc (IQR, 5.8-10.8 cc). Median endoleak volume per type of endoleak volume was as follows: type IB, 56 cc; type IC, 10.3 cc (IQR, 8.1-11.4 cc), type II, 10cc (IQR, 4.8-11.6 cc); and type III, 8.9 cc(IQR, 5.8-10.6 cc) (p>.1). All patients underwent endoleak repair.Endoleak secondary repair was required in 3 patients (20%). Those patients were found with higher endoleak volumes (10.6 cc [IQR,10.3-341.2cc]) when compared to patients that were repaired at a primary intervention (8.78 cc [IQR,5.7-10.6 cc]) (p=.07).

CONCLUSION

The frequency of endoleaks that required intervention after FEVAR using investigational devices was 7%. Type IC endoleaks were the most frequently found. Endoleaks with higher volume were found have higher risk for secondary endoleak repair.

CLINICAL RELEVANCE/APPLICATION

Endoleaks after endovascular repair of AAAs are frequent. For FFEVAR, the incidence and natural history of endoleaks are still under invetigation. This study assess the incidence of endoleaks and predictors of primary endoleak failure.

RC514-05 Endovascular Reconstruction Offers Non-Inferior Outcomes at Reduced Cost Compared to Surgical Bypass for TASC-II D Aorto-Iliac Occlusive Disease

Participants Roger T. Tomihama, MD, Loma Linda, CA (*Presenter*) Nothing to Disclose Joshua Gabel, MD, Loma Linda, CA (*Abstract Co-Author*) Nothing to Disclose Ahmed Abou-Zamzam, MD, Loma Linda, CA (*Abstract Co-Author*) Nothing to Disclose Theodore Teruya, MD, Loma Linda, CA (*Abstract Co-Author*) Nothing to Disclose Udo Oyoyo, Loma Linda, CA (*Abstract Co-Author*) Nothing to Disclose Sharon C. Kiang, MD, Loma Linda, CA (*Abstract Co-Author*) Nothing to Disclose

PURPOSE

To compare the clinical outcomes and cost of endovascular reconstruction of occlusive and near-occlusive disease of the aortic bifurcation to surgical bypass.

METHOD AND MATERIALS

Thirty-three consecutive patients with symptomatic TASC-II D Aorto-Iliac Occlusive Disease (AIOD) who underwent surgical bypass or endovascular reconstruction from 2012 to 2017 were retrospectively reviewed. Lesion characteristics, technical approach, survival, limb salvage, and patency were analyzed. Device, operating room, and length of stay costs were calculated based on rates provided by the Department of Veterans Affairs (VA) and compared between treatment groups.

RESULTS

Nineteen patients at prohibitive risk for open surgery underwent endovascular reconstruction, while thirteen underwent surgical bypass. Kissing stent technique was used in all patients for reconstruction of the aortic bifurcation. The endovascular group had decreased operative time (157 vs 245 minutes, p=0.004), blood loss (273 vs 763 milliliters, p=0.005), and peri-operative complications (5% vs 31%, p=0.045) compared to surgical bypass. At mean follow-up of 2.8 years, endovascular reconstruction compared to surgical bypass demonstrated non-inferior primary/primary-assisted patency (85% vs 85%, p=0.98), limb salvage (100% vs 92%, p=0.76), and survival (90% vs 85%, p=0.65). Endovascular device costs were \$4,223 greater then surgical bypass (p<0.001), but with operating room cost \$3,332 less then surgical bypass (p=0.001). Length of stay costs was \$13,580 less for patients undergoing endovascular reconstruction compared to surgery (p<0.001), and led to an overall reduction of \$11,706, in hospitalization costs in favor of endovascular reconstruction (p<0.001).

CONCLUSION

Patients with occlusive and near-occlusive disease of the aortic bifurcation treated with endovascular reconstruction achieve noninferior outcomes of patency, limb-salvage, and survival compared to surgical bypass at a mean 2.8 years. Decreased operative and length of stay costs associated with endovascular reconstruction produced an \$11,706 cost advantage relative to surgical bypass.

CLINICAL RELEVANCE/APPLICATION

Patients with occlusive and near-occlusive disease of the aortic bifurcation treated with endovascular reconstruction achieve noninferior clinical outcomes and average \$11,706 cost savings relative to surgical bypass.

RC514-06 Treatment of Visceral Aneurysms

Wednesday, Nov. 28 9:40AM - 10:00AM Room: S105AB

Participants

Jordan C. Tasse, MD, Chicago, IL (Presenter) Nothing to Disclose

LEARNING OBJECTIVES

1) Review the clinical presentation and diagnosis of visceral aneurysms. 2) Describe endovascular and surgical approaches to the management of visceral aneurysms. 3) Illustrate case based examples of their endovascular treatment.

RC514-07 Advanced Arterial Revascularization

Wednesday, Nov. 28 10:00AM - 10:20AM Room: S105AB

Participants Aseem Bhandari, MD, Savannah, GA (*Presenter*) Nothing to Disclose

LEARNING OBJECTIVES

View Learning Objectives under main course title.

RC514-08 Below-the-Knee Interventions

Wednesday, Nov. 28 10:30AM - 10:50AM Room: S105AB

Participants Ryan C. Schenning, MD, Portland, OR (*Presenter*) Nothing to Disclose

LEARNING OBJECTIVES

View Learning Objectives under main course title.

RC514-09 Association of Plasma Rcn2 Levels with Lower Extremity Arterial Calcification in Patients with Peripheral Arterial Disease Complicated with Type 2 Diabetes Mellitus

Wednesday, Nov. 28 10:50AM - 11:00AM Room: S105AB

Participants

Zhihui Chang, BMedSc, MMed, Shenyang, China (*Presenter*) Nothing to Disclose Zhaoyu Liu, MD, Shenyang, China (*Abstract Co-Author*) Nothing to Disclose

Jiahe Zheng, Shenyang, China (*Abstract Co-Author*) Nothing to Disclose Qiyong Guo, MD, Shenyang, China (*Abstract Co-Author*) Nothing to Disclose

PURPOSE

Vascular calcification is a prominent feature of both atherosclerosis and diabetes, and is clinically associated with outcomes of interventional treatment for peripheral arterial disease. Rcn2 is a key regulator of cytokine expression in arterial wall cells. Herein we examined the association of plasma Rcn2 levels with lower extremity arterial calcification in patients with peripheral arterial disease (PAD) complicated with type 2 diabetes mellitus(T2DM).

METHOD AND MATERIALS

This study had medical ethics committee approval, with waiver of informed consent. A total of 54 patients with T2DM and 38 nondiabetic patients were recruited. All patients have critical limb ischemia or intermittent claudication. Diagnosis of PAD was based on clinical ischemic symptoms, lower extremity arterial CT angiography showing stenosis or occlusion and ankle-brachial index (ABI). Plasma Rcn2 levels were measured using ELISA. Lower extremity artery calcification scores were measured on noncontrast computed tomography scans. Spearman's correlation testing was used to assess the relationship between Rcn2 level and calcification scores.

RESULTS

Patients with PAD complicated with T2DM had higher Rcn2 levels than non-diabetic patients. In subjects with PAD, Rcn2 level was associated with ABI. There was a significant correlation between the Rcn2 level and lower extremity artery calcification scores (R=0.69, p<0.01). Patients with critical limb ischemia had higher calcification scores than patients with intermittent claudication.

CONCLUSION

Plasma Rcn2 levels are associated with lower extremity arterial calcification in patients with peripheral arterial disease complicated with T2DM . Further research aimed at understanding the regulatory mechanism of Rcn2 in arterial calcification is warranted.

CLINICAL RELEVANCE/APPLICATION

Rcn2 is expected to be a new therapeutic target for the prevention and treatment of arterial calcification.

RC514-10 Retrograde Recanalization of the Celiac Trunk via the Pancreaticoduodenal Arcade: A Valid Alternative to an Antegrade Approach?

Wednesday, Nov. 28 11:00AM - 11:10AM Room: S105AB

Participants

Federico Pedersoli, MD, Aachen, Germany (*Presenter*) Nothing to Disclose Peter Isfort, MD, Aachen, Germany (*Abstract Co-Author*) Nothing to Disclose Markus Zimmermann, MD, Aachen, Germany (*Abstract Co-Author*) Nothing to Disclose Maximilian F. Schulze-Hagen, MD, Aachen, Germany (*Abstract Co-Author*) Nothing to Disclose Martin Liebl, MD, Aachen, Germany (*Abstract Co-Author*) Nothing to Disclose Fabian Goerg, Aachen, Germany (*Abstract Co-Author*) Nothing to Disclose Sebastian Keil, MD, Aachen, Germany (*Abstract Co-Author*) Nothing to Disclose Christiane K. Kuhl, MD, Aachen, Germany (*Abstract Co-Author*) Nothing to Disclose Philipp Bruners, MD, Aachen, Germany (*Abstract Co-Author*) Nothing to Disclose

For information about this presentation, contact:

fpedersoli@ukaachen.de

PURPOSE

Antegrade recanalization of a high-grade stenosis or short occlusion of the celiac trunk from the aorta often presents a challenge. In fact, in the absence of vascular stump ("flash-occlusions") or pronounced calcification of the aortic wall, an antegrade approach may remain unsuccessful. Therefore, we evaluated the feasibility of a retrograde access by the superior mesenteric artery, via the pancreaticoduodenal arcade and the common hepatic artery.

METHOD AND MATERIALS

A retrospective analysis of all patients, who underwent stent implantation in the celiac trunk from 01/2010 to 12/2017 was performed. Data on the indication of the intervention, the access, the material used, the stent model and the follow-up were collected from the hospital information system.

RESULTS

Successful stent implantation into the celiac trunk was performed in 34 patients. An antegrade passage of the occlusion or stenosis was not possible in 4/34 (12%) patients. In these cases, a 5F-catheter was placed in the proximal superior mesenteric artery and a 2.4 F microcatheter and micro-guidewire was used to cross the stenosis or occlusion via the pancreaticoduodenal arcade. Once the tip of the micro-wire crossed the lesion in the celiac trunk and entered into the aorta, it was caught with a snare, pulled out of the femoral introducer sheath and then used as a guide for the antegrade implantation of a balloon-expandable stent into the celiac trunk. Follow-up showed no complications related to the stent implantation; in particular, no signs of mesenteric ischemia.

CONCLUSION

Retrograde access to the celiac trunk via pancreaticoduodenal arcade is a valid alternative if antegrade access fails.

CLINICAL RELEVANCE/APPLICATION

Offering a valid option in case of difficult antegrade access to the celiac trunk.

RC514-11 Magnetic Particle Imaging (MPI)-Guided Percutaneus Transluminal Angioplasty in an Iliac Artery Phantom Model

Participants

Stefan M. Herz, MD, Wuerzburg, Germany (*Presenter*) Nothing to Disclose Patrick Vogel, Wurzburg, Germany (*Abstract Co-Author*) Nothing to Disclose Thomas Kampf, Wurzburg, Germany (*Abstract Co-Author*) Nothing to Disclose Martin A. Ruckert, Wurzburg, Germany (*Abstract Co-Author*) Nothing to Disclose Philipp Dietrich, Wurzburg, Germany (*Abstract Co-Author*) Nothing to Disclose Simon Veldhoen, MD, Wurzburg, Germany (*Abstract Co-Author*) Nothing to Disclose Aleksander Kosmala, Wurzburg, Germany (*Abstract Co-Author*) Nothing to Disclose Ralph Kickuth, MD, Bern, Switzerland (*Abstract Co-Author*) Nothing to Disclose Volker C. Behr, Wurzburg, Germany (*Abstract Co-Author*) Nothing to Disclose Thorsten A. Bley, MD, Hamburg, Germany (*Abstract Co-Author*) Nothing to Disclose

PURPOSE

The aim of this study was to assess the feasibility of real-time magnetic particle imaging (MPI)-guided percutaneous transluminal angioplasty (PTA) in-vitro and compare it to conventional X-ray guided PTA.

METHOD AND MATERIALS

MPI experiments were conducted on a custom-built MPI scanner (FOV: length 65 mm, diameter 29 mm; isotropic resolution $\sim 1-1.5$ mm; gradient strength ~ 3 T/m). Vascular stenosis phantoms (Fig. 1a) consisted of polyvinyl chloride (PVC) tubes with an inner diameter 8 mm prepared to form ~ 50 % stenoses. MPI angiography for visualization of stenoses and post-interventional results was performed using the SPIO contrast agent Ferucarbotran (10 mmol (Fe)/l). Balloon catheters and guidewires were visualized with MPI fluoroscopy using a custom-made Ferucarbotran-based lacquer marker (Fig. 1b). An online reconstruction algorithm for real-time imaging was implemented. X-ray based angiography was conducted on a floor mounted Artis zee Interventional Angiography System (Siemens Healthcare GmbH, Erlangen, Germany) using an iodine-based contrast agent (Imeron 300, dilution 1:4 with sodium chloride 0.9 % injection solution).

RESULTS

Visualization of stenosis phantoms and MPI-guided PTA procedures (4 frames/sec) were in concordance to the conventional PTA approach (Fig 1 c+d). Labeling of guidewires and balloon catheters allowed for precise tracking of endovascular instruments with MPI. The spatial resolution of MPI is still distinctly lower than the submillimeter resolution of state of the art X-ray fluoroscopes.

CONCLUSION

Real-time MPI-guided PTA in an iliac artery phantom model is feasible. Further research is necessary to improve MPI scanner hardware and SPIO design for cardiovascular interventions.

CLINICAL RELEVANCE/APPLICATION

Magnetic particle imaging is a promising new tomographic imaging method with the potential to provide radiation-free cardiovascular imaging and guided interventions.

RC514-12 Mesenteric Ischemia

Wednesday, Nov. 28 11:20AM - 11:40AM Room: S105AB

Participants Laura K. Findeiss, MD, Atlanta, GA (*Presenter*) Nothing to Disclose

LEARNING OBJECTIVES

View Learning Objectives under main course title.

RC514-13 Renovascular Occlusive Disease: Current Paradigm

Wednesday, Nov. 28 11:40AM - 12:00PM Room: S105AB

Participants

Bulent Arslan, MD, Chicago, IL (*Presenter*) Advisory Board, Medtronic plc; Advisory Board, Guerbet SA; Speakers Bureau, Biocompatibles International plc; Speakers Bureau, C. R. Bard, Inc; Advisory Board and Speakers Bureau, Boston Scientific Corporation; Speakers Bureau, Penumbra, Inc

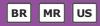
LEARNING OBJECTIVES

View Learning Objectives under main course title.



BI-RADS Interactive Challenge (Interactive Game)

Wednesday, Nov. 28 8:30AM - 10:00AM Room: N227B



AMA PRA Category 1 Credits ™: 1.50 ARRT Category A+ Credit: 1.75

Participants

Jay R. Parikh, MD, Houston, TX (Moderator) Nothing to Disclose

GENERAL INFORMATION

This interactive session will use RSNA Diagnosis Live[™]. Please bring your charged mobile wireless device (phone, tablet or laptop) to participate.

Sub-Events

RC515A Mammography

Participants Cindy S. Lee, MD, Garden City, NY (*Presenter*) Nothing to Disclose

For information about this presentation, contact:

Cindy.Lee3@nyumc.org

LEARNING OBJECTIVES

1) To define BIRADS terms used to describe mammography findings and recognize common appearances of malignant and benign disease.

ABSTRACT

This case-based session will review a variety of imaging findings at mammography, appropriate use of BI-RADS descriptors and categories, as well as highlight potential pitfalls and strategies to avoid them.

Active Handout:Cindy S. Lee

http://abstract.rsna.org/uploads/2018/18000473/RSNA 2018 DBT Handout RC515A.pdf

RC515B Case-based Session on Ultrasound

Participants Ana P. Lourenco, MD, Providence, RI (*Presenter*) Nothing to Disclose

For information about this presentation, contact:

alourenco@lifespan.org

LEARNING OBJECTIVES

1) Apply appropriate BI-RADS descriptors and categories to a variety of benign and malignant lesions on ultrasound. 2) Describe how certain imaging features may predict pathology.

ABSTRACT

This case-based session will review a variety imaging findings at US, appropriate use of BI-RADS descriptors and categories, as well as highlight potential pitfalls and strategies to avoid them.

Active Handout: Ana P. Lourenco

http://abstract.rsna.org/uploads/2018/18000474/Lourenco.RSNA.US RC515B.pdf

RC515C Case-based Session on MRI

Participants

Elizabeth S. McDonald, MD, Philadelphia, PA (Presenter) Nothing to Disclose

LEARNING OBJECTIVES

1) Define BIRADS terms used to describe MRI findings and recognize common appearances of malignant and benign disease.

RC515D Audit and Outcomes Monitoring

Participants Jay R. Parikh, MD, Houston, TX (*Presenter*) Nothing to Disclose

LEARNING OBJECTIVES

1) Describe the basic clinically relevant mammography medical outcomes audit based on BIRADS. 2) Strategies to monitor outcomes and provide radiologist feedback.

ABSTRACT

Bi-RADS enables annual the basic clnically relevant medical outcomes audit, which can be used to monitor outcomes and provide radioloigsts feedback.



Parental/FMLA Leave in Residency: A Panel Discussion (In Conjunction with the American Association for Women Radiologists)

Wednesday, Nov. 28 8:30AM - 10:00AM Room: E353A



AMA PRA Category 1 Credits ™: 1.50 ARRT Category A+ Credit: 0

Participants

Cheri L. Canon, MD, Birmingham, AL (*Presenter*) Royalties, The McGraw-Hill Companies Lori A. Deitte, MD, Nashville, TN (*Presenter*) Nothing to Disclose Allison M. Grayev, MD, Madison, WI (*Presenter*) Nothing to Disclose

For information about this presentation, contact:

ccanon@uabmc.edu

LEARNING OBJECTIVES

1) Compare parental leave policies.



Emerging Technology: PET/MRI Update 2018

Wednesday, Nov. 28 8:30AM - 10:00AM Room: S505AB



AMA PRA Category 1 Credits ™: 1.50 ARRT Category A+ Credit: 1.75

FDA Discussions may include off-label uses.

Participants

Rathan M. Subramaniam, MD, PhD, Dallas, TX (*Moderator*) Consultant, Blue Earth Diagnostics Ltd; Speaker, Blue Earth Diagnostics Ltd

For information about this presentation, contact:

rathan.subramaniam@utsouthwestern.edu

LEARNING OBJECTIVES

1) To discuss opportunities of PET/MRI in clinical practice and research. 2) To discuss challenges of PET/MRI in clinical practice and research.

Sub-Events

RC517A PET/MRI: Update 2018

Participants

Rathan M. Subramaniam, MD,PhD, Dallas, TX (*Presenter*) Consultant, Blue Earth Diagnostics Ltd; Speaker, Blue Earth Diagnostics Ltd

For information about this presentation, contact:

rathan.subramaniam @utsouthwestern.edu

LEARNING OBJECTIVES

1) To discuss the status of PET/MRI in clinical practice in 2018 and the opportunities and challenges in implementation.

RC517B PET/MRI Update 2018: Clinical Practice Implementation - Pearls

Participants

Geoffrey B. Johnson, MD, PhD, Rochester, MN (Presenter) Research Grant, General Electric Company; Research Grant, Pfizer Inc

Honored Educators

Presenters or authors on this event have been recognized as RSNA Honored Educators for participating in multiple qualifying educational activities. Honored Educators are invested in furthering the profession of radiology by delivering high-quality educational content in their field of study. Learn how you can become an honored educator by visiting the website at: https://www.rsna.org/Honored-Educator-Award/ Geoffrey B. Johnson, MD,PhD - 2015 Honored EducatorGeoffrey B. Johnson, MD,PhD - 2017 Honored Educator

RC517C PET/MRI Update 2018: Clinical Applications - Brain and Head and Neck

Participants

Alexander Drzezga, MD, Cologne, Germany (*Presenter*) Consultant, Siemens AG; Consultant, Bayer AG; Consultant, General Electric Company; Consultant, Eli Lilly and Company; Consultant, The Piramal Group; Speakers Bureau, Siemens AG; Speakers Bureau, Bayer AG; Speakers Bureau, General Electric Company; Speakers Bureau, Eli Lilly and Company; Speakers Bureau, The Piramal Group

LEARNING OBJECTIVES

1) Review relevant clinical applications for PET/MR in the diagnostic work-up of disorders of the brain. 2) Review strengths of PET/MR for disorders of the head and neck. 3) Understand the value of different currently available tracers for neuroimaging and oncological applications. 4) Review challenges and limitations of PET/MR in brain/head&neck and expected future developments.

RC517D PET/MRI Update 2018: Clinical Applications - Body

Participants

Thomas A. Hope, MD, San Francisco, CA (Presenter) Research support, General Electric Company

For information about this presentation, contact:

thomas.hope@ucsf.edu

LEARNING OBJECTIVES

1) Review common current applications for abdominopelvic oncoloaic PET/MRI. including hepatic malignancies. rectal cancer. and

cervical cancer. 2) Understand the role of novel tracers in prostate cancer (PSMA PET) and neuroendocrine tumors (somatostatin receptor PET). The presentation will focus on prostate cancer as an application. 3) Present the current limitations and future advances in PET/MRI that will help increase the clinical acceptance and applicability of body PET/MRI.

RC517E PET/MRI Update 2018: Clinical Applications - Cardiac

Participants

Pamela K. Woodard, MD, Saint Louis, MO (*Presenter*) Research agreement, Siemens AG; Research, Eli Lilly and Company; Research, F. Hoffmann-La Roche Ltd; ; ; ; ; ;

For information about this presentation, contact:

woodardp@wustl.edu

LEARNING OBJECTIVES

Discuss clinical cardiac PET/MR imaging applications; applications will include myocardial perfusion and viability, nonischemic cardiomyopathy, and tumor assessment.

RC517F PET/MRI Update 2018: Physics

Participants

Georges El Fakhri, PhD, Boston, MA (Presenter) Nothing to Disclose

LEARNING OBJECTIVES

1) Understand the challenges and opportunities afforded by simultaneous PET/MR. 2) Understand the role of PET/MR in imaging myocardial membrane potential.



Metabolic Tumor Imaging: Current and Beyond

Wednesday, Nov. 28 8:30AM - 10:00AM Room: N229



FDA Discussions may include off-label uses.

Participants

Evis Sala, MD, PhD, Cambridge, United Kingdom (Moderator) Nothing to Disclose

LEARNING OBJECTIVES

Learn about he new PET tracers and they new potential clinical applications.
 Review the added value of PET/MRI in oncology.
 Learn about the current and future applications of hyperpolarised MRI.

Sub-Events

RC518A PET Tracers: Which Ones Will Be Next to Make it to Clinical Practice?

Participants

Jason S. Lewis, PhD, New York, NY (*Presenter*) Shareholder, pHLIP, Inc; Research support, MabVax Therapeutics, Inc; Research support, Eli Lilly and Company; Research support, Sapience Therapeutics; Research support, Telix Pharmaceuticals

LEARNING OBJECTIVES

1) To have an appreciation for some of the latest PET tracers in clinical research in oncology. 2) Understand the PET and radiotherapy agents currently FDA approved and those undergoing the approval process. 3) Understand the next generation of PET tracers and molecular imaging agents that could be the next standard-of-care imaging probes.

RC518B PET/MRI: The Added Value in Oncology

Participants

Hebert Alberto Vargas, MD, Cambridge, United Kingdom (Presenter) Nothing to Disclose

LEARNING OBJECTIVES

1) To understand the concept of value in imaging and how it relates to PET/MR technology. 2) To discuss the need for research specifically geared toward assessing the value of PET/MRI in oncology.

RC518C Hyperpolarized MRI: Current and Future Applications

Participants

Ferdia A. Gallagher, PhD, FRCR, Cambridge, United Kingdom (*Presenter*) Research support, General Electric Company; Research support, GlaxoSmithKline plc

For information about this presentation, contact:

fag1000@cam.ac.uk

LEARNING OBJECTIVES

1) To explore the role of metabolism in cancer development. 2) To understand how these changes in metabolism can be exploited using hyperpolarised 13C-pyruvate. 3) To review the current evidence for hyperpolarised carbon-13 imaging in oncology. 4) To understand potential clinical applications for hyperpolarised carbon-13 imaging. 5) To consider the role of new hyperpolarised molecules in oncology.

ABSTRACT

There is increasing evidence to support a role for metabolism in tumor development; for example, deregulation of cellular energetics is now considered to be one of the key hallmarks of cancer. Changes in tumor metabolism over time are now known to be early biomarkers of successful response to chemotherapy and radiotherapy. There are a number of imaging methods that have been used to probe cancer metabolism: the most widely available is 18F-fluorodeoxyglucose (FDG), an analogue of glucose, used in PET. Hyperpolarized carbon-13 MRI (13C-MRI) is an emerging molecular imaging technique for studying cellular metabolism, particularly in the field of oncology. This method allows non-invasive measurements of tissue metabolism in real-time. To date, the most promising probe used in conjunction with hyperpolarized MRI has been 13C-labelled pyruvate: pyruvate is metabolized into lactate in normal tissue in the absence of oxygen, but in tumors this occurs very rapidly even in the presence of oxygen. Results from many animal models have shown that there is a reduction in the metabolism of pyruvate following successful treatment with chemotherapy. Tumor lactate labelling has also been shown to correlate with the grade of some tumor types. There are now a small number of sites performing human hyperpolarized carbon-13 MRI imaging. This talk will discuss the progress that has been made in this field within the area of oncology and potential clinical applications.



Fundamentals of Imaging for the Radiation Oncologist

Wednesday, Nov. 28 8:30AM - 10:00AM Room: S104A



AMA PRA Category 1 Credits ™: 1.50 ARRT Category A+ Credit: 1.75

Participants

Stanley L. Liauw, MD, Chicago, IL (Moderator) Nothing to Disclose

For information about this presentation, contact:

sliauw@uchicago.edu

Sub-Events

RC520A Fundamentals of Imaging of Liver Cancer in Radiation Oncology

Participants

Michael I. Lock, MD, FRCPC, London, ON (Presenter) Speaker, sanofi-aventis Group

LEARNING OBJECTIVES

1) Provide a step-by-step method to distinguish recurrence from normal radiation changes. 2) Appraise new research to better select MRI sequences to localize tumors. 3) Provide an image review of common errors in imaging post radiation.

ABSTRACT

Imaging changes after treatment with radiation can be difficult and misleading. Recent evidence provides insight into better timing of imaging, appropriate MRI sequences (these sequences often differ from sequences used by radiologists) and imaging features that are associated with a higher risk of recurrence.

RC520B Fundamentals of Imaging of Lung Cancer in Radiation Oncology

Participants

Candice A. Johnstone, MD, Milwaukee, WI (Presenter) Nothing to Disclose

For information about this presentation, contact:

cjohnstone@mcw.edu

LEARNING OBJECTIVES

1) Define the most appropriate uses for the use of PET-CT in lung cancer. 2) Identify situations when imaging is sufficient for mediastinal staging. 3) Describe new imaging techniques and their application to lung cancer treatment.

RC520C Fundamentals of Imaging of Gynecologic Cancer in Radiation Oncology

Participants

Eric Leung, MD, FRCPC, Toronto, ON (Presenter) Nothing to Disclose

LEARNING OBJECTIVES

1) To review imaging modalities for staging, planning and response of gynaecological cancer treatments with radiation therapy. 2) To review imaging techniques in three-dimensional based brachytherapy for locally advanced gynaecological cancers. 3) To review imaging techniques for stereotactic radiation therapy of gynaecological cancers. 4) To review functional imaging techniques for gynaecological cancers and radiation treatment.

RC520D Fundamentals of Imaging of CNS Tumors in Radiation Oncology

Participants

Hui-Kuo G. Shu, MD, PhD, Atlanta, GA (*Presenter*) Speakers Bureau, Varian Medical Systems, Inc; Stockholder, Medtronic plc; Stockholder, Apple Inc; Stockholder, ICON plc; Stockholder, Raytheon

For information about this presentation, contact:

hgshu@emory.edu

LEARNING OBJECTIVES

 List the imaging modalities most often used by the radiation oncologist in the management of CNS tumors. 2) Explain how specific CNS imaging techniques are utilized to assess the extent of disease prior to initiation of radiation therapy (upfront staging).
 Describe various imaging evaluations of CNS tumors after radiation therapy for longitudinal response assessment with attention to interpretation of specific results.

ABSTRACT

Radiation therapy (RT) is critical for the overall management of many central nervous system (CNS) tumors. Advances in radiation treatment planning, with techniques such as intensity modulated radiation therapy, volumetric modulated arc therapy, and stereotactic radiosurgery, now allow the delivery of highly conformal doses with very high precision. These techniques rely on high-resolution 3-dimensional anatomic imaging modalities such as computed tomography (CT) and magnetic resonance imaging (MRI) scans to accurately and reliably define CNS targets and avoidance structures. The integration of cross sectional imaging into CNS radiation oncology has directly translated into improvements in the therapeutic window of RT, and the union between radiation oncology and imaging is only expected to grow stronger. In addition to standard imaging such as CT and MRI scans, advanced imaging techniques including diffusion/perfusion/spectroscopic MRIs and positron emission tomography (PET) scans with novel tracers are being used to provide additional insight into CNS tumor biology and behavior beyond anatomy. Together, standard and advanced imaging modalities hold significant potential to improve future RT delivery and response assessment. In this talk, we will discuss the current utilization of standard/advanced imaging for CNS malignancies from a radiation oncology perspective as well as discuss the implications of novel MRI and PET modalities currently under investigation.



Advances in CT: Technologies, Applications, Operations-Functional CT

Wednesday, Nov. 28 8:30AM - 10:00AM Room: E351



AMA PRA Category 1 Credits ™: 1.50 ARRT Category A+ Credit: 1.75

Participants

Ehsan Samei, PhD, Durham, NC (*Coordinator*) Research Grant, General Electric Company; Research Grant, Siemens AG; Advisory Board, medInt Holdings, LLC; License agreement, 12 Sigma Technologies; License agreement, Gammex, Inc Lifeng Yu, PhD, Chicago, IL (*Coordinator*) Nothing to Disclose

LEARNING OBJECTIVES

1) Comprehend the principles of CT Perfusion imaging in stroke and cancer applications. 2) Apply the principles to discern errors that my occur in perfusion calculation. 3) Design scanning protocols for CT Perfusion imaging of stroke and cancer. 4) Apply dose saving techniques to reduce radiation dose. 5) Discuss the application of CT Perfusion imaging in stroke and cancer with examples. 6) Comprehend the theoretical basis and pitfalls of each myocardial CTP method (qualitative, semi-quantitative and quantitative). 7) Assess the sources and solutions of various image artifacts in myocardial CTP. 8) Evaluate the effectiveness of radiation dose reduction methods for low dose quantitative myocardial CTP. 9) Develop the optimal myocardial CTP protocol for assessing high-risk coronary artery disease. 10) Assess the recent advances in quantitative CTP for imaging myocardial edema and scar and their potential applications to guide therapy in post infarction settings.

ABSTRACT

CT has become a leading medical imaging modality, thanks to its superb spatial and temporal resolution to depict anatomical details. New advances have enabled extending the technology to depict physiological information. This has enabled a wide and expanding range of clinical applications. These advances are highlighted in this multi-session course. The course offers a comprehensive and topical depiction of these advances with material covering CT system innovations, CT operation, CT performance characterization, functional and quantitative applications, and CT systems devised for specific anatomical applications. The sessions include advances in CT system hardware and software, CT performance optimization, CT practice management and monitoring, spectral CT techniques, quantitative CT techniques, functional CT methods, and special CT use in breast, musculoskeletal, and interventional applications.

Sub-Events

RC521A Contrast Administration for Cardiovascular Imaging and Beyond

Participants

Dominik Fleischmann, MD, Stanford, CA (Presenter) Research Grant, Siemens AG

RC521B Perfusion Techniques and Applications-Stroke and Cancer

Participants

Ting-Yim Lee, MSc, PhD, London, ON (Presenter) License agreement, General Electric Company

LEARNING OBJECTIVES

1) Comprehend the principles of CT Perfusion imaging in stroke and cancer applications. 2) Apply the principles to discern errors that my occur in perfusion calculation. 3) Design scanning protocols for CT Perfusion imaging of stroke and cancer. 4) Apply dose saving techniques to reduce radiation dose. 5) Discuss the application of CT Perfusion imaging in stroke and cancer with examples.

RC521C Perfusion Techniques and Applications-Cardiac

Participants Aaron So, PhD, London, ON (*Presenter*) Nothing to Disclose

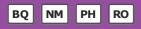
LEARNING OBJECTIVES

1) Comprehend the theoretical basis and pitfalls of each myocardial CTP method (qualitative, semi-quantitative and quantitative). 2) Assess the sources and solutions of various image artifacts in myocardial CTP. 3) Evaluate the effectiveness of radiation dose reduction methods for low dose quantitative myocardial CTP. 4) Develop the optimal myocardial CTP protocol for assessing high-risk coronary artery disease. 5) Assess the recent advances in quantitative CTP for imaging myocardial edema and scar and their potential applications to guide therapy in post infarction settings.



Advanced PET Imaging for Radiotherapy Planning and Response Assessment

Wednesday, Nov. 28 8:30AM - 10:00AM Room: N226



AMA PRA Category 1 Credits ™: 1.50 ARRT Category A+ Credit: 1.75

Participants

Paul E. Kinahan, PhD, Seattle, WA (Moderator) Research Grant, General Electric Company; Co-founder, PET/X LLC

Sub-Events

RC522A State of the Art in PET Imaging

Participants

Paul E. Kinahan, PhD, Seattle, WA (Presenter) Research Grant, General Electric Company; Co-founder, PET/X LLC

LEARNING OBJECTIVES

1) Understand the connections between the capabilities of PET imaging and clinical and research uses. 2) Become familiar with recent technical advances in PET imaging and tradeoffs. 3) Gain awareness of initiative in quantitative imaging for clinical trials.

RC522B Technical Challenges in the Integration of PET Imaging into Radiotherapy Treatment Planning

Participants

Stephen R. Bowen, PhD, Seattle, WA (Presenter) Nothing to Disclose

For information about this presentation, contact:

srbowen@uw.edu

LEARNING OBJECTIVES

1) Understand the differences between diagnostic and treatment planning PET/CT imaging technical requirements. 2) Become familiar with the source and propagation of technical errors in PET/CT-guided radiation therapy. 3) Gain awareness of technical design elements in PET/CT-guided radiation therapy clinical trials.



Optimization and Technology in Interventional Radiology

Wednesday, Nov. 28 8:30AM - 10:00AM Room: S403B



AMA PRA Category 1 Credits ™: 1.50 ARRT Category A+ Credit: 1.75

FDA Discussions may include off-label uses.

Participants

William F. Sensakovic, PhD, Scottsdale, AZ (*Coordinator*) Speaker, Bayer AG; Research Grant, Mazor Robotics Ltd; Founder, Telerad Physics Teaching, LLC

Thaddeus A. Wilson, PhD, Madison, WI (Coordinator) Nothing to Disclose

For information about this presentation, contact:

wfsensak@gmail.com

LEARNING OBJECTIVES

1) Apply techniques to optimize dose in the interventional setting. 2) Identify opportunities where ionizing radiation can be replaced by ultrasound to guide interventional procedures. 3) Understand new CT interventional techniques that will open new fields of CT intervention for percutaneous and intravascular interventions. 4) Describe a 500X dose reduced CT fluoroscopy mode. 5) Describe a method for quantitative high frame rate CTA that provides vascular velocity and flow information to help plan and evaluate CT vascular interventions.

Sub-Events

RC523A Dose Optimization in the Interventional Suite

Participants

Robert G. Dixon, MD, Chapel Hill, NC (Presenter) Nothing to Disclose

For information about this presentation, contact:

bob_dixon@med.unc.edu

LEARNING OBJECTIVES

1. Review the importance of dose optimization in the angiography suite. 2. Discuss basic concepts that will help to build a culture of safety at your institution. 3. Identify simple, practical steps that operators can take to protect patients, staff and themselves in the IR suite.

RC523B Using Ultrasound in Place of CT and Fluoroscopy in the Interventional Suite

Participants

Patrick Warren, MD, Columbus, OH (Presenter) Nothing to Disclose

LEARNING OBJECTIVES

1) Discuss skills, techniques, and pitfalls of invasive sonography. 2) Discuss basic skills involved in utilizing ultrasound guidance in lieu of CT fluoroscopy or conventional fluoroscopy during minimally invasive percutaneous procedures in order to minimize radiation exposure to patients and healthcare providers. 3) Incorporate these component skill sets into further life-long learning for expansion of competency and implementation into clinical interventional practice.

RC523C Advances in Interventional Use of CT

Participants

Charles A. Mistretta, PhD, Madison, WI (*Presenter*) Founder, Mistretta Medical Intellectual Property Licensing Activities; Research, Siemens AG; Co-Founder, LiteRay Medical LLC

For information about this presentation, contact:

camistre@wisc.edu

LEARNING OBJECTIVES

1) To familiarize attendees with new CT interventional techniques that will open new fields of CT intervention for percutaneous and intravascular interventions. 2) To describe a 500X dose reduced CT fluoroscopy mode. 3) To describe a method for quantitative high frame rate CTA that provides vascular velocity and flow information to help plan and evaluate CT vascular interventions.

ABSTRACT

We will summarize recent developments in C-Arm 4D DSA that have now been extended to conventional CT. These include a 500X dose reduced CT fluoroscopy mode and 4D CT DSA that provides quantitative velocity and flow information from 30 CTA volumes

per second. These modes in combination, promise to provide new opportunities for ultra low dose artifact-free percutaneous needle placement and CT vascular intervention including real time intra-luminal views.



How to Turn Your Abstract into an Award-winning Publication: Tips from the Editors of the RSNA Journals

Wednesday, Nov. 28 8:30AM - 10:00AM Room: S402AB



AMA PRA Category 1 Credits ™: 1.50 ARRT Category A+ Credit: 1.75

Sub-Events

RC524A How to Publish a Great Paper in RADIOLOGY

Participants

David A. Bluemke, MD, PhD, Bethesda, MD (Presenter) Nothing to Disclose

For information about this presentation, contact:

dbluemke@rsna.org

LEARNING OBJECTIVES

1) Describe the elements of a scientific manuscript that are necessary to achieve publication. 2) Identify methods for creating effective scientific manuscripts that increase the likelihood of acceptance by peer reviewed journals. 3) Describe methods to improve the writing of scientific abstracts and manuscripts, in order to clearly and effectively communication your results and new information in the field.

ABSTRACT

The peer-review process for scientific publications is the international standard for scientific advancement in your career. Although you may have the most innovative or novel scientific breakthrough, it remains necessary to publish your ideas in order to advance the field. Much effort is placed on obtaining funding and generating the data to prove your idea. But there is often less attention paid to methods of publishing your scientific breakthrough. Effort and initiative is needed to translate your ideas into a manuscript that can be read and interpreted by your peers. In this seminar, the editors of RSNA journals will describe the publication process, from the starting point of submission, to peer review to editorial board review and eventual publication. Techniques that help authors write effective manuscripts and communicate their ideas will be illustrated. The critical elements of a scientific manuscript, including the title, abstract and main body of the paper will be discussed. The overall goal of this seminar is to help your manuscript be eligible for acceptance at the leading manuscripts in the field of imaging.

RC524B Creating Manuscripts for Radiology and RadioGraphics

Participants Jeffrey S. Klein, MD, Burlington, VT (*Presenter*) Nothing to Disclose

For information about this presentation, contact:

jklein@rsna.org

LEARNING OBJECTIVES

1) Explain the processes that RadioGraphics uses to identify content for potential publication. 2) List the required elements of a manuscript submitted to RadioGraphics. 3) Describe the journal's peer-review and decision processes. 4) Show how an accepted manuscript is produced for publication.

ABSTRACT

RadioGraphics is unique in that the majority of content published in the journal is solicited from education exhibits displayed at the RSNA annual meeting. The editor of RadioGraphics will review the process that the journal uses to identify appropriate content in the various radiology subspecialties, safety and quality, and informatics, as well as medical physics and radiation oncology, including the consideration of unsolicited materials. The proper components of a RadioGraphics submission, including online-only interactive education content, will be detailed. The peer review process, acceptance/revision/rejection decision process will be described and the production of accepted materials reviewed.



Mini-course: Image Interpretation Science - Perception in the Clinic

Wednesday, Nov. 28 8:30AM - 10:00AM Room: S103AB

PH

AMA PRA Category 1 Credits ™: 1.50 ARRT Category A+ Credit: 1.75

Participants

Elizabeth A. Krupinski, PhD, Atlanta, GA (*Coordinator*) Nothing to Disclose Ehsan Samei, PhD, Durham, NC (*Coordinator*) Research Grant, General Electric Company; Research Grant, Siemens AG; Advisory Board, medInt Holdings, LLC; License agreement, 12 Sigma Technologies; License agreement, Gammex, Inc

For information about this presentation, contact:

ekrupin@emory.edu

LEARNING OBJECTIVES

1) Describe how fatigue impacts diagnostic accuracy. 2) Describe how fatigue impacts the efficiency with which cases are interpreted. 3) Provide ways to avoid & ameliorate fatigue. 4) Provide an overview of the role of volumetric imaging in radiology. 5) Describe the perceptual challenges in interpreting volumetric data. 6) Review evidence on differences in visual search between 2D & 3D image sets. 7) Define image quality and its most common metrics. 8) Present the impact of image resolution on diagnostics performance. 9) Present the impact of image noise and dose on diagnostic performance.

ABSTRACT

Medical images constitute a core portion of the information physicians utilize to render diagnostic and treatment decisions. At a fundamental level, the diagnostic process involves two aspects - visually inspecting the image (perception) and rendering an interpretation (cognition). Key indications of expert interpretation of medical images are consistent, accurate and efficient diagnostic performance, but how do we know when someone has attained the level of training required to be considered an expert? How do we know the best way to present images to the clinician in order to optimize accuracy and efficiency? The advent of digital imaging in many clinical specialties, including radiology, pathology and dermatology, has dramatically changed the way that clinicians view images, how residents are trained, and thus potentially the way they interpret image information, emphasizing our need to understand how clinicians interact with the information in an image during the interpretation process. With improved understanding we can develop ways to further improve decision-making and thus improve patient care.

Sub-Events

RC525A Impact of Fatigue on Radiologists' Performance

Participants Elizabeth A. Krupinski, PhD, Atlanta, GA (*Presenter*) Nothing to Disclose

For information about this presentation, contact:

ekrupin@emory.edu

LEARNING OBJECTIVES

1) Describe how fatigue impacts diagnostic accuracy. 2) Describe how fatigue impacts the efficiency with which cases are interpreted. 3) Provide ways to avoid & ameliorate fatigue.

ABSTRACT

Medical images constitute a core portion of the information physicians utilize to render diagnostic and treatment decisions. At a fundamental level, the diagnostic process involves two aspects - visually inspecting the image (perception) and rendering an interpretation (cognition). Key indications of expert interpretation of medical images are consistent, accurate and efficient diagnostic performance, but how do we know when someone has attained the level of training required to be considered an expert? How do we know the best way to present images to the clinician in order to optimize accuracy and efficiency? The advent of digital imaging in many clinical specialties, including radiology, pathology and dermatology, has dramatically changed the way that clinicians view images, how residents are trained, and thus potentially the way they interpret image information, emphasizing our need to understand how clinicians interact with the information in an image during the interpretation process. With improved understanding we can develop ways to further improve decision-making and thus improve patient care.

Honored Educators

Presenters or authors on this event have been recognized as RSNA Honored Educators for participating in multiple qualifying educational activities. Honored Educators are invested in furthering the profession of radiology by delivering high-quality educational content in their field of study. Learn how you can become an honored educator by visiting the website at: https://www.rsna.org/Honored-Educator-Award/ Elizabeth A. Krupinski, PhD - 2017 Honored Educator

RC525B Perception of Volumetric Image Data

Geoffrey D. Rubin, MD, Durham, NC (*Presenter*) Consultant, Fovia, Inc; Consultant, HeartFlow, Inc; Consultant, General Electric Company;

LEARNING OBJECTIVES

1) Understand how volumetric images acquired from CT, MRI or PET differ from more commonly studies 2-D projections such as radiographs and mammograms. 2) Discuss recent investigations focused upon unraveling the unique aspects of volumetric image perception and how they might impact diagnostic performance.

RC525C Role of Image Quality in Visual and Computational Perception

Participants

Justin B. Solomon, PhD, Durham, NC (*Presenter*) License agreement, Sun Nuclear Corporation; License agreement, 12 Sigma Technologies

Ehsan Samei, PhD, Durham, NC (*Presenter*) Research Grant, General Electric Company; Research Grant, Siemens AG; Advisory Board, medInt Holdings, LLC; License agreement, 12 Sigma Technologies; License agreement, Gammex, Inc

For information about this presentation, contact:

justin.solomon@duke.edu

LEARNING OBJECTIVES

1) Define image quality and its most common metrics. 2) Present the impact of image resolution on diagnostics performance. 3) Present the impact of image noise and dose on diagnostic performance.

ABSTRACT

This talk will define basic image quality concepts such as resolution, contrast, and noise, and describe how such concepts are measured and quantified in medical images. Further, the impact of resolution, contrast, and noise on human interpretation of medical images will be discussed. Examples will be mostly focused on CT but the concepts are applicable to any modality. A special focus will be given to the relationship between the detectability of low-contrast image features and radiation dose in CT.



Comparative Effectiveness Research: Translating Science into Health Policy and Practice

Wednesday, Nov. 28 8:30AM - 10:00AM Room: E261



AMA PRA Category 1 Credits ™: 1.50 ARRT Category A+ Credit: 1.75

Participants

Jason N. Itri, MD, PhD, Winston-Salem, NC (Moderator) Nothing to Disclose

LEARNING OBJECTIVES

1) Detail the process for identifying high-priority areas for CER. 2) Discuss the scientific methods used in CER. 3) Describe how CER influences health policy in the era of value-based health care.

ABSTRACT

Despite various diagnostic and treatment options available to patients, practical information to help patients and providers choose the most effective options for a particular population is often not available or accessible, which contributes to regional variations in clinical practice and negatively impacts patient outcomes. Comparative effectiveness research (CER) is one of the key approaches to address this gap, designed to generate and synthesize evidence that compares the benefits and harms of alternative methods to prevent, diagnose, treat, and monitor a clinical condition, or to improve delivery of care. CER is playing an increasingly critical role in guiding health care policy and practice in order to achieve the aims of improving the health of populations, reducing the cost of healthcare, and improving the patient experience. This course will introduce participants to the key principles of CER using examples such as screening chest CT for lung cancer, lumbar spine MRI for low back pain, and imaging for breast cancer screening.

Sub-Events

RC527A NLST and Chest CT for Lung Cancer

Participants

Mitchell D. Schnall, MD, PhD, Philadelphia, PA (Presenter) Nothing to Disclose

LEARNING OBJECTIVES

1) Understand the conduct and results of the National Lung Cancer Screening trials. 2) Learn how a comparative effectiveness clinical trial results can impact healthcare policy. 3) Learn the limitation of a clinical trial to predict clinical impact.

Honored Educators

Presenters or authors on this event have been recognized as RSNA Honored Educators for participating in multiple qualifying educational activities. Honored Educators are invested in furthering the profession of radiology by delivering high-quality educational content in their field of study. Learn how you can become an honored educator by visiting the website at: https://www.rsna.org/Honored-Educator-Award/ Mitchell D. Schnall, MD, PhD - 2013 Honored Educator

RC527B Imaging for Breast Cancer Screening

Participants

Constance D. Lehman, MD, PhD, Boston, MA (*Presenter*) Research Grant, General Electric Company; Medical Advisory Board, General Electric Company

LEARNING OBJECTIVES

1) Summarize the evidence of performance of breast cancer screening imaging tests including potential benefits and harms. 2) Review the cost effective research findings for breast cancer screening imaging tests. 3) Discuss future of breast cancer screening in era of value-based health care policy.

RC527C MRI for Low Back Pain

Participants

Jeffrey G. Jarvik, MD, Seattle, WA (*Presenter*) Consultant, Wolters Kluwer nv; Co-editor, Springer Nature; Royalties, Springer Nature

For information about this presentation, contact:

jarvikj@uw.edu

LEARNING OBJECTIVES

1) Review the evidence that has led to much of imaging for low back pain being considered 'low value care'. 2) Discuss an evidence-based approach to reporting lumbar MRI findings. 3) Discuss the evidence for including epidemiological data in lumbar MRI reports.

ABSTRACT

Low back pain an Institute of Modicine priority condition for comparative offectiveness recearch is of major public health

Low back pain, an institute or medicine priority condition for comparative effectiveness research, is or major public health importance. Imaging is frequently performed as part of the diagnostic evaluation and is an important contributor to the cost of back pain care. Even without back pain, magnetic resonance (MR) imaging of the lumbar spine frequently reveals findings such as disc desiccation or bulging. Patients and their providers may attribute greater importance to these findings, which are often age-related, than they should, because they do not have an appropriate frame of reference in which to interpret the findings. These 'incidental' findings may initiate a cascade of events leading possibly even to surgery, without improving patient outcomes. Understanding evidence-based recommendations regarding when to obtain imaging can help to reduce inappropriate examinations that could lead to unnecessary additional procedures. Standardized nomenclature as well as inserting epidemiological benchmarks into imaging reports may also improve the process of care, reduce subsequent tests and treatments and possibly even improve patient outcomes. Inserting epidemiological benchmarks in lumbar spine imaging reports has been preliminarily shown to reduce subsequent diagnostic and therapeutic interventions, including MR and CT, opioid prescriptions, spinal injections and surgery. The rationale is that the epidemiologic data may provide a context for both physicians and patients to better interpret imaging findings. The longterm public health significance is high. Through simple, inexpensive interventions, radiologists may be able to substantially reduce unnecessary and expensive care for back pain.

Honored Educators

Presenters or authors on this event have been recognized as RSNA Honored Educators for participating in multiple qualifying educational activities. Honored Educators are invested in furthering the profession of radiology by delivering high-quality educational content in their field of study. Learn how you can become an honored educator by visiting the website at: https://www.rsna.org/Honored-Educator-Award/ Jeffrey G. Jarvik, MD - 2017 Honored EducatorJeffrey G. Jarvik, MD - 2018 Honored Educator



The Abbreviated Liver MRI Imaging Protocol

Wednesday, Nov. 28 8:30AM - 10:00AM Room: S102CD



AMA PRA Category 1 Credits ™: 1.50 ARRT Category A+ Credit: 1.75

FDA Discussions may include off-label uses.

Participants

Hero K. Hussain, MD, Ann Arbor, MI (Moderator) Nothing to Disclose

Sub-Events

RC529A Developing Cost-Effective Abbreviated Liver MRI Protocols

Participants

Pari Pandharipande, MD, MPH, Boston, MA (Presenter) Research Grant, Medical Imaging & Technology Alliance

LEARNING OBJECTIVES

1) Define cost-effectiveness analysis in the context of different imaging protocols. 2) Describe a path by which abbreviated MRI protocols could improve population health outcomes.

RC529B The Abbreviated Standard Liver Protocol

Participants

Scott B. Reeder, MD, PhD, Madison, WI (*Presenter*) Institutional research support, General Electric Company; Institutional research support, Bracco Group; Founder, Calimetrix, LLC; Shareholder, Elucent Medical; Consultant, ArTara

LEARNING OBJECTIVES

Understand emerging strategies for limited liver MRI protocols.
 Describe at least three examples of limited liver MRI protocols.
 Be familiar with the challenges with implementing limited MRI protocols.

RC529C The Abbreviated Liver Protocol for the Detection of Metastasis

Participants

Angela M. Riddell, MBBS, London, United Kingdom (Presenter) Nothing to Disclose

For information about this presentation, contact:

Angela.Riddell@rmh.nhs.uk

LEARNING OBJECTIVES

1) Explain the essential sequences required within an abbreviated protocol for the detection of liver metastases. 2) Compare the diagnostic performance of an abbreviated protocol versus standard multiparametric liver protocol. 3) Identify pitfalls/challenges for the abbreviated liver protocol.

RC529D The Abbreviated Liver Protocol for Quantitative Evaluation of Diffuse Liver Disease

Participants

Takeshi Yokoo, MD, PhD, Dallas, TX (Presenter) Nothing to Disclose

For information about this presentation, contact:

takeshi.yokoo@utsouthwestern.edu

LEARNING OBJECTIVES

1) Develop an abbreviated protocol for quantitative evaluation of diffuse liver disease. 2) Define clinical indications for the abbreviated protocol examination. 3) Identify quantitative maps of hepatic fat, iron, and stiffness. 4) Quantitatively estimate the severity of hepatic steatosis, siderosis, and fibrosis.

RC529E The Abbreviated Liver Protocol for Screening for Hepatocellular Carcinoma Using Hepatobiliary Contrast

Participants

Bachir Taouli, MD, New York, NY (Presenter) Research Grant, Guerbet SA; Research Grant, Bayer AG

For information about this presentation, contact:

bachir.taouli@mountsinai.org

LEARNING OBJECTIVES

1) Review current guidelines for liver cancer screening. 2) Review the limitations of ultrasound for liver cancer screening. 3) Review gadoxetic acid-enhanced abbreviated MRI protocol and early results for liver cancer screening.

ABSTRACT

Hepatocellular carcinoma (HCC) is the 2nd leading cause of cancer-related death worldwide, and the fastest growing cause of cancer death in the USA. The most important risk factor for HCC is cirrhosis. In this presentation, we will discuss the performance of ultrasound for HCC screening and surveillance and we will review recent developments in the use of gadoxetic-enhanced abbreviated MRI protocols for HCC screening and surveillance.



Imaging Utilization, Clinical Decision Support, and Appropriateness

Wednesday, Nov. 28 8:30AM - 10:00AM Room: E263

LM

AMA PRA Category 1 Credits ™: 1.50 ARRT Category A+ Credit: 1.75

Participants

Yoshimi Anzai, MD, Salt Lake City, UT (Moderator) Nothing to Disclose

Sub-Events

RC532A Imaging Utilization: Past, Present, and Future

Participants

David C. Levin, MD, Philadelphia, PA (Presenter) Consultant, HealthHelp, LLC; Board Member, Outpatient Imaging Affiliates, LLC

For information about this presentation, contact:

david.levin@jefferson.edu

LEARNING OBJECTIVES

1) Understand the overall trends in imaging during the last 12 years. 2) Understand the trends in utilization of each of the major imaging modalities over the last 12 years. 3) Assess the various factors that might cause imaging use to increase or decrease in the coming years.

RC532B Variations in Medicare Imaging: A Data-Driven Approach

Participants

Andrew B. Rosenkrantz, MD, New York, NY (Presenter) Nothing to Disclose

LEARNING OBJECTIVES

1) Understand the importance from a policy perspective of recognizing sources of variation in imaging utilization. 2) Explore a spectrum of sources of variation in imaging utilization. 3) Describe associations between variation in utilization of imaging and other categories of healthcare services.

RC532C Clinical Decision Support for Radiology Order Entry: Challenges and Opportunities

Participants

Charles E. Kahn JR, MD, Philadelphia, PA (Presenter) Nothing to Disclose

For information about this presentation, contact:

ckahn@upenn.edu

LEARNING OBJECTIVES

1) Describe the requirements of the Protecting Access to Medicare Act (PAMA). 2) Define some of the challenges of clinical decision support (CDS) for radiology order entry. 3) Explore early results using order-entry CDS. 4) Identify opportunities to use imaging CDS to improve clinical practice.

Honored Educators

Presenters or authors on this event have been recognized as RSNA Honored Educators for participating in multiple qualifying educational activities. Honored Educators are invested in furthering the profession of radiology by delivering high-quality educational content in their field of study. Learn how you can become an honored educator by visiting the website at: https://www.rsna.org/Honored-Educator-Award/ Charles E. Kahn JR, MD - 2012 Honored EducatorCharles E. Kahn JR, MD - 2018 Honored Educator

RC532D High Value Practice Academic Alliance

Participants Pamela T. Johnson, MD, Baltimore, MD (*Presenter*) Consultant, Oliver Wyman

For information about this presentation, contact:

PamelaJohnson@jhmi.edu

LEARNING OBJECTIVES

1) Understand the barriers to value-based quality improvement. 2) Recognize the importance of cross-specialty collaboration for effective performance improvement initiatives. 3) Understand the power of cross-institutional collaboration to efficiently advance performance improvement. 4) Recognize the importance of disseminating value-based quality improvement through publication and

presentations at national meetings, with emphasis on safety outcomes data.

ABSTRACT

This session reviews strategies to effectively increase radiology value on a national scale, based on our experience with the High Value Practice Academic Alliance, a national consortium of >85 academic medical centers.

Honored Educators

Presenters or authors on this event have been recognized as RSNA Honored Educators for participating in multiple qualifying educational activities. Honored Educators are invested in furthering the profession of radiology by delivering high-quality educational content in their field of study. Learn how you can become an honored educator by visiting the website at: https://www.rsna.org/Honored-Educator-Award/ Pamela T. Johnson, MD - 2016 Honored Educator



Vertebral Augmentation (Hands-on)

Wednesday, Nov. 28 8:30AM - 10:00AM Room: E260



AMA PRA Category 1 Credits ™: 1.50 ARRT Category A+ Credit: 1.75

Participants

A. Orlando Ortiz, MD, MBA, Mineola, NY (*Presenter*) Nothing to Disclose Bassem A. Georgy, MD, MSc, San Diego, CA (*Presenter*) Consultant, Johnson & Johnson; Consultant, Merit Medical Systems, Inc; Consultant, Medtronic plc; Stockholder, Spine Solutions, Inc; ; Allan L. Brook, MD, Bronx, NY (*Presenter*) Nothing to Disclose Todd S. Miller, MD, Bronx, NY (*Presenter*) Nothing to Disclose Afshin Gangi, MD, PhD, Strasbourg, France (*Presenter*) Proctor, BTG International Ltd; Proctor, Galil Medical Ltd

For information about this presentation, contact:

gangi@unistra.fr

tmiller@montefiore.org

LEARNING OBJECTIVES

Discuss appropriate algorithms for patient selection.
 Review anatomic and technical considerations for vertebral augmentation.
 Present an update of the recent advances in vertebral augmentation including sacroplasty.
 Emphasize safety issues and how to avoid complications.
 Understand the applications of vertebral augmentation in osteoporotic and neoplastic spine pathology.
 Update participants with respect to advances in equipment and biomaterials.

ABSTRACT

1. Patient selection for vertebral augmentation Indications and Contraindications 2. New devices and techniques in vertebral augmentation 3. Vertebral augmentation for osteoporotic and pathologic vertebral compression fractures 4. Sacroplasty (sacral augmentation) 5. Complications avoidance 6. Efficacy Vertebral augmentation is an image-guided (fluoroscopy or CT) percutaneous procedure in which a bone needle is inserted into a painful osteoporotic or pathologic fracture within the spinal axis. Biopsy, cavity creation or lesion ablation may then be performed under imaging guidance depending on the nature of the pathology that is being treated. Subsequently a radioopaque implant, usually an acrylic bone cement, is carefully injected into the vertebra or sacral ala under imagining guidance, These procedures have been shown to provide pain relief by stabilizing the fractured vertebra or sacral. As with any other invasive procedure, they carry a small risk (<<1%) of complication including bleeding, infection, neurovacular injury, or cement embolus. Appropriate patient seleciton and a detailed understanding of the technical aspects of the procedure along with active clinical patient follow-up are paramount to a successful outcome. This workshop will utilize short lectures, case examples and interactive audience participation in order to further explore critical topics in vertebral augmentation.



Liver Elastography (Hands-on)

Wednesday, Nov. 28 8:30AM - 10:00AM Room: E264

GI US

AMA PRA Category 1 Credits ™: 1.50 ARRT Category A+ Credit: 1.75

Participants

Richard G. Barr, MD, PhD, Campbell, OH (Presenter) Consultant, Siemens AG; Consultant, Koninklijke Philips NV; Research Grant, Siemens AG; Research Grant, SuperSonic Imagine; Speakers Bureau, Koninklijke Philips NV; Research Grant, Bracco Group; Speakers Bureau, Siemens AG; Consultant, Canon Medical Systems Corporation; Research Grant, Esaote SpA; Research Grant, BK Ultrasound; Research Grant, Hitachi, Ltd Nitin G. Chaubal, MD, MBBS, Mumbai, India (Presenter) Nothing to Disclose Chander Lulla, MBBS, Mumbai, India (Presenter) Nothing to Disclose Mirko D'Onofrio, MD, Verona, Italy (Presenter) Speaker, Bracco Group; Speaker, Siemens AG; Consultant, Siemens AG; Speaker, Hitachi, Ltd Carlo Filice, MD, Pavia, Italy (Presenter) Research Grant, Shenzhen Mindray Bio-Medical Electronics Co, Ltd; Research Grant, Hitachi, Ltd; Research Grant, Esaote SpA; Research Grant, Canon Medical Systems Corporation; Speaker, Shenzhen Mindray Bio-Medical Electronics Co, Ltd Vito Cantisani, MD, Rome, Italy (Presenter) Speaker, Canon Medical Systems Corporation; Speaker, Bracco Group; Speaker, Samsung Electronics Co, Ltd; Fabrizio Calliada, MD, Pavia, Italy (Presenter) Research Grant, Canon Medical Systems Corporation; Speakers Bureau, Hitachi, Ltd; Speakers Bureau, Shenzhen Mindray Bio-Medical Electronics Co, Ltd Ann E. Podrasky, MD, Miami, FL (Presenter) Consultant, Siemens AG Michelle L. Robbin, MD, Birmingham, AL (Presenter) Consultant, Koninklijke Philips NV; Speaker, Koninklijke Philips NV; Hisham A. Tchelepi, MD, Los Angeles, CA (Presenter) Nothing to Disclose Norihisa Yada, MD, Kyoto, Japan (Presenter) Nothing to Disclose Laura Maiocchi, MD, Pavia, Italy (Presenter) Nothing to Disclose Patrick Warren, MD, Columbus, OH (Presenter) Nothing to Disclose Maija Radzina, MD, PhD, Riga, Latvia (Presenter) Nothing to Disclose Anil Chauhan, MD, Philadelphia, PA (Presenter) Nothing to Disclose Raffaella Lissandrin, Pavia, Italy (Presenter) Nothing to Disclose Giovanna Ferraioli, MD, Pavia, Italy (Presenter) Speaker, Koninklijke Philips NV; Speaker, Hitachi Ltd; Speaker, Canon Medical Systems Corporation; Speaker, Shenzhen Mindray Bio-Medical Electronics Co, Ltd Cheng Fang, MBBS, FRCR, London, United Kingdom (Presenter) Nothing to Disclose Giuseppe Schillizzi, Roma, Italy (Presenter) Nothing to Disclose Valerio Forte, MD, Rome, Italy (Presenter) Nothing to Disclose Gregorio Alagna, Rome, Italy (Presenter) Nothing to Disclose Valeria de Soccio, JD, Rome, Italy (Presenter) Nothing to Disclose Daniele Fresilli, Roma, Italy (Presenter) Nothing to Disclose For information about this presentation, contact: riaclinic@gmail.com

thaneultrasound@gmail.com

mirko.donofrio@univr.it

giovanna.ferraioli@unipv.it

vito.cantisani@uniroma1.it

daniele.fresilli@hotmail.it

mrobbin@uabmc.edu

LEARNING OBJECTIVES

1) Improve basic knowledge and skills relevant to clinical practice in Liver elastography of the participants. 2) Teach how to practice liver elastography. 3) Show live how to do a proper examination, providing tips and tricks and updating current knowledge on different techniques. 4) Practical hands-on and slide presentation with key messages will be used.

Honored Educators

Presenters or authors on this event have been recognized as RSNA Honored Educators for participating in multiple qualifying educational activities. Honored Educators are invested in furthering the profession of radiology by delivering high-quality educational content in their field of study. Learn how you can become an honored educator by visiting the website at: https://www.rsna.org/Honored-Educator-Award/ Richard G. Barr, MD, PhD - 2017 Honored Educator



Deep Learning: Applying Machine Learning to Multi-disciplinary Precision Medicine Data Sets

Wednesday, Nov. 28 8:30AM - 10:00AM Room: E451B



AMA PRA Category 1 Credits ™: 1.50 ARRT Category A+ Credit: 1.75

FDA Discussions may include off-label uses.

Participants

Paula M. Jacobs, PhD, Bethesda, MD (Moderator) Nothing to Disclose

Maryellen L. Giger, PhD, Chicago, IL (*Presenter*) Stockholder, Hologic, Inc; Shareholder, Quantitative Insights, Inc; Shareholder, QView Medical, Inc; Co-founder, Quantitative Insights, Inc; Royalties, Hologic, Inc; Royalties, General Electric Company; Royalties, MEDIAN Technologies; Royalties, Riverain Technologies, LLC; Royalties, Mitsubishi Corporation; Royalties, Canon Medical Systems Corporation

John B. Freymann, BS, Rockville, MD (*Presenter*) Nothing to Disclose Joel Saltz, MD, PhD, Stony Brook, NY (*Presenter*) Nothing to Disclose Hugo Aerts, PhD, Boston, MA (*Presenter*) Stockholder, Sphera Inc

For information about this presentation, contact:

Paula.Jacobs@nih.gov

john.freymann@nih.gov

m-giger@uchicago.edu

LEARNING OBJECTIVES

1) Understand the strategy NIH National Cancer Institute is making to link clinical imaging with other existing patient-case 'metadata' archives. 2) Learn to navigate the patient-specific database silos (genetics, proteomics, clinical demographics) so as to strengthen Machine Learning research. 3) By specific use-case examples attendees will comprehend the advantage such imaging and disparate-type metadata links offer to clinically relevant cancer research.

ABSTRACT

Abstract: This didactic session will provide clinician researchers with examples of ongoing machine learning research in imaging combined with clinical and 'omics data sets, along with examples of where to find and how to link existing cancer image archive cases to other public-access stored databases that contain same-patient demographics, genetics, proteomic, and pathology images. Many of these disparate data types may be presently unfamiliar to imagers - such as mass spectroscopy data that arises from cellular proteomic analysis that propel the need for urgently forming new cross-disciplinary research teams. These datasets, often stored separately by different professional specialty teams, constitute critical complementary elements ultimately needed for reliable Machine Learning. This session pivots out from the clinical images available in the NCI Cancer Imaging Archive (TCIA) collections that acts as the point of origin for linking same-patient demographics, pathology, proteomics, and genetic data so that machine learning efforts can be more scientifically robust.



Next Generation Reporting: Informatics to Improve the Value of Reporting

Wednesday, Nov. 28 8:30AM - 10:00AM Room: S504AB



AMA PRA Category 1 Credits ™: 1.50 ARRT Category A+ Credit: 1.75

Participants

Arun Krishnaraj, MD, MPH, Charlottesville, VA (Moderator) Nothing to Disclose

LEARNING OBJECTIVES

1) Identify unmet needs of current and future practices with regards to radiology reporting. 2) Apply existing and emerging informatics applications to improve report generation, including a focus on patient centered reporting. 3) Demonstrate an understanding of how best to apply emerging machine intelligence tools to create structured automated recommendations.

Sub-Events

RC554A The Actionable Patient Facing Report

Participants

Arun Krishnaraj, MD, MPH, Charlottesville, VA (Presenter) Nothing to Disclose

LEARNING OBJECTIVES

1) Appreciate the current state of radiology reporting in the United States. 2) Identify areas for improvement in reporting. 3) Demonstrate an understanding of the potential of patient portals. 4) Understand how patient facing actionable reports can lead to better care through shared decision making

RC554B The Multimedia Report: Ready for Prime Time?

Participants

Cree M. Gaskin, MD, Charlottesville, VA (*Presenter*) Author with royalties, Oxford University Press; Author with royalties, Thieme Medical Publishers, Inc; Research Grant, Carestream Health, Inc;

For information about this presentation, contact:

cree@virginia.edu

LEARNING OBJECTIVES

1) Identify characteristics of an interactive multimedia radiology report. 2) Comprehend the value of improved communication that occurs with interactive multimedia reporting. 3) Describe barriers to overcome during the implementation of interactive multimedia reporting and integration of advanced reports into the electronic health record.

RC554C Interactive Reporting

Participants

Les R. Folio, MPH,DO, Bethesda, MD (Presenter) Institutional research agreement, Carestream Health, Inc

For information about this presentation, contact:

Les.Folio@nih.gov

LEARNING OBJECTIVES

1) Comprehend the difference between plain text and interactive multimedia radiology reports. 2) Identify characteristics and components suitable for an interactive multimedia radiology report. 3) Demonstrate objective evidence of radiology report value using interactive reports now that we can analyze click through behaviours of hyperlinked text.

ABSTRACT

For the past several years, the NIH Clinical Center has been routinely producing multimedia-enhanced interactive reports (Folio L. Multimedia Reports. Radiographics. April/ May 2018) in which radiologist reports contain hyperlinked text, directing clinicians to the corresponding image annotation (most often two-diameter measurements). Our prior studies have also demonstrated notable time savings for oncologists (three times faster) when they use the hyperlinked target lesion measurements for their patients (Folio L. RSNA 2015) as they spend significantly less time "hunting" for measurements in the previous text-only reports. Bookmark tables within our PACS (VuePACS V12, Carestream Health, Rochester, NY) contain fields where "radiologist assistants" (RAs) can label target lesions. In one ongoing study (Toscano A. SCBT.MR 2018), RAs simulate an AI workflow where target lesions are measured before radiologists open the exam for interpretation. This improves target lesion. Selection and measurement concordance while saving radiologists time by not having to identify or measure these lesions. Once verified, radiologists import the active annotation as a link into our report by dictating the word "hyperlink," which minimizes the potential transcription error of three sets of numbers (measurement, series and image numbers) and other metadata (e.g. x,y image and z table space, comparison of current with prior measurements for RECIST calculations, lesion measurement creator). We have followed adoption of hyperlinks since we started the capability and showed a rapid rise of use and that body radiologists use the most hyperlinks (about 80% of all CT), followed by

body MR, PET CT and nueroradiology. We also collect data on use of annotations, with two-diameter the most frequent, followed by linear, ovals then arrows (least frequent). Preliminary work indicates that two-diameter and ovals better guide bounding boxes for deep learning with the annotations directly associated with the the hyperlinked text. Lastly, we have been analyzing clinician click-through behaviors where we can objectively demonstrate report value as a function of number of clicks on linked text, thus verifying clinician interaction with radiologist reports. We can also analyze radiologists' clicks on prior report text and noted that body radiologists (for example) frequently click on these reports while dictating their interpretations.

RC554D Structured Automated Recommendations: Reporting in the Era of Artificial Intelligence

Participants

Tarik K. Alkasab, MD, PhD, Boston, MA (Presenter) Nothing to Disclose



RCB41

Getting Stuff Done: A Mindful Approach to Personal Productivity

Wednesday, Nov. 28 8:30AM - 10:00AM Room: S401CD

IN

AMA PRA Category 1 Credits ™: 1.50 ARRT Category A+ Credit: 1.75

Participants

Puneet Bhargava, MD, Seattle, WA (*Moderator*) Nothing to Disclose Matthew B. Morgan, MD, Sandy, UT (*Presenter*) Consultant, Reed Elsevier Puneet Bhargava, MD, Seattle, WA (*Presenter*) Nothing to Disclose

For information about this presentation, contact:

Bhargp@uw.edu

LEARNING OBJECTIVES

1) Introduce the concept of "Getting Things Done.' Learn the concepts of Inbox Zero and other email management techniques. 2) Using tools such as note-taking applications, citation and password managers.3) Using self-inquiry techniques, review how to make meaningful and powerful changes in how we engage with technology.

Active Handout: Puneet Bhargava

http://abstract.rsna.org/uploads/2018/18001638/Productivity Primer RCB41.pdf

Honored Educators

Presenters or authors on this event have been recognized as RSNA Honored Educators for participating in multiple qualifying educational activities. Honored Educators are invested in furthering the profession of radiology by delivering high-quality educational content in their field of study. Learn how you can become an honored educator by visiting the website at: https://www.rsna.org/Honored-Educator-Award/ Puneet Bhargava, MD - 2015 Honored Educator



RCC41

Advanced Cybersecurity for Imaging Departments and Imagers: Threats, Vulnerabilities, and Best Practices

Wednesday, Nov. 28 8:30AM - 10:00AM Room: S501ABC



CME credit is not available for this session. ARRT Category A Credit: 1.75

Participants

Kevin McDonald, Rochester, MN (Moderator) Nothing to Disclose

LEARNING OBJECTIVES

Describe common imaging device vulnerabilities. 2) Explain possible patient safety impacts of cyber attacks. 3) Explain the possible institutional impacts of cyber attacks. 4) List the technical, environmental and cultural barriers in improving the cyber security of imaging devices. 5) Contrast the items in the C-I-A triad. 6) List high value cybersecurity remediation and mitigations.
 Zist the steps to creating an imaging device cybersecurity program. 8) Identify available cybersecurity resources.

Sub-Events

RCC41A Medical Device Security in a Connected World

Participants

Kevin McDonald, Rochester, MN (Presenter) Nothing to Disclose

LEARNING OBJECTIVES

1) Identity the common cybersecurity threat actors. 2) Describe the state of cybersecurity in healthcare. 3) List common catagories of security vulnerabilities. 4) Describe cybersecurity challanges with medical devices.

RCC41B Medical Device Cybersecurity and the FDA

Participants

Suzanne B. Schwartz, MD, Silver Spring, MD (Presenter) Nothing to Disclose

RCC41C Federal Lead for the Industrial Control Systems Vulnerability Management and Coordination

Participants Jay Angus, Oak Brook, IL (*Presenter*)



MSRT42

ASRT@RSNA 2018: Tips and Tricks - Radiation Dose Aspects in Oncologic CT Imaging

Wednesday, Nov. 28 9:20AM - 10:20AM Room: N230B



AMA PRA Category 1 Credit ™: 1.00 ARRT Category A+ Credit: 1.00

Participants

Dianna D. Cody, PhD, Houston, TX (*Presenter*) In-kind support, General Electric Company; Reviewer, ACR CT accreditation program; Researcher, Gammex, Inc

LEARNING OBJECTIVES

1) Better understand 'routine' CT imaging performed in a cancer center. 2) How this particular cancer center approaches abdominal CT imaging without IV contrast. 3) Appreciate scan options for CT imaging of very large patients. 4) Comprehend implementation of dual-energy CT for oncology.

ABSTRACT

The management of CT radiation exposure for cancer patients presents a difficult dilemma. We know that each exposure has a small probability of inducing radiation damage, but we must weigh that knowledge against the fact that the patient already has cancer, and may have a reduced life expectancy as a result. Patient management decisions often hinge on a detailed appreciation of the patient's present condition, and CT can provide critical information in this respect. In our practice, the concern for short-term survival typically supersedes the long term and complex risk associated with CT dose. The concept of what is 'routine' CT imaging at our oncology center will be explored, with a focus on our most frequently performed exams and typical scan parameters. CT dose metrics will be reviewed and compared to naitonal benchmarks for several routine CT exams. Our approach to abdominal CT protocols designed for use without IV contrast will be covered, as well as several options for imaging our very large cancer patients. How we have implemented dual-energy CT, and its benefits, will also be illustrated.



MSCP42

Case-based Review of Pediatric Radiology (Interactive Session)

Wednesday, Nov. 28 10:30AM - 12:00PM Room: E450B



AMA PRA Category 1 Credits ™: 1.50 ARRT Category A+ Credit: 1.75

Participants

Ricardo Restrepo, MD, Miami, FL (Director) Nothing to Disclose

Sub-Events

MSCP42A Pediatric Spine Disorders

Participants

Thierry Huisman, MD, Baltimore, MD (Presenter) Nothing to Disclose

For information about this presentation, contact:

thuisma1@jhmi.edu

LEARNING OBJECTIVES

1) Review the unique biomechanical and imaging presentation of the developing pediatric spine. 2) Review key features of pediatric spine trauma. 3) Present a brief introduction into congenital versus acquired spine disorders.

ABSTRACT

The normal development and variations of the pediatric spinal column will be discused, age specific biomechanical properties and resultant variable patterns of accidental and non-accidental injury will be reviewed. In addition, a brief introduction will be given on differentiating acquired from congenital spine and spinal cord pathologies using a case based approach.

MSCP42B Pediatric Pulmonary Disorders

Participants

Mark C. Liszewski, MD, Bronx, NY (Presenter) Grant, Carestream Health, Inc; Advisory Board, Carestream Health, Inc

For information about this presentation, contact:

mliszews@montefiore.org

LEARNING OBJECTIVES

1) Describe the imaging findings of several pediatric pulmonary disorders. 2) Differentiate between disorders with similar findings. 3) Recommend appropriate management based on the imaging features.

ABSTRACT

Congenital and acquired pediatric pulmonary cases will be presented. Discussion will include: 1) description of the imaging features for each condition, 2) tips for differentiating between conditions with similar imaging findings, 3) up-to-date recommendations for management and follow-up for each condition.

MSCP42C Pediatric Head and Neck Disorders

Participants Amy F. Juliano, MD, BOSTON, MA (*Presenter*) Nothing to Disclose

MSCP42D Pediatric Musculoskeletal Disorders

Participants Ricardo Restrepo, MD, Miami, FL (*Presenter*) Nothing to Disclose

For information about this presentation, contact:

ricardo.restrepo@nicklaushealth.org

LEARNING OBJECTIVES

1) Recognize normal variants in the pediatric musculoskeletal system and distinguish them from disease processes. 2) Be familiar with MR imaging findings in patients with chronic non bacterial osteomyelitis. 3) Differentiate musculoskeletal neoplasms from infections.

ABSTRACT

A series of pediatric musculoskeletal cases will be presented to illustrate:1- normal variants that can be confused with pathology2-MR imaging spectrum of chronic non bacterial osteomyelitis (CNO)3- Neoplasms that can mimic infections and viceversa



MSES42

Essentials of GI Imaging

Wednesday, Nov. 28 10:30AM - 12:00PM Room: S100AB

GI

AMA PRA Category 1 Credits ™: 1.50 ARRT Category A+ Credit: 1.75

Sub-Events

MSES42A Management of Incidental Pancreatic Cysts

Participants

Desiree E. Morgan, MD, Birmingham, AL (Presenter) Institutional Research Grant, General Electric Company

For information about this presentation, contact:

dmorgan@uabmc.edu

LEARNING OBJECTIVES

1) Identify typical imaging findings of cystic pancreatic lesions. 2) Be familiar with imaging evaluation and clinical management strategies for incidentally detected cystic pancreas lesions. 3) Detect and uniformly describe imaging features of pancreatic cystic lesions that indicate an increased risk for malignancy.

MSES42B Management of Incidental Liver Findings

Participants

Richard M. Gore, MD, Evanston, IL (Presenter) Nothing to Disclose

For information about this presentation, contact:

rgore@northshore.org

LEARNING OBJECTIVES

1) Understand the prevalence of incidental liver lesions in the general population as well as high risk patients. 2) Review the imaging characteristics of the most common incidental liver lesions. 3) Appreciate which liver lesions can be ignored, which lesions need to be followed, and which lesions need immediate evaluation.

MSES42C Approach to a Focal Lesion in the Cirrhotic Liver

Participants

Giuseppe Brancatelli, MD, Palermo, Italy (Presenter) Speaker, Bayer AG; Speaker, Guerbet SA; Advisory Committee, Guerbet SA

For information about this presentation, contact:

gbranca@yahoo.com

LEARNING OBJECTIVES

1) Describe the vascular patterns of typical and atypical hepatocellular carcinoma. 2) Identify the major and ancillary features for the diagnosis of hepatocellular carcinoma. 3) List the most common lesions occurring in the cirrhotic liver beyond hepatocellular carcinoma.

ABSTRACT

The enrolment of patients with chronic liver disease into surveillance programs has determined a steady increase in the number of small hepatic masses being detected. In addition, technological advances have improved the spatial, contrast and temporal resolution of imaging modalities allowing for higher rates of detection. However, detection and characterization of a lesion in a cirrhotic liver is oftentimes a challenging task, due to the intrinsic features of a fibrotic/cirrhotic organ and to a different epidemiology in comparison to the noncirrhotic population. When a nodular lesion is larger than 1 cm and shows enhancement in the hepatic arterial phase and washout either in the portal venous or delayed phase, it can be confidently diagnosed as HCC. However, small HCC frequently presents with atypical findings, such as lack of enhancement, lack of washout or no capsule. Furthermore, HCC <1cm grows very slowly; therefore, stability (i.e. lack of growth) over a few months does not entirely rule out malignancy, and a negative biopsy is not helpful due to the high false-negative sampling rate. In these instances, two possible options are 1) further imaging with a different technique or 2) imaging follow-up. While most lesions in a cirrhotic liver are hepatocellular, a wide array of other observations can be encountered, such as haemangioma, nodule-like arterial phase hyperenhancement, focal fibrosis, cholangiocarcinoma and metastases.

MSES42D Non-invasive Diagnosis of Liver Fibrosis: Why and How

Participants Amir Borhani, MD, Pittsburgh, PA (*Presenter*) Consultant, Guerbet SA; Author, Reed Elsevier borhaniaa@upmc.edu

LEARNING OBJECTIVES

1) Explain the importance of non-invasive assessment of liver fibrosis in management of different disease processes. 2) List morphologic features of advanced fibrosis on ultrasound, CT, and MRI and discuss the sensitivity and specificity of these signs. 3) Discuss different elastography techniques and their role in non-invasive assessment of liver fibrosis.



MSRO42

BOOST: Lymphoma-Oncology Anatomy and Case-based Multidisciplinary Review (Interactive Session)

Wednesday, Nov. 28 10:30AM - 12:00PM Room: S103CD



AMA PRA Category 1 Credits ™: 1.50 ARRT Category A+ Credit: 1.75

FDA Discussions may include off-label uses.

Participants

Chelsea C. Pinnix, MD, PhD, Houston, TX (*Moderator*) Research Grant, Merck & Co, Inc; Consultant, Global One Inc; Speaker, International Journal of Radiation Oncology, Biology & Physics Jurgen Rademaker, MD, New York, NY (*Presenter*) Nothing to Disclose Bradford Hoppe, MD, Jacksonville, FL (*Presenter*) Nothing to Disclose Alison M. Friedmann, MD, Boston, MA (*Presenter*) Nothing to Disclose

LEARNING OBJECTIVES

1) Case-based review of staging and treatment response in lymphoma (CT, PET, MRI).



MSSR42

RSNA/ESR Sports Imaging Symposium: Lower Extremity Sports Injuries (Interactive Session)

Wednesday, Nov. 28 10:30AM - 12:00PM Room: E352



AMA PRA Category 1 Credits ™: 1.50 ARRT Category A+ Credit: 1.75

Participants

Laura W. Bancroft, MD, Orlando, FL (*Moderator*) Author with royalties, Wolters Kluwer nv; Speaker, World Class CME; Editor, Thieme Medical Publishers, Inc; Travel support, Thieme Medical Publishers, Inc; ; Andrew J. Grainger, MRCP, FRCR, Leeds, United Kingdom (*Moderator*) Consultant, Levicept Ltd; Director, The LivingCare Group;

Sub-Events

MSSR42A Sports-related Injuries of the Knee: What Does the Orthopedic Surgeon Need to Know?

Participants

Theodore T. Miller, MD, New York, NY (Presenter) Nothing to Disclose

For information about this presentation, contact:

millertt@hss.edu

LEARNING OBJECTIVES

1) To be able to describe features of meniscal tears, ACL tears, and cartilage abnormalities that should be included in the MRI report. 2) To be able to recognize common sports-related injury patterns of the knee.

MSSR42B Multimodality Imaging of the Foot and Ankle Injuries in the Athlete

Participants

Andrew J. Grainger, MRCP, FRCR, Leeds, United Kingdom (Presenter) Consultant, Levicept Ltd; Director, The LivingCare Group;

For information about this presentation, contact:

andrewgrainger@nhs.net

LEARNING OBJECTIVES

1) To appreciate the different and often contributory roles that imaging modalities have in the foot and ankle. 2) To recognize the most common ligamentous and tendon injuries in the ankle. 3) To understand how common patterns of injury relate to the mechanisms involved.

ABSTRACT

Abstract: Ankle injuries are common in many sports and the complicated anatomy of the ankle joint can be challenging the reporting radiologist. The ankle joint itself is a synovial hinge joint, but important movement for ankle function also occurs at the joints of the hind and midfoot which are also susceptible to injury. In addition to conventional radiographs, CT, MRI and ultrasound all have important roles to play in the diagnosis of foot and ankle injuries in the athlete. The ligamentous and tendon structures about the ankle are generally superficial in nature and readily amenable to assessment with ultrasound where assessment can be enhanced due to the dynamic capabilities of the technique. While MRI also demonstrates these structures, it has advantages for assessing deeper joint structures such as the chondral surfaces and bones. The complex 3d anatomy of the foot and ankle means that conventional radiographs can struggle to demonstrate bone injury which means CT also has an important role to play. This lecture will focus on the use of these imaging modalities for the assessment of acute and chronic ligamentous and tendon injury. Emphasis will be put on the mechanisms of injury and how they determine the resultant patterns of injury and the imaging appearances.

Active Handout: Andrew J. Grainger

http://abstract.rsna.org/uploads/2018/18001000/Foot&Ankle notesMSSR42B.pdf

MSSR42C Interactive Case Discussion

Participants

Theodore T. Miller, MD, New York, NY (*Presenter*) Nothing to Disclose Andrew J. Grainger, MRCP, FRCR, Leeds, United Kingdom (*Presenter*) Consultant, Levicept Ltd; Director, The LivingCare Group;

For information about this presentation, contact:

andrewgrainger@nhs.net

LEARNING OBJECTIVES

1) To appreciate common patterns of athletic injury in the knee. 2) To become familiar with the techniques available and imaging appearances of the knee, foot and ankle athletic injury. 3) To consolidate the knowledge gained from the session with interactive cases of lower limb athletic injury.



RCA42

From Texture Analysis to Deep Learning for Lesion Characterization (Hands-on)

Wednesday, Nov. 28 10:30AM - 12:00PM Room: S401AB



AMA PRA Category 1 Credits ™: 1.50 ARRT Category A+ Credit: 1.75

Participants

Kevin Mader, DPhil,MSc, Basel, Switzerland (*Moderator*) Employee, 4Quant Ltd; Shareholder, 4Quant Ltd Kevin Mader, DPhil,MSc, Basel, Switzerland (*Presenter*) Employee, 4Quant Ltd; Shareholder, 4Quant Ltd Barbaros S. Erdal, PhD, Columbus, OH (*Presenter*) Nothing to Disclose Joshy Cyriac, Basel, Switzerland (*Presenter*) Nothing to Disclose

LEARNING OBJECTIVES

1) Review the basic principles of machine learning. 2) Learn what texture analysis is and how to apply it to medical imaging. 3) Understand how to combine texture analysis and machine learning for lesion classification tasks.

ABSTRACT

During this course, an introduction to machine learning and image texture analysis will be provided through hands on examples. Participants will use open source as well as freely available commercial platforms in order to achieve tasks such as image feature extraction, statistical analysis, building models, and validating them. Imaging samples will include both 2D and 3D datasets from a variety of modalities (CT, PET, MR). The course will begin with a brief overview of important concepts and links to more detailed references. The concepts will then be directly applied in visual, easily understood workflows where the participants will see how the images are processed, features and textures are extracted and how publication ready statistics and models can be built and tested.



RCB42

Getting Stuff Done: A Hands-on Technology Workshop to Enhance Personal Productivity (Hands-on)

Wednesday, Nov. 28 10:30AM - 12:00PM Room: S401CD

IN

AMA PRA Category 1 Credits ™: 1.50 ARRT Category A+ Credit: 1.75

Participants

Puneet Bhargava, MD, Seattle, WA (*Moderator*) Nothing to Disclose Matthew B. Morgan, MD, Sandy, UT (*Presenter*) Consultant, Reed Elsevier Puneet Bhargava, MD, Seattle, WA (*Presenter*) Nothing to Disclose Amanda Lackey, MD, Springfield, MO (*Presenter*) Nothing to Disclose Tarun Pandey, MD, FRCR, Little Rock, AR (*Presenter*) Nothing to Disclose

For information about this presentation, contact:

Bhargp@uw.edu

LEARNING OBJECTIVES

1) Introduce the concept of "Getting Things Done.' Learn the concepts of Inbox Zero and other email management techniques. 2) Using tools such as note-taking applications, citation and password managers.3) Using self-inquiry techniques, review how to make meaningful and powerful changes in how we engage with technology.

Active Handout:Puneet Bhargava

http://abstract.rsna.org/uploads/2018/17002645/Productivity Primer RCB42.pdf

Active Handout:Tarun Pandey

http://abstract.rsna.org/uploads/2018/17002645/Pandey_RSNA 2018 Productivity Exercises FINAL RCB22.pdf

Honored Educators

Presenters or authors on this event have been recognized as RSNA Honored Educators for participating in multiple qualifying educational activities. Honored Educators are invested in furthering the profession of radiology by delivering high-quality educational content in their field of study. Learn how you can become an honored educator by visiting the website at: https://www.rsna.org/Honored-Educator-Award/ Puneet Bhargava, MD - 2015 Honored Educator



RCC42

Medical 3D Printing Operations and Applications II

Wednesday, Nov. 28 10:30AM - 12:00PM Room: S501ABC

IN

AMA PRA Category 1 Credits ™: 1.50 ARRT Category A+ Credit: 1.25

Participants

Kenneth C. Wang, MD, PhD, Ellicott City, MD (*Moderator*) Co-founder, DexNote, LLC; Software support, 3D Systems, Inc Jonathan M. Morris, MD, Rochester, MN (*Moderator*) Nothing to Disclose

Sub-Events

RCC42A Neural Applications of 3D Printing

Participants Edward P. Quigley III, MD,PhD, Salt Lake City, UT (*Presenter*) Nothing to Disclose

RCC42B Establishing 3D Medical Labs at the VA

Participants

Beth A. Ripley, MD, PhD, Seattle, WA (Presenter) Nothing to Disclose

LEARNING OBJECTIVES

Understand why training in computer technologies such as 3D modeling and 3D printing is increasingly critical to resident training.
 Learn how to develop methods for instruction in 3D technologies. 3) Identify potential opportunities and resources for resident training.

RCC42C Cardiac Applications in 3D Medical Printing

Participants

Justin R. Ryan, PhD, SAN DIEGO, CA (Presenter) Nothing to Disclose

LEARNING OBJECTIVES

1) Describe the need for 3D printing for congenital heart disease. 2) Describe basic segmentation tools for congenital heart modeling. 3) Describe challenges and possible solutions for common issues in CHD segmentation.

RCC42D **3D Printing in Europe**

Participants

Philipp Brantner, MD, Basel, Switzerland (Presenter) Nothing to Disclose

LEARNING OBJECTIVES

1) List several sites that leverage 3D printing in Europe. 2) Describe common use cases of 3D printing in European hospitals. 3) Explain differences in 3D printing in Europe compared to the North Americas.

RCC42E 3D Printing in Craniofacial Surgery

Participants

Jonathan M. Morris, MD, Rochester, MN (Presenter) Nothing to Disclose

LEARNING OBJECTIVES

Discuss the Clinical Applications of 3D Printing in Craniomaxillofacial Reconstruction.
 Discuss Simolation of Rare Events Utilizing 3D Printing.
 Become familiar with the concept of bio-compatibility and sterilization techniques as they relate to 3D printed parts.
 Become awere of the varied types of 3D printing technology including benefits and limitations.



SSK01

Breast Imaging (Digital Breast Tomosynthesis: Screening and Diagnostic Indications)

Wednesday, Nov. 28 10:30AM - 12:00PM Room: E451A

BR

AMA PRA Category 1 Credits ™: 1.50 ARRT Category A+ Credit: 1.75

FDA Discussions may include off-label uses.

Participants

Sarah M. Friedewald, MD, Chicago, IL (*Moderator*) Consultant, Hologic, Inc; Research Grant, Hologic, Inc; Susan Weinstein, MD, Philadelphia, PA (*Moderator*) Nothing to Disclose

Sub-Events

SSK01-01 Blinded Observer Study: "Virtual" Full-Dose (VFD) Digital Breast Tomosynthesis (DBT) Images Derived from Reduced-Dose Acquisitions versus Clinical Full-Dose DBT Images

Participants

Junchi Liu, MS, Chicago, IL (*Abstract Co-Author*) Nothing to Disclose Syed Ammar Qadir, Chicago, IL (*Abstract Co-Author*) Nothing to Disclose Amin Zarshenas, MSc, Chicago, IL (*Abstract Co-Author*) Nothing to Disclose Limin Yang, MD, PhD, Iowa City, IA (*Abstract Co-Author*) Nothing to Disclose Laurie L. Fajardo, MD, MBA, Park City, UT (*Abstract Co-Author*) Consultant, Hologic, Inc; Consultant, Siemens AG; Consultant, FUJIFILM Holdings Corporation; Kenji Suzuki, PhD, Chicago, IL (*Presenter*) Royalties, General Electric Company; Royalties, Hologic, Inc; Royalties, MEDIAN Technologies; Royalties, Riverain Technologies, LLC; Royalties, Canon Medical Systems Corporation; Royalties, Misubishi Corporation; Royalties, AlgoMedica, Inc

For information about this presentation, contact:

jliu118@hawk.iit.edu

PURPOSE

We developed a deep-learning-based "virtual" higher-dose (VHD) technology for radiation dose reduction in DBT. The purpose of our study was to compare the image quality of our VFD images generated from half-dose acquisitions to that of real clinical full-dose images in DBT.

METHOD AND MATERIALS

Our deep-learning-based VHD technology employed our original patched-based neural network convolutional deep learning to convert lower-dose (LD) to higher-dose (HD) tomosynthesis images. To evaluate our VHD technology, we collected half-dose (50% of the standard dose: 32±14 mAs at 33±5 kVp) and full-dose (100% of the standard dose: 68±23 mAs at 33±5 kVp) images of 51 clinical screening cases with a DBT system (Selenia Dimensions, Hologic, Inc, Bedford, MA) at University of Iowa Hospitals & Clinics. We applied our VHD technology to the 51 cases to convert half-dose images to VFD images. We invited 35 breast radiologists to participate in our observer rating study to rate and distinguish blinded VFD and real full-dose DBT images of 10 of the 51 cases. A VFD image and its corresponding real full-dose image were shown on two clinical LCD monitors (EIZO RadiForce GX540) in a blinded manner. Radiologists were asked to rate the image quality on a 0-to-100 scale and to provide their choices as to which one was better in image quality.

RESULTS

Among the 35 breast radiologists, 21 (60%) radiologists either preferred our VFD DBT images over the real full-dose images or could not distinguish between the two in our observer rating study. The mean scores of the image quality of our VFD images and the real full-dose images were 83.2 ± 3.2 and 84.0 ± 3.0 , respectively. The difference in image quality between VFD and real-full dose images was not statistically significant (p=0.37).

CONCLUSION

Our blinded observer study with 35 breast radiologists demonstrated that our deep-learning-based VFD images generated from halfdose acquisitions were equivalent to real full-dose DBT images. Thus, our VHD technology achieved 50% dose reduction without sacrificing the image quality.

CLINICAL RELEVANCE/APPLICATION

Substantial radiation dose reduction with the observer-study-proven VHD technology would benefit patients by reducing the lifetime risk of radiation-induced cancer from DBT screening.

SSK01-02 Comparison of DM/Tomosynthesis and Synthesized DM/Tomosynthesis False Negative Cancers in a Population-Based Breast Cancer-Screening Program

Wednesday, Nov. 28 10:40AM - 10:50AM Room: E451A

Awards

Student Travel Stipend Award

Participants

Samantha P. Zuckerman, MD, Philadelphia, PA (*Presenter*) Nothing to Disclose Rebecca Hubbard, Philadelphia, PA (*Abstract Co-Author*) Nothing to Disclose Elizabeth S. McDonald, MD, Philadelphia, PA (*Abstract Co-Author*) Nothing to Disclose Susan Weinstein, MD, Philadelphia, PA (*Abstract Co-Author*) Nothing to Disclose Lauren Pantalone, BS, Philadelphia, PA (*Abstract Co-Author*) Nothing to Disclose Marie Synnestvedt, Philadelphia, PA (*Abstract Co-Author*) Nothing to Disclose Emily F. Conant, MD, Philadelphia, PA (*Abstract Co-Author*) Nothing to Disclose Consultant, iCAD, Inc; Speaker, iiCME

For information about this presentation, contact:

samantha.zuckerman@uphs.upenn.edu

PURPOSE

Synthesized 2D imaging (s2D) is replacing 2D digital mammography (DM) in digital breast tomosynthesis (DBT) screening to reduce radiation dose. However, there have been reports of decreased rates of detection of in situ carcinomas with s2D/DBT screening. The purpose of this study is to compare screening outcomes as well as false negative rates and lesion types in DM/DBT versus s2D/DBT screening.

METHOD AND MATERIALS

Recall rate percentage (RR), cancer detection (CDR) and false negative (FN) rates per 1000 screened, false negative cancer subtype (invasive versus in situ) and the method of detection of the false negative cancer (symptomatic versus by another imaging modality) were compared for 37,184 women screened with DM/DBT from 1/3/2011-1/6/2015 and 37,996 women screened with s2D/DBT from 1/7/2015-1/6/2018. Differences were compared using chi-squared tests at the standard a=0.05 significance level with Yates correction. All statistical tests were two-sided.

RESULTS

RR decreased with s2D/DBT versus DM/DBT screening - 6.9% versus 8.9% (p<0.001). CDR for DM/DBT and s2D/DBT screening were not statistically different (6.0/1000 vs. 5.5/1000, p=0.37). However, FN rate doubled for s2D/DBT (0.84/1000, n=32) versus DM/DBT screening (0.40/1000, n=15), p=0.02. While not statistically significant, there was a trend of more asymptomatic FN cancers detected by other modalities (i.e., MR, US, CT) in the s2D cohort than in the DM/DBT cohort (13/32 (41%) versus 5/15 (33%), p=0.11) and a trend of higher proportion of DCIS in the s2D cohort than in the DM cohort (9/32 (28%) versus 3/15 (20%), p=0.16).

CONCLUSION

s2D/DBT maintains CDR with the benefit of decreased recall rates. However, the FN rate increased with s2D/DBT compared to DM/DBT with both in situ and invasive FN cancers increased in the s2D cohort. While not statistically significant, a greater proportion of s2D FN cancers were detected by other modalities in asymptomatic patients. The increase in false negative rates is multifactorial and may be intrinsically related to the new technology and/or a learning curve in implementing the s2D technology.

CLINICAL RELEVANCE/APPLICATION

The replacement of DM with s2D in a large DBT breast cancer screening program maintained cancer detection rates and decreased recall rates, but increased false negative rates.

SSK01-03 Integration of Digital Breast Tomosynthesis into Breast Cancer Screening Practices in the United States: A Comparative Modeling Analysis

Wednesday, Nov. 28 10:50AM - 11:00AM Room: E451A

Participants

Kathryn Lowry, MD, Seattle, WA (*Presenter*) Nothing to Disclose Natasha K. Stout, PhD, Boston, MA (*Abstract Co-Author*) Nothing to Disclose Oguzhan Alagoz, PhD, Madison, WI (*Abstract Co-Author*) Consultant, Renaissance Rx Elizabeth S. Burnside, MD,MPH, Madison, WI (*Abstract Co-Author*) Dr. Burnside has a research grant from Hologic Emily F. Conant, MD, Philadelphia, PA (*Abstract Co-Author*) Grant, Hologic, Inc; Consultant, Hologic, Inc; Grant, iCAD, Inc; Consultant, iCAD, Inc; Speaker, iiCME Karla Kerlikowske, MD, San Francisco, CA (*Abstract Co-Author*) Nothing to Disclose Diana Miglioretti, PhD, Seattle, WA (*Abstract Co-Author*) Nothing to Disclose Diana Miglioretti, PhD, Seattle, WA (*Abstract Co-Author*) Nothing to Disclose Anna N. Tosteson, Lebanon, NH (*Abstract Co-Author*) Nothing to Disclose Martin J. Yaffe, PhD, Toronto, ON (*Abstract Co-Author*) Nothing to Disclose Martin J. Yaffe, PhD, Toronto, ON (*Abstract Co-Author*) Research collaboration, General Electric Company; Shareholder, Volpara Health Technologies Limited; Co-founder, Mammographic Physics Inc; Research Consultant, BHR Pharma LLC Clyde Schechter, Bronx, NY (*Abstract Co-Author*) Nothing to Disclose Amy Trentham-Dietz, Madison, WI (*Abstract Co-Author*) Nothing to Disclose

PURPOSE

To project long-term outcomes and cost-effectiveness of transitioning from breast cancer screening using digital mammography (DM) to digital mammography with digital breast tomosynthesis (DBT) in the United States.

Two established breast cancer models were used to simulate two scenarios: complete transition from DM to DBT for all women ages 40+ between 2011-2020 versus continued use of DM alone. Screening utilization was based on observed dissemination patterns from national surveillance datasets. We assumed current screening and treatment patterns continued, and women were followed for their remaining lifetimes. DM and DBT performance was based on screening data from the NCI's Population Based Research Optimizing Screening through Personalized Regimen (PROSPR) consortium from 2011-2014. Costs and quality of life weights were based on US national averages and published literature. Outcomes included life-years (LY), quality-adjusted life-years (QALYs), breast cancer deaths, false positive exams (FP), costs (2017 US\$) and incremental cost-effectiveness ratios (ICER). Analyses were performed from the payer perspective. Results were summarized within and across models.

RESULTS

Transition to DBT had the greatest impact on FP screening mammograms, which reduced FP exams by 278-288/1,000 women. The small difference in test sensitivity observed in the PROSPR data translated to minimal differences in breast cancer deaths and LY gains, with a reduction in deaths from 0 to 0.03/1,000 women and LY gains from -1 to 0.05 years/1,000 women. Total costs increased by \$5.64-\$5.66 million, with ICERs of \$193,634-\$217,532/QALY with DBT relative to DM. In sensitivity analyses, ICERs were sensitive to both the test performance and costs of screening DBT. For example, ICERs decreased to \$141,043/QALY with 2% absolute improvement in DBT sensitivity; ICERs decreased to \$163,092/QALY and \$59,872 with \$20 and \$40 reductions in cost of DBT exams, respectively.

CONCLUSION

The transition from DM to DBT for routine breast cancer screening in the U.S. reduces FP results, but substantially increases costs assuming current estimates of performance and reimbursement rates.

CLINICAL RELEVANCE/APPLICATION

Digital breast tomosynthesis for routine breast cancer screening in the U.S. reduces false positive exams, but substantially increases costs based on current estimates of performance and reimbursement rates.

SSK01-04 Interval Cancers at Digital Breast Tomosynthesis (DBT) and Full-Field Digital Mammography (FFDM) in a Hybrid Imaging Environment

Wednesday, Nov. 28 11:00AM - 11:10AM Room: E451A

Participants

Gunjan M. Senapati, MD, Boston, MA (*Presenter*) Nothing to Disclose Aijia Wang, Boston, MA (*Abstract Co-Author*) Nothing to Disclose Pragya A. Dang, MD, Boston, MA (*Abstract Co-Author*) Nothing to Disclose Sona A. Chikarmane, MD, Boston, MA (*Abstract Co-Author*) Nothing to Disclose Ivan Ip, MD, MPH, Brookline, MA (*Abstract Co-Author*) Nothing to Disclose Ronilda Lacson, MD, PhD, Brookline, MA (*Abstract Co-Author*) Nothing to Disclose Ramin Khorasani, MD, Boston, MA (*Abstract Co-Author*) Nothing to Disclose Catherine S. Giess, MD, Wellesley, MA (*Abstract Co-Author*) Nothing to Disclose

For information about this presentation, contact:

gsenapati@bwh.harvard.edu

PURPOSE

To review imaging features and histopathology of interval cancers (IC) on screening full-field digital mammography (FFDM) and screening digital breast tomosynthesis (DBT) in a hybrid imaging environment.

METHOD AND MATERIALS

This HIPAA-compliant IRB approved retrospective review of consecutive screening exams (9,828 DBT and 41,713 FFDM exams) from October 2012-September 2014 identified interval cancers by cross reference to the institutional cancer registry. Interval cancer was defined as cancer detected within 365 days of a negative screening exam. During the study period a hybrid imaging environment for screening existed, using both FFDM and DBT. Three breast radiologists reviewed prior mammograms of all IC in consensus. Cancers were classified as missed (actionable), minimal signs (non-actionable), or true negative. Mammographic lesion features and breast density were described. Electronic medical record review of patient demographics and histopathology was performed. Percentages were compared using Fisher's exact test.

RESULTS

There were 34 interval cancers (20 FFDM, 14 DBT). IC were considered missed, actionable in 2/20 (10%) FFDM and 2/14 (14%) DBT; minimal signs, non-actionable in 3/20 (15%) FFDM and 0/14 (0%) DBT, and true negative in 15/20 (75%) FFDM and 12/14 (86%) DBT (p-value = 0.4061). Of the 5 cancers visible (2 missed, 3 minimal signs) on prior FFDM, 3 were asymmetries, 1 calcifications, and 1 architectural distortion. Both cancers visible (both missed) on prior DBT were spiculated masses. Most IC on both FFDM and DBT were moderate-to-high grade invasive carcinoma (n=29): 17/20 (85%) FFDM and 12/14 (86%) DBT (p-value = 0.9999). 1 case of pure intermediate grade DCIS, presenting as nipple discharge, was missed on FFDM; the remaining four, 2 FFDM and 2 DBT, were grade 1 invasive carcinoma. Most IC were in Category 3 and 4 dense breasts (n=26): 15/20 (75%) FFDM and 11/14 (79%) DBT (p-value = 0.9999).

CONCLUSION

In this hybrid FFDM/DBT screening environment, most IC are mammographically occult at prior imaging, occur in dense breast tissue, and are moderate to high grade invasive cancers.

CLINICAL RELEVANCE/APPLICATION

Because FFDM and DBT techniques both rely on lesion morphology for detection, IC on each technique have similarities, occurring in dense tissue and with moderate to high grade invasive histopathology.

Honored Educators

Presenters or authors on this event have been recognized as RSNA Honored Educators for participating in multiple qualifying

educational activities. Honored Educators are invested in furthering the profession of radiology by delivering high-quality educational content in their field of study. Learn how you can become an honored educator by visiting the website at: https://www.rsna.org/Honored-Educator-Award/ Catherine S. Giess, MD - 2015 Honored EducatorCatherine S. Giess, MD - 2017 Honored Educator

SSK01-05 Evidence Supporting Digital Breast Tomosynthesis as Primary Mammographic Screening Tool: Sustained Improved Outcomes over 7 Consecutive Years

Wednesday, Nov. 28 11:10AM - 11:20AM Room: E451A

Participants

Liane E. Philpotts, MD, New Haven, CT (*Presenter*) Consultant, Hologic, Inc Tamara Y. Carroll, MD, Seattle, WA (*Abstract Co-Author*) Nothing to Disclose Madhavi Raghu, MD, New Haven, CT (*Abstract Co-Author*) Nothing to Disclose

For information about this presentation, contact:

liane.philpotts@yale.edu

PURPOSE

Digital breast tomosynthesis (DBT) has shown promise in multiple individual, multi-institutional and population based practices to improve screening metrics, particularly reduce recall rates and improve cancer detection. The sustainability of the early results has not yet been well demonstrated. Long term results are needed to demonstrate if the technology is the preferred screening tool compared with 2D full field digital mammography (FFDM). The purpose of this study was to assess screening metrics with DBT over a 7 year period.

METHOD AND MATERIALS

DBT screening (Dimensions, Hologic, Inc, Bedford, MA) was offered to all women free of charge at a dedicated academic breast center starting in August 2011 and 3 out-patient satellite offices that obtained DBT units in the following years. Over a 7 year period, 124,669 screening DBT exams were performed. Screening metrics were obtained from the breast imaging electronic database (PenRad, MN) and assessed by one-year intervals starting in August 2011. Recall rate (RR), Cancer detection rate (CRD), positive predictive value of screening recall (PPV1) and of biopsy (PPV3) were assessed. Comparison with historic 2D rates (8/1/08 though 7/31/11) were performed.

RESULTS

The RR was significantly reduced over 2D and showed a decreasing trend for each consecutive year: 7.9%, 8.8%, 7.8%, 7.5%, 6.9%, 6.7%, 6.2% (2D = 11.4) (p<0.0001). The CDR (per 1000) showed a stable trend that was statistically significantly improved over 2D: 5.8, 5.2, 5.4, 5.6, 6.6, 5.6, 5.1 (2D = 3.8)(p<.0001). The PPV1 showed a sustained significant improvement over 2D: 7.2, 5.8, 7.0, 7.5, 9.5, 8.4, 8.2 (2D=3.3) (p<.0001). The PPV3 also showed a striking significant increase over 2D and an upward trend over consecutive DBT years: 35%, 31%, 36%, 37%, 47%, 42%, 44% (2D=29%) (p<0.05).

CONCLUSION

Screening metrics with DBT over 7 years were sustainably significantly improved over 2D rates and further demonstrate favorable trends of improvement over time. This may reflect learning curve and/or increasing availability of prior comparison tomosynthesis exams.

CLINICAL RELEVANCE/APPLICATION

The sustained use of DBT demonstrates that there are fewer false positive screening recalls and biopsies which is essential for shifting the harms and benefits of screening.

SSK01-06 Impact of Using Digital Breast Tomosynthesis in Diagnostic Mammography

Wednesday, Nov. 28 11:20AM - 11:30AM Room: E451A

Participants

Emily Ambinder, MD, MSc, Baltimore, MD (*Presenter*) Nothing to Disclose Lisa A. Mullen, MD, Cockeysville, MD (*Abstract Co-Author*) Nothing to Disclose Delaram Shakoor, MD, Baltimore, MD (*Abstract Co-Author*) Nothing to Disclose Kelly Myers, MD, New York, NY (*Abstract Co-Author*) Nothing to Disclose Eniola T. Falomo, MD, Baltimore, MD (*Abstract Co-Author*) Nothing to Disclose Susan C. Harvey, MD, Lutherville, MD (*Abstract Co-Author*) Consultant, Hologic, Inc Consultant, IBM Corporation

For information about this presentation, contact:

emcinto8@jhmi.edu

PURPOSE

The use of digital breast tomosynthesis (DBT) in the screening setting has been shown to decrease recall rate and improve cancer detection. This study evaluates the impact of using DBT in the diagnostic setting at a large academic institution.

METHOD AND MATERIALS

All diagnostic mammograms performed from 7/1/2013 to 8/24/2017 were reviewed. Diagnostic mammograms performed to further evaluate calcifications were excluded, as spot magnification views, rather than DBT views, are typically used for diagnostic evaluation in these cases. Studies were divided into two groups: those performed with at least one DBT view and those performed with only full field digital mammography (FFDM). We compared the frequency of a negative/benign assessment (BI-RADS 1 or 2), a probably benign assessment (BI-RADS 3), and a suspicious or highly suspicious assessment (BI-RADS 4 or 5) between the two groups. We also compared positive predictive value 2 and cancer detection rate between the two groups. The Chi-squared test was used for statistical analysis.

12,324 studies were included in the DBT group and 11,775 studies were included in the FFDM group. There was a significantly higher percentage of BI-RADS 1 or 2 assessments (77.8% vs. 74.9%, p<0.001) and a significantly lower percentage of BI-RADS 3 assessments (10.6% vs. 12.9%, p<0.001) in the DBT group compared to the FFDM group. There was no significant change in the percentage of BI-RADS 4 or 5 assessments (biopsy recommendations) between the two groups (12.1% vs. 11.6%, p=0.20). Both PPV2 and CDR were significantly higher for studies performed with DBT compared to FFDM (PPV2: 36.1 vs. 26.6, p<0.001; CDR: 41.8 vs. 32.3, p<0.001).

CONCLUSION

In our study, using DBT in the diagnostic setting led to more studies being assessed as normal with less frequent need for shortterm follow-up, implying decreased associated cost of follow-up and decreased stress and anxiety for patients. While the number of biopsy recommendations was similar between the groups, PPV2 and CDR increased when DBT views were included, suggesting improved accuracy of biopsy recommendations.

CLINICAL RELEVANCE/APPLICATION

Routine use of digital breast tomosynthesis for diagnostic mammography may result in more confident assessments, and could lead to resource savings and improved patient-centered care.

SSK01-07 Architectural Distortion (AD) on Digital Breast Tomosynthesis (DBT): Outcomes, Histopathology, and Predictive Features of Malignancy

Wednesday, Nov. 28 11:30AM - 11:40AM Room: E451A

Participants

Sona A. Chikarmane, MD, Boston, MA (*Presenter*) Nothing to Disclose Christine M. Denison, MD, Boston, MA (*Abstract Co-Author*) Nothing to Disclose Gunjan M. Senapati, MD, Boston, MA (*Abstract Co-Author*) Nothing to Disclose Ronilda Lacson, MD, PhD, Brookline, MA (*Abstract Co-Author*) Nothing to Disclose Ramin Khorasani, MD, Boston, MA (*Abstract Co-Author*) Nothing to Disclose Catherine S. Giess, MD, Wellesley, MA (*Abstract Co-Author*) Nothing to Disclose

For information about this presentation, contact:

cdenison@bwh.harvard.edu

PURPOSE

1) To determine histopathologic outcomes for architectural distortion (AD) detected on tomoshynthesis (3D) mammography, (2) to investigate imaging features predictive of malignancy.

METHOD AND MATERIALS

A HIPAA-compliant IRB approved retrospective review of a mammography screening database between 12/2012-5/2015 identified 297 consecutive screening mammograms classified as BI-RADS 0 for AD. All breast imaging available for cases classified as BI-RADS 4 and 5 at diagnostic work-up were reviewed in consensus by 3 breast radiologists. Imaging features and biopsy accuracy were assessed. Medical records were reviewed for patient demographics, histopathology and follow-up imaging. Chi-square tests were performed with <0.05 significance.

RESULTS

Of 297 BI-RADS category 0 screening detected AD on DBT, 45 (15.2%) were subsequently categorized as BI-RADS category 4-5. Cases were excluded if the finding was a mass rather than AD alone (n=3) or if no pathology results were available (n=2). Within the study population of 40 cases, 20/40 (50%) were malignant (18/20 [90%] invasive, 2/20 [10%] ductal carcinoma in situ), 3/40 (7.5%) atypical ductal hyperplasia, and 17/40 (42.5%) benign. 31/40 (77.5%) cases of AD were visible on 3D only and 9/40 (22.5%) were seen on 2D and 3D. Malignancy was found in 15/31 (48.4%) 3D only AD and 5/9 (56%) AD visible on 2D and 3D (p=1.00). While presence of a sonographic correlate did not increase likelihood of malignancy (US correlate in 33 cases [17 benign, 16 malignant] and no US correlate in 7 cases [3 benign, 4 malignant] [p=1.00]), the specific finding of a mass was more likely malignant than non-mass findings (17 masses [4 benign, 13 malignant] and 16 non-mass [13 benign, 3 malignant] [p=0.0016]. Diagnostic MRI was performed in 7/40 (17.5%) cases, of which 3/7 (1 malignant, 2 benign) had a correlate for AD and 4/7 (0 malignant) did not.

CONCLUSION

The majority of AD cases in this series were seen on 3D only, although risk of malignancy for 3D only visible compared to 2D plus 3D visible was similar. AD is more likely to represent invasive disease than in situ and is more likely malignant if a sonographic mass is present. Given the high malignancy rate, negative US or breast MRI should not obviate the need for biopsy of mammographic detected AD.

CLINICAL RELEVANCE/APPLICATION

Given the high malignancy rate associated with AD detected on 3D mammography, lack of US or MRI correlate should not obviate biopsy.

Honored Educators

Presenters or authors on this event have been recognized as RSNA Honored Educators for participating in multiple qualifying educational activities. Honored Educators are invested in furthering the profession of radiology by delivering high-quality educational content in their field of study. Learn how you can become an honored educator by visiting the website at: https://www.rsna.org/Honored-Educator-Award/ Catherine S. Giess, MD - 2015 Honored EducatorCatherine S. Giess, MD - 2017 Honored Educator

SSK01-08 Evaluating the Clinical Performance of Stationary 3D Mammography

Wednesday, Nov. 28 11:40AM - 11:50AM Room: E451A

Awards

Student Travel Stipend Award

Participants Connor Puett, Chapel Hill, NC (*Presenter*) Nothing to Disclose Christy Inscoe, MS, BS, Chapel Hill, NC (*Abstract Co-Author*) Nothing to Disclose Beilin Jia, Chapel Hill, NC (*Abstract Co-Author*) Nothing to Disclose Connie E. Kim, MD, Durham, NC (*Abstract Co-Author*) Spouse, Consultant, ClarVista Medical, Inc Spouse, Royalties, Leica Biosystems Nussloch GmbH Spouse, Intellectual property, Leica Biosystems Nussloch GmbH Sora C. Yoon, MD, Durham, NC (*Abstract Co-Author*) Nothing to Disclose Ruth Walsh, MD, Durham, NC (*Abstract Co-Author*) Nothing to Disclose Suk Jung Kim, Seoul, Korea, Republic Of (*Abstract Co-Author*) Nothing to Disclose Cherie M. Kuzmiak, DO, Chapel Hill, NC (*Abstract Co-Author*) Research Grant, Delphinus Medical Technologies, Inc Donglin Zeng, PhD, Chapel Hill, NC (*Abstract Co-Author*) Nothing to Disclose Jianping Lu, Chapel Hill, NC (*Abstract Co-Author*) Board of Directors, XinRay Systems Inc Yueh Z. Lee, MD,PhD, Chapel Hill, NC (*Abstract Co-Author*) Board of Directors, XinRay Systems Inc

For information about this presentation, contact:

connor_puett@med.unc.edu

PURPOSE

The purpose of this study was to assess the clinical performance of *stationary* 3D mammography, which is a new approach to digital breast tomosynthesis that uses a fixed array of carbon nanotube-based x-ray sources to acquire the projection views.

METHOD AND MATERIALS

Women with a suspicious abnormality (BIRADS 4 lesion) identified by screening digital mammography were recruited for the study, which involved imaging by *stationary* 3D mammography prior to biopsy. Pre-clinical testing has demonstrated that *stationary* 3D mammography offers a higher spatial resolution than commercially-available 3D mammography devices, since it solves the problem of source blur. In this study, the *stationary* 3D mammography device collected 15 projections over an angular span of 28°. Four radiologists were asked to evaluate the likelihood of malignancy and rate breast density (BIRADS 1-4) when interpreting the standard mammography and *stationary* 3D mammography images. Using pathology as ground truth, reader performance was quantified as the area under the receiver operating characteristic curve (AUC), while multivariate analysis with a fitted linear mixed-effect model was used to relate breast density to reader performance.

RESULTS

43 women [average age: 56.7 (35 to 83) years] provided a lesion-enhanced image set, in which malignancy was found to be present in 28% of participants by pathology. On average, readers were more accurate identifying malignancy when interpreting the *stationary* 3D mammography images compared to the standard mammograms, as demonstrated by the significantly higher (p<0.0001) mean AUC for *stationary* 3D mammography. This higher accuracy was present and statistically-significant across the full range of breast densities.

CONCLUSION

In this first-in-human study, readers were more likely to identify malignancy correctly when interpreting *stationary* 3D mammography images compared to the standard digital mammogram. Given these encouraging findings, as well as the results of pre-clinical testing, future trials are being designed to compare the performance of *stationary* 3D mammography to commercially-available 3D mammography devices in the clinic.

CLINICAL RELEVANCE/APPLICATION

Stationary 3D mammography may prove to be a valuable clinical tool, as readers were more accurate identifying malignancy when interpreting its images compared to the standard digital mammogram.

SSK01-09 Molecular Characterization of Breast Cancers: Could It Change Potential Overdiagnosis Analysis?

Wednesday, Nov. 28 11:50AM - 12:00PM Room: E451A

Participants

Francesca Caumo, MD, Padua, Italy (*Presenter*) Nothing to Disclose Gisella Gennaro, PhD, Padua, Italy (*Abstract Co-Author*) Nothing to Disclose Giovanna Romanucci, Verona, Italy (*Abstract Co-Author*) Nothing to Disclose Marco Zappa, Firenze, Italy (*Abstract Co-Author*) Nothing to Disclose

PURPOSE

To compare the amount of potentially overdiagnosed breast cancers in two screening populations using tomosynthesis (DBT) and digital mammography (FFDM) considering only tumor stage or also molecular features.

METHOD AND MATERIALS

Cancers detected within a prospective screening trials using DBT were compared with those obtained from an historical FFDM screening cohort. The amount of potentially overdiagnosed breast cancers in the two cohorts was calculated according to two different assumptions: (1) stages 0 and 1 cancers (DCIS, IDCs, ILCs); (2) considering low-grade DCIS and IDCs/ILCs that are simultaneously grade 1, stage IA or IB, luminal A subtype. Rates (Fisher exact test) were used to compare the two hypotheses of potential overdiagnosis. A p-value lower than 0.05 was considered statistically significant. The same analysis was performed on the complementary subgroups for the two hypotheses: (1) stage > 1 tumors; (2) any other combination of features with the exception of that defined with the second assumption.

RESULTS

Cancers detected in the two screening populations was 322 from the DBT trial and 153 from the FFDM cohort. Considering only tumor stage, cancers potentially overdiagnosed were 268 with DBT and 116 with FFDM, equivalent to 83.2% and 75.8%, respectively. Comparing rates, DBT found 7.9/1000 stage 0/1 cancers vs. 4.0/1000 found by FFDM (P<0.0001), with an incidence rate ratio (IRR) equal to 1.99 (95%CI = [1.60-2.50]. Rates of cancers with stage >1 were 1.6/1000 with DBT vs. 1.3/1000 with FFDM, not significantly different (P=0.2817); the IRR was 1.26 (95%CI = [0.81-1.97]). Including in the definition of potentially overdiagnosed cancers also molecular features, the numbers become 61/322 (18.9%) with DBT and 13/153 (8.5%) with FFDM; rates of overdiagnosed cancers with the second assumption were 1.8/1000 with DBT and 0.4/1000 with FFDM (P<0.0001) corresponding to an IRR of 4.04 (95%CI = [2.20-8.02]). Rates of any other cancers (not overdiagnosed) were 7.7/1000 with DBT vs. 4.8/1000 with FFDM (P<0.0001), with an IRR of 1.61 [95%CI = [1.30-1.99]].

CONCLUSION

DBT increased the amount of potentially overdiagnosed cancers with both definitions. However, the second assumption (inclusion of stage, grade, and molecular features) showed that cancers detected by DBT were mostly not overdiagnosed.

CLINICAL RELEVANCE/APPLICATION

Overdiagnosis by DBT is overestimated using only cancer stage as metric for overdiagnosis.



SSK02

Breast Imaging (Artificial Intelligence)

Wednesday, Nov. 28 10:30AM - 12:00PM Room: E451B



AMA PRA Category 1 Credits ™: 1.50 ARRT Category A+ Credit: 1.75

FDA Discussions may include off-label uses.

Participants

Despina Kontos, PhD, Philadelphia, PA (*Moderator*) Nothing to Disclose

Maryellen L. Giger, PhD, Chicago, IL (*Moderator*) Stockholder, Hologic, Inc; Shareholder, Quantitative Insights, Inc; Shareholder, QView Medical, Inc; Co-founder, Quantitative Insights, Inc; Royalties, Hologic, Inc; Royalties, General Electric Company; Royalties, MEDIAN Technologies; Royalties, Riverain Technologies, LLC; Royalties, Mitsubishi Corporation; Royalties, Canon Medical Systems Corporation

Sub-Events

SSK02-01 Using Deep Convolutional Neural Networks to Predict Readers' Estimates of Mammographic Density from Raw and Processed Mammographic Images

Participants

Georgia Ionescu, Manchester, United Kingdom (*Abstract Co-Author*) Nothing to Disclose Martin Fergie, Manchester, United Kingdom (*Abstract Co-Author*) Nothing to Disclose Michael Berks, Manchester, United Kingdom (*Abstract Co-Author*) Nothing to Disclose Elaine Harkness, PhD, Manchester, United Kingdom (*Abstract Co-Author*) Nothing to Disclose Johan Hulleman, Manchester, United Kingdom (*Abstract Co-Author*) Nothing to Disclose Adam Brentnall, London, United Kingdom (*Abstract Co-Author*) Nothing to Disclose Jack Cuzick, London, United Kingdom (*Abstract Co-Author*) Nothing to Disclose Gareth Evans, Manchester, United Kingdom (*Abstract Co-Author*) Nothing to Disclose Susan M. Astley, PhD, Manchester, United Kingdom (*Presenter*) Nothing to Disclose

PURPOSE

Mean percentage density assessed visually by two independent readers using Visual Analogue Scales (VAS) has a strong association with breast cancer risk, but is resource-intensive and impractical for stratified screening. We describe a fully-automated method for predicting this mammographic percent density measure from raw (for processing) or processed (for presentation) mammograms, and compare association of predicted VAS score with risk.

METHOD AND MATERIALS

Convolutional Neural Networks (CNNs) were trained using 67520 whole-image mammograms from 16968 women, each labelled with the average VAS score of two independent readers. The networks learned a mapping between mammographic appearance and mammographic density so that they can predict density for unseen images. To evaluate its use for risk assessment, we tested on case-control datasets of contralateral mammograms of screen detected cancers (SDC) and prior screening mammograms of women with cancers detected subsequently. Each cancer was matched to three controls on age, menopausal status, parity, HRT and BMI. The test datasets contained 366 cancers (SDC) and 338 (priors). Odds ratios between the top and bottom quintile were derived, and matched concordance indices were estimated. All images were acquired on GE Senographe systems, and none of the images from the case-control test sets were used in the training process.

RESULTS

For density estimates derived from raw images, odds ratios of cancer in the highest vs lowest quintile were 3.07 (95%CI: 1.97 - 4.77) for SDC and 3.52 (2.22 - 5.58) for priors, with matched concordance indices of 0.59 (0.55 - 0.64) and 0.61 (0.58 - 0.65) respectively. For processed images we obtained odds ratios of 3.22 (2.06 - 5.03) for SDC and 3.65 (2.27 - 5.88) for priors. Matched concordance indices were 0.58 (0.53 - 0.62) for SDC and 0.61 (0.57 - 0.65) for priors.

CONCLUSION

Our fully automated method demonstrated encouraging results on both raw and processed mammographic images, indicating that either image type could be used for screening stratification.

CLINICAL RELEVANCE/APPLICATION

Mammographic density is one of the most important risk factors for breast cancer. Our fully automated method could provide a pragmatic solution for population-based stratified screening.

SSK02-02 Breast Density Classification with Deep Convolutional Neural (DCN) Networks Utilizing 200,000 Screening Mammograms

Wednesday, Nov. 28 10:40AM - 10:50AM Room: E451B

Krzysztof J. Geras, New York City, NY (*Abstract Co-Author*) Nothing to Disclose Eric Kim, MD, New York, NY (*Presenter*) Nothing to Disclose Nan Wu, New York City, NY (*Abstract Co-Author*) Nothing to Disclose Yiqiu Shen, New York City, NY (*Abstract Co-Author*) Nothing to Disclose Jingyi Su, New York City, NY (*Abstract Co-Author*) Nothing to Disclose Sungheon Kim, PhD, New York, NY (*Abstract Co-Author*) Nothing to Disclose Stacey Wolfson, New York, NY (*Abstract Co-Author*) Nothing to Disclose Linda Moy, MD, New York, NY (*Abstract Co-Author*) Nothing to Disclose Kyunghyun Cho, New York City, NY (*Abstract Co-Author*) Nothing to Disclose

For information about this presentation, contact:

kime18@nyumc.org

PURPOSE

To develop a DCN network to reliably assess mammographic breast density

METHOD AND MATERIALS

In this retrospective study, we trained a multi-column DCN network on 200,000 digital screening mammograms performed at our institution from 2010-2016 to assess breast density. We extracted the textual reports associated with each exam to obtain the breast density as determined by the original interpreting radiologist. The algorithm was trained on 80% of the data sets, validated on a separate 10%, and tested on the remaining 10%. Once this convolutional neural network classifier was trained, we performed a reader study comparing our model to 3 radiologists. All readers independently evaluated the breast density in 100 mammograms in a randomized order. Breast density was assessed using the conventional BI-RADS categories: Class 0 - fatty, Class 1 - scattered fibroglandular densities, Class 2 - heterogeneously dense, and Class 3 - extremely dense. Performance of the model and the readers were assessed using the area under the ROC curve (AUC). Kappa score was used to assess for intra-observer and inter-observer variability.

RESULTS

Both the radiologists and our DCN model achieved a fair agreement (k = 0.34 - 0.51) with the labels in the reader study. The agreement between the predictions of our model and the labels in the data were higher (k = 0.65 - 0.72) compared to the interobserver agreement between the radiologists. There was higher agreement for the fatty and extremely dense breast tissue. Comparing our CNN model to an average of the radiologists, the CNN achieved AUC of 0.934 (class 0: 0.971, class 1: 0.859, class 2: 0.905 and class 3: 1.000) while the radiologists achieved an AUC of 0.892 (class 0: 0.960, class 1: 0.812, class 2: 0.807 and class 3: 0.990) (Figure 1).

CONCLUSION

The level of agreement between the trained classifier and the classes in the data was found to be similar to that between the radiologists and the classes in the data, as well as among the radiologists.

CLINICAL RELEVANCE/APPLICATION

The classifier provides quantitative, reproducible prediction of breast density, while there is often poor intra-reader and inter-reader correlation in the qualitative assessment of breast density.

SSK02-03 Improving Radiologists' Breast Cancer Detection with Mammography Using a Deep Learning-Based Computer System for Decision Support

Wednesday, Nov. 28 10:50AM - 11:00AM Room: E451B

Participants

Alejandro Rodriguez-Ruiz, Nijmegen, Netherlands (*Abstract Co-Author*) Nothing to Disclose Elizabeth A. Krupinski, PhD, Atlanta, GA (*Abstract Co-Author*) Nothing to Disclose Jan-Jurre Mordang, MSc, Nijmegen, Netherlands (*Abstract Co-Author*) Nothing to Disclose Kathy J. Schilling Colletta, MD, Boca Raton, FL (*Abstract Co-Author*) Nothing to Disclose Sylvia H. Heywang-Koebrunner, MD, Munich, Germany (*Abstract Co-Author*) Nothing to Disclose Ioannis Sechopoulos, PhD, Atlanta, GA (*Abstract Co-Author*) Research Grant, Siemens AG; Research Grant, Canon Medical Systems Corporation; Speakers Bureau, Siemens AG; Scientific Advisory Board, Fischer Medical Ritse M. Mann, MD, PhD, Nijmegen, Netherlands (*Presenter*) Researcher, Siemens AG; Researcher, Seno Medical Instruments, Inc; Researcher, Identification Solutions, Inc; Researcher, Micrima Limited; Researcher, Medtronic plc; Scientific Advisor, ScreenPoint Medical BV; Scientific Advisor, Transonic Imaging, Inc; Stockholder, Transonic Imaging, Inc

For information about this presentation, contact:

ritse.mann@radboudumc.nl

PURPOSE

To compare the breast cancer detection performance of radiologists reading mammography exams unaided versus reading using an interactive deep learning-based computer system for decision support (DS).

METHOD AND MATERIALS

A retrospective, fully-crossed (two sessions >4 weeks apart), multi-reader multi-case (MRMC) study was performed. 240 cases (100 cancers, 40 false positive recalls, 100 normals) were scored by 14 MQSA-qualified radiologists, once with and once without using DS. For each case, a forced BI-RADS® score and a level of suspicion (1-100) were provided. When reading with the DS system (Transpara, Screenpoint Medical, Nijmegen, The Netherlands), radiologists could activate the DS for a specific breast region by clicking on it and the system then displayed a cancer likelihood score (1-100). Additionally, traditional computer-aided detection was available to prompt calcification and soft tissue lesion markers. Area under the receiver operating characteristic curve (AUC), specificity and sensitivity, and reading time were compared using MRMC Analysis of Variance.

On average, with the DS system, the AUC increased significantly from 0.866 to 0.886 (P=0.0019) compared to unaided reading. Sensitivity increased from 83% to 86% (P=0.046), while specificity only slightly improved from 77% to 79% (P=0.061). Considering lesion type, AUC increased for soft tissue lesions (0.886 to 0.902, P=0.033), and calcifications (0.878 to 0.898, not significant, P=0.1021). Reading time per case was similar in both situations (unaided = 146 s, with DS = 149 s, P=0.147). As a stand-alone, the computer system had an equal detection performance (AUC=0.887) than the average of radiologists (P=0.333).

CONCLUSION

Radiologists significantly improved their cancer detection in mammography when using a deep learning-based computer system for decision support without taking more time.

CLINICAL RELEVANCE/APPLICATION

The use of decision support might prevent overlook and interpretation errors that are relatively common in the reading of mammography. The increase in performance when concurrently using DS does not lengthen radiologists reading time per case, as opposed to traditional computer-aided detection systems. The use of single-reading in combination with the computer system might achieve a performance similar to double human reading considering that the stand-alone performance of the system is similar to the average of radiologists.

Honored Educators

Presenters or authors on this event have been recognized as RSNA Honored Educators for participating in multiple qualifying educational activities. Honored Educators are invested in furthering the profession of radiology by delivering high-quality educational content in their field of study. Learn how you can become an honored educator by visiting the website at: https://www.rsna.org/Honored-Educator-Award/ Elizabeth A. Krupinski, PhD - 2017 Honored Educator

SSK02-04 Data-Driven Imaging Biomarker for Breast Cancer Screening in Mammography-Reader Study

Wednesday, Nov. 28 11:00AM - 11:10AM Room: E451B

Participants

Eun-Kyung Kim, MD, Seoul, Korea, Republic Of (*Abstract Co-Author*) Nothing to Disclose Hyo-Eun Kim, Seoul, Korea, Republic Of (*Abstract Co-Author*) Employee, Lunit Inc Hak Hee Kim, MD, Seoul, Korea, Republic Of (*Abstract Co-Author*) Nothing to Disclose Boo-Kyung Han, MD, PhD, Seoul, Korea, Republic Of (*Abstract Co-Author*) Nothing to Disclose Jung Yin Huh, MD, Seoul, Korea, Republic Of (*Presenter*) employee, Lunit Inc. Kyunghwa Han, PhD, Seoul, Korea, Republic Of (*Abstract Co-Author*) Nothing to Disclose

For information about this presentation, contact:

ekkim@yuhs.ac

PURPOSE

Previously, we demonstrated data-driven imaging biomarker in mammography (DIB-MMG; an imaging biomarker that is derived from large-scale mammography data by using deep learning technology) for detection of malignant lesions. Now, we assess the feasibility of DIB-MMG as a diagnosis-support-tool for radiologists.

METHOD AND MATERIALS

Total 96,191 exams of 4-view digital mammograms were retrospectively collected from two institutions. All cancer exams were proven by biopsy. Benign exams were proven by biopsy or at least 1 year of follow-up mammography, and normal exams were proven by at least 1 year of follow-up mammography. 90,637 exams of training data (16,086 cancer, 31,237 benign, and 43,314 normal exams) and 5,554 exams of test data (1,692 cancer, 2,780 benign, 1,082 normal cases) were used for developing the DIB-MMG. Sensitivity, specificity, and AUC of the final DIB-MMG on the test data were 82.6%, 93.3%, and 0.94, respectively. Total 120 exams of mammograms (38 cancer and 82 non-cancer exams) were independently collected for reader study, and five radiologists participated. For each exam, readers first read the exam without the help of DIB-MMG and Task-1) annotate the most suspicious lesion with DMIST 7-pt scores and Task-2) decide recall or not per breast. After reading of each exam, readers modify their decision based on the heat-map of DIB-MMG which denotes the likelihood of malignancy.

RESULTS

Per-breast standalone performance of DIB-MMG for 120 exams was 0.942 of AUC in Task-1, and 89.7% of sensitivity, 89.6% of specificity in Task-2. Average performance of five radiologists without DIB-MMG was 0.807 of AUC in Task-1, and 70.8% of sensitivity, 86.2% of specificity in Task-2. With DIB-MMG, the average performance was improved to 0.879 of AUC (p=0.024) in Task-1, and 79.5% of sensitivity, 86.5% of specificity in Task-2. Fig.1 shows exemplary DIB-MMG heat-maps.

CONCLUSION

This retrospective reader study showed the potential of DIB-MMG as a diagnosis support tool for radiologists in breast cancer screening. Further clinical validation with prospective study is needed.

CLINICAL RELEVANCE/APPLICATION

DIB-MMG is purely based on data-driven features from a large-scale mammography data instead of manually designed features of conventional computer-aided detection (CAD) algorithms. With further clinical validation, DIB-MMG can be practically used as a diagnosis support tool for radiologists in breast cancer screening.

SSK02-05 Generative Neural Network Inserting or Removing Cancer into Mammograms Fools Radiologists and Deep Learning Alike: Example of an Adversarial Attack

Wednesday, Nov. 28 11:10AM - 11:20AM Room: E451B

Participants Anton S. Becker, MD, Zurich, Switzerland (*Presenter*) Nothing to Disclose Lukas Jendele, Oberengstringen, Switzerland (*Abstract Co-Author*) Nothing to Disclose Ondrej Skopek, Oberengstringen, Switzerland (*Abstract Co-Author*) Nothing to Disclose Soleen Ghafoor, MD, Zurich, Switzerland (*Abstract Co-Author*) Nothing to Disclose Nicole Berger, MD, Zurich, Switzerland (*Abstract Co-Author*) Nothing to Disclose Magda Marcon, MD, Zurich, Switzerland (*Abstract Co-Author*) Nothing to Disclose Ender Konukoglu, Sophia Antipolis, France (*Abstract Co-Author*) Nothing to Disclose

For information about this presentation, contact:

anton@becker.md

PURPOSE

To investigate whether a cycle-consistent generative adversarial network (CycleGAN) can insert or remove cancer-specific features into mammographic images in a realistic fashion.

METHOD AND MATERIALS

From two publicly available datasets (BCDR and INbreast) 680 mammographic images from 334 patients were selected, 318 of which exhibited potentially cancerous masses, and 362 were healthy controls. We trained a CycleGAN, using two pairs of generator and discriminator networks to convert cancerous breast images to healthy and back, and vice versa for the controls, without the need for paired images. The network, implemented in TensorFlow, was trained for 40 epochs on an augmented dataset enlarged ten-fold by random rotation, scaling, and contrast perturbations. To investigate how realistic the images appear, we randomly selected 20 image pairs of original and generated images, and 10 single images of each category (60 images in total). The images were presented to three radiologists (5 and 3 years of experience, and PGY-5 resident) who rated them on a 5-point Likert-like scale and had to indicate whether the image was real or generated/modified. The readout was analysed with a receiver-operating-characteristics (ROC) analysis, performance was expressed as area under the ROC curve (AUC).

RESULTS

For the most experienced radiologist, the modifications introduced by CycleGAN reduced diagnostic performance, with the AUC dropping from 0.85 to 0.63 (p=0.06), respectively, while the two less experienced ones seemed unaffected at a lower baseline performance (AUC 0.75 vs. 0.77 and 0.67 vs. 0.69). None of the radiologists could reliably detect which images were real and which were modified by CycleGAN (AUC 0.50-0.66).

CONCLUSION

CycleGAN can inject or remove malignant features into mammographic images while retaining their realistic appearance. These artificial modifications may lead to false diagnoses.

CLINICAL RELEVANCE/APPLICATION

Modern adversarial attacks may go undetected by humans as well as deep learning algorithms, and could be used in cyber warfare. It is vital to secure healthcare devices and information systems against such attacks mediated by neural networks.

SSK02-06 Deep Learning for Detection of Breast Cancer and Negative Screening Exams Using an In-House Million Mammogram Dataset

Wednesday, Nov. 28 11:20AM - 11:30AM Room: E451B

Participants

Hari Trivedi, MD, San Francisco, CA (*Presenter*) Nothing to Disclose Peter Chang, MD, San Francisco, CA (*Abstract Co-Author*) Nothing to Disclose Dmytro Lituiev, San Francisco, CA (*Abstract Co-Author*) Nothing to Disclose April Liang, San Francisco, CA (*Abstract Co-Author*) Nothing to Disclose Maryam Panahiazar, San Francisco, CA (*Abstract Co-Author*) Nothing to Disclose Jae Ho Sohn, MD, San Francisco, CA (*Abstract Co-Author*) Nothing to Disclose Yunn-Yi Chen, MD, San Francisco, CA (*Abstract Co-Author*) Nothing to Disclose Benjamin L. Franc, MD, Sacramento, CA (*Abstract Co-Author*) Nothing to Disclose Bonnie N. Joe, MD, PhD, San Francisco, CA (*Abstract Co-Author*) Nothing to Disclose Dexter Hadley, San Francisco, CA (*Abstract Co-Author*) Nothing to Disclose

For information about this presentation, contact:

hari.trivedi@gmail.com

PURPOSE

Breast cancer is the second leading cause of cancer death in women in the US. Screening mammography is effective for early detection, however suffers from unnecessary recall imaging and biopsies. Deep learning shows promise in medical image recognition tasks, but requires large-scale, robustly-annotated datasets. We expand upon our previously described end-to-end process of constructing a million mammogram dataset using routine clinical data and present results of two preliminary deep learning models for cancer detection and the identification of true negative images.

METHOD AND MATERIALS

923,685 DICOM images and 37,730 free-text pathology reports were used to generate an in-house database labeled with groundtruth pathology results. The first deep learning model was created for cancer detection only in biopsy proven specimens - the most difficult subset of data as each image contained a suspicious finding. The model was comprised of two components: patch-based pre-training and end-to-end fine tuning. Training set size was 34,390 images (12,251 positive, 22,139 negative), and test set size was 6,778 images equally split. The second model was designed to have a high NPV for screening and diagnostic studies. An attention-based object detection network was used, with potential abnormalities identified by a region-proposal network and resolved by a separate head classifier network. The model was trained with 359,574 images (4,738 positive, 354,837 negative).

RESULTS

The first model achieved an AUC of 0.81, sensitivity of 0.764, and specificity of 0.797. The second model when tested on 100 positive and 100 negative cases achieved an AUC of 0.90, sensitivity of .866, and specificity of .873. If the test cases were

changed to a more clinically relevant distribution of 99% benign and 1% cancer, the AUC increased to 0.96.

CONCLUSION

We demonstrate the efficacy of deep learning for mammography in both cancer detection and the identification of negative studies. Future work includes enrichment of the dataset with further clinical data such as history of breast cancer, prior surgeries, and hormone replacement therapy. We also aim to improve model performance and efficiency through novel model architectures.

CLINICAL RELEVANCE/APPLICATION

We develop novel deep learning models for mammography using routine clinical data from a single institution with the potential to decrease recall imaging and unnecessary biopsies.

SSK02-07 Improved Cancer Detection using Artificial Intelligence: A Retrospective Evaluation of Missed Cancers on Mammography

Wednesday, Nov. 28 11:30AM - 11:40AM Room: E451B

Participants

Alyssa T. Watanabe, MD, Manhattan Beach, CA (*Presenter*) Consultant, CureMetrix, Inc Vivian Lim, MD, La Jolla, CA (*Abstract Co-Author*) Consultant, CureMetrix, Inc Jenna I. Liu, MD, La Jolla, CA (*Abstract Co-Author*) Consultant, Curemetrix, Inc Eric Weise, La Jolla, CA (*Abstract Co-Author*) Software developer, CureMetrix, Inc; Chi Yung Chim, La Jolla, CA (*Abstract Co-Author*) Researcher, CureMetrix, Inc William G. Bradley JR, MD, PhD, La Jolla, CA (*Abstract Co-Author*) Officer, CureMetrix, Inc Christopher E. Comstock, MD, New York, NY (*Abstract Co-Author*) Nothing to Disclose

For information about this presentation, contact:

alyssa90266@gmail.com

PURPOSE

To determine whether artificial intelligence-based (AI) software can be used to improve radiologists' sensitivity in breast cancer screening and detection.

METHOD AND MATERIALS

A set of 2-D Digital Mammograms originally interpreted with R2 ImageChecker CAD (Hologic, Sunnyvale, CA) and performed between October 2011 to March 2017 was collected from a community facility. Of the 317 cancer patients with available prior mammograms, 139 had retrospective findings, and 90 of those were deemed actionable. A blinded retrospective study was performed with a panel of seven radiologists comprised of false negative actionable mammograms obtained up to 5.8 years prior to diagnosis and 32 normal studies. Each radiologist viewed the cases without and then with benefit of cmAssist TM (CureMetrix, La Jolla, CA) AI based computer-aided detection (AI-CAD) flags and neuScore TM (quantitative AI-based probability for malignancy of flagged lesions, 1-100 scale). Reader decision making changes in true and false positive recalls with and without AI were analyzed.

RESULTS

All radiologists showed a significant improvement in their cancer detection rate (CDR) with the use of AI-CAD and neuScore (p =0.0069, C.I. = 95%). With the assistance of AI software, the sensitivity of less experienced general radiologists improved to a level higher than a fellowship-trained academic mammographer. The readers detected between 25% and 71% (mean 51%) of the early cancers without assistance. With AI software results,, overall reader CDR was 41% to 76% (mean 62%). Overall, there was less than 1% increase in the readers' false positive recalls with use of the AI software.

CONCLUSION

There was a statistically significant improvement in radiologists' sensitivity for cancer detection in this enriched data set of primarily false negative mammograms with the benefit of the AI-CAD with neuScore. The percentage increase in CDR for the radiologists in the reader panel, ranged from 6% to 64% (mean 27%) with the use of AI-CAD, with negligible increase in false positive recalls.

CLINICAL RELEVANCE/APPLICATION

This study shows a measurable, significant benefit for radiologists in mammography interpretation with the use of artificial intelligence (AI) based computer-aided detection software with quantitative scoring. The use of AI in clinical practice may potentially expedite workflow, enhance earlier detection of cancer, and reduce false negative mammograms.

SSK02-08 Data-Driven Imaging Biomarker for Breast Cancer Screening in Digital Breast Tomosynthesis

Wednesday, Nov. 28 11:40AM - 11:50AM Room: E451B

Participants

Sungwon Kim, MD, Seoul, Korea, Republic Of (*Presenter*) Nothing to Disclose Hyo-Eun Kim, Seoul, Korea, Republic Of (*Abstract Co-Author*) Employee, Lunit Inc Jin Chung, MD, Seoul, Korea, Republic Of (*Abstract Co-Author*) Nothing to Disclose Jee Eun Lee, MD, Seoul, Korea, Republic Of (*Abstract Co-Author*) Nothing to Disclose Minsung Kim, MD, Seoul, Korea, Republic Of (*Abstract Co-Author*) Nothing to Disclose Eun-Kyung Kim, MD, Seoul, Korea, Republic Of (*Abstract Co-Author*) Employee, Lunit Inc

For information about this presentation, contact:

dinbe@yuhs.ac

PURPOSE

To assess feasibility of a data-driven imaging biomarker in digital breast tomosynthesis (DIB-DBT) using the deep learning technology and evaluate its potential for detection of breast cancer.

METHOD AND MATERIALS

We retrospectively collected 49,577 exams of 4-view digital mammograms (MMG) and 1,196 exams of 4-view digital breast tomosynthesis images (DBT) from a single institution. We also collected 41 (10 cancer, 16 benign, 15 normal) exams of 4-view DBT retrospectively from another institution for external validation. 49,577 exams of MMG consists of 47,719 (5,599 cancer, 17,971 benign, and 24,149 normal) and independent 1,858 (619 cancer, 620 benign, 619 normal) exams of training and validation data, respectively. 1,196 exams of DBT consists of 996 (822 cancer, 40 benign, 134 normal) and independent 200 (120 cancer, 30 benign, 50 normal) exams of training and validation data, respectively. Previously, we assessed the feasibility of DIB-MMG as a screening tool for breast cancer detection in mammograms through external validation and pilot reader study. Thus, we exploit DIB-MMG for developing DIB-DBT in this study. Training of DIB-DBT consists of two stages - semi-supervised pre-training with partially-annotated large-scale MMG followed by fully-supervised fine-tuning with fully-annotated small-scale DBT. Residual network for image recognition is used as a baseline model. Diagnostic accuracy of DIB-DBT was assessed using receiver operating characteristic analysis.

RESULTS

Area under the curve (AUC) on the internal validation dataset of DIB-DBT with and without the pre-training stage of DIB-MMG was 0.9227 and 0.9081, respectively. AUC of the external validation dataset of DIB-DBT with and without the pre-training stage of DIB-MMG was 0.9710 and 0.9232, respectively.

CONCLUSION

This study showed the feasibility of DIB-DBT as a screening tool for breast cancer detection in DBT. This research also showed the potential of DIB-MMG as a base model for DIB-DBT. Further clinical validation of DIB-DBT is needed for using it as a reliable screening tool for breast cancer screening.

CLINICAL RELEVANCE/APPLICATION

With further clinical validation, DIB-DBT could be practically used as a second-reader to help radiologists detecting and diagnosing breast cancer in DBT efficiently.

SSK02-09 Improved Performance of Machine Learning-Based Analysis of Mammography by Using Digital Breast Tomosynthesis Versus 2D Mammography

Wednesday, Nov. 28 11:50AM - 12:00PM Room: E451B

Participants

Bill Lotter, Boston, MA (Abstract Co-Author) Officer, DeepHealth Inc

Jerrold L. Boxerman, MD, PhD, Providence, RI (Abstract Co-Author) Nothing to Disclose

A. Gregory Sorensen, MD, Belmont, MA (*Presenter*) Employee, DeepHealth, Inc; Board member, IMRIS Inc; Board member, Siemens AG; Board member, Fusion Healthcare Staffing; Board member, DFB Healthcare Acquisitions, Inc; Board member, inviCRO, LLC;

For information about this presentation, contact:

sorensen@deep.health

PURPOSE

Digital Breast Tomosynthesis (DBT) has been shown to be clinically superior to both full-field digital mammography and synthetic two-dimensional mammography (2D) for breast cancer detection. However, few studies to date have compared machine learning (ML) algorithmic performance in DBT versus 2D in large data sets. Technically, the much larger size of a DBT acquisition could actually be a hindrance for training convolutional neural networks (CNNs), for example via overfitting. Such technical issues could in turn imply impracticality of ML for DBT or a need for much larger training datasets. We sought to implement CNNs for both DBT and synthetic 2D X-ray mammograms and compare their performance.

METHOD AND MATERIALS

We compiled two separate datasets consisting of de-identified images and linked reports, collected from multiple mammography centers following an IRB-approved protocol. Data originated from equipment from the same manufacturer across all sites, and included presentation DBT and synthetic 2D images. We developed a novel CNN architecture and trained this model on the first dataset consisting of 22,000 DBT studies (323 cases of confirmed malignancy), where radiology reports and MQSA outcome data were used as estimates of ground truth. To simulate a more realistic evaluation scenario, the CNN was then tested on the second dataset collected from a different center. Using a test set of 1,750 screening DBT studies (94 confirmed cancers), receiver operating characteristic (ROC) curves and the corresponding area-under-the-curve (AUC) were calculated on both the full DBT study, and on just the synthetic 2D data alone.

RESULTS

AUC values for performance on the test dataset were: 2D: 0.894. DBT: 0.915. (p < 0.01 for difference between 2D and DBT on the full test dataset). At typical operating points (sensitivity 0.75 to 0.90) this corresponds to an average 19.6% relative decrease in model callback rates for the model (e.g., at sensitivity=0.8, from ~15% to ~11%).

CONCLUSION

ML can be applied successfully to DBT and results in improved performance over synthetic 2D mammography.

CLINICAL RELEVANCE/APPLICATION

Machine learning could play an important role in screening mammography, not only for traditional 2D mammography, but also when used with DBT; thus, ML is not in conflict with DBT but complementary and could further improve breast cancer screening performance.



SSK03

Cardiac (CT, MRI and PET: General Topics)

Wednesday, Nov. 28 10:30AM - 12:00PM Room: S102CD



AMA PRA Category 1 Credits ™: 1.50 ARRT Category A+ Credit: 1.75

FDA Discussions may include off-label uses.

Participants

Satinder P. Singh, MD, Birmingham, AL (*Moderator*) Nothing to Disclose Jens Bremerich, MD, Basel, Switzerland (*Moderator*) Nothing to Disclose Jadranka Stojanovska, MD, Ann Arbor, MI (*Moderator*) Nothing to Disclose

Sub-Events

SSK03-01 Predictive Value of Cardiac CT, Cardiac MR, and Transthoracic Echocardiography for Cardioembolic Stroke Recurrence

Participants

Simon S. Martin, MD, Frankfurt, Germany (*Presenter*) Nothing to Disclose Francesco Lavra, MD, Cagliari, Italy (*Abstract Co-Author*) Nothing to Disclose Carlo N. De Cecco, MD, PhD, Atlanta, GA (*Abstract Co-Author*) Research Grant, Siemens AG Akos Varga-Szemes, MD, PhD, Charleston, SC (*Abstract Co-Author*) Research Grant, Siemens AG Luca Saba, MD, Cagliari, Italy (*Abstract Co-Author*) Nothing to Disclose U. Joseph Schoepf, MD, Charleston, SC (*Abstract Co-Author*) Research Grant, Astellas Group; Research Grant, Bayer AG; Research Grant, Siemens AG; Research support, Bayer AG; Consultant, Guerbet SA; Consultant, General Electric Company; Consultant, HeartFlow, Inc; Consultant, Bayer AG; Consultant, Siemens AG; ; ; Marly van Assen, MSc, Charleston, SC (*Abstract Co-Author*) Nothing to Disclose Brian E. Jacobs, BS, Charleston, SC (*Abstract Co-Author*) Nothing to Disclose Marco Scarabello, MD, Milan, Italy (*Abstract Co-Author*) Nothing to Disclose Parkwood Griffith, Charleston, SC (*Abstract Co-Author*) Nothing to Disclose Marwen Eid, MD, Charleston, SC (*Abstract Co-Author*) Nothing to Disclose

For information about this presentation, contact:

schoepf@musc.edu

PURPOSE

To determine the sensitivity, specificity, and predictive value of cardiac CT angiography (cCTA), cardiac MR (CMR), and transthoracic echocardiography (TTE) for stroke recurrence in patients with suspected cardioembolic stroke.

METHOD AND MATERIALS

163 patients (55% men, 61.9±16.9 years) with suspected cardioembolic stroke who underwent TTE, CMR, or cCTA between January 2013 and May 2017 were retrospectively analyzed. The presence of left atrial thrombus, left ventricular thrombus, complex aortic plaque, cardiac tumors, and valvular vegetation was evaluated. The patient electronic medical records were used to determine if the patient suffered a recurrent stroke. The sensitivity, specificity, positive predictive value (PPV), and negative predictive value (NPV) were calculated for each imaging modality and the diagnostic accuracy was compared using receiver operating characteristic analysis.

RESULTS

cCTA was performed in 82 patients, CMR in 81 patients, and TTE in 151 patients. 28 recurrent strokes occurred (cCTA- n=14; CMR- n=14; TTE- n=26). The sensitivity, specificity, PPV and NPV were: 14%, 79%, 12.5%, and 81.5% for CMR; 28.5%, 88.2%, 33.3%, and 85.7% for cCTA; and 11.5%, 88.8%, 17.6%, and 82.8% for TTE. There was no significant difference in diagnostic accuracy between CMR (0.53, 95% CI [0.42, 0.64]), cCTA (0.56, 95% CI [0.43, 0.69]), and TTE (0.50, 95% CI [0.43, 0.57]).

CONCLUSION

cCTA, CMR, and TTE demonstrated comparably high specificity and NPV for the exclusion of cardioembolic stroke recurrence.

CLINICAL RELEVANCE/APPLICATION

The comparable performance of cCTA, CMR, and TTE in predicting recurrent cardioembolic stroke allows physicians to choose a preferred imaging modality for patients with suspected cardioembolic stroke.

SSK03-02 Quantitative Assessment of Myocardial Infarction with Computed Tomography (CT) Using a Bolus Contrast Injection Scheme: Comparison Between Extravascular Contrast Distribution Volume (ECDV) and Extracellular Volume Fraction (ECV)

Participants Jie Yu, Wuhan, China (*Presenter*) Nothing to Disclose Ping Han, MD, Wuhan, China (*Abstract Co-Author*) Nothing to Disclose Ting-Yim Lee, MSc, PhD, London, ON (*Abstract Co-Author*) License agreement, General Electric Company Aaron So, PhD, London, ON (*Abstract Co-Author*) Nothing to Disclose

For information about this presentation, contact:

aso@robarts.ca

PURPOSE

Myocardial viability can be assessed with CT by delineating the infarcted tissue with a higher degree of contrast retention in the late phase after bolus injection of iodinated contrast. In this study, we investigated the effectiveness of two metrics for the quantification of late iodine enhancement in myocardium for viability assessment.

METHOD AND MATERIALS

Reperfused acute myocardial infarction was induced in four farm pigs with 1-hr occlusion of the left anterior ascending artery (LAD) with a balloon catheter, and CT studies were performed within 2 weeks after the interventional procedure. After bolus injection of contrast at 3 mL/s and 0.7 mg/kg followed by saline flush, a 4-phase dynamic acquisition covering 10 min was performed with a GE Healthcare Revolution CT scanner at 100 kV, 100 mA, 280 ms/rot: 1st phase: 22 axial scans every 1-2 diastoles; 2nd: 6 scans every 15 s; 3rd: 4 scans every 30 s; 4th: 6 scans every 60 s. Dynamic images were analyzed with a model-based deconvolution approach, with the modified Johnson-Wilson-Lee tracer kinetic model used to describe the contrast exchange among the cellular and interstitial and vascular spaces in myocardium to derive ECDV in ml/g. The difference images were also generated by subtracting the images acquired at 10 min post contrast injection by the baseline images to obtain enhancement in the myocardium (Δ HUmyo) and left ventricular blood pool (Δ HUblood). ECV was then calculated as (1-Hematocrit)·(Δ HUmyo/ Δ HUblood). ECDV and ECV in normal (LCx territory) and infarcted myocardium (LAD territory) were compared.

RESULTS

Mean ECV in normal and infarcted myocardium were 0.27 ± 0.11 and 0.52 ± 0.11 respectively. The corresponding mean ECDV calculated from the dynamic images covered up to 3 min post contrast injection were 0.28 ± 0.07 ml/g and 0.60 ± 0.10 ml/g respectively. Infarcted myocardium exhibited a higher percentage increase in ECDV from normal myocardium (114%) compared to ECV (93%).

CONCLUSION

ECDV may be a more sensitive marker of myocardial viability compared to ECV due to the larger difference exhibited between the normal and infarcted tissues, and can be measured with only 1/3 of the time required for ECV (3 min vs. 10 min post contrast injection).

CLINICAL RELEVANCE/APPLICATION

With bolus contrast injection, ECDV measurement could provide a faster and more reliable assessment of myocardial viability after acute myocardial infarction compared to conventional ECV measurement.

SSK03-03 Feasibility of Myocardial Extracellular Volume Fraction Quantification Using Dual-Energy CT

Wednesday, Nov. 28 10:50AM - 11:00AM Room: S102CD

Participants

Marly van Assen, MSc, Charleston, SC (*Abstract Co-Author*) Nothing to Disclose Parkwood Griffith, Charleston, SC (*Presenter*) Nothing to Disclose Carlo N. De Cecco, MD, PhD, Atlanta, GA (*Abstract Co-Author*) Research Grant, Siemens AG Pooyan Sahbaee, Malvern, PA (*Abstract Co-Author*) Employee, Siemens AG Matthijs Oudkerk, MD, PhD, Groningen, Netherlands (*Abstract Co-Author*) Nothing to Disclose U. Joseph Schoepf, MD, Charleston, SC (*Abstract Co-Author*) Research Grant, Astellas Group; Research Grant, Bayer AG; Research Grant, Siemens AG; Research support, Bayer AG; Consultant, Guerbet SA; Consultant, General Electric Company; Consultant, HeartFlow, Inc; Consultant, Bayer AG; Consultant, Siemens AG; ; ; Marwen Eid, MD, Charleston, SC (*Abstract Co-Author*) Nothing to Disclose Rozemarijn Vliegenthart, MD, PhD, Groningen, Netherlands (*Abstract Co-Author*) Instutional Research Grant, Siemens AG Brian E. Jacobs, BS, Charleston, SC (*Abstract Co-Author*) Nothing to Disclose Akos Varga-Szemes, MD, PhD, Charleston, SC (*Abstract Co-Author*) Research Grant, Siemens AG

For information about this presentation, contact:

schoepf@musc.edu

PURPOSE

To assess the feasibility of Dual Energy CT (DECT) to derive myocardial extracellular volume (ECV) and detect ECV differences without the need for a true non-contrast scan compared to Single Energy CT (SECT) results.

METHOD AND MATERIALS

A total of 35 patients were included in this IRB-approved, HIPAA-compliant study; 8 control patients, 17 infarct patients (focal fibrosis), and 10 cardiomyopathy patients (diffuse fibrosis). All scans were acquired using a 2nd or 3rd generation dual source CT system. A true non-contrast and delayed acquisition were used to calculate SECT-ECV, while only the delayed acquisition in dual energy mode and derived virtual non-contrast images were used to calculate DECT-ECV. In the control and diffuse fibrotic groups, a region of interest (ROI) encompassing the entire left ventricular myocardium was used to calculate ECV. Two ROIs were placed in the focal fibrotic group; one in normal myocardium and one in fibrotic myocardium.

RESULTS

The median ECV was 33.4% (IQR, 30.1-37.4) for the SECT approach and 34.9% (IQR, 31.2-39.2) for the DECT approach (p =

0.401). For both SECT-ECV and DECT-ECV, focal fibrotic and diffuse fibrotic tissue had significantly higher ECV values compared to normal myocardium (all p < 0.021). No systematic bias was observed between SECT and DECT measurements, with limits of agreement calculated at \pm 9.4% (p = 0.348). The DECT acquisition had a lower radiation dose than the SECT scan by 1.1 mSv (p < 0.001), which was likely caused by the absence of the true non-contrast acquisition in the DECT approach.

CONCLUSION

Measurement of ECV with only a delayed acquisition is feasible using the DECT approach. The DECT approach provides similar results at a lower radiation dose compared to a SECT protocol.

CLINICAL RELEVANCE/APPLICATION

This study demonstrates the feasibility of DECT for myocardial ECV measurements using only a delayed acquisition, thus eliminating the need for a true non-contrast scan and consequently reducing radiation dose.

SSK03-04 Accuracy of Myocardial Blood Flow Quantification with Dual-source CT: Validation in Human Using 150-Water PET

Wednesday, Nov. 28 11:00AM - 11:10AM Room: S102CD

Participants

Masafumi Takafuji, Tsu, Japan (*Presenter*) Nothing to Disclose Kakuya Kitagawa, MD, PhD, Tsu, Japan (*Abstract Co-Author*) Nothing to Disclose Yasutaka Ichikawa, MD, Tsu, Japan (*Abstract Co-Author*) Nothing to Disclose Masaki Ishida, MD, PhD, Tsu, Japan (*Abstract Co-Author*) Nothing to Disclose Yoshitaka Goto, MD, Tsu, Japan (*Abstract Co-Author*) Nothing to Disclose Satoshi Nakamura, MD, Tsu, Japan (*Abstract Co-Author*) Nothing to Disclose Hajime Sakuma, MD, Tsu, Japan (*Abstract Co-Author*) Nothing to Disclose Group; Research Grant, FUJIFILM Holdings Corporation; Research Grant, Siemens AG; Research Grant, Nihon Medi-Physics Co, Ltd; Speakers Bureau, Bayer AG

For information about this presentation, contact:

masa-tkfj@clin.medic.mie-u.ac.jp

PURPOSE

Myocardial CT perfusion has emerged as a potential method for absolute quantification of myocardial blood flow (MBF). However, there is no standardized technique for CT MBF quantification, and dual-source CT MBF values have never been compared against positron emission tomography (PET), which is an established technique for non-invasive quantification of MBF. The aim of this study was to assess the accuracy and usefulness of absolute MBF values quantified with dual-source CT by comparing them with those quantified with 150-water PET.

METHOD AND MATERIALS

Dynamic CT perfusion and 150-water PET were performed in 26 patients (70+/-9 years, 22 male) with known/suspected coronary artery disease with a median interval of 48 days (interquartile range: 29-73 days). Hyperemic MBF in AHA 16 segments were quantified with a dual-source CT and its dedicated software (Force/VPCT body, Siemens). For the quantification of hyperemic MBF using 150-water PET, non-commercial software (Carimas) was used. Comparison of hyperemic MBF quantified by CT and PET was performed on segment (n=377), vessel (n=77), and patient (n=26) levels after exclusion of 7 segments out of FOV and 32 segments with transmural myocardial infarction.

RESULTS

CT results showed excellent linear correlation with PET results at segment (r=0.87, p<0.0001), vessel (r=0.91, p<0.0001), and patient level (r=0.93, p<0.0001). Area under the receiver-operating characteristics curve for detecting reduced MBF (<2.3 mL/min/g) on 150-water PET was 0.88, 0.91, and 0.92 at segment, vessel, and patient level, respectively. Although CT demonstrated significantly lower hyperemic MBF than PET (1.16 \pm 0.29 mL/min/g vs 2.46 \pm 1.56 mL/min/g, p<0.0001), there was good per-vessel sensitivity (79.5%), specificity (92.1%), negative predictive value (81.4%) and positive predictive value (91.2%) for diagnosing reduced PET-derived MBF with a CT-derived MBF cutoff value of 1.09 mL/min/g.

CONCLUSION

Hyperemic MBF quantified by CT demonstrated excellent correlation with MBF estimated by 15O-water PET, and yielded high diagnostic accuracy for detecting abnormal perfusion.

CLINICAL RELEVANCE/APPLICATION

CT MBF quantification has potential to provide objective assessment of perfusion abnormality in patients with known or suspected CAD with high accuracy comparable to 15O-water PET.

SSK03-05 Relationship Between Epicardial Adipose Tissue and Coronary Vascular Function in Patients with Normal Myocardial Perfusion by 82Rb PET/TC

Wednesday, Nov. 28 11:10AM - 11:20AM Room: S102CD

Participants

Massimo Imbriaco, MD, Napoli, Italy (*Presenter*) Nothing to Disclose Andrea Ponsiglione, MD, Naples, Italy (*Abstract Co-Author*) Nothing to Disclose Carmela Nappi, MD, Naples, Italy (*Abstract Co-Author*) Nothing to Disclose Serena Dell'Aversana, MD, San Marcellino, Italy (*Abstract Co-Author*) Nothing to Disclose Marta Puglia, Napoli, Italy (*Abstract Co-Author*) Nothing to Disclose Ludovica D'Acierno, Napoli, Italy (*Abstract Co-Author*) Nothing to Disclose Alberto Cuocolo, Napoli, Italy (*Abstract Co-Author*) Nothing to Disclose

For information about this presentation, contact:

PURPOSE

We assessed the relationship between epicardial adipose tissue (EAT) and coronary flow reserve (CFR) in patients with suspected or known coronary artery disease (CAD) and normal myocardial perfusion imaging (MPI).

METHOD AND MATERIALS

The overall population consisted of 272 subjects referred for the evaluation of suspected or known CAD to stress-rest 82Rb PET/CT and showing normal MPI. CAC score was measured according to the Agatston method. Using unenhanced CT images for CAC, EAT volume was measured (cm3). The ln(CAC+1) score and lnEAT transformation were used to reduce heteroscedasticity. Myocardial perfusion was assessed using standardized segmentation of 17 myocardial regions. The summed stress, summed rest and summed difference scores were automatically calculated. Myocardial perfusion was considered normal when the summed stress score was <3. Absolute myocardial blood flow (MBF) was computed (in milliliters per minute per gram) from the dynamic rest and stress imaging series. CFR was defined as the ratio of hyperemic to baseline MBF; CFR 2 was considered reduced.

RESULTS

In the overall population, 95 (35%) patients showed reduced and 177 (65%) normal CFR. Compared to patients with normal CFR, those with reduced CFR were older ($60\pm11 \text{ vs. } 67\pm9, P<0.05$) and showed higher values of ln(CAC+1) ($3.9\pm3 \text{ vs. } 4.7\pm3, P<0.05$) and lnEAT volume ($4.5\pm1 \text{ vs. } 4.7\pm1, P<0.05$). At univariable logistic regression analysis age, ln(CAC+1) and lnEAT resulted significant predictors of reduced CFR. At multivariable analysis, only age and lnEAT volume were independently associated with reduced CFR (hazard ratio 1.05 and 1.89 and 95% confidence interval 1.02-1.08 and 1.01-3.54, P<0.005). The addition of lnEAT to clinical data significantly increased the global chi-square of the model (from 23.8 to 28.6, P<0.05) in predicting reduced CFR.

CONCLUSION

In patients with suspected and known CAD and normal myocardial perfusion, age and EAT are strongly associated with reduced CFR confirming that visceral fat depot may directly influence coronary vascular function. Thus, EAT evaluation may play a major role in the identification of coronary vascular dysfunction in patients with normal perfusion.

CLINICAL RELEVANCE/APPLICATION

In patients with suspected and known CAD and normal myocardial perfusion, age and EAT are associated with impaired CFR confirming that visceral fat may directly influence coronary vascular function.

SSK03-06 Beyond CT-Fractional Flow Reserve (FFR): Non-Invasive Assessment of Instantaneous Wave Free Ratio (iFR), Coronary Flow Reserve (CFR) and Hyperemic Stenosis Resistance Index (HSR) from CTA

Wednesday, Nov. 28 11:20AM - 11:30AM Room: S102CD

Participants

Andreas Giannopoulos, MD, Zurich, Switzerland (*Abstract Co-Author*) Nothing to Disclose Anji Tang, Boston, MA (*Abstract Co-Author*) Nothing to Disclose Frank J. Rybicki III, MD, PhD, Ottawa, ON (*Abstract Co-Author*) Medical Director, Imagia Cybernetics Inc Dimitris Mitsouras, PhD, Boston, MA (*Presenter*) Research Grant, Canon Medical Systems Corporation;

For information about this presentation, contact:

dmitsouras@alum.mit.edu

PURPOSE

Although FFR can be assessed by CTA, patient management in the cathlab uses eg, iFR to avoid pharmacologic stress, or CFR and HSR to assess other factors associated with increased risk of major adverse cardiac events, such as microvascular disease or endothelial dysfunction. Estimating these metrics from CTA requires matched baseline and hyperemic simulations (ie, stress simulated using results obtained from rest simulation), which no technology to date provides. We sought to determine if coupling rest/stress computational fluid dynamics (CFD) simulations from CTA is feasible, and whether resulting metrics agree with known relationships of those metrics to reference-standard FFR.

METHOD AND MATERIALS

Rest-stress hemodynamics from CTA were performed for 50 patients with invasive FFR in intermediate lesions in <90d of CTA. Rest CFD was performed using only CTA data (myocardial mass, Murray's law). Stress CFD was then performed by coupling the epicardial arteries to a microvascular resistance model using the resistances estimated by the rest CFD for each myocardial territory. Hemodynamic metrics were calculated at the same location as invasive FFR as follows: CT-FFR=stress P/aortic stress P; CT-iFR=rest P/aortic rest P; CT-CFR from average peak velocity (APV), CFR=stress APV/rest APV; and CT-HSR=(aortic stress P-stress P)/stress APV. Correlation to FFR and receiver operating characteristic area-under-the-curve (AUC) to predict FFR<=0.8 was determined for each metric.

RESULTS

Target lesion DS was 46.8±8.7%, and 40% had FFR<=0.8. Pearson correlations against invasive FFR of CT-FFR, CT-IFR, CT-CFR and CT-HSR were r=0.70, 0.69, 0.35, and -0.71, respectively (all p<0.01). Diagnostic accuracy to detect FFR<=0.8 was 0.87 (95%CI:0.77-0.98), 0.86 (95%CI:0.75-0.97), 0.72 (95%CI:0.56-0.88), and 0.9 (95%CI:0.8-0.99), respectively. These match reported relationships between invasive FFR and iFR, CFR and HSR (eg, Pearson r~0.75 for iFR and r~0.34 for CFR compared to FFR, and AUC of FFR to predict significant HSR of ~0.94).

CONCLUSION

Coupling baseline and hyperemic simulations enables key physiologic parameters dependent on both pressure and flow to be estimated non-invasively from standard retrospective CTA.

CLINICAL RELEVANCE/APPLICATION

Evaluation of coronary artery disease by CTA can non-invasively assess coronary physiology beyond FFR, delivering key physiologic

information that is used in clinical decision making for patients with angina

Honored Educators

Presenters or authors on this event have been recognized as RSNA Honored Educators for participating in multiple qualifying educational activities. Honored Educators are invested in furthering the profession of radiology by delivering high-quality educational content in their field of study. Learn how you can become an honored educator by visiting the website at: https://www.rsna.org/Honored-Educator-Award/ Frank J. Rybicki III, MD, PhD - 2016 Honored Educator

SSK03-07 Feasibility of Coronary Flow and Velocity Measurement using 4D CTA Reconstruction

Wednesday, Nov. 28 11:30AM - 11:40AM Room: S102CD

Participants

Martin Wagner, PhD, Madison, WI (Presenter) Owner, LiteRay Medical LLC

Paul F. Laeseke, MD, PhD, Madison, WI (*Abstract Co-Author*) Consultant, NeuWave Medical, Inc; Shareholder, Elucent Medical; Shareholder, HistoSononics; Shareholder, McGinley Orthopaedics

Fred T. Lee JR, MD, Madison, WI (*Abstract Co-Author*) Consultant, NeuWave Medical, Inc Stockholder, HistoSonics, Inc Michael Speidel, PhD, Madison, WI (*Abstract Co-Author*) Nothing to Disclose

Charles M. Strother, MD, Madison, WI (*Abstract Co-Author*) Research Consultant, Siemens AG Research support, Siemens AG License agreement, Siemens AG

Charles A. Mistretta, PhD, Madison, WI (*Abstract Co-Author*) Founder, Mistretta Medical Intellectual Property Licensing Activities; Research, Siemens AG; Co-Founder, LiteRay Medical LLC

For information about this presentation, contact:

mwagner9@wisc.edu

PURPOSE

Commercially available CT scanners can achieve gantry rotation times of 0.3 s (~3 frames per second). However, the temporal resolution might not be sufficient to calculate blood flow and velocity in the coronary arteries, which are important for the diagnosis of coronary artery disease (CAD). Currently, ~1000 projection images are acquired during each gantry rotation. The purpose of this study was to determine the feasibility of a new reconstruction technique called 4D CTA, which calculates a 3D time frame for each projection image and therefore provides high temporal resolution for flow calculations in the coronary arteries.

METHOD AND MATERIALS

The previously described 4D DSA technique (Davis, 2013) was extended for the time-resolved 3D reconstruction of coronary arteries (CA). A pig study was retrospectively analyzed, where continuous axial CT acquisitions (64 slices) were performed with a 0.4 s gantry rotation time over a period of 50 s during intravenous contrast injection. A 3D image of the vasculature was reconstructed using a short scan (235 degrees) during diastole and the CA were manually segmented. A constrained back-projection was then performed for each projection image to create a 3D time frame. The reconstructed time attenuation curves were used to calculate the blood flow and velocity in the CA based on the mean transit time. The velocity and flow values were compared to values from literature and the flow conservation was determined.

RESULTS

In the first order branches, the average diameter, velocity and flow were 4.12 mm (3.28 mm), 110.43 mm/s (128 mm/s), and 1.44 ml/s (1.07 ml/s) respectively. The same measurements for the second order branches were 1.31 mm (1.70 mm), 63.34 mm/s (46.10 mm/s) and, 0.32 ml/s (0.10 ml/s) respectively. Values given in brackets are from literature as reported in Kassab et al. (1997) The flow conservation in the measured branches of the CA was 96.71 %.

CONCLUSION

Calculated coronary arterial velocity and flow correlated well with previously reported values from the literature suggesting that flow determination from 4D CTA is feasible. Additionally, the high flow conservation shows that the calculated values are consistent.

CLINICAL RELEVANCE/APPLICATION

The presented technique could provide both anatomical and functional information in diagnostic settings as well as cath labs using existing CT systems to detect pathologies of the coronary arteries.

SSK03-08 Deep Learning Reconstruction of Non-Contrast Magnetic Resonance Coronary Angiography at 3T Machine

Wednesday, Nov. 28 11:40AM - 11:50AM Room: S102CD

Participants

Daisuke Utsunomiya, MD, Kumamoto, Japan (*Presenter*) Nothing to Disclose Masafumi Kidoh, Kumamoto, Japan (*Abstract Co-Author*) Nothing to Disclose Kosuke Morita, Kumamoto, Japan (*Abstract Co-Author*) Nothing to Disclose Seitaro Oda, MD, Kumamoto, Japan (*Abstract Co-Author*) Nothing to Disclose Takeshi Nakaura, MD, Kumamoto, Japan (*Abstract Co-Author*) Nothing to Disclose Yasuyuki Yamashita, MD, Kumamoto, Japan (*Abstract Co-Author*) Consultant, DAIICHI SANKYO Group Yuichi Yamashita, Otawara, Japan (*Abstract Co-Author*) Employee, Canon Medical Systems Corporation

PURPOSE

Dedicated T2 preparation pulse have enabled non-contrast magnetic resonance coronary angiography (MRCA) at 3T system; however, the vascular contrast-to-noise ratio (CNR) is still inadequate for clinical use. The deep learning reconstruction (DLR) is a novel technique to improve the image quality. The purpose of this study was to investigate the effects of DLR on the image quality of 3T non-contrast MRCA.

We enrolled 10 volunteers (2 female, mean age 48 years) with no known coronary artery disease. Non-contrast MRCA was performed on a 3T MR scanner (Galan 3T ZGO, Canon medical) with following parameters: 3D fast FE, TR/TE =5.3/1.9ms, flip angle = 12°, slice thickness = 1.7mm with ECG trigger and real time motion correction. DLR images at moderate level and high level were generated by using dedicated workstation. In the quantitative evaluation, we measured signal-to-noise ratio of 3 coronary vessels (proximal and distal segments). In the qualitative evaluation, the 2 observers graded the vessel visualization and artifacts on a 4-point scale (worst, 1; best, 4).

RESULTS

The CNR (original MRCA) was 31 ± 7 and 16 ± 5 in the proximal and distal vessel, respectively. The corresponding CNR (moderatelevel DLR) was 46 ± 9 and 24 ± 10 ; and the CNR (high-level DLR) was 85 ± 20 and 45 ± 14 . The visual scores for overall image quality and image noise were significantly better in DLR images than original images. The vessel sharpness scores were comparable among 3 reconstructions (3.4, 3.8, and 3.8 for original, moderate DLR, and high DLR, respectively). The visual scores for image noise/graininess was significantly better in DLR (2.4, 3.8, and 4.0 for original, moderate DLR, and high DLR, respectively).

CONCLUSION

Non-contrast MRCA at 3T using DLR provides higher CNR without degrading the vessel sharpness.

CLINICAL RELEVANCE/APPLICATION

The deep learning reconstruction technique contributes in improved visualization of coronary arteries in non-contrast MR coronary angiography, enabling noninvasive scrutiny of the heart.

SSK03-09 Clinical and Transthoracic Echocardiography Predictors of Non-Detectable Left Ventricular Thrombus: When Is Cardiac Magnetic Resonance Necessary

Wednesday, Nov. 28 11:50AM - 12:00PM Room: S102CD

Participants

Rolf Symons, MD, Leuven, Belgium (*Presenter*) Nothing to Disclose Jan Verduyckt, Leuven, Belgium (*Abstract Co-Author*) Nothing to Disclose Davide Curione, Roma, Italy (*Abstract Co-Author*) Nothing to Disclose Steven Dymarkowski, MD, Leuven, Belgium (*Abstract Co-Author*) Nothing to Disclose Jan G. Bogaert, MD, Leuven, Belgium (*Abstract Co-Author*) Nothing to Disclose

For information about this presentation, contact:

rolf.symons@uzleuven.be

PURPOSE

Currently, transthoracic echocardiography (TTE) remains the most commonly used technique for the identification of LV thrombi. However, not all thrombi are visualized with TTE. Therefore, the purpose of our study was to identify predictors of unsuccessful TTE thrombus visualization and to develop a risk score to stratify which patients may benefit from cardiac magnetic resonance (CMR) to reliably detect or exclude LV thrombus.

METHOD AND MATERIALS

We performed a retrospective search of our CMR database including 10300 patients and identified 118 patients with LV thrombus and a time interval between CMR and TTE of <72h. Univariate logistic regression analysis was used to assess the association between baseline characteristics and TTE parameters with the primary endpoint (i.e. unsuccessful LV thrombus visualization on TTE). Variables with P<0.10 at univariate analysis were included as covariates in the multivariate logistic regression analysis. Receiver-operating characteristic (ROC) curve analysis was performed to examine differences in performance of each variable for prediction of the primary endpoint. A two-sided P-value<0.05 was considered to represent a significant difference.

RESULTS

In multivariate analysis, body mass index (BMI), LV end-diastolic diameter (EDD), and mitral valve regurgitation (MVR) were identified as significant predictors of unsuccessful LV thrombus visualization by TTE (all P<0.001). ROC analysis showed BMI >=26.9 kg/m2, LVEDD >=52 mm, and MVR >=2/4 to be the optimal cutoff points for prediction of the primary endpoint. The combination of the independent predictors allowed generation of a gradient response risk score of unsuccessful LV thrombus visualization by TTE (0/3 present: 0% missed; 1/3 present: 33.3% missed; 2/3 present: 79.5% missed; 3/3 present: 100% missed) (P<0.001).

CONCLUSION

Individual clinical and TTE parameters can predict the sensitivity of TTE for the successful detection of LV thrombus in heart disease. By using the presented risk score, a cost-effective strategy may be implemented by selectively referring patients to CMR when these risk factors are present.

CLINICAL RELEVANCE/APPLICATION

Clinical and TTE parameters can predict unsuccessful detection of LV thrombus in heart disease. These findings may lead to a costeffective referral of certain patients to CMR to rule out LV thrombus.



SSK04

Cardiac (Valves Imaging and Intervention)

Wednesday, Nov. 28 10:30AM - 12:00PM Room: S103AB



AMA PRA Category 1 Credits ™: 1.50 ARRT Category A+ Credit: 1.75

FDA Discussions may include off-label uses.

Participants

Jill E. Jacobs, MD, New York, NY (Moderator) Nothing to Disclose

Jonathon A. Leipsic, MD, Vancouver, BC (*Moderator*) Speakers Bureau, General Electric Company; Speakers Bureau, Edwards Lifesciences Corporation; Consultant, Heartflow, Inc; Consultant, Circle Cardiovascular Imaging Inc; Consultant, Edwards Lifesciences Corporation; Consultant, Neovasc Inc; Consultant, Samsung Electronics Co, Ltd; Consultant, Koninklijke Philips NV; Consultant, Arineta Ltd; Consultant, Pi-Cardia Ltd;

Robert C. Gilkeson, MD, Cleveland, OH (*Moderator*) Research Consultant, Riverain Technologies, LLC; Research support, Koninklijke Philips NV; Research support, Siemens AG; Research support, General Electric Company

Sub-Events

SSK04-01 Morphologic and Hemodynamic Characteristics of Low-Flow, Low-Gradient Aortic Stenosis: Cardiac CT and Echocardiography.

Participants

Sejin Choi, MD, Seoul, Korea, Republic Of (*Abstract Co-Author*) Nothing to Disclose Hyun Jung Koo, MD, Seoul, Korea, Republic Of (*Presenter*) Nothing to Disclose Dong Hyun Yang, MD, Seoul, Korea, Republic Of (*Abstract Co-Author*) Nothing to Disclose Joon-Won Kang, MD, Seoul, Korea, Republic Of (*Abstract Co-Author*) Nothing to Disclose

For information about this presentation, contact:

elfin19@gmail.com

PURPOSE

Aortic stenosis(AS) have a quite proportion of low-flow, low-gradient(LF/LG) AS, defined as small aortic valve area(AVA<1.0cm2) but a low mean pressure gradient(PG<40mmHg) and low flow(stroke volume<35ml/m2). Diagnosis of AS has been based on a valve area, mean PG and a peak flow velocity measured on echocardiography. However, there was a discrepancy between the measured AVA on cardiac CT and degree of AS on echocardiography. The purpose of this study was to evaluate the discrepancy between CT and echocardiography, and show the role of CT to detect LF/LG AS.

METHOD AND MATERIALS

Between June 2011 and Mar 2016, 465 patients with AS underwent CT for preoperative evaluation of aortic valve replacement. On CT, aortic annulus, AVA and aortic root size were measured. Clinical information including echocardiography findings was retrospectively collected. On echocardiography, severe AS was defined as peak velocity >4 m/s or mean PG <40mmHg. On CT, severe AS was defined as AVA <1.0 cm2. Patients were classified into four groups: Group 1) severe AS on both CT and echocardiography (n=282); Group 2) Severe AS on CT alone (n=49); Group 3) Severe AS on echocardiography alone (n=99); and Group 4) non-severe AS on both CT and echocardiography (n=35). Echocardiography and CT findings were compared among the groups.

RESULTS

AVA in both group 1 and 2 were similar (0.8 and 0.8cm2, respectively, P=0.99). However, in group 2, left ventricular ejection fraction (LVEF) (59.3 vs. 54.1%, P=0.02) and mean PG (67.5 vs. 28.5mmHg, P<0.001) ware significantly low compared to those in group 1, suggests LF/LG severe AS. Peak velocity was also smaller in group 2 (5.2 vs. 3.1m/s, P<0.001). LV mass index and B-type natriuretic peptide were no significant difference among the four groups.

CONCLUSION

In 32% of patients who required AVR due to AS, there was a discrepancy between the measured AVA on CT and degree of AS on echocardiography. Patients who showed peak velocity <4m/s or mean PG <40mmHg on echocardiography and AVA<1.0cm2 on CT show significantly lower EF, peak velocity, and mean PG, which suggests characters of LF/LG AS. CT may be useful to detect LF/LG AS.

CLINICAL RELEVANCE/APPLICATION

Since echocardiography is useful for functional evaluation of LV and CT can accurately measure the AVA, we can accurately evaluate the characteristics of AS using both modalities. The use of two modalities may help to risk stratify AS patients and to make therapeutic decision.

SSK04-02 Bioprosthesis Thrombosis After Transcatheter Aortic Valve Replacement: Cardiac Computed Tomography Findings

Participants

Hyun Jung Koo, MD, Seoul, Korea, Republic Of (*Presenter*) Nothing to Disclose Joon-Won Kang, MD, Seoul, Korea, Republic Of (*Abstract Co-Author*) Nothing to Disclose Dong Hyun Yang, MD, Seoul, Korea, Republic Of (*Abstract Co-Author*) Nothing to Disclose Jooae Choe, MD, Seoul, Korea, Republic Of (*Abstract Co-Author*) Nothing to Disclose

For information about this presentation, contact:

donghyun.yang@gmail.com

PURPOSE

To evaluate post-transcatheter aortic valve replacement (TAVR) findings such as thrombosis and leaflet dysfunction using cardiac computed tomography.

METHOD AND MATERIALS

Among 397 post-TAVR patients, 133 patients underwent cardiac CT. After excluding immediate post-TAVR CT, 49 patients (23 CoreValve, 23 Sapien XT, and 3 Sapien 3) with CT obtained more than one month after TAVR were retrospectively reviewed. Leaflet opening limitation, bioprosthesis thrombosis, leaflet degeneration, and stent eccentricity were analyzed. Baseline immediate and follow-up echocardiography parameters were collected and analyzed.

RESULTS

Median intervals between TAVR and CT was 13 months (range: 9.4 - 24.5 months). Minimal subvalvular rim-like soft tissue thickening (n= 27, 55%) and mild thickening of leaflets (n=2, 4%) are detected, but the patients are asymptomatic without hemodynamic disturbance. Leaflet opening limitation is noted in 11 (22%, 7 mild, 3 moderate, and 1 severe reduction) patients, however, there was no correlation with echocardiography parameters. TAV thrombosis is noted in 9 (18%) patients. In the patients with TAV thrombosis, transvalvular peak velocity (2.9 vs. 2.5 m/sec) and pressure gradient (20.7 vs. 13.6 m/sec) are higher than the others, but without statistical significance (P<0.05). One patient who showed highest peak velocity and pressure gradient on echocardiography (5.4 m/sec and 71 mmHg) had extensive subvalvular and valvular soft tissue thickening on CT even though she have managed with intense anticoagulation. One infective endocarditis is occur. The smaller the size of the stent lumen at the valve level, the more the peak velocity and pressure gradient increases (r=-0.4, P=0.008).

CONCLUSION

Leaflet thrombosis, subvalvular soft tissue thickening and leaflet opening limitation following TAVR is not uncommon findings in patients who performed cardiac CT. Cardiac CT can demonstrate post-TAVR findings such as subvalvular soft tissue, valve thrombosis, leaflet opening limitation and stent lumen size.

CLINICAL RELEVANCE/APPLICATION

Although the majority of patients who present leaflet thrombosis, subvalvular soft tissue thickening or leaflet opening limitation following TAVR show subclinical conditions without hemodynamic disturbance on echocardiography, follow-up cardiac CT may help to detect early complications of TAVR.

SSK04-03 Dynamic Evaluation of 3D Mitral Annular Anatomy in Primary and Functional Mitral Regurgitation Patients Using Multiphase Cardiac CT: Implications for Trans-catheter Mitral Valve Replacement Planning

Wednesday, Nov. 28 10:50AM - 11:00AM Room: S103AB

Participants

Asim Rizvi, MD, Rochester, MN (*Presenter*) Nothing to Disclose Shuai Leng, PHD, Rochester, MN (*Abstract Co-Author*) License agreement, Bayer AG Shivaram Poigai Arunachalam, PhD, Rochester, MN (*Abstract Co-Author*) Nothing to Disclose Nikkole Weber, Rochester, MN (*Abstract Co-Author*) Nothing to Disclose Emily Sheedy, Rochester, MN (*Abstract Co-Author*) Nothing to Disclose Ian T. Mark, MD, Rochester, MN (*Abstract Co-Author*) Nothing to Disclose Mackram Eleid, Rochester, MN (*Abstract Co-Author*) Nothing to Disclose Cynthia H. McCollough, PhD, Rochester, MN (*Abstract Co-Author*) Research Grant, Siemens AG Eric E. Williamson, MD, Rochester, MN (*Abstract Co-Author*) Nothing to Disclose

For information about this presentation, contact:

RIZVI.ASIM@MAYO.EDU

PURPOSE

To date, there is a relative lack of data regarding the use of CT to characterize dynamic geometry of the mitral valve (MV) in patients with MV disease. The aims of this study are: 1) to obtain 3D CT measurements of the mitral annulus throughout the cardiac cycle using a prototype mitral evaluation tool, and 2) to compare these measurements among patients with primary mitral regurgitation (PMR), functional (secondary) MR (FMR), and control patients without MR.

METHOD AND MATERIALS

Patients were retrospectively identified who underwent ECG-gated cardiac CT using a dual-source scanner (SOMATOM Definition, Siemens Healthcare). Multiphasic CT data was loaded into our prototype software. Multiple anatomical parameters were recorded in 3D space throughout the cardiac cycle (0-95%, at 5% increments), and included: annular circumference, planar surface area (PSA), anterior-posterior (A-P) or inter-commissural diameter, anterolateral-posteromedial (AL-PM) or septo-lateral diameter, and annular ellipticity. Comparisons were made among the three groups, with p<0.01 considered statistically significant.

RESULTS

A total of 145 subjects (age: 63.5±14.0 years, 64% males) were included in this study: 50 control, 50 with PMR, and 45 with FMR.

Mitral annular dimensions were significantly higher in the PMR group, followed by FMR and control groups, with circumference (144±11 vs. 131±14 vs. 117±8mm), PSA (1533±247 vs. 1229±269 vs. 1005±142mm2), A-P diameter (38±4 vs. 35±5 vs. 32±2mm), and AL-PM diameter (47±4 vs 41±4 vs. 39±3mm) (all p<0.001). Notably, different patterns were observed among the three groups regarding the change in annular dimensions across cardiac phases, with FMR maintaining relatively similar size while control and PMR both had substantial size changes, but with maximal and minimal sizes at different cardiac phases. However, no statistically significant difference was demonstrated for annular ellipticity among control versus pathological groups (p>0.01).

CONCLUSION

Multiphase cardiac CT affords assessment of mitral annular dynamicity in response to various types of MV disease. The dramatic variability in annular dimensions across the cardiac cycle demonstrates the significance of obtaining multiphasic 3D measurements.

CLINICAL RELEVANCE/APPLICATION

Multiphase ECG-gated cardiac CT offers dynamic, pre-procedural evaluation of complex 3D mitral valve geometry for catheterguided prostheses in patients with various types of mitral valve disease.

SSK04-04 Differentiation of Pannus From Other Prosthetic Valve Abnormalities Using Computed Tomography Texture Analysis

Wednesday, Nov. 28 11:00AM - 11:10AM Room: S103AB

Participants

Kyungsun Nam, MD, Seoul, Korea, Republic Of (*Presenter*) Nothing to Disclose Young Joo Suh, MD, Seoul, Korea, Republic Of (*Abstract Co-Author*) Nothing to Disclose Sang Joon Park, PhD, Seoul, Korea, Republic Of (*Abstract Co-Author*) Nothing to Disclose Young Jin Kim, MD, Seoul, Korea, Republic Of (*Abstract Co-Author*) Nothing to Disclose Dong Jin Im, Seoul, Korea, Republic Of (*Abstract Co-Author*) Nothing to Disclose Yoo Jin Hong, MD, Seoul, Korea, Republic Of (*Abstract Co-Author*) Nothing to Disclose Hye-Jeong Lee, MD, Seoul, Korea, Republic Of (*Abstract Co-Author*) Nothing to Disclose Jin Hur, MD, Seoul, Korea, Republic Of (*Abstract Co-Author*) Nothing to Disclose Byoung Wook Choi, MD, Seoul, Korea, Republic Of (*Abstract Co-Author*) Nothing to Disclose

PURPOSE

The purpose of this study was to determine whether quantitative computed tomography (CT) texture analysis features can differentiate the cause of prosthetic valve obstruction (PVO) in patients who had undergone prosthetic valve replacement.

METHOD AND MATERIALS

We retrospectively included 46 subprosthetic masses in 39 patients who were clinically suspected prosthetic valve dysfunction and underwent cardiac CT scan from March 2010 to December 2017. The cause of PVO was assessed by redo-surgery and follow-up imaging findings as standard reference, and classified as pannus, thrombus or vegetation. CT texture analysis was performed with drawing region-of-interests of subprosthetic mass using an in-house texture analysis software and features such as first-order statistics, size and volume, and gray-level co-occurrence matrix (GLCM) features were extracted. Features on texture analysis were compared between two groups (pannus vs. thrombus or vegetation) using Mann-Whitney U test. Logistic regression analysis was performed to investigate association between quantitative CT features and pannus formation.

RESULTS

Of 46 subprosthetic masses, there were 19 cases with pannus, 14 cases with thrombus, and 13 cases with vegetation. Patients with pannus tended to be female, and had higher mean and standard deviation of CT attenuation, percentile value of the cumulative histogram (Perc25, 50, 75, 90, 95), and GLCM features (moments and contrast), and smaller volume, with statistical significance (P<0.05).On multivariate logistic regression analysis, mean CT attenuation (OR: 5.71; 95% CI: 0.48, 68.43; p=0.1691), volume (OR: 5.52; 95% CI: 0.88, 34.59; p=0.068), GLCM moments and GLCM contrast (OR: 6.00; 95% CI: 0.72, 50.40; p=0.0987 and OR: 12.07; 95% CI: 1.31, 110.90; p=0.0277) of subprosthetic mass were significantly associated with pannus.

CONCLUSION

Quantitative features on CT texture analysis may help differentiating pannus from thrombus or vegetation in patients with suspected PVO.

CLINICAL RELEVANCE/APPLICATION

Quantitative CT texture analysis can differentiate pannus from other causes of prosthetic valve obstruction and may diminish the subjectivity of visual analysis.

SSK04-05 CT Virtual Endoscopic Findings of Bicuspid Aortic Valve in Patients with Severe Aortic Stenosis: Comparison with Surgical Diagnosis

Wednesday, Nov. 28 11:10AM - 11:20AM Room: S103AB

Participants

Hidenobu Takagi, MD, PhD, Morioka, Japan (*Presenter*) Nothing to Disclose Makoto Orii, Morioka, Japan (*Abstract Co-Author*) Nothing to Disclose Takuya Chiba, Morioka, Japan (*Abstract Co-Author*) Nothing to Disclose Hajime Kin, MD, Morioka, Japan (*Abstract Co-Author*) Nothing to Disclose Ryoichi Tanaka, MD, Morioka, Japan (*Abstract Co-Author*) Research Grant, Canon Medical Systems Corporation Kunihiro Yoshioka, MD, Morioka, Japan (*Abstract Co-Author*) Research Grant, Canon Medical Systems Corporation

For information about this presentation, contact:

hdnb69tkg@gmail.com

PURPOSE

CT has been known to have high diagnostic accuracy for bicuspid aortic valve (BAV). However, CT findings of BAV remain unclear.

The aim of our study was to evaluate diagnostic characteristics of CT findings for BAV compared with surgical diagnosis as the reference standard.

METHOD AND MATERIALS

This retrospective study included 112 consecutive patients with severe aortic stenosis who underwent preoperative cardiac CT, followed by surgical aortic valve replacement (57% woman, mean age, 70 years [range, 27-92]). All CT images were acquired using retrospective ECG-gated helical scan, from the aortic arch to the heart. Optimal stationary systolic and diastolic phase images were reconstructed at the slice thickness of 0.5 mm, and surgical-view virtual endoscopic images were reconstructed on a workstation. CT findings included shape of orifice (oval or the letter 'Y') and the number of leaflet (2 or 3) on systolic images, and balance of leaflet size (central angle of >= 150^{-9} or $120-149^{\circ}$ in the largest leaflet) and the number of commissure (2 or 3) on diastolic images. For each CT findings, oval orifice, 2 leaflets, central angle of >= 150° or 2 commissures were defined as BAV.

RESULTS

BAV was surgically found in 37% (41/112) of patients. Accuracy, sensitivity, specificity and area under the curve (AUC) (95% confidence interval) for the detection of BAV were as follows; number of leaflets, 0.86 (0.80-0.87), 0.98 (0.91-1.00), 0.79 (0.69-0.83) and 0.88 (0.82-0.93); orifice shape, 0.93 (0.87-0.96), 0.93 (0.82-1.00) 0.93 (0.87-0.99) and 0.93 (0.86-0.96); central angle, 0.92 (0.86-0.95), 0.76 (0.59-0.88), 0.98 (0.95-1.00) and 0.87 (0.79-0.93); and number of commissures, 0.87 (0.81-0.87), 0.63 (0.46-0.78), 1.00 (1.00-1.00) and 0.82 (0.73-0.88), respectively. Although there was no difference in accuracy (p = 0.147 by Cochran's Q test), sensitivity of the number of commissure or specificity of number of leaflet were the lowest among the CT findings (adjusted p < 0.05 for all by post-hoc Dunn's test with Bonferroni correction, respectively). AUC of number of commissure was lower than orifice shape and central angle (p < 0.05 for both by DeLong's test).

CONCLUSION

Although CT findings have high accuracy for detection of BAV, number of commissure showed lower sensitivity and AUC, and number of leaflet showed lower specificity.

CLINICAL RELEVANCE/APPLICATION

Knowledge of morphological CT characteristics of BAV may help diagnosis in patients with severe aortic valve stenosis.

SSK04-06 3D Printing of the Aortic Annulus Based on Cardiovascular Computed Tomography: Preliminary Experience in Pre-Procedural Planning for Aortic Valve Sizing

Wednesday, Nov. 28 11:20AM - 11:30AM Room: S103AB

Participants

Marco Gatti, MD, Turin, Italy (*Presenter*) Nothing to Disclose Riccardo Faletti, Turin, Italy (*Abstract Co-Author*) Nothing to Disclose Aurelio Cosentino, MD, Torino, Italy (*Abstract Co-Author*) Nothing to Disclose Laura Bergamasco, Turin, Italy (*Abstract Co-Author*) Nothing to Disclose Stefano Salizzoni, Torino, Italy (*Abstract Co-Author*) Nothing to Disclose Erik Cura Stura, Turin, Italy (*Abstract Co-Author*) Nothing to Disclose Domenica Garabello, Torino, Italy (*Abstract Co-Author*) Nothing to Disclose Giovanni Pennisi, Turin, Italy (*Abstract Co-Author*) Nothing to Disclose Simona Veglia, Torino, Italy (*Abstract Co-Author*) Nothing to Disclose Davini Ottavio, Torino, Italy (*Abstract Co-Author*) Nothing to Disclose Mauro Rinaldi, Torino, Italy (*Abstract Co-Author*) Nothing to Disclose Paolo Fonio, MD, Vercelli, Italy (*Abstract Co-Author*) Nothing to Disclose

For information about this presentation, contact:

marcogatti17@gmail.com

PURPOSE

to determine reliability and reproducibility of measurements of aortic annulus in 3D models printed from cardiovascular computed tomography (CCT) images.

METHOD AND MATERIALS

Retrospective study on the records of 20 patients who underwent aortic valve replacement (AVR) with pre-surgery annulus assessment by CCT and intra-operative sizing by Hegar dilators (IOS). 3D models were fabricated by fused deposition modelling of thermoplastic polyurethane filaments. For each patient, two 3D models were independently segmented, modelled and printed by two blinded "manufacturers": a radiologist and a radiology technician. Two blinded cardiac surgeons performed the annulus diameter measurements by Hegar dilators on the two sets of models. Matched data from different measurements were analyzed with Wilcoxon test, Bland-Altmann plot and within-subject ANOVA.

RESULTS

No significant differences were found among the measurements made by each cardiac surgeon on the same 3D model (p=0.48) or on the 3D models printed by different manufacturers (p=0.25); also, no intraobserver variability (p=0.46). The annulus diameter measured on 3D models showed good agreement with the reference CCT measurement (p=0.68) and IOH sizing (p=0.11). Time and cost per model were: model creation 10-15 min; printing time 60 min; post-processing 5min; material cost 1 euro.

CONCLUSION

3D printing of aortic annulus can offer reliable, not expensive patient-specific information to be used in the pre-operative planning of AVR or TAVI.

CLINICAL RELEVANCE/APPLICATION

3D models of aortic annulus printed from CCT may offer a reliable, not expensive, patient-specific pre-operative planning opportunity: they provide the final user with a unique interactive platform for both visual and tactile experiences, which are critical

for simulation of the procedure, but are not available in imaging data per se.

SSK04-07 Improving the Diagnostic Performance of 18F-FDG PET/CT in Prosthetic Heart Valve Endocarditis

Wednesday, Nov. 28 11:30AM - 11:40AM Room: S103AB

Participants

Laurens E. Swart, MD, Rotterdam, Netherlands (Abstract Co-Author) Nothing to Disclose Anna Gomes, MD, Groningen, Netherlands (Abstract Co-Author) Nothing to Disclose Asbjorn Scholtens, MD, Amersfoort, Netherlands (Abstract Co-Author) Nothing to Disclose Bhanu Sinha, MD, PhD, Groningen, Netherlands (Abstract Co-Author) Nothing to Disclose Wilco Tanis, The Hague, Netherlands (Abstract Co-Author) Nothing to Disclose Marnix G. Lam, MD, Utrecht, Netherlands (Abstract Co-Author) Nothing to Disclose Maureen van der Vlugt, Nijmegen, Netherlands (Abstract Co-Author) Nothing to Disclose Sebastian Streukens, Maastricht, Netherlands (Abstract Co-Author) Nothing to Disclose Erik Aarntzen, Nijmegen, Netherlands (Abstract Co-Author) Nothing to Disclose Jan Bucerius, New York, NY (Abstract Co-Author) Nothing to Disclose Sander van Assen, Hoogeveen, Netherlands (Abstract Co-Author) Nothing to Disclose Chantal Bleeker-Rovers, Nijmegen, Netherlands (Abstract Co-Author) Nothing to Disclose Peter Paul van Geel, Groningen, Netherlands (Abstract Co-Author) Nothing to Disclose Gabriel P. Krestin, MD, PhD, Rotterdam, Netherlands (Abstract Co-Author) Nothing to Disclose Joost P. van Melle, Groningen, Netherlands (Abstract Co-Author) Nothing to Disclose Jolien Roos - Hesselink, Rotterdam, Netherlands (Abstract Co-Author) Nothing to Disclose Riemer Slart, MD, PhD, Groningen, Netherlands (Abstract Co-Author) Nothing to Disclose Andor Glaudemans, Groningen, Netherlands (Abstract Co-Author) Nothing to Disclose Ricardo P. Budde, MD, PhD, Utrecht, Netherlands (Presenter) Nothing to Disclose

For information about this presentation, contact:

l.swart@erasmusmc.nl

PURPOSE

18F-Fluorodeoxyglucose (FDG) Positron-Emission Tomography/Computed Tomography (PET/CT) was recently introduced as a new tool for the diagnosis of prosthetic heart valve (PV) endocarditis (PVE). Previous studies reporting a modest diagnostic accuracy may have been hampered by unstandardized image acquisition and assessment, as well as several confounders. The aim of this study was to improve the diagnostic performance of FDG PET/CT in patients suspected of PVE by identifying and eliminating possible confounders, using both visual and standardized quantitative assessments.

METHOD AND MATERIALS

In this multicentre study, 160 patients with a PV who underwent FDG PET/CT for suspicion of PVE, as well as 77 patients with a PV who underwent FDG PET/CT for other indications (negative control group), were included. Their scans were reassessed by two independent observers blinded to all clinical data, both visually and quantitatively on EARL reconstructions. Confounders were identified using a binomial regression model, and subsequently eliminated.

RESULTS

Visual assessment of FDG PET/CT had a sensitivity/specificity/PPV/NPV for PVE of 74%/91%/89%/78%, respectively. Low inflammatory activity (CRP <40mg/L) at the time of imaging and use of surgical adhesives during PV implantation were significant confounders, while recent valve implantation was not. After elimination of significant confounders, diagnostic performance values of the visual assessment increased to 91%/95%/95%/91%. As a semi-quantitative measure of FDG uptake, an EARL-standardized SUVratio of >=2.0 was a 100% sensitive and 91% specific predictor of PVE.

CONCLUSION

Both visual and quantitative assessment of FDG PET/CT have a high diagnostic accuracy in patients suspected of PVE. FDG PET/CT should be implemented early in the diagnostic work-up to prevent negative confounding effects of low inflammatory activity (e.g. due to prolonged antibiotic therapy). As a quantitative measure of FDG uptake, an EARL-standardized SUVratio of >=2.0 is a 14 100% sensitive and 91% specific predictor of PVE. Recent valve implantation was not a significant predictor of false positive interpretations, but surgical adhesives used during implantation were.

CLINICAL RELEVANCE/APPLICATION

FDG PET/CT should be implemented early in the diagnostic work-up to prevent negative confounding effects of low inflammatory activity.

SSK04-08 Aortic Regurgitation in Hypertrophic Cardiomyopathy: A Cardiac Magnetic Resonance Study

Wednesday, Nov. 28 11:40AM - 11:50AM Room: S103AB

Participants

Zixian Chen, MD, Lanzhou, China (*Presenter*) Nothing to Disclose Minjie Lu, MD, PhD, Beijing, China (*Abstract Co-Author*) Nothing to Disclose Shihua Zhao, Beijing, China (*Abstract Co-Author*) Nothing to Disclose Junqiang Lei, Lanzhou, China (*Abstract Co-Author*) Nothing to Disclose Shunlin Guo, DDS, Lanzhou, China (*Abstract Co-Author*) Nothing to Disclose

For information about this presentation, contact:

chenzxcmr@163.com

PURPOSE

We sought to investigate the prevalence, mechanism and risk factors of AR in patients with HCM by cardiac magnetic resonance(CMR).

METHOD AND MATERIALS

This is an retrospective study of 105 consecutive patients (49±16 years, 70% male) with HCM who underwent CMR between April to November, 2017. Cardiac morphological, functional paremeters and AR were evaluated by multi-plane cine images and velocityencoded phase contrast images.Patients were divided into 2 groups by AR. The clinical and CMR characteristics were compared between the 2 groups, and predictors of AR assessed on multivariable logistic regression analysis.

RESULTS

AR was identified in 38 (36%) HCM patients including 25 (66%) with left ventricle outflow tract obstruction (LVOTO). AR was also more prevalent in obstruction group than that in non-obstruction group (52% vs. 23%, p=0.002). Patients with AR showed older age (58± 11 vs. 45±16 years, P<0.001), the higher prevalence of hypertension, mitral regurgitation (MR) and aortic valve thickening (55% vs. 33%, P=0.03; 90% vs.61%, P=0.006 and 40% vs. 9%, P<0.001, respectively). The distance of interventricular septum that protruded into the LVOT(D1), anterior mitral leaflet (AML) and left atrial diameter were greater and LVOT effective width (D3) were shorter in patients with AR than without it (13.5± 4.4 vs.10.6±4.0 mm, P=0.001; 25.5± 3.6 vs. 23.5±4.1mm, P=0.013 and 43.6± 8.6 vs. 39.1± 8.4mm, P=0.01; 10.2±5.3 vs. 13.7±5.9mm, P=0.003, respectively). On multivariable logistic regression analysis, the independent risk factors of AR were LVOTO and age.

CONCLUSION

This study has demonstrated that AR is not an uncommon consequence secondary to HCM. Age and LVOTO are the most probably risk factors of this pathophysiology consequence.

CLINICAL RELEVANCE/APPLICATION

(dealing with CMR) 'AR is a quite common comorbidity of HCM especially in patients with LVOTO . An earlier and better control of blood pressure and relieving LVOTO are required as early as possible to delay the progress of aortic valvular degeneration.'

SSK04-09 T1 Mapping as a Predictor for Persisting Valvular Cardiomyopathy in Patients with Chronic Aortic Regurgitation After Aortic Valve Repair

Wednesday, Nov. 28 11:50AM - 12:00PM Room: S103AB

Participants

Martin Sinn, Hamburg, Germany (*Presenter*) Nothing to Disclose Johannes Petersen, MD, Innsbruck, Austria (*Abstract Co-Author*) Nothing to Disclose Niklas Neumann, MD, Hamburg, Germany (*Abstract Co-Author*) Nothing to Disclose Gunnar K. Lund, MD, Hamburg, Germany (*Abstract Co-Author*) Nothing to Disclose Hermann Reichenspurner, MD, Hamburg, Germany (*Abstract Co-Author*) Nothing to Disclose Shiho Naito, Hamburg, Germany (*Abstract Co-Author*) Nothing to Disclose Tatiana Gross, MD, Hamburg, Germany (*Abstract Co-Author*) Nothing to Disclose Alexander Lenz, MD, Hamburg, Germany (*Abstract Co-Author*) Nothing to Disclose Gerhard B. Adam, MD, Hamburg, Germany (*Abstract Co-Author*) Nothing to Disclose Evaldas Girdauskas, MD, Hamburg, Germany (*Abstract Co-Author*) Nothing to Disclose Peter Bannas, MD, Hamburg, Germany (*Abstract Co-Author*) Nothing to Disclose

For information about this presentation, contact:

m.sinn@uke.de

PURPOSE

Left ventricular (LV) dysfunction is associated with poor prognosis in patients presenting with chronic aortic regurgitation. Unfortunately, LV-dysfunction often persists even after successful aortic valve (AV) repair. We aimed to evaluate the value of native T1 mapping by cardiac MRI as a predictor of valvular cardiomyopathy in patients with severe aortic regurgitation.

METHOD AND MATERIALS

31 consecutive patients (mean age 49.5±11.5 years, 52% men) with severe bicuspid (n=18) or tricuspid (n=13) aortic valve regurgitation and without previous history of coronary artery disease underwent 1.5 Tesla cardiac MR imaging. Native T1 mapping was performed using a modified Look-Locker inversion-recovery (MOLLI) sequence for quantification of diffuse interstitial myocardial fibrosis prior to AV repair and correlated with echocardiographic LV parameters before and after surgery.

RESULTS

Mean native T1 relaxation time of myocardium was 1025±44 ms (range: 898-1109 ms). There was no significant correlation between native T1 and preoperative LVEF (r=-0.1, p=0.6), LVEDD (r=-0.2, p=0.4), LVESD (r=-0.03, p=0.9), LVEDV (r=-0.02, p=0.9) and regurgitation fraction (r=-0.17, p=0.6). Fourteen patients (45%) had a postoperative decrease in LVEF more than 10% as compared to preoperative LVEF values. These fourteen patients showed significantly longer preoperative native T1 as compared to native T1 of patients with preserved postoperative LVEF (1056 \pm 32 ms vs. 1019 \pm 40 ms, p=0.03).

CONCLUSION

Native T1 mapping might be a promising predictor of postoperative LVEF decrease after AV repair for chronic severe aortic regurgitation.

CLINICAL RELEVANCE/APPLICATION

T1 mapping before aortic valve repair may guide and optimize aortic valve repair surgery in the future.



SSK05

Science Session with Keynote: Chest (Artificial Intelligence/Deep Learning)

Wednesday, Nov. 28 10:30AM - 12:00PM Room: N227B



AMA PRA Category 1 Credits ™: 1.50 ARRT Category A+ Credit: 1.75

Participants

Bram Van Ginneken, PhD, Nijmegen, Netherlands (*Moderator*) Stockholder, Thirona BV; Co-founder, Thirona BV; Research Grant, Varian Medical Systems, Inc; Research Grant, Canon Medical Systems Corporation Carol C. Wu, MD, Bellaire, TX (*Moderator*) Author, Reed Elsevier

Sub-Events

SSK05-01 Chest Keynote Speaker: AI and Machine Learning in Thoracic Imaging

Participants

Bram Van Ginneken, PhD, Nijmegen, Netherlands (*Presenter*) Stockholder, Thirona BV; Co-founder, Thirona BV; Research Grant, Varian Medical Systems, Inc; Research Grant, Canon Medical Systems Corporation

SSK05-02 Application of Deep Learning for Risk Stratification of Pulmonary Nodules

Wednesday, Nov. 28 10:40AM - 10:50AM Room: N227B

Participants

Seyoun Park, Baltimore, MD (*Presenter*) Nothing to Disclose Linda C. Chu, MD, Baltimore, MD (*Abstract Co-Author*) Nothing to Disclose Cheng Ting Lin, MD, Baltimore, MD (*Abstract Co-Author*) Nothing to Disclose Alan Yuille, Baltimore, MD (*Abstract Co-Author*) Nothing to Disclose Elliot K. Fishman, MD, Baltimore, MD (*Abstract Co-Author*) Institutional Grant support, Siemens AG; Institutional Grant support, General Electric Company; Co-founder, HipGraphics, Inc

For information about this presentation, contact:

spark139@jhmi.edu

PURPOSE

The low dose CT (LDCT) screening criteria used in National Lung Screening Trial (NLST) has a 26.6% false positive rate at baseline. Even when updated more stringent Lung RADS criteria was retrospectively applied to the NLST data, the false positive rate remained at 12.8%. Deep learning, a form of artificial intelligence, has the potential to improve risk stratification of pulmonary nodules. The purpose of this study is compare the performance of deep learning vs. radiologists in the risk stratification of pulmonary nodules.

METHOD AND MATERIALS

264 patients with one solid nodule reported in NLST database up to 20mm (mean±standard deviation: 7.5±3.4mm) in size (223 benign, 41 malignant) were retrospectively selected from the NLST baseline LDCT (T0). All malignant nodules were confirmed pathologically and benign nodules were diagnosed based on pathology or clinical follow-up by NLST investigators. The nodules were semi-automatically segmented using our in-house software. 3D deep convolutional networks (CNN) was used for the deep learning classification of malignancy based on 64x64x64 input patch bounding intramodular and perinodular areas. 4-fold cross-validation was performed. Data augmentation by scaling and rotating was used to increase the number of training dataset. Two radiologists who were blinded to the diagnosis reviewed the cases independently and scored the nodules based on Lung RADS criteria. Scores 1 and 2 were considered negative and scores >= 3 were considered positive.

RESULTS

The selected cohort was 62.0±5.1 year-old-patients at T0 (150 male and 114 female). The average accuracy, sensitivity, and specificity of the review of radiologists were 0.67, 0.73, and 0.67, respectively. 4-fold cross validation result of deep learning was 0.88, 0.90, and 0.88 in the same terms of accuracy, sensitivity, and specificity. Especially, the false positive rate showed significant improvement from 0.33 to 0.12, which represents to reduce false positive cases from 73 to 27, using CNN.

CONCLUSION

Deep learning achieved improved sensitivity, specificity, and accuracy in risk stratification of pulmonary nodules compared with radiologists.

CLINICAL RELEVANCE/APPLICATION

Deep learning can improve the accuracy in risk stratification of pulmonary nodules compared with radiologists. This has the potential of achieving earlier cancer detection and reducing unnecessary work up in the lung screening population.

Honored Educators

Presenters or authors on this event have been recognized as RSNA Honored Educators for participating in multiple qualifying

educational activities. Honored Educators are invested in furthering the profession of radiology by delivering high-quality educational content in their field of study. Learn how you can become an honored educator by visiting the website at: https://www.rsna.org/Honored-Educator-Award/ Elliot K. Fishman, MD - 2012 Honored EducatorElliot K. Fishman, MD - 2014 Honored EducatorElliot K. Fishman, MD - 2016 Honored EducatorElliot K. Fishman, MD - 2018 Honored Educator

SSK05-03 Deep Learning with Convolutional Neural Network for the Differentiation of Pathologic Grades in Lung Adenocarcinomas

Wednesday, Nov. 28 10:50AM - 11:00AM Room: N227B

Participants

Hyun-Ju Lee, MD, PhD, Seoul, Korea, Republic Of (*Presenter*) Nothing to Disclose Young Jae Kim, PhD, Incheon, Korea, Republic Of (*Abstract Co-Author*) Nothing to Disclose Kwang Gi Kim, PhD, Incheon, Korea, Republic Of (*Abstract Co-Author*) Nothing to Disclose Ju G. Nam, MD, Seoul, Korea, Republic Of (*Abstract Co-Author*) Nothing to Disclose Young Joo Suh, MD, Seoul, Korea, Republic Of (*Abstract Co-Author*) Nothing to Disclose Heekyung Kim, Seoul, Korea, Republic Of (*Abstract Co-Author*) Nothing to Disclose Young Tae Kim, MD, PhD, Seoul, Korea, Republic Of (*Abstract Co-Author*) Nothing to Disclose Yoon Kyung Jeon, Seoul, Korea, Republic Of (*Abstract Co-Author*) Nothing to Disclose

For information about this presentation, contact:

lee.hyunju.rad@gmail.com

PURPOSE

To investigate the diagnostic performance of a deep learning method with a convolutional neural network (CNN) for the differentiation of pathologic grades in lung adenocarcinomas (ADs) manifesting as solitary lung nodules.

METHOD AND MATERIALS

This clinical retrospective study comprised preoperative CT image sets of lung ADs pathologically confirmed to be one of three grades (grade A, patterns with low metastatic potential [AIS, MIA, and lepidic-predominant]; grade B, patterns with intermediate metastatic potential [acinar and papillary]; and grade C, patterns with high metastatic potential [solid and micropapillary]). Supervised training was performed using 26,321 CT images (2390 sets) obtained between 2014 and 2016 (a total of 1066 image sets; 278, 718, and 70 nodules for grades A, B, and C, respectively; 609 enhanced and 457 non-enhanced). Image sets were augmented (rotated, parallel-shifted, strongly enlarged, and horizontal flipped images were generated from the original images) by a factor of 4 in images from grade A tumors and by a factor of 8 from grade C tumors. A CNN composed of 151 convolutional, two maximum pooling, and one fully connected layers was tested using independent 1268 image sets (762 enhanced and 506 non-enhanced) obtained between 2007 and 2013 (578 men and 690 women; mean age, 62.7 years ± 10.1; mean mass size, 23.5 mm ± 14.4; 400, 709, and 159 lung ADs of grades A, B, and C, respectively). Accuracy in categorizing lung ADs using the CNN model and the area under the ROC curve (AUC) for differentiating grades A vs. B+C, grade A vs. B, grade A vs. C, and grade B vs. C were calculated.

RESULTS

For the differentiation of grades A vs. B+C, diagnostic accuracy was 79.1% and AUC was 0.77 in the test data. For differentiating grades A vs. B, A vs. C, and B vs. C, diagnostic accuracies were 73.4%, 78.8%, 70.1% and AUCs were 0.77, 0.91, and 0.62, respectively.

CONCLUSION

Deep learning with CNN demonstrated high diagnostic performance in differentiating the pathologic grade of lung ADs.

CLINICAL RELEVANCE/APPLICATION

The CNN model can be useful in differentiating the pathologic grade of lung ADs, however, further study is warranted to correlate patients' prognoses with the output of CNN.

SSK05-04 Deep Machine Learning for Automatic Analysis of Chest X-Rays: Effect of Clinically Relevant Pathology Class Label Definition

Wednesday, Nov. 28 11:00AM - 11:10AM Room: N227B

Participants

Anas Ż. Abidin, MS, Rochester, NY (*Presenter*) Nothing to Disclose Adora M. D'Souza, MSc, Rochester, NY (*Abstract Co-Author*) Nothing to Disclose Axel Wismueller, MD, PhD, Rochester, NY (*Abstract Co-Author*) Nothing to Disclose

PURPOSE

To quantitatively analyze the effect of radiologically relevant pathology class label definition on deep machine learning results for automatic analysis of chest x-rays.

METHOD AND MATERIALS

With >100,000 frontal-view chest radiographs, the ChestX-ray14 data (Wang et al, 2017) is currently the largest publicly available annotated dataset for automatic chest x-ray analysis. Annotations consist of one or more of 14 thoracic pathology labels, e.g. Consolidation (C), Infiltration (I), Pneumonia (P) and 11 others. As radiologists cannot distinguish between C, I and P based on imaging findings alone, the stratification of these 'Opacity' entities into separate classes suggests a non-existent crispness of reported pathology class labels. To circumvent this key limitation of the ChestX-ray14 dataset and to investigate its effect on machine learning performance, we resampled data belonging to the 3 'Opacity' and 'No findings' classes, resulting in a 2-class classification problem with 63,000 chest x-rays. Images were resized to 10242 without preserving aspect ratio. Ensuring strict training/test (80%/20%) data separation, we fine-tuned a pre-trained ResNet-34 convolutional neural network with batch normalization, cross-entropy loss function, and last layer sigmoid activation. We also performed classification for all 14 individual pathology labels using the full dataset. Diagnostic accuracy was quantified using Area Under the receiver operating characteristics

RESULTS

For 'Opacity/No Findings' classification, we obtained AUC=0.78. This is close to the best performance obtained for original labels I, C, P with AUCs of 0.72, 0.81, 0.73, respectively. For the remaining 11 class labels, AUCs were comparable to, and for some labels, slightly better than the best published results of current state-of-the art methods (Rajpurkar et al 2017).

CONCLUSION

Our results suggest that radiologically relevant pathology label definition is important for training deep machine learning systems for automatic chest x-ray analysis, as it can influence their performance. Merging visually indistinguishable pathology classes can address a key limitation of the ChestX-ray14 data by alleviating the effect of 'structured noise'.

CLINICAL RELEVANCE/APPLICATION

It is critical that the datasets being used for training artificial intelligence recapitulate the characteristics of datasets encountered in a radiology setting as closely as possible.

SSK05-05 Evaluating the Use of a Deep Learning Algorithm for Radiology Quality Assurance in Out-Patient Chest X-Ray Reporting

Wednesday, Nov. 28 11:10AM - 11:20AM Room: N227B

Participants

Amit K. Sahu, MBBS, MD, New Delhi, India (Presenter) Nothing to Disclose Bharat Aggarwal, MBBS, MD, New Delhi, India (Abstract Co-Author) Nothing to Disclose Anandamoyee Dhar, New Delhi, India (Abstract Co-Author) Nothing to Disclose Gaurav Kapoor, MBBS, MD, Haryana, India (Abstract Co-Author) Nothing to Disclose Pooja Rao, MBBS, PhD, Mumbai, India (Abstract Co-Author) Employee, Qure.ai

For information about this presentation, contact:

drsahuamit@gmail.com

PURPOSE

To evaluate the accuracy of a deep learning algorithm - 1. To assist with screening of chest X-rays in the wellness check/primary care setting with predominantly normal X-rays 2. To help optimize the quality assurance (QA) process by selecting X-rays for review

METHOD AND MATERIALS

For this retrospective study, we used 3945 de-identified chest X-rays with the accompanying radiologist reports, randomly selected from the natural distribution of scans from adult patients attending OPD for a wellness check at 5 urban centers. Language processing algorithms were used to extract an initial ground truth of either 'normal' or 'abnormal' from the report impressions. A commercial deep learning-based chest X-ray screening system was then evaluated versus this ground truth. X-rays with a discordance between the original radiology report and the algorithm output were re-read by a panel of 3 radiologists. The majority opinion of the 3 radiologists was used as a new ground truth, to evaluate accuracy on this discordant set.

RESULTS

3274 of 3945 (82.9%) X-rays were normal, based on the original radiology report. Algorithm accuracy on the original dataset was 80%, with an AUC of 0.8, sensitivity of 0.63 and specificity of 0.83 on the detection of abnormal X-rays. Of the 789 discordant Xrays, 405were read by the panel of 3 radiologists. On this discordant dataset, the 3 radiologist-consensus agreed with the algorithm results in 64.9% of the cases, and with the original radiology report in the remaining 35.1%.

CONCLUSION

Among the discordant scans, the consensus ground truth was closer to the algorithm results than to the original report. Deep learning algorithms can effectively select chest X-rays for review during radiology quality control

CLINICAL RELEVANCE/APPLICATION

Artificial intelligence algorithms can be used for automated selection of chest X-rays for review during the radiology QA process, potentially increasing its effectiveness.

SSK05-06 Performance Validation of a Deep Learning-Based Automatic Detection Algorithm for Major Thoracic **Abnormalities on Chest Radiographs**

Wednesday, Nov. 28 11:20AM - 11:30AM Room: N227B

Participants

Eui Jin Hwang, Seoul, Korea, Republic Of (Presenter) Nothing to Disclose Sunggyun Park, Seoul, Korea, Republic Of (Abstract Co-Author) Employee, Lunit Inc So Young Choi, MD, Daejeon, Korea, Republic Of (Abstract Co-Author) Nothing to Disclose Jong Hyuk Lee, MD, Seoul, Korea, Republic Of (Abstract Co-Author) Nothing to Disclose Jin Mo Goo, MD, PhD, Seoul, Korea, Republic Of (Abstract Co-Author) Research Grant, Samsung Electronics Co, Ltd; Research Grant, Lunit Inc

Chang Min Park, MD, PhD, Seoul, Korea, Republic Of (Abstract Co-Author) Nothing to Disclose

For information about this presentation, contact:

ken921004@hotmail.com

PURPOSE

To evaluate the performance of a deep learning-based automatic detection (DLAD) algorithm for major thoracic abnormalities

including malignant pulmonary nodules/masses, tuberculosis, pneumonia, and pneumothorax on chest radiographs (CRs) in comparison with physicians.

METHOD AND MATERIALS

DLAD was developed using a 27-layer deep convolutional neural network. External validation of its diagnostic performance was conducted using 2 separate datasets from 2 institutions (normal: abnormal = 97:103 and 100:84). For comparison with physicians, an observer performance test was conducted using 1 of the datasets including 15 physicians (5 non-radiology physicians, 5 board-certified radiologists, 5 thoracic radiologists). All physicians reviewed each CR twice, without and with DLAD, and determined the presence of clinically significant thoracic abnormalities on a 5-point scale. Performance measurements were done using area under the receiver operating characteristic (ROC) curves for image-wise classification and area under the alternative free-response ROC curves for lesion-wise localization.

RESULTS

Image-wise classification performances of DLAD for abnormal CRs were 0.983 and 0.993 and lesion-wise localization performances were 0.974 and 0.985 on the two external validation datasets. Without DLAD, average classification performances of non-radiology physicians, board-certified radiologists, and thoracic radiologists were 0.813, 0.896, and 0.932, and average localization performances were 0.781, 0.870, and 0.907, respectively. DLAD demonstrated significantly higher performance in image-wise classification and lesion-wise localization compared with all reader groups (all Ps < 0.05). With DLAD, physicians' diagnostic performances were significantly improved in classification (0.904, 0.939, 0.958; all Ps <0.05) and localization (0.873, 0.919, 0.938; all Ps < 0.05) in all reader groups.

CONCLUSION

DLAD demonstrated excellent performance in image-wise classification and lesion-wise localization on CRs with major thoracic abnormalities, outperforming physicians, and enhancing the physician's diagnostic performance when used as a second reader.

CLINICAL RELEVANCE/APPLICATION

Our DLAD algorithm can accurately classify abnormal CRs and localize abnormal findings, and has the potential to improve diagnostic accuracy, patients' safety, and clinical workflow efficacy.

SSK05-07 Deep Learning-Based Automatic Detection Algorithm for the Detection of Major Thoracic Abnormalities on Chest Radiographs

Wednesday, Nov. 28 11:30AM - 11:40AM Room: N227B

Participants

Sunggyun Park, Seoul, Korea, Republic Of (*Presenter*) Employee, Lunit Inc Jaehong Aum, Seoul, Korea, Republic Of (*Abstract Co-Author*) Employee, Lunit Inc Chang Min Park, MD, PhD, Seoul, Korea, Republic Of (*Abstract Co-Author*) Nothing to Disclose Eui Jin Hwang, Seoul, Korea, Republic Of (*Abstract Co-Author*) Nothing to Disclose Jong Hyuk Lee, MD, Seoul, Korea, Republic Of (*Abstract Co-Author*) Nothing to Disclose Minsung Kim, MD, Seoul, Korea, Republic Of (*Abstract Co-Author*) Nothing to Disclose

For information about this presentation, contact:

sgpark@lunit.io

PURPOSE

To develop a deep learning-based automatic detection (DLAD) algorithm for major thoracic abnormalities including nodule/mass, tuberculosis (TB), pneumonia and pneumothorax on chest radiographs (CRs) using a large-scale CR dataset and evaluate its diagnostic performance.

METHOD AND MATERIALS

We collected a total of 89,832 CRs comprising 54,221 normal CRs and 35,641 abnormal CRs with major thoracic abnormalities including malignant pulmonary nodules/masses (n=13,925), pulmonary TB (n=6,798), pneumonia (n=6,903) and pneumothorax (n=8,015). Thereafter, all CRs were randomly split into three datasets; training dataset (n=84,072; 53,393 normal and 30,679 abnormal CRs), validation dataset (n=750; 300 normal and 450 abnormal CRs), and test dataset (n=750; 300 normal and 450 abnormal CRs). DLAD was designed using deep convolutional network consisting of 27 layers and 12 residual connections, and trained with 71,376 label-only CRs and 12,696 annotated CRs for which 15 thoracic radiologists marked the locations of the individual abnormalities. Diagnostic performance of the DLAD was investigated using receiver-operating characteristic (ROC) curve analysis for per-CR classification performance and jackknife alternative free-response receiver-operating characteristic (JAFROC) curve analysis for per-lesion detection performance. All CRs in the validation and test datasets were annotated by 5 out of 15 thoracic radiologists, and the final determination of the location of each abnormality was made by majority decision.

RESULTS

In the test dataset, DLAD showed an area under the ROC curve (AUC) of 0.9811 for per-CR classification performance and an area under the JAFROC curve of 0.9656 for per-lesion detection performance. The AUCs and JAFROCs of each disease category were 0.9674 and 0.9494 for malignant pulmonary nodule/mass, 0.9902 and 0.9742 for tuberculosis, 0.9854 and 0.9740 for pneumonia, and 0.9937 and 0.9800 for pneumothorax, respectively.

CONCLUSION

Our deep learning-based automatic detection algorithm demonstrated excellent, cutting-edge performances both in terms of differentiating normal and abnormal CRs and localizing individual abnormalities on CRs.

CLINICAL RELEVANCE/APPLICATION

DLAD can augment the diagnostic performance of radiologists both in terms of image-wise diagnosis and lesion-wise detection, thereby improving diagnostic accuracy, patients' safety, and work-flow efficacy.

"Change" versus "No-Change": Can Machine Learning Driven Algorithm Detect Stability or Change in Chest Radiographs?

Wednesday, Nov. 28 11:40AM - 11:50AM Room: N227B

Ramandeep Singh, MBBS, Boston, MA (*Presenter*) Nothing to Disclose Fatemeh Homayounieh, MD, Chelsea, MA (*Abstract Co-Author*) Nothing to Disclose Subba R. Digumarthy, MD, Boston, MA (*Abstract Co-Author*) Nothing to Disclose Chayanin Nitiwarangkul, MD, Boston, MA (*Abstract Co-Author*) Nothing to Disclose Atul Padole, MD, Boston, MA (*Abstract Co-Author*) Nothing to Disclose Mannudeep K. Kalra, MD, Boston, MA (*Abstract Co-Author*) Research Grant, Siemens AG; Research Grant, Canon Medical Systems Corporation John A. Patti, MD, Boston, MA (*Abstract Co-Author*) Nothing to Disclose Amita Sharma, MBBS, Boston, MA (*Abstract Co-Author*) Nothing to Disclose Manoj D. Tadepalli, BEng, Mumbai, India (*Abstract Co-Author*) Employee, Qure.ai Jo-Anne O. Shepard, MD, Boston, MA (*Abstract Co-Author*) Nothing to Disclose

PURPOSE

Chest radiograph is the most commonly performed imaging; changes, or lack thereof, of radiographic findings have tremendous implications on patient care. We compared accuracy of machine learning (ML) algorithm (Qure AI) and thoracic radiologists for assessing stability or change in findings over serial chest radiographs.

METHOD AND MATERIALS

We parsed the publicly available, de-identified, frontal-view chest radiographs from the NIH to identify 300 baseline and follow-up radiographs from 150 adult patients both with and without change in radiographic findings. Two thoracic radiologists reviewed all 300 radiographs to establish ground truth for radiographic findings [such as pleural effusions (EF), lung opacities (LO), hilar prominence (HP), and cardiomegaly (CM)]. All radiographs were processed with Qure AI ML to generate prediction scores and heat maps for each finding. Then, two different thoracic (test R1 and R2) radiologists independently recorded their findings, unaware of the ground truth and ML findings. Data were analyzed to determine accuracy and area under curve with free-choice receiver operating characteristics (FROC) analyses.

RESULTS

Respective percentage changes in findings on follow-up radiographs for EF, CM, HP and LO were 15% (21/138), 9% (13/150), 5% (8/150), 25% (33/132) for ground truth; 20% (28/138), 13% (20/150), 12% (18/150), 27% (36/132) for R1; 19% (26/138), 7% (11/150), 4.7% (7/150), 25% (33/132) for R2; and 25% (34/138), 23% (34/150), 23% (35/150), 40% (53/132) for ML. The AUC of ML algorithm for detecting lack of change in findings were 0.867 (EF), 0.904 (C), 0.872 (HP), 0.742 (LO). Accuracy of ML for detecting change in radiographic findings was also high with corresponding AUC of 0.804 (EF), 0.923 (C), 0.839 (HP), 0.758 (LO). Although both test radiologists had AUC similar to ML for stable radiographic findings, their AUC [0.867-0.878 (EF), 0.815-0.904 (CM), 0.635-0.872 (HP), 0.742-0.854 (LO) for change in findings were lower compared to corresponding AUC for ML.

CONCLUSION

ML algorithm can accurately predict stability and change in radiographic findings on follow up radiographs. Its accuracy varies across different types of findings, and is highest for cardiomegaly and lowest for lung opacities.

CLINICAL RELEVANCE/APPLICATION

ML can enable stratification of chest radiographs on basis of change or stability of findings, thus expediting interpretation of radiographs with important changes.

Honored Educators

Presenters or authors on this event have been recognized as RSNA Honored Educators for participating in multiple qualifying educational activities. Honored Educators are invested in furthering the profession of radiology by delivering high-quality educational content in their field of study. Learn how you can become an honored educator by visiting the website at: https://www.rsna.org/Honored-Educator-Award/ Subba R. Digumarthy, MD - 2013 Honored Educator

SSK05-09 Assessment of Endotracheal Tube Position on Chest Radiographs using Deep Learning

Wednesday, Nov. 28 11:50AM - 12:00PM Room: N227B

Participants

Paras Lakhani, MD, Philadelphia, PA (*Presenter*) Nothing to Disclose Adam E. Flanders, MD, Philadelphia, PA (*Abstract Co-Author*) Nothing to Disclose Baskaran Sundaram, MRCP, FRCR, Philadelphia, PA (*Abstract Co-Author*) Nothing to Disclose Maansi R. Parekh, MBBS, Philadelphia, PA (*Abstract Co-Author*) Nothing to Disclose Achala Donuru, MD, Philadelphia, PA (*Abstract Co-Author*) Nothing to Disclose Vijay M. Rao, MD, Philadelphia, PA (*Abstract Co-Author*) Nothing to Disclose Richard J. Gorniak, MD, Philadelphia, PA (*Abstract Co-Author*) Consultant, BioClinica, Inc; Consultant, Medtronic plc

For information about this presentation, contact:

paras.lakhani@jefferson.edu

PURPOSE

Assess the efficacy of deep learning in determining endotracheal tube (ETT) position on chest radiographs.

METHOD AND MATERIALS

23,079 de-identified frontal chest radiographs with an ETT were split into 12 categories, which included bronchial insertion, and distance from the carina at 1.0cm intervals (e.g. 0.0-0.9cm, 1.0-1.9cm...) and lastly >=10cm. Ground truth ETT position was determined by two board certified radiologists (original author and a second radiologist for QA confirmation). Images were split into

training (80%, 18467 images), validation (10%, 2306 images), and test (10%, 2306 images). The ETT was re-measured on 100 random images from the test data to assess inter-observer variability. The pretrained Inception V3 convolutional neural network was utilized to a) predict ETT distance from the carina in cm and b) categorize images as low ETT (< 2cm of carina), satisfactory (2-7cm above carina), or high (>= 7cm above carina). Image normalization and auto-cropping about the carina was performed prior to model training. Real-time data augmentation was employed, and an ensemble of 10 Inception V3 models was used in the final classification. Receiver operating characteristic (ROC), area-under-the-curves (AUC), sensitivity and specificity on test data were used to assess the models.

RESULTS

The predicted ETT distance from carina had a mean difference of 0.79cm (\pm 0.56) from the ground truth, and the two radiologists had a mean difference of 0.44cm (\pm 0.44). On the test data, the AUC was 0.97 (95%CI: 0.96-0.98) for differentiating ETT<2cm from carina from all others. The AUC was 0.96 (95%CI: 0.95-0.98) for differentiating high ETT>=7cm from all others. 4 bronchial insertions and ETT 0-0.9cm from carina were missed of 385 true positives (sensitivity: 99.0%). There were 86 false positives of 1921 true negative cases (specificity: 95.5%). However, threshold cases near a category were sometimes missed; for example, 43 cases of 1-1.9cm above carina were misclassified as >=2cm above carina, usually as 2-3cm above carina. Similarly, threshold cases of 6-6.9cm were predicted as 7-7.9cm above carina or vice-versa. The sensitivity of the model drops to 87.8% when including these threshold cases as misclassified.

CONCLUSION

Deep learning shows promise in assessing ETT position and predicts postion within 1cm in most cases.

CLINICAL RELEVANCE/APPLICATION

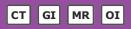
Automatic identification of ETT position may reduce time to identification of critical placement.



SSK06

Science Session with Keynote: Gastrointestinal (Colorectal Imaging)

Wednesday, Nov. 28 10:30AM - 12:00PM Room: S502AB



AMA PRA Category 1 Credits ™: 1.50 ARRT Category A+ Credit: 1.75

Participants

Marc J. Gollub, MD, New York, NY (*Moderator*) Nothing to Disclose Seong Ho Park, MD, Seoul, Korea, Republic Of (*Moderator*) Research Grant, DONGKOOK Pharmaceutical Co, Ltd; Research Grant, Central Medical Service Co, Ltd Cauray (Khatri, MD, Dallas, TX (*Moderator*) Nothing to Disclose

Gaurav Khatri, MD, Dallas, TX (Moderator) Nothing to Disclose

Sub-Events

SSK06-01 Gastrointestinal Keynote Speaker: Rectal Cancer Imaging

Participants Marc J. Gollub, MD, New York, NY (*Presenter*) Nothing to Disclose

SSK06-02 Feasibility Study of Dual-Energy Spectral CT for Differentiating Rectal Cancers with and Without Vascular Invasion

Wednesday, Nov. 28 10:40AM - 10:50AM Room: S502AB

Participants Rui Fan, huludao, China (*Abstract Co-Author*) Nothing to Disclose Mei-yu Sun, Dalian, China (*Abstract Co-Author*) Nothing to Disclose Meng Yao Wang, Dalian, China (*Abstract Co-Author*) Nothing to Disclose Xu Han, Da Lian, China (*Abstract Co-Author*) Nothing to Disclose Jianying Li, Beijing, China (*Abstract Co-Author*) Nothing to Disclose Jianying Li, Beijing, China (*Abstract Co-Author*) Employee, General Electric Company Ailian Liu, MD, Dalian, China (*Abstract Co-Author*) Nothing to Disclose Lijun Wang, Dalian, China (*Presenter*) Nothing to Disclose

For information about this presentation, contact:

329739283@qq.com

PURPOSE

The purpose of this study was to investigate the potential value of dual-energy CT (DECT) in differentiating vascular invasion rectal cancer from non-vascular invasion rectal cancer.

METHOD AND MATERIALS

90 consecutive untreated patients (56 men, 34 women; mean age, 62.95 years) were enrolled and underwent DECT before biopsy. DECT image metrics including iodine (water) concentration (IC) and effective atomic number (eff-Z) were measured. Data were analyzed statistically by the independent-samples t test and were correlated with pathological findings. The receiver operating characteristics (ROC) analysis was also carried to evaluate the efficacy of these parameters for differentiating rectal cancers with or without vascular invasion.

RESULTS

Pathological results showed that there were 41 vascular invasion rectal cancer and 49 non-vascular invasion rectal cancer. The IC values of the vascular invasion rectal cancer in the venous phase were 2.42 ± 0.55 mg/ml, significantly higher than that of the non-vascular invasion rectal cancer with 2.13 ± 0.52 mg/ml (P<0.05). The eff-Z of the vascular invasion rectal cancer in the venous phase was 17.85 \pm 3.731, which was also higher than that of the non-vascular invasion rectal cancer with 16.19 \pm 3.638 (P<0.05). However, there were no significant differences in those parameters in the arterial phase (P>0.05). Based on the ROC curves, the optimal cut off value for the IC was 2.25mg/ml which yielded a sensitivity of 70.7% and a specificity of 67.3% for differentiating rectal cancers with or without vascular invasion.

CONCLUSION

It is feasible to differentiate a vascular invasion rectal cancer from the non-vascular invasion rectal cancer using dual energy CT, especially the iodine concentration measurement in the venous phase.

CLINICAL RELEVANCE/APPLICATION

Dual energy CT appears to be an efficient CT technique for a possible method to evaluate vascular or non-vascular invasion of rectal cancer.

SSK06-03 Low Anterior Resection Syndrome (LARS): Imaging Characteristics of Rectal Cancer and Anorectal Anatomy

Participants

Xiao Zeng, Beijing, China (Presenter) Nothing to Disclose Fan Liu, Beijing, China (Abstract Co-Author) Nothing to Disclose Xiaoxuan Jia, MA, Beijing, China (Abstract Co-Author) Nothing to Disclose Chao Ding, Beijing, China (Abstract Co-Author) Nothing to Disclose Peng Guo, Beijing, China (Abstract Co-Author) Nothing to Disclose Nan Hong, MD, Beijing, China (Abstract Co-Author) Nothing to Disclose Yingjiang Ye, Beijing, China (Abstract Co-Author) Nothing to Disclose Yi Wang, MD, Beijing, China (Abstract Co-Author) Nothing to Disclose

For information about this presentation, contact:

zx333232@163.com

PURPOSE

To identify risk factors associated with LARS severity based on the imaging characteristics of rectal cancer and anorectal anatomy defined by magnetic resonance imaging (MRI) pre-operation.

METHOD AND MATERIALS

Between August 2016 and August 2017, patients who had pathological-proved rectal cancer and underwent low anterior resection (LAR) were collected in this retrospective study. Patients need to be followed-up at least 9months after operative. All patients were divided into non-major LARS group and major LARS group based on LARS score. The tumor morphological characteristics were measured and recorded as the following: the distance between tumor and anal margin, the distance between tumor and puborectal muscle, the length of tumor involvement, the tumor stage, the lymph nodes stage, and circumferential resection margin. In addition, morphological characteristics of rectal-anal canal were measured and recorded, including anorectal angle (ARA), levatoanal angle (LAA), levator plate angle, thickness of internal anal sphincter, levator plate angle(°), thickness of rectal wall(mm), thickness of obturator internus(mm), thickness of external anal sphincter (mm), thickness of internal anal sphincter(mm), thickness of puborectal muscle(mm), and thickness of illiosacrum muscle(mm). The differences of measurement between non-major and major LARS groups were analyzed by t-test and x2-test.

RESULTS

Thirty-three patients were enrolled in the final cohort including 22 patients (66.7%) with non-major LARS (score 0-20) and 11 patients (33.3%) with major LARS (score 30-42, n=11). The distances of tumor and anal margin and the distance of tumor and puborectal muscle of patients with major LARS was significantly lower than patients with non-major LARS (<= 7cm, P =0.017 and <= 5 cm P=0.009). The LAA and the ARA of patients with major LARS were larger than patient with non-major LARS and significances were seen (>=100°, P=0.049 and >=125°, P=0.025).

CONCLUSION

The lower tumor, larger ARA and LAA was identified as risk factors may be associated with major LARS for patients with rectal cancer after Low Anterior Resection.

CLINICAL RELEVANCE/APPLICATION

Identification of risk factors associated with LARS severity by MRI pre-operation may help surgeons change the strategy of operation to avoid LARS and, therefore, the life quality of patients may be improve after surgery.

SSK06-04 Preoperative Staging for Rectal Cancer: Comparison of Whole Body MR-PET and Standard Protocol

Wednesday, Nov. 28 11:00AM - 11:10AM Room: S502AB

Participants

Jeong Hee Yoon, MD, Seoul, Korea, Republic Of (Presenter) Research Grant, Bayer AG; Speaker, Koninklijke Philips NV; Speaker, Bayer AG

Won Chang, MD, Seoul, Korea, Republic Of (Abstract Co-Author) Nothing to Disclose

Hyun-Ju Lim, MD, Goyang, Korea, Republic Of (Abstract Co-Author) Nothing to Disclose

Hyo-Jin Kang, MD, Seoul, Korea, Republic Of (Abstract Co-Author) Nothing to Disclose

Keon Wook Kang, Seoul, Korea, Republic Of (Abstract Co-Author) Nothing to Disclose

Jeong Min Lee, MD, Seoul, Korea, Republic Of (Abstract Co-Author) Grant, Bayer AG Grant, General Electric Company Grant,

Koninklijke Philips NV Grant, STARmed Co, Ltd Grant, RF Medical Co, Ltd Grant, Samsung Electronics Co, Ltd Grant, Guerbet SA

PURPOSE

To measure the concordance of rectal cancer clinical staging between whole body MR-PET including dedicated liver and rectal MRI (WB MR-PET) and the current standard care protocol (chest/abdominopelvic CT and rectal MRI).

METHOD AND MATERIALS

This IRB-approved prospective study enrolled 71 patients (M:F = 43:28, mean age 60.9 years) with newly diagnosed mid to lower rectal cancer. Clinical staging and effective dose were compared between standard protocol and WB MR-PET protocol according to AJCC 7th staging. In addition, incidence of further study recommendation and incidental findings were recorded.

RESULTS

Regarding with the presence of metastasis, two protocols were consistent in 67.6% (48/71), and discordant in 4.2% (3/71). In the remaining 28.2% (20/71), standard protocol did not conclude presence or absence of metastasis or extent of metastasis (IVa or IVb) due to indeterminate lesions in lung, liver, or retroperitoneal lymph nodes. In these patients, standard protocol recommended followings for lesion characterization: chest CT follow up in 20% (4/20), liver MRI in 20% (4/20), PET-CT in 45% (9/20) and liver MRI with chest CT follow up for multiple indeterminate lesions in 15% (3/20). In these 20 patients, WB MR-PET protocol suggested presence or absence of metastasis in 25% (5/20) and 75% (15/20), respectively. Compared with clinical follow-up results within 6 months, 14 of 15 patients with WB MR-PET negative findings did not show metastasis. In 5 patients with WB MR-PET positive

findings, all liver lesions were correctly classified, but one false positive and one false negative cases for lung nodules were observed. There were 13 cases with incidental findings including incidentally detected tonsillar cancer with neck lymph node metastasis (n=1) and incidentally detected Warthin's tumor in the parotid gland (n=1). Effective dose was significantly lower in WB MR-PET than standard protocol (6.18 ± 1.06 mSv vs. 10.70 ± 5.45 mSv, P<0.0001).

CONCLUSION

WB MR-PET protocol showed low discrepancy rate with the standard protocol for metastasis evaluation in patients with rectal cancer and it served as problem-solving modality for indeterminate lesions.

CLINICAL RELEVANCE/APPLICATION

Compared with the standard protocol, WB MR-PET with dedicated rectal and liver MRI may facilitate the staging work-up with less inconvenience in a short period.

SSK06-05 Application of Dynamic Dual-Energy CT Imaging In Colorectal Cancer for Assessing the Correlation Between Blood Perfusion and Iodine Uptake on 320-Row Multidetector CT

Wednesday, Nov. 28 11:10AM - 11:20AM Room: S502AB

Participants

Dandan Wang, Shenyang, China (*Presenter*) Nothing to Disclose Yahong Luo, Shenyang, China (*Abstract Co-Author*) Nothing to Disclose Dong Ma, Shenyang, China (*Abstract Co-Author*) Nothing to Disclose Yu Tao SR, DO, Shenyang City, China (*Abstract Co-Author*) Nothing to Disclose Jing Wen, MD, Shenyang, China (*Abstract Co-Author*) Nothing to Disclose Fengjiao Cui, Shenyang, China (*Abstract Co-Author*) Nothing to Disclose Na Li, Shenyang, China (*Abstract Co-Author*) Nothing to Disclose Lin Li, Shenyang, China (*Abstract Co-Author*) Nothing to Disclose

For information about this presentation, contact:

m13940431957@163.com

PURPOSE

To evaluate the characteristics of blood perfusion and iodine uptake in colorectal cancer using dynamic dual-energy imaging on 320-row CT.

METHOD AND MATERIALS

29 patients with colonic adenocarcinoma diagnosed by colonoscopy were enrolled. Each patient was scanned for 10 dual-emerge acquisition phases, with 3-second intervals for 1 to 7 phases, 5-second intervals for 8 to 10 phases, and total scanning time was 53s. Iodine map and perfusion map were generated, and iodine uptake peak (IUP), arterial flow (AF, ml/min/100ml), blood volume (BV,ml/100ml) and permeability (ml/min/100ml) of tumor were measured.

RESULTS

The IUP, AF, BV and permeability of tumor were 71.46 \pm 2.19, 158.26 \pm 80.40, 17.33 \pm 17.80, 60.14 \pm 20.59, respectively. The IUP of tumor was significantly associated with the AF (r=0.440, P<0.05) and BV (r=0.382, P<0.05) There was no significant correlation between IUP and permeability(P>0.05). The average DLP of dynamic dual-energy CT imaging was 1104 mGy•cm with an effective radiation dose of 16.56 mSv.

CONCLUSION

Dynamic dual-energy CT imaging can generate dynamic iodine map and perfusion map at the same time. The correlations of iodine uptake peak and perfusion parameters AF and BV of colorectal cancer are significant.

CLINICAL RELEVANCE/APPLICATION

Dynamic dual-energy CT imaging of coloractal cancer provides iodine uptake and perfusion data in just one scan. It can be used to evaluate the hemodynamic characteristics of colorectal cancer and provide more diagnostic information for the clinical doctors.

SSK06-06 Predictors of Surgical Outcome, DFS and OS in Mid and Low Rectal Cancer Undergoing Laparoscopic Resection After Neoadjuvant Chemoradiation Therapy: Impact of Pretreatment and Re Staging MRI

Wednesday, Nov. 28 11:20AM - 11:30AM Room: S502AB

Participants

Laurene Aupin, Saint-Maur=des-Fosses, France (*Presenter*) Nothing to Disclose Frederic Pigneur, MD, Creteil, France (*Abstract Co-Author*) Nothing to Disclose Rasha Alani, Creteil, France (*Abstract Co-Author*) Nothing to Disclose Aleix Martinez-Perez, Valencia, Spain (*Abstract Co-Author*) Nothing to Disclose Giulio Cesare Vitali, Geneve, Switzerland (*Abstract Co-Author*) Nothing to Disclose Frilippo Landi, Barcelona, Spain (*Abstract Co-Author*) Nothing to Disclose Frederic Ris, Geneve, Switzerland (*Abstract Co-Author*) Nothing to Disclose Frederic Ris, Geneve, Switzerland (*Abstract Co-Author*) Nothing to Disclose Fracesco Brunetti, Creteil, France (*Abstract Co-Author*) Nothing to Disclose Nicola De'Angelis, Creteil, France (*Abstract Co-Author*) Nothing to Disclose Alain Luciani, MD,PhD, Creteil, France (*Abstract Co-Author*) Research Consultant, Bracco Group; Research Grant, Bracco Group; Research Consultant, General Electric Company; Research Consultant, Siemens AG

PURPOSE

To assess (1) the impact of restaging MRI as a predictor of surgical difficulties and survival and (2) the diagnostic accuracy of restaging MRI against final pathological assessment.

METHOD AND MATERIALS

Between 1/2010 and 1/2016, patients with histologically proven locally advanced (AJCC stages I to IIIc) rectal cancer of the mid or lower third of the rectum, who underwent MRI including DWI before (pre-treatment MRI) and after neo-adjuvant chemo-radiotherapy (re-staging MRI) followed by either elective laparoscopic anterior resection (LAR) with total mesorectal excision or laparoscopic abdominoperineal (L-APR) resection were included. Pelvimetry was performed on pre-treatment MRI providing transverse, sagittal, angles and surface measures. On pre and post-treatment MRI, T stage, N stage and EMVI status were assessed. On re-staging MRI, the MR tumor regression grade score (mrTRG) was determined. Sensitivity, specificity, PPV and NPV of restaging MRI for mrTRG prediction were assessed. Binary, multimodal, or linear regression analyses were performed to assess predictors of surgical difficulties (i.e., estimated on operative time, blood loss, and conversion rate) and surgical success (i.e., postoperative complications and successful resection rate).

RESULTS

170 patients (mean age 59±13) were included. Tumor volume and tumor height on re-staging MRI were associated respectively with operative time and blood loss. Conversion was predicted by tumor volume, interischial distance and pubic tubercle height. A circumferential resection margin> 2 mm was found as a protector of postoperative complications and unsuccessfull resection. The quality of the surgical resection was found as a predictor of overall and disease-free survival. On re-staging MRI, the PPV of ymrT for ypT0 stage, ypT1/T2 stages, and ypT3/T4 staging was 83%, 55.7% and 68.8% respectively. The PPV of ymrN for ypN0 and ypN+ staging was 87.7% and 62.5% respectively. The sensitivity, specificity, PPV, and NPV of ymrEMVI was respectively 68.4%, 78.8%, 28.8% and 95.2%. The sensitivity and specificity of tumor regression grade (mrTRG) 1 to identify pathologic complete response was 76.9% and 89.3%, respectively, with a PPV of 68.2% and NPV of 92.8%.

CONCLUSION

Pelvimetry and re-staging MRI may be useful to predict surgical difficulties and surgical outcomes.

CLINICAL RELEVANCE/APPLICATION

Pelvimetry and re-staging MRI can predict outcome in rectal cancer.

SSK06-07 The Tram Track Sign and the Railroad to Complete Response after Neoadjuvant Therapy in Rectal Cancer

Wednesday, Nov. 28 11:30AM - 11:40AM Room: S502AB

Participants

Ines A. Santiago, MD, Lisbon, Portugal (*Abstract Co-Author*) Nothing to Disclose Maria Joao Barata, Lisbon, Portugal (*Abstract Co-Author*) Nothing to Disclose Hugo Rio-Tinto, Lisbon, Portugal (*Presenter*) Nothing to Disclose Oriol Pares, Lisbon, Portugal (*Abstract Co-Author*) Nothing to Disclose Nuno Figueiredo, Lisbon, Portugal (*Abstract Co-Author*) Nothing to Disclose Celso Matos, MD, Lisbon, Portugal (*Abstract Co-Author*) Nothing to Disclose

For information about this presentation, contact:

ines.santiago@neuro.fchampalimaud.org

PURPOSE

To measure the diagnostic performance of the tram track sign for the identification of sustained complete response (SCR) after neoadjuvant therapy on re-staging magnetic resonance (MR) T2-weighted imaging (T2-WI) in patients with locally advanced rectal cancer.

METHOD AND MATERIALS

Institutional review board approval was obtained for this retrospective study and patient informed consent requirement was waived. Fifty-eight consecutive patients with locally advanced rectal cancer who underwent neoadjuvant therapy were enrolled. Two radiologists blindly and independently reviewed restaging pelvic MRs and analyzed 3 features: a distinct morphologic pattern of tumour response - the tram track sign (TTS) -characterized by the presence of 2 hypointense rims at previous tumour location separated by a variable amount of homogeneously intermediate or high signal intensity on T2-WI; the relative proportion of intermediate signal intensity on T2-WI; and the relative proportion of high signal intensity on high b-value diffusion-weighted images (DWI). Endoscopic response grading from the same timepoint was retrieved. Qui-Square test was employed in search for any associations between SCR and TTS, T2-WI, DWI or endoscopy. Interrater agreement of MR parameters was estimated using Cohen's Kappa statistic (k).

RESULTS

TTS was significantly associated with SCR, with specificity=0.97/0.97, sensitivity=0.52/0.64, PPV=0.93/0.94, NPV=0.73/0.78 and AuROC=0.78/0.83, for observers 1/2, respectively. DWI was significantly associated with SCR for observer 2, with specificity=0.76, sensitivity=0.60, PPV=0.65, NPV=0.71 and AuROC=0.69. No significant differences were found for T2-WI or endoscopy. Interobserver agreement was substantial for TTS (k=0.69), moderate for DWI (k=0.46) and poor for T2-WI (k=0.17).

CONCLUSION

The tram track sign is a specific and reliable tool for the early identification of SCR after neoadjuvant therapy in rectal cancer. Its diagnostic performance exceeds that of endoscopy and conventional T2-WI and DWI assessment.

CLINICAL RELEVANCE/APPLICATION

The tram track sign may outperform standard T2-WI, DWI and endoscopic assessment in the early identification of sustained complete response after neoadjuvant therapy in rectal cancer.

SSK06-08 Diffusion-Weighted MR-Volumetry and High-Resolution MR-Volumetry Association with Lymphovascular Invasion and N-Stages in Resectable Rectal Cancer

Participants Hao Liu, Chengdu, China (*Abstract Co-Author*) Nothing to Disclose Hang Li, Chengdu, China (*Abstract Co-Author*) Nothing to Disclose Xiao-Li Chen, Chengdu, China (*Abstract Co-Author*) Nothing to Disclose Hong Pu, Chengdu, China (*Abstract Co-Author*) Nothing to Disclose Guo-Hui Xu, Chengdu, China (*Presenter*) Nothing to Disclose

For information about this presentation, contact:

lihang111222@126.com

PURPOSE

Purpose: To determine whether diffusion-weighted imaging (DWI)-volumetry and high-resolution T2-weighted imaging (T2WI) MR-volumetry could predict lymphovascular invasion (LVI) and N-stages in resectable rectal cancer.

METHOD AND MATERIALS

Materials & Methods: 50 consecutive patients with rectal cancer who underwent radical surgery in 1-week after DWI and highresolution T2WI were retrospectively identified. Gross tumor volume (GTV) was evaluated on DWI and high-resolution T2WI. Univariate and multivariate analyses were performed to determine whether GTV could predict LVI and lymph node metastasis (LNM). Mann-Whitney U test was performed to compare GTV among N-stages. Cutoffs of GTV were investigated using area under the receiver operating characteristic curve (AUC) analysis for predicting LVI and N-stages.

RESULTS

Results: DWI-GTV and T2WI-GTV increased with LVI (r=0.750 and 0.710,P<0.0001,respectively) and increasing of N stage(r=0.780 and 0.755,P<0.0001,respectively). Univariate analysis showed DWI-GTV and T2WI-GTV could predict LVI (P<0.0001). Multivariate analyses indicated only DWI-GTV as an independent risk factor of LVI (P=0.005, odds ratio=1.207) and LNM (P=0.005, odds ratio=1.420). The Mann-Whitney U test showed DWI-GTV and T2WI-GTV could distinguish N0 from N1, N0 from N1-2, N0-1 from N2 (P<0.0001). DWI-GTV could predict LVI (cutoff,11.05cm3;AUC,0.899), and distinguish N0 from N1 (cutoff,10.86cm3;AUC,0.865), N0 from N1-2 (cutoff,10.46cm3;AUC,0.934), N0-1 from N2 (cutoff,12.25cm3;AUC,0.932). T2WI-GTV could predict LVI (cutoff,13.36cm3; AUC,0.911), N0-1 from N2 (cutoff,20.43cm3; AUC,0.927).

CONCLUSION

Conclusion: High-resolution T2WI-GTV and DWI-GTV of resectable rectal cancer were correlated well with the LVI and LNM, but the latter is a potentially more promising non-invasive technique that can help predict the preoperative LVI and distinguishing N-stages.

CLINICAL RELEVANCE/APPLICATION

Diffusion-weighted MR-volumetry of resectable rectal cancer are correlated well with the lymphovascular invasion and lymph node metastasis, and is recommended as a potentially more promising non-invasive technique for predicting the preoperative lymphovascular invasion and distinguishing N-stages.

SSK06-09 Comparison of Polyp Surface Tagging Performance of Barium plus Diatrizoate Meglumine/Diatrizoate Sodium Solution versus Barium plus Iohexol during CT Colonography

Wednesday, Nov. 28 11:50AM - 12:00PM Room: S502AB

Participants

Matthew A. Barish, MD, Stony Brook, NY (*Abstract Co-Author*) Stockholder, Blackford Analysis Ltd Marc Pomeroy, Stony Brook, NY (*Abstract Co-Author*) Nothing to Disclose Adam Khan, MD, Stony Brook, NY (*Abstract Co-Author*) Nothing to Disclose Kiyon Naser-Tavakolian, MD, Stony Brook, NY (*Abstract Co-Author*) Nothing to Disclose Jie Yang, Stony Brook, NY (*Abstract Co-Author*) Nothing to Disclose Jerrin Varghese, MD, Stony Brook, NY (*Abstract Co-Author*) Nothing to Disclose Jerome Z. Liang, PhD, Stony Brook, NY (*Abstract Co-Author*) Nothing to Disclose David H. Kim, MD, Middleton, WI (*Abstract Co-Author*) Shareholder, Cellectar Biosciences, Inc; Shareholder, Elucent Medical; Perry J. Pickhardt, MD, Madison, WI (*Abstract Co-Author*) Stockholder, SHINE Medical Technologies, Inc; Stockholder, Elucent Medical; Advisor, Bracco Group; Musa A. Mufti, MD, MBBS, Stony Brook, NY (*Presenter*) Nothing to Disclose

PURPOSE

The detection of polyps at CT colonography (CTC), especially serrated adenomas, is contingent on polyp surface tagging. The purpose of this study is to investigate differences in surface tagging performance of barium when combined with either diatrizoate meglumine/diatrizoate sodium solution (DM-DS) versus iohexol.

METHOD AND MATERIALS

A retrospective review was conducted of 338 polyps detected at CTC with two different tagging regimens: barium plus either DM-DS or iohexol. The degree of coating of each polyp was graded on a 0-4 scale (no coating to heavy coating) and correlated to polyp histologic subtype and tagging agent. Polyp histology was classified into: hyperplastic, sessile serrated or non-serrated adenoma. Performance of coating scores were analyzed with univariate logistic regression and Wilcoxon rank sum tests.

RESULTS

338 polyps were included, 255 tagged with DM-DS and 83 with iohexol. Across all polyps, coating score of SSA (3±2) was significantly higher than in NSA (1±3) (p<.0001). However, the coating score was only significantly higher for SSA compared with NSA within the DM-DS group (3±2 versus 1±2) (p<.0001). No statistical difference was seen for the iohexol group (3±1 versus 1±3) (p=.0603). Using all polyps (and in sub-analysis of DM-DS and iohexol groups) there was a statistically significant difference in tagging of SSA (N=70) versus benign HP (N=71) (p < .0001). Of note, there is a significantly higher percentage of serrated adenomas compared with all adenomas (30.8%, 61/198) detected in the DM-DS group compared with iohexol group (15.3%, 9/59)

CONCLUSION

CT colonography using both an iodine and barium oral tagging regimen allows for detection of polyps by the presence of surface tagging. We demonstrated that DM-DS demonstrates a significantly higher coating score of serrated adenomas when compared with non-serrated adenomas. Although a similar difference was seen for iohexol, it was not statistically significant. Of concern, there is a significantly higher percentage of serrated adenomas (as compared to all adenomas) detected in the DM-DS group. This may suggest a lower sensitivity for serrated adenomas with iohexol.

CLINICAL RELEVANCE/APPLICATION

Combined with barium, DM-DS results in greater surface tagging of serrated compared with nonserrated adenomas. Although no difference in tagging was seen, Iohexol resulted in lower SSA detection.

Honored Educators

Presenters or authors on this event have been recognized as RSNA Honored Educators for participating in multiple qualifying educational activities. Honored Educators are invested in furthering the profession of radiology by delivering high-quality educational content in their field of study. Learn how you can become an honored educator by visiting the website at: https://www.rsna.org/Honored-Educator-Award/ Perry J. Pickhardt, MD - 2014 Honored EducatorPerry J. Pickhardt, MD - 2018 Honored Educator



SSK07

Gastrointestinal (Liver Diffuse Disease, Steatosis)

Wednesday, Nov. 28 10:30AM - 12:00PM Room: S402AB



AMA PRA Category 1 Credits ™: 1.50 ARRT Category A+ Credit: 1.75

FDA Discussions may include off-label uses.

Participants

Cynthia S. Santillan, MD, San Diego, CA (*Moderator*) Consultant, Robarts Clinical Trials, Inc Jason A. Pietryga, MD, Riverside, RI (*Moderator*) Nothing to Disclose Richard Tsai, MD, Saint Louis, MO (*Moderator*) Nothing to Disclose

Sub-Events

SSK07-01 Assessment of Fatty Liver Disease Using Twin Beam Dual-Energy CT Derived Fat Fraction

Participants Verena Hofmann, Basel, Switzerland (*Presenter*) Nothing to Disclose Aurelio Cosentino, MD, Torino, Italy (*Abstract Co-Author*) Nothing to Disclose Daniel Boll, Basel, Switzerland (*Abstract Co-Author*) Nothing to Disclose Markus M. Obmann, MD, San Francisco, CA (*Abstract Co-Author*) Nothing to Disclose Matthias Benz, MD, Basel, Switzerland (*Abstract Co-Author*) Nothing to Disclose

For information about this presentation, contact:

Verena.Hofmann@usb.ch

PURPOSE

The aim of this study was to compare parameters of liver fat quantification derived from single source twin beam dual energy computed tomography (deCT) and magnetic resonance imaging (MRI).

METHOD AND MATERIALS

We retrospectively analyzed 50 patients (28 male, 22 female, mean age 65 years) who underwent both abdomino-pelvic twin beam deCT (SOMATOM Definition Edge, Siemens, Germany) and abdominal MRI examinations. Region of interests were drawn on CT and MRI in each liver segment. The fat fraction (FF) and the virtual unenhanced attenuation values (VUE) derived from portal-venous phase deCT were quantified using commercially available software (Syngo.via, Siemens, Germany) and compared to the changes in signal intensity (SI) on in-phase (SIIP) and out-of-phase images (SIOP), as well as the signal intensity on the fat only images (SIF) (DIXON sequence). A p-value less than 0.05 was considered to indicate statistical significance.

RESULTS

456 of 459 liver segments were included in this analysis. 188 segments were classified as steatotic according to MRI. The FF in steatotic segments averaged $13.5\pm11\%$ compared to $2.2\pm7.9\%$ in non-steatotic segments (p<0.001). The FF was significantly correlated to the VUE attenuation vales (r=-0.94), changes in SIIP to SIOP (r=0.62), as well as SIF (r=0.5) (p<0.001). The color coded FF map readily indicated diffuse of focal fatty liver disease.

CONCLUSION

Quantitative analysis of liver fat fraction using single source twin beam dual energy computed tomography shows a strong correlation to the standard imaging parameters of fatty liver disease.

CLINICAL RELEVANCE/APPLICATION

Fatty liver disease should be reported due to increased risk for developing e.g. cirrhosis. Since steatosis can be easily missed on portal venous phase CT, deCT derived liver FF analysis improves the evaluation of liver parenchyma.

SSK07-02 Quantification of Fat in Hepatocellular Carcinoma (HCC) Using Multimaterial Decomposition (MMD) Analysis of Fast-Kilovolt-Peak Switching Dual-Energy CT Data: Comparison with Chemical Shift MR Imaging

Wednesday, Nov. 28 10:40AM - 10:50AM Room: S402AB

Participants

Takashi Ota, Suita, Japan (*Presenter*) Nothing to Disclose Masatoshi Hori, MD, Suita, Japan (*Abstract Co-Author*) Nothing to Disclose Kosuke Sasaki, MS, Hino, Japan (*Abstract Co-Author*) Employee, General Electric Company Hiromitsu Onishi, MD, Suita, Japan (*Abstract Co-Author*) Nothing to Disclose Atsushi Nakamoto, MD, Suita, Japan (*Abstract Co-Author*) Nothing to Disclose Noriyuki Tomiyama, MD,PhD, Suita, Japan (*Abstract Co-Author*) Research Grant, Canon Medical Systems Corporation Hideyuki Fukui, Suita, Japan (*Abstract Co-Author*) Nothing to Disclose Kazuya Ogawa, Suita, Japan (*Abstract Co-Author*) Nothing to Disclose Mitsuaki Tatsumi, MD, PhD, Suita, Japan (*Abstract Co-Author*) Nothing to Disclose

PURPOSE

Recent study showed that the multimaterial decomposition (MMD) analysis can accurately quantify hepatic fat in dual-energy CT (DECT) data. However, intratumoral fat quantification in hepatocellular carcinoma (HCC) by the MMD algorithm has not been evaluated yet, although there are some differences in component materials between liver parenchyma and HCC. The purpose of the study was to quantify HCC fat with the MMD algorithm using DECT, comparing with chemical shift MRI.

METHOD AND MATERIALS

Thirty-one consecutive patients having HCC (22 males; 9 females, mean age 66.5 ± 7 years) underwent non-enhanced and fourphases dynamic contrast-enhanced DECT (80 and 140 kVp) and MRI before liver surgery. Fat volume fraction (FVFDECT) images were generated by using the MMD algorithm on DECT data to quantify HCC fat and liver fat. Additionally, fat fraction (FFMRI) were measured for HCC and liver on dual-echo sequence using 1.5 or 3T MRI. The correlation between FVFDECT and FFMRI was evaluated using Pearson's correlation test. Real non-contrast-enhanced FVFDECT were compared with four-phases contrast enhanced FVFDECT to prove the reproducibility of MMD by using one-way ANOVA.

RESULTS

FVFDECT and FFMRI exhibited moderate correlations for HCC in all phases (r = 0.51, 0.47, 0.42, 0.47, 0.45, respectively; all *P* <0.05), and strong correlations for liver parencyma in all phases (r = 0.68, 0.65, 0.71, 0.72, 0.72, respectively; all *P* <0.05). Those correlation coefficients were significantly higher in the liver than in HCC for each phase (P = 0.005, 0.004, <0.001, <0.001, <0.001, respectively). FVFDECT did not differ significantly in all comparisons of scan phases regarding HCC fat or liver fat quantification by one-way ANOVA (P = 0.41, 0.81, respectively).

CONCLUSION

The MMD algorithm quantifying intratumoral fat in DECT images is reproducible across scan phases. However, correlation between FVFDECT and FFMRI was significantly lower for HCC than that for liver parenchyma.

CLINICAL RELEVANCE/APPLICATION

The MMD algorithm might eliminate the need for non-contrast CT scan to measure FVF because of its reproducibility, however, it is needed further technological improvement to quantify HCC fat.

SSK07-03 Non-Invasive MR Index for the Detection of Non-Alcoholic Steatohepatitis (NASH) in Patients with Non-Alcoholic Fatty Liver Disease (NAFLD)

Wednesday, Nov. 28 10:50AM - 11:00AM Room: S402AB

Participants

Jeong Woo Kim, MD, Seoul, Korea, Republic Of (*Presenter*) Nothing to Disclose Chang Hee Lee, MD, Seoul, Korea, Republic Of (*Abstract Co-Author*) Nothing to Disclose Yang Shin Park, MD, Seoul, Korea, Republic Of (*Abstract Co-Author*) Nothing to Disclose Kyeong Ah Kim, MD, Seoul, Korea, Republic Of (*Abstract Co-Author*) Nothing to Disclose Cheol Min Park, MD, Seoul, Korea, Republic Of (*Abstract Co-Author*) Nothing to Disclose

For information about this presentation, contact:

chlee86@korea.ac.kr

PURPOSE

To evaluate feasibility of MRI to predict NASH and to develop non-invasive MR index for the detection of NASH in patients with NAFLD

METHOD AND MATERIALS

This prospective study was approved by our IRB and the written informed consent was obtained from each patient. 47 patients with NAFLD who were scheduled to undergo or underwent US-guided parenchymal liver biopsy within 6 months were included. Biopsy specimens were graded according to SAF scoring system - semi-quantitative score of Steatosis (0-3), Activity [lobular inflammation (0-2)+ballooning (0-2)], and Fibrosis (0-4) - as NASH group (steatosis score>=1, activity score>=2, any fibrosis score) and non-NASH group. All patients underwent gadoxetic acid-enhanced MRI including MR spectroscopy (MRS), MR elastography (MRE), and T1 mapping. The diagnostic performance of MRS, MRE and T1 mapping for grading steatosis, activity, and fibrosis was evaluated by using ROC curve analysis. Non-invasive MR index, combination of liver signal fat fraction (FF), liver stiffness (LS) value, and T1 relaxation time, was developed for the prediction of SAF score using linear regression analysis. R-squared (R2) was obtained by plotting the predicted value against the observed value. The optimal cut-off value of SAF score differentiating NASH group from non-NASH group was determined using ROC curve analysis. Using the cut-off value, the diagnostic performance of MR index for the detection of NASH was evaluated.

RESULTS

20 NASH patients and 27 non-NASH patients were included. Using MRS, MRE, T1 mapping, the mean AUC for grading steatosis, fibrosis, and activity was 0.870, 0.951, and 0.664, respectively. Non-invasive MR index combining FF, LS value, and T1 relaxation time was $-3.819 + 0.037 \times FF + 1.4 \times LS$ value $+ 0.004 \times T1$ relaxation time. R-squared (R2) was 0.67. Cut-off value of SAF score differentiating NASH group from non-NASH group was 6. Using the cut-off value, MR index provided sensitivity of 84.2% and specificity of 82.1% for detecting NASH in patients with NAFLD.

CONCLUSION

Non-invasive MR index combining FF, LS value, and T1 relaxation time have high diagnostic performance for detecting NASH in patients with NAFLD.

CLINICAL RELEVANCE/APPLICATION

liver bionous a current cold standard for differentiating NACH from simple staateesis, has several drawbacks including invasiveness

sampling error, and cost. Non-invasive MR index may help detect NASH in patients with NAFLD.

SSK07-04 Association between Hepatic Magnetic Resonance Elastography-Based Mechanical Properties and Histologic Measures in Adults with Nonalcoholic Fatty Liver Disease without Liver Fibrosis

Wednesday, Nov. 28 11:00AM - 11:10AM Room: S402AB

Participants

Yali Qu, San Diego, CA (Presenter) Nothing to Disclose

Michael S. Middleton, MD, PhD, San Diego, CA (*Abstract Co-Author*) Institutional research contract, Alexion Pharmaceuticals, Inc; Institutional research contract, AstraZeneca PLC; Institutional research contract, BioClinica, Inc; Institutional research contract, Biomedical Systems; Consultant, Bracco Group; Institutional research contract, Bristol-Myers Squibb Company; Institutional research contract, Enanta; Institutional research contract, Galmed Pharmaceuticals Ltd; Institutional consultant contract, Genentech; Institutional research contract, General Electric Company; Institutional research contract, Gilead Sciences, Inc; Institutional research contract, Guerbet SA; Institutional research contract, ICON plc; Institutional research contract, Intercept Pharmaceuticals, Inc; Consultant, Kowa Company, Ltd; Consultant, MEDIAN Technologies; Consultant, IBM Corporation; Consultant, Novo Nordisk AS; Institutional research contract, Pfizer Inc; Stockholder, Pfizer Inc; Institutional research contract, Shire plc; Institutional research contract, Synageva; Institutional research contract, Siemens AG; Institutional research contract, VirtualScopics, Inc

Rohit Loomba, MD, MSc, La Jolla, CA (*Abstract Co-Author*) Grant, Adheron; Grant, Arora; Grant, Bristol-Myers Squibb Company; Grant, DAIICHI SANKYO Group; Grant, Galectin; Grant, Galmed Pharmaceuticals Ltd; Grant, General Electric Company; Grant, GENFIT SA; Grant, Gilead Sciences, Inc; Grant, Immuron Ltd; Grant, Intercept Pharmaceuticals, Inc; Grant, Janseen Inc; Grant, Kinemed; Grant, Madrigal Pharmaceuticals, Inc; Grant, Merck & Co, Inc; Grant, NGM Biopharmaceuticals, Inc; Grant, Promega Corporation Inc; Grant, Siemens AG; Grant, Sirius; Grant, Tobira Therapeutics, Inc

Meng Yin, PhD, Rochester, MN (Abstract Co-Author) Intellectual property, Magnetic Resonance Innovations, Inc; Stockholder, Resoundant, Inc

Jun Chen, PhD, Rochester, MN (Abstract Co-Author) Intellectual property, Magnetic Resonance Innovations, Inc Stockholder, Resoundant, Inc

Kevin J. Glaser, Rochester, MN (Abstract Co-Author) Intellectual property, Magnetic Resonance Elastography Technology; Stockholder, Resoundant, Inc

Jonathan C. Hooker, BS, San Diego, CA (Abstract Co-Author) Nothing to Disclose

Tanya Wolfson, MS, San Diego, CA (Abstract Co-Author) Nothing to Disclose

Yesenia Covarrubias, MS, La Jolla, CA (Abstract Co-Author) Nothing to Disclose

Ethan Sy, BS, San Diego, CA (Abstract Co-Author) Nothing to Disclose

Jeffrey B. Schwimmer, MD, San Diego, CA (Abstract Co-Author) Nothing to Disclose

Emily D. Bass, MA, San Diego, CA (Abstract Co-Author) Nothing to Disclose

Anthony Gamst, PhD, San Diego, CA (Abstract Co-Author) Nothing to Disclose

Yingzhen Zhang, MD, La Jolla, CA (Abstract Co-Author) Postdoctoral Research Fellowship, General Electric Company

Bin Song, MD, Chengdu, China (Abstract Co-Author) Nothing to Disclose

Scott B. Reeder, MD, PhD, Madison, WI (*Abstract Co-Author*) Institutional research support, General Electric Company; Institutional research support, Bracco Group; Founder, Calimetrix, LLC; Shareholder, Elucent Medical; Consultant, ArTara

Richard L. Ehman, MD, Rochester, MN (Abstract Co-Author) CEO, Resoundant, Inc Stockholder, Resoundant, Inc

Claude B. Sirlin, MD, San Diego, CA (*Abstract Co-Author*) Research Grant, Gilead Sciences, Inc; Research Grant, General Electric Company; Research Grant, Siemens AG; Research Grant, Bayer AG; Research Grant, ACR Innovation; Research Grant, Koninklijke Philips NV; Research Grant, Celgene Corporation; Consultant, General Electric Company; Consultant, Bayer AG; Consultant, Boehringer Ingelheim GmbH; Consultant, AMRA AB; Consultant, Fulcrum Therapeutics; Consultant, IBM Corporation; Consultant, Exact Sciences Corporation; Advisory Board, AMRA AB; Advisory Board, Guerbet SA; Advisory Board, VirtualScopics, Inc; Speakers Bureau, General Electric Company; Author, Medscape, LLC; Author, Resoundant, Inc; Lab service agreement, Gilead Sciences, Inc; Lab service agreement, ICON plc; Lab service agreement, Intercept Pharmaceuticals, Inc; Lab service agreement, Shire plc; Lab service agreement, Takeda Pharmaceutical Company Limited; Lab service agreement, sanofi-aventis Group; Lab service agreement, Johnson & Johnson; Lab service agreement, NuSirt Biopharma, Inc; Contract, Epigenomics; Contract, Arterys Inc

For information about this presentation, contact:

yaliquwestchina@gmai.com

PURPOSE

To investigate the association between hepatic magnetic resonance elastography (MRE)-based mechanical properties and histology in adults with known or suspected nonalcoholic fatty liver disease (NAFLD) with histology-confirmed absence of liver fibrosis.

METHOD AND MATERIALS

This IRB-approved, HIPAA-compliant, cross-sectional secondary analysis of prospective clinical trials included adults who underwent liver biopsy to assess known or suspected NAFLD and had no liver fibrosis histologically. Subjects were included who had undergone 2D, or both 2D and 3D MRE, and hepatic proton density fat fraction (PDFF) imaging at 3T. Mechanical properties included magnitude of the shear modulus ('shear stiffness') ($|G^*|$), and for 3D MRE, also storage modulus (G'), loss modulus (G'), shear attenuation and damping ratio ($\zeta = G/2G'$). Histologic features were scored (Nonalcoholic Steatohepatitis Clinical Research Network system). The association between mechanical parameters, and steatosis, inflammation, and ballooning was assessed using Wilcoxon-Mann-Whitney tests or Kruskal-Wallis tests. Spearman's correlation analyses were performed to assess association between mechanical parameters and age, BMI, and PDFF. Adjustment for multiple comparisons was not applied as this was an exploratory study.

RESULTS

89 subjects met the inclusion criteria (52 women; mean age 49 yrs; mean body mass index [BMI] 31 kg/m2), 77 of whom also had 3D MRE. $|G^*|$ measured by 2D MRE and G' measured by 3D MRE were significantly higher for patients with inflammation grade >=2 vs. grade <=1 (2.58±0.61 vs. 2.27±0.29 kPa, p=0.033 and 0.42±0.12 vs. 0.36±0.11 kPa, p=0.042, respectively). Hepatic G' and G' by 3D MRE and $|G^*|$ by both 2D and 3D MRE increased with age; correlation coefficients ranged from 0.25 to 0.31 (all p<0.03). No 2D or 3D hepatic MRE mechanical parameter had a significant association with BMI, MRI-PDFF, steatosis, or ballooning (p>=0.10). In patients with known or suspected NAFLD but with histology-confirmed absence of liver fibrosis, moderate to severe inflammation is associated with elevated hepatic shear stiffness measured by 2D MRE and loss modulus measured by 3D MRE. In this series, increasing age is associated with higher shear stiffness and hepatic storage and loss moduli.

CLINICAL RELEVANCE/APPLICATION

MRE-measured biomarkers show promise for detecting significant inflammation before the onset of fibrosis in NAFLD.

Honored Educators

Presenters or authors on this event have been recognized as RSNA Honored Educators for participating in multiple qualifying educational activities. Honored Educators are invested in furthering the profession of radiology by delivering high-quality educational content in their field of study. Learn how you can become an honored educator by visiting the website at: https://www.rsna.org/Honored-Educator-Award/ Richard L. Ehman, MD - 2016 Honored Educator

SSK07-05 Long-Term and Short-Term Repeatabilities of Hepatic Proton Density Fat Fraction Measurements across Field Strengths: Human and Phantom Studies

Wednesday, Nov. 28 11:10AM - 11:20AM Room: S402AB

Participants

Hye Jin Kim, MD, Suwon, Korea, Republic Of (*Abstract Co-Author*) Nothing to Disclose Bohyun Kim, MD, Suwon, Korea, Republic Of (*Presenter*) Research Grant, Bracco Group Jimi Huh, MD, Suwon, Korea, Republic Of (*Abstract Co-Author*) Nothing to Disclose Jei Hee Lee, MD, Suwon, Korea, Republic Of (*Abstract Co-Author*) Nothing to Disclose Jai Keun Kim, MD, PhD, Suwonsi, Korea, Republic Of (*Abstract Co-Author*) Nothing to Disclose

PURPOSE

To assess the long- and short-term repeatabilities of MR-based proton density fat fraction (PDFF) measurements across MR field strengths in nonalcoholic fatty liver disease (NAFLD) subjects and a phantom.

METHOD AND MATERIALS

A phantom consisted of 10 test tubes containing 3-50% of lard underwent MR-PDFF scans on 1.5T (Signa HDxt; GE) and 3.0T (Discovery 750 W; GE) units within a day and a 14-day interval, in addition to MR spectroscopy. For clinical scan, 20 prospectivelyenrolled clinically NAFLD patients underwent the same MR-PDFF scans. All subjects were asked to refrain from consuming excessive fatty meal or alcohol during the recess. A commercially available PDFF pulse sequence (IDEAL IQ, GE) was used for all scans. To estimate PDFF, two radiologists independently drew 1 cm2 circular region of interests on each Couinaud segment. The repeatability of PDFF measurements was assessed by within-subject coefficient of variation (wCV). The correlation of PDFF measurements and field strengths was evaluated.

RESULTS

In the phantom, MRS- and PDFF-measured FF showed excellent correlation in both 1.5T and 3.0T (r2=0.906 and 0.927). PDFFmeasured FF across field strengths showed strong correlation (r2=0.996) with mean difference of 1.1% and 95% limits of agreement ranging \pm 0.1 on Bland-Altman analysis. Within-day and two-week wCVs were 0.3-0.6% and 1.6% for 1.5T, 0.1-0.3% and 2% for 3.0T, 2.9-5.9% and 4.2-4.7% for across field strengths. In human, the mean \pm SD of the BMI and PDFF at 3.0T was 27.5 kg/m2 \pm 5.2 and 15.6% \pm 11.4 (range, 2.72-42.3%). PDFF-measured FF across field strengths showed strong correlation, with r2=0.995 and 0.996 for the same day, and 0.98 and 0.99 for two weeks interval. Within-day and two-week wCVs were 0.7-0.9% and 4.6% for 1.5T, 1.5-2.2% and 4.6% for 3.0 T, and 3.4-3.7% and 5.2-5.5% for across field strengths. Interobserver agreement for pooled PDFF measurement was excellent with intraclass correlation coefficient reaching 0.99.

CONCLUSION

MR-PDFF measured FF is highly reproducible across field strengths, readers, and 2-week interval. Based on the phantom and clinical scans, FF change in proportion of >5% indicates a true change in a longitudinal follow-up across field strengths.

CLINICAL RELEVANCE/APPLICATION

MR-PDFF scan is a reliable method for the longitudinal follow-up of NAFLD patients regardless of MR field strengths. Interval FF change in proportion of >5% indicates a true change across field strengths.

SSK07-06 Prediction of Hepatic Steatosis Using Sonographic Features

Wednesday, Nov. 28 11:20AM - 11:30AM Room: S402AB

Participants

Cheng W. Hong, MD, MS, San Diego, CA (Presenter) Nothing to Disclose Austin T. Marsh, MD, La Jolla, CA (Abstract Co-Author) Nothing to Disclose Tanya Wolfson, MS, San Diego, CA (Abstract Co-Author) Nothing to Disclose Jeremy S. Paige, MD, PhD, San Diego, CA (Abstract Co-Author) Nothing to Disclose Soudabeh Fazeli Dehkordy, San Diego, CA (Abstract Co-Author) Nothing to Disclose Alexandra A. Schlein, BS, San Diego, CA (Abstract Co-Author) Nothing to Disclose Elise Housman, San Diego, CA (Abstract Co-Author) Nothing to Disclose Lisa Deiranieh, San Diego, CA (Abstract Co-Author) Nothing to Disclose Charles Q. Li, MD, San Diego, CA (Abstract Co-Author) Nothing to Disclose Ashish P. Wasnik, MD, Ann Arbor, MI (Abstract Co-Author) Nothing to Disclose Hyun-Jung Jang, MD, Toronto, ON (Abstract Co-Author) Nothing to Disclose Christoph F. Dietrich, MD, Bad Mergentheim, Germany (Abstract Co-Author) Nothing to Disclose Fabio Piscaglia, Bologna, Italy (Abstract Co-Author) Research support, Bracco Group Speaker, Bayer AG Advisory Board, Bayer AG Speaker, Siemens AG Giovanna Casola, MD, San Diego, CA (Abstract Co-Author) Nothing to Disclose Mary K. O'Boyle, MD, La Jolla, CA (Abstract Co-Author) Nothing to Disclose Katherine M. Richman, MD, La Jolla, CA (Abstract Co-Author) Nothing to Disclose

Mark Valasek, San Diego, CA (Abstract Co-Author) Nothing to Disclose

Michael P. Andre, PhD, La Jolla, CA (Abstract Co-Author) Researcher, Siemens AG

Rohit Loomba, MD, MSc, La Jolla, CA (*Abstract Co-Author*) Grant, Adheron; Grant, Arora; Grant, Bristol-Myers Squibb Company; Grant, DAIICHI SANKYO Group; Grant, Galectin; Grant, Galmed Pharmaceuticals Ltd; Grant, General Electric Company; Grant, GENFIT SA; Grant, Gilead Sciences, Inc; Grant, Immuron Ltd; Grant, Intercept Pharmaceuticals, Inc; Grant, Janseen Inc; Grant, Kinemed; Grant, Madrigal Pharmaceuticals, Inc; Grant, Merck & Co, Inc; Grant, NGM Biopharmaceuticals, Inc; Grant, Promega Corporation Inc; Grant, Siemens AG; Grant, Sirius; Grant, Tobira Therapeutics, Inc

Claude B. Sirlin, MD, San Diego, CA (*Abstract Co-Author*) Research Grant, Gilead Sciences, Inc; Research Grant, General Electric Company; Research Grant, Siemens AG; Research Grant, Bayer AG; Research Grant, ACR Innovation; Research Grant, Koninklijke Philips NV; Research Grant, Celgene Corporation; Consultant, General Electric Company; Consultant, Bayer AG; Consultant, Boehringer Ingelheim GmbH; Consultant, AMRA AB; Consultant, Fulcrum Therapeutics; Consultant, IBM Corporation; Consultant, Exact Sciences Corporation; Advisory Board, AMRA AB; Advisory Board, Guerbet SA; Advisory Board, VirtualScopics, Inc; Speakers Bureau, General Electric Company; Author, Medscape, LLC; Author, Resoundant, Inc; Lab service agreement, Gilead Sciences, Inc; Lab service agreement, ICON plc; Lab service agreement, Intercept Pharmaceuticals, Inc; Lab service agreement, Shire plc; Lab service agreement, Takeda Pharmaceutical Company Limited; Lab service agreement, sanofi-aventis Group; Lab service agreement, Johnson & Johnson; Lab service agreement, NuSirt Biopharma, Inc; Contract, Epigenomics; Contract, Arterys Inc

For information about this presentation, contact:

cwhong@ucsd.edu

PURPOSE

Eight sonographic imaging features have been proposed to assess hepatic steatosis on conventional ultrasound (CUS). However, there is little guidance on applying these features towards a composite assessment. The purpose of this study is to explore the use of decision rules for assessing hepatic steatosis using sonographic features.

METHOD AND MATERIALS

This is a prospective study of adult patients with known or suspected hepatic steatosis. CUS images were acquired using a standardized protocol (Siemens S3000, 6C1HD transducer). Each patient was included twice in the image bank. Eight radiologists independently graded 8 features on ordinal scales (large hepatic vein blurring, main right portal vein blurring, anterior posterior right portal vein blurring, liver-kidney contrast, posterior beam attenuation, diaphragm definition, focal fat sparing, and liver echotexture) and overall impression of steatosis severity. Seven readers were academic faculty with liver ultrasound expertise, and one was a fourth year resident. Intra-reader agreement was computed using repeat exams. Features with highest agreement were selected as predictors for biopsy-based steatosis (dichotomized into grades 0 and 1 vs. grades 2 and 3) using a Classification and Regression Tree (CART) analysis. The classification accuracy of the decision rule was compared to that of the overall impression in predicting steatosis severity.

RESULTS

40 patients (16 male, 24 female; mean age 55 \pm 12 years) were included. The features with the highest reader agreement included in the CART regression were large hepatic vein blurring, liver-kidney contrast, posterior beam attenuation, and focal fat sparing. The CART used only large hepatic vein blurring, and achieved 74% accuracy (59% sensitivity, 86% specificity) for grade 2 or 3 steatosis. The radiologists' overall impression achieved 68% accuracy (83% sensitivity, 57% specificity). There was no significant difference in accuracy.

CONCLUSION

Large hepatic vein blurring may be the sonographic feature most predictive of hepatic steatosis. Accuracy was comparable to that of the radiologists' overall impression, and achieved higher specificity at the cost of lower sensitivity.

CLINICAL RELEVANCE/APPLICATION

Large hepatic vein blurring may be the sonographic feature most predictive of histological hepatic steatosis. If validated in future studies, additional emphasis should be placed on this feature during clinical practice.

SSK07-07 Quantification of Steatosis Using an Ultrasound Generated Hepato-Renal Index (HRI)

Wednesday, Nov. 28 11:30AM - 11:40AM Room: S402AB

Participants Stephen I. Johnson, MD, Jefferson, LA (*Presenter*) Nothing to Disclose Edward I. Bluth, MD, New Orleans, LA (*Abstract Co-Author*) Nothing to Disclose

For information about this presentation, contact:

stephen.johnson@ochsner.org

PURPOSE

Hepatorenal index (HRI) has been shown by Marshall et al (AJR Am J Roentgenol 2012; 199:997-1002) to be an effective, noninvasive ultrasound tool to screen patients for the presence of > 5% hepatic steatosis. The aim of this study was to further refine this HRI tool in order to stratify patients according to their degree of liver steatosis (< 5%, between 5%-20%, and > 20% steatosis).

METHOD AND MATERIALS

We carried out a retrospective review of 174 consecutive patients from 2015-2017 who had abdominal ultrasounds and a subsequent random liver biopsy within a month. The HRI was calculated and compared with the percent steatosis as assessed by histology.

RESULTS

HRI of 1.57 corresponded with > 20% steatosis with a sensitivity of 0.92, specificity of 0.83, negative predictive value of 0.96 and positive predictive value of 0.73. The HRI value of >5% steatosis was updated to 1.41 and corresponded with a sensitivity of 0.94,

specificity of 0.96, negative predictive value of 0.93, and positive predictive value of 0.96.

CONCLUSION

HRI can accurately place patients into categories of less than 5%, between 5%-20%, and greater than 20% steatosis.

CLINICAL RELEVANCE/APPLICATION

HRI is non-invasive, cheap tool which is free of side effects that can be used to accurately follow changes in steatosis over time and determine if therapeutic interventions are being successful and if disease is progressing or regressing.

SSK07-08 Non-Invasive Ultrasonographic Index for the Detection of Non-Alcoholic Steatohepatitis (NASH) in Patients with Non-Alcoholic Fatty Liver Disease (NAFLD)

Wednesday, Nov. 28 11:40AM - 11:50AM Room: S402AB

Participants

Jeong Woo Kim, MD, Seoul, Korea, Republic Of (*Presenter*) Nothing to Disclose Chang Hee Lee, MD, Seoul, Korea, Republic Of (*Abstract Co-Author*) Nothing to Disclose Jongmee Lee, Seoul, Korea, Republic Of (*Abstract Co-Author*) Nothing to Disclose Jae Woong Choi, MD, Seoul, Korea, Republic Of (*Abstract Co-Author*) Nothing to Disclose Kyeong Ah Kim, MD, Seoul, Korea, Republic Of (*Abstract Co-Author*) Nothing to Disclose Cheol Min Park, MD, Seoul, Korea, Republic Of (*Abstract Co-Author*) Nothing to Disclose

For information about this presentation, contact:

chlee86@korea.ac.kr

PURPOSE

1. To evaluate feasibility of US for the prediction of NASH in patients with NAFLD2. To compare diagnostic performance between index using shear wave elastography (SWE) with hepatic/renal echo intensity ratio (H/R ratio) and index using transient elastography (TE, FibroScan®) with controlled attenuation parameter (CAP) for the detection of NASH in patients with NAFLD

METHOD AND MATERIALS

This retrospective study was approved by our IRB and the requirement for informed consent was waived. 55 patients with NAFLD who underwent US-guided parenchymal liver biopsy, SWE with H/R ratio, and TE with CAP were included. Biopsy specimens were reviewed for histologic grading and NAFLD Activity Score (NAS) - the unweighted sum of scores for steatosis (0-3), lobular inflammation (0-3), and hepatocellular ballooning (0-2) - was calculated based on the NASH-CRN criteria. Patients were classified according to the NAS as NASH group (NAS>=5) and non-NASH group (NAS<5). The diagnostic performance of SWE, TE, H/R ratio, and CAP for grading fibrosis and steatosis was evaluated using ROC curve analysis with obtaining the AUC. Using linear regression analysis, indices were developed for the prediction of NAS using SWE with H/R ratio and TE with CAP, respectively. The diagnostic performance was evaluated and compared between two indices using ROC curve analysis.

RESULTS

24 NASH and 31 non-NASH patients were included. The AUC for grading >=G2 and >=G3 steatosis were 0.879 and 0.842 using H/R ratio, and 0.604 and 0.563 using CAP. The AUC for grading >=F1, >=F2, >=F3, and >=F4 fibrosis were 0.653, 0.747, 0.861, and 0.816 using SWE, and 0.742, 0.824, 0.858, and 0.880 using TE. Index using SWE with H/R ratio was $2.374 + 0.091 \times SWE + 0.356 \times H/R$ ratio (Index 1). Index using TE with CAP was $5.251 + 0.035 \times TE - 0.005 \times CAP$ (Index 2). In ROC curve analysis, index 1 showed higher tendency of AUC than index 2 (0.767 vs. 0.655, p=0.13) with corresponding sensitivity of 62.5% and specificity of 80.7%.

CONCLUSION

Index using SWE with H/R ratio have higher diagnostic performance than index using TE with CAP although statistically insignificant.

CLINICAL RELEVANCE/APPLICATION

Liver biopsy, which is a current gold standard for differentiating NASH from simple steatsosis, has several disadvantages including invasiveness, sampling error, and cost. Non-invasive US index using SWE and H/R ratio may help predict NASH in patients with NAFLD.

SSK07-09 Viscosity and Viscoelasticity Measurement in Patients with Nonalcoholic Fatty Liver Disease Using Shear Wave Ultrasound Elastography

Wednesday, Nov. 28 11:50AM - 12:00PM Room: S402AB

Participants Katsutoshi Sugimoto, MD, PhD, Tokyo, Japan (*Presenter*) Nothing to Disclose Hirohito Takeuchi, Tokyo, Japan (*Abstract Co-Author*) Nothing to Disclose Takao Itoi, Tokyo, Japan (*Abstract Co-Author*) Nothing to Disclose

For information about this presentation, contact:

sugimoto@tokyo-med.ac.jp

PURPOSE

To investigate the usefulness of the shear wave (SW) speed (related to viscoelasticity), dispersion slope (related to viscosity), and attenuation value (related to the degree of steatosis) obtained using a new ultrasound (US) elastography system in patients with histologically confirmed nonalcoholic fatty liver disease (NAFLD).

METHOD AND MATERIALS

A US-based SW imaging system (Aplio i800; Canon Medical Systems) was used to measure three US parameters: SW speed (m/s),

dispersion slope ([m/s]/kHz), and attenuation value (dB/cm/MHz). These parameters were compared against liver histopathologic findings such as fibrosis, ballooning, lobular inflammation, and steatosis as assessed by the NAFLD Activity Score in 24 patients diagnosed with NAFLD.

RESULTS

In univariate analysis, SW speed was significantly correlated with fibrosis (Spearman's rank correlation coefficient: ρ =0.77, P<0.01) and ballooning (ρ =0.59, P<0.01). Dispersion slope was significantly correlated with lobular inflammation (ρ =0.58, P<0.01), ballooning (ρ =0.53, P<0.01), and fibrosis (ρ =0.46, P=0.02). Attenuation value was significantly correlated with steatosis (ρ =0.71, P<0.01). In multivariable analysis with histologic features as independent variables, SW speed was significantly correlated with fibrosis (P<0.05), and dispersion slope was significantly correlated with lobular inflammation (P<0.05). However, attenuation value was not significantly correlated with steatosis (P=0.07).

CONCLUSION

SW speed is more useful than dispersion slope for predicting the degree of fibrosis, and dispersion slope is more useful than SW speed for predicting the degree of necroinflammation.

CLINICAL RELEVANCE/APPLICATION

Dispersion slope, which reflects viscosity, may provide additional pathophysiological insight into NAFLD.



SSK08

Gastrointestinal (Dual-Energy CT Techniques)

Wednesday, Nov. 28 10:30AM - 12:00PM Room: S404CD



AMA PRA Category 1 Credits ™: 1.50 ARRT Category A+ Credit: 1.75

FDA Discussions may include off-label uses.

Participants

Bhavik N. Patel, MD,MBA, Stanford, CA (*Moderator*) Nothing to Disclose Lakshmi Ananthakrishnan, MD, Irving, TX (*Moderator*) Nothing to Disclose Priya R. Bhosale, MD, Bellaire, TX (*Moderator*) Nothing to Disclose

Sub-Events

SSK08-01 Application of Dual-Energy Spectral CT in the Quantitative Study of Blood Flow in Cirrhotic and Healthy Livers

Participants Zhanli Ren, Xianyang, China (*Presenter*) Nothing to Disclose Taiping He, Xianyang, China (*Abstract Co-Author*) Nothing to Disclose

For information about this presentation, contact:

395654582@qq.com

PURPOSE

To evaluate the application of material decomposition technique in spectral CT imaging in the quantitative study of blood flow in patients with liver cirrhosis and patients with healthy liver.

METHOD AND MATERIALS

30 patients with liver cirrhosis diagnosed clinically were enrolled as the study group while 30 abdominal patients whose liver and portal vein enhancement examination were normal as a control group.All patients underwent Spectral CT imaging and iodine-based material decomposition (MD) images were reconstructed. The iodine concentration (IC) was measured in five liver lobes (Caudate, left lateral, left inner, right anterior and right posterior) in both the arterial phase (AP) and portal venous phase (VP) on the iodine-based MD images. The average and total iodine concentrations of the liver were calculated, as well as the arterial iodine fraction (AIF=ICAP/ICVP) and the portal venous iodine concentration (PVIC=ICVP - ICAP). These parameters between the two groups were statistically compared by using independent sample t test.

RESULTS

The iodine concentrations in the five liver lobes in patients with liver cirrhosis were the same in AP (P>0.05), but the iodine concentrations of study group in portal venous phase were statistically lower than those of the control group (P<0.05). The average IC ($6.02\pm2.12mg/ml$) and total IC ($33.74\pm10.84mg/ml$) in the liver parenchyma in AP of liver cirrhosis were statistically the same as those in the control group (5.85 ± 1.79 and $33.04\pm9.28mg/ml$) (P>0.05); while the average IC ($19.42\pm3.28mg/ml$) and the total IC ($99.83\pm16.65mg/ml$) in VP of liver cirrhosis were lower than those in the control group (22.82 ± 3.83 and $117.27\pm19.45mg/ml$) (P<0.05) (Table 1). The AIF values were the same for the two groups, while the portal venous iodine concentrations in liver cirrhosis were lower than the control group (P < 0.05) (Table 2).

CONCLUSION

The material decomposition technology in Spectral CT can be used to assess the change and difference of blood flow between liver cirrhosis and healthy liver.

CLINICAL RELEVANCE/APPLICATION

The material decomposition technology in Spectral CT may be used to provide more evidence for early diagnosis of liver cirrhosis.

SSK08-02 Influence of Radiation Dose on Quantitative Tumor Measurements Using a Dual-Source, Single-Energy CT Acquisition

Wednesday, Nov. 28 10:40AM - 10:50AM Room: S404CD

Participants

Mathias Meyer, Durham, NC (*Presenter*) Researcher, Siemens AG; Researcher, Bracco Group Federica Vernuccio, MD, Palermo, Italy (*Abstract Co-Author*) Research support, Siemens AG Fernando Gonzalez, Santiago, Chile (*Abstract Co-Author*) Nothing to Disclose Hans-Christoph R. Becker, MD, PhD, Stanford, CA (*Abstract Co-Author*) Nothing to Disclose Bhavik N. Patel, MD, MBA, Stanford, CA (*Abstract Co-Author*) Nothing to Disclose Rendon C. Nelson, MD, Durham, NC (*Abstract Co-Author*) Research Consultant, General Electric Company; Research Consultant, Nemoto Kyorindo Co, Ltd; Consultant, VoxelMetrix, LLC; Co-owner, VoxelMetrix, LLC; Advisory Board, Bracco Group; Advisory Board, Guerbet SA; Research Grant, Nemoto Kyorindo Co, Ltd; Speakers Bureau, Bracco Group; Royalties, Wolters Kluwer nv Daniele Marin, MD, Durham, NC (*Abstract Co-Author*) Research support, Siemens AG

PURPOSE

To determine the effect of different dose levels on quantitative tumour measurements from one dual-source, single-energy CT (DSCT) acquisition.

METHOD AND MATERIALS

A total of 23 patients with 39 metastatic liver lesions were enrolled in this HIPAA-compliant and IRB approved study. Patient underwent a clinically indicated DSCT of the abdomen with reconstruction of seven radiation dose levels (25%, 37.5%, 50%, 63.5%, 75%, 88.5% as well as a 100% corresponding to a diagnostic CT dose level scan [mean CTDIvol 10.4mGy]) by using different combination of projection data of the two tubes from a single DSCT acquisition. CT data were reconstructed using a second-generation iterative reconstruction algorithm. For each dose level, unidimensional measurements of tumor size according to RECIST 1.1 criteria were obtained by four independent and blinded readers using a conventional manual approach, as well as a semi-automated approach using two commercially available lesion segmentation tools (Syngo.Via, Siemens Healthineers and Mint lesion, Mint Medical GmbH). All readers repeated lesion measurements after 4 weeks for measurement of intra-reader variability. The measurements obtained at 100% dose served as the reference standard for each reader.

RESULTS

There was an excellent intra-reader correlation of $r_2=0.93$ (range: 0.93 - 0.94 for all readers) with an intra-reader measurement error of 7.2% 7.9% (range 4.9%-8.6%). For the 25% dose level datasets the inter-reader measurement error was statistically significantly higher compared to the 75% datasets, for both the readers and semi-automatic software algorithms (p<0.0252). Of note, the overall intra-reader measurement error (7.2% 7.9%) was significantly higher than the overall measurement error for different dose levels (6.3% 6.3%) (p=0.001).

CONCLUSION

Our data suggest that reductions in radiation dose up to 72.5% may not significantly affect manual and semi-automated unidimensional measurements of tumor size. Intra- and inter-reader variability affected unidimensional measurements of tumor size statistically significantly more than a decrease radiation dose.

CLINICAL RELEVANCE/APPLICATION

CT scans with a dose level of 37.5% allow for a high reproducible and accuracy of quantitative tumour measurements, potentially reducing cumulative radiation exposure of oncological staging CTs.

SSK08-05 Virtual Monoenergetic Images from Spectral Detector CT for Visualization of Hypodense Liver Lesions: Contrast Blooming Vice Versa-Proof of Concept in a 3D-Printed Phantom and Evaluation in Patients

Wednesday, Nov. 28 11:10AM - 11:20AM Room: S404CD

Awards

Student Travel Stipend Award

Participants

Nils Grosse Hokamp, MD, Cleveland, OH (*Presenter*) Nothing to Disclose Verena Obmann, MD, Cleveland, OH (*Abstract Co-Author*) Nothing to Disclose Rivka Kessner, MD, Cleveland, OH (*Abstract Co-Author*) Nothing to Disclose Robert C. Gilkeson, MD, Cleveland, OH (*Abstract Co-Author*) Research Consultant, Riverain Technologies, LLC; Research support, Koninklijke Philips NV; Research support, Siemens AG; Research support, General Electric Company Stefan Haneder, MD, Cologne, Germany (*Abstract Co-Author*) Nothing to Disclose Elias Kikano, MD, Cleveland, OH (*Abstract Co-Author*) Nothing to Disclose Thorsten Persigehl, MD, New York, NY (*Abstract Co-Author*) Nothing to Disclose Nikhil H. Ramaiya, MD, Jamaica Plain, MA (*Abstract Co-Author*) Nothing to Disclose

For information about this presentation, contact:

nils.grosse-hokamp@uk-koeln.de

PURPOSE

There is a well-known boost of iodine associated-attenuation in low keV virtual monoenergetic images (VMI_low) which is frequently used to improve visualization of lesions and structures that take up contrast media (e.g. hemangiomas, hypervascular metastases or vessels in CT-angiography). This study aimed to evaluate this contrast vice versa: Does improved attenuation of the liver parenchyma allow for improved visualization of little or none-enhancing lesions?

METHOD AND MATERIALS

For the phantom portion a 3D-printed phantom mimicking the shape of a human liver exhibiting a lesion in its center was designed and printed. Both, parenchyma- and lesion-mimic were filled with iodine-solutions of different concentrations exhibiting an attenuation of 80, 100, 120 HU for parenchyma- and 0, 40, 60 HU for lesion-mimics. Further, a total of 75 patients with MRI or follow-up proven cysts and/or hypodense metastases was included. Imaging was performed on a spectral detector CT scanner (SDCT) and VMI of 40-120 keV as well as conventional images (CI) were reconstructed. Regions of interest were placed in lesion and parenchyma (-mimics) on CI and transferred to VMI. Signal- and contrast-to-noise ratio were calculated. Data was statistically assessed using ANOVA with Tukey's posthoc to adjust for multiple comparisons.

RESULTS

In phantoms, S/CNR was significantly higher in VMI_low. A cyst (0HU lesion mimic) in highly attenuating liver parenchyma (120HU) on CI yielded a CNR of 6.4 ± 0.8 ; using 40keV images, mildly hypodense lesions in poorly attenuating liver parenchyma exhibited a similar CNR (5.8 ± 0.9 ; p<=0.05). The same tendency was observed in patients, again cysts in CI yielded similar values as metastases in VMI_low (4.4 ± 1.2 and 3.9 ± 1.8 , respectively, p<=0.05).

CONCLUSION

The improved attenuation of the liver outweighs increasing in attenuation of the lesion itself. Hence, VMI_low from SDCT allow for an improved visualization of hypodense focal liver lesions exploiting the concept of contrast blooming vice versa.

CLINICAL RELEVANCE/APPLICATION

Low keV VMI should be considered when screening after focal liver lesions, irrespective of the expected imaging characteristic.

Honored Educators

Presenters or authors on this event have been recognized as RSNA Honored Educators for participating in multiple qualifying educational activities. Honored Educators are invested in furthering the profession of radiology by delivering high-quality educational content in their field of study. Learn how you can become an honored educator by visiting the website at: https://www.rsna.org/Honored-Educator-Award/ Nikhil H. Ramaiya, MD - 2017 Honored Educator

SSK08-06 Quantification of the Liver-Iron Fraction Using Spectral CT Imaging and Material Decomposition Technique: A Vitro Experiment Study

Wednesday, Nov. 28 11:20AM - 11:30AM Room: S404CD

Participants

Tingting Xie JR, MD, Shenzhen, China (*Presenter*) Nothing to Disclose Guanxun Cheng, Shenzhen, China (*Abstract Co-Author*) Nothing to Disclose

PURPOSE

Our first goal was to build in vitro liver-iron model in order to provide a phantom for iron content quantification in study. The second goal was to evaluate the feasibility and accuracy of using spectral imaging and material decomposition techniques for iron density quantification to provide a basis for the precise iron quantification in clinical use.

METHOD AND MATERIALS

Liver-iron mixture samples were prepared as described. A total of six homogeneous liver-iron mixed samples with a iron content of 0, 3.125, 6.25, 12.5, 25, 50 mg/mL. All samples were scanned on a GE Revolution CT scanner using GSI mode with rapid tube voltage switching between 80-140 kVp, and with tube current 200mA, 320mA, 485mA respectively. After the CT scan reconstructed imaging data were processed with GSI imaging analysis software package for material decomposition and characterization. Iron concentration (on iron-water bases,Unit:mg/mL) was measured. The difference of measured iron concentration(VIC) between 3 groups of tube currents was analyzed by one-way ANOVA. A linear regression was performed to analyze the relationship between the VIC and the actual iron concentration.

RESULTS

(1) We had successfully developed models in vitro for iron content quantification. (2) There was no significant difference in VIC between 3 tube current groups, P=0.999, F=0.001. (3) The model showed good linear relationship between the measured iron concentration and actual iron concentration. And the linear correlation equation was y=2.177x-2.820, $R^2 = 0.995$, P<0.001, F=3186.883.

CONCLUSION

(1) Spectral imaging and material decomposition techniques were demonstrated to provide accurate and reliable measurement of iron content for liver-iron model, which will contribute to the development of clinical iron content quantification assays. (2) The quantification of the liver-iron fraction was not affected by radiation dose.

CLINICAL RELEVANCE/APPLICATION

This study demonstrated the feasibility of using CT spectral imaging and material decomposition techniques to precisely quantify the iron concentrations. The advantages of this quantitative method are non-invasive, high accuracy, without additional scanning, and the technique can be used to guide the treatment of relieving iron overload in hereditary hemochromatosis and acquired hemochromatosis, and assist the diagnosis of canceration of liver cirrhosis nodules.

SSK08-07 The Influence of Liver Fat Deposition on the Quantification of the Liver-Iron Fraction Using Spectral CT Imaging and Material Decomposition Technique: A Vitro Experiment Study

Wednesday, Nov. 28 11:30AM - 11:40AM Room: S404CD

Participants

Tingting Xie JR, MD, Shenzhen, China (*Presenter*) Nothing to Disclose Guanxun Cheng, Shenzhen, China (*Abstract Co-Author*) Nothing to Disclose

PURPOSE

Our first goal was to build in vitro liver iron- fat deposition model in order to provide a phantom for iron content quantification in study. The second goal was to evaluate the feasibility and accuracy of using spectral imaging and material decomposition techniques for iron density quantification under the condition of simultaneous fat deposition and iron deposition in the liver.

METHOD AND MATERIALS

Liver-iron-fat mixture samples were prepared as described. A total of 18 samples(3 groups) of homogeneous liver-iron mixed samples with iron concentration gradient of 0, 10, 20, 30, 40, 50 mg/mL were prepared(group A, B and C), group A, B and C added fat with volume percentage of 10%, 30% and 60% respectively. All samples were scanned on a GE Revolution CT scanner using GSI mode with rapid tube voltage switching between 80-140 kVp, tube current 485mA. After the CT scan reconstructed imaging data were processed with GSI imaging analysis software package for material decomposition and characterization. Iron concentration (on iron-fat bases) measured with consistent regions of interest (ROIs) and statistical analysis. A linear regression was performed to analyze the relationship between the measured iron concentration and the actual iron concentration.

RESULTS

(1) We had successfully developed liver iron- fat models in vitro. The designed iron concentration range covered clinical iron content in liver, and the fat volume ratio of 10%, 30% and 60% simulated the mild, moderate and severe fatty liver respectively. (2) The model showed good linear relationship between the measured iron concentration and actual iron concentration. And the linear correlation equation were yA=0.575x-11.222, ($R^2=0.927$, P=0.005, F=52.038), yB=0.848x-2.303($R^2=0.884$, P=0.011, F=31.481), yC=0.788x-9.998($R^2=0.949$, P=0.003, F=76.068).

CONCLUSION

(1) Spectral imaging and material decomposition techniques were demonstrated to provide accurate and reliable measurement of iron content for liver-iron-fat model. (2) Fat affect the results of measured iron concentration.

CLINICAL RELEVANCE/APPLICATION

This study demonstrated the feasibility of using CT spectral imaging and material decomposition techniques to precisely quantify the iron concentrations under the condition of simultaneous fat deposition and iron deposition, and can be used to guide the treatment of relieving iron overload in hereditary hemochromatosis and acquired hemochromatosis.

SSK08-08 Dual Energy CT Iodine Maps for Response Assessment in Colorectal Liver Metastases (CLM) Treated With a Multikinase Inhibitor (MKI) with Anti-Angiogenic Activity

Wednesday, Nov. 28 11:40AM - 11:50AM Room: S404CD

Participants

Uday Patel, London, United Kingdom (*Presenter*) Nothing to Disclose Khurum Khan, London, United Kingdom (*Abstract Co-Author*) Nothing to Disclose Ed McDonagh, MSc, London, United Kingdom (*Abstract Co-Author*) Nothing to Disclose David Cunningham, MD, MRCP, Sutton, United Kingdom (*Abstract Co-Author*) Nothing to Disclose Dow-Mu Koh, MD,FRCR, Sutton, United Kingdom (*Abstract Co-Author*) Nothing to Disclose Maria Antonietta Bali, MD, PhD, Brussel, Belgium (*Abstract Co-Author*) Nothing to Disclose

For information about this presentation, contact:

udaypatel2@nhs.net

PURPOSE

To assess changes in quantitative CT iodine maps in patients with CLM treated with a MKI with known anti-angiogenic activity and to assess their relationships with treatment outcomes.

METHOD AND MATERIALS

After IRB approval, 28 patients with CLM were prospectively consented and underwent dual energy CT studies on a Siemens SOMATOM CT scanner before and at 8 weeks after treatment. Iodine maps were generated from 3 mm dual energy CT images acquired in the arterial and portovenous phases. In each patient, regions of interest were drawn around a target hepatic metastasis to record the average iodine uptake before and after treatment, as well as the absolute and percentage change in iodine uptake after treatment. Results were compared between responders and non-responders, defined by RECIST 1.1 and clinical criteria. The diagnostic performance of CT iodine uptake for identifying responders was assessed by ROC analysis, and the relationship to overall survival (OS) was evaluated by Kaplan-Meier analysis.

RESULTS

Of the 28 patients, 16 patients were responders and 12 non-responders. Across the entire cohort, a significant decrease in the median averaged iodine uptake after treatment in arterial (17.06 vs. 7.86, p<0.0002) and portovenous phases (20.34 vs. 14.06, p<0.0001) was observed. However, there was no significant difference in the mean absolute or percentage decrease in iodine uptake on arterial (-6 vs -4.5, p=0.82 and -65 vs -38, p=0.22) or portovenous (-8.4 vs -6.1, p=0.10 and -41 vs -28, p=0.17) phase between the two groups. A -33.6% reduction in iodine uptake showed 68.8% sensitivity and 81.8% specificity for identifying responders, but this threshold showed no relationship with OS (36 vs. 29 weeks, p=0.3278).

CONCLUSION

A significant decrease in iodine uptake was observed across the study cohort on arterial and portovenous phase CT after antiangiogenic therapy. Notwithstanding with small numbers, a significant difference in CT iodine uptake between responders and nonresponder was not observed thus the technique cannot be used to inform treatment decisions at this stage.

CLINICAL RELEVANCE/APPLICATION

Dual energy CT iodine maps can not yet be used for response assessment in colorectal liver metastases treated with antiangiogenic agents.

SSK08-09 How Reliable are CT-Based Measurements of Iodine Concentration? A Comparison of the Minimum Detectable Concentration Difference Among Single-Source and Dual-Source Dual-Energy CT

Wednesday, Nov. 28 11:50AM - 12:00PM Room: S404CD

Participants

Andre Euler, MD, Durham, NC (Presenter) Fellowship funded, General Electric Company

Justin B. Solomon, PhD, Durham, NC (Abstract Co-Author) License agreement, Sun Nuclear Corporation; License agreement, 12 Sigma Technologies

Maciej A. Mazurowski, MS, PhD, Durham, NC (Abstract Co-Author) Nothing to Disclose

Ehsan Samei, PhD, Durham, NC (*Abstract Co-Author*) Research Grant, General Electric Company; Research Grant, Siemens AG; Advisory Board, medInt Holdings, LLC; License agreement, 12 Sigma Technologies; License agreement, Gammex, Inc Rendon C. Nelson, MD, Durham, NC (*Abstract Co-Author*) Research Consultant, General Electric Company; Research Consultant, Nemoto Kyorindo Co, Ltd; Consultant, VoxelMetrix, LLC; Co-owner, VoxelMetrix, LLC; Advisory Board, Bracco Group; Advisory Board, Guerbet SA; Research Grant, Nemoto Kyorindo Co, Ltd; Speakers Bureau, Bracco Group; Royalties, Wolters Kluwer nv

euler.rad@gmail.com

PURPOSE

To assess the impact of scan- and patient-related factors on the error and the minimum detectable difference in iodine concentration among a wide range of different imaging conditions for second- and third-generation single-source fast kV-switching and dual-source dual-energy CT (DECT).

METHOD AND MATERIALS

Lesions of nine iodine concentrations (0.2 - 4 mgI/mL) were emulated in a 3D-printed phantom of medium and large size. Each combination of concentration and size was scanned in dual-energy mode on four different second- and third-generation single-source (SS) fast-kV switching and dual-source (DS) DECTs. Radiation doses were 7, 10 mGy (medium size) and 10, 13, 16 mGy (large size). Iodine maps were reconstructed with FBP and vendor-specific iterative reconstruction algorithms. ROI measurements of iodine concentration were made from each reconstructed iodine map with an automated script (243,000 total measurements). Absolute error of iodine quantification (E) was calculated. Multivariate regression models determined the influence of CT scanner condition, iodine concentration, phantom size, radiation dose, and reconstruction algorithm on E. Minimum detectable difference in iodine concentration, Dmin, was estimated for each pair of imaging conditions (including inter- and intra-condition comparisons). For a given pair of imaging conditions, Dmin was defined as the minimum difference in iodine concentration in which measured differences 95% of the time.

RESULTS

The iodine quantification error E was significantly lower in third-generation compared to second-generation DECT platforms (P<0.001). E significantly increased with increasing phantom size and decreasing radiation dose for all CT scanner conditions (P<0.001). Iodine concentration only significantly affected E for SS DECT (P<0.001). The minimum intra- and interconditional detectable difference in iodine concentration depended on patient- and scan-related factors and ranged from 0.4 mgI/mL to 1.5 mgI/mL

CONCLUSION

Patient- and scan-related factors have a significant impact on the error and minimum detectable difference in iodine concentration within and among second- and third-generation SS fast kV-switching and DS DECT.

CLINICAL RELEVANCE/APPLICATION

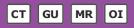
To inform radiologists about the impact of patient- and scan-related factors and the high error range of DECT-based iodine quantification when patients are imaged under different conditions.



SSK09

Genitourinary (Renal Masses)

Wednesday, Nov. 28 10:30AM - 12:00PM Room: N226



AMA PRA Category 1 Credits ™: 1.50 ARRT Category A+ Credit: 1.75

Participants

Atul B. Shinagare, MD, Boston, MA (*Moderator*) Advisory Board, Arog Pharmaceuticals, Inc; Research Grant, GTx, Inc Erick M. Remer, MD, Cleveland, OH (*Moderator*) Travel support, Bracco Group

Sub-Events

SSK09-01 Application of Deep-Learning Neural Network Model in Differentiation of Clear Cell Renal Carcinoma from Benign Oncocytoma Lesions

Participants

Faraz Farhadi, Bethesda, MD (*Presenter*) Nothing to Disclose Ziyue Xu, PhD, Bethesda, MD (*Abstract Co-Author*) Nothing to Disclose Dakai Jin, PhD, Bethesda, MD (*Abstract Co-Author*) Nothing to Disclose Ahmad Shafiei, MD, Bethesda, MD (*Abstract Co-Author*) Nothing to Disclose Uyen Hoang, Bethesda, MD (*Abstract Co-Author*) Nothing to Disclose Moozhan Nikpanah, Bethesda, MD (*Abstract Co-Author*) Nothing to Disclose Mojdeh Mirmomen, Bethesda, MD (*Abstract Co-Author*) Nothing to Disclose W. Marston Linehan, MD, Bethesda, MD (*Abstract Co-Author*) Nothing to Disclose Elizabeth C. Jones, MD, Bethesda, MD (*Abstract Co-Author*) Nothing to Disclose Daniel J. Mollura, MD, Bethesda, MD (*Abstract Co-Author*) Nothing to Disclose Ashkan A. Malayeri, MD, Bethesda, MD (*Abstract Co-Author*) Nothing to Disclose

For information about this presentation, contact:

Faraz.Farhadi@nih.gov

PURPOSE

To use feature representations based on deep convolutional neural network in differentiating Clear Cell Renal Cell Carcinoma (ccRCC) from Oncocytoma lesions on MRI T2-weighted images.

METHOD AND MATERIALS

94 ccRCCs from 31 patients (12 males, 19 females) and 37 Oncocytoma lesions from 9 patients (6 males, 3 females) were identified from an institutional urologic oncology database. Weighted-T2 MR images taken within 6 months prior to surgery were selected for analysis. Lesions were segmented on every slice. Local square ROIs around each lesion were extracted and resized to 224x224 as neural network inputs. Deep residual network ResNet-101 pre-trained on ImageNet dataset was then used as feature extractor without fine-tuning. Using feature representations from ResNet, the corresponding lesion slices were then classified into either ccRCC or Oncocytoma using Support Vector Machine. Performance was reported based on five-fold cross-validation classification results. Accuracy at the lesion level was calculated based on the majority (> 50%) of correctly predicted class for all the slices in one lesion. If the number of correctly predicted slices is equal to the number of incorrectly predicted slices, then the entire lesion is considered to be incorrectly classified.

RESULTS

Out of a total of 407 slices, our model showed an overall accuracy of 78.62% in detecting Oncocytoma from Clear Cell RCCs. At the lesion level, 80 out of 94 (85%) ccRCC lesions and 23 out of 37 (62%) of oncocytoma lesions were correctly identified. The model showed an overall accuracy of 78.63%.

CONCLUSION

Deep Learning with CNN showed promising diagnostic performance in differentiation of Oncocytoma lesions from Clear Cell RCC.

CLINICAL RELEVANCE/APPLICATION

Our training model can be used as support information in the differential diagnosis between Oncocytoma and Clear Cell.

SSK09-02 Semantic Modeling of Fat Poor Angiomyolipoma (fp-AML) on Multiphase Contrast-Enhanced CTs

Wednesday, Nov. 28 10:40AM - 10:50AM Room: N226

Participants

Yaqin Zhang, MD,PhD, Zhuhai, China (*Presenter*) Nothing to Disclose Yao Lu, Guangzhou, China (*Abstract Co-Author*) Nothing to Disclose Chuan Zhou, PhD, Ann Arbor, MI (*Abstract Co-Author*) Nothing to Disclose Jun Wei, PhD, Ann Arbor, MI (*Abstract Co-Author*) Nothing to Disclose Hong Shan, PhD,MD, Zhuhai, China (*Abstract Co-Author*) Nothing to Disclose

For information about this presentation, contact:

zhyaqin@mail.sysu.edu.cn

PURPOSE

To investigate the efficacy of noninvasive models in which clinical and radiographic descriptors were fused to differentiate the fp-AMLs from clear cell renal cell carcinoma (ccRCCs) in multiphase contrast-enhanced CT images.

METHOD AND MATERIALS

With IRB approval, we retrospectively collected patients at two academic hospitals (A and B) from Jan. 2006 to Dec. 2016 in Guangdong, China. All patients were clinically diagnosed with one suspicious ccRCC on multiphase contrast-enhanced CT acquired at least 30 days before surgical resection. Histopathologic data was served as ground truth. For model selection, we collected 118 cases (13 of 20 fpAMLs diameter <= 4cm and 46 of 98 ccRCCs diameter <= 4cm) at hospital A. An experienced radiologist identified the locations of lesions by examining all available information including the CTs and clinical reports, and provided descriptors of the lesion shapes, gray-level information as well as lesion margins. Twenty-four features including 5 clinical (gender, age, red blood cell in urine, white blood cell in urine, and symptom) and 19 radiographic descriptors were used. LASSO was used for feature selection and fp-AML prediction. To evaluate the efficacy of the developed fp-AML model, an independent set of 63 cases including 15cases (13 diameter <= 4cm) fp-AMLs and 48 (22 diameter <= 4cm) ccRCCs were collected from hospital B. Four additional radiologists independently provided the radiographic descriptors on multiphase CTs as well as the binary diagnostic decision of each lesion for baseline comparison.

RESULTS

On test set, the diagnosis accuracies of four readers were 0.74, 0.73, 0.71 and 0.90 while the models' achieved 0.81, 0.83, 0.87 and 0.92, respectively. Comparing to baselines, the improvements with models were 9.5%, 13.7%, 22.5% and 2.2%, respectively. For small lesions (diameter <= 4cm), the readers' accuracies were 0.57, 0.60, 0.57 and 0.89 while the models' were 0.74, 0.71, 0.83 and0.91, correspondingly. The improvements were 29.8%, 18.3%, 45.6% and 2.2%, respectively.

CONCLUSION

Multiple reader study found that the semantic model improved the diagnostic accuracies of fp-AMLs and the bigger improvement were observed for small lesion.

CLINICAL RELEVANCE/APPLICATION

The noninvasive diagnosis of fp-AMLs from ccRCCs is a challenging task in clinical practice. The semantic modeling has the potential to improve the diagnostic accuracy of fp-AMLs.

SSK09-03 Comparison of Computed Tomography (CT), Magnetic Resonance Imaging (MRI), and Contrast-Enhanced Ultrasound (CEUS) in the Evaluation of Unclear Renal Lesions: A 10-Year Single Center Experience

Wednesday, Nov. 28 10:50AM - 11:00AM Room: N226

Participants

Johannes Ruebenthaler, MD, Munich, Germany (*Presenter*) Nothing to Disclose Dirk-Andre Clevert, MD, Muenchen, Germany (*Abstract Co-Author*) Speaker, Siemens AG; Speaker, Koninklijke Philips NV; Speaker,

Bracco Group; Speaker, Samsung Electronics Co, Ltd;

PURPOSE

To compare the sensitivity and specificity of contrast-enhanced ultrasound (CEUS), computed tomography (CT) and magnetic resonance imaging (MRI) in the evaluation of unclear renal lesions to the histopathological outcome.

METHOD AND MATERIALS

A total of 255 patients with a single unclear renal mass with initial imaging studies between 2005 and 2015 were included. Patient ages ranged from 18 to 86 with (mean age 62 years; SD \pm 13). CEUS (255 patients), CT (88 out of 255 patients; 34.5%) and MRI (36 out of 255 patients; 14.1%) were used for determining malignancy or benignancy and initial findings were correlated with the histopathological outcome. Out of the 255 renal masses a total of 212 lesions were malignant (83.1%) and 43 were benign (16.9%). Diagnostic accuracy was tested by using histopathology as the gold standard.

RESULTS

CEUS showed a sensitivity of 99.1% (95% confidence interval (CI): 96.7%, 99.9%), a specificity of 80.5% (95% CI: 65.1%, 91.2%), a positive predictive value (PPV) of 96.4% (95% CI: 93.0%, 98.4%) and a negative predictive value (NPV) of 94.3% (95% CI: 80.8%, 99.3%). CT showed a sensitivity of 97.1% (95% CI: 89.9%, 99.6%), a specificity of 47.4% (95% CI: 24.4%, 71.1%), PPV of 87.0% (95% CI: 77.4%, 93.6%) and a NPV of 81.8% (95% CI: 48.2%, 97.7%). MRI showed a sensitivity of 96.4% (95% CI: 81.7%, 99.9%), a specificity of 75.0% (95% CI: 34.9%, 96.8%), a PPV)of 93.1% (95% CI: 77.2%, 99.2%) and a NPV of 85.7% (95% CI: 42.1%, 99.6%). Out of 212 malignant lesions 130 clear cell renal carcinomas, 59 papillary renal cell carcinomas, 7 chromophobe renal cell carcinomas, 4 combined clear cell and papillary renal cell carcinomas and 12 other malignant lesions were diagnosed. Out of 43 benign lesions 10 angiomyolipomas, 3 oncocytomas, 8 benign cysts and 22 other benign lesions were diagnosed. Using CEUS, 10 lesions were falsely identified as malignant or benign: 8 lesions were false positive and 2 lesions false negative. The 8 false-positive lesions included 5 oncocytomas or angiomyolipomas and 3 Bosniak category III cystic lesions.

CONCLUSION

CEUS is an useful method which can be additionally used to clinically differentiate between malignant and benign renal lesions. CEUS shows a comparable sensitivity, specificity, PPV and NPV to CT and MRI.

CLINICAL RELEVANCE/APPLICATION

CEUS can be easily performed during clinical routine for the evaluation of unclear renal lesions as a complementary imaging method.

SSK09-04 Diagnosis of Fuhrman Nuclear Grade in T1a Clear Cell Renal Cell Carcinomas on MRI: Can We

Accurately Differentiate High Grade from Low Grade Disease to Better Guide Management?

Wednesday, Nov. 28 11:00AM - 11:10AM Room: N226

Awards

Student Travel Stipend Award

Participants Kevin G. Moran, MBBCh, MD, Ottawa, ON (*Presenter*) Nothing to Disclose Nicola Schieda, MD, Ottawa, ON (*Abstract Co-Author*) Nothing to Disclose Trevor A. Flood, MD, FRCPC, Ottawa, ON (*Abstract Co-Author*) Nothing to Disclose Robert Lim, MD, Ottawa, ON (*Abstract Co-Author*) Nothing to Disclose Matthew D. McInnes, MD, PhD, Ottawa, ON (*Abstract Co-Author*) Nothing to Disclose

For information about this presentation, contact:

nschieda@toh.on.ca

PURPOSE

Multi-parametric (mp) MRI is accurate to diagnose clear cell renal cell carcinoma (cc-RCC). T1a cc-RCC is typically treated radically; however, low-grade tumors may be candidates for active surveillance. Fuhrman nuclear grading (FNG) of cc-RCC with biopsy is not accurate and this study evaluated mp-MRI to differentiate low from high-grade cc-RCC.

METHOD AND MATERIALS

42 consecutive solid <4cm cc-RCC with mp-MRI before nephrectomy between 2013 and 2017 (low-grade=FNG 1 [N=4] or 2 [N=27] and high-grade=FNG 3 [N=11]) were identified. Size, apparent diffusion coefficient (ADC), enhancement wash-in and wash-out (WI/WO) ratios and, chemical-shift signal-intensity index (SI-index) were measured. Subjectively, two blinded radiologists assessed for: 1) intracellular lipid (SI drop on opposed-phase MRI), 2) hemorrhage and 3) homogeneity. Discrepancies were resolved by consensus. Comparisons were performed using logistic regression and Chi-square and accuracy assessed using ROC.

RESULTS

Mean lesion size was 24 ± 7 (13-39) mm with no difference by FNG (p=0.45). 35.5% (11/31) low-grade tumors showed intracellular lipid compared to 9.1% (1/11) high-grade tumors (p=0.009). Agreement was moderate (K=0.65). SI-index was higher in low grade tumors (9.8 ± 34.4 versus 5.2 ± 19.9), p=0.283. Hemorrhage and homogeneity did not differ between groups (p>0.05). Mean ADC was higher in low-grade tumors (0.860 ± 0.142 versus 0.787 ± 0.229 mm2/sec) with significant differences observed for 10th centile ADC (p<0.001). WI index was higher in low-grade tumors for corticomedullary (p=0.019) and nephrographic phase (p=0.027) with no differences in WO. Presence of lipid was specific for diagnosis of low-grade disease (90.9% [58.7-98.8]) with low sensitivity (35.5% [19.2-54.6]). Logistic regression model combining presence of intracellular lipid, SIindex, ADC and WI yielded area under curve=0.79 (CI 0.62-0.96) with better accuracy (p=0.007, improved sensitivity=75.0% but lowered specificity=73.7%) compared to subjective assessment of lipid content alone.

CONCLUSION

Intracellular lipid in T1a clear cell RCC on MRI is highly specific for low-grade disease but with low sensitivity. Combining presence of lipid with ADC, SI-index and enhancement features improved accuracy of diagnosis.

CLINICAL RELEVANCE/APPLICATION

Multi-parametric MRI is accurate to differentiate low-grade and high-grade solid T1a clear cell tumors which may better inform management decisions.

SSK09-05 Radiogenomic Association Study Between PET/MR Imaging Features and Regional Histological and Gene Expression Status of Primary Clear Cell Renal Cell Carcinoma

Wednesday, Nov. 28 11:10AM - 11:20AM Room: N226

Participants

Sheng-Che Hung, MD, Chapel Hill, NC (*Presenter*) Nothing to Disclose Qingbo Yin, Dalian, China (*Abstract Co-Author*) Nothing to Disclose Julia R. Fielding, MD, Dallas, TX (*Abstract Co-Author*) Nothing to Disclose Amir H. Khandani, MD, Chapel Hill, NC (*Abstract Co-Author*) Consultant, Progenics Pharmaceuticals, Inc; Consultant, F. Hoffmann-La Roche Ltd; Michael Woods, Chapel Hill, NC (*Abstract Co-Author*) Nothing to Disclose Matthew Milowsky, MD, Chapel Hill, NC (*Abstract Co-Author*) Nothing to Disclose Eric Wallen, MD, Chapel Hill, NC (*Abstract Co-Author*) Nothing to Disclose Wendy K. Rathmell, Nashville, TN (*Abstract Co-Author*) Nothing to Disclose Dinggang Shen, Chapel Hill, NC (*Abstract Co-Author*) Nothing to Disclose Weili Lin, PhD, Chapel Hill, NC (*Abstract Co-Author*) Nothing to Disclose

For information about this presentation, contact:

shengche@med.unc.edu

PURPOSE

To discern potential associations between various imaging features and regionally altered histological and gene expression status of primary clear cell renal cell carcinomas (ccRCC) using a hybrid positron emission tomography/magnetic resonance (PET/MR) system.

METHOD AND MATERIALS

Between 2012 and 2013, eighteen ccRCC patients underwent presurgical PET/MR imaging. Ten histologically-confirmed ccRCC were included for subsequent analysis. Twenty-three regions-of-interest (ROIs) within primary tumors were pre-surgically defined using PET/MR images. Tissue samples of these ROIs were obtained during nephrectomy and sent for histological and microarray analyses.

Four images dataset, including Dixon fat and water images, dynamic contrast enhancement (DCE) from MR imaging and standard uptake value (SUV) from PET, were coregistered, and then radiomic imaging features were extracted from the pre-defined ROIs. Associations between these radiomic features, SUV, and 12 key selected genetic expressions of ccRCC were analyzed using sparse canonical correlation analysis.

RESULTS

Our study highlighted that combined structural and functional information from MRI and PET provides significant moderate to strong correlations between radiomic features and 8 of the selected genetic expressions, including FBP-1, BAP1, VHL, MUC4, PECAM1, PBRM1, TSC1, and MUC1 (P = 0.041). PET provides the highest loadings for the explanations of the radiomic correlations of expressions of PECAM1, while DCE in expressions of FBP-1, VHL, and PBRM1, and Dixon images in expressions of BAP1, MUC4, and TSC1.

CONCLUSION

Our study revealed the associations between PET/MR image features and regional variation of relevant biological features, underscoring the potential utility of PET/MR for discerning regional genetic variability in ccRCC.

CLINICAL RELEVANCE/APPLICATION

PET/MR identifies associations between radiomic features and genetic expressions. Knowledge on radiogenomic associations facilitates non-invasive mapping of tumor heterogeneity and selection of personalized treatments.

SSK09-06 Radiologically-Defined Tumor Necrosis in Clear Cell Renal Cell Carcinoma as a Surrogate of Pathologically-Defined Tumor Necrosis, Staging, and as a Size-Independent Prognostic Biomarker

Wednesday, Nov. 28 11:20AM - 11:30AM Room: N226

Participants

Firas Ś. Ahmed, MBChB, MPH, New York, NY (*Presenter*) Nothing to Disclose Lyndon Luk, MD, New York, NY (*Abstract Co-Author*) Nothing to Disclose Hiram Shaish, MD, New York, NY (*Abstract Co-Author*) Nothing to Disclose Xiaotao Guo, PHD, New York, NY (*Abstract Co-Author*) Nothing to Disclose Hao Yang, New York, NY (*Abstract Co-Author*) Nothing to Disclose A Ari Hakimi, MD, New York, NY (*Abstract Co-Author*) Nothing to Disclose Binsheng Zhao, DSc, New York, NY (*Abstract Co-Author*) License agreement, Varian Medical Systems, Inc; Royalties, Varian Medical Systems, Inc; License agreement, Keosys SAS; License agreement, Hinacom Software and Technology, Ltd; Oguz Akin, MD, New York, NY (*Abstract Co-Author*) Nothing to Disclose Lawrence H. Schwartz, MD, New York, NY (*Abstract Co-Author*) Committee member, Celgene Corporation Committee member, Novartis AG Committee member, ICON plc Committee member, BioClinica, Inc

For information about this presentation, contact:

f.ahmed05@fulbrightmail.org

PURPOSE

Pathologically defined tumor necrosis (PDTN) in clear cell renal cell carcinoma (ccRCC) has been considered as a prognostic factor. We aimed to measure radiologically-defined tumor necrosis (RDTN) of ccRCC and explore its association with PDTN, stage/grade, and with survival outcomes in a multi-institutional cohort.

METHOD AND MATERIALS

183 patients with ccRCC form The Cancer Genome Atlas (TCGA) with available contrast enhanced CT imaging were included in this study. Quantitative imaging methods were used to measure the volume of non-enhancing component of ccRCC (representing necrotic volume) based on the change of attenuation values of each tumor pixel between pre-contrast and postcontrast imaging. The percent of tumor necrosis ((necrotic volume/whole ccRCC volume) x 100) was used as a size-independent variable to represent RDTN. Associations of RDTN with pathological stage/grade were tested using Wilcoxon signed-rank test and with survival outcomes using Kaplan-Meier's curves and Cox regression analyses.

RESULTS

Median RDTN was 8% (interquartile range 3% - 17%) in this cohort. RDTN was higher in ccRCC with PDTN than those without (11% versus 7%; p-value= 0.042). There was no significant association between RDTN and pathological grading (p-value= 0.057). However, RDTN was higher in patients with AJCC pathological stage II, III, and IV in comparison with stage I (11% versus 5%; p-value<0.001). Patients with higher RDTN (>=median) had higher incidence of cancer recurrence after resection (Log-rank test p-value<0.001) and higher incidence of cancer-specific mortality (Log-rank test p-value<0.001). Controlling for age at diagnosis and stage of disease in a multivariable Cox-regresion model, patients with higher RDTN continued to have higher cancer recurrence and worse cancer-specific survival (Odds Ratios= 4.6 and 2.8; p-values= 0.003 and 0.020).

CONCLUSION

RDTN in ccRCC can be a surrogate to pathologically defined TN. Additionally, RDTN is associated with pathological staging and an important independent prognosticator.

CLINICAL RELEVANCE/APPLICATION

Radiologically-defined tumor necrosis in clear cell renal cell carcinoma conveys additional clinically-relevant information regarding tumor stage and prognosis.

SSK09-07 Developing a Sex-Specific Stratification System for Renal Cell Carcinoma Patients Using CT-Based Abdominal Fat and Muscle Quantification and Tumor Molecular Phenotyping

Wednesday, Nov. 28 11:30AM - 11:40AM Room: N226

Muhammad Naeem, MBBS, Saint Louis, MO (*Abstract Co-Author*) Nothing to Disclose Gerard K. Nguyen, MD, St. Louis, MO (*Abstract Co-Author*) Nothing to Disclose Vincent M. Mellnick, MD, Saint Louis, MO (*Abstract Co-Author*) Nothing to Disclose Joseph E. Ippolito, MD, PhD, Saint Louis, MO (*Presenter*) Nothing to Disclose

For information about this presentation, contact:

ippolitoj@wustl.edu

PURPOSE

Imaging biomarkers of metabolism such as tumor glucose uptake, patient muscle mass, and patient visceral fat have the ability to predict outcomes in cancer patients. Recent evidence has demonstrated sex differences in these metabolic measurements both on the imaging and the molecular levels. We wanted to determine if muscle mass and visceral fat measured by CT and molecular profiling of tumor glycolytic metabolism could be combined to develop a multiparametric sex-specific stratification system for RCC patients.

METHOD AND MATERIALS

This study included 222 patients with clear cell RCC included within The Cancer Genome Atlas (TCGA) and Cancer Imaging Archive (TCIA). The abdominal fat and glycolytic subtyping of patients were performed and used as published previously [PMID: 29558292] and combined with muscle quantification in this study. Abdominal fat was segmented into visceral, subcutaneous, and total fat areas as well as the normalized relative visceral fat area (visceral fat/total fat ratio, or rVFA). Glycolytic gene expression profiling of the tumors using TCGA data was used to metabolically classify the tumors. CT-based muscle mass and density measurements of the psoas muscle at L3 were performed. Biomarker optimization analyses were conducted to identify imaging metric thresholds that maximally stratified the patients based upon overall survival (OS).

RESULTS

The average psoas muscle area measured more in men than women (1171 vs 679.5 mm2) [p<0.0001]. The average psoas muscle density also measured more in men than women (41.1 vs 38.5 HU) [p=0.045]. Increased muscle area (>442 mm2 for women and >784 mm2 for men) was associated with increased OS (men p=0.002, women p=0.001). However, increased psoas density (>48.1 HU) was prognostic only for women; in this cohort, only 1/11 women died compared to the <48.1 HU group that experienced 29/66 deaths [p=0.02]. Combining rVFA, glycolysis and muscle area resulted in the identification of three sex-specific survival groups (Figure 1). Although all three variables contributed to female stratification (p<0.0001), male stratification was driven by glycolysis and muscle area (p=0.001).

CONCLUSION

Abdominal CT measurement of muscle and fat in tandem with molecular features of tumors predicts sex-specific outcomes in RCC patients.

CLINICAL RELEVANCE/APPLICATION

Sex differences in patient and tumor metabolism may provide a new risk-stratification system for patients with clear cell RCC.

Honored Educators

Presenters or authors on this event have been recognized as RSNA Honored Educators for participating in multiple qualifying educational activities. Honored Educators are invested in furthering the profession of radiology by delivering high-quality educational content in their field of study. Learn how you can become an honored educator by visiting the website at: https://www.rsna.org/Honored-Educator-Award/ Vincent M. Mellnick, MD - 2016 Honored EducatorVincent M. Mellnick, MD - 2018 Honored Educator

SSK09-08 Baseline CT Texture Feature of Metastatic Clear Cell Renal Cell Carcinoma Correlates with Sunitinib Therapy Response

Wednesday, Nov. 28 11:40AM - 11:50AM Room: N226

Participants Yichen Wang, MD, Beijing, China (*Presenter*) Nothing to Disclose Yan Chen, MD, Beijing, China (*Abstract Co-Author*) Nothing to Disclose Fei Xu, Beijing, China (*Abstract Co-Author*) Nothing to Disclose

For information about this presentation, contact:

annietiger1988@163.com

PURPOSE

Our study aimed to analyze tumor's baseline CT texture features and evaluate the correlation with first-line Sunitinib therapy response in metastatic clear cell renal cell carcinoma patients.

METHOD AND MATERIALS

Jan 2013 to July 2016, 48 metastatic RCC patients who received first line Sunitinib undertook abdominal CT scan before treatment. Forty-two patients were included. Clinical information (age, gender, surgery, MSCKK score and Heng's score, metastasis) and pathological information (tumor diameter, Fuhrmann grade, tumor thrombus) were collected. We collected 30 unenhanced CT images, 30 corticomedullary phase CT images and 36 nephrographic phase CT images from these patients. 2D CT texture parameters were generated from the image with the largest tumor diameter using histogram analysis and spatial gray-level dependence matrices (GLCM and RLM), respectively. Patients were divided into respond group (CR+PR) and non-respond group (SD+PD) according to RECIST criteria. We compared the CT texture feature, clinical and pathological parameters between two groups. We further assess the CT texture parameters with progression-free survival (PFS) using Kaplan-Meier analysis and Cox regression model.

RESULTS

Age ander tymer diameter and elinical progratic scores (MEVCC and Hands score) had no difference between respond and non

Age, gender, turnor diameter and clinical prognostic scores (MSKCC and nengs score) had no dimenence between respond and nonrespond group. Gray-level nonuniformity (GLN) from unenhanced and corticomedullary phase CT in respond group was significantly smaller than non-respond group (p<0.05). Logistic regression showed that GLN from unenhanced (p<0.05, OR 0.98(0.97, 0.99)) and corticomedullary phase CT (p<0.05, OR 0.96(0.94, 0.99)) independently associated with therapy response. GLN from unenhanced CT had AUC of 0.76(P<0.05, sensitivity 84.2%, specificity 63.6%); GLN from corticomedullary phase CT had AUC of 0.77 (P<0.05, sensitivity 73.7%, specificity 73.7%). Cox regression model showed that both GLN from unenhanced (p<0.05, HR 1.008(1.003,1.013)) and corticomedullary phase CT(p<0.05, HR 1.012(1.002,1.022)) had significant correlation with PFS.

CONCLUSION

For metastatic patients who received Sunitinib therapy, baseline CT texture parameter Gray-length nonuniformity reflecting tumor heterogeneity correlate with therapy response and PFS.

CLINICAL RELEVANCE/APPLICATION

CT texture parameter reflecting tumor heterogeneity has the potential to predict targeted therapy response before treatment in metastatic clear cell renal cell carcinoma.

SSK09-09 Role of Non-Target Disease and New Lesions as Defined by RECIST 1.1 in Determining Radiological Progression in Renal Cell Carcinoma

Wednesday, Nov. 28 11:50AM - 12:00PM Room: N226

Participants

Heidi Coy, Los Angeles, CA (*Presenter*) Nothing to Disclose
Michael L. Douek, MD, MBA, Los Angeles, CA (*Abstract Co-Author*) Nothing to Disclose
Hyung J. Kim, PhD, Los Angeles, CA (*Abstract Co-Author*) Research Consultant, MedQIA Imaging Core Laboratory
Matthew S. Brown, PhD, Los Angeles, CA (*Abstract Co-Author*) Nothing to Disclose
Kathleen Ruchalski, MD, Santa Monica, CA (*Abstract Co-Author*) Nothing to Disclose
Antonio J. Gutierrez, MD, Los Angeles, CA (*Abstract Co-Author*) Nothing to Disclose
Victor F. Sai, MD, Los Angeles, CA (*Abstract Co-Author*) Nothing to Disclose
Maitraya K. Patel, MD, Los Angeles, CA (*Abstract Co-Author*) Nothing to Disclose
Daniel J. Margolis, MD, Los Angeles, CA (*Abstract Co-Author*) Nothing to Disclose
Daniel J. Margolis, MD, Los Angeles, CA (*Abstract Co-Author*) Nothing to Disclose
Steven S. Raman, MD, Santa Monica, CA (*Abstract Co-Author*) Nothing to Disclose

For information about this presentation, contact:

hcoy@mednet.ucla.edu

PURPOSE

Progression free survival (PFS) based on RECIST 1.1 (R1.1) is still the most accepted primary end point for Phase III trials in renal cell carcinoma. Guidelines to assess tumor response based on changes in target lesions (TG) are quantifiable and established. However, guidelines to assess tumor response based on non-target (NT) or new lesions (NL) are qualitative and subject to interobserver variation. The purpose of our study was to retrospectively assess the most common criteria for determination of progressive disease (PD) assessed using R1.1 and how these progression events impact PFS.

METHOD AND MATERIALS

We conducted a secondary analysis of a cohort of patients enrolled in a Phase III global multi-center open label trial who were randomized 1:1 to open label anti-VEGFR tyrosine kinase inhibitor (TKI) therapies. All patients had previously progressed after having received prior VEGFR therapy and had measurable disease at screening (SCR). A chest CT, and either a CT or MRI of the abdomen and pelvis were acquired at SCR and every 8 weeks and interpreted at an imaging core laboratory for PD using R1.1. Kaplan-Meier plots, Holm's multiple comparisons and log-rank tests were performed to compare the median PFS for each R1.1 measurement assessment.

RESULTS

We analyzed 395 subjects with a mean age of 60.7 years (SD \pm 10.0). The mean number of follow-up visits was 4.9 (SD \pm 1.8) with a mean of 6.59 (SD \pm 3.70) months enrolled. PD was determined by growth of target (TG) lesions in 126 (32%) subjects (median PFS (mPFS) 5.44 months, IQR 3.87) appearance of a new lesion (NL) in 105 (27%) subjects (mPFS 3.61 months, IQR 3.60), and unequivocal progression of a non-target (NT) lesion in 73(18%) subjects (mPFS 2.79 months, IQR 3.54). The remaining subjects had PD determined by a combination of assessments: 33 (8%) by TG+NT (mPFS 3.54 months, IQR 3.70), 27(7%) by NT +NL (mPFS 3.74 months, IQR 2.48), 23(6%) by TG +NL (mPFS 3.64 months, IQR 5.38), and 8(2%) by TG+NT+NL (mPFS 4.52 months, IQR 4.98).

CONCLUSION

TG disease contributed to PD determination in less than 50% of patients and NT and NL were the most common criteria that defined PD, with a significant decrease in PFS compared to those patients who had PD determine by TG alone.

CLINICAL RELEVANCE/APPLICATION

In R1.1 assessment of metastatic RCC, both NT and NL alone, or in combination, are the dominant contributors to PD and may need updated R1.1 guidelines for NT and NL progression



SSK10

Genitourinary (PI-RADS)

Wednesday, Nov. 28 10:30AM - 12:00PM Room: N228



AMA PRA Category 1 Credits ™: 1.50 ARRT Category A+ Credit: 1.75

Participants

Nelly Tan, MD, Loma Linda, CA (*Moderator*) Nothing to Disclose Ronaldo H. Baroni, MD, Sao Paulo, Brazil (*Moderator*) Nothing to Disclose

Sub-Events

SSK10-01 Can 3+1=5? Evaluation of Dynamic Contrast Enhanced (DCE)-MRI "Upgraded" PI-RADS Version 2 Assessment Category 3 Peripheral Zone Observations: Should Size Impact the Final Assessment Category?

Participants

Sabarish Narayanasamy, MBBS,MD, Ottawa, ON (*Abstract Co-Author*) Nothing to Disclose Nicola Schieda, MD, Ottawa, ON (*Abstract Co-Author*) Nothing to Disclose Satheesh Krishna, MD, Ottawa, ON (*Presenter*) Nothing to Disclose Trevor A. Flood, MD, FRCPC, Ottawa, ON (*Abstract Co-Author*) Nothing to Disclose Matthew D. McInnes, MD, PhD, Ottawa, ON (*Abstract Co-Author*) Nothing to Disclose

For information about this presentation, contact:

nschieda@toh.on.ca

PURPOSE

PI-RADS v2 peripheral zone (PZ) observations considered indeterminate on diffusion-weighted imaging (assessment category 3) can be upgraded by 1 when showing early, focal and asymmetric hyper-enhancement on DCE-MRI. It is unclear whether upgraded category 3 PZ observations measuring >15 mm should be scored as category 4 or 5 lesions. This study evaluates DCE-MRI upgraded PI-RADS v2 PZ observations compared to other category 4 and 5 lesions and compares upgraded observations stratified by size when correlated to extra-prostatic extension (EPE), seminal vesicle invasion (SVI) and Gleason score (GS).

METHOD AND MATERIALS

With IRB approval, 230 men with mp-MRI before radical prostatectomy (RP) between 2013 and 2017 and with mp-MRI-RP maps confirming location of PZ dominant tumor foci were evaluated. Two blinded radiologists assigned PI-RADSv2 scores at independent review, then, both radiologists later jointly reviewed observations which were upgraded by abnormal DCE-MRI and discrepancies were resolved by consensus. Size of tumors was measured on axial T2-weighted MRI. Comparisons were performed using ANOVA and Chi-square.

RESULTS

9.1% (21/230) of tumors were upgraded by DCE, with size of upgraded tumors13 \pm 5 (6-24) mm. Upgraded tumors had lower EPE (52.4% [11/21]) and SVI (4.8% [1/21]) versus non-upgraded PIRADSv2 score 4 or 5 tumors (EPE 67.5% [141/209], SVI 22.0% [46/209]), p=0.16 and 0.06. 85.7% (18/21) of upgraded tumors had Gleason score (GS)=7 with 14.3% (3/21) GS >7. Assigning PI-RADSv2 score to upgraded lesions based on size, 23.8% (5/21) would be score 5 (size 16-24mm) and the remaining 76.2% (16/21) score 4. All five score 5 upgraded tumors (100% [5/5]) had EPE, 25% (1/5) had SVI and 40% (2/5) had GS >7. In upgraded lesions measuring <15 mm, 31.3% (5/16) had EPE, none had SVI and only one patient had GS >7.

CONCLUSION

Peripheral zone tumors which are upgraded by DCE-MRI are less aggressive compared to non-upgraded score 4 and 5 tumors with lower rates of EPE, SVI and GS>7. In upgraded tumors measuring >15 mm, an assessment category of 5 is appropriate due to higher rates of EPE, SVI and high-risk Gleason score compared to upgraded tumors measuring <15 mm.

CLINICAL RELEVANCE/APPLICATION

DCE-MRI upgraded PZ tumors are less aggressive than non-upgraded score 4 or 5 tumors; however, DCE-MRI upgraded peripheral zone observations measuring >15 mm should be assigned assessment category 5.

SSK10-02 Optimizing MRI-Based Size Thresholds for Prostate Cancer Lesions: Peripheral Zone Cancers are More Predictable than Transition Zone Tumors

Wednesday, Nov. 28 10:40AM - 10:50AM Room: N228

Participants Samy Mahjoub, MD, Berlin, Germany (*Presenter*) Nothing to Disclose Alexander D. Baur, MD, Berlin, Germany (*Abstract Co-Author*) Speaker, Bayer AG Julian Lenk, Berlin, Germany (*Abstract Co-Author*) Nothing to Disclose Madhuri Rudolph, Berlin, Germany (*Abstract Co-Author*) Nothing to Disclose Hannes Cash, Berlin, Germany (Abstract Co-Author) Nothing to Disclose

Patrick Asbach, MD, Berlin, Germany (Abstract Co-Author) Nothing to Disclose

Bernd K. Hamm III, MD, Berlin, Germany (*Abstract Co-Author*) Research Consultant, Canon Medical Systems Corporation; Stockholder, Siemens AG; Stockholder, General Electric Company; Research Grant, Canon Medical Systems Corporation; Research Grant, Koninklijke Philips NV; Research Grant, Siemens AG; Research Grant, General Electric Company; Research Grant, Elbit Imaging Ltd; Research Grant, Bayer AG; Research Grant, Guerbet SA; Research Grant, Bracco Group; Research Grant, B. Braun Melsungen AG; Research Grant, KRAUTH medical KG; Research Grant, Boston Scientific Corporation; Equipment support, Elbit Imaging Ltd; Investigator, CMC Contrast AB

Tobias Penzkofer, MD, Berlin, Germany (Abstract Co-Author) Nothing to Disclose

PURPOSE

To evaluate if thresholds based on tumor size on MR Imaging can successfully stratify prostate cancers by their aggressiveness separated by their zone of origin. Goal was improve the currently applied PI-RADS 4 vs. 5 differentiation criterion.

METHOD AND MATERIALS

The MRI datasets of 152 patients who underwent 3 T MRI imaging and subsequent systematic and MRI/TRUS-fusion biopsy were re-read in a fully informed setting by three radiologists. All patients hat prostate cancer confirmed on histopathology. All retrospectively identifiable tumors were measured on T2 for lesions originating in the transition zone and on DWI for lesions from the peripheral zone and tabulated against their respective Gleason grade.

RESULTS

151 lesions were measurable in peripheral zone (n=111) and transition zone (n=40) with the following distribution: Gleason 3+3: 36, 3+4: 29, 3+5: 1, 4+3: 36, 4+4: 37, 4+5: 11, 5+5: 1. Looking at different size thresholds, rates of aggressive cancers (defined as Gleason 3+4 and above) in the peripheral zone were 75% (threshold=0.5 cm), 77% (threshold=1.0 cm), 87% (threshold=1.5 cm), 90% (threshold=2 cm) and 100% (threshold=2.5 cm). In the transition zone rates of aggressive cancer were 55% (threshold=0.5 cm), 57% (threshold=1 cm), 55% (threshold=1.5 cm), 57% (threshold=2.0 cm) and 86% (threshold=2.5 cm), 100% were reached at a threshold of 3 cm. Ten lesions were located in the anterior stroma, which were excluded due to small subgroup numbers.

CONCLUSION

Size thresholds can be used to stratify prostate cancer to some extent. Considering peripheral zone and transition zone separately, there was a clearer separation of clinically significant/aggressive tumors in peripheral zone cancers compared to transition zone cancers. Conversely, even low threshold lesions of 0.5 cm and below can harbor clinically significant cancers. Future versions of PI-RADS should therefore consider different cut-offs for peripheral zone and transition zone cancers. Furthermore, additional criteria - other than size - could add value to the differentiation between PIRADS 4 and 5. A clear separation as in BI-RADS 4a-c (2-9%, 10-50%, 50-95%) on the basis of size seems currently unfeasible.

CLINICAL RELEVANCE/APPLICATION

Adopting different size cut-offs for transition zone and peripheral tumors could be warranted. Additional characteristics - other than size - will likely be needed to stratify between PI-RADS 4 and 5 lesions.

SSK10-03 PI-RADS v2 based Characteristics of Missed Prostate Cancer Lesions on 3T Multiparametric-MRI Based on 518 Patients using Whole Mount Histopathology Reference

Wednesday, Nov. 28 10:50AM - 11:00AM Room: N228

Participants

Amirhossein Mohammadian Bajgiran, MD, Los Angeles, CA (*Presenter*) Nothing to Disclose Sohrab Afshari Mirak, MD, Los Angeles, CA (*Abstract Co-Author*) Nothing to Disclose Sepideh Shakeri, Los Angeles, CA (*Abstract Co-Author*) Nothing to Disclose Ely R. Felker, MD, Los Angeles, CA (*Abstract Co-Author*) Nothing to Disclose Danielle Ponzini, Los Angeles, CA (*Abstract Co-Author*) Nothing to Disclose Preeti Ahuja, PhD, Los Angeles, CA (*Abstract Co-Author*) Nothing to Disclose Anthony Sisk, DO, Los Angeles, CA (*Abstract Co-Author*) Nothing to Disclose Robert E. Reiter, MD, Los Angeles, CA (*Abstract Co-Author*) Nothing to Disclose David S. Lu, MD, Los Angeles, CA (*Abstract Co-Author*) Nothing to Disclose David S. Lu, MD, Los Angeles, CA (*Abstract Co-Author*) Nothing to Disclose Solver S. Raman, MD, Santa Monica, CA (*Abstract Co-Author*) Nothing to Disclose

For information about this presentation, contact:

ambajgiran@ucla.edu

PURPOSE

To determine the characteristics of missed prostate cancer (PCa) lesions on 3TmpMRI using a whole mount histopathology (WMHP) as a standard of reference.

METHOD AND MATERIALS

With IRB approval & HIPAA compliance, the study cohort comprised 518 consecutive men who underwent robotic prostatectomy between Dec 2009 & May 2017. Clinical, 3TmpMRI (T2-weighted imaging, diffusion-weighted imaging (DWI), & dynamic contrastenhanced (DCE) imaging) & WMHP features were analyzed. A structural report system, based on PI-RADS v2, was used. MRI detected lesions were matched with previously finalized WMHP in a joint session by a genitourinary radiologist and pathologist. MRI lesion detection rate was calculated. After the multidisciplinary sessions, patients without any detected PCa lesion in 3TmpMRI, but with at least one lesion >1 cm on WMHP, were retrospectively reviewed & assigned a PI-RADS v2 score.

RESULTS

In 518 patients with 1085 PCa foci on WMHP, 51.9% (563) lesions were missed & 48.1% (522) detected. Of the 563 missed lesions, 71.4% & 21.7% were graded as GS=3+3 & GS=3+4 respectively, while only 4.4% & 2.5% were graded as GS=4+3 & GS=8-10. The proportion of PCa with GS>7 was significantly lower among missed tumors compared to detected ones(p=0.001). Missed foci were

significantly smaller than detected ones in both overall $(0.9 \pm 0.7 \text{ cm vs}. 2.1 \pm 0.9 \text{ cm})$ & index $(1.5 \pm 0.8 \text{ cm vs} 2.0 \pm 0.9 \text{ cm})$ lesion subcohorts(p =0.001). Of overall & index missed lesions 34.4% & 71.2% were >1 cm. In 13.7% (71/518) of patients without an MR detected lesion, a total of 151 lesions were detected on WMHP, of which 70(47 %) were >1 cm. On retrospective review of these lesions, 42.8% (30), 18.5% (13), 20% (14), 10%(7), 7%(5), were PI-RADS V2 1, 2, 3, 4 & 5 respectively. Evaluation of 27% (19) of these lesions was limited by hemorrhage or susceptibility artifact or geometric distortion. Overall, 5.9% (31/518) of patients with clinically significant (CS) PCa lesions were totally missed in 3TmpMRI.

CONCLUSION

On 3TmpMRI, most missed PCa lesions were small & low grade. Although there were some large & high grade missed lesions on 3TmpMRI, the number of missed patients with CS lesion were small & detection for these patients was excellent.

CLINICAL RELEVANCE/APPLICATION

Number of missed patients with CS lesion were small and detection for these patients was excellent. 3T MRI can be use for every patients with PCa suspicious perior to biopsy and surgery.

SSK10-04 Yield of Concurrent Systemic Biopsy During MRI-Guided Targeted Biopsy According to PI-RADS Version 2 in Patients with Suspicious Prostate Cancer

Wednesday, Nov. 28 11:00AM - 11:10AM Room: N228

Participants

Chuhyun Kim, Seoul, Korea, Republic Of (*Presenter*) Nothing to Disclose Chan Kyo Kim, MD, PhD, Seoul, Korea, Republic Of (*Abstract Co-Author*) Nothing to Disclose Jung Jae Park, Daejeon, Korea, Republic Of (*Abstract Co-Author*) Nothing to Disclose Sung Yoon Park, Seoul, Korea, Republic Of (*Abstract Co-Author*) Nothing to Disclose

For information about this presentation, contact:

chankyokim@skku.edu

PURPOSE

Few studies have reported the value of concurrent systemic biopsy during MRI-guided targeted biopsy according to PI-RADS version 2 (v2). We aimed to investigate the yield of concurrent systemic biopsy during MRI-guided targeted biopsy based on PI-RADS v2 interpretations in patients with suspicious prostate cancer (PCa).

METHOD AND MATERIALS

285 consecutive patients with suspicious PCa who performed initial (n = 154) or repeated prostate biopsies (n =131) were enrolled in this retrospective study. All patients underwent prebiopsy 3-T multiparametric MRI, and performed MRI-transrectal ultrasound (TRUS) fusion targeted biopsy regarding PI-RADS v2 category 3-5 lesions and concurrent systemic standard biopsy. Detection rates of all PCa and clinically significant cancer (CSC) were evaluated based on the index lesion in each patient. Biopsy-based definition of CSC was Gleason score (GS) >= 3 + 4.

RESULTS

In all 351 target lesions (peripheral zone [PZ] = 215, transition zone [TZ] = 130, and both = 6), distributions of PI-RADS category 3, 4, and 5 lesions were 86, 177 and 88, respectively. Detection rates of all PCa and CSCs were 39.6% (139/351) and 29.6% (104/351), respectively. As each PI-RADS scoring, detection rates of all PCa and CSCs were 7% and 4.7% for category 3, 36.2% and 24.3% for category 4, and 78.4% and 64.8% for category 5. Regarding each PI-RADS category 4 and 5 lesion, CSC detection rates in PZ were 64.7% (33/51) and 92.9% (26/28), while detection rates of insignificant PCa in TZ were 23.1% (3/13) and 28.6% (10/35). In 49 patients (17.2%), systemic biopsy contained the highest GS cancer compared to targeted biopsy: 22 patients with positive targeted and positive systemic biopsy, and 27 patients with negative targeted biopsy and positive systemic biopsy. Of 88 patients with PI-RADS category 5 lesions, 15 (17%) had the highest GS cancer in systemic biopsy: PZ (n = 6), TZ (n = 8) and both (n = 1).

CONCLUSION

When performing a MRI-guided targeted biopsy based on PI-RADS v2, concurrent systemic biopsy cannot be abandoned in patients with suspicious PCa due to potential harboring more aggressive cancer.

CLINICAL RELEVANCE/APPLICATION

Although MRI-guided targeted biopsy regarding PI-RADS v2 category 4 or 5 lesion demonstrates excellent detection rates of all PCa and CSCs, concurrent systemic biopsy should be performed because of potential harboring more aggressive cancer.

SSK10-05 PI-RADS 3/Total Lesion Ratio is Associated with Clinically-Significant Prostate Cancer in Patients with Equivocal Risk Lesions on Multi-Parametric Magnetic Resonance Imaging

Wednesday, Nov. 28 11:10AM - 11:20AM Room: N228

Participants

Kamyar Ghabili Amirkhiz, MD, New Haven, CT (*Abstract Co-Author*) Nothing to Disclose Matthew Swallow, New Haven, CT (*Abstract Co-Author*) Nothing to Disclose Michael Leapman, New Haven, CT (*Abstract Co-Author*) Nothing to Disclose Preston Sprenkle, New Haven, CT (*Abstract Co-Author*) Nothing to Disclose Jeffrey C. Weinreb, MD, New Haven, CT (*Abstract Co-Author*) Consultant, Bracco Group; Author, Siemens AG Nariman Nezami, MD, New Haven, CT (*Presenter*) Nothing to Disclose

For information about this presentation, contact:

kamyar.ghabili@yale.edu

PURPOSE

Prostate imaging reporting and data system (PI-RADS) category 3 (P3) provides an equivocal assessment of prostate cancer. We aimed to investigate multi-parametric magnetic resonance imaging (mpMRI) parameters including the ratio of P3-to-total regions of interest (ROI) that may assist in identifying patients with P3 lesions harboring clinically-significant prostate cancer (csPCa).

METHOD AND MATERIALS

We retrospectively queried our institutional mpMRI-ultrasound fusion (targeted) biopsy database to identify patients without a prior diagnosis of prostate cancer and with at least one P3 lesion on mpMRI who underwent targeted biopsy during Feb 2015-Oct 2017. mpMRI findings were assessed, including prostate and P3 volumes, number of ROIs, and P3-to-total ROIs ratio (P3 lesion volume/total ROIs volumes). Logistic regression and receiver operating characteristics curves with area under the curve (AUC) were used to assess the ability of clinical and mpMRI characteristics to predict csPCa, defined as any Gleason score (GS)>=7 cancer or GS 6 cancer in >2 cores or >50% of any positive core from targeted biopsy of the P3 lesion.

RESULTS

Of 132 men with at least one P3 lesion, 31 (23.4%) had csPCa on the biopsy of P3 lesions. Patients with csPCa in P3 lesions had smaller prostate volumes (p=0.002), lower P3/total ROIs ratios (p=0.002), and higher numbers of total ROIs (p=0.009). Compared with patients who had a P3/total ROIs ratio >0.58, men with ratios <0.58 were more likely to be diagnosed with csPCa in a P3 lesion (53.3% vs 12%, p<0.001). Using a threshold of 0.58, P3/total ROIs ratio was 69% sensitive and 79% specific for csPCa in a P3 lesion. On multivariable analysis, smaller prostate volume (OR 1.04, 95%CI 1.01-1.07, p=0.02) and lower P3/total ROIs ratio (OR 1.04, 95%CI 1.01-1.07, p=0.03) were associated with an increased risk of csPCa in P3 lesions. P3/total ROIs ratio and prostate volume (both AUC 0.70) were superior to prostate-specific antigen (PSA) density (AUC 0.66) for the prediction of csPCa in P3 lesions.

CONCLUSION

P3/total ROIs ratio and prostate volume outperformed PSA density in and were associated with detecting csPCa in P3 lesions. P3/total ROIs ratio could be used to avoid 79% of unnecessary biopsies of a P3 lesion in men with multiple ROIs on mpMRI.

CLINICAL RELEVANCE/APPLICATION

PI-RADS 3/total ROIs ratio might have a potentially significant clinical implication in the setting of equivocal-risk lesions on mpMRI.

Honored Educators

Presenters or authors on this event have been recognized as RSNA Honored Educators for participating in multiple qualifying educational activities. Honored Educators are invested in furthering the profession of radiology by delivering high-quality educational content in their field of study. Learn how you can become an honored educator by visiting the website at: https://www.rsna.org/Honored-Educator-Award/ Jeffrey C. Weinreb, MD - 2018 Honored Educator

SSK10-06 Interobserver Agreement of PI-RADS v2 Lexicon Among Radiologists with Different Levels of Experience

Wednesday, Nov. 28 11:20AM - 11:30AM Room: N228

Participants

Thais Mussi, MD,PhD, Sao Paulo, Brazil (*Presenter*) Nothing to Disclose Fernando I. Yamauchi, MD, Sao Paulo, Brazil (*Abstract Co-Author*) Nothing to Disclose Tatiana Martins, MD, Belo Horizonte, Brazil (*Abstract Co-Author*) Nothing to Disclose Cassia F. Tridente, MD, Sao Paulo, Brazil (*Abstract Co-Author*) Nothing to Disclose Victor M. Tonso, MD, Catanduva, Brazil (*Abstract Co-Author*) Nothing to Disclose Layra R. Leao, Sao Paulo, Brazil (*Abstract Co-Author*) Nothing to Disclose Daniel C. Luz, MD, Brazil, Brazil (*Abstract Co-Author*) Nothing to Disclose Debora Z. Recchimuzzi, MD, Sao Paulo, Brazil (*Abstract Co-Author*) Nothing to Disclose Adriano Tachibana, MD, Sao Paulo, Brazil (*Abstract Co-Author*) Nothing to Disclose Ronaldo H. Baroni, MD, Sao Paulo, Brazil (*Abstract Co-Author*) Nothing to Disclose

For information about this presentation, contact:

thaiscaldara@gmail.com

PURPOSE

To determine the interobserver agreement of the PI-RADS version 2 lexicon.

METHOD AND MATERIALS

Retrospective IRB approved study. Eight radiologists, with different levels of experience and blinded to clinical data and original multiparametric MRI reports, evaluated a total of 160 lesions, 130 from peripheral zone (PZ) and 30 from transition zone (TZ). On T2w imaging, signs of definite extraprostatic extension or invasive behavior were assessed, for both TZ and PZ lesions. For TZ lesions, the following additional features on T2w imaging were assessed: circumscribed versus obscured margins, encapsulation, heterogeneous versus homogeneous, moderately hypointense and lenticular shape. On DWI and ADC map, the following features were assessed, for both PZ and TZ: focal versus indistinct, marked hyperintensity on high-b-value DWI, and marked hypointensity on ADC map. Finally, on DCE images the readers assigned presence or absence of early enhancement in the lesion/region of the lesion.

RESULTS

Of the five features evaluated on PZ lesions, only definite extraprostatic extension or invasive behavior on T2w had good agreement (AC1= 0.80). All other features (focal versus indistinct on ADC map and DWI, marked hyperintensity on high-b-value DWI, marked hypointensity on ADC map, and presence or not of early enhancement in the lesion/region of the lesion on DCE) had fair agreement (AC1= 0.32 to 0.40). Of the eight features evaluated on TZ lesions, two had good agreement: definite extraprostatic extension or invasive behavior (AC1= 0.77) and moderately/marked hypointensity on T2w (AC1= 0.67). Four features had moderate agreement: encapsulation and lenticular shape on T2w, focal (not indistinct) on ADC map and DWI, and marked hypointensity on ADC map (AC1= 0.45 to 0.60). The four other features had fair agreement: heterogeneous (not homogeneous) and circumscribed (not obscured) margins on T2w, marked hyperintensity on high-b-value DWI, and presence or not of early

enhancement in the lesion/region of the lesion (AC1= 0.30 to 0.38).

CONCLUSION

PI-RADS v2 lexicon ranged from fair to good interobserver agreement. The best agreements were observed for definitive EPE or invasive behavior on T2w on PZ and TZ.

CLINICAL RELEVANCE/APPLICATION

To evaluate the reproducibility of PI-RADS v2 lexicon is essential for clinical use.

SSK10-07 Comparison of Multi and Single Zonal True Positive Index Prostate Cancer Lesions with 3T Multiparametric MRI and Whole Mount Histopathology Correlation in 408 Patients

Wednesday, Nov. 28 11:30AM - 11:40AM Room: N228

Participants

Sohrab Afshari Mirak, MD, Los Angeles, CA (*Presenter*) Nothing to Disclose Amirhossein Mohammadian Bajgiran, MD, Los Angeles, CA (*Abstract Co-Author*) Nothing to Disclose Sepideh Shakeri, Los Angeles, CA (*Abstract Co-Author*) Nothing to Disclose Ely R. Felker, MD, Los Angeles, CA (*Abstract Co-Author*) Nothing to Disclose Danielle Ponzini, Los Angeles, CA (*Abstract Co-Author*) Nothing to Disclose Preeti Ahuja, PhD, Los Angeles, CA (*Abstract Co-Author*) Nothing to Disclose Anthony Sisk, DO, Los Angeles, CA (*Abstract Co-Author*) Nothing to Disclose Robert E. Reiter, MD, Los Angeles, CA (*Abstract Co-Author*) Nothing to Disclose David S. Lu, MD, Los Angeles, CA (*Abstract Co-Author*) Nothing to Disclose Johnson; Research Grant, Johnson & Johnson; Consultant, Bayer AG; Research Grant, Bayer AG; Speaker, Bayer AG Steven S. Raman, MD, Santa Monica, CA (*Abstract Co-Author*) Nothing to Disclose

For information about this presentation, contact:

safsharimirak@mednet.ucla.edu

PURPOSE

To investigate the clinical, 3T multiparametric MRI (3T mpMRI) and histopathologic characteristics of multi and single zone true positive index prostate cancer (PCa) lesions with whole mount histopathology (WMHP) as reference standard.

METHOD AND MATERIALS

In this HIPAA-compliant, IRB-approved study, we evaluated a cohort of 408 men with both 3T mpMRI and WMHP before and after robotic prostatectomy from 12/2009 to 10/2017. A genitourinary (GU) radiologist and GU pathologist matched all WMHP PCa lesions with PI-RADSv2 based detected lesions on 3T mpMRI. The clinical, MRI and WMHP characteristics of true positive index lesions between multi zone (present in both transition (TZ) and peripheral zone (PZ)) and single zone (present in either TZ or PZ) PCa lesions were determined and compared using Chi-square and Mann-Whitney U test in SPSS v24.

RESULTS

Patients' mean age was 62.2±7 years with median PSA of 6.3 (IQR 4.25). 9.3% (38/408) of the lesions were located in both TZ and PZ, 19.4% (79/408) in TZ and 71.3% (291/408) in PZ. Tumor size was slightly but significantly (P=0.002) higher for multi zone lesions (median 2.5cm) compared to TZ lesions (median 2.3cm) and PZ lesions (median 2.1cm). PSA was significantly higher (P= 0.001) in multi zone (7.7 ng/ml) and TZ PCa lesions (7.65 ng/ml) compared to PZ lesions (6 ng/ml). Multi zone lesions had a significantly higher proportion of PI-RADSv2 score 5 (55.3%) compared to TZ lesions (44.3%) and PZ lesions (33.7%) (p<0.001). Other parameters such as PSA density, prostate volume, tumor grading (Gleason score) and staging were similar between single and multi zone lesions.

CONCLUSION

Although multi zone PCa lesions may have more aggressive 3T mpMRI and clinical characteristics, however the grading and staging of the tumors on WMHP are similar to single zone lesions.

CLINICAL RELEVANCE/APPLICATION

Multi zone PCa lesions are associated with more aggressive clinical and MRI features with similar pathologic characteristics compared to single zone PCa lesions.

SSK10-08 Are Qualitative or Quantitative Analysis of DCE the Key to Success in the Grading and Detection of Prostate Cancer?

Wednesday, Nov. 28 11:40AM - 11:50AM Room: N228

..

Participants

Farid Ziayee, Dusseldorf, Germany (*Abstract Co-Author*) Nothing to Disclose Lars Schimmoeller, MD, Dusseldorf, Germany (*Presenter*) Nothing to Disclose Tim Ullrich, Duesseldorf, Germany (*Abstract Co-Author*) Nothing to Disclose Michael Quentin, MD, Dusseldorf, Germany (*Abstract Co-Author*) Nothing to Disclose Christian Arsov, MD, Duesseldorf, Germany (*Abstract Co-Author*) Nothing to Disclose Gerald Antoch, MD, Duesseldorf, Germany (*Abstract Co-Author*) Nothing to Disclose

PURPOSE

The primary purpose of this study was to evaluate the performance of (semi-)quantitative analysis of dynamic contrast-enhanced MRI (DCE) in the detection of prostate cancer (PCa) in comparison to qualitative analysis. The secondary purpose of this study was to find out if any of the methods could distinguish clinically significant PCa from insignificant PCa.

. . .

METHOD AND MATERIALS

DCE data of 103 consecutive patients with multi-parametric MRI (T2WI, DWI, DCE) and subsequent MRI-(in-bore)-biopsy of the prostate were retrospectively analyzed. Qualitative analysis of DCE (after PIRADS v2 criteria), semiquantitative analysis (curve type after PIRADS v1 criteria) and quantitative (Ktrans, kep after Tofts) analysis of in total 206 lesions (87 cancer positive and 119 benign lesions) were performed. Cancer detection, discrimination of significant cancer, and localization was assessed and compared to histopathologic findings.

RESULTS

Subdivided in peripheral zone (PZ) and transition zone (TZ) Ktrans (p<0.01; p=0.04) and Kep (p=0.04, p<0.01) were significantly different between PCa and benign lesions. The PI-RADS v2 overall score could discriminate PCa and benign lesions in both, PZ and TZ (p<0.01), whereas PI-RADS single scores of DCE could differentiate PCa better in PZ (p<0.01) than in TZ (p=0.5). None perfusion parameter could differentiate between insignificant and significant (>=3+4=7) PCa (p=0.5-0.8).

CONCLUSION

PI-RADS v2 criteria for DCE discriminate well between benign lesions and PCa in the peripheral zone. Qualitative (curve type) and quantitative parameters (Ktrans, Kep) provide no additional improvement in PCa detection compared to PI-RADS scoring alone. DCE-MRI alone did not allow differentiation between significant and insignificant PCa.

CLINICAL RELEVANCE/APPLICATION

DCE and PI-RADS v2 criteria enable an improvement of PCa detection especially in the peripheral zone, central zone, and anterior stroma; therefore DCE should not be omitted for primary PCA detection. With limitations quantitative analysis can detect PCa, but the additional diagnostic relevance of quantitative parameters is limited. PI-RADS criteria for DCE in transition zone needs to be optimized for PCa detection.

SSK10-09 Is Biopsy Justified in Prostate Patients Assigned to PI-RADS Category 3?

Wednesday, Nov. 28 11:50AM - 12:00PM Room: N228

Participants

Tim Ullrich, Duesseldorf, Germany (*Presenter*) Nothing to Disclose Lars Schimmoeller, MD, Dusseldorf, Germany (*Abstract Co-Author*) Nothing to Disclose Nina Laqua, Dusseldorf, Germany (*Abstract Co-Author*) Nothing to Disclose Frederic Dietzel, Dusseldorf, Germany (*Abstract Co-Author*) Nothing to Disclose Michael Quentin, MD, Dusseldorf, Germany (*Abstract Co-Author*) Nothing to Disclose Gerald Antoch, MD, Duesseldorf, Germany (*Abstract Co-Author*) Nothing to Disclose Dirk Blondin, MD, Duesseldorf, Germany (*Abstract Co-Author*) Nothing to Disclose Christian Arsov, MD, Duesseldorf, Germany (*Abstract Co-Author*) Nothing to Disclose Robert Rabenalt, Duesseldorf, Germany (*Abstract Co-Author*) Nothing to Disclose Peter Albers, MD, PhD, Duesseldorf, Germany (*Abstract Co-Author*) Nothing to Disclose

For information about this presentation, contact:

Lars.schimmoeller@med.uni-duesseldorf.de

PURPOSE

To systematically analyze patients with PI-RADS-3-lesions (called 'equivocal' according to PI-RADS v2) in multiparametric prostate MRI (mp-MRI) and MR-targeted plus systematic transrectal ultrasound-guided (TRUS-GB) biopsies as reference standard.

METHOD AND MATERIALS

One hundred and twenty consecutive patients assigned to PI-RADS assessment category 3 after mp-MRI (T2WI, DWI, DCE-MRI) at 3T and subsequent targeted MRI/US fusion-guided (FUS-GB) plus systematic 12-core TRUS-GB were retrospectively included in this study. As endpoints prostate cancer (PCa) detection rates, distribution of Gleason scores, location of PCa, and risk stratification by subgroup analyses were defined.

RESULTS

PCa was detected in 13 of 118 patients (detection rate 11%) including five patients with a Gleason score (GS) >=3+4=7 (4.2%). 1.4% of the lesions within the transition zone (3/212) and 9.4% within the peripheral zone (6/64) were positive for PCa. Patients with PCa showed in 54% MRI patterns of peripheral prostatitis combined with diffuse stromal hyperplasia. Prostate volume was significantly lower in PCa patients (p=0.015), whereas differences in PSA levels were not statistically significant (p=0.87). PSA density was higher in patients with PCa (0.19 vs. 0.12 ng/ml/ml).

CONCLUSION

PCa with a GS >=3+4=7 can be detected in mp-MRI with a high degree of certainty. In patients assigned to PI-RADS category 3 low-grade PCa (GS 3+3=6) can occur, but GS >=4+3=7 PCa is very unlikely. Therefore, primarily follow-up MRI is justified in these patients to avoid overtreatment of clinically insignificant PCa. In patients with a combination of MRI aspects of extensive prostatitis and diffuse stromal hyperplasia, low prostate volume, and/or high PSA density biopsy might be considered.

CLINICAL RELEVANCE/APPLICATION

Patients with PI-RADS 3 lesions can safely be managed by follow-up MRI as "test-of-time" approach without immediate biopsy, especially if lesions are located in the transition zone. This recommendation may apply specifically to patients with low PSA density and without MRI features of peripheral prostatitis combined with diffuse stromal hyperplasia.



SSK11

Health Service, Policy and Research (Value, Outcomes and Risk)

Wednesday, Nov. 28 10:30AM - 12:00PM Room: S104A



AMA PRA Category 1 Credits ™: 1.50 ARRT Category A+ Credit: 1.75

FDA Discussions may include off-label uses.

Participants

Stephen Hobbs, MD, Lexington, KY (*Moderator*) Author with royalties, Wolters Kluwer nv Seon-Kyu Lee, MD, PhD, Chicago, IL (*Moderator*) Nothing to Disclose Bhavya R. Shah, MD, Dallas, TX (*Moderator*) Nothing to Disclose

Sub-Events

SSK11-01 Financial Implications of Oral Contrast Administration Prior to Abdominopelvic CT for Non-Traumatic Abdominal Pain in the Emergency Department: A Time-Driven Activity-based Costing Analysis

Participants

Prasad R. Shankar, MD, Ann Arbor, MI (*Presenter*) Nothing to Disclose Marta E. Heilbrun, MD, Salt Lake City, UT (*Abstract Co-Author*) Nothing to Disclose Kushal Parikh, MD, Ann Arbor, MI (*Abstract Co-Author*) Nothing to Disclose Alexis Flake, Ann Arbor, MI (*Abstract Co-Author*) Nothing to Disclose Emily Herbstman, Ann Arbor, MI (*Abstract Co-Author*) Nothing to Disclose Trevor Hoffman, Ann Arbor, MI (*Abstract Co-Author*) Nothing to Disclose Benjamin Sweeny, Ann Arbor, MI (*Abstract Co-Author*) Nothing to Disclose Renee Havey, Ann Arbor, MI (*Abstract Co-Author*) Nothing to Disclose Steven Kronick, MD, Ann Arbor, MI (*Abstract Co-Author*) Nothing to Disclose Matthew S. Davenport, MD, Ann Arbor, MI (*Abstract Co-Author*) Nothing to Disclose

PURPOSE

To quantify the time and monetary cost associated with oral contrast administration prior to abdominopelvic CT for patients with non-traumatic abdominal pain in the emergency department (ED). A secondary aim was to assess the cost savings associated with a new institutional policy change for oral contrast administration in this population.

METHOD AND MATERIALS

A HIPAA-complaint, IRB-approved time-driven activity-based costing analysis was performed using both prospective time-studies and retrospective data obtained in a quaternary care center. Retrospective data spanned a 1-year period (1/1/2016-12/31/2016). A process map was generated. Exam volume-related data, labor costs, and material costs were determined and applied to a basecase model. Univariate and multivariate sensitivity analyses were conducted. Multivariate analysis was used to estimate the cost savings associated with a policy change eliminating oral contrast for patients with BMI >=25, no prior abdominal surgery <=30 days, and no inflammatory bowel disease.

RESULTS

The baseline oral contrast utilization rate was 86% (4,541/5,263). The annual base-case cost estimate for oral contrast administration was \$155,173. In multivariate analyses, this ranged from \$20,034 - \$672,469. The model was most sensitive to volume of cases requiring oral contrast and passive ED costs during contrast consumption. The median time cost of oral contrast consumption was 33 minutes (IQR: 23-43 minutes) for barium sulfate suspension and 62 minutes (IQR: 43-81 minutes) for diatrizoate meglumine-sodium. Applying parameters from the new policy change reduced the annual cost by 52% (cost saving: \$73,709).

CONCLUSION

Time and monetary costs associated with oral contrast administration prior to abdominopelvic CT in the ED should be balanced with its potential diagnostic benefits to ensure high-quality patient care and healthcare cost stewardship. Our multi-departmental collaborative policy change is estimated to halve hospital costs associated in ED oral contrast administration.

CLINICAL RELEVANCE/APPLICATION

Time and monetary costs associated with oral contrast administration prior to abdominopelvic CT in the ED should be balanced with diagnostic benefits to ensure high-quality patient care and healthcare cost stewardship.

SSK11-02 Testing for Verification Bias in Reported Malignancy Risks for Side-Branch Intraductal Papillary Mucinous Neoplasms: A Simulation Modeling Approach

Wednesday, Nov. 28 10:40AM - 10:50AM Room: S104A

Anna P. Lietz, BA, Boston, MA (*Abstract Co-Author*) Nothing to Disclose Sarah Mercaldo, PhD, Boston, MA (*Abstract Co-Author*) Nothing to Disclose Mary Linton B. Peters, MD,MS, Boston, MA (*Abstract Co-Author*) Speaker, Bayer AG; Travel support, Halozyme Therapeutics, Inc; Travel support, AstraZeneca PLC Chin Hur, MD, Boston, MA (*Abstract Co-Author*) Nothing to Disclose Chung Yin Kong, PhD, Boston, MA (*Abstract Co-Author*) Nothing to Disclose Brian M. Wolpin, MD, Boston, MA (*Abstract Co-Author*) Nothing to Disclose Alec J. Megibow, MD, New York, NY (*Abstract Co-Author*) Consultant, Bracco Group

Lincoln L. Berland, MD, Birmingham, AL (Abstract Co-Author) Consultant, Nuance Communications, Inc

Amy Knudsen, PhD, Boston, MA (*Abstract Co-Author*) Spouse, Employee, ZOLL Medical Corporation; Board of Directors, Miracor Medical, SA

Pari Pandharipande, MD, MPH, Boston, MA (Presenter) Research Grant, Medical Imaging & Technology Alliance

For information about this presentation, contact:

davis@mgh-ita.org

PURPOSE

To test for the possibility that published malignancy risks for side-branch intraductal papillary mucinous neoplasms (SBIPMN) are overestimates, likely due to verification bias.

METHOD AND MATERIALS

We tested for possible verification bias using simulation modeling techniques. First, in age-defined hypothetical cohorts of one million persons, we projected the frequency of pancreatic ductal adenocarcinoma (PDAC) arising from SBIPMNs over five years using published estimates of their prevalence (4.4%) and rate of malignant transformation (1.9%). Second, we projected the total number of PDAC cases in corresponding cohorts over the same time horizon using national cancer registry data (SEER). For each cohort, we determined if the percentage of all PDAC cases that arose from SBIPMNs (i.e., of SBIPMN-associated PDAC cases) was clinically plausible, invoking an upper limit of 10% to define plausibility, as estimated from the literature. Model assumptions and parameter uncertainty were evaluated in sensitivity analysis.

RESULTS

Across all cohorts, percentages of SBIPMN-associated PDAC greatly exceeded 10%. In the base case (mean age=56 years), 88% of PDAC cases arose from SBIPMNs (874/989). In the oldest cohort evaluated (mean age=75 years), this estimate was 82% (1,549/1,882). In a secondary analysis, we found that if an upper limit threshold of 10% for SBIPMN-associated PDAC was imposed, the model-predicted rate of malignancy for SBIPMN would be <0.21% over a five-year time horizon, substantially lower than most literature-based estimates.

CONCLUSION

Our results suggest that reported malignancy risks associated with SBIPMNs are likely to be overestimates, and imply the presence of verification bias.

CLINICAL RELEVANCE/APPLICATION

Our results highlight the uncertainty surrounding the natural history of SBIPMNs and underscore the importance of each patient's individual circumstance when making decisions regarding follow-up or treatment of SBIPMN.

SSK11-03 Automatic Evaluation of Routine Computed Tomography Scans for Prediction of Osteoporotic Fractures

Wednesday, Nov. 28 10:50AM - 11:00AM Room: S104A

Participants

Noa Dagan, MD, MPH, Tel Aviv, Israel (*Presenter*) Nothing to Disclose Eldad Elnekave, MD, Shefayim, Israel (*Abstract Co-Author*) Employee, Zebra Medical Vision Ltd Noam Barda, Tel Aviv, Israel (*Abstract Co-Author*) Nothing to Disclose Orna Bregman-Amitai, BSC, Shefayim, Israel (*Abstract Co-Author*) Employee, Zebra Medical Vision Ltd Amir Bar, Berkeley, CA (*Abstract Co-Author*) Employee, Zebra Medical Vision Ltd Eitan Bachmat, PhD, Beer Sheva, Israel (*Abstract Co-Author*) Nothing to Disclose Ran Balicer, MD,PhD, Tel Aviv, Israel (*Abstract Co-Author*) Nothing to Disclose

For information about this presentation, contact:

NoaDa@clalit.org.il

PURPOSE

Osteoporotic (OP) fractures cause major morbidity and mortality. The clinical importance of fracture risk predictors such as FRAX is well established, and they are integrated into treatment guidelines. However, FRAX is underutilized due to lack of physician time, awareness, and availability of the 18 required inputs. The study's purpose is to establish whether OP fracture risk scores can be produced automatically from routine CTs using an artificial-intelligence based algorithm, and to compare their predictive ability to that of FRAX.

METHOD AND MATERIALS

Members of a healthcare provider aged 50-90, who underwent routine chest or abdomen CTs prior to July 2012 (index date), were divided to train and test sets. An algorithm scored each CT for bone mineral density (BMD) and presence of vertebral compression fractures. Five-year fracture risk scores were assessed as of the index date by: FRAX (module without DXA), CT (based on the algorithm markers and metadata of age and sex), and combined FRAX-CT. Models' discrimination was evaluated using area under the ROC curve (AUC), by comparing the models' outputs to major OP and hip fracture incidence during a 5-years follow-up period (until 2017). Missing FRAX inputs were completed using 10 imputed data sets. Significance was evaluated using 500 bootstrap samples per data set.

RESULTS

A total of 48,227 individuals were analyzed, of these, 5,106 (10.6%) and 1,901 (3.9%) suffered major OP and hip fractures during follow-up, respectively. Missing values occurred in 1.17% of the population. Compression fractures were identified in 7,521 (15.6%) CTs and abnormally low BMD was identified in 8,196 (17.0%). The AUCs of the FRAX, CT and combined models were 68.7%, 70.2% and 71.5% for major OP fractures, and 75.1%, 75.3% and 77.0% for hip fractures, respectively. All AUC differences were significant except those between the FRAX and CT models for hip fractures.

CONCLUSION

Fully automatic screening for OP fracture risk using routinely acquired CT scans achieves discrimination which is at least as good as the well-established FRAX model. If data for all FRAX inputs is available, the CT algorithmic score may be incorporated to further improve its predictive ability.

CLINICAL RELEVANCE/APPLICATION

OP fracture prediction scores can be added automatically to CT reports, and help identify people at high risk for fractures, who are currently missed due to under use of traditional prediction tools.

SSK11-04 Natural Language Processing at Work! Is There a Difference Between LI-RADS Category 3 to Category 5 Progression Assessment Between CT versus MR? A Retrospective Analysis of 1,887 Patients Who Underwent 5,082 Radiologic Exams for HCC Surveillance

Wednesday, Nov. 28 11:00AM - 11:10AM Room: S104A

Awards

Student Travel Stipend Award

Participants

Patricia I. Ojeda, MD, Seattle, WA (*Presenter*) Nothing to Disclose Rebecca J. Mieloszyk, PhD, Seattle, WA (*Abstract Co-Author*) Researcher, Radiology Solutions; Researcher, Koninklijke Philips NV Christopher Hall, PhD, Bothell, WA (*Abstract Co-Author*) Employee, Koninklijke Philips NV Akshay D. Baheti, MD, Mumbai, India (*Abstract Co-Author*) Nothing to Disclose Puneet Bhargava, MD, Seattle, WA (*Abstract Co-Author*) Nothing to Disclose

For information about this presentation, contact:

pojeda@uw.edu

PURPOSE

Using the Liver Imaging Reporting and Data System (LI-RADS), our purpose is to identify the proportion of liver lesions with indeterminate probability of hepatocellular carcinoma (HCC) (LI-RADS 3) which progress to high likelihood of HCC (LI-RADS 5) using a large patient cohort to compare the differences in progression between computed tomography (CT) versus magnetic resonance (MR) imaging.

METHOD AND MATERIALS

This is a retrospective, single-center, longitudinal study of 1,887 patients who underwent a total of 5,082 radiologic examinations for HCC surveillance. Examinations included CT and MR studies identified from 2010-2017 (CT 36.4%, MR 61.6%). The dates of imaging studies, modality type, and associated LI-RADS category assignments were automatically extracted from the original examination reports using natural language processing techniques. We calculated the proportions of lesions initially classified as LI-RADS Category 3 which progressed to LI-RADS Category 5 on both CT and MR.

RESULTS

On MR, a LI-RADS Category 3 lesion was 1.5 times more likely to be upgraded to LI-RADS Category 5 compared to CT (114/379 upgraded on MR vs. 43/217 upgraded on CT, p<0.01). While only 20% of CT LI-RADS Category 3 were upgraded to a LI-RADS Category 5, 30% of MR CT LI-RADS Category 3 were upgraded to a CT LI-RADS Category 5.

CONCLUSION

Our data suggests that MR is more likely to upgrade a LI-RADS Category 3 to LI-RADS Category 5 as compared to CT. Improved characterization of lesions definitely representing HCC (LI-RADS Category 5) has the potential to lead to earlier diagnosis and provide lead time for subsequent treatment optimization for these patients.

CLINICAL RELEVANCE/APPLICATION

Using natural language processing, 5,082 CT/MR liver protocol studies were analyzed. MR is more likely to upgrade a LI-RADS Category 3 lesion to Category 5 compared to CT and can provide additional lead time for treatment optimization.

Honored Educators

Presenters or authors on this event have been recognized as RSNA Honored Educators for participating in multiple qualifying educational activities. Honored Educators are invested in furthering the profession of radiology by delivering high-quality educational content in their field of study. Learn how you can become an honored educator by visiting the website at: https://www.rsna.org/Honored-Educator-Award/ Puneet Bhargava, MD - 2015 Honored Educator

SSK11-05 Reducing the Volume of Low-Value Outpatient MRI Joint Exams in Patients >55 Years of Age

Wednesday, Nov. 28 11:10AM - 11:20AM Room: S104A

Participants

Joshua Kandiah, BSC, Vancouver, BC (*Abstract Co-Author*) Nothing to Disclose Vivian Chan, MPH,PhD, Vancouver, BC (*Abstract Co-Author*) Nothing to Disclose Flora Dong, Vancouver, BC (*Abstract Co-Author*) Nothing to Disclose Jing Luo, MS,MA, Vancouver, BC (*Abstract Co-Author*) Nothing to Disclose Bruce B. Forster, MD, Vancouver, BC (*Abstract Co-Author*) Stockholder, Canada Diagnostic Centres James P. Nugent, BSC, Vancouver, BC (*Presenter*) Nothing to Disclose

For information about this presentation, contact:

joshua.kandiah@alumni.ubc.ca

PURPOSE

Knee pain is the most common orthopaedic indication for MRI, and is frequently caused by meniscal tears. Such tears increase in prevalence in the presence of osteoarthritis (OA), with one study showing that, of patients with significant OA, 63% with knee pain and 60% without symptoms have MRI evidence of meniscal tear. If surgery is required in patients with co-existent OA, it should be for joint replacement, which is evaluated with plain X-rays. Therefore, there are a considerable number of patients with significant OA that would not benefit from MRI. We attempt to determine if evaluation of OA via recent X-rays can reduce inappropriate MRI use in patients >55 years of age. Additionally, in our jurisdiction, CT arthrograms are used as surrogate tests for knee internal derangement because of long MRI wait times. Therefore, we attempt to determine if there will be a decrease in knee CT arthrograms as well.

METHOD AND MATERIALS

Our intervention required recent X-rays (within one year) for patients >55 years of age who were scheduled for outpatient MRI of the knee/hip/shoulder. A working group agreed upon red flags (i.e. neoplasm, infection) for which MRI would be indicated regardless. Through review of radiographs on PACS/digital media and use of the validated Kellgren-Lawrence (KL) OA scale, radiologists assessed the degree of OA, and thus the need for advanced imaging. A finding of significant OA (KL >2) without red flags would preclude MRI. Monthly averages of MRI and CT arthrogram requisitions were measured before (33 months) and following our intervention (14 months).

RESULTS

Post-intervention, the average monthly number of MRI requisitions decreased from 61 to 56 (P = 0.070) compared with the baseline. If MRI wait time is taken into consideration (9 months), the monthly average decreased to 40. The proportion of protocoled cases that were avoided was 17% (38/227). The average monthly number of knee CT arthrogram requisitions decreased from 21 to 12 (P = 0.004) following the intervention.

CONCLUSION

We were able to decrease the number of MRI and knee CT arthrogram exams in patients over 55 years of age with joint pain by implementing an evaluation for OA via recent X-ray imaging.

CLINICAL RELEVANCE/APPLICATION

Recent X-ray evaluation for osteoarthritis can prevent unnecessary MRI and is recommended for patients who are over 55 years of age and have joint pain.

SSK11-06 Second Thoughts: Emergency Clinicians See Value in Secondary Interpretations

Wednesday, Nov. 28 11:20AM - 11:30AM Room: S104A

Awards

Student Travel Stipend Award

Participants Dipan Danda, MD, Hamden, CT (*Presenter*) Nothing to Disclose Jonathan Mezrich, MD, New Haven, CT (*Abstract Co-Author*) Nothing to Disclose

For information about this presentation, contact:

dipan.danda@yale.edu

PURPOSE

As technological improvements have lead to increased transportability of imaging, and as facilities have begun to realize the costs, both in terms of liability and time, of offering curbside consults on outside imaging, many large institutions now offer complete secondary read radiology reports and attempt to monetize such efforts. But are clinicians ordering these secondary reads simply as part of their intake process, or is there any real benefit to the emergency physicians and trauma surgeons who obtain these secondary reports? This study seeks to evaluate the benefit of secondary reads, and how clinicians navigate issues regarding payment, reimaging and managing conflicting reports.

METHOD AND MATERIALS

An anonymous electronic survey regarding secondary interpretations and associated issues was circulated to 58 attending emergency physicians and trauma surgeons at Yale-New Haven Hospital. There were 26 responses, representing a 44.8% response rate.

RESULTS

80.8% of respondents requested secondary interpretations either always or most of the time. Over half of respondents cited trust in the house radiologist interpretation over the outside radiologist as the primary reason they requested secondary reads. 92.3% and 84.6% of respondents felt that the ability to obtain second interpretations improves patient care and facilitates disposition, respectively. Furthermore, 88.5% of respondents reported a reduced need to obtain additional imaging due to secondary reads. When presented with conflicting interpretations 65.4% of respondents rely on the in house interpretations while 26.9% consider obtaining further imaging. 96.2% of respondents were uncertain about whether insurance covered secondary reads, but 73.1% would continue to order them regardless.

CONCLUSION

Not only were secondary reads heavily utilized by respondents, but they were felt to influence patient care and aid in disposition,

suggesting that secondary reads have real clinical import. Most felt secondary interpretations reduced the need for more imaging even when presented with conflicting reads, suggesting benefits in resource utilization and minimization of radiation. Finally, most respondents would still request secondary interpretations despite being unaware if insurance covered these interpretations.

CLINICAL RELEVANCE/APPLICATION

This study should be of interest to all radiologists working at institutions which offer or are considering providing secondary reads.

SSK11-07 Emergency Radiology: An Underappreciated Source of Liability Risk

Wednesday, Nov. 28 11:30AM - 11:40AM Room: S104A

Participants

Jeffrey D. Robinson, MD, MBA, Seattle, WA (*Presenter*) Consultant, HealthHelp, LLC; President, Cleareview, Inc; Robert P. DeConde, MD, Seattle, WA (*Abstract Co-Author*) Nothing to Disclose Neerav R. Mehta, MD, Swarthmore, PA (*Abstract Co-Author*) Partner, Clearview, Inc Co-founder, NeuroCAD, LLC

For information about this presentation, contact:

jeff8rob@uw.edu

PURPOSE

Many studies examine the malpractice risk of radiologists in general, focusing on factors such as the type of error, modality and organ system. However, no publication has focused attention on the patient status as a differentiating factor. This study estimates the relative risk of liability action arising between inpatient, outpatient and emergency department exams.

METHOD AND MATERIALS

90 consecutive malpractice claims referred to a radiology-specific malpractice consulting company were reviewed. The site of service for the exam at issue was identified as Inpatient (IP), Outpatient(OP) or Emergency Department (ED). The Medicare Part B claims file was queried to establish the relative frequency of exams performed in each of these settings for 2016. A chi-squared test was used to compare the distributions of malpractice to Medicare claims. The odds ratio of legal action was calculated using the Medicare data as a proxy for the relative number of exams performed in the US for each patient status.

RESULTS

There were 12 IP, 33 OP and 45 ED malpractice claims. In 2016, Medicare beneficiaries claimed 29,124,475 IP, 78,430,930 OP and 22,356,328 ED exams. The distribution of patient status for malpractice claims differed from the Medicare claims file with a Chi-squared statistic of 67.9 (p<<0.01). The odds ratio of a malpractice claim was 4.89 (95%CI 2.58 - 9.24) for ED exams compared to IP, 4.78 (95%CI 3.05 - 7.50) compared to OP exams, and 0.98 (95%CI 0.51 - 1.90) for IP compared to OP exams.

CONCLUSION

This initial examination suggests that Emergency Radiology as it is currently practiced presents an increased risk of a malpractice claim compared to other aspects of the practice of radiology.

CLINICAL RELEVANCE/APPLICATION

Radiology practice groups might wish to consider forming a core radiology section whose members have interest, expertise and/or fellowship training in Emergency Radiology.

SSK11-08 Fully Automated Computer-Aided Detection Implementation in The Emergency Department for Detection of Pulmonary Nodules on CT: Effect on Workflow and Diagnostic Accuracy

Wednesday, Nov. 28 11:40AM - 11:50AM Room: S104A

Participants

Amirhossein Mozafarykhamseh, MD, Chicago, IL (*Presenter*) Grant, Siemens AG Tugce Agirlar Trabzonlu, MD, Chicago, IL (*Abstract Co-Author*) Grant, Siemens AG Pamela J. Lombardi, MD, Chicago, IL (*Abstract Co-Author*) Nothing to Disclose Rishi Agrawal, MD, Chicago, IL (*Abstract Co-Author*) Speakers Bureau, Boehringer Ingelheim GmbH Vahid Yaghmai, MD, Chicago, IL (*Abstract Co-Author*) Nothing to Disclose

PURPOSE

To assess the feasibility and added value of implementing fully automated computer-aided diagnosis (CAD) for detection of pulmonary nodules on CT angiography studies in emergency setting.

METHOD AND MATERIALS

We retrospectively reviewed a dataset of 48 emergency patients who underwent computed tomography pulmonary angiography (CTPA) for pulmonary embolism (PE) in September 2017. A cardiothoracic radiologist with 6 years experience (RAD1) and a third year radiology resident (RAD2) reviewed the scans separately to detect pulmonary nodules without CAD followed by CAD. CAD detection rate of nodules was also evaluated in the same reading session. CAD nodule detection was fully automated and required no additional processing time by RAD or technologist. The time spent by RAD to evaluate the image sets was measured for each case. Fisher's exact test and T-test were used to determine the differences between the rate of detection between the readers and the CAD.

RESULTS

CAD significantly increased the rate of RAD1 detection by 27% (2.23 vs. 1.75 nodule/scan, P<0.05). CAD significantly increased the rate of RAD2 detection by 34% (2.52 vs. 1.88 nodule/scan, P<0.05).

CONCLUSION

Routine utilization of CAD in the emergency setting is feasible and can improve detection rate of pulmonary nodules significantly.

CLINICAL RELEVANCE/APPLICATION

Computer aided detection can be considered as a useful adjunct tool which can optimize pulmonary nodule detection in emergency department CT scans.

Honored Educators

Presenters or authors on this event have been recognized as RSNA Honored Educators for participating in multiple qualifying educational activities. Honored Educators are invested in furthering the profession of radiology by delivering high-quality educational content in their field of study. Learn how you can become an honored educator by visiting the website at: https://www.rsna.org/Honored-Educator-Award/ Vahid Yaghmai, MD - 2012 Honored EducatorVahid Yaghmai, MD - 2015 Honored Educator

SSK11-09 Initial Experience with Silent Mode CDS

Wednesday, Nov. 28 11:50AM - 12:00PM Room: S104A

Awards

Student Travel Stipend Award

Participants Jessica G. Fried, MD, Philadelphia, PA (*Presenter*) Nothing to Disclose Charles E. Kahn JR, MD, Philadelphia, PA (*Abstract Co-Author*) Nothing to Disclose Hanna M. Zafar, MD, Philadelphia, PA (*Abstract Co-Author*) Nothing to Disclose

For information about this presentation, contact:

Jessica.Fried@uphs.upenn.edu

PURPOSE

The Protecting Access to Medicare Act of 2014 (PAMA) requires referring physicians to use clinical decision support (CDS) when ordering advancing imaging procedures. We sought to identify opportunities to improve use of radiology order entry CDS.

METHOD AND MATERIALS

All advanced diagnostic imaging orders placed at a 590-bed level II trauma teaching hospital were tracked silently in the CDS: clinicians were prompted to select a study indication from a drop-down menu at the time of order-entry that mapped to AUC categories, but no feedback was given to the ordering clinician. All orders placed in the first 30 days after CDS deployment were mapped to an AUC category. Orders which could not be categorized were reviewed manually to determine if an indication existed.

RESULTS

Of 39,533 advanced diagnostic imaging orders, 23,267 (59%) were not mapped to an indication. Most unmapped orders (16,440/23,267, 71%) used free-text study indications rather than the drop-down menu. Emergency Medicine (3,877/16,440, 24%) and Hematology/Oncology (3,410/16,440, 21%) had the highest free-text entry rates. Exams with the highest free text entry rates were CT Abdomen/Pelvis with IV contrast (1,693/16,440, 10%) and CT Head without IV contrast (1,527/16,440, 9%). Manual review of free-text study indications revealed that 3,132/3,220 (97%) could easily be matched to a single mapped indication in the CDS. The remaining one-third of orders that could not be mapped (6,827/23,267, 29%) reflected issues related to software build and best practice alert configuration.

CONCLUSION

Nearly two-thirds of advanced diagnostic imaging orders placed in the first month CDS was implemented could not be mapped to AUC; this was mainly due to free-text entry of study indication rather than use of drop down menus, although (97%) of free text entries could easily be matched to a single mapped indication in the CDS.

CLINICAL RELEVANCE/APPLICATION

Opportunities for improvement of electronic imaging decision support systems to support CMS PAMA can be identified prior to deployment through piloting of the system in a silent-mode setting.

Honored Educators

Presenters or authors on this event have been recognized as RSNA Honored Educators for participating in multiple qualifying educational activities. Honored Educators are invested in furthering the profession of radiology by delivering high-quality educational content in their field of study. Learn how you can become an honored educator by visiting the website at: https://www.rsna.org/Honored-Educator-Award/ Charles E. Kahn JR, MD - 2012 Honored EducatorCharles E. Kahn JR, MD - 2018 Honored Educator



SSK12

Molecular Imaging (New Tracers)

Wednesday, Nov. 28 10:30AM - 12:00PM Room: S504CD



AMA PRA Category 1 Credits ™: 1.50 ARRT Category A+ Credit: 1.75

FDA Discussions may include off-label uses.

Participants

Benjamin Larimer, PhD, Charlestown, MA (*Moderator*) Co-founder, Cytosite Biopharma Inc; Consultant, Cytosite Biopharma Inc; Stockholder, Cytosite Biopharma Inc

Christopher C. Riedl, MD, New York, NY (Moderator) Nothing to Disclose

Sub-Events

SSK12-01 Standardized Uptake Value Atlas: Physiological and Abnormal 68Ga-RM2 Uptake in Patients with Prostate Cancer

Participants

Lucia Baratto, Stanford, CA (*Presenter*) Nothing to Disclose Heying Duan, Stanford, CA (*Abstract Co-Author*) Nothing to Disclose Akira Toriihara, Stanford, CA (*Abstract Co-Author*) Nothing to Disclose Negin Hatami, Stanford, CA (*Abstract Co-Author*) Nothing to Disclose Sonya Y. Park, MD, Seoul, Korea, Republic Of (*Abstract Co-Author*) Nothing to Disclose Tomomi Nobashi, MD, PhD, Palo Alto, CA (*Abstract Co-Author*) Nothing to Disclose Andrei Iagaru, MD, Emerald Hills, CA (*Abstract Co-Author*) Research Grant, General Electric Company

For information about this presentation, contact:

lbaratto@stanford.edu

PURPOSE

To describe the distribution and range of physiological uptake of 68Ga-RM2 in patients with prostate cancer and to evaluate the spectrum of abnormal uptake using standardized uptake values (SUVs).

METHOD AND MATERIALS

We retrospectively reviewed images of 20 prostate cancer patients who performed either an 68Ga-RM2 PET/CT for primary diagnosis and staging (n=7) or 68Ga-RM2 PET/MRI for a biochemical recurrence (n=13). Two nuclear medicine physicians evaluated images using an AW workstation (GE Healthcare). SUVmax and SUVmean were measured in 24 normal anatomical structures for each patient. 68Ga-RM2 uptake values of each organ was classified as "none" if SUVmean value was less than of the aortic blood pool, "mild" if SUVmean was greater than SUVmean of aortic blood pool, but less than 2.5, "moderate" if SUVmean was between 2.5 and 5 and "intense" if SUVmean was greater than 5. Areas of focal increased 68Ga-RM2 uptake were also collected.

RESULTS

The highest activity was observed in bladder and renal collecting system, related to urinary excretion of radiotracer. The highest physiologic uptake was present in the pancreas (SUVmax 62.38 ± 13.74). Uptake in the kidney cortex, duodenum and esophagus was mostly classified as mild (average SUVmax of 3) and only few times as moderate. Uptake in the in the stomach wall, rectum and adrenal was mostly classified as not significant (average SUVmax of 2.5) and only few times as mild. Brain, adrenals, liver, spleen, bone, gluteal muscle and fat had not significant uptake. Sixteen avid foci of 68Ga-RM2 uptake were detected in 9 patients. Uptake was identified in the prostate bed (n=6), abdominopelvic and mediastinal lymphnodes (n=5 and n=2, respectively), skeleton (n=2) and lungs (n=1).

CONCLUSION

We presented data on patterns of physiological 68Ga-RM2 uptake in normal tissues with the aim of creating an atlas to improve the interpretation accuracy of 68Ga-RM2 PET scan. Our data also confirmed that 68Ga-RM2 is a promising tracer for the assessment of GRPr expression in prostate cancer patients. Further evaluation in a larger cohort are needed to confirm these data.

CLINICAL RELEVANCE/APPLICATION

68Ga-RM2 is a promising radiotracer for prostate cancer imaging. Atlas of 68Ga-RM2 would improve accuracy of imaging interpretation.

SSK12-02 A Fluorescent Glucose Analogue for Selective Imaging of Sodium-Dependent Glucose Transporters in Breast Cancer

Wednesday, Nov. 28 10:40AM - 10:50AM Room: S504CD

For information about this presentation, contact:

richard.agnes@case.edu

PURPOSE

Sodium-dependent glucose transporters (SGLTs) are emerging as biomarkers as well as a potential imaging and therapeutic target in a variety of human malignancies. Recently, we have developed a fluorescent glucose analog with a near infrared fluorophore attached at the carbon-6 position (6FGA) and have reported its cell uptake in cancer cells in vitro. With a goal towards clinical application, we are further characterizing 6FGA for cancer imaging including cell uptake mechanisms, transporter selectivity, and conditions for small animal imaging.

METHOD AND MATERIALS

6FGA was synthesized using click chemistry between 6-azido-glucose and alkyne cyanine 5.5. To assess SGLT-driven cellular uptake, MDA-MB-231 triple-negative breast cancer lines were incubated with 6FGA for 20 minutes in various conditions, including in the presence and absence of SGLT (phlorizin), SGLT2 (dapagliflozin), and GLUT (cytochalasin B) inhibitors as well as in presence and absence of the cotransported sodium ion. 6FGA cellular uptake was examined using confocal microscopy. 6FGA uptake in vivo in murine xenograft tumors that were grown and sectioned to 1 millimeter slices was examined by fluorescence imaging.

RESULTS

Western blots confirmed the expression of SGLT1 and SGLT2. In cell uptake studies, 6FGA accumulation in MDA-MB-231 cells was reduced by SGLT and SGLT2 but not by GLUT inhibitors. Further confirming the SGLT-driven uptake, 6FGA accumulation did not occur when the SGLT co-transported sodium ion was absent from the medium. The uptake in tumor slices was consistent with that in the cell studies in that it increases over time and did not wash out.

CONCLUSION

6FGA is emerging as promising tool for investigating SGLT in cancer cells and tumor tissues. Our preliminary cell uptake studies suggest that 6FGA uptake is mediated through SGLTs. Initial studies with tumor slices suggests feasibility and optimal conditions for in vivo imaging of tumor model in small animals.

CLINICAL RELEVANCE/APPLICATION

6FGA is a model towards designing new tracers for PET imaging to improve detection and treatment for SGLT cancers such as triple negative breast and metastatic prostate.

SSK12-04 Quantitative Magnetic Particle Imaging of Transplanted Ferumoxytol-Labeled Stem Cells

Wednesday, Nov. 28 11:00AM - 11:10AM Room: S504CD

Participants

Hossein Nejadnik, MD, PhD, Stanford, CA (*Presenter*) Nothing to Disclose Prachi Pandit, PhD, Alameda, CA (*Abstract Co-Author*) Stockholder, Magnetic Insight Inc; Employee, Magnetic Insight Inc Olga Lenkov, BSC, Stanford, CA (*Abstract Co-Author*) Nothing to Disclose Arian Pourmehdi Lahiji, Stanford, CA (*Abstract Co-Author*) Nothing to Disclose Ketan Yerneni, Stanford, CA (*Abstract Co-Author*) Nothing to Disclose Heike E. Daldrup-Link, MD, Palo Alto, CA (*Abstract Co-Author*) Nothing to Disclose

For information about this presentation, contact:

hnejadni@stanford.edu

PURPOSE

To evaluate, if ferumoxytol (Feraheme) can be used for in vivo detection and quantification of stem cell transplants with magnetic particle imaging (MPI).

METHOD AND MATERIALS

Mesenchymal stem cells (MSCs) were labeled with ferumoxytol (Feraheme) or ferucarbotran (Resovist/Vivotrax) and underwent magnetic particle imaging (MPI), magnetic resonance imaging (MRI), prussian blue staining and inductively coupled plasma (ICP) spectrometry. Unlabeled, ferumoxytol, and ferucarbotran-labeled MSCs were implanted in calvarial defects of eight mice and underwent MPI, MRI and histopathology. The iron concentration calculated according to the MPI signal intensity and T2* relaxation times of the three different groups were compared using an analysis of variance (ANOVA) with Bonferroni correction, and a p<0.05.

RESULTS

Compared to unlabeled controls, ferumoxytol and ferucarbotran labeled MSC showed significantly increased iron content, MPI signal and MRI signal. The ferumoxytol MPI signal was approximately 4x weaker compared to ferucarbotran at equimolar concentrations (p=0.0003) and approximately 1.5 times weaker for labeled cells when using optimized labeling protocols (p=0.002). In vivo, the MPI signal of ferumoxytol-labeled MSC decreased significantly between day 1 and day 14 (p=0.0124). This was confirmed by histopathology where we observed a decrease in Prussian blue stain of MSCs at the transplant site. The MRI signal of the same transplants did not change significantly during this observation period (p=0.93).

CONCLUSION

Ferumoxytol nanoparticles can be used for in vivo detection of stem cell transplants with MPI and provide quantitative information not attainable with MRI.

CLINICAL RELEVANCE/APPLICATION

Clinically applicable ferumoxytol can be detected with MPI, allowing accurate in vivo detection and quantification of labeled stem

cells, which is an important basis for clinical translation of MPI.

SSK12-05 18F-Labeled Magnetic Nanoparticles for the Assessment of Early Anti-angiogenic Therapy Effects in Triple Negative Breast Cancer Xenografts

Wednesday, Nov. 28 11:10AM - 11:20AM Room: S504CD

Participants

Yanshu Wang, Shanghai, China (*Presenter*) Nothing to Disclose Huanhuan Liu, Shanghai, China (*Abstract Co-Author*) Nothing to Disclose Jinning Li, BMedSc, Shanghai, China (*Abstract Co-Author*) Nothing to Disclose Dengbin Wang, Shanghai, China (*Abstract Co-Author*) Nothing to Disclose

For information about this presentation, contact:

wangyanshu_1992@sina.com

PURPOSE

To investigate the positron emission tomography/magnetic resonance imaging (PET/MRI) dual-modality imaging probe 18F-RGD-PAA-USPIO for the in vivo monitoring of avß3-integrin expression as biomarker of anti-angiogenic therapy effects in breast cancer xenografts model.

METHOD AND MATERIALS

A multimodal imaging agents 18F-RGD-PAA-USPIO nanoparticles was synthesized and tested in vitro and in vivo. Mice bearing MDA-MB-231 subcutaneous tumors were treated with bevacizumab or placebo(n=10/group,intraperitoneal injections of bevacizumab or a volume-equivalent placebo solution at the dose of 10 mg/kg every other day for 4 times). Tumor volumes were assessed with caliper measurements everyday. The animals were imaged with 18F-RGD-PAA-USPIO, the target-to-background ratio (TBR, VOImaxtumor/VOImeanmuscle, Δ TBR=TBRday7-TBRday0) and Δ T2 value(Δ T2=T2pre-contrast-T2post-contrast, $\Delta\Delta$ T2= Δ T2day7- Δ T2day0) were served as semiquantitative measure to determine the effect of bevacizumab. Imaging results were validated by ex vivo multiparametric immunohistochemistry with regard to microvascular density (CD31) and proliferation(Ki-67).

RESULTS

18F-RGD-PAA-USPIO did not cause cellular toxicity in MDA-MB-231 cell lines.Both small-animal PET and T2-weighted MRI show integrin specific delivery of 18F-RGD-PAA-USPIO. No intergroup difference in tumor volume development between day 0 and day 7 was observed (p=0.118).18F-RGD-PAA-USPIO binding was significantly reduced after bevacizumab compared with the control group shown both in PET/CT (Δ TBR,-0.65 ± 0.43 vs 0.66 ± 1.04,p=0.032) and MRI imaging ($\Delta\Delta$ T2,9.56 ± 4.14 vs 4.92 ± 6.10,p<0.01).Correspondingly,immunohistochemistry revealed a significantly lower microvascular density (CD31,15.19 ± 7.58 vs 42.90 ± 16.81,p<0.01), tumor cell proliferation (Ki-67,420.60 ± 113.67 vs 702.30 ± 119.62,p<0.01) in the therapy compared with the control group.

CONCLUSION

18F-RGD-PAA-USPIO can be use to monitor and evaluate the therapeutic effects of anti-angiogenesis agents on breast cancer model.

CLINICAL RELEVANCE/APPLICATION

(to dealing with PET/MRI) the multimodal imaging agents, 18F-RGD-PAA-USPIO, which are capable of simultaneously providing both PET and MRI information, can expand the applicability of PET/MRI dual modality imaging system.

SSK12-07 Fractional Excretion and Biodistribution of the Manganese-Based MRI Contrast Agent Mn-PyC3A in Rats

Wednesday, Nov. 28 11:30AM - 11:40AM Room: S504CD

Participants

Eric Gale, Charlestown, MA (*Abstract Co-Author*) Co-founder, Reveal Pharmaceuticals; Stockholder, Reveal Pharmaceuticals Ian Ramsay, BS, Charlestown, MA (*Abstract Co-Author*) Nothing to Disclose Peter D. Caravan, PhD, Charlestown, MA (*Presenter*) Research Grant, Pfizer Inc;

For information about this presentation, contact:

caravan@mgh.harvard.edu

PURPOSE

To determine the fractional excretion and biodistribution of manganese at 1 day and 7 days following injection of the manganesebased MRI contrast agent Mn-PyC3A in rats.

METHOD AND MATERIALS

All experiments were performed in accordance with the National Institutes of Health's Guide for the Care and Use of Laboratory Animals, 8th Edition, and were approved by the institutional animal care and use committee of Massachusetts General Hospital. [52Mn]Mn-PyC3A was prepared from an aliquot of a 0.5 M solution of Mn-PyC3A that was mixed with 3 mCi of 52MnCl2 (beta+, t1/2 = 5.56 d) at pH to 3.0. After stirring for 30 min, the pH was adjusted to 8.0 with N-methyl-D-glucamine and returned to the bulk 0.5 M solution. [52Mn]Mn-PyC3A (2.0 mmol/kg, 100 - 300 μ Ci) was administered via tail vein to Wistar Rats. Rats, equal numbers of males and females, were housed in metabolic cages and euthanized after 1 d (N=10) or 7 d (N=8), and the organs were harvested and 52Mn quantified by gamma counter. The fractional excretion into urine and feces was also determined.

RESULTS

One day after [52Mn]Mn-PyC3A injection, 0.36±0.11 percent of the injected dose (%ID) remains in the rat and this drops to 0.052±0.042% after seven days. These values are an order of magnitude lower than reported Gd-retention following injection of gadolinium based contrast agents (GBCAs) (Tweedle, Invest. Radiol 1995;30(6):372-380). [52Mn]Mn-PyC3A is eliminated

 $84.9\pm4.9\%$ into the urine and $15.1\pm4.9\%$ into the feces. Mass balance indicated that $97.5\pm3.9\%$ ID was recovered from the excreta, tissues, and GI contents 1 d after injection.

CONCLUSION

Mn-PyC3A is >99.6% eliminated from rats one day after, and >99.9% eliminated seven days after intravenous injection. Mn-PyC3A shows extremely low levels of metal retention after administration.

CLINICAL RELEVANCE/APPLICATION

Mn-PyC3A has been proposed as a Gd-free alternative for contrast enhanced MRI. Before clinical translation, it is important to establish whether there is manganese ion accumulation. These studies indicate that Mn-PyC3A is rapidly and efficiently eliminated from the body and prompt further development of this new contrast agent.

SSK12-08 A pH-sensitive Manganese Core Nanoparticle as the Tumor Targeting MR Contrast Agent: Comparison with Gd-DTPA in a Mouse Model

Wednesday, Nov. 28 11:40AM - 11:50AM Room: S504CD

Participants

Jiali Li, Wuhan, China (*Abstract Co-Author*) Nothing to Disclose Zhen Li, MD, PhD, Wuhan, China (*Presenter*) Nothing to Disclose Daoyu Hu, Wuhan, China (*Abstract Co-Author*) Nothing to Disclose Yaqi Shen, PhD, MD, Wuhan, China (*Abstract Co-Author*) Nothing to Disclose

PURPOSE

A novel manganese core nanoparticle designed as pH-sensitive MR contrast agent (L-EGCG-Mn), confirmed the tumor targeting properties in a mouse model. In vitro and in vivo MR properties were compared with Gd-DTPA.

METHOD AND MATERIALS

This study was approved by the local Animal Ethics Committee. The physicochemical properties of L-EGCG-Mn were characterized by dynamic light scattering, transmission electron microscopy(TEM), and near infrared fluorescence small animal living imaging. A serial of different concentration of L-EGCG-Mn dispersed in phosphate buffered saline(PBS) with different pH (pH=7.4, 6.8, 5.5) and Gd-DTPA solutions were evaluated at a 3 T MRI scanner, and the relaxivities (r1 and r2) were obtained for comparison in vitroanalysis. A total of eight Hepatoma-22 cells implanted mice (5 for L-EGCG-Mn;3 for Gd-DTPA) were scanned at a 3.0 T MRI with an animal coil. MR images of pre- and 30min, 1h, 2h, 4h after injection of L-EGCG-Mn and Gd-DTPA were acquired. The signal-to-noise ratio (SNR) and contrast-to-noise ratio (CNR) of tumor were calculated.

RESULTS

The particle size of L-EGCG-Mn was 277.4 \pm 5.5 nm and the zeta potential of it was -13.56 \pm 1.91mV, the negative zeta potential indicating a good biocompatibility. TEM images confirmed that L-EGCG-Mn incubated in pH=5.5 PBS expanded faster than that in pH=6.8 PBS. And the r1(r2) relaxivity of L-EGCG-Mn increased from 1.8(10.1) to 6.4(22.9) mM-1 · s-1 when the pH values decreased from 7.4 to 5.5, which was higher than Gd-DTPA (r1=4.7, r2=5.4 mM-1 · s-1). In H22 model mice, L-EGCG-Mn had significantly higher average CNR and SNR compared with Gd-DTPA for all acquired time point (P < 0.05 for all).

CONCLUSION

L-EGCG-Mn had promising pH sensitivity and superior enhancement properties, compared with Gd-DTPA in H22 model mice and vitro relaxivity analysis.

CLINICAL RELEVANCE/APPLICATION

L-EGCG-Mn with tumor-microenvironment changeable relaxivity may be an alternative to Gd-DTPA and overcome controversy regarding gadolinium-associated toxicity and retention in the clinical.

SSK12-09 First-Pass CMR Perfusion Imaging with a Novel Manganese Chelate Contrast Agent in Myocardial infarction: Comparison with Gd-DTPA

Wednesday, Nov. 28 11:50AM - 12:00PM Room: S504CD

Participants

Lingyi Wen Jr, MD, Chengdu, China (*Presenter*) Nothing to Disclose Zhigang Yang, MD, Chengdu, China (*Abstract Co-Author*) Nothing to Disclose Huayan Xu, Chengdu, China (*Abstract Co-Author*) Nothing to Disclose Kun Zhang, Chengdu, China (*Abstract Co-Author*) Nothing to Disclose Yingkun Guo, Chengdu, China (*Abstract Co-Author*) Nothing to Disclose

For information about this presentation, contact:

lizzievane@126.com

PURPOSE

To evaluate the feasibility of novel Mn2+ chelate to quantify myocardial perfusion in myocardial infarction (MI), by comparison with Gd-based First-pass perfusion MRI.

METHOD AND MATERIALS

We designed and synthesized an aza-semi-crown pentadentate chelator that formed manganese (Mn2+) complexes as a novel MRI contrast agent. MI was induced in 6 rabbits by permanent occlusion of left circumflex coronary artery. After 7days post-surgery, cine MRI, T1WI, T2WI, first-pass perfusion MRI were performed on a 3.0T clinical MRI scanner (Achieva, Philips, Andover, MA) with a clinical 8-channel knee coil. Dynamic signal changes on first-pass perfusion MRI was acquired using segmented turbo-FLASH sequence with 80 dynamic acquisitions. Three contiguous short-axis images was obtained after intravenous injection of gadolium (Gd-DTPA, Magnevist, Berlin, Germany) at 0.15 mmol/kg and Mn2+ chelate successively. A 120-minute washout period proceeded

between administration of contrast agents to ensure independent enhancement pattern. Short-axis cine images were analyzed for assessment of left ventricular (LV) volumes, ejection fractions (EF), first-perfusion images for slope, max signal intensity, time to peak, time to 50% max with dedicated software (Cmr42,Circle Cardiovascular Imaging Inc.,Calgary, Canada). The correlation between methods was evaluated with two-variable linear regression analysis, with Pearson correlation.

RESULTS

All rabbits survived after MRI scanning without significant differences in heart rate, LV end-diastolic volume, end-systolic volume and EF between baseline and after injection of Gd or Mn (p>0.05). First-pass perfusion MRI identified infarcted myocardial segments when compared with normal myocardial segments. When compared with normal myocardial segments, the slope, max signal intensity of infarcted myocardial segments decreased significantly, time to peak and time to 50% max extended (all p<0.05). All the perfusion parameters of infarcted and normal myocardial segments correlated well between Gd-based and Mn-based perfusion imaging (all p<0.05, r=0.43-0.72).

CONCLUSION

Our novel Mn2+ Chelate contrast agent is safe and reliable to visualize myocardial perfusion in myocardial infarction.

CLINICAL RELEVANCE/APPLICATION

Although still in the preclinical stage, the novel Mn2+ Chelate contrast agent may be useful for assessment of myocardial perfusion in myocardial infarction.



SSK13

Musculoskeletal (Advances in MR Imaging)

Wednesday, Nov. 28 10:30AM - 12:00PM Room: N229



AMA PRA Category 1 Credits ™: 1.50 ARRT Category A+ Credit: 1.75

Participants

Christine B. Chung, MD, La Jolla, CA (*Moderator*) Nothing to Disclose Gregory Chang, MD, New York, NY (*Moderator*) Nothing to Disclose

Sub-Events

SSK13-01 Lower Leg Muscle Activation during Walking and Running: Quantitative Muscle-specific Assessment of Microvascular Perfusion with Intravoxel Incoherent Motion (IVIM) MR Imaging

Participants

Pia M. Jungmann, MD, Zurich, Switzerland (*Presenter*) Nothing to Disclose Christian W. Pfirrmann, MD, MBA, Forch, Switzerland (*Abstract Co-Author*) Nothing to Disclose Christian Federau, Basel, Switzerland (*Abstract Co-Author*) Nothing to Disclose

PURPOSE

Little is known about muscle activation patterns during walking and running. Blood flow to skeletal muscles depends on the metabolic activity. Aim of this study was to non-invasively assess specific muscle activation of the lower limb after walking and running by using Intravoxel Incoherent Motion (IVIM) perfusion MRI.

METHOD AND MATERIALS

3T MR IVIM diffusion-weighted images of the lower extremities of 8 healthy female volunteers (mean age 27.5±5.7 years) were acquired at rest and immediately after walking and running, respectively. For IVIM measurements, a transverse monopolar pulsed gradient fat suppressed spin echo (SE) EPI sequence was used (9 b-values from 0 to 1000s/mm2, 3 orthogonal directions). In addition, anatomical transverse T1-weighted turbo SE images were acquired at rest. Entire muscles of the pelvis, thigh and lower leg were segmented. IVIM perfusion parameters f, D* and fD* and the diffusion coefficient D were obtained after standard two-steps fitting of the IVIM bi-exponential signal equation. Descriptive statistics, paired t-tests, multiple regression models and Pearson's correlations were used for statistical analyses.

RESULTS

Mean heart rates were 63 ± 3 min-1 at rest, 113 ± 14 min-1 during walking and 166 ± 14 min-1 during jogging. Microvascular blood-flow related fD* correlated significantly with heartrate while walking and running, respectively (P<0.05). Mean fD* of all muscles was significantly higher after running (2.18\pm0.98*10-3mm2/s, P<0.001) and after walking (1.99\pm0.80*10-3mm2/s, P<0.001) compared to rest (1.65\pm0.83*10-3mm2/s). Perfusion increase was gradual and most pronounced for the lower leg muscles (fD* increase of 60.8% after walking, 137.3% after running compared to rest, P<0.001) and for the feet muscles (78.4% and 181.4%, P<0.001) (Figure). Abductor muscles showed a higher microvascular perfusion than adductor muscles; quadriceps muscles showed a higher perfusion than hamstrings (P<0.05).

CONCLUSION

Non-invasive IVIM MRI is able to quantitatively measure local microvascular muscle perfusion in order to detect muscle activation patterns after walking and running.

CLINICAL RELEVANCE/APPLICATION

IVIM is a promising modality to non-invasively assess muscle physiology. It may potentially be of use to monitor changes in physiological microvascular muscle perfusion after training and to detect pathological muscle recruitment patterns.

SSK13-02 Evaluation of Role of Diffusion Weighted Imaging (DWI), Apparent Diffusion Coefficient (ADC) and Chemical Shift Imaging (CSI) in Distinguishing Benign versus Malignant Vertebral Body Lesions with Histopathological Correlation

Wednesday, Nov. 28 10:40AM - 10:50AM Room: N229

Participants

Gurudat R. Shenoy, MBBS, Bangalore, India (*Presenter*) Nothing to Disclose Rahul Sharma, MBBS, Bangalore, India (*Abstract Co-Author*) Nothing to Disclose Pankaj M. Kolhe, MBBS, Bangalore, India (*Abstract Co-Author*) Nothing to Disclose Aishwarya K. Mahendrakar, MBBS, Bangalore, India (*Abstract Co-Author*) Nothing to Disclose Prashanth Reddy, MBBS,MD, Bangalore, India (*Abstract Co-Author*) Nothing to Disclose Bharath B. Das, MD, MBBS, Bangalore, India (*Abstract Co-Author*) Nothing to Disclose Sankar Neelakantan, MD, Bangalore, India (*Abstract Co-Author*) Nothing to Disclose Bhavana Nagabhushana Reddy, MBBS, MD, Bangalore, India (*Abstract Co-Author*) Nothing to Disclose Sanjaya Viswamitra, MD, Bengaluru, India (*Abstract Co-Author*) Nothing to Disclose

For information about this presentation, contact:

s.gurudat@gmail.com

PURPOSE

To evaluate the role of qualitative DWI, qualitative CSI: quantitative DWI(ADC values) and quantitative CSI(Signal Intensity Ratio - SIR values) in the differentiation of benign and malignant vertebral lesions.

METHOD AND MATERIALS

44 patients of all age group of both sexes showing presence of vertebral fractures on MRI were included in study. We used the biopsy results or results of clinical and radiologic follow up for at least 6 months, as the gold standard to classify the vertebral fractures as benign or malignant. The presence of high SI of vertebral fractures on DWI were considered as diffusion restricting. ADC values acquired, by placing ROI in ADC maps over the areas within the vertebral fractures that were showing abnormal signal intensities on T1, T2 weighted and STIR. The SI of vertebral fractures were compared in in-phase and out-of-phase image and loss of signal on out-of-phase image was evaluated. Quantitative analysis was done by calculating SIR values of opposed-phase to in-phase, by placing ROI over the areas within the vertebral fractures on the in-phase images and corresponding areas on the out-of-phase images(that were of abnormal SI on T1, T2 weighted and STIR sequences). SIR = SI opposed-phase / SI in-phase.

RESULTS

Qualitative DWI resulted in sensitivity of 92.9%, specificity of 20%, PPV of 35.14%, NPV of 85.71% and accuracy of 43.2%. The mean ADCs for the benign (1.37 ± 0.22) compression fracture group were significantly higher than the malignant (0.94 ± 0.17) group, and ADC cutoff value of 1.085 resulted in sensitivity of 85.7%, specificity of 83.3%, PPV of 70.59%, NPV of 92.59% and accuracy of 84.1%. Qualitative CSI resulted in sensitivity of 92.9%, specificity of 53.3%, PPV of 48.15%, NPV of 94.12% and accuracy of 65.9%. The mean SIRs for the benign (0.67 ± 29) compression fracture group were significantly lower than SIR values for the malignant (1.12 ± 0.15) group and SIR cutoff value to be 0.97 was identified with sensitivity of 92.9%, specificity of 90%, PPV of 81.25%, NPV of 96.43% and accuracy of 90.9%.

CONCLUSION

Quantifying the loss of signal on out-of-phase imaging and quantifying diffusion on ADC maps, can be used in differentiation between benign and malignant vertebral compression fractures.

CLINICAL RELEVANCE/APPLICATION

Quantitative DWI and quantitative chemical shift imaging can differentiate between benign and malignant vertebral fractures and is recommended as part of a MR study.

SSK13-03 Asymmetric Muscle Recruitment of the Back during Exercise in Patients with Scoliosis Demonstrated with Intravoxel Incoherent Motion (IVIM) MR Perfusion Imaging: Preliminary Results

Wednesday, Nov. 28 10:50AM - 11:00AM Room: N229

Participants

Christian Federau, Basel, Switzerland (*Presenter*) Nothing to Disclose Daniela Kroismayr, Zurich, Switzerland (*Abstract Co-Author*) Nothing to Disclose Linda Dyer, Zurich, Switzerland (*Abstract Co-Author*) Nothing to Disclose Mazda Farshad, Zurich, Switzerland (*Abstract Co-Author*) Nothing to Disclose Christian W. Pfirrmann, MD, MBA, Forch, Switzerland (*Abstract Co-Author*) Nothing to Disclose

PURPOSE

It is thought that patients with scoliosis overuse the back muscle in the convexity of their scoliosis, which might worsen their condition. Because muscle activity increases local blood flow, muscle recruitment can be mapped using MR perfusion imaging. The purpose of this work was to study the muscular recruitment of back muscle during Roman chair exercise in patients with scoliosis using Intravoxel Incoherent Motion (IVIM), an imaging technique which extracts local and quantitative perfusion information from a diffusion weighted MRI sequence, without the need for an injection of a contrast agent.

METHOD AND MATERIALS

4 patients ($3/1 \text{ f/m}, 20 \pm 4y$) with scoliosis (Cobb angle $28 \pm 2^{\circ}$, range [25-30°]) were scanned at 3T first after observing a period of rest of 20 min, and then immediately after performing a symmetric back muscle exercise on a Roman chair, holding a 4kg dumbbell with both hands in the middle of the thorax, until exhaustion ($72 \pm 2s$). The IVIM diffusion-weighted sequence consisted of a spinecho with echo planar readout and monopolar pulsed gradients with 16 b-values ranging from 0-900s/mm2. The IVIM bi-exponential signal equation model was fitted using a C++ implementation of a standard two steps algorithms. A region of interest was drawn in the paraspinal muscles at the level of the convexity of the scoliosis on both sides. Statistical significance was assessed using paired Student t-test.

RESULTS

At rest, microvascular blood-flow related IVIM fD* was found larger in the paraspinal muscles on the side of convexity $(5.8\pm1.1\times10-3mm2/s)$ compared to the concavity $(4.3\pm1.5\times10-3mm2/s)$, but the difference was not significantly (p=0.11). After Roman chair muscle exercise, fD* increased significantly in the paraspinal muscles (p=0.001), and fD* was significantly larger in the paraspinal muscles on the side of convexity (7.7\pm0.8\times10-3mm2/s) compared to the concavity (5.3\pm1.0\times10-3mm2/s), p=0.001).

CONCLUSION

The preliminary data of this study demonstrates an asymmetric microvascular muscle perfusion pattern in the muscle of the back after exercise in patient with scoliosis.

CLINICAL RELEVANCE/APPLICATION

This study helps clarifying muscular recruitment of back muscle during exercise in patients with scoliosis, and could help to improve current physiotherapeutic and surgical treatment approaches.

SSK13-04 Diffusion Weighted Imaging of Musculoskeletal Infections: Quantitative ADC Analysis of Lower Extremity Superficial and Deep Infections

Wednesday, Nov. 28 11:00AM - 11:10AM Room: N229

Awards

Student Travel Stipend Award

Participants Raamis Khwaja, BS, Dallas, TX (*Presenter*) Nothing to Disclose Charisma DeSai, BS, Dallas, TX (*Abstract Co-Author*) Nothing to Disclose Anish Narayanan, BS, Irving, TX (*Abstract Co-Author*) Nothing to Disclose Yin Xi, PhD, Dallas, TX (*Abstract Co-Author*) Nothing to Disclose Avneesh Chhabra, MD, Dallas, TX (*Abstract Co-Author*) Consultant, ICON plc; Author with royalties, Wolters Kluwer nv; Author with royalties, Jaypee Brothers Medical Publishers Ltd

For information about this presentation, contact:

Avneesh.Chhabra@utsouthwestern.edu

PURPOSE

This study investigates the value of diffusion weighted imaging (DWI) and apparent diffusion coefficient (ADC) in the differential diagnosis of musculoskeletal infections and determines the region of interest (ROI) values for cellulitis, soft tissue abscess, osteitis, osteomyelitis and intraosseous abscesses in the lower extremity.

METHOD AND MATERIALS

The MRIs of sixty-two patients with musculoskeletal inflammation and/or infection were retrospectively evaluated through measurement of ROIs on DWI and ADC at the site of disease. Imaging was conducted between 2014 and 2017 with inclusion criteria of: adults 18-100 years, no metal in the field of view, extremity MRI scans with DWI imaging, and established reference standards of biopsy, surgery, and follow-up results. Patient cases were placed into six categories of infection: soft tissue edema, soft tissue cellulitis, soft tissue abscess, osteitis, osteomyelitis, and osteomyelitis with abscess. Diagnosis was based on a combination of pathology reports and clinical correlation (lab values, patient care notes, treatment regimen, time to resolution of symptoms). ROIs were measured by three readers trained by an experience musculoskeletal radiologist at the region of interest with minimum area of 1cm2. Statistical analysis of data was performed to measure inter-reader agreement with ICC and significance of ROI measurements on ADC with ANOVA to test for differences between the six categories of infection. The Bonferroni adjustment was applied to adjust the p value for multiple comparisons.

RESULTS

The mean ADC value of osteitis is 1.58 compared to 1.41 for osteomyelitis and 0.78 for intraosseous abscess with statistically significant difference (p < 0.02). Similarly, mean ADC value of soft tissue cellulitis is 1.70 and soft tissue abscess is 0.73 with statistically significant difference (p < 0.001). Intra-reader agreement was excellent with ICC of 0.93 and 0.96 between the three readers.

CONCLUSION

DWI and ROI measurements on ADC can reliably distinguish between osteitis, osteomyelitis and intraosseous abscess, as well as soft tissue abscess and soft tissue cellulitis.

CLINICAL RELEVANCE/APPLICATION

DWI and ADC measurements can distinguish between musculoskeletal infections and are recommended as part of the MRI studies and evaluation of these conditions.

SSK13-05 Diffusion MRI of Human Patellar Tendon: Initial Experience

Wednesday, Nov. 28 11:10AM - 11:20AM Room: N229

Participants

Kenneth T. Wengler, MS, Stony Brook, NY (*Abstract Co-Author*) Nothing to Disclose Takeshi Fukuda, MD, Stony Brook, NY (*Abstract Co-Author*) Nothing to Disclose Dharmesh Tank, MD, Stony Brook, NY (*Presenter*) Nothing to Disclose Mingqian Huang, MD, Syosset, NY (*Abstract Co-Author*) Nothing to Disclose David E. Komatsu, PhD, Stony Brook, NY (*Abstract Co-Author*) Nothing to Disclose James M. Paci, MD, Setauket- East Setauket, NY (*Abstract Co-Author*) Nothing to Disclose Elaine S. Gould, MD, Stony Brook, NY (*Abstract Co-Author*) Consultant, Endo International plc Mark E. Schweitzer, MD, Stony Brook, NY (*Abstract Co-Author*) Consultant, MMI Munich Medical International GmbH; Data Safety Monitoring Board, Histogenics Corporation Xiang He, PhD, Stony Brook, NY (*Abstract Co-Author*) Consultant, Endo International plc

PURPOSE

The patellar tendon (PT) is essential for knee extension. Patellar tendinopathy causes persistent anterior knee pain and occurs in \sim 14% of recreational athletes. Despite the high prevalence, no consensus treatment exists. PT microstructure and microcirculation play crucial roles in the progression of tendinopathy and tendon repair. Diffusion tensor imaging (DTI) and intravoxel incoherent motion (IVIM) imaging can assess the microstructure and microcirculation characteristics of biological tissue. However, the application of conventional diffusion MRI protocols to PT is challenged by short T2/T2* values (\sim 2ms) and the long TE (\sim 60ms) requirement. In this study, a stimulated-echo based short TE (\sim 15ms) diffusion protocol (ste-RS-EPI), originally developed for Achilles tendon, was applied to PT of healthy subjects. After validation, this technique can be readily adopted to assess treatment response in patellar tendinopathy.

METHOD AND MATERIALS

Six healthy subjects were recruited for this IRB approved study on a Siemens Prisma 3T magnet. Stimulated-echo diffusion

preparation with readout-segmented EPI (ste-RS-EPI) was adopted. To further boost tendon MR signal, magic angle effect was exploited by positioning PT ~55 degrees w.r.t. B0 direction. PT fractional anisotropy (FA), radial diffusivity (RD), axial diffusivity (AD), and mean diffusivity (MD) maps were generated with DTI Studio. PT diffusion coefficient (D), pseudo-diffusion coefficient (D*), and perfusion fraction (fp) were calculated using standard bi-exponential fit to the IVIM signal. The product of D* and fp was used as an indicator of intra-tendinous blood flow.

RESULTS

Ste-RS-EPI images achieved high signal and good image quality for the PT. The measured DTI and IVIM parameters (diffusivities in units of $\times 10-3$ mm2/s) in the PT were: AD (1.54±0.09), RD (1.01±0.06), MD (1.19±0.07), FA (0.29±0.02), fp (4.6±1.2%), and D* \times fp (36.6±6.9).

CONCLUSION

This preliminary study demonstrated the feasibility of the ste-RS-EPI DTI and IVIM protocols to assess patellar tendon microstructure and microcirculation. The estimated DTI and IVIM parameters in control subjects may serve as a baseline for subsequent studies on patients with clinical and subclinical patellar tendinopathy.

CLINICAL RELEVANCE/APPLICATION

The ste-RS-EPI DTI and IVIM techniques may be used for evaluation of tendinopathy and to quantitatively assess pathophysiological changes that occur as a result from various treatments.

SSK13-06 Diffusion Tensor Imaging With Quantitative Evaluation of Sciatic Nerve within the Pelvis in Patients with Non-Contributory Lumbar Spine Magnetic Resonance Imaging in Radiculopathy: Preliminary Results

Wednesday, Nov. 28 11:20AM - 11:30AM Room: N229

Participants

Matteo Catania, MD, Trieste, Italy (*Presenter*) Nothing to Disclose Giovanni Foti, MD, Negrar, Italy (*Abstract Co-Author*) Nothing to Disclose Luigi Romano, MD, Verona, Italy (*Abstract Co-Author*) Nothing to Disclose Alberto Beltramello, MD, Negrar, Italy (*Abstract Co-Author*) Nothing to Disclose Emanuele Demozzi, MD, Negrar, Italy (*Abstract Co-Author*) Nothing to Disclose Giovanni M. Carbognin, MD, Verona, Italy (*Abstract Co-Author*) Nothing to Disclose

For information about this presentation, contact:

matteocatania89@gmail.com

PURPOSE

Diffusion tensor imaging with quantitative evaluation of sciatic nerve within the pelvis in Patients with non-contributory lumbar spine magnetic resonance imaging in radiculopathy: preliminary results.

METHOD AND MATERIALS

This prospective institutional review board-approved study included 32 consecutive patients (11 males and 21 females; mean age of 41.2, range 19-52 years) studied between October 2016 and February 2018. The study population included 32 patients suffering from sciatica pain with negative lumbar MRI. All patients underwent DTI sequence of the pelvis (TR/TE 5800/97 ms; b=1000; slice thickness 3,5 mm; directions=20) by using a 1.5T scanner (Siemens Aera). DTI data were postprocessed on a dedicated offline workstation by two radiologists (25 and 11 years of experience, respectively) blinded to clinical data. Each radiologist placed two ROI on the nerve roots at three different levels within the pelvis on both side, and the mean value was used for further analysis. Clinical findings served as standard of reference. Diagnostic accuracy values of the FA numbers by using receiver operator curves (ROC) and relative area under the curve (AUC) were calculated. Inter-observer and intra-observer agreement were calculated with k-statistics. Continuous and categorical variables were evaluated by using t test and x2 or Fisher exact test, as appropriate. A value of p<0.05 was considered statistically significant

RESULTS

The lumbar nerve roots were visualized and FA values were calculated in all subjects. The FA values were significantly different between suffering nerve roots (178 ± 48 ; range 146-285) and spared side (296 ± 52 ; range 221-412) with a p value <0.001. The ROC curve analysis revealed an AUC of 0.816 (95% confidence interval: 0.682-0.874). By using a FA of 220 as cutoff to identify suffering nerve roots, the sensitivity, specificity, PPV and NPV and accuracy of DTI sequences were and 81.8, 95.4, 90.0, 91.3 and 90.9%, respectively. The interobserver and intraobsever agreement were near perfect (k=0.83 and k=0.81, respectively)

CONCLUSION

DTI can quantitatively demonstrate the presence of suffering sciatic nerve roots within the pelvis.

CLINICAL RELEVANCE/APPLICATION

DTI can quantitatively evaluate compressed nerve roots of sciatic nerve in patients with negative lumbar MRI. This sequences could be used to guide the identification of nerve compression site within the pelvis by means of a tailored MR study

SSK13-07 Comparison of Proton Density Fat Fraction, Simultaneous R2*, and Diffusion Weighted Image for Assessment of Focal Vertebral Bone Marrow Lesions

Wednesday, Nov. 28 11:30AM - 11:40AM Room: N229

Participants

Seong Woo Jeon, MD, Suwon, Korea, Republic Of (*Abstract Co-Author*) Nothing to Disclose Kyu-Sung Kwack, MD, PhD, Suwon, Korea, Republic Of (*Abstract Co-Author*) Nothing to Disclose Sunghoon Park, MD, Suwon, Korea, Republic Of (*Presenter*) Nothing to Disclose

PURPOSE

To investigate proton density fat fraction (PDFF), R2* and apparent diffusion coefficient (ADC) estimation for assessing focal vertebral bone marrow lesions.

METHOD AND MATERIALS

We retrospectively reviewed 182 spine MRIs performed in 119 patients with focal vertebral bone marrow lesions from November 2016 to February 2018. The lesions were divided into bone metastases and focal benign vertebral bone marrow lesions. The protocol consisted of routine clinical sequences followed by IDEAL-IQ and diffusion-weighted (DW) magnetic resonance (MR) imaging with 1.5T MR unit (Signa HDxt, GE Healthcare, Waukesha, WI). PDFF and R2* were performed using a quantitative chemical shift-based water-fat separation method known as IDEAL-IQ with a multi-echo gradient echo sequence. ADC (b = 0 and 800 s/mm2) was calculated with a monoexponential fitting of the DW image data. PDFF, R2*, and ADC were compared using the Mann-Whitney U test. Receiver operating characteristic (ROC) curve analysis was performed to assess the diagnostic performances for differentiating metastasis from benign vertebral bone marrow lesions.

RESULTS

In the comparison of diagnostic performance among parameters, the PDFF (AUC = 0.960; 95% confidence interval [CI], 0.921, 0.984) showed a significantly larger AUC as compared to the R2* (AUC = 0.667; 95 % CI, 0.593 - 0.735) and ADC (AUC = 0.754; 95 % CI, 0.685 - 0.815) value. The optimal cut-off value of fat fraction for predicting focal malignant vertebral bone marrow lesions was 9.0 %; at this threshold, sensitivity was 97.30 % and specificity was 91.55 %. All the PDFF, R2*, and ADC values sequences were in almost perfect agreement (r values > 0.8)

CONCLUSION

Our study shows that PDFF measurement can enable in differentiating focal vertebral bone marrow lesions, and may be more useful than DW MR imaging.

CLINICAL RELEVANCE/APPLICATION

PDFF can be the excellent diagnostic performance in differentiating focal vertebral bone marrow lesions and this examination recommend in the evaluation of suspected bone metastases.

SSK13-08 Quantitative Analysis with 3T Multiparametric MR imaging: Differentiation between Benign and Malignant Soft Tissue Tumors

Wednesday, Nov. 28 11:40AM - 11:50AM Room: N229

Participants

Seul Ki Lee, MD, Gyeonggi, Korea, Republic Of (*Presenter*) Research Grant, Dongkook Life Science Co, Ltd Won-Hee Jee, MD, Seoul, Korea, Republic Of (*Abstract Co-Author*) Research Grant, Bayer AG; Chan-Kwon Jung, Seoul, Korea, Republic Of (*Abstract Co-Author*) Nothing to Disclose Joon-Yong Jung, MD, Seoul, Korea, Republic Of (*Abstract Co-Author*) Nothing to Disclose Yohan Son, Seoul, Korea, Republic Of (*Abstract Co-Author*) Nothing to Disclose Munyoung Paek, Seoul, Korea, Republic Of (*Abstract Co-Author*) Nothing to Disclose Yang-Guk Chung, MD, Seoul, Korea, Republic Of (*Abstract Co-Author*) Nothing to Disclose

For information about this presentation, contact:

whjee12@gmail.com

PURPOSE

To determine the reliability and accuracy of 3T multiparametric magnetic resonance (MR) imaging in the differentiation between benign and malignant soft tissue tumors.

METHOD AND MATERIALS

This retrospective study was approved by the institutional review board and informed consent was waived. Sixty-eight patients with pathologically confirmed soft tissue tumors (35 benign and 33 malignant) who underwent 3T standard MR imaging, intravoxel incoherent motion (IVIM) diffusion-weighted MR imaging (DWI), and dynamic contrast-enhanced (DCE) MR imaging were enrolled with exclusion of lipoma and well-differentiated liposarcoma. IVIM parameters (true diffusion coefficient, D; pseudodiffusion coefficient, D*; perfusion fraction, f), apparent diffusion coefficient (ADC), and DCE parameters (transfer constant, Ktrans; rate constant, Kep; extravascular extracellular volume fraction, Ve; initial area under time-signal intensity curve, iAUC) were calculated by Syngovia software. All parameters were compared using Student's t test and multivariate logistic regression analysis. The receiver operating characteristic (ROC) curve with areas under the curve (AUC) was obtained.

RESULTS

ADC and D were significantly lower in malignant tumors than benign tumors ($1181.6\pm484.7 \text{ vs } 1472.3\pm349.1 \mu m^2/\text{sec}$; $1152.2\pm505.0 \text{ vs } 1414.9\pm373.8 \mu m^2/\text{sec}$; P<.05, respectively). Ktran, Kep, Ve, and iAUC were significantly different between malignant tumors and benign tumors ($211.3\pm158.2 \text{ vs } 92.4\pm67.0 10^3/\text{min}$; $775.9\pm528.9 \text{ vs } 311.5\pm230.4 10^3/\text{min}$; $31.7\pm17.3 \text{ vs } 43.9\pm28.2 \%$; $23.3\pm14.6 \text{ vs } 11.8\pm9.0 \%$, P<.05, respectively). The best discriminative parameters for prediction of malignant tumors versus benign tumors were ADC (odds ratio [OR]: 0.991, P=.046), Kep (OR: 1.004, P=.003) and iAUC (OR: 1.064, P=.048). The AUCs of ADC alone, ADC combined with Kep, and ADC combined Kep and iAUC were 0.738, 0.816, and 0.848, respectively.

CONCLUSION

ADC, Kep, and iAUC may be reliable and accurate parameters for the differentiation between benign and malignant soft tissue tumors at 3T multipamametic MR imaging.

CLINICAL RELEVANCE/APPLICATION

Multiparametric MR imaging is reliable and accurate in the differentiation between benign and malignant soft tissue tumors.

SSK13-09 Fat Suppression for Ultrashort Echo Time (UTE) Imaging Using Single Point Dixon Method

Participants

Hyungseok Jang, La Jolla, CA (*Presenter*) Nothing to Disclose Yajun Ma, San Diego, CA (*Abstract Co-Author*) Nothing to Disclose Saeed Jerban, PhD, San Diego, CA (*Abstract Co-Author*) Nothing to Disclose Tan Guo, MD, Beijing, China (*Abstract Co-Author*) Nothing to Disclose Wei Zhao, La Jolla, CA (*Abstract Co-Author*) Nothing to Disclose Eric Y. Chang, MD, San Diego, CA (*Abstract Co-Author*) Nothing to Disclose Jiang Du, PhD, San Diego, CA (*Abstract Co-Author*) Nothing to Disclose

For information about this presentation, contact:

h4jang@ucsd.edu

PURPOSE

Use of fat saturation (FS) pulses with UTE sequences can improve short T2 contrast but reduce short T2 signal, and two point Dixon (2p-Dixon) method can misestimate fat due to short T2* decay. We propose single point Dixon (1p-Dixon) method to suppress fat for high contrast UTE imaging of short T2 tissues.

METHOD AND MATERIALS

1p-Dixon technique directly decomposes fat and water from complex MR signals after correcting phase errors due to field inhomogeneity (Ma. JMRI 2008). The proposed method utilizes dual echo 3D UTE imaging, where UTE is followed by the 2nd TE (TE2), chosen flexibly. Fat is estimated by applying 1p-Dixon to the non-UTE image at TE2, and used to suppress fat in the UTE image. In-vivo experiments were performed in 3T (GE-MR750) with two healthy volunteers (left knee of male aged 36 and left ankle of male aged 26). Parameters for knee imaging were as follows: flip angle=15degree, TE1/TE2/TR=32µs/2.7ms/20ms, voxel size=0.6x0.6x3mm scan time=3min50sec. Parameters for ankle imaging were set same as above except: TE2 =2.9ms, voxel size=0.5x0.5x3mm scan time=5min30sec.

RESULTS

Since 2p-Dixon does not consider signal decay between UTE and TE2, the short T2* decay is misinterpreted as a contribution of fat signal partially nulling water signal. Therefore, in the knee imaging fat signal in tendon and bone was misestimated by 2p-Dixon method, while the 1p-Dixon method was not affected by the short T2* signal decay. Compared with FS, 1p-Dixon based approach showed strong signal intensity in the patellar and Achilles tendon with less spatial variation in the fat suppressed UTE images, while the UTE images with FS pulse exhibited lower intensity in the tendons with gradually varying signal. The pattern of signal variation in the UTE images with FS was very similar to the water images at TE2 where most of short T2 (especially bound water) signal already decayed, which implies broad-spectrum short T2 components were partially affected by the FS pulse.

CONCLUSION

We demonstrated feasibility of 1p-Dixon based fat suppression in UTE imaging, which has the advantage of flexible echo spacing and accurate fat estimation over 2p-Dixon. Moreover, the proposed method preserves short T2 (especially bound water) signal significantly better than FS method.

CLINICAL RELEVANCE/APPLICATION

The proposed method has potential to aid with various types of morphological and quantitative UTE imaging, such as T2* mapping or UTE-MT modeling.



SSK14

Nuclear Medicine (Lymphoma, Sarcoma and Melanoma)

Wednesday, Nov. 28 10:30AM - 12:00PM Room: S505AB



AMA PRA Category 1 Credits ™: 1.50 ARRT Category A+ Credit: 1.75

Participants

Helen R. Nadel, MD, Palo Alto, CA (*Moderator*) Nothing to Disclose Matthew S. Robertson, MD, Cleveland, OH (*Moderator*) Nothing to Disclose

Sub-Events

SSK14-01 Incremental Value of Interim 18F-FDG PET/CT over CT-Scan for Early Response Evaluation in Patients with Hodgkin Lymphoma Treated with Immune Checkpoint Inhibitors

Participants

Ai-ping Chen, Nanjing, China (*Presenter*) Nothing to Disclose Fatima-Zohra Mokrane, MD, Toulouse, France (*Abstract Co-Author*) Nothing to Disclose Lawrence H. Schwartz, MD, New York, NY (*Abstract Co-Author*) Committee member, Celgene Corporation Committee member, Novartis AG Committee member, ICON plc Committee member, BioClinica, Inc Romain-David Seban, Villejuif, France (*Abstract Co-Author*) Nothing to Disclose Samy Ammari, Villejuif, France (*Abstract Co-Author*) Nothing to Disclose Randy Yeh, MD, New York, NY (*Abstract Co-Author*) Nothing to Disclose Aurelien Marabelle, Villejuif, France (*Abstract Co-Author*) Nothing to Disclose Binsheng Zhao, DSc, New York, NY (*Abstract Co-Author*) License agreement, Varian Medical Systems, Inc; Royalties, Varian Medical Systems, Inc; License agreement, Keosys SAS; License agreement, Hinacom Software and Technology, Ltd; Roch Houot, Rennes, France (*Abstract Co-Author*) Nothing to Disclose Laurent Dercle, MD, New York, NY (*Abstract Co-Author*) Nothing to Disclose

For information about this presentation, contact:

laurent.dercle@gmail.com

PURPOSE

Anti-Programmed Death 1 (anti-PD1) antibody triggers new patterns of response and progression in patients with Hodgkin lymphoma (HL). We aimed to evaluate the incremental value of interim 18F-FDG PET/CT over CT scans in patients treated by anti-PD1.

METHOD AND MATERIALS

We retrospectively analyzed patients treated by anti-PD1 from 2013 to 2017. Concomitant 18F-FDG PET/CT and CT scans were acquired at baseline and upon treatment. A pair of radiologists classified blindly and independently patients as immune-responding or immune-refractory based on the first evaluation, using the International Harmonisation Project Cheson 2014 criteria and the Lymphoma Response to Immunomodulatory therapy Criteria (LYRIC) (2016 revised criteria).

RESULTS

Forty-four consecutive HL patients were included. Forty-four interim 18F-FDG PET/CT and CT scans were acquired at a median time of 3.7 months after anti-PD1 initiation. Radiologists classified patients as immune-responding or immune-refractory on both 18F-FDG PET/CT and CT-scan in 55.7% and 35.2% of cases, respectively. Radiologists experienced a significant incremental value of 18F-FDG PET/CT in 8.0% (95%CI: 3.3%-15.7%) of patients, whom were reclassified as immune-refractory (2.3%) or immune-responding (5.7%). Additionally, 18.2% (95%CI: 10.8%-27.8%) of patients were reclassified from PR on CT-scan to CR on PET.

CONCLUSION

CT-scan alone can reliably be used for response assessment in patients with HL treated with anti-PD1: radiologists correctly classified patients as immune-responding or immune-refractory in 92% of cases. However, interim 18F-FDG PET/CT showed clear incremental value to reclassify immune-responding patients from partial response to complete response, which is crucial for risk-adapted strategies.

CLINICAL RELEVANCE/APPLICATION

Interim 18F-FDG-PET/CT in HL patients treated with anti-PD1 supplied incremental value over CT-scan by reclassifying patients to immune-responding or complete response. This concept is crucial for risk-adapted therapeutic strategy.

SSK14-02 Impact of FDG-PET/CT on the Staging, Management and Outcomes of Patients with Presumed Limited Stage Hodgkin's Lymphoma and Aggressive Non-Hodgkin's Lymphoma

Wednesday, Nov. 28 10:40AM - 10:50AM Room: S505AB

Participants

Ur Metser, MD, FRCPC, Toronto, ON (*Presenter*) Nothing to Disclose Anca Prica, Toronto, ON (*Abstract Co-Author*) Nothing to Disclose

David C. Hodgson, MD, MPH, Toronto, ON (*Abstract Co-Author*) Nothing to Disclose Mindaugas Mozuraitis, Toronto, ON (*Abstract Co-Author*) Nothing to Disclose Maria Eberg, Toronto, ON (*Abstract Co-Author*) Nothing to Disclose Victor Mak, Toronto, ON (*Abstract Co-Author*) Nothing to Disclose Bo Green, Toronto, ON (*Abstract Co-Author*) Nothing to Disclose Amit Singnurkar, MD, Hamilton, ON (*Abstract Co-Author*) Nothing to Disclose Jill Dudebout, Kingston, ON (*Abstract Co-Author*) Nothing to Disclose Pamela Maccrostie, Toronto, ON (*Abstract Co-Author*) Nothing to Disclose Noam Tau, MD, Petah Tikva, Israel (*Abstract Co-Author*) Nothing to Disclose Nicole Mittmann, PhD, Toronto, ON (*Abstract Co-Author*) Nothing to Disclose

For information about this presentation, contact:

ur.metser@uhn.ca

PURPOSE

To determine the impact of positron-emission tomography/ computed tomography (PET/CT) on the staging, management and outcomes of patients with apparent limited-stage (LS) Hodgkin's lymphoma (HL) or aggressive non-Hodgkin's lymphoma (aNHL) being treated with curative intent.

METHOD AND MATERIALS

This single arm, prospective multicenter registry included patients with apparent LS HL or aNHL based on clinical data and CT, or with equivocal CT findings for advanced stage, being considered for curative-intent therapy. Pre-PET/CT treatment plan was compared to actual treatment received. Outcomes at 1 year post first line therapy included survival and second-line therapy initiation. These were compared to a historical control pool staged with CT alone. Administrative data sources were used to obtain and control for baseline characteristics using propensity score matching and regression adjustment. Outcomes were assessed using adjusted Cox proportional hazards regression and propensity score matching.

RESULTS

PET/CT upstaged 58/330 (17.6%) patients with HL and 92/520 (17.7%) patients with aNHL. Change in planned mode of therapy was seen in 119/266 (44.7%) patients with HL and 131/334 (39.2%) with aNHL (p<0.00001 for both). There was a lower 1-year mortality for aNHL patients with LS on PET compared to those with LS on CT (for propensity score matched cohort: HR, 0.34; 95% CI: 0.15, 0.74; p=0.0072). For patients with HL, no significant difference was found in survival or second-line therapy initiation at 1 year.

CONCLUSION

PET/CT upstaged >17% of patients with presumed LS aggressive lymphoma to advanced stage and planned management was altered in a significant proportion of patients. Patients with confirmed LS aNHL after PET/CT treated with curative intent had significantly better survival compared to the cohort of LS determined by CT.

CLINICAL RELEVANCE/APPLICATION

1. PET has a significant impact on the management of patients with HL and aNHL. 2. Patients with presumed limited stage aNHL on PET/CT treated with curative intent had a significantly better survival at one year compared to patients with presumed limited stage as determined by CT. 3. These results support the recent recommendation of the International Conference on Malignant Lymphoma in Lugano for the utilization of PET in the staging of patients with aggressive lymphoma.

SSK14-03 Altered Liver FDG Uptake in Lymphoma Patients with Chemotherapy Associated Hepatic Steatosis on PET/CT

Wednesday, Nov. 28 10:50AM - 11:00AM Room: S505AB

Participants

Yi W. Mo, Guangzhou, China (*Presenter*) Nothing to Disclose Yuan Hua Li, MD, Guangzhou, China (*Abstract Co-Author*) Nothing to Disclose Wen Long, Guangzhou, China (*Abstract Co-Author*) Nothing to Disclose Lu Li, Guangzhou, China (*Abstract Co-Author*) Nothing to Disclose Xu Zhang, Guangzhou, China (*Abstract Co-Author*) Nothing to Disclose Dan Lei, Guangzhou, China (*Abstract Co-Author*) Nothing to Disclose Wei Fan, Guangzhou, China (*Abstract Co-Author*) Nothing to Disclose

For information about this presentation, contact:

moyw@sysucc.org.cn

PURPOSE

To evaluate the prevalence of hepatic steatosis in lymphoma patients after chemotherapy; to reveal whether lymphoma patient with chemotherapy associated hepatic steatosis (CAHS) will change liver FDG uptake on PET/CT, compared to their baseline and to further study the relation between liver FDG uptake and severity of fatty liver.

METHOD AND MATERIALS

88 of 1647 lymphoma patients had been diagnosed fatty liver during or after chemotherapy from December 1, 2014, to June 30, 2017. 176 FDG PET/CT scans of the 88 lymphoma patients were reviewed retrospectively. These 88 lymphoma patients all had a normal liver before chemotherapy and then got hepatic steatosis after chemotherapy. Each patient had performed two PET/CT scans: baseline and post-chemotherapy. Paired t test was used to compare BMI, blood glucose (BG), liver SUVmax (SUVmax-I), liver average SUV (SUVave-I), liver SULmax (SULmax-I), aorta SUVmax (SUVmax-a), aorta average SUV (SUVave-a) and aorta SULmax (SULmax-a) between baseline and post-chemotherapy. CAHS was divided into three groups: mild-grade, moderate-grade, and severe-grade. The relationship within or between groups was assessed.

RESULTS

The prevalence of CAHS in lymphoma patients of our hospital was about 88/1647 (5.3%). After chemotherapy, 28 of 88 (31.8%) patients had increased liver SUVs, whereas 60 of 88 (68.2%) patients showed decreased liver SUVs. There were significant differences of mean liver SUVs between baseline and CAHS (baseline versus CAHS; SUVmax-I, 2.84 \pm 0.57 vs 2.57 \pm 0.64, P<0.00; SUVave-I, 2.17 \pm 0.43 vs 1.95 \pm 0.51, P=0.001; SULmax-I, 2.24 \pm 0.40 vs 2.0 \pm 0.41, P<0.001). BG had a slight decrease after chemotherapy (baseline versus CAHS; 5.5 \pm 1.2 vs 5.2 \pm 1.0, P=0.01). No difference was identified when the mean aorta SUVs and BMI for baseline were compared with those for CAHS (P>0.05). The patients with severe-grade of CAHS had significant lower liver SUV values, compared to those with mild-grade (P<0.05). And BMI showed no difference among the three groups of CAHS.

CONCLUSION

Increase of liver FDG uptake coexists with decrease. The severer the fatty liver is, the more likely the liver FDG uptake declines. The altered liver SUV due to CAHS might affect the response assessment and prognostic evaluation for lymphoma patients.

CLINICAL RELEVANCE/APPLICATION

(dealing with 18F-FDG PET/CT)'18F-FDG PET/CT is a powerful imaging technique and has become the standard for staging and response assessment of FDG-avid lymphomas'.

SSK14-04 Is Dual-Time Point 18F-FDG PET/CT Valuable for Differentiating Goitrous Hashimoto's Thyroiditis from Primary Thyroid Lymphoma?

Wednesday, Nov. 28 11:00AM - 11:10AM Room: S505AB

Participants

Kunihiro Nakada, Sapporo, Japan (*Presenter*) Nothing to Disclose Naoya Hattori, MD, PhD, Sapporo, Japan (*Abstract Co-Author*) Nothing to Disclose Hiroki Sugie, MD, Sapporo, Japan (*Abstract Co-Author*) Nothing to Disclose Noriyoshi Katoh, MD,PhD, Sapporo, Japan (*Abstract Co-Author*) Nothing to Disclose Masayuki Sakurai, Sapporo, Japan (*Abstract Co-Author*) Nothing to Disclose

For information about this presentation, contact:

metnakada@yahoo.co.jp

PURPOSE

Goitrous Hashimoto's thyroiditis (HT) occasionally shows diffusely increased F-18 fluorodeoxyglucose (FDG) uptake in the thyroid that it mimics primary thyroid lymphoma (PTL) on FDG-PET/CT i,ages. The aim of the study was to determine whether delayed imaging of FDG-PET/CT was valuable in differentiating PTL from HT.

METHOD AND MATERIALS

53 patients with HT, who were suspected of PTL due to enlarging goiter, underwent dual-time-point (60 \pm 5min and 120 \pm 10min after FDG injection) PET/CT scan using FDG combined with neck ultrasound (US) and US-guided core needle biopsy. Specimen of core needle biopsy was subjected to immunohistochemical staining (CD20,CD3,CD79a,Ki-67, etc.) along with H-E staining. Rearrangement of igH was also analyzed by PCR. In addition to visual assessment based on 5-point scale from The Lugano classification, the maximum standardized uptake value for the thyroid at the early image (SUV-E) and that at the delayed image (SUV-D) for the thyroid were determined. In addition, SUV increment (Δ SUV) was calculated by subtracting SUV-E from SUV-D. Those parameters were compared between patients with PTL and those with HT.

RESULTS

Pathological diagnosis was PTL in 36 (MALT lymphoma 31, DLBCL 5) and was HT in 17. 11 patients with PTL was excluded from analysis because they had either nodular FDG uptake in the thyroid or abnormal uptake in extrathyroidal area. The remaining 25 patients with PTL and all patients with HT showed diffusely increased thyroid FDG uptake on both the early and the delayed PET/CT images. There was no statistically significant difference between PTL and HT in 5-PS (early 4.4 vs. 4.2. delayed 4.1 vs. 4.0) as well as SUV-E and SUV-D (9.02 vs. 7.51, 8.28 vs. 6.54). 7 of 25 patients (28%) with PTL had plus values of Δ SUV while none but one (6%) with HT had plus value of Δ SUV. When plus value of Δ SUV was considered as a sign for PTL, PPV, NPV, and accuracy for PTL was 88%. 47%, and 55%, respectively.

CONCLUSION

Neither visual nor semi-quantitative analysis of dual tome-point FDG-PET/CT was helpful in differentiation HT from PTL among enlarging goiter. Needle biopsy may be the best strategy in differential diagnosis of HT with enlarging goiter.

CLINICAL RELEVANCE/APPLICATION

Addition of delayed imaging does not improve diagnostic performance of FDG-PET/CT in diffusely increased thyroidal uptake in enlarging goiter.

SSK14-05 Utility of Integrated 18F-FDG PET/MRI for Response Assessment of Isolated Limp Perfusion in Patients with Soft-Tissue Sarcomas

Wednesday, Nov. 28 11:10AM - 11:20AM Room: S505AB

Participants

Johannes Grueneisen, Essen, Germany (*Presenter*) Nothing to Disclose Ahmet Oernek, Essen, Germany (*Abstract Co-Author*) Nothing to Disclose Wolfgang Fendler, Munich, Germany (*Abstract Co-Author*) Nothing to Disclose Axel Wetter, Essen, Germany (*Abstract Co-Author*) Nothing to Disclose Nika Guberina, MD, Essen, Germany (*Abstract Co-Author*) Nothing to Disclose Lars Podleska, MD, Essen, Germany (*Abstract Co-Author*) Nothing to Disclose Ken Herrmann, Essen, Germany (*Abstract Co-Author*) Nothing to Disclose Biosciences; Consultant, Ipsen SA; Consultant, Siemens AG; Research Grant, Advanced Accelerator Applications SA; Research

Grant, Ipsen SA Lale Umutlu, MD, Essen, Germany (Abstract Co-Author) Consultant, Bayer AG

PURPOSE

To evaluate the diagnostic potential of simultaneously obtained PET- and MR-datasets for therapy response assessment of isolated limp perfusion with TNF-alpha and melphalan (TM-ILP) in patients with soft-tissue sarcomas.

METHOD AND MATERIALS

A total of 32 patients with histopathological confirmation of a soft-tissue sarcoma were prospectively enrolled for an integrated 18F-FDG PET/MRI examination before (1st scan) and after (2nd scan) neoadjuvant TM-ILP. In each examination morphological (tumor size) and metabolic (SUVmax, SUVpeak) parameters of the tumors were determined. Two readers analysed the datasets and assessed treatment response based on RECIST 1.1 and PERCIST criteria. Results from subsequent tumor resection served as reference standard and therapy response was determined based on the tumour regression grading scale of Salzer-Kuntschik.

RESULTS

Based on the reference standard, a total of 25 patients were classified as partial responder (PR) and 7 patients as stable disease (SD). Calculated mean values of the maximum tumor diameter, SUVmax and SUVpeak in patients with stable disease amounted to 62.4 ± 42.4 mm, 11.1 ± 7.9 and 9.1 ± 6.2 before and 59.5 ± 50.3 mm, 8.4 ± 5.3 and 6.7 ± 5.1 after treatment. The respective values in the responder group were 78.1 ± 65.6 mm, 11.9 ± 7.4 and 9.6 ± 6.1 , before and 71.1 ± 65.9 mm, 5.1 ± 3.1 and 3.9 ± 2.4 after treatment. Based on RECIST criteria, 25 patients were classified as SD and 6 patients as PR, whereas 1 patient showed progressive disease (PD). PERCIST criteria categorized 11 patients as SD, 20 patients as PR and one patient as PD. In accordance with PERCIST, a significantly higher number of patients (n = 23, 71.9%) could be correctly categorized as SD/PR, when compared to RECIST (n = 9, 28.1%; p < 0.005).

CONCLUSION

Our results demonstrate the significant discrepancy in morphological and metabolic response and underline the diagnostic superiority of 18F-FDG PET data over MRI for response assessment of neoadjuvant ILP in sarcoma patients.

CLINICAL RELEVANCE/APPLICATION

18F-FDG PET/MRI might enable more accurate therapy response assessment of isolated limp perfusion in patients with soft-tissue sarcomas when compared to MRI alone.

SSK14-06 Evaluation of 18F-FDG-PET/CT for Response Assessment in Patients with Advanced Melanoma Treated with Immune Checkpoint Inhibitors

Wednesday, Nov. 28 11:20AM - 11:30AM Room: S505AB

Participants

Dominique Fuser, MD, Saint Louis, MO (*Abstract Co-Author*) Nothing to Disclose Leonel Hernandez-Aya, St. Louis, MO (*Abstract Co-Author*) Nothing to Disclose Joyce C. Mhlanga, MBBCh, Portland, OR (*Abstract Co-Author*) Nothing to Disclose John Crandall, St. Louis, MO (*Abstract Co-Author*) Nothing to Disclose Lauren Ash, St. Louis, MO (*Abstract Co-Author*) Nothing to Disclose Richard L. Wahl, MD, Saint Louis, MO (*Abstract Co-Author*) Research Consultant, Nihon Medi-Physics Co, Ltd; Contract, WhiteRabbit.AI Inc Delphine L. Chen, MD, Saint Louis, MO (*Presenter*) Nothing to Disclose

For information about this presentation, contact:

fuserdominique@gmail.com

PURPOSE

Treatment with immune checkpoint inhibitors (ICI) have improved outcomes for patients with advanced melanoma. The aim of this retrospective study was to characterize the findings on 18F-FDG PET/CT that predict response in these patients.

METHOD AND MATERIALS

Ninety-seven patients with advanced melanoma treated with ICI were identified, with 70 having baseline (PET0) and interim 18F-FDG PET/CT studies (PET1, median 84 and range 19 to 181 days after cycle 1). Of these, 34 were treated with ipilimumab alone (N=17) or combined with nivolumab (N=17, analyzed together as the ipi cohort) and 36 with pembrolizumab (pembro cohort) alone. AutoPERCIST software was used to determine the SULpeak and SUVmax of the hottest lesion on each scan. Clinical assessment at the last office visit determined responders (R- partial response, stable, or no disease) and nonresponders (NR- progression) at a median 9.5 (range 0 to 61) months after PET1 for the ipi cohort and 5.5 months (range 0 to 20) for the pembro cohort. Repeated measures analysis of variance (SigmaPlot 12.5, Systat Software, Inc.) determined differences between PET0 and PET1 metrics among response categories by cohort. The Mann-Whitney rank sum test assessed for differences in the % change in each metric between response categories.

RESULTS

Thirteen R and 21 NR were identified in the ipi cohort and 26 R and 10 NR in the pembro cohort. Within the ipi R cohort, SULpeak (PET0 6.8 ± 5.1 , PET1 1.2 ± 2.4 , p=0.002) and SUVmax (PET0 9.9 ± 7.0 , PET1 2.0 ± 4.3 , p=0.002), were significantly different. The PET1 SULpeak (13 ± 12 , p=0.007) and SUVmax (19 ± 19 , p=0.006) of the NR was also significantly different from the R PET1 values. For the pembro NR cohort, SULpeak (PET0 6.2 ± 5.3 , PET1 10 ± 8.7 , p=0.017) and SUVmax (PET0 9.5 ± 9.1 , PET1 14 ± 12 , p=0.033) were significantly different, and the pembro R PET1 SULpeak (2.0 ± 3.6 , p<0.001) and SUVmax (3.4 ± 6.0 , p<0.001) were also significantly different from NR PET1 values. The % change in all metrics was significantly different between R and NR in both treatment cohorts.

CONCLUSION

Changes in the SULpeak and SUVmax of the hottest lesion on interim 18F-FDG PET/CT studies may be useful in predicting responders to ICI.

CLINICAL RELEVANCE/APPLICATION

Higher SULpeak and SUVmax values and lower % decrease in these parameters on interim 18F-FDG PET/CT scans during ICI treatment are predictors of poor treatment response.

Honored Educators

Presenters or authors on this event have been recognized as RSNA Honored Educators for participating in multiple qualifying educational activities. Honored Educators are invested in furthering the profession of radiology by delivering high-quality educational content in their field of study. Learn how you can become an honored educator by visiting the website at: https://www.rsna.org/Honored-Educator-Award/ Richard L. Wahl, MD - 2013 Honored Educator

SSK14-07 Is 18F-FDG PET/MR Including DWI an Alternative to Sentinel Lymph Node Biopsy in Initial N-Staging in Patients with Malignant Melanoma?

Wednesday, Nov. 28 11:30AM - 11:40AM Room: S505AB

Participants

Benedikt M. Schaarschmidt, MD, Essen, Germany (*Presenter*) Stockholder, Bayer AG; Stockholder, General Electric Company; Stockholder, Siemens AG; Stockholder, Teva Pharmaceutical Industries Ltd Johannes Grueneisen, Essen, Germany (*Abstract Co-Author*) Nothing to Disclose Lino Sawicki, MD, Dusseldorf, Germany (*Abstract Co-Author*) Nothing to Disclose Gerald Antoch, MD, Duesseldorf, Germany (*Abstract Co-Author*) Nothing to Disclose Thorsten D. Poeppel, Essen, Germany (*Abstract Co-Author*) Nothing to Disclose

PURPOSE

To compare 18F-fluordesoxyglucose positron emission tomography / computed tomography (18F-FDG PET/CT), 18F-FDG PET / magnetic resonance (18F-FDG PET/MR) as well as 18F-FDG PET/MR and diffusion weighted imaging (DWI) with sentinel lymph node biopsy (SLNB) in initial lymph node staging in patients with malignant melanoma.

METHOD AND MATERIALS

In this retrospective study, 52 patients with malignant melanoma (female: n=30, male: n=22, mean age 50.5y) that underwent 18F-FDG PET/CT and consecutive 18F-FDG PET/MRI including DWI prior to lymphoscintigraphy with single photon emission computed tomography / CT (SPECT/CT) and consecutive SLNB were included. By two readers, the status of the sentinel lymph nodes detected by SPECT/CT (benign/malignant) was assessed on 18F-FDG PET/CT, 18F-FDG PET/MR as well as 18F-FDG PET/MR and DWI images. In all modalities, increased tracer uptake in comparison to the background was considered as a sign of malignancy. In PET/MR, morphological criteria were considered as additional signs of malignancy. In 18F-FDG PET/MR and DWI, all of the aforementioned criteria and diffusion restriction were considered as signs of malignancy. Discrepancies were resolved in a consensus reading. Histopathologic results served as a reference standard to calculate sensitivity, specificity as well as positive (PPV) and negative predictive values (NPV).

RESULTS

In all patients, a total of 87 sentinel lymph nodes were detected by lymphoscintigraphy and SPECT/CT. According to histopathology, lymph nodes were metastatic. We found a sensitivity, specificity, PPV and NPV of 17.7%, 95.6%, 50.0% and 82.3% for PET/CT and of 23.5%, 96.9%, 66.7% and 82.3% for PET/MR. Additional DWI was available in 56 lymph nodes and led to two additional false positive findings, thus decreasing specificity of PET/MR and DWI.

CONCLUSION

Due to its low sensitivity and specificity, 18F-FDG PET/MR cannot be considered an alternative to SLNB in initial N-Staging in patients with malignant melanoma even if additional DWI is performed.

CLINICAL RELEVANCE/APPLICATION

18F-FDG PET/MR is inferior to SLNB in N-Staging in patients with malignant melanoma. Therefore, neither 18F-FDG PET/MR nor 18F-FDG PET/MR and DWI will be able to replace SLNB in clinical routine.

SSK14-08 Prognostic Value of 18F-FDG PET/CT in Intralesional Interleukin-2 Therapy for Cutaneous Metastatic Melanoma

Wednesday, Nov. 28 11:40AM - 11:50AM Room: S505AB

Participants

Rick Wray, MD, Sacramento, CA (*Presenter*) Nothing to Disclose Jason Kao, BS, Sacramento, CA (*Abstract Co-Author*) Nothing to Disclose Sarah Bateni, MD, Sacramento, CA (*Abstract Co-Author*) Nothing to Disclose Emanuel Maverakis, MD, Sacramento, CA (*Abstract Co-Author*) Nothing to Disclose Amanda Kirane, MD, Sacramento, CA (*Abstract Co-Author*) Nothing to Disclose

PURPOSE

Intralesional interleukin-2 (IL-2) therapy is an effective treatment for cutaneous metastatic melanoma even in cases refractory to multiple treatment modalities. 18F-FDG PET/CT is a valuable tool for diagnosis, staging and surveillance of melanoma, but its role in therapy assessment is unclear given the strong local inflammatory response in injected sites. This study investigates the prognostic value of 18F-FDG PET/CT for assessment of intralesional IL-2 in cutaneous metastatic melanoma.

METHOD AND MATERIALS

13 patients (10M/3F, 23 - 96 years) with Stage IIIC/IV cutaneous metastatic melanoma or stage IIB disease not amenable to surgical intervention had a total of 31 PET/CT scans performed at baseline, interim and completion time points while receiving variable injections of intralesional IL-2 (range, 1 - 20; mean 7.8) at variable doses (range 5 - 22 million units; mode 7). PET/CT scans were evaluated using maximum SUV (SUV max) and a 5 point scale (5PS): 1, no uptake; 2, uptake <= mediastinum; 3, uptake > mediastinum <= liver; 4, uptake moderately < liver; 5, uptake markedly > than liver. The 5PS was dichotomized to

negative (score 1, 2, and 3) or positive (score 4 and 5). The Kaplan-Meier (KM) method with log-rank test and Cox-regression analysis were performed.

RESULTS

Of the 31 scans, 17 were positive and 14 were negative. SUV max range, 1.3 -20.6 g/ml. Follow-up range, 8 - 51 months (median 15). Baseline scans with higher SUV max had a significantly lower PFS with hazard ratio (HR) of 1.55 (95% CI 1.001-1.33, p=0.048). KM curves demonstrated a trend of improved OS with lower SUVmax at baseline (p=0.11). Positive scans at completion trended toward lower OS with HR of 2.74, (p=0.48). The progression-free survival (PFS) was worse for positive groups at completion, HR of 12.12 (95%CI 1.22-120.49, p=0.03), with significant separation in KM curves (Log-rank, p=0.008).

CONCLUSION

18F-FDG PET/CT SUV max at baseline and qualitative therapy assessment at completion time points during intralesional IL-2 can predict PFS and show potential to predict OS, with larger sample size, in patients with cutaneous metastatic melanoma.

CLINICAL RELEVANCE/APPLICATION

A baseline PET/CT prior to intralesional IL-2 adds prognostic value. Additionally, using a qualitative therapy assessment method such as the 5PS increases the prognostic value of 18F-FDG PET/CT for therapy response in intralesional IL-2 treatment for cutaneous metastatic melanoma.

SSK14-09 Opportunistic Screening of FDG-PET/CT Reveals Undiagnosed Low Bone Mass in Patients Being Evaluated for Oncology Purposes

Wednesday, Nov. 28 11:50AM - 12:00PM Room: S505AB

Participants

Fernando U. Kay, MD, Dallas, TX (*Presenter*) Nothing to Disclose Edmund Dosnumu, Dallas, TX (*Abstract Co-Author*) Nothing to Disclose Vinh Ho, Dallas, TX (*Abstract Co-Author*) Nothing to Disclose Keenan Brown, Austin, TX (*Abstract Co-Author*) Employee, Mindways Software, Inc Stockholder, Mindways Software, Inc Orhan K. Oz, MD,PhD, Dallas, TX (*Abstract Co-Author*) Nothing to Disclose

For information about this presentation, contact:

fern and o.kay @ut south we stern.ed u

PURPOSE

To assess the prevalence of undetected low bone mineral density (BMD) in a cohort of patients undergoing PET/CT with opportunistic quantitative computed tomography (QCT).

METHOD AND MATERIALS

A retrospective survey was conducted to identify PET/CT studies obtained between Oct/2015 and Jan/2016 in a Biograph 64 scanner (Siemens). CT images were processed with the QCT Pro software (Mindways). A calibration CT scan was obtained in the same PET/CT scanner using the asynchronous Model 4 QCT Phantom. Two radiologists and a trained research technician performed the analyses of trabecular BMD at vertebral bodies L1 and L2. The American College of Radiology (ACR) criteria was used for diagnosing low BMD. Total BMD of femoral necks were measured on DXA-equivalent images (CTXA) of the hips and used to generate FRAX-scores for calculating absolute fracture risks. We obtained clinical data from institutional medical records. Requirement for signed informed consent was waived by the IRB.

RESULTS

Sixty-nine studies were identified, two studies excluded due to severe scoliosis and one excluded due to Schmörl node affecting the analysis. The final cohort comprised 66 subjects (20F/46M, mean age: 53.8, SD: 12.1). Mean coefficient of variation (CV) for trabecular BMD in L1-2 between the 3 readers was 1.2%. Distribution of subjects according to ACR category is shown in Table 1. Thirty-two percent (21/66) of subjects showed low lumbar spine BMD on QCT. Twenty-four percent (5/21) of subjects with low BMD on QCT had a prior DXA scan, all of which showing low BMD. None of the subjects with normal BMD on QCT had a prior DXA scan. Femoral neck BMD was assessed with CTXA in 20 of 66 subjects by one radiologist and the research technician. Mean CV between the readers was 6.1%. Fifteen percent (3/20) of the subjects had at least a 3% risk of hip fracture within 10 years. Only 33.3% (1/3) of these subjects had a prior diagnosis of low BMD.

CONCLUSION

Low BMD was an under recognized condition in our sample. Future analysis will correlate metabolic activity (FDGuptake) with bone mass.

CLINICAL RELEVANCE/APPLICATION

PET/CT provides a unique opportunity to screen patients for occult low BMD by leveraging the quantitative capabilities of CT. Identification of subjects at risk for future osteoporotic fractures may not only improve outcomes, but also decrease downstream costs.



SSK15

Neuroradiology (Stroke Imaging and Intervention)

Wednesday, Nov. 28 10:30AM - 12:00PM Room: E350



AMA PRA Category 1 Credits ™: 1.50 ARRT Category A+ Credit: 1.75

Participants

Bharathidasan Jagadeesan, MD, Minneapolis, MN (*Moderator*) Research Consultant, MicroVention Inc; Research Consultant, Medtronic plc; Research Consultant, CVRx

Salman Qureshi, MBChB, BSc, Sale, United Kingdom (Moderator) Nothing to Disclose

Sub-Events

SSK15-01 Distance to Thrombus in Stroke Due to Large Vessel Middle Cerebral Artery Occlusion

Participants

Daniel Apel, MSc, Munich, Germany (*Abstract Co-Author*) Nothing to Disclose Thomas Huber, MD, Munich, Germany (*Presenter*) Consultant, BrainLAB AG; Consultant, Smart Reporting GmbH Paul Reidler, MD, Munich, Germany (*Abstract Co-Author*) Nothing to Disclose Steffen Tiedt, Munich, Germany (*Abstract Co-Author*) Nothing to Disclose Frank Wollenweber, Munich, Germany (*Abstract Co-Author*) Nothing to Disclose Kolja Thierfelder, Munich, Germany (*Abstract Co-Author*) Nothing to Disclose Wolfgang G. Kunz, MD, Munich, Germany (*Abstract Co-Author*) Grant, Medtronic plc

For information about this presentation, contact:

Daniel.Apel@campus.lmu.de

PURPOSE

Endovascular thrombectomy (EVT) is supported by Level IA evidence for middle cerebral artery (MCA) M1 occlusion stroke, yet more distal occlusions lead to challenges in decision making. In stroke patients with large vessel MCA occlusion, distance to thrombus (DT) can be measured from the carotid T. We determined the value of DT in the context of established clinical and imaging parameters.

METHOD AND MATERIALS

We selected patients with isolated MCA occlusions (M1-M3) and follow-up-confirmed stroke. Two independent, blinded readers evaluated imaging. DT was measured as the distance from the carotid T to the proximal end of the thrombus on coronal CT angiography images. Established clinical and imaging parameters were assessed. Linear and ordinal regression analyses were performed to identify independent associations.

RESULTS

The study population of 162 patients had a median DT of 14.0 mm (interquartile range: 8.0-24.0mm). Dichotomizing the study population by median DT, patients with DT <=14.0 mm showed significantly higher median admission National Institutes of Health Stroke Scale scores (14 vs 9, p<0.001; NIHSS), no significant difference in median final infarction volumes (31 mL vs. 23 mL, p=0.224), but worse median modified Rankin Scale (mRS) scores at discharge (4 vs 3, p=0.004) and 90 days (5 vs 2, p=0.037). Patients with shorter DT had worse median non-contrast Alberta Stroke Program Early CT Scores (8 vs 9, p<0.001; NCCT-ASPECTS) and more frequently underwent EVT. When adjusted for age, sex, admission NIHSS, NCCT-ASPECTS, thrombolysis, EVT and DT, linear regression analyses revealed only significant associations of admission NIHSS (b=0.229, p=0.006) and NCCT-ASPECTS (b=-0.357, p<0.001) with final infarction volumes. In similarly adjusted ordinal regression analyses on clinical outcomes, only admission NIHSS was an independent predictor of discharge mRS (b=0.144, p<0.001) and 90-day mRS (b=0.137, p=0.004).

CONCLUSION

In this comprehensive analysis on the value of DT in acute stroke, DT was outperformed by existing imaging parameters for morphologic outcome prediction and had no independent predictive value for clinical outcomes.

CLINICAL RELEVANCE/APPLICATION

In stroke imaging, DT is a quantifiable occlusion parameter yet carries no independent predictive value. However, DT could be used to standardize selection for randomized EVT trials on M2 occlusions.

SSK15-02 MRI or CT Before Recanalization in Acute Ischemic Stroke: Impact on Clinical Workflow: Results from the THRACE Randomized Controlled Trial

Wednesday, Nov. 28 10:40AM - 10:50AM Room: E350

Corentin Provost, MD, Paris, France (*Presenter*) Nothing to Disclose Marc Soudant, Nancy, France (*Abstract Co-Author*) Nothing to Disclose Laurence Legrand, Paris, France (*Abstract Co-Author*) Nothing to Disclose Wagih Ben Hassen, MD, Paris, France (*Abstract Co-Author*) Nothing to Disclose Yu Xie, Nancy, France (*Abstract Co-Author*) Nothing to Disclose Sebastien Soize, Reims, France (*Abstract Co-Author*) Nothing to Disclose Romain Bourcier, Nantes, France (*Abstract Co-Author*) Nothing to Disclose Joseph Ben Zakoun, Paris, France (*Abstract Co-Author*) Nothing to Disclose Myriam Edjlali, Paris, France (*Abstract Co-Author*) Nothing to Disclose Gregoire Boulouis, MD, MSc, Lille, France (*Abstract Co-Author*) Nothing to Disclose Helene Raoult, MD, Rennes, France (*Abstract Co-Author*) Nothing to Disclose Francis Guillemin Sr, MD, Nancy, France (*Abstract Co-Author*) Nothing to Disclose Gregoire Naggara, MD, Paris, France (*Abstract Co-Author*) Nothing to Disclose Francis Guillemin Sr, France (*Abstract Co-Author*) Nothing to Disclose Grego Francis Guillemin Sr, MD, Nancy, France (*Abstract Co-Author*) Nothing to Disclose Francis Guillemin Sr, MD, Nancy, France (*Abstract Co-Author*) Nothing to Disclose Serge Bracard, Nancy, France (*Abstract Co-Author*) Nothing to Disclose Serge Bracard, Nancy, France (*Abstract Co-Author*) Nothing to Disclose

For information about this presentation, contact:

cyprovost@gmail.com

PURPOSE

To compare clinical workflow and functional outcome in acute ischemic stroke patients screened by Magnetic Resonance Imaging (MRI) or Computed Tomography (CT).

METHOD AND MATERIALS

Data were analyzed from THRACE, a multicenter, randomized, controlled trial that evaluated the efficacy of mechanical thrombectomy in addition to intravenous tissue-plasminogene activator (IV-tPA) in patients with acute ischemic stroke and proximal occlusion. Recruiting centers were free to use their routine MRI or CT stroke protocol before randomization. Brain imaging was performed within 4h of stroke onset. Workflow times were obtained from the trial database and extracted from Digital Imaging and Communications in Medicine (DICOM) metadata. All patients or their legal representative provided written informed consent.

RESULTS

403 patients were included: 300 based on MRI and 103 on CT. Median baseline National Institutes of Health Stroke Scale score was 18 in both groups. Time interval (median, interquartile range) from stroke onset to imaging was similar (MRI: 114 min (89-139); CT: 108 min (88-140); P = .23). MRI scan duration was overall longer (MRI: 13 min (10-16); CT/CT angiography: 9 min (7-12); P < .001), irrespective of the imaging protocol (without perfusion-weighted imaging [MRI: 12 min (10-15); CT: 7 min (2-11); P < .001] or with perfusion-weighted imaging [MRI: 16 min (15-19); CT: 10 min (8-13); P < .001]. Time from stroke onset to IV-tPA (MRI: 150 min (121-179); CT: 150 min (123-180); P = .31) and onset to entry in angiography suite (MRI: 200 min (170-250); CT: 213 min (180-246); P = .57) did not differ between groups. In the endovascular treatment arm, imaging modality of inclusion was not associated with unfavorable outcome (modified Rankin Score scale > 2) in multivariate analysis (MRI: odds ratio 0.72; 95% confidence interval: 0.33 - 1.54; P = .40).

CONCLUSION

In the THRACE trial, use of MRI at the acute phase of ischemic stroke did not delay treatment nor was associated with poorer functional outcome than CT after endovascular treatment.

CLINICAL RELEVANCE/APPLICATION

Efficient workflow allows to use MRI as a screening tool for stroke patients, without delay to treatment nor negative impact on clinical outcome.

SSK15-03 Focal Thinning in Remote Cortical Layers via Degeneration of Connecting Fibers Correlates with Clinical Outcome in Lacunar Infarct Patients

Wednesday, Nov. 28 10:50AM - 11:00AM Room: E350

Awards

Student Travel Stipend Award

Participants

Eyal Lotan, MD, New-York, NY (*Presenter*) Nothing to Disclose Ido Tavor, PhD, Tel-Aviv, Israel (*Abstract Co-Author*) Nothing to Disclose Daniel Barazany, PhD, Tel-Aviv, Israel (*Abstract Co-Author*) Nothing to Disclose Shani Ben-Amitai, Tel-Aviv, Israel (*Abstract Co-Author*) Nothing to Disclose Chen C. Hoffmann, MD, Ramat-Gan, Israel (*Abstract Co-Author*) Nothing to Disclose Galia Tsarfaty, MD, MPH, Ramat Gan, Israel (*Abstract Co-Author*) Nothing to Disclose Yaniv Assaf, Tel-Aviv, Israel (*Abstract Co-Author*) Nothing to Disclose David Tanne, MD, Tel-Aviv, Israel (*Abstract Co-Author*) Nothing to Disclose

PURPOSE

Ischemic infarcts have been observed to exert structural effects distant from the acute lesion itself, in remote, connected cortex. We aimed to extend this knowledge by exploring with in-vivo T1-relaxation 3T-MRI, surface-based cortical thickness analysis and tractography if (i) in patients with chronic lacunar infarct, involving the corticospinal tract, the cortical layers of the connected primary motor cortex are differently affected, and if (ii) these differences correlate with clinical symptomatology.

METHOD AND MATERIALS

Our cohort included patients (n=20) with history of chronic lacunar infarct, involving the posterior limb of the internal capsule or the corona radiata, with residual motor deficit, and healthy controls (n=15). T1-component probability maps, dividing the cortex into 5 laminar Gaussian-classes (noted L1-L5) were calculated, and tractography with lacunar infarcts as the seed areas to reconstruct the corticospinal tracts (CSTs) were performed.

RESULTS

Results demonstrated focal cortical thinning in the connected primary motor cortex (M1) and specifically only in its deepest L5class compared to the non-affected mirrored cortex (P<0.001 and P=0.0001, respectively). There was loss of microstructural integrity of the affected CST connecting the lacunar infarct to the M1 with significantly increased mean diffusivity (MD) and decreased fractional anisotropy (FA) compared to the non-affected hemisphere (P=0.002 and P=0.0002, respectively). Increased MD and decreased FA were associated with focal thinning in M1 and in its deepest L5-class in the affected compared to the nonaffected hemisphere (MD: P=0.07 and P=0.05, respectively; FA: P=0.02 and P=0.005, respectively). No significant difference was found between the laminar thickness pattern of the bilateral M1 or the microstructural integrity of the bilateral CSTs for the healthy subjects. Clinical scores were significantly correlated with microstructural damage of the CST and with thinning of both M1 and its deepest L5-class (P<0.05).

CONCLUSION

Our results support the concept of secondary neurodegeneration of Betz cells in layer V of connected M1, following a lacunar infarct affecting the CST, with a novel finding that the majority of the cortical thinning occurs in the deepest cortex.

CLINICAL RELEVANCE/APPLICATION

The severity of clinical symptoms is significantly correlated with the microstructural damage of the CST and with the connected M1 atrophy pattern.

SSK15-04 Clinical Decision Support Based on Automated Non-Contrast CT Density Measurements in Patients with Acute Ischemic Stroke

Wednesday, Nov. 28 11:00AM - 11:10AM Room: E350

Participants

Paul Reidler, MD, Munich, Germany (*Presenter*) Nothing to Disclose Daniel Puhr-Westerheide, MD, Munich, Germany (*Abstract Co-Author*) Nothing to Disclose Matthias P. Fabritius, MD, Munich, Germany (*Abstract Co-Author*) Nothing to Disclose Lukas Rotkopf, Munich, Germany (*Abstract Co-Author*) Nothing to Disclose Felix Schuler, Munich, Germany (*Abstract Co-Author*) Nothing to Disclose Wolfgang G. Kunz, MD, Munich, Germany (*Abstract Co-Author*) Nothing to Disclose Wolfgang G. Kunz, MD, Munich, Germany (*Abstract Co-Author*) Grant, Medtronic plc Daniel Apel, MSc, Munich, Germany (*Abstract Co-Author*) Nothing to Disclose Nils Daniel Forkert, Hamburg, Germany (*Abstract Co-Author*) Nothing to Disclose Steffen Tiedt, Munich, Germany (*Abstract Co-Author*) Nothing to Disclose Frank Wollenweber, Munich, Germany (*Abstract Co-Author*) Nothing to Disclose Kolja M. Thierfelder, MD,MSc, Rostock, Germany (*Abstract Co-Author*) Nothing to Disclose Andre Kemmling, MD, Luebeck, Germany (*Abstract Co-Author*) Nothing to Disclose

PURPOSE

To examine the clinical value of automated non-contrast CT (NCCT) density measurements in Alberta Stroke Program Early CT Score (ASPECTS) regions to support decision making in acute ischemic stroke.

METHOD AND MATERIALS

From a cohort of 1644 consecutive patients admitted for suspected stroke, we included patients with follow-up-confirmed middle cerebral artery infarction and available NCCT and CT perfusion (CTP) data. ASPECTS region density was assessed using automated software (Figure 1A). Relative Hounsfield units (rHU) were defined as the ratio of ipsilesional by contralesional region density. Extent of ischemic core was measured on CTP maps. Regression coefficients from a linear regression analysis on the association of regional rHU and infarction core volume were used as weighting factors to calculate a composite rHU score of all regions. Receiver operating characteristics (ROC) analyses were performed to test this score's discriminative value regarding time from symptom onset (TFSO) <=4.5h, current CTP trial selection criteria, and subacute stroke complications on follow-up imaging.

RESULTS

In total 121 patients were included. The composite rHU score resulted in significant classification of patients with TFSO<=4.5h (area under the curve [AUC]=0.721, p=0.018). Moreover, the score was able to classify patients who meet CTP selection criteria of ischemic core size <70mL and target mismatch >1.8 (AUC=0.759, p<0.001). The score discriminated between patients with and without subsequent space-occupying edema development (AUC=0.771, p<0.001). ROC curves are shown in Figure 1B. The score could not classify patients by occurrence of hemorrhagic infarction or parenchymal hematoma (both p>0.05).

CONCLUSION

The composite rHU score on NCCT allowed significant classification of patients with thrombolysis-eligible symptom onset times and current CTP imaging criteria for extended time window thrombectomy selection. The score also identified patients with subsequent space-occupying edema development.

CLINICAL RELEVANCE/APPLICATION

Automated NCCT density measurements have the potential to act as observer-independent imaging biomarkers that could support decision making in patients with unknown TFSO or in centers in which CTP is not available.

SSK15-05 Does IV-tPA Induce Thrombus Migration? A Retrospective Study Comparing Bridging Therapy and Thrombectomy Alone

Wednesday, Nov. 28 11:10AM - 11:20AM Room: E350

Participants Clara Cohen, Tours, France (*Presenter*) Nothing to Disclose Kathleen Gaillot, MD, Tours, France (*Abstract Co-Author*) Nothing to Disclose Kevin Janot, Tours, France (*Abstract Co-Author*) Nothing to Disclose Jean Philippe Cottier, MD,PhD, Tours, France (*Abstract Co-Author*) Nothing to Disclose Ana Paula Narata, Tours, France (*Abstract Co-Author*) Nothing to Disclose

For information about this presentation, contact:

clara.cohen.cc@gmail.com

PURPOSE

Thrombus migration (ThrMi) before mechanical thrombectomy (MT) is an epiphenomenon in acute ischemic stroke (AIS) treatment with few available data. The aim of this study is to evaluate ThrMi prior to MT in a bridging protocol (tPA-MT group) and standalone MT (MT group).

METHOD AND MATERIALS

205 consecutive AIS patients treated by MT (tPA and no tPA) were retrospectively analyzed. Distance between vessel origin and beginning of the thrombus on MRI (3D time of flight and/or contrast enhanced magnetic resonance angiography sequences) and digital-substracted-angiography (DSA) were measured in millimeters using a curve tool and the same anatomical parameters. DSA pixels were converted in millimeters by measuring 3 large vessels diameters in MRI and determining the ratio from pixels to millimeters.

RESULTS

129 patients were included in tPA-MT group, with ThrMi in 36.4%, and 76 patients in MT group, with ThrMi in 6.6% (p<0.0001). In tPA-MT group, 27 (20.9%) patients had a moderate migration between 5-10 millimeters, 11 (8.5%) patients had a distal migration of more than 10 millimeters or to another segment and 9 (7%) presented recanalization defined by spontaneous TICI score>=2B. In MT group, 69 (90.8%) patients had no ThrMi, moderate ThrMi in 6.6%, thrombus' extension in 2.6%; no patient presented distal migration or recanalization. The two groups had the same clinical prognosis (bleeding event at 48hours, NIHSS at discharge, mRS and death at 3 months). Number of device passes to reach thrombectomy was 1.40 (\pm 1.39) in tPA-MT group, 1.63 (\pm 1.09) in MT group, p=0.061.

CONCLUSION

IV thrombolysis seems to promote thrombus migration, present in 36.4% of patients in tPA-MT group compared to 6.6% of patients in MT group. This study adds more data concerning IV thrombolysis effects on AIS treatment when MT is also involved.

CLINICAL RELEVANCE/APPLICATION

(dealing with acute ischemic stroke) 'Before performing mechanical thrombectomy, the possibility of a thrombus migration favored by prior thrombolysis is an important data for neurointerventionalists.'

SSK15-06 Public Health and Cost Consequences of Treatment Delays in Endovascular Thrombectomy for Stroke Based on HERMES Collaboration Data

Wednesday, Nov. 28 11:20AM - 11:30AM Room: E350

Awards

Trainee Research Prize - Resident

Participants

Wolfgang G. Kunz, MD, Munich, Germany (Presenter) Grant, Medtronic plc Mohammed A. Almekhlafi, MD, MSc, Calgary, AB (Abstract Co-Author) Grant, Medtronic plc Bijoy Menon, MBBS, MD, Calgary, AB (Abstract Co-Author) Grant, Medtronic plc Jeffrey Saver, MD, Los Angeles, CA (Abstract Co-Author) Grant, Medtronic plc Diederik Dippel, Rotterdam, Netherlands (Abstract Co-Author) Research Grant, Stryker Corporation; Grant, Medtronic plc Mayank Goyal, MD, FRCPC, Calgary, AB (Abstract Co-Author) Grant, Medtronic plc; Consultant, Medtronic plc; Consultant, Stryker Corporation; Consultant, Terumo Corporation; Consultant, Cerenovus Tudor G. Jovin, MD, Pittsburgh, PA (Abstract Co-Author) Grant, Medtronic plc Antoni Davalos, MD, Barcelona, Spain (Abstract Co-Author) Grant, Medtronic plc Serge Bracard, Nancy, France (Abstract Co-Author) Grant, Medtronic plc Francis Guillemin Sr, MD, Nancy, France (Abstract Co-Author) Grant, Medtronic plc Bruce Campbell, Melbourne, Australia (Abstract Co-Author) Grant, Medtronic plc Peter Mitchell, Melbourne, Australia (Abstract Co-Author) Grant, Medtronic plc Phil White, MSc, MD, Newcastle-upon-Tyne, United Kingdom (Abstract Co-Author) Research Consultant, Terumo Corporation; Institutional Research funded, Terumo Corporation; Grant, Medtronic plc Keith Muir, MD, Glasgow, United Kingdom (Abstract Co-Author) Grant, Medtronic plc Scott Brown, PhD, St Louis, MN (Abstract Co-Author) Grant, Medtronic plc Andrew Demchuk, MD, Calgary, AB (Abstract Co-Author) Grant, Medtronic plc Michael D. Hill, MD, Calgary, AB (Abstract Co-Author) Grant, Medtronic plc Charles B. Majoie, MD, PhD, Amsterdam, Netherlands (Abstract Co-Author) Institutional Research Grant, Stryker Corporation

For information about this presentation, contact:

wolfgang.kunz@med.lmu.de

PURPOSE

The benefit that endovascular thrombectomy (EVT) offers to stroke patients with large vessel occlusions is highly time-dependent. Our aim was to determine the lifetime quality of life and cost consequences of delaying EVT administration for patients, the healthcare system, and the society.

METHOD AND MATERIALS

A Markov model estimated lifetime quality-adjusted life years (QALY) of EVT-treated patients and associated costs based on stroke onset to arterial puncture time (model structure in Figure 1). The analysis was performed from a United States perspective with two cost frameworks: 1) healthcare costs and 2) societal costs, which include productivity losses and costs of informal care given by family members. Input parameters were based on best available evidence (Table 1), including patient data from the 7-trial HERMES collaboration (ESCAPE, EXTEND-IA, MR CLEAN, REVASCAT, SWIFT PRIME, PISTE, THRACE; Figure 2). In addition to diminished functional outcomes with later EVT, the model also projects that a proportion of patients becomes EVT-ineligible over time. The lead analysis was conducted for stroke onset at 65 years. Probabilistic sensitivity analysis was performed.

RESULTS

Lifetime QALYs decreased for every hour of time delay until arterial puncture (Figure 3A). Within the first 6 hours of onset, every hour of delay resulted in an average loss of 0.69 QALYs. The healthcare and societal costs of each QALY yielded by EVT increased for every hour of time delay (Figure 3B). Within the first 6 hours of onset, every hour of delay increased the cost of QALYs yielded by EVT by \$5,310/QALY in healthcare costs and by \$7,914/QALY in societal costs. Within the first 3 hours of onset, a treatment delay of 2 hours - the amount typically associated with drip-and-ship compared to mothership care delivery - would result in an average loss of 1.7 QALYs per patient. In addition, this delay would result in an extra of about \$10,000/QALY gained incurred by the healthcare system and \$15,000/QALY gained incurred by the society.

CONCLUSION

Every hour of treatment delay in EVT for stroke reduces a patient's QALYs by almost three-quarters of a year and substantially increases healthcare and societal costs per QALY.

CLINICAL RELEVANCE/APPLICATION

Investments in healthcare policies and procedures to improve the efficiency of pre-hospital triage and in-hospital workflow for earlier treatment of stroke patients are likely highly cost-saving.

SSK15-07 Association Between Wall Characteristics of Atherosclerotic Middle Cerebral Artery with High-Resolution Magnetic Resonance Imaging and Infarction Pattern

Wednesday, Nov. 28 11:30AM - 11:40AM Room: E350

Participants

Yue Zhang, MD, Beijing, China (*Presenter*) Nothing to Disclose Qi Yang, MD, Los Angeles, CA (*Abstract Co-Author*) Nothing to Disclose Miao Zhang, Beijing, China (*Abstract Co-Author*) Nothing to Disclose Qingfeng Ma, Beijing, China (*Abstract Co-Author*) Nothing to Disclose Jie Lu, MD, PhD, Beijing, China (*Abstract Co-Author*) Nothing to Disclose

For information about this presentation, contact:

markweal_image@163.com

PURPOSE

To study the characteristics of atherosclerotic middle cerebral vascular wall by using 3.0 T high-resolution magnetic resonance imaging (HRMRI), explore the association between the characteristics of vascular wall and cerebral infarction, and predict the mechanism of infarction.

METHOD AND MATERIALS

Thirty-two patients with atherosclerotic patients were retrospectively enrolled and intracranial artery HRMRI was peformed. HRMRI protocol included a 3D T1 weighted technique known as inversion-recovery (IR) prepared SPACE. The plaque morphology, distribution, enhancement, stenosis degree and reconstruction index (positive reconstruction) of the middle cerebral artery were analyzed. Characteristics of acute infarct on diffusion weighted imaging (DWI) were categorized according to the number (single or multiple infarcts) and the pattern of cerebral infarcts(cortical,border zone, or perforating artery territory infarcts). The relationship between wall characteristics and infarction patterns was evaluated.

RESULTS

In the Thirty-two patients with acute infarction, twenty-one patients had multiple acute cerebral infarcts and eleven showed single acute cerebral infarcts. Border zone infarcts were the most common (16, 76.2%) among multiple acute infarcts. Eleven single infarcts were subcortical deep penetrating artery infarcts (11,100%). Thirty(93.8%) plaque were eccentric. Seven plaques (63.6%) in penetrating artery infarcts were located at the upper wall among single acute infarcts. Twelve plaques(75.0%) in border zone infarcts were located at the ventral wall among multiple acute infarcts. There was no significant difference in clinical data and laboratory examination of patients with single and multiple infarcts(P>0.05). The percentage of plaques located on the ventral wall, plaques with strong enhancement, pattern of PR reconstruction and degree of stenosis of the lumen in the multiple infarction were all significantly higher than those in the single infarction (P<0.05).

CONCLUSION

The strong enhancement plaque is associated with its vulnerability in the patients with intracranial MCA atherosclerosis. PR or obvious lumen stenosis were associated with artery to artery embolism. HR MRI provides insights into intracranial atherosclerosis, and predicting infarction patterns.

CLINICAL RELEVANCE/APPLICATION

HRMRI can provide insights into intracranial atherosclerosis, and predict infarction patterns.

SSK15-08 Deep Learning Based Quantitative Diagnosis of Ischemic Stroke on CT

Wednesday, Nov. 28 11:40AM - 11:50AM Room: E350

Awards

Student Travel Stipend Award

Participants Peter Chang, MD, San Francisco, CA (*Presenter*) Nothing to Disclose Richelle Roelandt L. Homo, Irvine, CA (*Abstract Co-Author*) Nothing to Disclose Christopher G. Filippi, MD, Grand Isle, VT (*Abstract Co-Author*) Research Consultant, Regeneron Pharmaceuticals, Inc Research Consultant, Syntactx, LLC Daniel S. Chow, MD, Orange, CA (*Abstract Co-Author*) Nothing to Disclose Christopher P. Hess, MD, PhD, Mill Valley, CA (Abstract Co-Author) Nothing to Disclose

For information about this presentation, contact:

pchang077@gmail.com

PURPOSE

To evaluate a deep learning based tool for quantitative and objective CT diagnosis of acute ischemia, benchmarked on a large population with CT/MR correlation.

METHOD AND MATERIALS

After IRB approval, all patients with suspected ischemia in a five-year interval (January 2013 to 2018) receiving a non-contrast head CT followed by MR within 48 hours were identified. For each patient, DWI was co-registered to CT after brain extraction. For all MR exams, regions of reduced diffusion were segmented by a custom deep learning algorithm and confirmed through visual inspection. A hybrid 3D/2D object localization network based on the faster R-CNN architecture was implemented using a feature pyramid backbone (Figure 1A-D). A region proposal network identified potential regions of infarct, and a separate head network quantified the primary CT findings of acute ischemia: gray-matter hypoattenuation and mass effect (Figure 1E-F). Network outputs are represented on a normalized scale from 0 to 1 based on finding severity. After training, population statistics for hypoattenuation and mass effect were used to create a nomogram of stroke risk.

RESULTS

A total of 4,382 patients with short-interval CT/MR were identified, 831 of which had DWI-confirmed ischemia, yielding 326,394 images across 8,764 exams for analysis. As quantified by the neural network, degree of hypoattenuation (0.68 vs. 0.21; p < 0.001) and mass effect (0.59 vs. 0.11; p < 0.001) was more severe in patients with ischemia vs. controls. A nomogram based on deep learning quantification of these findings predicted ischemia with AUC, accuracy, sensitivity, specificity, PPV and NPV of 0.823, 0.815, 0.729, 0.835, 0.508 and 0.929 respectively. By varying the thresholds for diagnosis, algorithm sensitivity/PPV for ischemia detection ranged between 0.91/0.14 to 0.33/0.89.

CONCLUSION

A deep learning tool is presented for completely objective assessment of hypoattenuation and mass effect in the setting of acute ischemia. A deep learning based nomogram of stroke risk as a function of these two variables yields a powerful and flexible tool for ischemia detection. Arguably, prediction errors from this entirely objective approach may primarily be attributed to limitations in CT technology.

CLINICAL RELEVANCE/APPLICATION

A deep learning enabled nomogram of stroke risk based on quantitative image findings yields a powerful and flexible tool for completely objective diagnosis of acute ischemia on CT.

SSK15-09 The Significant Difference of Plaque Characteristics in Middle Cerebral Artery between Ischemic Stroke Patients with Positive and Negative Penumbra Area: A Study of Intracranial Vessel Wall Imaging

Wednesday, Nov. 28 11:50AM - 12:00PM Room: E350

Participants

Song Liu, Tianjin, China (*Presenter*) Nothing to Disclose Ruowei Tang, Tianjin, China (*Abstract Co-Author*) Nothing to Disclose Weiwei Xie, Tianjin, China (*Abstract Co-Author*) Nothing to Disclose Shengting Chai, Tianjin, China (*Abstract Co-Author*) Nothing to Disclose Shuang Xia, MD, Tianjin, China (*Abstract Co-Author*) Nothing to Disclose

For information about this presentation, contact:

tjliusong0128@163.com

PURPOSE

The purpose of this study was to investigate the difference of plaque characteristics in middle cerebral artery assessed by Highresolution Vessel Wall Imaging (HRVWI) between patients with positive and negative penumbra area , and to identify the risk factors affected penumbra volumes.

METHOD AND MATERIALS

Sixty-seven patients (44 males; age, 59.33 ± 10.57 years) with severe stenosis in the unilateral middle cerebral artery were enrolled. Patients were assigned to two groups: Positive Penumbra (PP group) and Negative Penumbra (NP group). MRI data were collected on a 3T Siemens MAGNETOM Trio Tim, including High-Resolution T1-SPACE, and DSC-PWI. The plaque characteristics in MCA was measured in the T1-SPACE, and all the cross-sectional image slices of a stenotic MCA on T1-SPACE were analyzed, and plaque characteristics was calculated as follows: outer vessel wall area (OWA), lumen area (LA) and wall area (WA). Other extended parameters include normalized wall index (NWI), arterial remodeling, plaque length, configuration and enhanced behavior. The Mismatich volume was acquired using the RApid processing of PerfusIon and Diffusion (RAPID) software. Independent sample t test, Kruskal-Wallis H test and Chi-square test was performed in the difference of plaque characteristics in PP group and NP group. The relationship between the plaque characteristics and penumbra volume was calculated with Spearman's correlation or Kruskal-Wallis H test.

RESULTS

The results showed that eccentric plaques were observed 10 (37.04%) in PP group and 32 (80.00%) in NP group, which means significant difference was found between two groups (χ 2=12.72, p<0.001). There were no significant difference between two groups in WA (p=0.761), NWI (p=0.572), expansive remodeling (p=0.427), diffused plaque distribution (p=0.370) and enhancement (p=0.262). Patients with diffused plaque length had larger penumbra volume comparing with the focal one in PP group (Z=-2.754, p=0.005).

CONCLUSION

Plaque with eccentric distribution in MCA is a remarkable sign to predict the presence of penumbra. Based on the patients with positive penumbra, plaque with diffused plaque length hint the larger penumbra volume, which could be rescued by timely treatment.

CLINICAL RELEVANCE/APPLICATION

Plaque with eccentric distribution in MCA can predict the presence of penumbra area, and plaque with diffused length hint the larger penumbra volume, which could be rescued by timely treatment.



SSK16

Neuroradiology (Functional Neuroimaging)

Wednesday, Nov. 28 10:30AM - 12:00PM Room: E351



AMA PRA Category 1 Credits ™: 1.50 ARRT Category A+ Credit: 1.75

FDA Discussions may include off-label uses.

Participants

Greg Zaharchuk, MD, PhD, Stanford, CA (*Moderator*) Research Grant, General Electric Company; Stockholder, Subtle Medical; Shinji Naganawa, MD, Nagoya, Japan (*Moderator*) Nothing to Disclose

Sub-Events

SSK16-01 Functional Segmentation of Resting-State Brain Networks by Using Mutual Connectivity Analysis with Non-Metric Community Detection Methods

Participants

Adora M. D'Souza, MSc, Rochester, NY (*Abstract Co-Author*) Nothing to Disclose Anas Z. Abidin, MS, Rochester, NY (*Presenter*) Nothing to Disclose Axel Wismueller, MD, PhD, Rochester, NY (*Abstract Co-Author*) Nothing to Disclose

PURPOSE

To explore functional network identification using Mutual Connectivity Analysis (MCA) on resting-state functional MRI (rsfMRI) using non-metric community detection (CD) methods.

METHOD AND MATERIALS

We present the MCA computational framework to construct an affinity matrix characterizing mutual nonlinear predictability between each pair of voxel time-series in rsfMRI. The goal of MCA is to establish the degree of dynamic coupling between two time-series based on their ability to locally predict each other. Here, generalized radial basis function neural networks are used as non-linear time-series predictors. To recover their community structure, the resulting affinity matrices are subject to non-metric clustering using different CD approaches, namely the Louvain Method (LM), Agglomerative Clustering (AC) and Topographic Mapping of Proximity (TMP). We test our method on rsfMRI (1.5T, TR=0.5s, TE=40ms, 512 acquisitions) of four subjects, in which images from a finger tapping motor stimulation task were acquired as well. After pre-processing with motion correction and time-series detrending, recovered networks were compared with the localization aid from the motor stimulation task by computing the Dice Coefficient (DC) and the Area Under receiver operator characteristic Curve (AUC) in order to quantitatively evaluate the agreement between actual and recovered motor cortex network segmentations.

RESULTS

All three non-metric CD methods were able to recover bilateral motor cortices and the supplementary motor area with DC values of 0.57 (LM), 0.50 (AC), and 0.60 (TMP), respectively. High segmentation quality was confirmed by AUC values of 0.79 (LM), 0.86 (AC) and 0.85 (TMP), where statistically significant differences between the CD methods in their ability to perform functional motor cortex segmentation were not observed at a p<0.05 level.

CONCLUSION

Our results suggest that affinity matrices obtained using the model-free non-linear MCA approach can capture valuable information regarding the underlying brain network functional connectivity structure from rsfMRI data. Using this information, non-metric CD techniques can successfully perform functional segmentation of connected brain regions.

CLINICAL RELEVANCE/APPLICATION

Functional connectivity network identification at a rsfMRI voxel scale resolution using MCA can contribute to developing imaging biomarkers for diagnosis and therapy management of neurologic diseases.

SSK16-02 Functional Connectivity Measured By Functional Resting State MRI in Glioma Patients: Association with WHO Grade and Clinical Parameters

Wednesday, Nov. 28 10:40AM - 10:50AM Room: E351

Participants

Sophia Stoecklein, MD, Munich, Germany (*Abstract Co-Author*) Nothing to Disclose Veit Stoecklein, Munich, Germany (*Abstract Co-Author*) Nothing to Disclose Franziska Schoppe, MD, Munich, Germany (*Abstract Co-Author*) Nothing to Disclose Niklas Thon, Munich, Germany (*Abstract Co-Author*) Friedrich-Wilhelm Kreth, Munich, Germany (*Abstract Co-Author*) Birgit B. Ertl-Wagner, MD, Toronto, ON (*Abstract Co-Author*) Spouse, Stockholder, Siemens AG; ; Joerg-Christian Tonn, Munich, Germany (*Abstract Co-Author*) Nothing to Disclose Hesheng Liu, Charlestown, MA (*Abstract Co-Author*) Nothing to Disclose

Thomas Huber, MD, Munich, Germany (Presenter) Consultant, BrainLAB AG; Consultant, Smart Reporting GmbH

For information about this presentation, contact:

sophia.stoecklein@med.uni-muenchen.de

PURPOSE

Gliomas diffusely infiltrate the brain. We hypothesized that this could lead to disturbances in functional connectivity. We developed an individual measure for altered functional connectivity and aimed to establish association of this novel marker with aggressiveness of the tumor as indicated by WHO grade and IDH mutation status as well as clinical parameters, specifically neurocognitive performance and overall survival.

METHOD AND MATERIALS

34 patients with de-novo gliomas were prospectively included and resting state functional MRI (rsfMRI) data as well as 3D anatomical reference data were obtained at 3 Tesla. Neurocognition was tested using the Montreal Cognitive Assessment test. We developed a standardized score to evaluate the abnormality of functional connectivity by comparing each patient's data to data obtained from 1000 healthy individuals. Abnormality was quantified at each voxel of the brain, resulting in an individual measure for abnormality (abnormality score, AS). Statistical analysis was conducted adjusting for tumor volume, age and signal-to-noise ratio of the rsfMRI data.

RESULTS

13 patients were diagnosed with WHO grade II tumors, 6 with WHO grade III and 15 with WHO grade IV. 17 patients had IDH1/2mutations. We found that AS is significantly associated with WHO grade: patients with grade III and IV displayed higher AI than patients with grade II (p<0.01), with the strongest association seen in the non-lesional hemisphere (p=0.0294). Additionally, AS was significantly increased in patients with IDH-wildtype gliomas, again with strongest effects in the non-lesional hemisphere (p=0.013). Neurocognitive performance and AI was significantly correlated, this was most pronounced in the lesional hemisphere. 6 patients died within the follow-up period. We observed a trend towards association of overall survival with AI.

CONCLUSION

AS is a novel method to investigate functional connectivity on an individual basis. Especially in the non-lesional hemisphere, AI is significantly associated with WHO grade and IDH mutation status and correlates significantly with neurocognitive performance. Individual AS maps show the potential of this technique to gain information beyond conventional structural MRI.

CLINICAL RELEVANCE/APPLICATION

AI can detect widespread disturbances in functional connectivity which reach beyond the tumor visible on conventional MRI. AI might therefore be used to assess disease burden in glioma patients.

SSK16-03 Tumor-Induced Functional Reorganization of Language and Voxel-Based Morphometry of the Cortex: A Possible Window on Stemcells-Driven Plasticity

Wednesday, Nov. 28 10:50AM - 11:00AM Room: E351

Awards

Trainee Research Prize - Resident

Participants

Luca Pasquini, MD, Rome, Italy (*Presenter*) Nothing to Disclose Mehrnaz Jenabi, MS, Great Neck, NY (*Abstract Co-Author*) Nothing to Disclose Madeleine Gene, New York, NY (*Abstract Co-Author*) Nothing to Disclose Kyung K. Peck, PhD, New York, NY (*Abstract Co-Author*) Nothing to Disclose Alessandro Bozzao, Rome, Italy (*Abstract Co-Author*) Nothing to Disclose Andrei I. Holodny, MD, New York, NY (*Abstract Co-Author*) Nothing to Disclose

PURPOSE

Cortical thickening has been related to the process of learning in humans. fMRI has previously shown functional plasticity in patients with brain tumors. In this study, we retrospectively investigated the correlation between cortical morphometry and fMRI language activation in the non-dominant hemisphere of right-handed patients who have left brain tumors invading the Broca's area. Our aim was to test if tumor-induced language reorganization displayed a corresponding cortical thickening

METHOD AND MATERIALS

Patients with the following criteria were included: right handed, left tumor invading Broca's area, available fMRI, no previous irradiation, no surgery-related artifacts. The patients were divided in 2 groups by language dominance, assessed by hemispheric and Broca's laterality index. In a second analysis, we divided the patients with atypical language dominance by the results of intraoperative direct cortical stimulation of the inferior frontal gyrus. Structural data was analyzed to measure cortical thickness (or volume) with the FSL-VBM (Voxel-Based Morphometry) tool and compared between the groups

RESULTS

26 patients were included (13 left dominant, 13 atypical language dominant). VBM demonstrated a significant thickening of the right Broca's area analogue in patients with atypical language (p<0.05). The patients with neurosurgically-proven reorganization showed increased volume of the right hippocampal gray matter (p<0.05) and cortical gray matter in SMA and right insula (p<0.05)

CONCLUSION

Increased right-side Broca's area activation showed a corresponding cortical thickening. In the adult brain, structural plasticity is driven by the stem-cell located in the periventricular zone and the hippocampal perigranular zone (PGZ). The increased PGZ volume in patients with language reorganization to the right side may suggest that the compensatory increase in fMRI activation and the increased volume of the right language-related cortical structures is mediated by stem cells originating in the PGZ

CLINICAL RELEVANCE/APPLICATION

Our results address the mechanism of tumor-induced language reorganization, which may partly compensate the language deficits, by displaying cortical thickening of the right language areas and PGZ

SSK16-04 Cerebral Perfusion is Altered by Real-Time fMRI Neurofeedback-Directed Self-Regulation of the Primary Auditory Cortex

Wednesday, Nov. 28 11:00AM - 11:10AM Room: E351

Participants

Matthew S. Sherwood, PhD, Dayton, OH (*Presenter*) Research Consultant, DCS Corporation Emily E. Diller, MS, Indianapolis, IN (*Abstract Co-Author*) Nothing to Disclose Subhashini Ganapathy, PhD, Dayton, OH (*Abstract Co-Author*) Nothing to Disclose Kevin B. Bennett, PhD, Dayton, OH (*Abstract Co-Author*) Nothing to Disclose Jeremy Nelson, PhD, Lackland AFB, TX (*Abstract Co-Author*) Nothing to Disclose Jason G. Parker, PhD, Indianapolis, IN (*Abstract Co-Author*) Nothing to Disclose

For information about this presentation, contact:

matt.sherwood@wright.edu

PURPOSE

To determine the effects of real-time functional magnetic resonance imaging neurofeedback training (fMRI-NFT) of the primary auditory cortex (A1) on quantified cerebral perfusion (i.e., cerebral blood flow, CBF).

METHOD AND MATERIALS

18 healthy volunteers with hearing loss <40dB underwent 5 experimental sessions conducted using a 3T MRI. The first session started with a baseline measure of resting CBF using a 3D pseudo-continuous arterial spin labeling sequence. Next, fMRI-NFT was carried out by first implementing a single run of a simple auditory task with blocks of white noise stimulation with no auditory stimulation. Then, 2 runs of neurofeedback were completed where subjects were asked to relax and lower the displayed A1 activity in the presence of continuous white noise. The second, third, and fourth sessions only contained fMRI-NFT. On the fifth session, a final measure of CBF followed fMRI-NFT. A control group consisting of 8 subjects performed the same procedures except sham neurofeedback was yoked from the experimental group. The average deactivation in the target ROI was extracted from each fMRI-NFT run as a representative measure of A1 self-regulation performance. CBF maps were registered to a reference space. Permutation test model. The CBF maps were registered to a reference space. Permutation test ing compared the changes in CBF between groups on a voxel-wise basis using 1,000,000 permutations. The permutation test results were cluster-corrected for multiple comparisons.

RESULTS

A repeated-measures ANOVA revealed significant main effects of group (p = 0.029) and training (p = 0.0175) on A1 self-regulation performance. Those subjects most successful reportedly adopted mindfulness tasks associated with directed attention. The permutation analysis identified several regions with greater increased CBF in the experimental group including the left temporal lobe, bilateral parietal lobe, and bilateral frontal gyrus.

CONCLUSION

For the first time, changes in resting CBF have been observed following fMRI-NFT. CBF is coupled with metabolic activity and, thus, fMRI-NFT is likely altering resting metabolic rates which could be important in the treatment neurologic disorders such as chronic tinnitus.

CLINICAL RELEVANCE/APPLICATION

Our study indicates that fMRI neurofeedback may provide an innovative approach to augment resting metabolic activity which can be altered in neurologic disorders.

SSK16-05 Investigation of Functional Networks Changes Using Degree Centrality in Heavy Smokers

```
Wednesday, Nov. 28 11:10AM - 11:20AM Room: E351
```

Participants

Ke Xu, Zhengzhou, China (*Presenter*) Nothing to Disclose Yong Zhang, DO, Zhengzhou, China (*Abstract Co-Author*) Nothing to Disclose Jingliang Cheng, Zhengzhou, China (*Abstract Co-Author*) Nothing to Disclose

For information about this presentation, contact:

1043381896@qq.com

PURPOSE

To investigate the value of degree centrality (DC), a novel resting-state fMRI parameter, in voxel-wise whole-brain functional networks analysis in heavy smokers and mild smokers as compared with that in non-smokers.

METHOD AND MATERIALS

20 heavy smokers, 12 mild smokers, and 70 non-smokers served as normal controls were recruited, aged 20 to 55 years old, with an average (36.8 ± 2.5) years old. Their cognitive functions were evaluated by the fagerstrom test for nicotine dependence(FTND) and other clinical scales. The resting-state BOLD-fMRI datawere acquired and preprocessed. Analysis of DC map changes between the two smoking groups and the control group were performed by two sample t test. (threshold at P<0.05).

RESULTS

Compared with the control group, heavy smokers showed significantly reduced DC value in cerebrum, frontal lobe, pons, left posterior cingulate and left brainstem, increased DC value was observed in fusiform gyrus and temporal lobe. In mild smokers,

significantly reduced DC value was found in right superior occipital gyrus, left superior temporal gyrus and right angular gyrus.

CONCLUSION

Changes of DC value occurred in some region of brain in the two smoking groups when compared with the control group. It was indicated that DC, as a novel resting-state fMRI parameter in the voxel-wise whole-brain functional networks, might be an appealing alternative approach for further study on pathologic and neuropsychological states of heavy smokers.

CLINICAL RELEVANCE/APPLICATION

Changes of DC value occurred in some region of brain in the two smoking groups when compared with the control group. It was indicated that DC, as a novel resting-state fMRI parameter in the voxel-wise whole-brain functional networks, might be an appealing alternative approach for further study on pathologic and neuropsychological states of heavy smokers.

SSK16-06 Identification of Eloquent Cortex for Presurgical Planning Using Independent Component Analysis of Resting-State fMRI

Wednesday, Nov. 28 11:20AM - 11:30AM Room: E351

Participants

Gaurang V. Shah, MD, Ann Arbor, MI (*Presenter*) Nothing to Disclose Scott Peltier, Ann Arbor, MI (*Abstract Co-Author*) Nothing to Disclose

PURPOSE

In this study, presurgical patients with brain tumors were imaged. Task activation and resting-state ICA maps for motor and language networks were generated for all subjects and compared for spatial overlap.

METHOD AND MATERIALS

Subjects: 28 subjects undergoing presurgical planning were included in this study (18M/10F; 53 (±15) years old; heterogeneous pathologies, grade IV glioblastoma most common).MRI Acquisition: Task and resting-state fMRI scans were collected using a 3T Philips Ingenia MR scanner. Resting-state EPI parameters: TR/TE/FA = 2s/28ms/90, 64x64 matrix, 3.75x3.75x3.5 mm, 39 slices, 300 timepoints. Resting-state data were collected with eyes closed on all subjects. A single finger-tapping motor task and a verb generation task were acquired for functional activation localization in the motor and language networks, respectively.Data analysis: Motor and language task activation maps were generated using DynaSuite Neuro software (InVivo Diagnostic Imaging), thresholded at 0.05 significance. Resting-state network maps were generated using FastICA. For each subject, the ICA maps with highest spatial correlation with the task activation maps with the resting state networks was calculated. The Dice coefficient of spatial similarity was also calculated.

RESULTS

Testing state maps show good definition of the motor network, in agreement with the task activation maps; the second ICA component in some subjects added additional motor network information. The calculated motor task activation overlap with the resting state network was high across all subjects (0.73 ± 0.14), but the Dice coefficient was low (0.29 ± 0.14), indicating the resting-state networks contain the majority of task activation, but also extend farther spatially. The resting-state language ICA network has a high spatial overlap with the verb task activation (0.83 ± 0.17).

CONCLUSION

Th resulting resting-state maps compared well to task activation maps, with high percent of spatial overlap, without requiring an external task, with both motor and language networks identified from a single resting-state scan.

CLINICAL RELEVANCE/APPLICATION

This work examines identification of eloquent cortex using network identification in resting-state fMRI, which may complement and extend current clinical practice of using task fMRI.

SSK16-07 fMRI Guided Personalization of Cortical Parcellation Maps

Wednesday, Nov. 28 11:30AM - 11:40AM Room: E351

Participants

Mehmet S. Onay, BSC, Istanbul, Turkey (*Abstract Co-Author*) Nothing to Disclose Umut Kucukaslan, BSC, Istanbul, Turkey (*Abstract Co-Author*) Nothing to Disclose Cigdem Ulasoglu Yildiz, PhD, Istanbul, Turkey (*Abstract Co-Author*) Nothing to Disclose Burak Acar, PhD, Istanbul, Turkey (*Presenter*) Nothing to Disclose

For information about this presentation, contact:

acarbu@boun.edu.tr

PURPOSE

To personalize the 3D cortical parcellation of T1w MRI volumes to increase intra-parcel functional homogeneity by means of coregistered fMRI guidance.

METHOD AND MATERIALS

Inspired by the Demons Algorithm (Med. Image Anal., 2(3), pp 243-260,1998), we propose an iterative 3D deformation of the cortical parcellation map of a given subject, constrained to the cortex, to maximize the pairwise intra-parcel correlation coefficients (CCs) of fMRI BOLD signals (B). The co-registered T1w MRI, fMRI and (148 parcel, P) Destrieux cortical parcellation map are the inputs. The iterations are driven by a vector-field, F(rij), normal to boundary (rij) of Pi and Pj, and zero elsewhere. F is computed according to a local cost that takes into account the change in intra-parcel functional homogeneity and parcel volume change (ΔV). The former uses the CCs between the local signal, B(rij), and the parcel representative signals (Bi, Bj) defined as the inparcel B that is closest to the left principal singular vector of the matrix composed of parcel's B's. The latter is added with a

multiplicative factor λ . We used FreeSurfer and FSL for all co-registration and parcellation steps. We tested the algorithm on 5 normal subjects for λ =0 and 0.25, by measuring the mean of pairwise CCs between in-parcel B's and the mean B per parcel, before and after the algorithm, for each subject. Statistical significance is assessed with paired t-test of CCs per parcel per subject and mean values over subjects is reported. The mean of subject-wise minimum and maximum parcel volumes (Vmin, Vmax) are reported together with the percentage of parcels with ΔV >20%.

RESULTS

The initial mean intra-parcel CC of 0.43±0.04 was increased to 0.52±0.04 (0.51±0.04) with mean p-value 1.21e-5 (4.50e-5) for λ =0 (0.25). The mean [Vmin/Vmax] (mm3) was changed from [282.8/15747.1] to [592.7/10467.9] ([582.5/11136.8]) with 64% (57%) of parcels having Δ V>20% for λ =0 (0.25).

CONCLUSION

The proposed functionally homogeneizing personalization of cortical parcellations showed a statistically significant improvement in intra-parcel correlations accompanied by a decrease in parcel volume variation. Volume constraint with λ =0.25 does not affect the final intra-parcel CCs while limiting the volume change.

CLINICAL RELEVANCE/APPLICATION

fMRI guided personalization of 3D cortical parcellation maps significantly improves intra-parcel functional homogeneity, and can potentially improve brain network models.

SSK16-08 Sex Differences in Resting-State Cerebral Activity Alterations in Internet Gaming Disorder

Wednesday, Nov. 28 11:40AM - 11:50AM Room: E351

Participants

Yawen Sun, Shanghai, China (*Presenter*) Nothing to Disclose Xu Han, MD, Shanghai, China (*Abstract Co-Author*) Nothing to Disclose Yao Wang, Shanghai, China (*Abstract Co-Author*) Nothing to Disclose Weina Ding, Shanghai, China (*Abstract Co-Author*) Nothing to Disclose Yan Zhou, PhD, Shanghai, China (*Abstract Co-Author*) Nothing to Disclose Jianrong Xu, Shanghai, China (*Abstract Co-Author*) Nothing to Disclose

For information about this presentation, contact:

cjs1119@hotmail.com

PURPOSE

Although evidence has shown that the prevalence rates of Internet gaming disorder (IGD) differ between males and females, no study has examined whether such sex differences extend to brain function. This study aimed to explore the sex differences in resting-state cerebral activity alterations in IGD.

METHOD AND MATERIALS

Thirty male participants with IGD (IGDm), 23 female participants with IGD (IGDf), and 30 male and 22 female age-matched healthy controls (HC) underwent resting-state functional MRI. Maps of the amplitude of low-frequency fluctuation (ALFF) and functional connectivity (FC) were constructed. A two-factor ANCOVA model was constructed using SPM8, with sex (Male, Female) and diagnosis (IGD, HC) as the between-subject factors. When interaction effects occurred, post hoc pair-wise comparisons were performed using two-sample t-tests within the interaction masks. We used the Barratt Impulsiveness Scale-11 (BIS-11) to assess the behavioural inhibition function of the IGD participants. The correlations of the psychological scores with the ALFF and FC values were assessed using partial correlation analyses.

RESULTS

The ALFF values in the orbital part of left superior frontal gyrus (SFG) significantly decreased specifically in IGDm, which were negatively correlated with BIS-11 scores. IGDm also demonstrated lower connectivity between the orbital part of the left SFG and the posterior cingulate cortex, the right angular gyrus, and the right dorsolateral prefrontal cortex than HCm. Furthermore, IGDm had lower seed connectivity between the orbital part of the left SFG and the PCC than ICDf.

CONCLUSION

Our findings suggest that sex-specific regional- and network-level alterations exist in IGD, and the altered ALFF values in the SFG represent a clinically relevant biomarker for the behavioural inhibition function of IGDm.

CLINICAL RELEVANCE/APPLICATION

These neuroimaging findings can provide a comprehensive understanding of the neural basis of the sex-specific alterations in IGD.



SSK17

Physics (MR: Applications)

Wednesday, Nov. 28 10:30AM - 12:00PM Room: E353B



AMA PRA Category 1 Credits ™: 1.50 ARRT Category A+ Credit: 1.75

FDA Discussions may include off-label uses.

Participants

R. Jason Stafford, PhD, Houston, TX (*Moderator*) Nothing to Disclose Gregory S. Karczmar, PhD, Chicago, IL (*Moderator*) Nothing to Disclose Geoffrey D. Clarke, PhD, San Antonio, TX (*Moderator*) Nothing to Disclose

Sub-Events

SSK17-01 Quantitative Evaluation of Semimembranosus and Vastus Medialis in Knee Osteoarthritis by IDEAL

Participants Binamra Gurung, MBBS,MD, Tianjin, China (*Abstract Co-Author*) Nothing to Disclose Fei Fu, Tianjin, China (*Abstract Co-Author*) Nothing to Disclose Anwei He, Tianjin, China (*Presenter*) Nothing to Disclose

For information about this presentation, contact:

bnumra@gmail.com

PURPOSE

Iterative decomposition of water and fat with echo symmetry and least-square estimation (IDEAL) imaging has shown potential in assessment of degenerative changes in muscle. The purpose of this research was to evaluate changes in vastus medialis (VM) and semimembranosus (SM) .

METHOD AND MATERIALS

Eighty-one individuals were enrolled for measurement of water and fat IDEAL values in SM and VM. All of whom were divided into Group A consisting of 33 participants with no knee related symptoms, and Group B with 48 participants who had degenerative changes in their knees. IDEAL values of water and fat along with the area of the respective muscle were measured. Each measurement was taken in two different axial sections, the first was measured in the level of the superior border of the patella and second, in the level immediately after the superior border of patella. Independent T test was used to analyse the means of the IDEAL values (p value <0.05)

RESULTS

The IDEAL values for water and fat in VM and SM were greater in Group B with superiority in fat. Means of fat in VM of Group A was 121.56±41.92 and of Group B was 195.92±78.73. Likewise, means of fat in SM of Group A and B were 140.48±43.66 and 222.92±79.7, respectively. The area of VM in Group A and B appeared to have a significant difference rather than SM. Both VM and SM showed significant differences in fat of Group B. (p value=0.00)

CONCLUSION

Water and fat IDEAL values were found to be higher in degeneration group for both muscles with obvious increment in fat. Significant change in the area of VM was observed in degeneration group.

CLINICAL RELEVANCE/APPLICATION

IDEAL can be considered as a useful quantitative method for evaluation of fatty degeneration with severity in knee osteoarthritis.

SSK17-02 Manganese Dioxide-Based Nanoparticles for MR Imaging and Photothermal Anti-Cancer Therapy

Wednesday, Nov. 28 10:40AM - 10:50AM Room: E353B

Participants

Xiaoxuan Zhou, BS,MD, Hangzhou, China (*Presenter*) Nothing to Disclose Bin Xiao II, BS,PhD, Hangzhou, China (*Abstract Co-Author*) Nothing to Disclose Yuxin Han, PhD, Hangzhou, China (*Abstract Co-Author*) Nothing to Disclose Hongjie Hu, MD, Hangzhou, China (*Abstract Co-Author*) Nothing to Disclose Jianbin Tang, Hangzhou, China (*Abstract Co-Author*) Nothing to Disclose Youqing Shen, Hangzhou, China (*Abstract Co-Author*) Nothing to Disclose

For information about this presentation, contact:

misaki20@163.com

PURPOSE

Facile synthesis a manganese dioxide (MnO2)-based MRI contrast agent and in vivo evaluation of its photothermal breast cancer therapy.

METHOD AND MATERIALS

Bovine serum albumin (BSA)-MnO2-melanin-like-polymernanoparticle (BMD NP) was obtained via KMnO4-initiated in situ dopaminepolymerization induced self-assembly in the presence of BSA, and its size and r1 relaxivity were carefully measured. Mice injected with 4T1 breast cancer for MR imaging were randomly assigned into two groups; BMD NP and control group (DTPA-Gd). Images were acquired before injection and at 30, 60, 90, and 120 min post injection and then signal-to-noise ratio (SNRpost/SNRpre) at the tumor ring were quantitatively calculated. Mice bearing same tumors were randomized into the following four groups; BMD NP with/without photothermal therapy, PBS with/without photothermal therapy as control groups. The tumor sizes were measured and calculated every other day. All animal studies were performed in accordance with the guidelines established by the Institute for Experimental Animals of Zhejiang University.

RESULTS

BMD NP with a diameter of 60 nm and a high r1 relaxivity of 38.14 mM-1 s-1, which was incredibly 9 times higher than those of clinically used (Gd-DTPA). In vivo an obviously SNRpost/SNRpre at the tumor margin showed 1.57 times that of DTPA-Gd at 1h post injection, which provided detailed imaging features for precise diagnosis differentiation. The mice group treated both nanoparticle and irradiation exhibited excellent therapeutic efficacy in comparison the other three groups. The mice injected with BMD NP and irradiated by laser showed complete ablation without recurrence in 20 days, and the tumor-free period up to 60 days.

CONCLUSION

The BMD NP having excellent MRI contrasting capability and PTT efficacy plus its facile synthesis was a very promising theranostic agent for MRI-mediated photothermal anti-cancer therapy.

CLINICAL RELEVANCE/APPLICATION

The BMD NP exhibits MRI contrasting capability and photothermal anti-cancer therapy efficacy, which creates a novel theranostic methodology in evaluation and therapy of breast cancer.

SSK17-03 T1 Mapping for Myocardial Iron Overload in Thalassemia Major (TM) Patients: Time to Replace T2*

Wednesday, Nov. 28 10:50AM - 11:00AM Room: E353B

Participants

Aamish Kazi, MD, Mumbai, India (*Abstract Co-Author*) Nothing to Disclose Bhavin G. Jankharia, MD, Mumbai, India (*Abstract Co-Author*) Nothing to Disclose Nidhi M. Doshi, MBBS, MD, Mumbai, India (*Presenter*) Nothing to Disclose

For information about this presentation, contact:

bhavin@jankharia.com

kazi.aamish@gmail.com

CONCLUSION

T1 is possibly a better biomarker than T2, WB T2* and BB T2* to assess cardiac iron load at 3T.

Background

T2* at 1.5T is a clinically accepted biomarker for assessing cardiac siderosis. Cardiac T2* quantification at 3T is challenging due to increased artifacts & T2* shortening. Studies have shown that there is a linear relationship of T1 & T2 to T2* at 1.5 T & 3T indicating that T1 & T2 are potential alternative biomarkers. However, studies haven't explored the efficiency of these biomarkers in categorizing the severity of cardiac siderosis. In this study, we have explored the performance of T1,T2,white blood (WB) T2* & black blood (BB) T2* in categorizing in-vivo cardiac iron content at 3T.

Evaluation

Myocardial T1,T2, WB T2* & BB T2* maps of 103 patients with TM (age 20.5 \pm 13.5 years, 46 females),obtained at 3T MRI scanner (Ingenia, Philips, Netherlands), were retrospectively analysed. The quantitative imaging protocol included ECG gated single breath-hold Modified Look-Locker Inversion recovery sequence for native T1, Double Inversion Recovery (DIR) prepared multi-echo gradient echo BB T2*, DIR prepared GraSE for T2 & multi-echo gradient echo WB T2*. The values were measured by manually selecting ROIs on cardiac septum in a single mid ventricular short axis slice. Patients were categorized based on severity of cardiac siderosis as per WB T2* equivalent values at 1.5T as follows: Normal: > 20 ms, Mild:12 ms - 20 ms, Moderate: 8 ms - 12 ms & Severe: < 8 ms. Tukey test results for significant difference in mean values for Normal, Mild, Moderate & Severe patient groups was performed for each of the four sequences. A p-value of 0.01 was set as significant.

Discussion

Results indicate T1 to be the best biomarker among T1,T2,WB T2* & BB T2* in categorizing the severity of cardiac siderosis at 3T. Studies have shown that there is a linear relationship between T1, T2, WB T2* & BB T2* at 1.5T & 3T. This study shows that T1,T2,WB T2* and BB T2* linearly correlate with each other, confirming that T1 & T2 are potential alternative biomarkers to T2* on 3T. It demonstrates the effectiveness of each of these biomarkers in categorizing the disease severity, of which T1 shows better sensitivity than the others.

SSK17-04 Accurate Bound Water T1 Measurement Using 3D adiabatic Inversion Recovery Ultrashort Echo Time (3D IR-UTE) Imaging with Complete Suppression of Pore Water in Cortical Bone Accurate T1 Measurement of Bound Water in Cortical Bone Using 3D Adiabatic I

Wednesday, Nov. 28 11:00AM - 11:10AM Room: E353B

Yajun Ma, San Diego, CA (*Abstract Co-Author*) Nothing to Disclose Wei Zhao, La Jolla, CA (*Abstract Co-Author*) Nothing to Disclose Saeed Jerban, PhD, San Diego, CA (*Abstract Co-Author*) Nothing to Disclose Hyungseok Jang, La Jolla, CA (*Abstract Co-Author*) Nothing to Disclose Graeme M. Bydder, MBChB, San Diego, CA (*Abstract Co-Author*) Nothing to Disclose Jiang Du, PhD, San Diego, CA (*Abstract Co-Author*) Nothing to Disclose

For information about this presentation, contact:

guotan369@hotmail.com

PURPOSE

To accurately measure the bound water T1 of cortical bone ex vivo and in vivo using 3D IR-UTE imaging on a clinical 3T scanner.

METHOD AND MATERIALS

Six human tibia bone specimens (43 to 91 years) and the tibial mid-shaft of five male volunteers (26 to 73 years) were studied. A 3D adiabatic IR-UTE sequence with different TRs and inversion times (TI) was used to accurately calculate the nulling point of pore water in cortical bone at each TR. For the specimens 6 TRs (150, 200, 250, 300, 400, 500ms) were chosen with 7 TIs at each TR to cover the likely nulling points of pore water. For the volunteer study f4 TRs (150, 200, 300, 400ms) were chosen with 5 TIs at each TR. Each IR-UTE acquisition was performed with dual echoes (TE=32µs/2.5ms), flip angle=20°, FOV=8-10cm, slice thickness=4-6mm, reconstruction matrix=128×128, number of slices=10. The equation S=S0[1+(Q-1)×e^(-TI/T1)-Q×e^(-TI/T1)]/(1-Q×cosθ×e^(-TI/T1)) was used to calculate the nulling point of pore water. The specimens and volunteers were then scanned at different TRs using the IR-UTE with the calculated TI for nulling point at each TR. The bound water T1 of cortical bone was calculated from the different TR/TI combinations. The experiments were performed on a 3T MRI system using a 30ml solenoid coil and a 1.5 inch surface coil respectively.

RESULTS

The calculated TIs for nulling were 60.2±3.4ms, 76.3±3.3ms, 91.1±3.5ms, 104.3±3.4ms, 128.5±5.0ms and 148.7±6.5ms for TRs from 150 to 500ms in the specimen group. The mean bound water T1 of the bone specimens was 104.5±6.7ms. For the volunteers the nulling point TIs were 64.2±8.8ms, 81±10.3ms, 121.2±25.2ms and 148.8±28.1ms for TRs from 150 to 400ms respectively. The mean bound water T1 of the volunteer tibias was 98±8.8ms. The figure shows pure bound water and nulled pore water images with excellent inversion recovery fitting (for the pore water nulling time) and bound water T1 fitting in a specimen and a volunteer.

CONCLUSION

Our technique allows accurate determination of bound water T1 by completely nulling pore water signals in cortical bone and the use of variable TR/TI combinations. Measurement of bound water T1 without contamination from pore water has not previously been possible.

CLINICAL RELEVANCE/APPLICATION

Accurate measurement of bound water T1 provides a new biomarker for the assessment of cortical bone integrity and may assist with water fraction mapping and MT modeling in the study of bone diseases such as osteoporosis.

SSK17-05 MRI "Pharmacokinetics" of Gd Deposition: Quantitative Analysis of Serial Monthly Administration of Triple? Dose Gadopentetate Dimeglumine in 26 Multiple Sclerosis Patients Involving 13 Consecutive Monthly Triple-Doses

Wednesday, Nov. 28 11:10AM - 11:20AM Room: E353B

Participants

Reshma Munbodh, PHD, Farmington, CT (*Presenter*) Research support, Guerbet SA John J. Debevits IV, MD, Farmington, CT (*Abstract Co-Author*) Nothing to Disclose Lihong Wang, Farmington, CT (*Abstract Co-Author*) Institutional Grant, Quberbet Devin Bageac, Farmington, CT (*Abstract Co-Author*) Research funded, Guerbet SA David S. Karimeddini, MD, Farmington, CT (*Abstract Co-Author*) Institutional Grant, Guerbet SA Stuart D. Cook, MD, Newark, NJ (*Abstract Co-Author*) Nothing to Disclose Robert T. Naismith, St. Louis, MO (*Abstract Co-Author*) Consultant, Alkermes plc Consultant, Bayer AG Consultant, Biogen Idec Inc Consultant, Merck KGaA Consultant, F. Hoffmann-La Roche Ltd Consultant, sanofi-aventis Group Consultant, Mallinckrodt plc Consultant, Novartis AG Consultant, Pfizer Inc Paul A. DiCamillo, MD, PhD, Cleveland, OH (*Abstract Co-Author*) Nothing to Disclose Suhayl Dhib-Jalbut, New Brunswick, NJ (*Abstract Co-Author*) Institutional Grant, Guerbet SA PurPOSE

Studies on gadolinium (Gd) deposition and retention in the brain are limited by the lack of systematic administration of Gd inherent to most retrospective studies. Our purpose was to examine subjects who had been enrolled in a prospective trial for monitoring response to MS treatment (Wolansky L et. al. ACTRIMS 2006, Chicago) and received consecutive monthly triple-doses of gadopentetate dimeglumine.

METHOD AND MATERIALS

The cohort consisted of 26 patients who received 13 consecutive monthly triple doses (0.3 mmol/kg) of gadopentetate dimeglumine. 'Plain-T1' MR images were obtained at each monthly visit and studied for potential deposition from the prior month's Gd administration. Subjects were imaged with T1-weighted, proton-density (PD) and T2-weighted MRI at 14 time points (M1, M2 to M14). Gd deposition and retention were studied by evaluating intensity changes over time in the dentate nucleus, pulvinar, putamen, pallidum, caudate and corpus callosum. For each patient, these were manually segmented on the PD and T2 images at M14 and automatically registered to the T1 image at M14 as were the 13 preceding T1 images. Intensities in the sub-cortical structures on the bias-corrected, registered T1 images were then normalized to the mean intensity of the CC using the segmented structures as a mask. Longitudinal trends in Gd deposition and retention over time were evaluated using a Walds Wolfowitz runs test on the median of the normalized intensities over all patients. We also examined the intensity of the corpus callosum normalized

with respect to cerebrospinal fluid (CSF).

RESULTS

The dentate nucleus, caudate and pallidum showed an increasing trend (p < 0.05) in normalized intensity with respect to the corpus callosum over the 14 months (0.0055/month, 0.0022/month and 0.0023/month) indicating Gd deposition and retention in these structures with time. Intensity changes in the corpus callosum relative to CSF were not significant.

CONCLUSION

These findings demonstrate the rate of Gd deposition and retention in the brain after triple-dose administration of gadopentetate dimeglumine, monthly, for over a year.

CLINICAL RELEVANCE/APPLICATION

Though not linked with symptoms, Gd deposition in the brain has caused safety concerns. This pharmacokinetic study provides further scientific insight into the rate of MRI detectable deposition.

SSK17-06 The Effect of DCE-MRI Scanning Parameters on Parenchymal Enhancement of the Breast

Wednesday, Nov. 28 11:20AM - 11:30AM Room: E353B

Participants

Bas H. van der Velden, MSc, Utrecht, Netherlands (*Presenter*) Nothing to Disclose Michael J. van Rijssel, MSc, Utrecht, Netherlands (*Abstract Co-Author*) Nothing to Disclose Erik Verburg, Utrecht, Netherlands (*Abstract Co-Author*) Nothing to Disclose Hui Shan M. Chan, MSc, BA, Utrecht, Netherlands (*Abstract Co-Author*) Nothing to Disclose Claudette E. Loo, MD, Amsterdam, Netherlands (*Abstract Co-Author*) Nothing to Disclose Wouter B. Veldhuis, MD, PhD, Utrecht, Netherlands (*Abstract Co-Author*) Nothing to Disclose Carla H. van Gils, PhD, Utrecht, Netherlands (*Abstract Co-Author*) Software support, Volpara Health Technologies Limited Marielle E. Philippens, Utrecht, Netherlands (*Abstract Co-Author*) Nothing to Disclose Kenneth G. Gilhuijs, PhD, Amsterdam, Netherlands (*Abstract Co-Author*) Nothing to Disclose

For information about this presentation, contact:

bvelden2@umcutrecht.nl

PURPOSE

Background parenchymal enhancement (BPE) on breast DCE-MRI is increasingly used in cancer diagnosis, prognosis, and risk assessment. However, BPE, in particular quantitative measures, may be dependent on scanner and protocol, complicating pooling of results across studies. The purpose of this retrospective study was to explore the effect of differences in MRI protocol on parenchymal enhancement of the breast.

METHOD AND MATERIALS

We focused on contralateral parenchymal enhancement (CPE, Radiology 276.3(2015):675-685): CPE is the mean of the top-10% relative late enhancement in the parenchyma without lesions and has been associated with long-term survival. We performed simulations and tested these in four patient cohorts: the effect of flip angle (FA) and repetition time (TR) on CPE was simulated (Haacke, MRM 58.3(2007):463-472), and the effect of voxel size and slice thickness (resulting in differences in partial volume effect) was assessed by subsampling 50 scans from two databases (1.5T and 3T). Verification in clinical cohorts was done by comparing CPE distributions in four MRI cohorts: - cohort 1: 415 early breast cancer patients, 1.5T, FA=20°, TR=8.1ms, voxelsize=1.35x1.35x1.35mm - cohort 2: 100 advanced breast cancer patients, 3T, FA=20°, TR=8.1ms, voxelsize=1.21x1.21x1.69mm - cohort 3: 77 advanced breast cancer patients, 3T, FA=10°, TR=4.4ms, voxelsize=1.1x1.1x1.2mm - cohort 4: 150 women without breast cancer, 3T, FA=10°, TR=3.8ms, voxelsize=0.9x0.9x0.9mm

RESULTS

Analysis 1: Larger FA led to higher CPE, e.g. FA=15° at 1.5T yields CPE of 0.47 versus 0.23 at FA=5°. This was comparable at 3T. The opposite was observed for TR: larger TR yielded lower CPE. Analysis 2: Larger voxel size led to a decrease in CPE. Analysis 3: the distributions of CPE were not significantly different between the four cohorts (P=.496, KruskalWallis test) independent of scanner differences. Although FA and TR varied between datasets, the ratio between FA and TR was comparable.

CONCLUSION

We simulated the effect of MRI-protocol parameters on contralateral parenchymal enhancement in breast DCE-MRI. Although effects were present, implications for different cohorts appear to be limited when the ratio between flip angle and repetition time is comparable. This was confirmed by MRI scans of four different cohorts.

CLINICAL RELEVANCE/APPLICATION

Differences in MRI-protocol parameters should be taken into account when pooling parenchymal enhancement across studies.

SSK17-07 Acceleration of MR Imaging of Spine Using Compressed-SENSE: A Comparison with Existing Standard of Care Clinical Acquisition Methods

Wednesday, Nov. 28 11:30AM - 11:40AM Room: E353B

Participants

Harsh Mahajan, MD, MBBS, New Delhi, India (*Abstract Co-Author*) Nothing to Disclose Vidur Mahajan, MBBS, New Delhi, India (*Abstract Co-Author*) Nothing to Disclose Vasanthakumar Venugopal, MD, New Delhi, India (*Abstract Co-Author*) Nothing to Disclose Sriram Rajan, MD, New Delhi, India (*Presenter*) Nothing to Disclose Shoma M. Sharma SR, MD, New Delhi, India (*Abstract Co-Author*) Nothing to Disclose Murali Murugavel, PhD, New Delhi, India (*Abstract Co-Author*) Nothing to Disclose Rupsa Bhattacharjee, MENG, Gurgaon, India (*Abstract Co-Author*) Nothing to Disclose Indrajit Saha, PhD, Gurgaon, India (Abstract Co-Author) Employee, Koninklijke Philips NV

For information about this presentation, contact:

vidur@mahajanimaging.com

PURPOSE

To objectively evaluate the impact of Compressed-SENSE (CSENSE), a novel acquisition technique that combines compressed sensing with parallel imaging (or SENSE), on acquisition time and image quality in MR imaging of the spine.

METHOD AND MATERIALS

Current standard of care clinical axial T1 and T2-weighted acquisitions of the cervical and lumbo-sacral spine were modified to obtain higher acceleration with CSENSE (CSENSE factor 1.3999). Twenty-six patients were scanned both, with and without CSENSE, on a 3.0 T wide-bore MRI (Ingenia, Philips Healthcare). The images were anonymised and shared with three specialist MRI radiologists blinded to the acquisition type. Both sets of images were rated on a scale of 1 to 5 for image quality and delineation of specific structures including vertebral bodies, lateral recess, neural foramina, facet joints, cauda equina, nerve roots, spinal cord and paraspinal muscles. Disc abnormalities, foraminal stenosis, nerve root compression and facet joint degeneration were also rated. Dicom metadata was analysed to assess scan time acceleration (ratio of original time to CSENSE time).

RESULTS

Interrater agreement on image quality was compared between the Normal and CSENSE scans via a multivariate non-parametric Hotelling's T2 test. There was no statistically significant difference between Normal and CSENSE scans in the 12 measures evaluated by each radiologist (alpha < 0.001 level). Further, the mean percentage observed agreement between Normal and CSENSE scans for all three measures across the radiologists was 93%. The average time acceleration achieved using CSENSE on axial T1 was 1.41 and on axial T2 was 1.36 and the average time saved was 58 seconds (29%) and 50 seconds (26%) respectively.

CONCLUSION

There is no difference in image quality between current standard of care and CSENSE-based T1 and T2 axial MRI scans of the spine. Compressed-SENSE in the spine can reliably replace current axial T1 and T2 acquisitions without loss in image quality and with significant reduction in scan time.

CLINICAL RELEVANCE/APPLICATION

The potential for CSENSE to accelerate MRI acquisition without hampering image quality will increase patient throughput and patient compliance in MR scanning.

SSK17-08 Daily Qualitative and Quantitative Assessment of Magnetic Resonance Fingerprinting Using the American College of Radiology and Alzheimer's Disease Neuroimaging Initiative Phantoms

Wednesday, Nov. 28 11:40AM - 11:50AM Room: E353B

Participants

Sairam Geethanath, PhD, New York, NY (*Abstract Co-Author*) Nothing to Disclose Sachin Jambawalikar, PhD, New York, NY (*Abstract Co-Author*) Nothing to Disclose Rami Vanguri, PhD, New York, NY (*Abstract Co-Author*) Nothing to Disclose Michael Z. Liu, MS, New York, NY (*Abstract Co-Author*) Nothing to Disclose Miriam Klein, MS, New York, NY (*Presenter*) Nothing to Disclose Keerthi Sravan Ravi, BEng, New York, NY (*Abstract Co-Author*) Nothing to Disclose Maggie M. Fung, MEng, Bethesda, MD (*Abstract Co-Author*) Employee, General Electric Company Guido Buonincontri, Pisa, Italy (*Abstract Co-Author*) Nothing to Disclose

For information about this presentation, contact:

sg3606@columbia.edu

PURPOSE

Repeatability tests for robust T1/T2 measurements obtained from Magnetic Resonance Fingerprinting (MRF) based on inversion recovery requires approximately 5 hours. The goal of this study was to enable a 10-minute quality assurance protocol for MRF that could be employed on a daily basis prior to clinical studies. This involved investigating qualitative and quantitative measures of data consistency between multiple MRF scans and vendor/manufacturer supplied targets, demonstrated on in vitro Quality Assurance (QA) phantoms

RESULTS

MR signal intensity images for the ACR phantom from the SE and MRF acquisitions indicated similarity in contrast and resolution. The grid features indicated distortion due to gradient warps. The MRF implementation passed the positioning accuracy, ghosting and low contrast detectability as per the ACR guidelines. It failed tests with respect to resolution, slice thickness, geometric accuracy and signal uniformity. Relaxometric maps for the ADNI phantom from vendor supplied standard scans and MRF showed spatial correspondence. ROI analysis indicated variation of values within each ROI to be less than 13.5% whereas the variations in the repeats for each ROI was negligible. This indicated that the precision of measurements (T1) over repeats and spatial distribution of ROI were consistent. The accuracy of the measurements in the ROI varied as indicated significantly (<30% for T2, < 10% for T1) while the corresponding measures over repeats were consistent (< 1%). However, it must be noted that the ADNI phantom is primarily utilized for T1 measurements rather than T2. The MRF scans also involve variations due to the gridding reconstruction (such as the kernel size) of non-Cartesian k-space data. This is expected to impact the resolution, slice thickness and geometry accuracy tests. Incorporation of field maps into reconstruction may mitigate challenges with respect to signal uniformity, specifically in the context of spiral readouts and off-resonance challenges.

CONCLUSION

We have demonstrated a twelve minute QA protocol that could be used on a daily basis to enable measures of repeatability, accuracy and precision. We have utilized a VFA based T1- and FSE based T2-mapping schemes to enable shorter QA acquisition times. Prospective longitudinal data being currently pursued would enable insights into systemic errors and/or robustness of

implementation; thus providing higher confidence in MRF based studies at multiple sites. This is expected to aid in harmonization of MRF data between multiple sites and centers.

METHODS

An MRF implementation with 979 time points, 89 shot variable density spiral with 732 points was implemented on a GE 1.5T scanner. Spin Echo (SE) based structural imaging of the American College of Radiology (ACR) phantom was utilized for qualitative assessment with TR/TE = 500/20ms; 11 slices, 5mm slice thickness, in plane resolution of 1mm x 1mm. For comparison, MRF derived synthetic signal intensity data from the relaxation parameters was utilized. These were compared by two trained medical physicists with experience greater than five years. A 3D Fast Spoiled Gradient Recalled Echo Variable Flip Angle (2o, 5 o, 10 o, 20 o and 30 o) based T1 mapping with TR/TE = 6/1.4ms, 20 slices, 5mm slice thickness; and Fast Spin Echo based T2 mapping with eight echoes with TR/minimumTE = 1000/10ms with an echo spacing of 10.3ms, 20 slices, 5mm slice thickness were performed on the Alzheimer's Disease Neuroimaging Initiative (ADNI) Magphan EMR051 phantom (The Phantom Laboratory, NY) to obtain T1/T2 measurements. These were then compared to corresponding values determined by dictionary matched MRF scans that were repeated 5 times as part of test-retest experiments. Regions-of-interest (ROI) were drawn on specific spheres in the ADNI phantom to assess accuracy and precision of measurements. MATLAB (The Mathworks Inc., MA) based regression analysis was performed on conventionally obtained signal intensity images to determine T1/T2 maps. The total protocol time including the MRF scans was under twelve minutes.

PDF UPLOAD

http://abstract.rsna.org/uploads/2018/18015027/18015027_gi3k.pdf

SSK17-09 Simultaneous Measurement of T1, T2* and Fat Fraction for the Assessment of Non-Alcoholic Fatty Liver Disease

Wednesday, Nov. 28 11:50AM - 12:00PM Room: E353B

Participants Nicholas Rubert, PhD, Chicago, IL (*Presenter*) Nothing to Disclose Jie Deng, PhD, Chicago, IL (*Abstract Co-Author*) Nothing to Disclose

PURPOSE

This study assessed the feasibility of measuring T1 and T2* in the livers of patients exhibiting steatosis using a breath-hold dual flip-angle 3D GRE Dixon sequence.

METHOD AND MATERIALS

Imaging was performed on a 1.5T scanner. The proposed sequence consisted of two consecutive acquisitions of a 6-echo 3D GRE sequence with flip angle of 5° then 15°. From the acquisition at 5°, fat fraction (FF) and T2* were estimated at each voxel with a regularized fat-water separation algorithm. T1 of fat and water components of a voxel were then estimated in a separate step. In this step, a non-linear least squares fit of the signals at both flip angles to an equation incorporating sequence TR and fat and water T1 was performed with FF and T2* fixed. Three experiments were used to verify the performance of the algorithm: 1) A non-fat phantom containing nine vials each with different T1 and T2* values, was imaged with an inversion recovery (IR) and the proposed method. Mean T1 in an ROI within each vial was compared between the IR and proposed method. 2) Two healthy volunteers were imaged with the proposed method three times in rapid succession. Mean FF, T2*, and T1 within large ROI's in the livers of the volunteers were imaged with the proposed method. The proposed technique. Mean FF, T2*, and T1 within large ROI's in the livers of the patients were examined.

RESULTS

For the phantom experiments T1 in each of the 9 vials ranged from 353 to 1751 ms according to the IR method. Agreement with T1 by the proposed method was within 10% for all vials. For the repeatability study on healthy volunteers measurements of FF, T2*, and T1 all exhibited coefficient of variations of <6%. Among volunteers and patients, T1 was found to be uncorrelated with FF with R2 < .01 and weakly correlated with T2* with R2 of 0.47. FF in patients ranged from 3.2% to 34.2%, T1 from 342 to 956 ms, and T2* from 17 to 50 ms.

CONCLUSION

The proposed method demonstrates close agreement with IR measurements of T1 in a phantom and highly repeatable measurements among volunteers. T1 was found to yield independent information from either FF or T2* estimated in a routine Dixon imaging sequence.

CLINICAL RELEVANCE/APPLICATION

Liver T1 can be accurately estimated from a single breath-hold GRE MRI sequence when steatosis is present. T1 measurements may be useful for evaluation of inflammation and fibrosis in patients with NASH.



SSK18

Physics (CT: Image Quality)

Wednesday, Nov. 28 10:30AM - 12:00PM Room: E353C

AI CT PH SQ

AMA PRA Category 1 Credits ™: 1.50 ARRT Category A+ Credit: 1.75

FDA Discussions may include off-label uses.

Participants

Michael F. McNitt-Gray, PhD, Los Angeles, CA (*Moderator*) Institutional research agreement, Siemens AG; ; ; ; ; John M. Boone, PhD, Sacramento, CA (*Moderator*) Patent agreement, Isotropic Imaging Corporation Consultant, RadSite

Sub-Events

SSK18-01 Quantitative Impact of Denoising Strategies in Low-Dose CT

Participants

Juan Pablo Cruz Bastida, Madison, WI (*Presenter*) Nothing to Disclose Daniel Gomez-Cardona, PhD, Rochester , MN (*Abstract Co-Author*) Nothing to Disclose Ran Zhang, PhD, Madison, WI (*Abstract Co-Author*) Nothing to Disclose John W. Hayes, MS, Madison, WI (*Abstract Co-Author*) Nothing to Disclose Ke Li, PhD, Madison, WI (*Abstract Co-Author*) Nothing to Disclose Guang-Hong Chen, PhD, Madison, WI (*Abstract Co-Author*) Research funded, General Electric Company Research funded, Siemens AG

For information about this presentation, contact:

cruzbastida@wisc.edu

PURPOSE

CT number accuracy at low dose levels has been found to be strongly biased. It was demonstrated that the stochastic noise associated with photon detection is the root cause of inaccurate CT number. The purpose of this work is to investigate the impact of three different denoising strategies to alleviate CT number inaccuracy in FBP-based CT: image domain denoising, sinogram domain denoising and raw counts domain denoising.

METHOD AND MATERIALS

Data acquisition was performed in a benchtop CT system, which included a CdTe-based photon counting detector. A Catphan phantom, containing inserts of known composition, was scanned at 60 kV and two different CTDIw levels: 1.5 and 15 mGy. The acquired data was reconstructed using FBP with ramp filter. Locally adapted denoising diffusion filter was applied to the lowest dose data set, in image, sinogram and raw counts domain. The contrast of Teflon and LDPE inserts was measured in averaged images across repetitions. FBP reconstruction of the average raw counts at the highest dose was considered as reference.

RESULTS

Experimental results from in this study corroborate that CT number estimates are inaccurate at low dose levels. As a consequence, the contrast of inserts relative to the background is overestimated. Particularly, the contrast of the analyzed inserts is doubled in the lowest dose scans. After adapted denoising, only the strategy to perform denoise in the raw counts domain was successful in restoring the reference contrast values.

CONCLUSION

Results in this study suggest that locally adaptive denoising is an adequate methodology to preserve the quantitative accuracy of low dose CT when performed in the pre-log projection domain.

CLINICAL RELEVANCE/APPLICATION

Healthy tissue and disease characterization often rely on both absolute CT number and relative contrast, for example: liver and pancreatic steatosis, acute cerebral venous sinus thrombosis, etc. Dose reduction efforts in CT must be guided by both imaging performance and quantitative capabilities.

SSK18-02 Task-Based Image Quality Assessment of X-ray CT Using Convolutional Neural Networks

Wednesday, Nov. 28 10:40AM - 10:50AM Room: E353C

Participants

Felix K. Kopp, Munich, Germany (*Abstract Co-Author*) Nothing to Disclose Marco Catalano, Napoli, Italy (*Abstract Co-Author*) Nothing to Disclose Daniela Pfeiffer, MD, Munich, Germany (*Abstract Co-Author*) Nothing to Disclose Alexander A. Fingerle, MD, Munchen, Germany (*Abstract Co-Author*) Nothing to Disclose Ernst J. Rummeny, MD, Munich, Germany (*Abstract Co-Author*) Nothing to Disclose Peter B. Noel, PhD, Munich, Germany (*Presenter*) Nothing to Disclose

PURPOSE

The purpose of this study is the task-based image quality assessment of X-ray computed tomography.

METHOD AND MATERIALS

A phantom with contrast targets similar to lesions in a contrast enhanced liver (acrylic spheres, varying diameters, +30 HU) was repeatedly scanned with a computed tomography scanner. A board certified radiologist rated image patches containing the contrast targets with a confidence rating for the presence of the signal. Labeled image data were used to build several anthropomorphic model observers to predict the performance of the human observer: A neural network based on softmax regression (SR-MO) and a convolutional neural network (CNN-MO). Results were compared to a more traditional model observer, the channelized Hotelling observer (with Gabor channels and internal channel noise (CHOi)). The performance of the different model observers and the human observer were evaluated with a receiver operating characteristic curve analysis. The machine learning based model observers were trained with two different strategies: A) building a separate model for each lesion size; B) building one model that was applied to lesions of all sizes.

RESULTS

Machine learning based model observers as well as the CHOI and the human observer were highly correlated at each lesion size and dose level. With strategy A, Pearson's product-moment correlation coefficients r were 0.961 (95% confidence interval (CI): 0.863-0.989) for SR-MO and 0.974 (95% CI: 0.907-0.993) for CNN-MO. Mean absolute percentage differences (MAPD) between the model observer and the human observer were 1.1% for SR-MO and 1.0% for CNN-MO. With strategy B, r was 0.956 (95% CI: 0.845-0.988) for SR and 0.958 (95% CI: 0.854-0.989) for CNN. For CHOi, r was 0.971 (95% CI: 0.897-0.992). MAPD were 2.0% for SR-MO and 1.5% for CNN-MO. For the CHOi the MAPD was 1.9%.

CONCLUSION

Machine learning based model observers can accurately predict the performance of a human observer for all lesion sizes and dose levels in the evaluated signal detection task.

CLINICAL RELEVANCE/APPLICATION

Model observers are widely used in research regarding the development and optimization of medical imaging devices. Our results show that machine learning based model observers can accurately predict the performance of a human observer in a signal detection task for CT.

SSK18-03 DestreakNet: A Deep Convolutional Neural Network to Reduce Metal Streak Artifacts in CT Images

Wednesday, Nov. 28 10:50AM - 11:00AM Room: E353C

Participants

Lars Gjesteby, Troy, NY (*Presenter*) Nothing to Disclose Hongming Shan, Troy, NY (*Abstract Co-Author*) Research Grant, General Electric Company Qingsong Yang, Troy, NY (*Abstract Co-Author*) Nothing to Disclose Yan Xi, Shanghai, China (*Abstract Co-Author*) Employee, UEG Medical Imaging Yannan Jin, MSC, Erlangen, Germany (*Abstract Co-Author*) Employee, General Electric Company Bernhard Claus, PhD, Niskayuna, NY (*Abstract Co-Author*) Nothing to Disclose Bruno De Man, PhD, Niskayuna, NY (*Abstract Co-Author*) Employee, General Electric Company Ge Wang, PhD, troy, NY (*Abstract Co-Author*) Nothing to Disclose

For information about this presentation, contact:

ge-wang@ieee.org

PURPOSE

To design and train a deep convolutional neural network to reduce metal artifacts in CT images.

METHOD AND MATERIALS

Our network structure (DestreakNet) consists of two parallel streams, each with 20 residual units. In each residual unit, there are two convolution layers with batch normalization (BN) and rectified linear unit (ReLU) activation. The network is trained on the residual error between the input and output of the unit. The outputs of both streams are merged in the network's feature space, and then passed through nine more convolution layers to yield a final output. A mean squared error (MSE) and a perceptual loss function were both investigated for network optimization. All training, testing, and validation datasets were generated using CatSim, an industrial-grade CT simulator. Real data from the Visible Human Project were used to create voxelized phantoms of pelvic and spinal regions with and without metal implants. For initial correction, CT images were reconstructed using the state-of-the-art NMAR algorithm. The reconstructed images without metal were the ground truth and target of the network. From full-size images, approximately 150,000 patches of size 56x56 were extracted for training. Patches from the NMAR images were input to one network stream and patches from uncorrected CT images were input to the other to harness complimentary features simultaneously.

RESULTS

To validate the network performance, hip and spine images withheld from training were used. In a hip case, the image quality metrics including structural similarity index (SSIM) and peak signal-to-noise ratio (PSNR) were calculated for all images in reference to the artifact-free truth. The SSIM and PSNR were 0.2382 and 9.1830, respectively, for the initial uncorrected reconstruction image, 0.7014 and 18.8975 for the NMAR-corrected image, 0.8636 and 23.8582 for DestreakNet with MSE loss, and 0.8264 and 22.1685 for DestreakNet with perceptual loss.

CONCLUSION

Our network substantially reduced metal streak artifacts that remained in the CT image after initial correction by the NMAR algorithm.

CLINICAL RELEVANCE/APPLICATION

Our proposed data-driven metal artifact reduction method may provide sufficient image quality in radiation therapy planning, which requires accurate tumor characterization near implants for precise dose delivery.

SSK18-04 Patient-Specific Local Noise Power Spectrum Measurement via a Deep-Learning Generative Adversarial Network

Wednesday, Nov. 28 11:00AM - 11:10AM Room: E353C

Participants Chengzhu Zhang, BS, Madison, WI (*Presenter*) Nothing to Disclose Daniel Gomez-Cardona, PhD, Rochester , MN (*Abstract Co-Author*) Nothing to Disclose Yinsheng Li, BEng, Madison, WI (*Abstract Co-Author*) Nothing to Disclose Juan Montoya, Madison, WI (*Abstract Co-Author*) Nothing to Disclose Guang-Hong Chen, PhD, Madison, WI (*Abstract Co-Author*) Research funded, General Electric Company Research funded, Siemens AG

For information about this presentation, contact:

czhang553@wisc.edu

PURPOSE

With the increased use of low-dose CT techniques which are characterized for its highly shift-variant noise properties, the measurement of the noise power spectrum (NPS) has become challenging and time consuming since current solutions require multiple scans of a given clinical scenario. In this work, a deep-learning generative adversarial network (GAN) was developed to address this challenge and provide a fast and accurate way to measure patient-specific local NPS.

METHOD AND MATERIALS

GANs were utilized to learn a mapping from white noise input to output CT noise realizations with correct CT noise correlations from a single local uniform ROI. To achieve this, a two-stage training strategy was implemented. In the pre-training stage, repeated scans of a quality assurance phantom were performed to extract 1600 (64x64) local MBIR noise-only images used as labels to train the network. This network characterized the noise magnitude and correlation in labels and was able to generate 64x64 noise-only images with similar characteristics as the input. For the next stage, a single scan of an anthropomorphic phantom was used for fine-tuning, while repeated scans were used for validation. First, a 101x101 ROI was extracted from a single MBIR image, detrended, and augmented to obtain 128 (64x64) training labels and fine-tune the pre-trained GANs. To validate the GAN-generated noise images, their NPS was compared to the NPS from the physical ensemble of repeated scans in terms of overall RMSE, noise magnitude, and mean frequency across 30 trials. This patient-specific approach was applied to clinical data reconstructed with MBIR (same patient at two doses) to assess the estimated NPS in terms of noise magnitude and coarseness.

RESULTS

The overall RMSE between the GAN-generated NPS and the physical NPS was 0.83 HU2mm2. The mean percent discrepancy for their noise magnitude and mean frequency were 4.51% and 3.62%, respectively. The runtime for the fine-tuning stage was <100s and 1s to generate 250 noise images.

CONCLUSION

It was demonstrated that GANs can characterize CT noise in terms of magnitude and coarseness and generate multiple noise realizations with comparable characteristics from a single noise realization.

CLINICAL RELEVANCE/APPLICATION

A fast and accurate way to estimate patient-specific local NPS was provided and can be easily adapted to any given CT system. This is an essential step towards patient-specific image quality assessment.

SSK18-05 Multi-Kernel Synthesis for CT Images Using a Deep Convolutional Neural Network

Wednesday, Nov. 28 11:10AM - 11:20AM Room: E353C

Awards

Trainee Research Prize - Fellow

Participants Andrew Missert, PHD, Rochester, MN (*Presenter*) Nothing to Disclose Shuai Leng, PHD, Rochester, MN (*Abstract Co-Author*) License agreement, Bayer AG Lifeng Yu, PhD, Chicago, IL (*Abstract Co-Author*) Nothing to Disclose Cynthia H. McCollough, PhD, Rochester, MN (*Abstract Co-Author*) Research Grant, Siemens AG

For information about this presentation, contact:

Missert.Andrew@mayo.edu

PURPOSE

To produce a single synthetic image that combines the best qualities of images reconstructed with different kernels using a deep convolutional neural network (CNN).

METHOD AND MATERIALS

A CNN was trained from scratch to synthesize multiple input images, each produced with a different reconstruction kernel, into a single output image that exhibits improved image qualities (in terms of high sharpness and low noise levels) compared to each input individually. The CNN architecture was based on the ResNet design, and consisted of repeated blocks of residual units with a total of 32 convolutional layers. The CNN inputs consisted of three images produced by soft (B10), medium-sharp (B45), and sharp (B70) kernels that were stacked in the channel dimension. The CNN output was treated as a perturbation that was added to the sharp-kernel input, which reduced the required training time. The network was trained using supervised learning with both full-dose and simulated quarter-dose abdominal CT images. The simulated quarter-dose images obtained from different kernels were used as the

network input, and the corresponding full-dose images reconstructed with a sharp kernel were used as the ground truth to evaluate a mean-squared-error loss function. The network was trained on 500,000 example images of various sizes that were cropped from ten abdominal CT exams. After training, the performance was evaluated by comparing input and output images using a reserved set of full-dose abdominal, chest, and phantom CT scans that were not used in the network training.

RESULTS

The synthetic images improved the signal-to-noise ratio by 338% compared to the sharp kernel images, without observable blurring of sharp edges. No perceptible artificial texture was introduced that detracted from the natural appearance of the synthetic image. The algorithm was robust enough to be applied to multiple tissue types, including the bones, lungs, and liver.

CONCLUSION

An artificial neural network can be used to combine images from multiple reconstruction kernels into a single synthetic image that exhibits both low noise and a high degree of sharpness.

CLINICAL RELEVANCE/APPLICATION

CT Images from different reconstruction kernels can be merged using a neural network into a single image with superior qualities that can be used for reading multiple tissue types simultaneously.

SSK18-06 Correlation Between 2D Channelized Hoteling Observer in a Uniform Water Background and Human Observers in a Patient Liver Background for Low-Contrast Lesion Detection and Localization in CT

Wednesday, Nov. 28 11:20AM - 11:30AM Room: E353C

Participants

Hao Gong, PhD, Rochester,, MN (*Presenter*) Nothing to Disclose Lifeng Yu, PhD, Chicago, IL (*Abstract Co-Author*) Nothing to Disclose Shuai Leng, PHD, Rochester, MN (*Abstract Co-Author*) License agreement, Bayer AG Michael L. Wells, MD, Rochester, MN (*Abstract Co-Author*) Nothing to Disclose Joel G. Fletcher, MD, Rochester, MN (*Abstract Co-Author*) Grant, Siemens AG; Consultant, Medtronic plc; ; Cynthia H. McCollough, PhD, Rochester, MN (*Abstract Co-Author*) Research Grant, Siemens AG

For information about this presentation, contact:

Gong.Hao@mayo.edu

PURPOSE

To investigate the correlation between 2D channelized Hoteling observer (CHO) performance in a uniform water background (with single-slice viewing mode) and human observer (HO) performance in a patient liver background (with multi-slice scrolling viewing mode) for a low-contrast liver lesion detection and localization task when lesion location is uncertain.

METHOD AND MATERIALS

Seven routine dose abdominal patient scans (mean CTDIvol 12.6 mGy) were retrospectively collected. Patient scans at half and quarter of routine dose were simulated using a projection-based noise insertion tool. An abdomen-sized water phantom was repeatedly scanned (n = 10) on the same scanner. Lesion models generated from real metastatic liver lesions (size 7, 9 and 11 mm, and contrast 15, 20, and 25 HU) were inserted into both phantom and patient images using a projection-based method. CT images were created using filtered-back-projection (FBP) and iterative reconstruction (IR). Region-of-interests (ROIs) around lesions were extracted to generate trials for CHO and HO studies. Centers of the ROIs were shifted to randomly distribute lesion locations in the ROIs. A 2D CHO with 12 Gabor channels was applied to phantom images. Two subspecialized radiologists (10 and 25 years of experience) performed HO studies on patient images. For each trial, they localized lesions by scrolling through multiple slices. The performance of CHO and HO was compared across 12 experimental conditions with varying dose, lesion characteristics, and reconstruction types. Area under the receiver operating characteristic (ROC) curve and localization ROC curve were used as figure of merits for CHO and HO performance.

RESULTS

2D CHO performance in phantom images correlated well with HO performance in patient liver images (Pearson correlation coefficients 0.960 (p = 0.0023) and 0.984 (p = 0.0004) for detection and localization, respectively) for all conditions . No statistically significant difference was observed in Bland-Altman agreement analysis.

CONCLUSION

It is possible to use a simple single-slice viewing CHO and uniform water phantom to assess performance for realistic CT detection and localization tasks in patient liver backgrounds.

CLINICAL RELEVANCE/APPLICATION

Single-slice 2D CHO with Gabor channels provides a convenient tool to evaluate diagnostic performance and optimize abdominal CT scanning protocols.

Honored Educators

Presenters or authors on this event have been recognized as RSNA Honored Educators for participating in multiple qualifying educational activities. Honored Educators are invested in furthering the profession of radiology by delivering high-quality educational content in their field of study. Learn how you can become an honored educator by visiting the website at: https://www.rsna.org/Honored-Educator-Award/ Michael L. Wells, MD - 2017 Honored Educator

SSK18-07 Can Deep Learning Unseat Iterative Reconstruction for Low-Dose CT?

Wednesday, Nov. 28 11:30AM - 11:40AM Room: E353C

Participants Hongming Shan, Troy, NY (*Presenter*) Research Grant, General Electric Company Atul Padole, MD, Boston, MA (*Abstract Co-Author*) Nothing to Disclose Mannudeep K. Kalra, MD, Boston, MA (*Abstract Co-Author*) Research Grant, Siemens AG; Research Grant, Canon Medical Systems Corporation Uwe Kruger, Troy, NY (*Abstract Co-Author*) Nothing to Disclose Wenxiang Cong, Albany, NY (*Abstract Co-Author*) Nothing to Disclose Ge Wang, PhD, troy, NY (*Abstract Co-Author*) Nothing to Disclose

For information about this presentation, contact:

wangg6@rpi.edu

PURPOSE

Although widely applied in clinical practice, studies have reported that iterative reconstruction (IR) alters image appearance, and can adversely affect low contrast lesions. The purpose of this project is to systematically compare commercial/clinical iterative reconstructions by major vendors with FBP-reconstruction-based deep learning (FBP-DL) reconstruction for low-dose chest and abdomen CT exams.

METHOD AND MATERIALS

Our study included 80 low-dose chest and abdomen CT exams from three major CT vendors (de-identified). We created a neural network including 4 convolutional and 4 deconvolutional layers, each of the layers contains 32 filters except for the last layer with only 1 filter. For preserving image features, former feature-maps were reused at latter layers by three conveying-paths. The rectified linear unit was used for each layer. The network was optimized in the Wasserstein generative adversarial network framework with an additional perceptual loss. 128K normal- and low-dose FBP image patches from the MGH dataset were used in training our network. Image quality metrics including peak signal-to-noise ratio (PSNR) and structural similarity index (SSIM) were calculated for all the images in reference to the normal-dose FBP images. Also, a blinded reader study was designed to evaluate the image quality. Then, the Wilcoxon signed-rank test was used to compare FBP-DL with commercially available state-of-the-art IR techniques.

RESULTS

FBP-DL achieves a significantly better image quality and performance than commercially available IR images evaluated by PSNR and SSIM for all the selected vendors. Also, the reader study demonstrated that FBP-DL images had superior visibility of small and subtle structures with lower noise and less severe artifacts as compared to the IR counterparts. In addition to that, deep learning is computationally more efficient than IR.

CONCLUSION

The deep learning method has a great potential to outperform the commercial/clinical iterative reconstruction for low-dose CT. An integrated deep learning workflow from raw data to final images/radiomics is under active development.

CLINICAL RELEVANCE/APPLICATION

Emerging deep learning-based CT methods may provide a superior diagnostic performance in routine clinical applications.

SSK18-08 Reference-Based Image-Detail and Noise Texture Metrics for CT Image Quality Assessment

Wednesday, Nov. 28 11:40AM - 11:50AM Room: E353C

Participants

Sathish Ramani, Niskayuna, NY (*Abstract Co-Author*) Employee, General Electric Company Lin Fu, PhD, Niskayuan, NY (*Abstract Co-Author*) Employee, General Electric Company Bruno De Man, PhD, Niskayuna, NY (*Presenter*) Employee, General Electric Company

PURPOSE

Task-based image quality metrics are the gold-standard in evaluating and comparing the performance of imaging algorithms. Nevertheless, algorithm designers still benefit from lower-level more direct metrics reflecting the actual image presentation. Traditional noise and spatial resolution metrics are coming short for non-linear iterative reconstruction approaches. This work proposes quantitative metrics for separately assessing object-detail, artifact-level and noise texture based on a gold-standard reference.

METHOD AND MATERIALS

A phantom constructed from a freshly-cut turkey was scanned 117 times at 120 kV and 200 mA. FBP images were reconstructed and averaged over the scans to obtain a noise-free reference image Z, from which a noisy sinogram S was simulated. Model-Based Image Reconstruction (MBIR) images at varying regularization strengths, β , were reconstructed from S. For an MBIR-image M, the object-detail metric was computed as a normalized covariance between M and Z. Artifact metric was computed as the normalized energy of the difference between M and its geometric-projection along Z. Histogram and spectral density shapes of the residue R=M-Z, were used to assess noise texture.

RESULTS

With increasing β , noise decreased in M at the expense of loss of image features: the object-detail metric monotonically decreased correspondingly. Artifact metric exhibited a minimum and increased either way due to high noise at low β or loss of image features at high β . Histogram of R evolved from being broad with long tails (high noise at low β) to being narrow (nearly no noise at high β). The spectral density of R evolved from exhibiting high-frequency behavior (high noise at low β) to being predominantly low-frequency in nature (noise with long spatial correlation at low β).

CONCLUSION

The proposed metrics captured expected behavior of MBIR at varying strengths indicating their validity. These metrics can be helpful in judging preservation of image features and evaluation of artifact-level and noise texture for CT algorithm development and tuning.

CT iterative reconstruction was introduced a decade ago and is continuing to be improved. The proposed image quality evaluation methods are useful for algorithm designers to achieve the best possible tuning of CT algorithms before clinical deployment.

SSK18-09 Task Based Image Quality in Virtual Monoenergetic Images Across 3 Generations of Scanner Models

Wednesday, Nov. 28 11:50AM - 12:00PM Room: E353C

Participants

Jayasai R. Rajagopal, BA, Durham, NC (*Presenter*) Nothing to Disclose Yakun Zhang, MS, Durham, NC (*Abstract Co-Author*) Nothing to Disclose Juan Carlos Ramirez-Giraldo, PhD, St Louis, MO (*Abstract Co-Author*) Employee, Siemens AG Ehsan Samei, PhD, Durham, NC (*Abstract Co-Author*) Research Grant, General Electric Company; Research Grant, Siemens AG; Advisory Board, medInt Holdings, LLC; License agreement, 12 Sigma Technologies; License agreement, Gammex, Inc

For information about this presentation, contact:

yakun.zhang@duke.edu

PURPOSE

To use task-based metrics to assess the impact of patient size, beam spectra separation, and radiation exposure on image quality for virtual monoenergetic images (VMIs) across three scanner platforms.

METHOD AND MATERIALS

This study used a commercially available phantom with iodine, soft tissue and calcium inserts (Gammex Multi Energy CT phantom). The phantom was configured with additional fat rings simulating five different sizes (20, 30, 35, 40, and 50 cm diameter). All scans used radiation exposures of 4, 8, 16, and 24 mGy, and were repeated on three DECT platforms from one manufacturer (Siemens Force, Flash and Edge). VMIs were reconstructed at 50, 70 keV and 150 keV. Noise and image texture in terms of average frequency of the noise power spectra (Favg) and the contrast-dependent spatial resolution in terms of the 50% amplitude of the iodine-task transfer function (F50) were calculated. A task-specific detectability index (d') was calculated for iodine inserts using a 5 mm Gaussian circular disk as the task.

RESULTS

The Favg and F50 decreased with increasing phantom size. For 100/150Sn kV on Force scanner, Favg was 0.31, 0.30, 0.27, and 0.25 mm-1 for the 20, 30, 35, 40 cm sizes; F50 was 0.43, 0.43, 0.37, 0.32 mm-1, respectively. For the same phantom size, the Favg appeared to be insensitive to changes in acquisition spectra separations, but F50 increased with increasing spectra separation. Different keVs did not affect either Favg or F50, but affected the noise magnitude and contrast, and thus the detectability index. d' for the 15 mg/ml iodine insert had an average of 23% increase for all sizes and kV combinations when keV decreased from 70 to 50. At 70 keV, the larger spectra separation (80/150Sn kV) led to an increase in d' compared to less spectra separation (100/150Sn kV) at round 10% for the 20 and 30 cm phantoms, but only 3% higher d' for the 35 and 40 cm phantoms. For a fixed keV, image contrast, Favg, and F50 were relatively insensitive to changes in radiation exposure for sizes below 40cm.

CONCLUSION

The system behaved non-linearly for different phantom sizes and spectra separation. Task based metrics was able to capture the characteristics of the VMIs. Highest detectability was achieved with larger spectra separation and for smaller sizes.

CLINICAL RELEVANCE/APPLICATION

Highest iodine detectability for the VMIs was achieved with larger spectra separation and for smaller sizes.



SSK19

Science Session with Keynote: Radiation Oncology (Outcomes, Palliation, Sarcoma)

Wednesday, Nov. 28 10:30AM - 12:00PM Room: S504AB

RO

AMA PRA Category 1 Credits ™: 1.50 ARRT Category A+ Credit: 1.75

FDA Discussions may include off-label uses.

Participants

Carryn Anderson, MD, Iowa City, IA (*Moderator*) Nothing to Disclose Edward Y. Kim, MD, Seattle, WA (*Moderator*) Nothing to Disclose

Sub-Events

SSK19-01 The Safety and Efficacy of Interstitial 125I Seeds Implantation Brachytherapy for Metastatic Epidural Spinal Cord Compression

Participants

Chaojie Li, MD, Shanghai, China (Presenter) Nothing to Disclose

PURPOSE

To investigate the safety and efficacy of 125I seeds interstitial implantation for metastatic epidural spinal cord compression (MESCC) and the life quality of the patients.

METHOD AND MATERIALS

From April 2009 to May 2015, 28 patients who met the inclusion criteria were retrospectively reviewed. The number of 125I seeds implanted ranged from 7 to 62 with specific activity of 0.5 to 0.8 mCi. The post-plan showed that the tumor matched peripheral dose (MPD) were 80-140 Gy. Follow-up ranged from 1 to 32 months with a median of 18 months. Visual analogue scale (VAS), karnofsky performance scale (KPS) and motor performance were measured before and after treatment.

RESULTS

All patients tolerated seed implantation well. All patients were obviously alleviated pain. VAS scores of patients decreased from 4.89 ± 1.52 before treatment to 1.61 ± 1.20 after treatment, and KPS scores increased from 73.93 ± 12.27 to 86.76 ± 10.90 , both differences were statistically significant(P<0.05). The 1-, 2-, 3- year local control rates were 77%, 34%, and 14%, respectively, with a median of 19 months (7-32 months). The 1-, 2-, 3- year survival rates were 81%, 54%, and 14%, respectively, with a median of 25 months. 7(100%) nonwalking patients regained motor ability. No myelopathies or other neurologic sequelae were encountered.

CONCLUSION

Interstitial 125I seeds implantation brachytherapy was a promising local therapy and an alternative and palliative way to treat MESCC.

CLINICAL RELEVANCE/APPLICATION

To investigate the safety and efficacy of 125I seeds interstitial implantation for metastatic epidural spinal cord compression (MESCC) and the life quality of the patients.

SSK19-02 Cancer-Related Anxiety Following Definitive Treatment of Localized Prostate Cancer: A Population-Based Cohort Study

Wednesday, Nov. 28 10:40AM - 10:50AM Room: S504AB

Awards

Student Travel Stipend Award

Participants

Dominic Moon, MD, Chapel Hill, NC (*Presenter*) Nothing to Disclose Ram Basak, Chapel Hill, NC (*Abstract Co-Author*) Nothing to Disclose Deborah Usinger, Chapel Hill, NC (*Abstract Co-Author*) Nothing to Disclose Sarah Walden, Chapel Hill, NC (*Abstract Co-Author*) Nothing to Disclose Ronald Chen, MD, Chapel Hill, NC (*Abstract Co-Author*) Consultant, Accuray Incorporated

PURPOSE

Psychological distress following localized prostate cancer treatment is not well-understood. We assessed cancer-specific anxiety post-treatment and factors associated with increase in anxiety level.

METHOD AND MATERIALS

Population-based prospective cohort of newly diagnosed localized prostate cancer patients were enrolled from 1/2011 to 6/2013. A

total of 838 patients who received definitive treatment with radical prostatectomy (RP) or radiotherapy (RT) were analyzed. Patients with recurrence after treatment were excluded. Cancer-related anxiety one year post-treatment was assessed using the validated Memorial Anxiety Scale for Prostate Cancer (MAX-PC) questionnaire, which consists of 3 subscales: recurrence anxiety, PSA anxiety, and prostate cancer anxiety. Multivariable linear regression assessed factors associated with anxiety.

RESULTS

Median age was 64 and 74% were White. In this cohort, 53%, 25%, 11%, and 11% of patients received RP, conventional RT, stereotactic body RT, and brachytherapy, respectively. Multivariable analysis showed that White men had lower recurrence anxiety, PSA anxiety, and prostate cancer anxiety than non-White men (all p<0.001), while older men had less PSA anxiety and prostate cancer anxiety compared to younger men (p=0.002 and p=0.001, respectively). Patients with high risk prostate cancer had increased recurrence anxiety than those with low risk disease (p=0.04). Compared to men receiving RP, those receiving brachytherapy and conventional RT had borderline significant increase in recurrence anxiety and PSA anxiety, respectively (both p=0.05). Frequency of post-treatment PSA testing and last PSA value were not associated with level of anxiety.

CONCLUSION

White men and older patients overall had less cancer-related anxiety, while high risk patients had increased recurrence anxiety.

CLINICAL RELEVANCE/APPLICATION

Better understanding of factors associated with prostate cancer-related anxiety may aid in counseling patients to improve psychological well-being after definitive treatment.

SSK19-03 Evaluation of Prognostic Factors of Bone Metastasis Treated By Radiotherapy: A Single-Institution Experience

Wednesday, Nov. 28 10:50AM - 11:00AM Room: S504AB

Participants

Nana Shimoyachi, Kanazawa, Japan (*Presenter*) Nothing to Disclose Tomoyasu Kumano, Ishikawa, Japan (*Abstract Co-Author*) Nothing to Disclose Shigeyuki Takamatsu, MD, PhD, Kanazawa, Japan (*Abstract Co-Author*) Nothing to Disclose Aki Kanazawa, Chiba, Japan (*Abstract Co-Author*) Nothing to Disclose Takayuki Sakurai, Kanazawa, Japan (*Abstract Co-Author*) Nothing to Disclose Yoko Taima, MD, Kanazawa, Japan (*Abstract Co-Author*) Nothing to Disclose Sae Miyashita, Kanazawa, Japan (*Abstract Co-Author*) Nothing to Disclose Toshifumi Gabata, MD, PhD, Kanazawa, Japan (*Abstract Co-Author*) Nothing to Disclose

PURPOSE

We investigated the prognostic factors of bone metastases treated by radiotherapy and evaluated the efficacy of prognostic scoring systems in our institution.

METHOD AND MATERIALS

Between April 2011 and December 2016, 288 patients were evaluated (median age, 64 years). The median follow-up period was 11months. The common primary lesion was lung cancer (22%), liver cancer (12%) and prostate cancer (10%). We investigated the overall survival (OS) for all patients using Kaplan-Meier Method and the verification of prognostic prediction using Katagiri score and number of risk factor method (NRF). Katagiri score is scoring system using 6 factors; primary site, metastasis other than bone, poor PS, previous chemotherapy, multiple bone metastasis and abnormality of laboratory data. On the other hand, NRF uses only 3 factors; non-breast cancer, metastases other than bone, and KPS =2). Also, we analyzed factors (gender, age, primary lesion, PS, multiple bone metastases, previous chemotherapy, metastasis other than bone) by a multivariate analysis using the Cox proportional hazards model.

RESULTS

The OS rate for all patients was 42% at 1 year and median survival time was 9 months. In Katagiri score, 190 patients could be scored. The OS rate after 1 year was 79% for low risk (score0-3) and 51% for intermediate risk (score4-6). The OS rates for high risk (score7-10) after 6 months and 1 year were 43% and 19%, respectively. In NRF, all patients could be scored. Patients with a prognostic score of =3, the survival rate was 37% at 6 months, and only 18% at 1 year. Both Katagiri score and NRF, the significant differences are recognized between each all three groups. A multivariate analysis showed the significant prognostic factors for PS, primary lesion, previous chemotherapy, metastasis other than bone. Our results don't contradict the factors of previous studies.

CONCLUSION

We could investigate significant prognostic factors in our institution and show the validity of the prognostic scoring system previously reported.

CLINICAL RELEVANCE/APPLICATION

We could investigate the significant prognostic factors for radiotherapy of bone metastases and show the validity of the prognostic scoring systems (Katagiri score and number of risk factor method).

SSK19-05 Radiation Oncology Keynote Speaker: Sarcoma Keynote

Wednesday, Nov. 28 11:10AM - 11:20AM Room: S504AB

Participants

Matthew B. Spraker, MD, PhD, Saint Louis, MO (Presenter) Nothing to Disclose

SSK19-06 Planar and SPECT/CT Imaging in Human Immunodeficiency Virus (HIV) Subjects Diagnosed with Kaposi Sarcoma Using Intravenous 99mTc-tilmanocept

Wednesday, Nov. 28 11:20AM - 11:30AM Room: S504AB

Participants

Frederick O. Cope, PhD, Dublin, OH (*Abstract Co-Author*) Employee, Navidea Biopharmaceuticals, Inc; Stockholder, Navidea Biopharmaceuticals, Inc

Bonnie Abbruzzese, MS, Dublin, OH (Abstract Co-Author) Employee, Navidea Biopharmaceuticals, Inc

Allison Kissling, Dublin, OH (Abstract Co-Author) Nothing to Disclose

Rachael Hershey, Dublin, OH (Abstract Co-Author) Nothing to Disclose

- Carley Hartings, Dublin, OH (*Abstract Co-Author*) Nothing to Disclose David Ralph, PhD, Dublin, OH (*Presenter*) Nothing to Disclose
- Ahmad Ismail, Dublin, OH (*Abstract Co-Author*) Nothing to Disclose

Izabela Gierach, Dublin, OH (*Abstract Co-Author*) Nothing to Disclose

Michael Blue, MD, Dublin, OK (Abstract Co-Author) Nothing to Disclose

Matthew Haynam, Dublin, OH (Abstract Co-Author) Nothing to Disclose

Hannah Bailey, Dublin, OH (Abstract Co-Author) Nothing to Disclose

Christopher Gabelmann, Dublin, PR (Abstract Co-Author) Nothing to Disclose

Katherine Repp, Dublin, OH (Abstract Co-Author) Nothing to Disclose

Vasiliki Stamatopoulou, San Francisco, CA (Abstract Co-Author) Nothing to Disclose

Kenneth Gao, San Francisco, CA (Abstract Co-Author) Nothing to Disclose

Kieron Leslie, San Francisco, CA (Abstract Co-Author) Nothing to Disclose

Spencer C. Behr, MD, Burlingame, CA (*Abstract Co-Author*) Research Grant, General Electric Company Consultant, General Electric Company Consultant, Navidea Biopharmaceuticals, Inc Grant, Navidea Biopharmaceuticals, Inc Toby Maurer, San Francisco, CA (*Abstract Co-Author*) Nothing to Disclose

For information about this presentation, contact:

fcope@navidea.com

PURPOSE

To demonstrate Kaposi Sarcoma (KS) lesion imaging by planar and SPECT/CT of cutaneous and subcutaneous KS-associated lesions using 99mTc-tilmanocept (TCT). Such imaging may augment current clinical and biopsies evaluation of KS patients.

METHOD AND MATERIALS

In previous work, we confirmed that Tumor-associated Macrophages (TAMs) and KS cells express the macrophage mannose receptor (CD206), which is the receptor target for TCT. Here we present the first results from a Phase I open-label, dose escalation clinical study of TCT imaging in KS patients. Four subjects with biopsy confirmed cutaneous KS lesions (3 HIV+) were administrated 100 µg of tilmanocept radiolabeled with 5 mCi of 99mTc by intravenous injection (IV) followed by planar and SPECT/CT imaging of areas of interest. Images were acquired at 60 to 75 and 150 to 210 minutes post-injection and were visually cross-examined for uptake in cutaneous and presumably subcutaneous lesions.

RESULTS

IV injection of TCT was well-tolerated. No drug-related adverse events were observed. Uptake on SPECT/CT images was observed in cutaneous lesions of the feet and lower legs as well as suspected subcutaneous lesions of the same regions. All SPECT/CT images were compared to the photographs of KS lesions and other targeted areas of the body taken prior TCT administration. Overall, SPECT/CT imaging revealed highly specific TCT localization in the KS-affected area. Some of the results showed presumptive TCT localization in lymphatic vessels along legs.

CONCLUSION

Results suggest that TCT is a valuable immunodiagnostic agent for imaging of cutaneous and presumably subcutaneous KS lesions. The results shows that this method would improve the accuracy of disease staging in KS patients. TCT imaging may also contribute to monitoring the efficacy of KS therapies.

CLINICAL RELEVANCE/APPLICATION

This is a first attempt of merging TCT imaging data of cutaneous and presumably subcutaneous sites of KS-associated lesions in HIV subjects diagnosed with KS-lesions tissues biopsy results obtained from pathology labs and external medical evaluation of the lesions. Currently, TCT is a first highly specific immunodiagnostic agent, which was proven to support KS evaluation without drug-related adverse events.

Honored Educators

Presenters or authors on this event have been recognized as RSNA Honored Educators for participating in multiple qualifying educational activities. Honored Educators are invested in furthering the profession of radiology by delivering high-quality educational content in their field of study. Learn how you can become an honored educator by visiting the website at: https://www.rsna.org/Honored-Educator-Award/ Spencer C. Behr, MD - 2017 Honored Educator

SSK19-07 Impact of Lymph Node Dissection and Surgical Margins on Survival Outcomes for Definitive Local Surgery in the Setting of Stage IV Soft Tissue Sarcoma of the Extremity at Presentation: An NCDB Analysis

Wednesday, Nov. 28 11:30AM - 11:40AM Room: S504AB

Awards

Student Travel Stipend Award

Participants

Mustafa Abugideiri, MD, Atlanta, GA (*Presenter*) Nothing to Disclose Jeffrey Switchenko, PhD, Atlanta, GA (*Abstract Co-Author*) Nothing to Disclose Sibo Tian, New Brunswick, NJ (*Abstract Co-Author*) Nothing to Disclose Nicholas A. Madden, Atlanta, GA (*Abstract Co-Author*) Nothing to Disclose Robert Press, MD, Atlanta, GA (*Abstract Co-Author*) Nothing to Disclose Matthew J. Ferris, Atlanta, GA (*Abstract Co-Author*) Nothing to Disclose Zachary Buchwald, MD, PhD, Atlanta, GA (*Abstract Co-Author*) Nothing to Disclose Jaymin Jhaveri, MD, Atlanta, GA (*Abstract Co-Author*) Nothing to Disclose Jim Zhong, MD, Atlanta, GA (*Abstract Co-Author*) Nothing to Disclose Madhusmita Behera, Atlanta, GA (*Abstract Co-Author*) Nothing to Disclose David Monson, Atlanta, GA (*Abstract Co-Author*) Nothing to Disclose Jolinta Lin, Atlanta, GA (*Abstract Co-Author*) Nothing to Disclose Jerome C. Landry, MD, Atlanta, GA (*Abstract Co-Author*) Nothing to Disclose Karen D. Godette, MD, Atlanta, GA (*Abstract Co-Author*) Nothing to Disclose Pretesh Patel, Atlanta, GA (*Abstract Co-Author*) Nothing to Disclose

PURPOSE

For select patients with stage IV soft tissue sarcoma of the extremity (STSE), definitive surgery to the primary site (SP) is a treatment option as per NCCN and other modalities, such as radiotherapy (R), chemotherapy (C), and metastasectomy (M) can be added to the treatment regimen. We sought to compare the oncologic outcomes of such patients treated with SP in the National Cancer Data Base (NCDB).

METHOD AND MATERIALS

In the NCDB, patients with stage IV STSE who received SP from 2004-2014 with complete treatment records were identified. Survival distributions were estimated using the Kaplan-Meier method and compared using log-rank tests. Covariates were compared using chi-squared tests or ANOVA.

RESULTS

1,291 patients met entry criteria. 5-yr overall survival (OS5) was best for patients treated with metastasectomy (SP+M+/-C+/-R) at 31.4% compared to 20.7% for those treated with other non-surgical adjuvant therapies (SP+C, SP+R, SP+C+R) and 16.2% following SP alone (p<0.0001). Patients with adipocytic tumors had the best OS5 at 29.4% with a median OS of 2.4 years (p=0.0003). On multivariable analysis (MVA), higher Charlson-Deyo score trended with inferior OS (HR 1.20 [95% CI: 0.99-1.45], p=0.07). Patients with well-differentiated tumors had better OS (HR 0.40 [95% CI: 0.17-0.93], p=0.033). 17% of patients had lymph node sampling and this was associated with improved OS (HR 0.75 [95% CI: 0.59-0.94], p=0.014) on MVA. In addition, 27.4% of patients had positive surgical margins, and this was associated with worse OS (HR 1.56 [95% CI: 1.29-1.88], p<0.001). Tumors greater than 10-15cm (HR 1.69 [95% CI: (1.26-2.27) p<0.001) and tumors >15cm (HR 2.04 [95% CI: (1.53-2.73) p<0.001) were predictive for worse OS compared to tumors less than 5cm.

CONCLUSION

In this analysis of a national cancer database, negative surgical margins and lymph node dissection were both associated with prolonged overall survival in patients with stage IV STSE undergoing resection of the primary sarcoma. Metastasectomy was also associated with longer survival is this group. These hypothesis generating data warrant further study.

CLINICAL RELEVANCE/APPLICATION

Surgeons should consider lymph node dissections and re-resections for positive margins in patients with stage IV STSE undergoing resection of the primary sarcoma as both associated with prolonged overall survival. Metastasectomy was also associated with longer survival is this group.

SSK19-08 Radiomic Models of Pathological Markers of Sarcoma, Including Grade and Translocation Status

Wednesday, Nov. 28 11:40AM - 11:50AM Room: S504AB

Awards

Student Travel Stipend Award

Participants

Kevin C. Ball, DO, Milwaukee, WI (*Presenter*) Nothing to Disclose
Matthew B. Spraker, MD, PhD, Saint Louis, MO (*Abstract Co-Author*) Nothing to Disclose
Daniel S. Hippe, MS, Seattle, WA (*Abstract Co-Author*) Research Grant, Koninklijke Philips NV; Research Grant, General Electric
Company; Research Grant, Canon Medical Systems Corporation; Research Grant, Siemens AG
Landon Wootton, PHD, Seattle, WA (*Abstract Co-Author*) Nothing to Disclose
Robert Ricciotti, MD, Seattle, WA (*Abstract Co-Author*) Nothing to Disclose
Jose G. Mantilla, MD, Seattle, WA (*Abstract Co-Author*) Nothing to Disclose
Jan C. Peeken, Munich, Germany (*Abstract Co-Author*) Nothing to Disclose
Stephanie E. Combs, MD, Heidelberg, Germany (*Abstract Co-Author*) Research Grant, Schering-Plough Corporation Advisory Board, Schering-Plough Corporation Speaker, Schering-Plough Corporation
Edward Y. Kim, MD, Seattle, WA (*Abstract Co-Author*) Nothing to Disclose
Matthew J. Nyflot, PhD, Seattle, WA (*Abstract Co-Author*) Nothing to Disclose

PURPOSE

Soft tissue sarcomas (STS) are traditionally classified by tumor grade, and recently more complex pathologic markers such as translocation status have become of interest. Radiographic correlates may help determine tumor grade and detect targetable mutations, and radiomic features have been correlated to pathologic markers in other tumor types. We examined associations between radiomic features extracted from magnetic resonance images (MRI) of sarcoma with tumor grade and translocation status.

METHOD AND MATERIALS

A retrospective analysis of 199 patients (age>14 years) with histology-confirmed STS was performed. 30 radiomic features (histogram, Haralick, neighborhood difference, and zone size features) were extracted from T1-weighted contrast-enhanced MRI in the tumor volume. FNCLCC grade and translocation status were determined by expert pathologist review. Associations between patients who were grade 1+2 vs 3 and patients with translocation vs no translocation with radiomic features were investigated using univariate logistic regression. P-values were adjusted for multiple comparisons via permutation-based stepdown (A=0.05 for each feature).

RESULTS

101 patients (51%) had grade three STS, and 52 patients (26%) had known translocation. Patients with translocated tumors were younger (42 vs 56 years, p<0.001) with lower grade tumors (p<0.001). Before adjustment, 4 variables were associated with translocation status and 14 radiomic variables were associated with tumor grade. After adjustment, no features were significantly associated with translocation status but 3 features retained significant association with tumor grade (variance, odds ratio [OR]: 0.6, p=0.045; dissimilarity, OR: 0.6, p=0.002; and contrast OR: 0.6, p=0.035).

CONCLUSION

These results suggest translocation-driven STS occur more frequently in younger individuals and are associated with lower grade tumors. Radiomic features examined were not associated with translocation status but were significantly associated with FNCLCC tumor grading of STS. The results suggest radiomic-pathologic models might provide value for patient management in sarcoma in the future.

CLINICAL RELEVANCE/APPLICATION

Radiomic analysis of conventional imaging modalities may elucidate noninvasive sarcoma biomarkers that complement current classification systems.

SSK19-09 A Radiomics Model for Preoperative Metastasis Prediction for Soft-Tissue Sarcomas

Wednesday, Nov. 28 11:50AM - 12:00PM Room: S504AB

Participants

Wenzhe Zhao, Xian, China (*Presenter*) Nothing to Disclose Xin Huang, Xian, China (*Abstract Co-Author*) Nothing to Disclose Yiming Wang, Xi an, China (*Abstract Co-Author*) Nothing to Disclose Wang Yuan, Shaanxi, China (*Abstract Co-Author*) Nothing to Disclose Jianxin Guo, Xian, China (*Abstract Co-Author*) Nothing to Disclose Jian Yang, Xian, China (*Abstract Co-Author*) Nothing to Disclose

PURPOSE

To develop and validate a radiomics model based on multimodality images (PET, CT, T1-weighted and T2-weighted MRI) for the early evaluation of the metastasis risk in patients with soft-tissue sarcomas (STSs).

METHOD AND MATERIALS

In this retrospective study, a total of 51 patients with histologically confirmed STSs and clinically followed up for the metastasis were enrolled. Among the 51 patients, 35 were selected randomly as the primary cohort to build the prediction model, while the remaining 16 patients were used to test the prediction power of model. A total of 474 radiomics features were extracted from the single modality image for each patient. Feature selection was performed in 3 steps using Mann-Whitney U test, intra-class Spearman Rank Correlation test and Least absolute shrinkage and selection operator (LASSO) regression. Radiomics signature was developed based on each single modality images or their combinations. Delong test was used to detect the difference levels between the different radiomics signatures. The performance was assessed in discrimination of area under the curve (AUC) and clinical utility using 4-fold cross-validation.

RESULTS

The AUC for radiomics signatures in the primary cohort based on CT, T1-weighted MRI, T2-weighted MRI and PET individually was 0.71, 0.70, 0.80 and 0.73, respectively. In contrast, the AUC for the validation cohort based on CT, T1-weighted MRI, T2-weighted MRI and PET individually was 0.75, 0.82, 0.83 and 0.73, respectively. The combination of the radiomics signatures from CT, T2-weighted MRI and PET images improved AUC, with the optimal performance reached AUC of 0.87 for the training cohort, as well as 0.88 for the validation cohort. Besides, P<0.05 from Delong test showed significant differences between the combination of CT, MRI and PET and others. In addition, decision curve analysis confirmed the clinical usefulness of the multimodality model.

CONCLUSION

A radiomics model, based on CT, T2-weighted MRI and PET images improves the accuracy for the early evaluation of the metastasis risk in patients with STSs.

CLINICAL RELEVANCE/APPLICATION

The non-invasive radiomics model combining CT, T2-weighted MRI and PET images could be used to predict metastasis risk in patients with STSs.



SSK20

Vascular Interventional (Ablation)

Wednesday, Nov. 28 10:30AM - 12:00PM Room: E353A



AMA PRA Category 1 Credits ™: 1.50 ARRT Category A+ Credit: 1.75

FDA Discussions may include off-label uses.

Participants

D. T. Johnson, MD, PhD, South San Francisco, CA (*Moderator*) Speaker, Surefire Medical, Inc; Consultant, Surefire Medical, Inc; Advisory Board, Bristol-Myers Squibb Company; Speaker, BTG International Ltd; Advisory Board, Boston Scientific Corporation; Advisory Board, Merck & Co, Inc; Advisory Board, Dova Pharmaceuticals

Sub-Events

SSK20-01 MIRA Study: Microwave versus Radiofrequency Ablation of Hepatocellular Carcinoma - A Randomized Trial

Participants

Thomas J. Vogl, MD, PhD, Frankfurt, Germany (*Presenter*) Nothing to Disclose Lena-Maria Klohmann, Frankfurt, Germany (*Abstract Co-Author*) Nothing to Disclose Tatjana Gruber-Rouh, Frankfurt Am Main, Germany (*Abstract Co-Author*) Nothing to Disclose Renate M. Hammerstingl, MD, Frankfurt Am Main, Germany (*Abstract Co-Author*) Nothing to Disclose Yousef Jaraysa, Frankfurt, Germany (*Abstract Co-Author*) Nothing to Disclose Nour-Eldin A. Nour-Eldin, MD, PhD, Frankfurt Am Main, Germany (*Abstract Co-Author*) Nothing to Disclose

For information about this presentation, contact:

T.Vogl@em.uni-frankfurt.de

PURPOSE

To prospectively determine and compare therapy response and safety of microwave (MWA) ablation and radiofrequency ablation (RFA) of hepatocellular carcinoma (HCC) in a randomized trial.

METHOD AND MATERIALS

In this prospective study 50 patients (39 males/11 females; mean 64 years; range 42-82; SD 9.98) underwent CT-guided thermal ablation: 25 received RFA and 25 MWA. Using MRI the location of the HCC and changes in size, volume, necrotic area, diffusion and ADC value in the malignant tissue were evaluated. First MRI control took place before treatment with thermal ablation. The follow-up contained MRI controls 24 hours after ablation and then within 12 months in 3-month intervals.

RESULTS

50 HCC lesions with a mean diameter of 2.05 cm (range 0.62-5 cm: MWA 2.22 cm, RFA 1.84 cm) were treated with thermal ablation. The mean volume 24 hours after ablation was 49.2 cm3: 69.9 cm3 for MWA and 28.3 cm3 for RFA. Complete ablation was recorded in 94.0% (47/50): 100% (18/18) in the MWA group and 88.0% (22/25) in the RFA group. Local recurrence rate wihtin one year for both groups was 6.0% (3/50) and local recurrences were only documented in the RFA group. The recurrence rate for new malignant formations occurred at the control MRI 6 months after the ablation. 12.0% (6/50) of the patients underwent thermal ablation before taking part in this trial, 14% (7/50) again recieved a treatment with thermal ablation in other segments of the liver while being part of this trial. The mortality rate for this trial amounted to 8% (4/50): 4% (1/25) for the MWA group and 12% (3/25) for the RFA group. The survival rate after one year for both groups ws 92%: 96% for the MWA group and 88% for the RFA group. Major complications were not noticed.

CONCLUSION

The first data of the MIRA trial document no significant differences in mortality or complication rates between RFA and MWA. The study shows that thermal treatment with MWA generates greater ablation volumes. 1-year follow-up of the MWA group shows a lower rate of local recurrences and the 1-year survival rate is a little higher.

CLINICAL RELEVANCE/APPLICATION

MWA provdes greater ablation volume versus RFA with a lower rate of local recurrences.

SSK20-02 MR-Guided High Intensity Focused Ultrasound (MRgFUS) For the Treatment of Oligometastatic Prostate Cancer Bone Metastasis: Can Sound Waves Downstage Cancer Spread?

Wednesday, Nov. 28 10:40AM - 10:50AM Room: E353A

Awards Student Travel Stipend Award

Participants

Andrea Leonardi, MD, Roma, Italy (*Abstract Co-Author*) Nothing to Disclose Alessandro Napoli, MD, Rome, Italy (*Abstract Co-Author*) Nothing to Disclose Fabrizio Andrani, MD, Roma, Italy (*Presenter*) Nothing to Disclose Roberto Scipione, MD, Rome, Italy (*Abstract Co-Author*) Nothing to Disclose Hans Peter Erasmus, Rome, Italy (*Abstract Co-Author*) Nothing to Disclose Carlo Catalano, MD, Rome, Italy (*Abstract Co-Author*) Nothing to Disclose Carola Palla, MD, Rome, Italy (*Abstract Co-Author*) Nothing to Disclose

For information about this presentation, contact:

andrea.leonardi1988@gmail.com

PURPOSE

With improvements in diagnostic modalities such as functional imaging, oligometastatic prostate cancer is being diagnosed with greater frequency than ever before. Our aim was to determine MRgFUS ability to downstage patients with oligometastatic bone disease with single session of non-invasive metastasis-directed therapy.

METHOD AND MATERIALS

The study was designed with intention-to-treat metastatic bone lesions. Patients were enrolled if they had accessible bone metastasis and could safely undergo MRgFUS (InSightec, Israel). Baseline measurable characteristics included dynamic contrast enhanced MRI study (Gd-BOPTA, Bracco; GE 750 3T magnet) with semiquantitative perfusion analysis, PSA level (ng/ml) and choline PET (SUV). Measurable variables were obtained at treatment time, 3 months, 12 months, 24 and 36 months follow-up.

RESULTS

23 patients fulfilled the inclusion criteria and safely underwent MRgFUS procedure of metastatic bone ablations. Lesions were located in the pelvis (13), scapula (4) and long bones (6). At baseline all lesions showed a significant DCE perfusion (highly vascular) with mean perfusion reduction of 88% at 3 months follow-up (CI: 100-50; p<0.001) stable at subsequent follow-up scans. Similarly PSA levels decreased from a mean baseline of 19 (ng/ml) to 7.1, 2.9, 2.1 and 1.9, at 3-12-24 and 36 months respectively. SUV values showed similar trend with reduction from baseline (mean 8.9 to 3.0, 2.3, 1.7 and 1.3: p<0.001). In all patients single MRgFUS session was appropriate without any major or minor adverse events reported.

CONCLUSION

MRgFUS is a totally non-invasive procedure that can obtain nearly complete bone ablation in patients with oligometastatic prostate disease. The technique features a radiation-free approach that can be of incremental value in long-survivor subset on oncological patients, significantly reducing risk of toxic effects.

CLINICAL RELEVANCE/APPLICATION

MRgFUS could be routinely introduced as a treatment option for oligometastatic bone disease non responding to conventional treatment.

SSK20-03 Modified ABLATE-Score (mABLATE): A Specific Nephrometric Score to Predict Complications and Relapses in Percutaneous Cryoablation of Renal Lesions

Wednesday, Nov. 28 10:50AM - 11:00AM Room: E353A

Participants

Maurizio Papa, MD, Milan, Italy (*Presenter*) Nothing to Disclose Andrea Losa, MD, Milano, Italy (*Abstract Co-Author*) Nothing to Disclose Nazareno Suardi, Milan, Italy (*Abstract Co-Author*) Nothing to Disclose Giulia Agostini, Milan, Italy (*Abstract Co-Author*) Nothing to Disclose Fraco Gaboardi, MD, Milan, Italy (*Abstract Co-Author*) Nothing to Disclose Gianpiero Cardone, MD, Milano, Italy (*Abstract Co-Author*) Nothing to Disclose

For information about this presentation, contact:

papa.maurizio@hsr.it

PURPOSE

RENAL ed mRENAL scores have been validated on predicting adverse events and relapses in percutaneous treatments of renal lesions. However these scores remain of surgical origin. The aim of this work is to obtain a specific score (mABLATE) to quantify the risk of complications and relapses in percutaneous kidney ablation procedures

METHOD AND MATERIALS

Taking inspiration from the paper 'AJR 2014;202:894-903' with some changes based on our practical experience, a score was built trying to take into account the real difficulties faced in percutaneous treatment of renal lesions(Fig.1) .The mABLATE was retrospectively assessed on 60 cryoablations to evaluate its predictive value for complications (all procedures) and relapses (malign histology). Logistic regression was used to predict complication incidence;Cox regression was used for relapses;ROC analysis was used to evaluate the accuracy of the three different scores

RESULTS

Among 60 renal lesions treated with cryoablation technique we experienced 3 bleedings with anemia(5%), 2 of them treated with angiographic embolization(3%). Among 51 lesions with malignant histology (MH) we experienced 7 relapeses(13.7%) between 2 and 17 months from treatment, with a mean FU of 19,3 months. Mean MH RENAL score: 7.2pts. Mean relapsed RENAL score: 7.71pts. Mean MH mRENAL score: 7.26. Mean relapsed mRENAL score: 8pts. Mean MH mABLATE score: 4.98. Mean relapsed mABLATE score: 8.07pts. The Cox regression analysis for Renal (p=0.35) and mRENAL (p=0.29) showed a lack of predictive value for relapses.On the contrary the mABLATE score was found to be an independent predictor of relapses(HR 1,56; p=0,001).The predictive accuracy based on the ROC analysis of the mABLATE showed an AUC of 89.1%(vs 61,5% for mRENAL and 58,8% for RENAL).In the logistic regression analysis none of the three scores showed statistic significance in predicting complications(p>0.05),likely due to the small number of adverse events

CONCLUSION

The mABLATE score showed to be a better predictor of relapses than RENAL and mRENAL. All three scores showed a lack of statistic significance in predicting complications likely conditioned by the small number of complications occurred in our population.

CLINICAL RELEVANCE/APPLICATION

At the moment surgical (RENAL) or surgical modified (mRENAL) scores are used to quantify risks in percutaneous kidney ablations; a specific score (mABLATE) better performs in this task.

SSK20-04 Image-Guided Radiofrequency Hyperthermia-Enhanced Local Chemotherapy of Hepatic Tumors: The Underlying Molecular Mechanisms

Wednesday, Nov. 28 11:00AM - 11:10AM Room: E353A

Participants

Kun Qian, Wuhan, China (*Presenter*) Nothing to Disclose Feng Zhang, MD, Seattle, WA (*Abstract Co-Author*) Nothing to Disclose Minjiang Chen, Seattle, WA (*Abstract Co-Author*) Nothing to Disclose Yiming Zhou, Seattle, WA (*Abstract Co-Author*) Nothing to Disclose Qiaoyou Weng, Seattle, WA (*Abstract Co-Author*) Nothing to Disclose Qiang Li, Seattle, WA (*Abstract Co-Author*) Nothing to Disclose Peicheng Li, MD, Seattle, WA (*Abstract Co-Author*) Nothing to Disclose Chuansheng Zheng, Wuhan, China (*Abstract Co-Author*) Nothing to Disclose Xiaoming Yang, MD, PhD, Mercer Island, WA (*Abstract Co-Author*) Nothing to Disclose

For information about this presentation, contact:

kunchien@uw.edu

PURPOSE

To investigate the treatment effects and mechanisms of image-guided radiofrequency hyperthermia (RHF)-enhanced interventional chemotherapy of hepatic tumors.

METHOD AND MATERIALS

This study included two portions: (1) in-vitro experiments with VX2 tumor cell lines for establishing 'proof-of-principle' of the innovative concept; and (2) in-vivo experiment using rabbit models with orthotopic hepatic VX2 tumors to validate the feasibility of the new interventional technique. VX2 cell lines and animals were randomly assigned to four treatment groups (n=6/group): (i) combination therapy with 5- μ M Doxorubicin plus RFH; (ii) Doxorubicin-only; (iii) RFH-only; and (iv) saline. Viability and doxorubicin uptake and distribution, as well as proliferation rate of VX2 cells, were evaluated using flow cytometer, fluorescence microscopy, and MTS assay, while potential molecular mechanism via the heat shock protein (HSP70) pathway was investigated using western blot and immunohistochemistry.

RESULTS

Of in-vitro experiments, microscopy showed an increased doxorubicin concentration in tumor cells, which correlated to significantly higher HSP70 expression in combination therapy (1.28 ± 0.13), compared to other control treatments (0.15 ± 0.03 , 0.64 ± 0.13 , 0.83 ± 0.10 , p<0.05). Of in-vivo experiments, immunohistochemistry staining demonstrated a significant increase of HSP 70-positive signaling (1.47 ± 0.13) in combination therapy, compared to the control treatments, as verified in western blot analysis as well (0.16 ± 0.04 , 0.51 ± 0.13 , 0.74 ± 0.11 , p<0.01). In addition, a significant increase of tumor apoptosis and necrosis was found in combination therapy in comparison to other controls with Ki-67 and TUNEL staining (p < .001).

CONCLUSION

Image-guided interventional RFH-enhanced local chemotherapy can effectively eradicate hepatic tumors, via the molecular mechanisms of activating HSP70 pathway, as well as enhancing the doxorubicin penetration and tumor apoptosis, which thus inhibits tumor growth and prevents tumor metastasis efficiently. This technical development may open the new avenues for effective treatment of malignancies, not only in the liver but also in other solid organs through the integration of image-guided interventional oncology, RF technology, and direct intratumoral therapies.

CLINICAL RELEVANCE/APPLICATION

An underlying way and its mechanisms to enhanced doxorubicin effects in tumor margin after RFA.

SSK20-05 Early Assessment of Post-Radiofrequency Ablation with CT Perfusion Imaging in Rabbit VX2 Liver Tumor

Wednesday, Nov. 28 11:10AM - 11:20AM Room: E353A

Participants Li Qian, MD, Wuhan, China (*Presenter*) Nothing to Disclose Ping Han, MD, Wuhan, China (*Abstract Co-Author*) Nothing to Disclose

For information about this presentation, contact:

lipb37@163.com

PURPOSE

To evaluate the diagnostic potential of CT perfusion, and assess the characteristics of the quantitative parameters for discriminating the residual/recurrent tumors from the benign periablational enhancement (BPE) after radiofrequency ablation (RFA) in the rabbits liver VX2 tumor models, with pathological results as the standard.

METHOD AND MATERIALS

This protocol was approved by the Institutional Animal Care and Use Committee at our institution. Twenty eight V/V2 tumer were

Inis protocol was approved by the institutional Annual Care and use Connictee at our institution. Twenty-eight VA2 tunor were implanted into the livers of 28 rabbits by the laparotomy method, then were treated with RFA while confirmed the existence of tumors by enhanced CT. On days 1, 3, 7, 14 after RFA, seven animals were randomly chosen for CT perfusion. Pathology exam was performed immediately after the completion of post-RFA CT perfusion. The perfusion parameters were observed both in BPE and residual/recurrent tumors, including blood flow (BF), blood volume (BV), time to peak (TTP), permeability (P), hepatic arterial perfusion (ALP), portal vein perfusion (PVP) and hepatic perfusion index (HPI), along with the profile of time-density curves (TDCs) and pseudo-color images of parameters, and compared with the pathology results.

RESULTS

26/28 rabbits successfully underwent CT perfusion while 6/26 lesions were confirmed to be residual/recurrent tumors. The TDCs of BPE were mainly speed-up curves(15/26), whereas were speed-up-speed-down (3/6) and speed-up-platforms (2/6) types in residual/recurrent tumors. The PVP values of BPE were significantly higher than residual/recurrent tumors in all the different time groups, and the HPI values were significantly lower in BPE than in residual/recurrent tumors (P < 0.01). These characteristics of CT perfusion parameters were consistent with the pathological changes.

CONCLUSION

The TDCs and PVP and HPI parameters have the potential to indicate BPE and residual/recurrent tumors effectively in the early postoperative RFA treatment. Thus it can be seen that CT perfusion has more advantages, with greater efficacy in monitoring therapeutic effect response early after RFA treatment.

CLINICAL RELEVANCE/APPLICATION

To evaluate the diagnostic potential of CTP as an appropriate and timely postoperative radiographic evaluation in monitoring RFA efficacy

SSK20-06 TACE plus RFA versus Surgical Resection for Single 3 to 5 Cm HCC: Propensity Score Matching Analysis

Wednesday, Nov. 28 11:20AM - 11:30AM Room: E353A

Participants

Hyo-Jae Lee, Gwangju, Korea, Republic Of (*Abstract Co-Author*) Nothing to Disclose Jin Woong Kim, MD, Gwangju, Korea, Republic Of (*Presenter*) Nothing to Disclose Hyung Joong Kim, MD,PhD, Seoul, Korea, Republic Of (*Abstract Co-Author*) Nothing to Disclose Young Hoe Hur, Jeollanam-Do, Korea, Republic Of (*Abstract Co-Author*) Nothing to Disclose Eun Ju Yoon, Kwangju, Korea, Republic Of (*Abstract Co-Author*) Nothing to Disclose Eunsol Im, Gwangju, Korea, Republic Of (*Abstract Co-Author*) Nothing to Disclose Jong Eun Lee, Gwangju, Korea, Republic Of (*Abstract Co-Author*) Nothing to Disclose Seul Gi Choi, Gwangju, Korea, Republic Of (*Abstract Co-Author*) Nothing to Disclose

For information about this presentation, contact:

jw4249@hanmail.net

PURPOSE

To compare long-term therapeutic outcome for single nodular 3-5 cm HCC between transcatheter arterial chemoembolization with radiofrequency ablation (TACE+RFA) and surgical resection (SR).

METHOD AND MATERIALS

139 patients treated with SR and 60 patients treated with TACE+RFA were enrolled. Long term therapeutic outcomes including local tumor progression (LTP), intrahepatic distant recurrence (IDR), disease-free survival (DFS), and overall survival (OS) rates were evaluated between two groups before and after propensity-score matching. Major complications and length of hospital stay were also investigated.

RESULTS

1-, 3-, and 5-year LTP rates were 1.8%, 3.9%, and 8.1% in TACE+RFA and 4.3%, 8.1%, and 9.3% in SR, respectively (P = .444). 1-, 3-, and 5-year IDR rates were 6.7%, 31.7%, and 41.6% in TACE+RFA and 14.4%, 38.0%, and 51.3% in SR, respectively (P = .188). 1-, 3-, and 5-year DFS rates were 88.1%, 65.3%, and 49.0% in TACE+RFA and 84.2%, 58.2%, and 46.5% in SR, respectively (P = .446). 1-, 3-, and 5-year OS rates were 95.0%, 73.5%, and 54.0% in TACE+RFA and 97.1%, 87.4%, and 75.0% in SR, respectively (P = .055). After matching (n = 52), there was no difference in therapeutic outcomes between groups (P = .349, P = .127, P = .253, P = .878, respectively). SR showed higher complication rates and significant longer hospital stay than TACE+RFA (P = .015 and P < .001).

CONCLUSION

TACE+RFA may be a feasible treatment for single 3-5 cm HCC with comparable therapeutic outcomes with SR and more efficiency in terms of hospital stay.

CLINICAL RELEVANCE/APPLICATION

Before and after matching, there were no significant differences in long-term therapeutic outcomes between TACE plus RFA and SR groups. Therefore, TACE plus RFA may be an alternative treatment for single 3-5 cm HCCs with an expectation of similar outcomes.

SSK20-07 Outcomes of Thermal Ablation versus Surgery for Hepatocellular Carcinoma

Wednesday, Nov. 28 11:30AM - 11:40AM Room: E353A

Participants

Johannes Uhlig, Goettingen, Germany (*Presenter*) Nothing to Disclose Cortlandt Sellers, New Haven, CT (*Abstract Co-Author*) Nothing to Disclose Tamar Taddei, MD, New Haven, CT (*Abstract Co-Author*) Nothing to Disclose Stacey M. Stein, MD, New Haven, CT (*Abstract Co-Author*) Nothing to Disclose

Hyun S. Kim, MD, New Haven, CT (Abstract Co-Author) Nothing to Disclose

For information about this presentation, contact:

johannes.uhlig@med.uni-goettingen.de

PURPOSE

To compare outcomes of radiofrequency ablation (RFA) and cryoablation (CRA) versus surgical resection for hepatocellular cancer (HCC).

METHOD AND MATERIALS

The National Cancer Database was analyzed for HCC diagnosed from 2004-2015. Patients treated with thermal ablation, comprising RFA and CRA, or surgical wedge/segmental resection were included. Exclusion criteria were radiotherapy, age <18, and unknown survival status. Patients were 1:1 propensity score matched to account for confounders. In the matched cohort, duration of hospital stay, 30d unplanned hospital readmission, 30d/90d survival and 3-month postoperative overall survival were compared.

RESULTS

The study included 17,091 patients; 10,092 received RFA (59%), 243 CRA (1.4%) and 6,756 surgery (39.6%). Caucasian race, Medicare insurance, higher income, higher comorbidity indices, lower tumor stage, and treatment at academic centers were associated with an increased likelihood of thermal ablation. The matched cohort comprised 6,212 patients, 3,106 treated with thermal ablation and 3,106 with surgery, and demonstrated a balanced distribution of confounders. In the matched cohort, postoperative outcomes were superior for thermal ablation: hospital stay was short (mean 2.5d vs. 67d, p<0.001) and unplanned readmission low (2.9% vs. 4.9%, p=0.006). Mortality (30d/ 90d) was lower for thermal ablation (0% vs. 3.8%; 0% vs. 7.5%; each p<0.001). Three-month postoperative survival was superior for thermal ablation versus surgery (HR=0.75, 95% CI: 0.61-0.91, p=0.003). No significant difference was evident comparing postoperative outcomes of RFA to CRA (mean hospital stay 2.5d vs. 2.3d, p=0.96; unplanned hospital readmission rate 2.6% vs. 2.7%, p=1; 3 month postoperative survival HR= 1.41, 95% CI: 0.58 -3.5, p=0.466).

CONCLUSION

Thermal ablation provides superior short-term outcomes to surgical resection of HCC with shorter hospital stay, lower unplanned readmission rates, and superior 3-month postoperative survival. Prospective randomized trials contrasting both modalities are warranted to assess whether this advantage translates into comparable long-term survival.

CLINICAL RELEVANCE/APPLICATION

For treatment of HCC, thermal ablation provides superior short-term outcomes compared to surgical resection, including shorter hospital stay, fewer readmissions and improved 3-month overall survival.

SSK20-08 Combined Local Thermal Ablation and Chemoembolization in Irresectable or Recurrent Intrahepatic Cholangiocarcinoma, Impact on Local Tumor Control and Overall Survival

Wednesday, Nov. 28 11:40AM - 11:50AM Room: E353A

Participants

Elsayed M. Elhawash, BMedSc,MS, Frankfurt Am Main, Germany (*Presenter*) Nothing to Disclose Nour-Eldin A. Nour-Eldin, MD,PhD, Frankfurt Am Main, Germany (*Abstract Co-Author*) Nothing to Disclose Thomas J. Vogl, MD, PhD, Frankfurt, Germany (*Abstract Co-Author*) Nothing to Disclose Nagy N. Naguib, MD, MSc, Frankfurt Am Main, Germany (*Abstract Co-Author*) Nothing to Disclose Sherif E. Hegab, MD, Alexandria, Egypt (*Abstract Co-Author*) Nothing to Disclose Amr Abdel-Kerim I, PhD,MSc, Alexandria, Egypt (*Abstract Co-Author*) Nothing to Disclose Adel Ramadan, MD, Alexandria, Egypt (*Abstract Co-Author*) Nothing to Disclose Leona Alizadeh, Frankfurt, Germany (*Abstract Co-Author*) Nothing to Disclose Annette Zinn I, Frankfurt, Germany (*Abstract Co-Author*) Nothing to Disclose Tatjana Gruber-Rouh, Frankfurt Am Main, Germany (*Abstract Co-Author*) Nothing to Disclose

For information about this presentation, contact:

elsayedelhawash@yahoo.com

PURPOSE

To retrospectively evaluate the combined role of local thermal ablation and transarterial-chemoembolization in cases of irresectable or recurrent intrahepatic choloangiocarcinoma.

METHOD AND MATERIALS

Retrospective analysis for 30 patients with CCC from Januar 2007 till December 2017, in which 11 males (36.7 %) and 19 (63.3 %) females with mean age 59.2 years (25-86) with either irresectable (20/30, 66.66%) or recurrent lesions (10/30, 33.33%) managed by at least three sessions of TACE (3-26, mean 9) with local thermal ablation for overall 65 lesions with mean size 21 mm (10-74) with either laser (4/65, 6.2%), radiofrequency (8/65, 12.3%) or microwave (53/65, 81.5%) devices, with mean ablation time (8 minutes /1-27 min.) and mean Watt 640 (45-2095) at mean treatment duration 17.5 months (2-88 months). Follow up using CEMRI to evaluate local tumor control based on modified Response Evaluation Criteria for Solid Tumors (mRECIST) and the survival was evaluated using Kaplan-Meier method.

RESULTS

The mean survival was 33.4 months (CI: 22.7-44.2). The initial local tumor response following 3 TACE was 10% stable (SD), 80% partial response (PR), 10 % progressive (LR) and 0% complete remission (CR). The final effect was 13.3% SD, 16.7% PR, 63.3% LR and 6.7% CR. Local lesion response following thermal ablation was either complete resolution of the targeted lesion in 39/65 lesions (60%) or incomplete response at 26/65 (40%). Two patients (2/30 = 6.6%) developed local non-life threating complications following thermal ablation. Significant correlation has been found between the size of the targeted lesion and the response with better results at diameter ranging from 10-50 mm. However no significant correlation was found between the device type or the amount of watt used and the ablation outcome.

CONCLUSION

Combined targeted local liver therapy has a potentiality to provide a therapeutic option for irresectable or recurrent cholangiocarcinoma and may affect the overall patients' survival as well with better local results for smaller ablated lesions.

CLINICAL RELEVANCE/APPLICATION

Combined TACE and local Ablation therapy of irresectable or recurrent CCC provide the potentiality for local tumor control and improvement of survival rates.

SSK20-09 MRI-Guided High Intensity Focused Ultrasound in the Treatment of Osteoid Osteoma: Long-Term Outcomes

Wednesday, Nov. 28 11:50AM - 12:00PM Room: E353A

Awards

Student Travel Stipend Award

Participants

Fabrizio Andrani, MD, Roma, Italy (*Presenter*) Nothing to Disclose Alessandro Napoli, MD, Rome, Italy (*Abstract Co-Author*) Nothing to Disclose Roberto Scipione, MD, Rome, Italy (*Abstract Co-Author*) Nothing to Disclose Carola Palla, MD, Rome, Italy (*Abstract Co-Author*) Nothing to Disclose Hans Peter Erasmus, Rome, Italy (*Abstract Co-Author*) Nothing to Disclose Carlo Catalano, MD, Rome, Italy (*Abstract Co-Author*) Nothing to Disclose Andrea Leonardi, MD, Roma, Italy (*Abstract Co-Author*) Nothing to Disclose

PURPOSE

To evaluate clinical and radiological long-term outcomes after non-invasive radiation-free ablation of osteoid osteoma with MRIguided high intensity focused ultrasound (MRgFUS).

METHOD AND MATERIALS

50 patients with clinical and radiological diagnosis of osteoid osteoma eligible for MRgFUS and anaesthesia, were enrolled in this dual-centre prospective observational study. Osteoid osteomas with vertebral location were excluded as considered inaccessible. MrgFUS was performed using InSightec ExAblate 2100 system. Safety, clinical effectiveness and durability of treatment were evaluated in terms of rate of complications, Visual Analogue Scale (VAS) pain score reduction and stability of results over time, respectively. Tumour control (nidus ablation) at dynamic contrast enhanced MR imaging (Discovery 750, GE; Gd-BOPTA, Bracco) was considered as secondary outcome. All patients underwent a minimum follow-up period of 5 years.

RESULTS

Out of 55 subjects screened for recruitment, 50 were eligible to treatment and underwent to MRgFUS. A complete and durable response was achieved in 80% of cases at 5-years follow-up. Median VAS pain score dropped from 8 (IQR 7-9) to 0 at 1-week, and at all subsequent follow-up check points (1 month, 1 and 5 years). Also scores evaluating interference of pain with sleep, physical and daily activities showed similar improvement after treatment. Among subjects with partial response (20%), 5 received a second treatment (3 with CT-guided Radiofrequency Ablation, 2 with MRgFUS), and 5 did not need any other treatment. All re-treated patients achieved 0 VAS score. Overall, 87% of patients after MRgFUS treatment reached and maintained a stable 0 VAS score during follow-up. At 5-year MRI osteoid osteoma showed no vascularization in 36/47 patients (77%) treated with MRgFUS alone.

CONCLUSION

MRgFUS is a safe, effective and durable option in the treatment of non-spinal osteoid osteoma.

CLINICAL RELEVANCE/APPLICATION

This technique provides relevant advantages in the treatment of this impairing disease affecting mostly young population: no ionizing radiation, no incisions or needles, and, so far, no complications. Our results demonstrate the clinical and radiological long-term resolution of MRgFUS which should be the first-line treatment option for accessible osteoid osteoma.



MSRT43

ASRT@RSNA 2018: Radiologist Assistants-Who We Are and How We Can Help

Wednesday, Nov. 28 10:40AM - 11:40AM Room: N230B

от

AMA PRA Category 1 Credit ™: 1.00 ARRT Category A+ Credit: 1.00

Participants

Joann T. Yokley, RRA,BS, Greensboro, NC (*Presenter*) Nothing to Disclose Vicki Sanders, Wichita Falls, TX (*Presenter*) Nothing to Disclose Travis N. Prowant, MS, RT, Richmond, VA (*Presenter*) Nothing to Disclose Wesley Shay, New York, NY (*Presenter*) Nothing to Disclose Paige Mebus, New York, NY (*Presenter*) Nothing to Disclose

For information about this presentation, contact:

mebusp@mskcc.org

LEARNING OBJECTIVES

1) Describe RA education and clinical training. 2) Identify issues with legislation, reimbursement, and supervision. 3) Identify beneficial use of RA in a variety of fluoroscopy exams, interventional procedures, interventional radiology clinic, and breast imaging centers. 4) Explain how the RA is used to enhance overall patient care, provide continuity of care, and maximize efficiency. 5) Show the satisfaction current radiologists have when employing radiologist assistants.

ABSTRACT

As radiologic technologists with advanced training in radiological procedures, image assessment, patient management and assessment, Radiologist Assistants (RAs) are physician extenders specifically designed for the medical imaging environment. RAs practice under the supervision of the radiologist: to perform non-invasive and invasive medical imaging procedures; evaluate, manage, and educate patients; communicate radiologist findings with other members of the healthcare team; and act as patient navigators for the imaging department. Due to RAs' specialized education and training, they maximize efficiency and workflow, provide quality patient care, and maintain high standards of radiation safety.



RCA43

Image to 3D Prints: How 3D Printing Works (Hands-on)

Wednesday, Nov. 28 12:30PM - 2:00PM Room: S401AB

IN

AMA PRA Category 1 Credits ™: 1.50 ARRT Category A+ Credit: 1.75

Participants

Beth A. Ripley, MD, PhD, Seattle, WA (*Presenter*) Nothing to Disclose Tatiana Kelil, MD, San Francisco, CA (*Presenter*) Nothing to Disclose Dmitry Levin, Seattle, WA (*Presenter*) Nothing to Disclose Anish Ghodadra, MD, New Haven, CT (*Presenter*) Advisory Board, axial3D Limited

For information about this presentation, contact:

beth.ripley2@va.gov

LEARNING OBJECTIVES

1) Describe optimal CT and MRI protocols for 3D printing. 2) Explain basic software requirements for converting DICOM images to 3D-printable .STL (standard tessellation language) files. 3) Recognize some common 3D printing artifacts. 4) Apply basic 3D printed model post-processing techniques learned during the session, including UV curing and support material removal.

Honored Educators

Presenters or authors on this event have been recognized as RSNA Honored Educators for participating in multiple qualifying educational activities. Honored Educators are invested in furthering the profession of radiology by delivering high-quality educational content in their field of study. Learn how you can become an honored educator by visiting the website at: https://www.rsna.org/Honored-Educator-Award/ Tatiana Kelil, MD - 2017 Honored Educator



RCC43

AI, Radiomics, Text Mining, and More: 2018's Key Advances in Imaging Informatics

Wednesday, Nov. 28 12:30PM - 2:00PM Room: S501ABC



AMA PRA Category 1 Credits ™: 1.50 ARRT Category A+ Credit: 1.75

Participants

Charles E. Kahn JR, MD, Philadelphia, PA (*Moderator*) Nothing to Disclose Charles E. Kahn JR, MD, Philadelphia, PA (*Presenter*) Nothing to Disclose William Hsu, PhD, Los Angeles, CA (*Presenter*) Research Grant, Siemens AG

For information about this presentation, contact:

ckahn@upenn.edu

LEARNING OBJECTIVES

1) Identify the year's most important advances in imaging informatics. 2) Describe the ways in which Artificial Intelligence (AI) and machine learning are impacting radiology. 3) Define how radiomics, radiogenomics, and 'big data' have added to our knowledge of radiology.

ABSTRACT

The field of imaging informatics continues to advance rapidly. Machine learning, a form of artificial intelligence (AI), has improved the ability to detect image features, make diagnoses, and assess prognosis from image data. Radiomics - which generates highdimensionality datasets from radiology images - provides insights to support precision medicine. Novel approaches have improved sharing of images and image-derived findings with patients and clinicians. Current research efforts go beyond pixel data to integrate imaging with other biomedical data, standardize imaging workflows, and improve the quality and utility of image-derived information in clinical practice. This session reviews key advances in imaging informatics research published this past year.

Honored Educators

Presenters or authors on this event have been recognized as RSNA Honored Educators for participating in multiple qualifying educational activities. Honored Educators are invested in furthering the profession of radiology by delivering high-quality educational content in their field of study. Learn how you can become an honored educator by visiting the website at: https://www.rsna.org/Honored-Educator-Award/ Charles E. Kahn JR, MD - 2012 Honored EducatorCharles E. Kahn JR, MD - 2018 Honored Educator



MSRT44

ASRT@RSNA 2018: Hindsight is 20/20 - The Earliest Appearance of Breast Cancer

Wednesday, Nov. 28 1:00PM - 2:00PM Room: N230B



AMA PRA Category 1 Credit [™]: 1.00 ARRT Category A+ Credit: 1.00

Participants

Rita Gidwaney, MD, San Rafael, CA (Presenter) Nothing to Disclose

LEARNING OBJECTIVES

1) To review some of the key imaging features on mammography, tomosynthesis, ultrasound and MRI of detecting early breast cancer. 2) To review common pitfalls in breast imaging and how to avoid them in the future. 3) To be better equipped at handling such hindsight wisdom cases in your own practice.

ABSTRACT

This session will review how our advanced technology can help us detect the earliest signs of breast cancer, using mammography, tomosynthesis, ultrasound and MRI, but also how positioning and technique can play a huge role in cancer detection. We will examine cases and look at the pattern of how pathology develops in the breast, both malignant and benign. Common image aquisition and interpretation pitfalls will be reviewed as well. The session will also discuss ways of evaluating such cases in our practices to achieve the best patient outcomes, in spite of hindsight wisdom.



MSCT41

Case-based Review of Thoracic Radiology (Interactive Session)

Wednesday, Nov. 28 1:30PM - 3:00PM Room: S406A



AMA PRA Category 1 Credits ™: 1.50 ARRT Category A+ Credit: 1.75

Participants

Diana Litmanovich, MD, Haifa, Israel (Director) Nothing to Disclose

LEARNING OBJECTIVES

1) Identify CT features of benign solitary pulmonary nodules. 2) List morphologic features of solitary nodules that suggest malignancy. 3) Review current recommendations for management of incidentally-detected small lung nodules. 4) Recognize common mechanisms of intrathoracic metastatic spread with focus on pulmonary metastases. 5) Familiarize with pertinent imaging features and patterns of metastatic disease on CT. 6) Illustrate how to narrow the differential diagnosis regarding the primary site of malignancy. 7) Assess utility of imaging findings for diagnosis, prognosis and directing therapy of metastatic disease. 8) Describe intrathoracic calcification by location and identify those with characteristic morphology. 9) Identify signs of malignant pleural disease on CT examinations.

ABSTRACT

Solitary pulmonary nodules are among the most common diagnostic problems facing radiologists who interpret chest CT examinations. This component of the course will review technical considerations of CT of lung nodules, the characteristics of benign nodules and those CT features of SPNs that are concerning for malignancy. The evidence-based approach to small nodules detected incidentally on chest CT examinations will be reviewed, with a focus on the 2017 Fleischner Society guidelines for management of these lesions. Metastatic disease to the thorax is commonly encountered in clinical practice and can have a wide range of imaging manifestations. CT is typically used to detect the abnormality, guide diagnostic procedures and therapy, as well as assess treatment response. This presentation will review cases that illustrate main pathological mechanisms of metastatic spread to the chest, and imaging patterns on CT, characteristic for specific categories of primary malignancies, with focus on pulmonary metastases. Prognostic implications and available therapeutic options will be reviewed. Intrathoracic calcification is most often the result of prior granulomatous infection. Other intrathoracic calcifications will be presented by location: solitary pulmonary nodule, multiple pulmonary nodules, diffuse parenchymal involvement, lymph node and pleura. The differential diagnosis includes malignant, metabolic, occupational, and idiopathic causes often with subtle differences in morphology that can be used to correctly diagnose these conditions. Malignant pleural disease can manifest as an isolated pleural effusion, a pleural effusion with uneven pleural thickening or more rarely by presence of isolated small pleural nodules, which is named dry pleural dissemination

Sub-Events

MSCT41A Many Faces of Pulmonary Nodule

Participants

Jeffrey S. Klein, MD, Burlington, VT (Presenter) Nothing to Disclose

For information about this presentation, contact:

jklein@rsna.org

LEARNING OBJECTIVES

1) Identify CT features of benign solitary pulmonary nodules. 2) List morphologic features of solitary nodules that suggest malignancy. 3) Review current recommendations for management of incidentally-detected small lung nodules. 4) Recognize common mechanisms of intrathoracic metastatic spread with focus on pulmonary metastases. 5) Familiarize with pertinent imaging features and patterns of metastatic disease on CT. 6) Illustrate how to narrow the differential diagnosis regarding the primary site of malignancy. 7) Assess utility of imaging findings for diagnosis, prognosis and directing therapy of metastatic disease. 8) Describe intrathoracic calcification by location and identify those with characteristic morphology. 9) Identify signs of malignant pleural disease on CT examinations.

ABSTRACT

Solitary pulmonary nodules are among the most common diagnostic problems facing radiologists who interpret chest CT examinations. This component of the course will review technical considerations of CT of lung nodules, the characteristics of benign nodules and those CT features of SPNs that are concerning for malignancy. The evidence-based approach to small nodules detected incidentally on chest CT examinations will be reviewed, with a focus on the 2017 Fleischner Society guidelines for management of these lesions. Metastatic disease to the thorax is commonly encountered in clinical practice and can have a wide range of imaging manifestations. CT is typically used to detect the abnormality, guide diagnostic procedures and therapy, as well as assess treatment response. This presentation will review cases that illustrate main pathological mechanisms of metastatic so functions and available therapeutic options will be reviewed. Intrathoracic calcification is most often the result of prior granulomatous infection. Other intrathoracic calcifications will be presented by location: solitary pulmonary nodule, multiple pulmonary nodules, diffuse parenchymal involvement, lymph node and pleura. The differential diagnosis includes malignant, metabolic, occupational, and idiopathic causes often with subtle differences in morphology that can be used to correctly diagnose these conditions. Malignant pleural disease can manifest as an isolated pleural effusion, a pleural effusion with uneven pleural

thickening or more rarely by presence of isolated small pleural nodules, which is named dry pleural dissemination

MSCT41B Many Faces of Metastatic Diseases to the Chest

Participants Maya Galperin-Aizenberg, MD, Philadelphia, PA (*Presenter*) Nothing to Disclose

For information about this presentation, contact:

Maya.Galperin-Aizenberg@uphs.upenn.edu

LEARNING OBJECTIVES

1) Identify CT features of benign solitary pulmonary nodules. 2) List morphologic features of solitary nodules that suggest malignancy. 3) Review current recommendations for management of incidentally-detected small lung nodules. 4) Recognize common mechanisms of intrathoracic metastatic spread with focus on pulmonary metastases. 5) Familiarize with pertinent imaging features and patterns of metastatic disease on CT. 6) Illustrate how to narrow the differential diagnosis regarding the primary site of malignancy. 7) Assess utility of imaging findings for diagnosis, prognosis and directing therapy of metastatic disease. 8) Describe intrathoracic calcification by location and identify those with characteristic morphology. 9) Identify signs of malignant pleural disease on CT examinations.

ABSTRACT

Solitary pulmonary nodules are among the most common diagnostic problems facing radiologists who interpret chest CT examinations. This component of the course will review technical considerations of CT of lung nodules, the characteristics of benign nodules and those CT features of SPNs that are concerning for malignancy. The evidence-based approach to small nodules detected incidentally on chest CT examinations will be reviewed, with a focus on the 2017 Fleischner Society guidelines for management of these lesions. Metastatic disease to the thorax is commonly encountered in clinical practice and can have a wide range of imaging manifestations. CT is typically used to detect the abnormality, guide diagnostic procedures and therapy, as well as assess treatment response. This presentation will review cases that illustrate main pathological mechanisms of metastatic spread to the chest, and imaging patterns on CT, characteristic for specific categories of primary malignancies, with focus on pulmonary metastases. Prognostic implications and available therapeutic options will be reviewed. Intrathoracic calcification is most often the result of prior granulomatous infection. Other intrathoracic calcifications will be presented by location: solitary pulmonary nodule, multiple pulmonary nodules, diffuse parenchymal involvement, lymph node and pleura. The differential diagnosis includes malignant, metabolic, occupational, and idiopathic causes often with subtle differences in morphology that can be used to correctly diagnose these conditions. Malignant pleural disease can manifest as an isolated pleural effusion, a pleural effusion with uneven pleural thickening or more rarely by presence of isolated small pleural nodules, which is named dry pleural dissemination

MSCT41C Many Faces of Thoracic Calcifications

Participants

Cristopher A. Meyer, MD, Madison, WI (Presenter) Investor, Elucent Medical; Consultant, NIOSH Certified B-reader

For information about this presentation, contact:

cmeyer2@uwhealth.org

LEARNING OBJECTIVES

1) Identify the cause of diffuse lung parenchymal calcification based on morphology and distribution. 2) Describe the differential diagnosis for calcified mediastinal lymph nodes. 3) Be familiar with the entities of pleural plaque and pseudo-plaque in occupational exposure.

MSCT41D Many Faces of Pleural Disease

Participants

Marie-Pierre Revel, Paris, France (Presenter) Nothing to Disclose

LEARNING OBJECTIVES

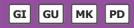
1) Identify CT features of benign solitary pulmonary nodules. 2) List morphologic features of solitary nodules that suggest malignancy. 3) Review current recommendations for management of incidentally-detected small lung nodules. 4) Recognize common mechanisms of intrathoracic metastatic spread with focus on pulmonary metastases. 5) Familiarize with pertinent imaging features and patterns of metastatic disease on CT. 6) Illustrate how to narrow the differential diagnosis regarding the primary site of malignancy. 7) Assess utility of imaging findings for diagnosis, prognosis and directing therapy of metastatic disease. 8) Describe intrathoracic calcification by location and identify those with characteristic morphology. 9) Identify signs of malignant pleural disease on CT examinations.



MSES43

Essentials of Pediatric Imaging

Wednesday, Nov. 28 1:30PM - 3:00PM Room: S100AB



AMA PRA Category 1 Credits ™: 1.50 ARRT Category A+ Credit: 1.75

Sub-Events

MSES43A Pediatric Abdominal Radiography

Participants

Steven J. Kraus, MD, Cincinnati, OH (Presenter) Author, Reed Elsevier

For information about this presentation, contact:

steven.kraus@cchmc.org

LEARNING OBJECTIVES

1) Have an alternative, organized approach to the interpretation of the abdominal radiograph in children. 2) Detect abnormalities of the abdomen on radiographs that may not have been detected previously. 3) Have a practical differential diagnosis of abnormalities detected on abdominal radiographs in children.

ABSTRACT

Abdominal imaging in children today is very sophisticated, with advances in techniques that do not involve exposure to radiation such as Ultrasonography (US) and Magnetic Resonance Imaging (MRI), as well as techniques which do expose children to radiation, namely Computed Tomography (CT). However, with all the advances in radiologic imaging techniques today, the most commonly performed abdominal imaging exam in a large academic children's hospital is the abdominal radiograph. However, if one would poll pediatric radiologists or even general radiologists today, one would probably find that the abdominal radiograph is the least favorite exam to interpret and most radiologists would probably admit that it is the hardest exam to interpret well. Cross sectional imaging such as US, MRI, and CT are so much easier because of the detailed anatomy in 3 dimensions, 4 for US if watching real-time US clips. An organized approach to the interpretation of the abdominal radiograph with a thorough knowledge of the pathologic processes of different age groups and patient demographics is very helpful in arriving at a diagnosis or differential diagnosis in many cases and can be helpful to the referring physicians of both inpatients and outpatients alike.

MSES43B Congenital Renal Anomalies

Participants

Katharine L. Hopkins, MD, Portland, OR (Presenter) Nothing to Disclose

LEARNING OBJECTIVES

1) Name ten categories of congenital renal anomaly that are likely to be encountered in general radiology practice. 2) Identify the distinguishing imaging features of up to three congenital renal anomalies in each category. 3) Develop appropriate strategies for management and follow-up of congenital renal anomalies.

MSES43C Complications of Pediatric Fractures

Participants

Arthur B. Meyers, MD, Orlando, FL (Presenter) Author with royalties, Reed Elsevier; Editor with royalties, Reed Elsevier

LEARNING OBJECTIVES

1) Identify the direct and indirect imaging findings of physeal bridge formation. 2) Calculate the percentage of physeal involvement of a bridge on MRI. 3) List the indications for treatment of physeal bridges.

ABSTRACT

Fractures in skeletally immature children often involve the physis. These injuries can lead to osseous bridge formation across the physis that may cause longitudinal growth disturbances or angular deformities leading to substantial disability. Risk factors for bridge formation after an injury include: the severity of the injury, the child's growth potential, the anatomic site of the fracture and the type of fracture. Complications arising from bridge formation depend upon the location of the bridge within the physis and the anatomic location within the pediatric skeleton. Imaging of children after physeal injury is important for the diagnosis of growth arrest and for the characterization of the size and location of physeal bridges for treatment planning. There is also an important role for imaging in the evaluation of complications caused by physeal bridges and in the post treatment evaluation of these children.

MSES43D Imaging Tumors of Pediatric Spine

Participants Laura L. Hayes, MD, Pensacola, FL (*Presenter*) Nothing to Disclose

For information about this presentation, contact:

LEARNING OBJECTIVES

1) To be able to identify and classify tumors of the pediatric spine. 2) To understand how to use and apply the knowledge gained by using advanced imaging techniques to study the pediatric spine in the setting of malignancy.

ABSTRACT

There are a wide variety of tumors involving the pediatric spine. In this session, we will review the types and imaging appearances of spinal lesions. Special attention will be given to the use of diffusion-weighted imaging of the spine in these children.



MSRO43

BOOST: Pediatric CNS Tumors and Diagnostic Dilemmas after Radiation Therapy (Interactive Session)

Wednesday, Nov. 28 1:30PM - 2:30PM Room: S103CD



AMA PRA Category 1 Credit ™: 1.00 ARRT Category A+ Credit: 1.00

Participants

Edward Y. Kim, MD, Seattle, WA (*Moderator*) Nothing to Disclose Kenneth Wong, MD, Los Angeles, CA (*Presenter*) Nothing to Disclose Benita Tamrazi, MD, South Pasadena, CA (*Presenter*) Nothing to Disclose

For information about this presentation, contact:

kewong@chla.usc.edu

LEARNING OBJECTIVES

1) Discuss the basic epidemiology, diagnostic workup, and evaluation of a child with a suspected CNS tumor. 2) Select and apply the different therapeutic alternatives in radiation therapy delivery for pediatric CNS cancers. 3) Identify advanced imaging modalities to resolve diagnostic dilemmas after radiation therapy for pediatric CNS tumors.



MSSR43

RSNA/ESR Sports Imaging Symposium: Musculoskeletal Interventional Procedures (Interactive Session)

Wednesday, Nov. 28 1:30PM - 3:00PM Room: E352



AMA PRA Category 1 Credits ™: 1.50 ARRT Category A+ Credit: 1.75

Participants

Laura W. Bancroft, MD, Orlando, FL (*Moderator*) Author with royalties, Wolters Kluwer nv; Speaker, World Class CME; Editor, Thieme Medical Publishers, Inc; Travel support, Thieme Medical Publishers, Inc; ; Andrew J. Grainger, MRCP, FRCR, Leeds, United Kingdom (*Moderator*) Consultant, Levicept Ltd; Director, The LivingCare Group;

Sub-Events

MSSR43A Diagnostic and Therapeutic Injections in the Athlete: Pearls and Pitfalls

Participants

Philippe A. Peetrons, MD, Brussels, Belgium (Presenter) Research Consultant, Canon Medical Systems Corporation

LEARNING OBJECTIVES

1) To become familiar with the most common requests and indications for sports-related injuries. 2) The learn about technical considerations for performing MSK injections. 3) To understand reasons to delay injections or avoid certain injectables.

ABSTRACT

The main pitfall is from far an mistake in the diagnosis done before sending the patient to the ultrasound guided treatment. Good examination and looking carefully to the examinations done before is mandatory. Among pearls, some innovative technique for injecting will be shown, such as Trapezo-metacarpal joint, sternoclavicular joint, Morton's neuroma, subtalar joint, hip and shoulder joints, carpal tunnel and de Quervain tenosynovitis. Treatment of nerve injuries will also be depicted and illustrated. Some tips will be given for ganglia tretment

MSSR43B Injectables, Percutaneous Tendon Fenestration and Tenotomy: Clinical Outcomes and Current Evidence

Participants

Jon A. Jacobson, MD, Ann Arbor, MI (*Presenter*) Research Consultant, BioClinica, Inc; Advisory Board, General Electric Company; Advisory Board, Koninklijke Philips NV; Royalties, Reed Elsevier

For information about this presentation, contact:

jjacobsn@umich.edu

LEARNING OBJECTIVES

1) To be aware of the indications and benefits of available injectables used to treat sports-related injuries. 2) To learn about technical considerations for performing tendon fenestration and tenotomy. 3) To become familiar with current evidence on results of MSK procedures in the literature.

Honored Educators

Presenters or authors on this event have been recognized as RSNA Honored Educators for participating in multiple qualifying educational activities. Honored Educators are invested in furthering the profession of radiology by delivering high-quality educational content in their field of study. Learn how you can become an honored educator by visiting the website at: https://www.rsna.org/Honored-Educator-Award/ Jon A. Jacobson, MD - 2012 Honored EducatorJon A. Jacobson, MD - 2017 Honored Educator

MSSR43C Interactive Case Discussion

Participants

Philippe A. Peetrons, MD, Brussels, Belgium (*Presenter*) Research Consultant, Canon Medical Systems Corporation Jon A. Jacobson, MD, Ann Arbor, MI (*Presenter*) Research Consultant, BioClinica, Inc; Advisory Board, General Electric Company; Advisory Board, Koninklijke Philips NV; Royalties, Reed Elsevier

For information about this presentation, contact:

jjacobsn@umich.edu

LEARNING OBJECTIVES

1) To learn the targeted approach to injecting joints, ligaments, tendons and tendon sheaths. 2) To appreciate pitfalls to avoid in MSK procedures for treatment of sports-related injuries. 3) To understand evidence-based data on various MSK procedures in order to give patients realistic expectations after treatment.

Presenters or authors on this event have been recognized as RSNA Honored Educators for participating in multiple qualifying educational activities. Honored Educators are invested in furthering the profession of radiology by delivering high-quality educational content in their field of study. Learn how you can become an honored educator by visiting the website at: https://www.rsna.org/Honored-Educator-Award/ Jon A. Jacobson, MD - 2012 Honored EducatorJon A. Jacobson, MD - 2017 Honored Educator



PS40

Wednesday Plenary Session

Wednesday, Nov. 28 1:30PM - 2:45PM Room: E450A

RO

AMA PRA Category 1 Credits ™: 1.25 ARRT Category A+ Credit: .75

Participants

Vijay M. Rao, MD, Philadelphia, PA (Presenter) Nothing to Disclose

Sub-Events PS40A	Announcement of Education Exhibit Awards
PS40B	Announcement of Quality Improvement Report Awards
PS40C	Dedication of the Annual Oration in Radiation Oncology to the Memory of Seymour H. Levitt, MD (1928-2017)
PS40D	Annual Oration in Radiation Oncology: Radiotherapy to Convert the Tumor Into an In Situ Vaccine

Participants

Silvia C. Formenti, MD, New York, NY (*Presenter*) Research Grant, Bristol-Myers Squibb Company; Research Grant, Varian Medical Systems, Inc; Research Grant, Johnson & Johnson; Research Grant, Regeneron Pharmaceuticals, Inc; Research Grant, Eisai Co, Ltd; Research Grant, Merck & Co, Inc; Speaker, Bristol-Myers Squibb Company; Speaker, Varian Medical Systems, Inc; Speaker, Johnson & Johnson; Speaker, Regeneron Pharmaceuticals, Inc; Speaker, Johnson & Johnson; Speaker, Regeneron Pharmaceuticals, Inc; Speaker, Eisai Co, Ltd; Speaker, Merck & Co, Inc; Speaker, Elekta AB; Speaker, GlaxoSmithKline plc; Speaker, AstraZeneca PLC; Speaker, Dynavax Technologies Corporation Edward Y. Kim, MD, Seattle, WA (*Introduction*) Nothing to Disclose

Abstract

Optimal delineation of the target and real-time visualization of organ movement have converged radiology and radiation oncology to achieve a more and more precise and effective delivery of cytotoxic ionizing radiation. This partnership between our two disciplines continues in the era of cancer immunotherapy. Radiotherapy has revealed an ideal adjuvant to cancer immunotherapy, because of its ability to convert the irradiated tumor into an individualized, in situ vaccine. When successful at immunizing, radiotherapy evokes T cell memory, and induces effects outside the treated field, defined as abscopal effects (responses at a distant, synchronous, unirradiated established tumor or metastasis). In the setting of clinical cancer, however, abscopal effects are extremely rare, because of immune-suppressive characteristic of established solid tumors (Curr Probl Cancer 40;25-37, 2016). Thus, strategies to exploit the pro-immunogenic effects of radiotherapy require combination with immunotherapy: experiments in several syngeneic mouse models that mimic the setting of advanced cancer have demonstrated promise of combining radiation with immune checkpoint blockade (Clin Cancer Res. 2005;11:728-734). Radiation can compensate tumors with a low mutational load, by inducing de novo T cell priming to multiple tumor antigens and therefore, achieve responses in the absence of pre-existing neoantigens with anedoctal clinical examples confirming the preclinical data (Trends Cancer 2016:2,6:286-294). Currently, multiple clinical trials are exploring optimal regimes of radiotherapy and immunotherapy, with some initial success. The issue of dose and fractionation seems to be particularly relevant to abscopal responses. A mechanism underlying the dose dependence of abscopal response was recently elucidated (Nature Communications 2017; Jun 9;8:15618). In mice bearing bilateral TSA murine breast carcinoma when combined with ICB a single dose of 20 or 30Gy achieved comparable in field control to that of a regimen of 8GyX3 fractions, but only the fractionated regimen induced abscopal responses. Radiation-generated double strands (ds) DNA fragments reach the cytoplasm of irradiated cells where they are "sensed" by the cGAS/STING pathway (cGAS=cyclic GMP-AMP synthase and its adaptor protein STING= stimulator of interferon genes, aka transmembrane protein 173 - TMEM173). cGAS binds cytosolic dsDNA to initiate interferon (IFN-I) responses upon STING stimulation, resulting in dendritic cell recruitment and cross-priming of effector T-cells, the key steps to convert the tumor into an in situ vaccine. When tested in multiple carcinoma murine and human carcinoma cells as the radiation dose per fraction increases, cytosolic dsDNA was found to accumulate to a threshold above which induction of three prime repair exonuclease 1 (Trex1) occurred, an enzyme that degrades cytoplasmic DNA. Single doses in excess of 10-12Gy induced Trex1 to rapidly degrade cytosolic dsDNA, the substrate for cGAS/STING. As a result, signaling to induce IFN was abrogated, impairing RT-induced abscopal effects. Consideration to these findings suggest that a hypo-fractionated regimen, ideally with 3-5 doses of less than 10-12 Gy each, should be used when radiotherapy is combined with immunotherapy. Finally, non-invasive strategies to follow the kinetics of tumor immune-infiltration are warranted. Image co-registration and total body monitoring of immune response are investigational priorities that once again converge radiology and radiation oncology.



SPHA41

Hospital Administrators Symposium

Wednesday, Nov. 28 1:30PM - 4:50PM Room: S105AB



ARRT Category A+ Credits: 4.00 AMA PRA Category 1 Credits ™: 3.25

Participants

Gregory N. Nicola, MD, River Edge, NJ (Moderator) Nothing to Disclose

LEARNING OBJECTIVES

1) Cover a broad range of topics geared towards phyician and non-phyician hospital administrators ranging from regulatory to operational.

Sub-Events

SPHA41A Putting the Patient First in the Radiology Department

Participants Keith D. Hentel, MD, MS, New York, NY (*Presenter*) Nothing to Disclose

For information about this presentation, contact:

keh9003@med.cornell.edu

LEARNING OBJECTIVES

1) Identify potential benefits of putting patients first in the radiology department. 2) Apply new techniques and develop programs to enhance the patient experience.

ABSTRACT

Patient experience is an important part of patient centered care and increasingly important from a reimbursement perspective. Using the patient experience as a framework for operations, practices may improve operational efficiency as well as improve the value of the care provided. Examples of such efforts will be provided to illustrate how such a framework may be useful.

SPHA41B Implementing Advanced Imaging Decision Support in the Ambulatory Setting

Participants

Robert Cooke, Redding, CT (Presenter) Vice President, National Decision Support Company

SPHA41C Hospital Consolidation and Quality of Care

Participants

David J. Seidenwurm, MD, Carmichael, CA (*Presenter*) Shareholder, Sutter Medical Group ; Shareholder, RASMG Medical Group ; Director, RASMG Medical Group; Expert Witness, Medical Legal

LEARNING OBJECTIVES

1) Understand vertical integration. 2) Understand degrees of integration. 3) Understand the positive impact of vertical integration on quality.

ABSTRACT

Vertical integration among clinicians, payers and facilities offer opportunities to improve value in healthcare. Factors including simpler customer experience, narrow networks with aligned incentives, transparent information flows, improved patient satisfaction may contribute. Objective demonstrations of improved quality with vertical integration at the plan level suggest that this is an empirically verifiable phenomenon, not just a theoretical possibility.

SPHA41D Q&A

Participants David J. Seidenwurm, MD, Carmichael, CA (*Presenter*) Shareholder, Sutter Medical Group ; Shareholder, RASMG Medical Group ; Director, RASMG Medical Group; Expert Witness, Medical Legal Robert Cooke, Redding, CT (*Presenter*) Vice President, National Decision Support Company Keith D. Hentel, MD, MS, New York, NY (*Presenter*) Nothing to Disclose

SPHA41E Quality Payment Program Little Known Facts

Participants Wendy Lomers, MBA, Longview, TX (*Presenter*) Principal, Acclaim Radiology Management

LEARNING OBJECTIVES

4) To be a surger of subblables in the MIDC

1) TO become aware of subtleties in the MIPS program allowing them to better understand MIPS reporting options and scoring.

SPHA41F Operational Decisions Necessary for an Effective Endovascular Stroke Program

Participants

Ramon G. Gonzalez, MD, PhD, Boston, MA (Presenter) Nothing to Disclose

LEARNING OBJECTIVES

1) Understand the physiological changes that occur in acute stroke patients with large vessel occlusions. 2) Identify the most important variables needed to select ischemic stroke patients for endovascular thrombectomy. 3) Know the most reliable neuroimaging methods to identify the key stroke variables needed for interventional triage. 4) Review the available options for creating a hub and spoke endovascular stroke program.

SPHA41G Operationalizing Culture of Safety: Moving from Concept to Reality

Participants

Jennifer C. Broder, MD, Burlington, MA (Presenter) Nothing to Disclose

For information about this presentation, contact:

jennifer.c.broder@lahey.org

LEARNING OBJECTIVES

1) List activities that help managers implement Just Culture. 2) Identify opportunities for frontline staff to engage in patient safety activities. 3) Describe how leadership can demonstrate commitment to improving patient safety.

ABSTRACT

Establishing a strong 'culture of safety' is integral to providing high quality and safe care, but how do you really make that happen in your department? This session will move beyond theory to share practical activities that can be implemented to establish and reinforce patient safety as a primary goal. Active practice of Just Culture, engagement of frontline staff, and visibility of leadership commitment to patient safety will be discussed.

SPHA41H Q&A

Participants Ramon G. Gonzalez, MD, PhD, Boston, MA (*Presenter*) Nothing to Disclose Jennifer C. Broder, MD, Burlington, MA (*Presenter*) Nothing to Disclose Wendy Lomers, MBA, Longview, TX (*Presenter*) Principal, Acclaim Radiology Management



VSIO41

Interventional Oncology Series: Colon and Neuroendocrine Liver Mets

Wednesday, Nov. 28 1:30PM - 6:00PM Room: S405AB



AMA PRA Category 1 Credits ™: 4.00 ARRT Category A+ Credits: 5.00

FDA Discussions may include off-label uses.

Participants

Sarah B. White, MD,MS, Philadelphia, PA (*Moderator*) Research support, Guerbet SA; Research support, Siemens AG; Consultant, Guerbet SA; Consultant, BSC; Consultant, Cook Group Incorporated

Constantinos T. Sofocleous, MD, PhD, New York, NY (*Moderator*) Consultant, General Electric Company; Consultant, Johnson & Johnson; Consultant Terumo; ; Research Support: BTG, Ethicon J&J; ; ;

LEARNING OBJECTIVES

1) Defining the role and timing of LDT in the care of patients with liver dominant metastatic neuroendocrine. 2) Determining the appropriate pre-procedural work-up for patients undergoing LDT and absolute contraindications. 3) Understand the complications and adverse events that can occur due to LDT.

Sub-Events

VSI041-01 Surgical Resection for Colorectal Liver Metastases

Wednesday, Nov. 28 1:30PM - 1:50PM Room: S405AB

Participants

Robert E. Roses, MD, Philadelphia, PA (Presenter) Nothing to Disclose

VSI041-02 Ablation for Colorectal Liver Metastases

Wednesday, Nov. 28 1:50PM - 2:10PM Room: S405AB

Participants

Constantinos T. Sofocleous, MD, PhD, New York, NY (*Presenter*) Consultant, General Electric Company; Consultant, Johnson & Johnson; Consultant Terumo; ; Research Support: BTG, Ethicon J&J; ; ;

For information about this presentation, contact:

sofoclec@mskcc.org

LEARNING OBJECTIVES

- Optimal Use of Ablation in the treatment of colon cancer liver metastases- Evidence based use of thermal ablation- Review of recent literature and guidelines- Clinical and technical Considerations- Impact of Technique on outcomes- Comparisons to surgery-Genetic consideration in ablation technique- Alternative image guided therapies when Ablation with margins is not feasible

VSIO41-03 The Role of MicroRNA-196a-5p/IkBa/NFKB in Transitional Area Tumor Rapid Progress After Radiofrequency Ablation of Colorectal Liver Metastases and Mechanism Research

Wednesday, Nov. 28 2:10PM - 2:20PM Room: S405AB

Participants

He Xin, Shenyang, China (Presenter) Nothing to Disclose

PURPOSE

To research the mechanism of the transitional area tumor rapid:progress after radiofrequency ablation of colorectal liver metastases.

METHOD AND MATERIALS

1. Establish a single metastatic colon cancer model in BALB/c nude mice liver, draw materials after RFA. 2. The basis express of miR-196a in different CRC cells; The influence of miR-196a to proliferation, migration and EMT of CRC cells; The influence of NF-KB to EMT of CRC cells; MiR-196a impacts migration of CRC cells through NF-KB.

RESULTS

High expression of the miR-196a in the experimental group of animal model; In the cell experiment, high expression of the miR-196a in the CRC cells, miR-196a promotes proliferation, migration and EMT of CRC cells, we verify the targeted relationship of miR-196a and IKBA by Dual-Luciferase, MiR-196a promotes migration of CRC cells through NF-KB.

CONCLUSION

Ma waife that MiaraDNA 1062 En/TVDA/NEVD aromates transitional area tumar ranid arearmas after radiafraguance ablation of

we verify that MICTORINA-190a-59/1KBA/INFKB promotes transitional area tumor rapid:progress after radiofrequency ablation of colorectal liver metastases, this project research results will help to reveal the core factor of the transitional area tumor rapid:progress after RFA of colorectal liver metastases, put forward targeted intervention treatment method and targets, it has great significance to improve the overall prognosis and survival rate of colorectal cancer liver metastases.

CLINICAL RELEVANCE/APPLICATION

This project research results will help to reveal the core factor of the transitional area tumor rapid:progress after RFA of colorectal liver metastases, put forward targeted intervention treatment method and targets, it has great significance to improve the overall prognosis and survival rate of colorectal cancer liver metastases.

VSI041-04 SBRT for Colorectal Liver Metastases

Wednesday, Nov. 28 2:20PM - 2:50PM Room: S405AB

Participants

Mary Ú. Feng, MD, San Francisco, CA (*Presenter*) Self: Consultant, Varian, Inc and RefleXion Medical Inc; Spouse (Felix Feng, MD), Advisory Boards Dendreon, Janssen, Bayer, Sanofi, Ferring, EMD Serono, Medivation/Astellas, Blue Earth Diagnostics, Progenics; Spouse, honorarium Clovis

For information about this presentation, contact:

Mary.feng@ucsf.edu

LEARNING OBJECTIVES

To review outcomes for SBRTTo describe the logistics of SBRTTo describe the patient experience with SBRT

VSI041-05 Comparing Survival Outcomes of Radioembolization for Liver Metastases from Right versus Left-Sided Colon Cancer

Wednesday, Nov. 28 2:50PM - 3:00PM Room: S405AB

Participants

Ronald A. Mora, MD, Chicago, IL (*Presenter*) Nothing to Disclose Ahmed Gabr, MD, MBBCh, Chicago, IL (*Abstract Co-Author*) Nothing to Disclose Rehan Ali, MBBS, Forest Park, IL (*Abstract Co-Author*) Nothing to Disclose Ali Al Asadi, BS, Chicago, IL (*Abstract Co-Author*) Nothing to Disclose Samdeep Mouli, MD, Chicago, IL (*Abstract Co-Author*) Nothing to Disclose Ahsun Riaz, MD, Chicago, IL (*Abstract Co-Author*) Nothing to Disclose Riad Salem, MD, MBA, Chicago, IL (*Abstract Co-Author*) Research Consultant, BTG International Ltd; Research Grant, BTG International Ltd; Consultant, Eisai Co, Ltd; Consultant, Exelixis, Inc; Consultant, Bristol-Myers Squibb Company; Consultant, Dove;

Robert J. Lewandowski, MD, Chicago, IL (*Abstract Co-Author*) Consultant, BTG International Ltd; Advisory Board, Boston Scientific Corporation; Consultant, Cook Group Incorporated; Advisory Board, ABK Biomedical Inc; Advisory Board, Accurate Medical; Consultant, C. R. Bard, Inc;

For information about this presentation, contact:

ronald.mora@northwestern.edu

PURPOSE

Advanced stage presentation with earlier hepatic metastases and worse prognosis has been reported for right-sided colorectal carcinoma (CRC) compared to left-sided CRC. In this study, we aimed to compare survival outcomes in patients with left vs. right-sided metastatic colorectal cancer (mCRC) to the liver treated with Yttrium-90 radioembolization (Y90).

METHOD AND MATERIALS

With IRB approval, we searched our prospectively acquired database for patients with mCRC to the liver treated with glass microsphere radioembolization between 2003-2014. Overall survival (OS) was calculated from the dates of primary colon cancer diagnosis, development of hepatic metastasis and Y90 treatment. Survival plots were estimated using Kaplan-Meier Method. Log-rank test was used to compare the survival of right vs left-sided mCRC

RESULTS

120 patients had left-sided CRC and 61 had right-sided CRC. Mean age was 59 (95% CI: 57-61) years in left sided vs. 62 (95% CI 60-66) in right sided mCRC patients (P=0.04). There was no statistical difference in time to development of hepatic metastases among left sided (15 months) vs. right sided (16 months) mCRC (P=0.1). There was a significant difference in time from date of liver metastases to Y90 for left sided (21 months) vs. right sided (13 months) (P=0.002). OS (95%CI) from date of diagnosis of primary CRC was 53 (47-63) vs. 37 (26-66) months for left and right mCRC respectively (P=0.1). OS (95%CI) from the time of development of hepatic metastasis was 48 (39-54) months for left sided vs. 24 (20.6-40.5) months for right sided CRC (P=0.0093). OS (95%CI) from the date of first Y90 treatment was 14 (10.6-16) and 8.6 (4.5-14.3) months for the left and right mCRC, respectively (P=0.06). In patients with tumor burden <25%, median OS (95%CI) was 14.5 (13-22.5) and 11.5 (5.5-20) months for left and right mCRC respectively (P=0.2).

CONCLUSION

There is significant clinical interest in outcomes of mCRC depending on side of origin. Given the limitations of lead-time bias, as well as the possibility of an underpowered analysis, we are unable to demonstrate an OS difference from Y90 by side. Further work is underway.

CLINICAL RELEVANCE/APPLICATION

OS benefits may be demonstrated if earlier diagnoses of mCRC is made and there may be possibility of survival difference due to radioembolization depending on the site of origin.

VSI041-06 PRO: Y90 Only in Salvage Setting. My Data Do Not Support Earlier Administration Outside of a Clinical Trial!

Wednesday, Nov. 28 3:00PM - 3:20PM Room: S405AB

Participants

James Thomas, MD, Milwaukee, WI (Presenter) Nothing to Disclose

VSI041-07 CON: Y90 Can Be Given in Earlier Line in Selected Patients: Choosing Your Data!

Wednesday, Nov. 28 3:20PM - 3:40PM Room: S405AB

Participants

Robert J. Lewandowski, MD, Chicago, IL (*Presenter*) Consultant, BTG International Ltd; Advisory Board, Boston Scientific Corporation; Consultant, Cook Group Incorporated; Advisory Board, ABK Biomedical Inc; Advisory Board, Accurate Medical; Consultant, C. R. Bard, Inc;

For information about this presentation, contact:

r-lewandowski@northwestern.edu

LEARNING OBJECTIVES

1) Review contemporary data for radioembolization in mCRC. 2) Understand potential benefits of combining systemic therapy + radioembolization. 3) Consider scenarios where radioembolization may be useful early in disease course for mCRC.

VSI041-08 Discussion/Rebuttal

Wednesday, Nov. 28 3:40PM - 4:00PM Room: S405AB

VSIO41-09 Survival of Patients with Non-Resectable, Chemotherapy-Resistant Colorectal Liver Metastases Undergoing Conventional Lipiodol-Based Transarterial Chemoembolization (cTACE) Prior to Thermal Ablation: Palliative versus Neoadjuvant Intention

Wednesday, Nov. 28 4:00PM - 4:10PM Room: S405AB

Participants

Thomas J. Vogl, MD, PhD, Frankfurt, Germany (*Presenter*) Nothing to Disclose Maximilian Lahrsow, Frankfurt, Germany (*Abstract Co-Author*) Nothing to Disclose Tatjana Gruber-Rouh, Frankfurt Am Main, Germany (*Abstract Co-Author*) Nothing to Disclose Nour-Eldin A. Nour-Eldin, MD,PhD, Frankfurt Am Main, Germany (*Abstract Co-Author*) Nothing to Disclose Nagy N. Naguib, MD, MSc, Frankfurt Am Main, Germany (*Abstract Co-Author*) Nothing to Disclose

For information about this presentation, contact:

T.Vogl@em.uni-frankfurt.de

PURPOSE

To determine overall (OS) and progression-free survival (PFS) for conventional transarterial chemoembolization (cTACE) alone and in combination with percutaneous thermal ablation in patients with non-resectable, chemotherapy-resistant colorectal cancer liver metastases (CRLM).

METHOD AND MATERIALS

The study included 452 patients undergoing 2,654 repetitive conventional transarterial chemoembolization (cTACE) treatments of CRLM. 233 patients had palliative treatment using only cTACE, and 219 patients had neoadjuvant treatment with cTACE and subsequent thermal ablation (either microwave ablation or laser-induced thermotherapy). The chemotherapeutic agents used in either single, double or triple combination included Mitomycin C, Gemcitabine, Irinotecan, and Cisplatin. Several factor were analyzed to determine their prognositc value regarding OS and PFS.

RESULTS

Palliative use of cTACE resulted in a median OS and PFS of 12.6 and 5.9 months, whereas the neoadjuvant use of cTACE showed a median OS and PFS of 25.8 and 10.8 months, respectively. The differences in OS and PFS between the two groups were statistically significant (p<0.001). Extrahepatic metastases were a significant prognostic factor in OS and PFS of the palliative and neoadjuvant group. In addition, number, location, and mean size of metastases were significant prognostic factors for OS and PFS in the neoadjuvant group. Sex, primary tumor location, T- and N-parameters of the TNM staging system, time of appearance of liver metastases, ablation method, and patient age did not have a significant impact on OS and PFS in either patient group. The most distinct response to cTACE was observed in metastases that were treated with a triple combination of chemotherapy (p=0.021).

CONCLUSION

cTACE is an effective treatment option in advanced non-resectable CRLM. Chemoembolization followed by ablation further increases survival rates. A triple combination of chemotherapy improves response to cTACE.

CLINICAL RELEVANCE/APPLICATION

Triple combination of chemotherapy in cTACE followed improves the clinical outcome of patients with CRLM in both the neoadjuvant and palliative group.

VSI041-10 Systemic Therapies for NET

Wednesday, Nov. 28 4:30PM - 4:50PM Room: S405AB

Participants

Emily Bergsland, MD, San Francisco, CA (*Presenter*) Institutional research support, Lexicon Pharmaceuticals, Inc Institutional research support, Novartis AG Consultant, Ipsen SA Consultant, Lexicon Pharmaceuticals, Inc

LEARNING OBJECTIVES

1) Review the epidemiology and classification of gastroenteropancreatic neuroendocrine tumors (GEPNETS). 2) Discuss the value of somatostatin analogs for the treatment of GEPNETS. 3) Summarize the role of additional systemic treatment options, including peptide receptor radionuclide therapy, for metastatic GEPNETS. 4) Examine commonly applied treatment algorithms for advanced GEPNETS.

VSIO41-11 PRRT for NET

Wednesday, Nov. 28 4:50PM - 5:10PM Room: S405AB

Participants

Lisa Bodei, MD, PhD, New York, NY (Presenter) Consultant, AAA; Consultant, Ipsen SA; Speaker, AAA

LEARNING OBJECTIVES

On successful completion of this activity, participants should be able to describe (A) the technique, efficacy and tolerability profile of Peptide Receptor Radionuclide Therapy (PRRT) with 177Lu-DOTATATE therapy in neuroendocrine tumors (NETs); (B) the role and appropriate use of PRRT in NET management; and (C) special uses of PRRT and new perspectives.

VSIO41-12 High-Quality Imaging and Dosimetry of Yttrium-90 (90Y) Radioembolization Using a SiPM-Based PET/CT Scanner

Wednesday, Nov. 28 5:10PM - 5:20PM Room: S405AB

Participants

Heying Duan, Stanford, CA (Presenter) Nothing to Disclose

Mohamed H. Khalaf, Stanford, CA (Abstract Co-Author) Nothing to Disclose

Lucia Baratto, Stanford, CA (Abstract Co-Author) Nothing to Disclose

Daniel Y. Sze, MD, PhD, Stanford, CA (*Abstract Co-Author*) Consultant, Amgen Inc; Consultant, AstraZeneca PLC; Consultant, Bristol-Myers Squibb Company; Consultant, BTG International Ltd; Consultant, Eisai Co, Ltd; Consultant, Embolx, Inc; Consultant, W. L. Gore & Associates, Inc; Consultant, Johnson & Johnson; Consultant, Terumo Corporation; Medical Advisory Board, Boston Scientific Corporation; Medical Advisory Board, Koli Medical; Medical Advisory Board, Radguard Medical, Inc; Shareholder, Confluent Medical; Shareholder, Proteus Digital Health

Shyam Srinivas, MD, PhD, Cleveland, OH (Abstract Co-Author) Nothing to Disclose

Andrei Iagaru, MD, Emerald Hills, CA (Abstract Co-Author) Research Grant, General Electric Company

For information about this presentation, contact:

heying@stanford.edu

PURPOSE

Yttrium-90 radioembolization (RE) is a treatment modality for hepatic malignancies. Personalized dosimetry aims for maximum treatment and low toxicity. Dose calculation methods are based on empirical evidence with regards to efficacy and safety, but do not take radiation absorbed dose in tumor or normal liver tissue into account. We assessed the accuracy for distribution and dosimetry and compared absorbed dose in tumor and normal liver tissue in pre- and post-therapy imaging. Furthermore, image quality of 90Y post RE scans using a SiPM-based PET/CT was compared to standard of care pre-therapy 99mTc MAA SPECT/CT.

METHOD AND MATERIALS

We analyzed 99mTc MAA SPECT/CT and 90Y PET/CT images using SurePlan (MIM) software. Tumor volume and normal liver tissue were contoured on the pre-therapy diagnostic CT and then registered to 99mTc MAA SPECT/CT and 90Y PET/CT respectively. Image quality was evaluated using the 5-point Likert scale by two experienced nuclear medicine physicians.

RESULTS

Eleven patients were treated with a median administered activity of 2.73 GBq. Mean tumor dose in 99mTc MAA SPECT/CT was 81.8 Gy versus 83.82 Gy in 90Y PET/CT. There was no significant difference between Tumor-SPECT/CT and Tumor-90Y PET/CT doses (t = -.335, p=0.740). On average, Tumor-SPECT/CT scores were 2 Gy lower than tumor-90Y PET/CT doses (95% CI [-20, 15]). For normal liver tissue, a mean dose of 26.8 Gy was found in the 99mTc MAA SPECT/CT images and 18.6 Gy for 90Y PET/CT (t= 1.260, p=0.236). On average, normal liver tissue doses in 99mTc MAA SPECT/CT were 8 Gy higher than 90Y PET/CT doses (95% CI [-6, 22]). For 90Y PET/CT imaging, the best image quality was found at 20 min scan time (Likert-Scale 4.5 ± 0.5) vs. 15 min Likert-Scale 4 ± 0.6 and 10 min Likert-Scale 2 ± 0.6.

CONCLUSION

Our preliminary data show excellent image quality from digital 90Y PET/CT at a reduced scan time of 20 minutes. MIM software computed no significant divergent tumor or normal liver tissue doses for 99mTc MAA SPECT/CT or 90Y PET/CT. However, more patients have to be evaluated to confirm these findings. The faster imaging time may allow for inclusion of 90Y PET/CT in routine clinical workflows.

CLINICAL RELEVANCE/APPLICATION

The faster imaging time on digital 90Y PET/CT with excellent image quality may allow inclusion of it in routine clinical workflows.

VSI041-13 Arterially Directed Therapy for Metastatic Neuroendocrine Tumor

Participants

Sarah B. White, MD,MS, Philadelphia, PA (*Presenter*) Research support, Guerbet SA; Research support, Siemens AG; Consultant, Guerbet SA; Consultant, BSC; Consultant, Cook Group Incorporated

LEARNING OBJECTIVES

The objective of this lecture is improve knowledge of mNET patients in the following areas: I. Initial clinical assessment a. Optimal imaging modalities i. CT vs. MRI b. Eligibility for and timing of liver directed therapy i. ECOG status, % tumor burden, tumor vascularity ii. Bilioenteric manipulation II. Conventional Transarterial Chemoembolization (cTACE) a. Drug/oil emulsion with particle embolic III. Drug Eluting Bead Transarterial Chemoembolization (DEB-TACE) a. Micron sized beads loaded with Doxorubicin IV. Radioembolization a. Safety and efficacy b. Complications V. Post treatment care and follow-up a. Post-embolization syndrome i. Clinical management b. Timing of follow-up imaging

VSIO41-14 Tumor Board Cases

Wednesday, Nov. 28 5:40PM - 6:00PM Room: S405AB



MSRT45

ASRT@RSNA 2018: CT Colonography - The New Kid on the Block

Wednesday, Nov. 28 2:20PM - 3:20PM Room: N230B



AMA PRA Category 1 Credit ™: 1.00 ARRT Category A+ Credit: 1.00

Participants

Travis N. Prowant, MS, RT, Richmond, VA (Presenter) Nothing to Disclose

LEARNING OBJECTIVES

1) Recognize the vital role of CT Colonography (CTC) in colorectal cancer screening for the US population. 2) Explain aspects and procedural details of a single-center CTC program managed by a radiologist assistant. 3) Examine departmental resources required to establish and develop a CTC program. 4) Justify the use of a radiologist assistant to enhance involvement of radiologists in being at the forefront of colorectal screening in a safe, efficient and cost-effective manner.

ABSTRACT

Although technically not new in terms of how long CT Colonography (CTC) has been performed, it is potentially new to the procedural realm of the Radiologist Assistant (RA). Through routine practice analysis of Radiologist Assistant work in the United States, a variety of common fluoroscopic examinations have been identified as less commonly performed in recent years such as the barium enema, which has traditionally been considered the "gold standard" for colon screening in Radiology. In 2016, the US Preventive Services Task Force approved CTC as a colorectal screening option available to patients in what was viewed as a truly under-utilized preventive health strategy. To that end, the American Gastroenterological Association, the American College of Radiology and the American Cancer Society have also approved CTC use with equivalent sensitivity to optical colonoscopy for detecting significant colorectal polyps or cancers. CTC is a minimally invasive, patient-centric, low-dose CT examination of the color that can be performed without the use of sedation and minimal risk of perforation or side effect and has been proven to increase adherence rates and attracts more patients that may have otherwise not chosen to get screened. As a physician extender that can safely and successfully perform and manage the CTC from start to finish, the Radiologist Assistant is uniquely poised to enhance the patient experience and, in the meantime, allow the radiologist to tend to critical interpretations and other physician-specific duties. The Radiologist Assistant can be a vital part of colorectal screening programs around the country. Involve one today!



RCA44

Advanced AI Tools for Radiologist-driven Mining of Imaging and Hospital-based Data Sets for Developing and Testing Hypothesis from Clinical Practice (Hands-on)

Wednesday, Nov. 28 2:30PM - 4:00PM Room: S401AB



AMA PRA Category 1 Credits ™: 1.50 ARRT Category A+ Credit: 0

FDA Discussions may include off-label uses.

Participants

Jaron Chong, MD, Montreal, QC (Moderator) Nothing to Disclose

Dimitris Mitsouras, PhD, Boston, MA (Moderator) Research Grant, Canon Medical Systems Corporation;

An Tang, MD, Montreal, QC (*Presenter*) Research Consultant, Imagia Cybernetics Inc; Speaker, Siemens AG; Speaker, Eli Lilly and Company

Leonid Chepelev, MD, PhD, Ottawa, ON (*Presenter*) Nothing to Disclose Adnan M. Sheikh, MD, Ottawa, ON (*Presenter*) Nothing to Disclose Betty Anne Schwarz, PhD, Ottawa, ON (*Presenter*) Nothing to Disclose

For information about this presentation, contact:

an.tang@umontreal.ca

dmitsouras@alum.mit.edu

LEARNING OBJECTIVES

1) Understand how to use NLP based tools in the clinical setting. 2) Interact with the AI to improve its training potential. 3) Assess those properties of data needed for optimized AI training. 4) Make conclusions regarding evidence for a biomarker in a particular data set.

ABSTRACT

This course fills a large unmet educational gap in hands-on learning using real clinical data set and active Deep Learning software. Hands-on actual clinical data will be accessed by clinical arenas that are well recognized by RSNA attendees and for which there is data and applications that will be available in a cloud-based format. The entirety of the program will run on RSNA computers already available for hands-on courses.



RCC44

Cinematic Rendering: Principles, Pearls, and Clinical Applications

Wednesday, Nov. 28 2:30PM - 4:00PM Room: S501ABC

IN

AMA PRA Category 1 Credits ™: 1.50 ARRT Category A+ Credit: 1.75

FDA Discussions may include off-label uses.

Participants

Elliot K. Fishman, MD, Baltimore, MD (*Moderator*) Institutional Grant support, Siemens AG; Institutional Grant support, General Electric Company; Co-founder, HipGraphics, Inc

Steven P. Rowe, MD, PhD , Baltimore, MD (Presenter) Research funded, Progenics Pharmaceuticals, Inc

Elliot K. Fishman, MD, Baltimore, MD (*Presenter*) Institutional Grant support, Siemens AG; Institutional Grant support, General Electric Company; Co-founder, HipGraphics, Inc

Linda C. Chu, MD, Baltimore, MD (Presenter) Nothing to Disclose

For information about this presentation, contact:

efishman@jhmi.edu

lindachu@jhmi.edu

LEARNING OBJECTIVES

1) Understand the principles of cinematic rendering and how it differs from classic 3D techniques like volume rendering and maximum intensity projection (MIP) techniques. 2) Understand the potential role of cinematic rendering in applications ranging from oncology to trauma to vascular imaging. 3) Understand the role of cinematic rendering in specific applications in the pancreas, liver, kidneys and cardiovascular imaging.

ABSTRACT

Cinematic Rendering (CR) represents an advance in volume visualization with a high fidelity display of CT data. The technique has evolved with the introduction of faster GPU's at a lower cost and these GPU;s being used for medical imaging. In this refresher course we will discuss the basic principles of Cinematic Rendering and its advantages over classic volume rendering (VR) and maximum intensity projection technique (MIP). Case studies illustrating the advantages and disadvantages of each techniques will be discussed and illustrated. We will also discuss the range of current clinical applications focusing on oncology (pancreas, liver, kidney, small bowel, musculoskeletal trauma, cardiothoracic imaging and vascular imaging.

Honored Educators

Presenters or authors on this event have been recognized as RSNA Honored Educators for participating in multiple qualifying educational activities. Honored Educators are invested in furthering the profession of radiology by delivering high-quality educational content in their field of study. Learn how you can become an honored educator by visiting the website at: https://www.rsna.org/Honored-Educator-Award/ Elliot K. Fishman, MD - 2012 Honored EducatorElliot K. Fishman, MD - 2014 Honored EducatorElliot K. Fishman, MD - 2016 Honored EducatorElliot K. Fishman, MD - 2018 Honored Educator



MSRO44

BOOST: Advanced Techniques in Image-guided Therapy (Interactive Session)

Wednesday, Nov. 28 3:00PM - 4:15PM Room: S103CD



AMA PRA Category 1 Credits ™: 1.25 ARRT Category A+ Credits: 1.50

Participants

Theodore S. Hong, MD, Boston, MA (*Presenter*) Nothing to Disclose Susanna I. Lee, MD,PhD, Boston, MA (*Presenter*) Editor, Wolters Kluwer nv Homer A. Macapinlac, MD, Houston, TX (*Presenter*) Nothing to Disclose Peter Balter, PhD, Houston, TX (*Presenter*) Research Grant, Varian Medical Systems, Inc; Research Grant, RaySearch Laboratories AB

For information about this presentation, contact:

slee0@mgh.harvard.edu

LEARNING OBJECTIVES

1) Explain and apply modern CT and MR imaging technologies and PET tracers for treatment planning of solid malignancies in the chest, abdomen and pelvis. 2) Explain and apply the modern techniques in radiotherapy safely and effectively in the chest, abdomen and pelvis.

ABSTRACT

The last decade has seen emergence of important advances in locoregional cancer therapy. Use of functional imaging and advanced radiatiotherapy often integrated with targeted chemotherapy have improved patient outcomes. This course will present the underlying principles in diffusion MRI, novel MR contrast agents, PET-MR and dual energy CT. PET tracers to be discussed are F-18 FDG, widely used for most solid tumors; C-11 choline/F-18 Fluciclovine for prostate cancer and Ga-68-DOTATATE for neuroendocrine tumors. Advanced radiotherapy techniques such as Image Guided Radiotherapy (IGRT), Intensity Modulated Radiation Therapy (IMRT), and Stereotactic Body Radiation Therapy (SBRT) using image guidance with X-ray, CT, MRI and PET will be described.

Honored Educators

Presenters or authors on this event have been recognized as RSNA Honored Educators for participating in multiple qualifying educational activities. Honored Educators are invested in furthering the profession of radiology by delivering high-quality educational content in their field of study. Learn how you can become an honored educator by visiting the website at: https://www.rsna.org/Honored-Educator-Award/ Susanna I. Lee, MD,PhD - 2013 Honored Educator



SPOR41

AOSR-RSNA Joint Symposium

Wednesday, Nov. 28 3:00PM - 4:30PM Room: S504AB



AMA PRA Category 1 Credits ™: 1.50 ARRT Category A+ Credit: 1.75

Sub-Events

SPOR41A Imaging Landmarks: Primary Tumor Evaluation

Participants

Hugh D. Curtin, MD, Boston, MA (Presenter) Nothing to Disclose

For information about this presentation, contact:

Hugh_Curtin@meei.harvard.edu

LEARNING OBJECTIVES

1) Assess bone involvment and understand its significance in tumor assessment. 2) Understand the assessment of perineural spread using the second division of the trigeminal as a model. 3) Understand the special considerations at various subsites including retromolar trigone, tonsillar pillar, and larynx.

ABSTRACT

Most tumors of the head and neck are identified by clinical examination. This is particularly true of squamous cell carcinoma of the mucosa. Imaging is done to identify deep extension. This includes assessment of bone invasion which has a very important role in determining therapy. Extension of tumor along nerves or perineural spread carries tumor beyond potential resection margins and is important in radiation planning. Assessment of perineural spread uses fat pads located at various foramina as well as abnomrality of a foramen itself. Fat is usually present at the exit of skull base foramina as well as at more peripheral foramina such as the infraorbital foramen, mandibular foramen etc. CSF is usually located at the endocranial end of a foramen. In larynx cancer spread into the paraglottic space and involvment of the cartilage is important in planning therapy. This session will explore basic principles and imaging advantages and disadvantages in various types of tumor analysis

SPOR41B Staging the Lymph Nodes

Participants Hiroya Ojiri, MD, Tokyo, Japan (*Presenter*) Nothing to Disclose

For information about this presentation, contact:

ojiri@jikei.ac.jp

LEARNING OBJECTIVES

1) To stage regional lymph nodes in patients with head and neck cancer by standard morphological criteria. 2) To explain strengths and weakness of each criterion in assessment of metastatic nodal diseases. 3) To combine morpho-functional information to maximize benefits of multimodality imaging approach.

ABSTRACT

Regional nodal metastasis is the most important negative prognosticator in patients with head and neck cancer. It's, therefore, very important to assess as reliably as possible if the patient has regional metastatic disease by imaging. We need to combine morphofunctional information to obtain the best results because imaging is based on morphological as well as functional criteria. These will be explained in the lecture.

SPOR41C Post Treatment Surveillance

Participants

Barton F. Branstetter IV, MD, Pittsburgh, PA (Presenter) Nothing to Disclose

LEARNING OBJECTIVES

1) List the goals of surveillance imaging for recurrent head and neck cancer. 2) Describe the advantages and disadvantages of different surveillance modalities and frequencies. 3) Apply the NIRADS scheme to surveillance scans in the setting of head and neck cancer.

ABSTRACT

Patients with squamous cell carincoma of the head and neck undergo extensive clinical surveillance to detect recurrent tumor as soon as possible. Radiologic surveillance is also of critical importance, but the details, including frequency, timing, and modality, not universally agreed upon. This lecture will delineate the goals of radiologic surveillance, review the literature on the subject, and discuss new tools to assist radiologists who interpet these scans.

SPOR41D Special Considerations in Nasopharynx Carcinoma

Participants Vincent F. Chong, MD, FRCR, Singapore, Singapore (*Presenter*) Nothing to Disclose

LEARNING OBJECTIVES

1) To identify the pertient anatomy of nasopharynx relevant to tumor mapping. 2) To describe the pathways tumor spread. 3) To apply appropriate radiological examinations for accurate staging.



SSM01

Breast Imaging (Interventional Techniques and Path Correlation)

Wednesday, Nov. 28 3:00PM - 4:00PM Room: E351

BR

AMA PRA Category 1 Credit ™: 1.00 ARRT Category A+ Credit: 1.00

Participants

Michael A. Cohen, MD, Atlanta, GA (*Moderator*) Nothing to Disclose Gary J. Whitman, MD, Houston, TX (*Moderator*) Nothing to Disclose

Sub-Events

SSM01-01 Cryoablation as a Primary Treatment of Low-Risk Breast Cancers: An Interim Update of the Ice 3 Trial

Wednesday, Nov. 28 3:00PM - 3:10PM Room: E351

Participants

Kenneth R. Tomkovich, MD, Freehold, NJ (Presenter) Consultant, Scion Medical Technologies, LLC;

For information about this presentation, contact:

ktomkovich@princetonradiology.com

PURPOSE

The Ice 3 Trial is the first of its kind large scale multi center trial in the world to assess image guided cryoablation as a primary treatment for breast cancer without surgical lumpectomy. We report updated interim results and important imaging findings.

METHOD AND MATERIALS

This HIPPA compliant and IRB approved trial seeks enrollment of between 150 and 200 patients for cryoablation of low risk carcinoma of the breast. The study is limited to female patients ages 60 and over with biopsy proven primary, unifocal cancer. Cancers must measure 1.5cm or less with tumor prognostic panels that are ER+/PR+ or ER+/PR- and HER 2-. All patients underwent ultrasound guided cryoablation using the IceSense 3 system (IceCure Medical). Following local anesthesia, patients underwent a freeze, thaw, freeze cycle of cryoablation with the goal of a visible ice ball producing at least a 10mm margin of ice around the tumor. Patients will be followed for recurrence with mammography at 6 and 12 months and then annually for 5 years. Additional imaging with MRI or Ultrasound may be utilized as needed but is not a requirement. All patients have the option of post cryoablation chemotherapy, hormone therapy and or radiation therapy as clinically indicated. Patients will not undergo surgical lumpectomy following cryoablation.

RESULTS

A total of 157 patients have been treated with since enrollment began in October 2014 at 17 participating centers across the United States. Patients ranged from 60-90 years of age. Tumor sizes ranged from 3 to 15mm. No serious adverse events were reported. There has been 100% procedural success. All patients have had at least 6 months follow up. 78 patients have had at least 24 months follow up. 24 patients have had at least 36 months follow up. There has been no recurrence in 156/157 patients with at least 6 months follow up (99.4% success rate). Common imaging findings include fat necrosis, scarring and a mammographic "halo" effect.

CONCLUSION

Cryoablation of the breast is safe and well tolerated with a 100% initial procedural success rate. The overall clinical success rate for 157 patients with at least 6 months follow up is 99.4%. Long term results are also promising.

CLINICAL RELEVANCE/APPLICATION

Interim results suggest that cryoablation is a safe and effective primary treatment for women with small low risk breast cancers as an alternative to surgical lumpectomy.

SSM01-02 Do Eligibility Criteria for Ductal Carcinoma in Situ (DCIS) Active Surveillance Trials Identify Patients at Low Risk for Upgrade to Invasive Carcinoma?

Wednesday, Nov. 28 3:10PM - 3:20PM Room: E351

Participants

Manisha Bahl, MD,MPH, Boston, MA (*Presenter*) Nothing to Disclose Tawakalitu Oseni, Boston, MA (*Abstract Co-Author*) Nothing to Disclose Charmi Vijapura, MD, Iowa City, IA (*Abstract Co-Author*) Nothing to Disclose Niveditha Pinnamaneni, MD, New York, NY (*Abstract Co-Author*) Nothing to Disclose Constance D. Lehman, MD,PhD, Boston, MA (*Abstract Co-Author*) Research Grant, General Electric Company; Medical Advisory Board, General Electric Company

For information about this presentation, contact:

mbahl1@mgh.harvard.edu

PURPOSE

Due to concerns regarding overtreatment of ductal carcinoma in situ (DCIS), randomized controlled trials are currently underway in the United States and Europe to determine the safety and efficacy of active surveillance versus usual care for women with DCIS. The purpose of this study is to determine upgrade rates of DCIS at core needle biopsy to invasive carcinoma at surgical excision among women who meet eligibility criteria for three active surveillance trials.

METHOD AND MATERIALS

In this IRB-approved and HIPAA-compliant study, a retrospective review was performed of consecutive female patients diagnosed with DCIS at vacuum-assisted core needle biopsy from 2007 to 2016. Medical records were reviewed for mode of presentation, imaging findings, core biopsy pathology results, and surgical outcomes. DCIS cases were classified based on eligibility criteria for the COMET, LORD, and LORIS Trials. Of note, eligibility for the LORIS Trial also requires real-time central pathology review with features not routinely reported and thus not captured in this retrospective study.

RESULTS

Over a ten-year period, 1378 patients were diagnosed with unilateral DCIS at core biopsy and 12 were diagnosed with bilateral DCIS, for a total of 1390 patients (mean age 57, range 27-89) with 1402 cases of DCIS. 79.8% (n=1119) were detected on screening mammography. 17.3% of cases (n=243) were low nuclear grade, 47.2% (n=662) were intermediate nuclear grade, 26.2% (n=368) were high nuclear grade, and 9.2% (n=129) were unreported. The overall upgrade rate to invasive disease was 19.1% (268/1402). 485 were eligible for the COMET Trial, 163 for the LORD Trial, and 489 for the LORIS Trial. The rates of upgrade to invasive carcinoma were 12.2% (59/485), 7.4% (12/163), and 12.5% (61/489) for the COMET, LORD, and LORIS Trials, respectively. Of the 69 cases that upgraded to invasive carcinoma, 31.9% (n=22) upgraded to microinvasive disease (less than or equal to 1 mm) and 91.3% (n=63) were node-negative.

CONCLUSION

The upgrade rates for women with DCIS who meet eligibility criteria for active surveillance trials range from 7.4 to 12.5%. Of the upgraded cases, nearly one-third were microinvasive disease and more than 90% were node-negative.

CLINICAL RELEVANCE/APPLICATION

The risk of missing occult invasive carcinoma in women eligible for active surveillance trials ranges from 7.4 to 12.5%, and the majority of these cancers have favorable biologic profiles.

SSM01-03 Role of Vacuum Assisted Excision (VAE) in Managing Ductal Atypia Such as Flat Epithelial Atypia (FEA) and Atypical Intraductal Epithelial Proliferation (AIDP)

Wednesday, Nov. 28 3:20PM - 3:30PM Room: E351

Participants

Nisha Sharma, MBChB, Leeds, United Kingdom (*Presenter*) Nothing to Disclose Isobel Haigh, Leeds, United Kingdom (*Abstract Co-Author*) Nothing to Disclose

For information about this presentation, contact:

nisha.sharma2@nhs.net

PURPOSE

It is recognised that surgical excision for B3 lesions is considered over treatment and vacuum excision (VAE) is playing a role in managing these lesions.. In Europe and USA ductal atypia is still treated with surgical excision. In the UK ductal atypia is managed with vacuum excision rather than surgical excision.

METHOD AND MATERIALS

Retrospective audit performed from a prospective database of all B3 lesions identified through the Breast Screening Programme. All cases of pure ductal atypia, including AIDP and FEA were identified from April 2009 to March 2016. The mode of biopsy and upgrade rate were recorded and follow up data obtained until March 2018.

RESULTS

268990 women were screened from April 2009 to March 2016, of which 12434 were recalled to assessment (4.6%). 5582 biopsies were performed of which 688 were B3 lesions (12.3%). Ductal atypias (FEA and AIDP) (excluding papilloma and radial scars with ductal atypias) accounted for 39.8% of the biopsies. 69% (190/274) were managed with vacuum assisted excsion (VAE) and annual mammographic follow-up or routine screening surveillance. 3% (7/190) developed a cancer during surveillance period, of which 4 were in the same quadrant. 13% (35/274) were upgraded to malignancy following VAE and were treated with therapeutic surgery. 2 developed further cancer on surveillance in the same breast. 8% (21/274) had a vacuum excision and a surgical biopsy due to radiological or pathological concern and 14/21 was benign and 7/21 upgraded to malignancy. One case developed cancer in the contralateral breast on cancer follow up. 8% (22/274) had a surgical diagnostic biopsy instead of vacuum excision and 13/22 were benign and 9/22 were upgraded to malignancy. 2% (6/274) did not go on to have either vacuum excision or surgery due to co-morbidities. 2 developed cancer on surveillance. 12/274 (4%) developed malignancy during surveillance period of which 8/274 were in the same breast.

CONCLUSION

Our study shows that managing ductal atypia with vacuum assisted excision (VAE) is a safe alternative to surgical excision as a primary intervention but multidisciplinary review is important to determine if further surgery is required. Vacuum excision allowed 13% of our women to have a therapeutic surgery as preoperative diagnosis of malignancy was made and 69% avoided surgery altogether.

Vacuum assisted excision is a safe alternative to surgical biopsy in managing ductal atypias

SSM01-04 Papillary Breast Lesions Without Atypia Diagnosed by Core Biopsy: Should They Be Surgically Excised?

Wednesday, Nov. 28 3:30PM - 3:40PM Room: E351

Participants

Sarah Dhundass, MD, Saint Cloud, France (*Presenter*) Nothing to Disclose Pascal Cherel, Saint Cloud, France (*Abstract Co-Author*) Nothing to Disclose Adriana Langer, MD, Saint Cloud, France (*Abstract Co-Author*) Nothing to Disclose

PURPOSE

To evaluate the upgrade rate of benign papilloma without atypia diagnosed after core needle biopsy (CNB) or Vacuum assisted biopsy (VAB) in order to determine whether they should require surgical excision or not.

METHOD AND MATERIALS

Histological results of 15615 biopsy procedures were reviewed from January 2001 to December 2014 in our institution. Sampling methods included large gauge VAB by ultrasonographic (US) or stereotaxic guidance and US guided 14G CNB. A total of 179 papillary lesions without atypia that were diagnosed in 159 women were included: 121 had surgical excision following initial detection and 58 underwent imaging surveillance. Initial histological results were compared to the histological results after surgery or to the follow up findings. Statistical analysis was performed to evaluate the association of clinical and radiological variables with the upgrade rate to malignancy.

RESULTS

After exclusion of patients lost to follow up, 158 lesions have been analyzed. 90 were diagnosed by VAB and 68 by CNB. Surgical excision revealed 7 malignant lesions (6 DCIS and 1 carcinoma). The upgrade rate to malignancy was 4.4%. Among the 42 followed up patients, two necessitated secondary surgery, one of them corresponded to a malignant lesion (45 months after biopsy). The median follow-up period was 30 months (6-93). The upgrade rate was statistically higher in the group diagnosed with CNB 8.9% vs 1.1% in the VAB group (p=0.042). Age, history of cancer, size of the lesion, ultrasound and mammographic findings including BIRADS category were not associated with underestimation of malignancy (p>0.05).

CONCLUSION

Papilloma without atypia detected with VAB could not require surgery (upgrade rate 1.1%) if the excision is complete but should be radiologically followed up at least 5 years to screen for potential biopsy site changes. Papilloma without atypia diagnosed with CNB require surgical excision as the risk of coexisting carcinoma is significantly higher (8.9% in our study)

CLINICAL RELEVANCE/APPLICATION

Papilloma without atypia diagnosed with vacuum assisted biopsy can be radiologically followed up given the low rate of underestimation.

SSM01-05 Follow-Up Outcomes of BI-RADS Category 3 Solid Nodules Identified on Screening and Diagnostic Breast Ultrasound

Wednesday, Nov. 28 3:40PM - 3:50PM Room: E351

Awards

Student Travel Stipend Award

Participants Joanna Marie D. Choa, MD, Taguig, Philippines (*Presenter*) Nothing to Disclose Anna Lyn C. Egwolf, MD, Taguig, Philippines (*Abstract Co-Author*) Nothing to Disclose

For information about this presentation, contact:

choa.jmd@gmail.com

PURPOSE

Our study aims to determine significant difference in BI-RADS category from initial imaging to its subsequent follow-up and the minimum length of time that the BI-RADS category will change for solid nodules. Our study also wants to assess the characteristics and growth pattern of BI-RADS category 3 solid nodules.

METHOD AND MATERIALS

We did a retrospective cohort study reviewing patient reports across a 10-year follow-up period. All solid nodules with at least 2 follow-up ultrasound imaging within a minimum of 22 months were included. Patients were segregated into 2 groups by age: one group below 40 years old and another group age 40 years old and above. Mammogram results were not viewed. Patients with known carcinoma and those with other lesions having a higher BI-RADS assessment in either breast were excluded. Nodule size, characteristics, and BI-RADS score for each follow-up were obtained. We employed ANOVA for repeated measures for statistical analysis.

RESULTS

A total of 511 nodules (5.1% of identified solid nodules) were included and showed no significant difference in BI-RADS scores over the course of 2 follow-ups, regardless of age. Significant change was identified at the sixth and seventh follow-ups with downgrading of BI-RADS scores to 2. Significant changes in size between the second and third follow-up and comparing the first with the third follow-up were appreciated in patients 40 years old and above. Patients in this study were also found out to have an average interval between follow-up imaging of 14.39 months. The minimum length of time for a BI-RADS category 3 solid nodule to become category 4 on follow-up was approximately 1 year (354 days). Only 1 out of the total 511 nodules turned out malignant, 44 months after initial imaging.

CONCLUSION

There is no significant change between BI-RADS scores of solid nodules regardless of age within a 2-year follow-up period. The minimum time for change in BI-RADS from 3 to 4 is about 1 year. Low patient compliance to BI-RADS category 3 follow-up guidelines should be taken into consideration in formulating institutional protocols in the management of these solid nodules.

CLINICAL RELEVANCE/APPLICATION

Patient compliance to follow-up recommendations of BI-RADS category 3 solid nodules is very low, hence can be re-classified as category 2 and follow an annual schedule of follow-up imaging. Only 1 out of 511 nodules turned out malignant after 44 months (\sim 0.2%, low turn-out rate).

SSM01-06 Comparison of Upright Digital Breast Tomosynthesis-Guided Vacuum-Assisted Biopsy with Conventional Prone Stereotactic Vacuum-Assisted Biopsy

Wednesday, Nov. 28 3:50PM - 4:00PM Room: E351

Participants

Mary Maunglay, MD, Pontiac, MI (*Abstract Co-Author*) Nothing to Disclose Manisha Bahl, MD,MPH, Boston, MA (*Presenter*) Nothing to Disclose Helen Anne D'Alessandro, MD, Boston, MA (*Abstract Co-Author*) Nothing to Disclose Constance D. Lehman, MD,PhD, Boston, MA (*Abstract Co-Author*) Research Grant, General Electric Company; Medical Advisory Board, General Electric Company

For information about this presentation, contact:

mbahl1@mgh.harvard.edu

PURPOSE

Breast imaging practices are rapidly transitioning from digital 2D mammography (DM) to digital breast tomosynthesis (DBT), but there is limited research on the clinical performance of DBT-guided vacuum-assisted breast biopsy (VABB). The purpose of this study was to compare the performance of upright DBT VABB to that of conventional prone stereotactic (PS) VABB.

METHOD AND MATERIALS

In this IRB-approved and HIPAA-compliant study, a retrospective review was performed of consecutive patients who underwent PS VABB from August 2014 to December 2015 (PS VABB group) and DBT VABB from February 2016 to June 2017 (DBT VABB group). Tissue sampling methods and materials (9-gauge needles) were the same for PS VABB and DBT VABB. Student's *t*-tests and chi-square tests were used to compare the following variables between the PS VABB and DBT VABB groups: sampling success, procedure times, exposures, lesion types, histologic results, and complications.

RESULTS

Over a 17-month period before the introduction of DBT VABB, 444 PS VABBs in 410 patients (mean age 57, range 32-84) were performed (PS VABB group). Over a 17-month period after complete integration of DBT VABB, 709 DBT VABBs in 682 patients (mean age 58, range 23-90) were performed (DBT VABB group). Technical success was achieved for more lesions with DBT VABB than PS VABB (98.4% [698/709] vs 93.2% [414/444], p<0.001). Mean procedure time was shorter with DBT VABB (12 vs 28 minutes, p<0.001), and significantly fewer exposures were acquired with DBT VABB (3 vs 11, p<0.001). A higher percentage of lesions biopsied with DBT VABB were non-calcified lesions (eg, architectural distortion, asymmetry, and mass) (29.5% [206/698] with DBT VABB vs 3.1% [13/414] with PS VABB, p<0.001). There were no differences in the distribution of histologic results (benign, high-risk, or malignant) (p=0.94). No major complications were observed in either group. Two patients in the DBT VABB group (2/682, 0.3%) experienced self-limited vasovagal symptoms.

CONCLUSION

DBT VABB has higher technical success than PS VABB and can be performed in less than half the time and with less than one third of the radiation. In addition, more distortions and asymmetries are amenable to biopsy with DBT VABB.

CLINICAL RELEVANCE/APPLICATION

Clinical performance of DBT VABB is superior to PS VABB. DBT VABB can replace PS VABB for routine use in patients with suspicious findings identified on DBT alone and on conventional DM.



SSM02

Science Session with Keynote: Breast Imaging (Risk-Based Screening: Should We Do It?)

Wednesday, Nov. 28 3:00PM - 4:00PM Room: E350



AMA PRA Category 1 Credit ™: 1.00 ARRT Category A+ Credit: 1.00

Participants

Elizabeth A. Morris, MD, New York, NY (*Moderator*) Nothing to Disclose Daniel B. Kopans, MD, Waban, MA (*Moderator*) Royalties, Cook Group Incorporated; Research Consultant, Deep Health; Scientific Advisory Board, Dart, Inc

Sub-Events

SSM02-01 Breast Keynote Speaker: Risk Based Screening

Wednesday, Nov. 28 3:00PM - 3:10PM Room: E350

Participants Elizabeth A. Morris, MD, New York, NY (*Presenter*) Nothing to Disclose

SSM02-02 Risk-Based Screening Mammography for Women Age <40: Outcomes from the National Mammography Database

Wednesday, Nov. 28 3:10PM - 3:20PM Room: E350

Participants

Cindy S. Lee, MD, Garden City, NY (*Presenter*) Nothing to Disclose Heidi Ashih, PhD, Reston, VA (*Abstract Co-Author*) Nothing to Disclose Debapriya Sengupta, MBBS,MPH, Reston, VA (*Abstract Co-Author*) Nothing to Disclose Edward A. Sickles, MD, San Francisco, CA (*Abstract Co-Author*) Nothing to Disclose Margarita L. Zuley, MD, Pittsburgh, PA (*Abstract Co-Author*) Investigator, Hologic, Inc Etta D. Pisano, MD, Charleston, SC (*Abstract Co-Author*) Researcher, Freenome Holdings Inc; Researcher, Real Imaging Ltd; Researcher, Therapixel; Researcher, DeepHealth, Inc; Researcher, ToDos

For information about this presentation, contact:

Cindy.Lee3@nyumc.org

PURPOSE

There is insufficient large-scale evidence supporting screening mammography in women <40 years with risk factors. This study compares risk-based screening of women ages 30-39 versus women age 40-49 with no known risk factors, using screening mammography performance metrics from the National Mammography Database (NMD).

METHOD AND MATERIALS

This HIPAA compliant and IRB approved study analyzed data from 150 mammography facilities in 31 states in the NMD. The NMD collects clinical practice data including self-reported patient demographics, clinical findings, screening mammography interpretation and biopsy results. Patients were stratified by 5-year age intervals and specific risk factors for breast cancer: family history of breast cancer (any first degree relative regardless of age), personal history of breast cancer and breast density of heterogeneously or extremely dense (C or D). Prior mammography were identified by patient date of birth and facility-assigned identification number. Four performance metrics for screening mammography were calculated for each age and risk group: recall rate, cancer detection rate, and positive predictive values for biopsy recommended (PPV2) and biopsy performed (PPV3).

RESULTS

5,772,730 screening mammograms were performed between January 2008 and December 2015 in 2,647,315 women. Overall, mean cancer detection rate was 3.7 per 1000 (95% CI: 3.65-3.75), recall rate was 9.8% (9.8-9.8%), PPV2 was 20.1% (19.9-20.4%), and PPV3 was 28.2% (27.0-28.5%). Overall, women age 30-34 and 35-39 had similar cancer detection rates, recall rates and PPVs, with the presence of the three evaluated risk factors associated with significantly higher cancer detection rates. Moreover, compared to a population currently recommended for screening mammography in the USA (age 40-44 with no known risk factors), incidence screening (at least one prior screening examination) of women ages 30-39 with tthe three evaluated risk factors has similar cancer detection rates and recall rates.

CONCLUSION

Women ages 30-39 with 3 specific risk factors should benefit by starting screening at age 30 instead of the age 40 start recommended for average-risk women.

CLINICAL RELEVANCE/APPLICATION

Women

SSM02-03 A Deep-Learning Breast Cancer Risk Prediction Network: Trained on the Population-based Swedish CSAW Data

Wednesday, Nov. 28 3:20PM - 3:30PM Room: E350

Participants

Fredrik Strand, MD,PhD, Stockholm, Sweden (*Presenter*) Nothing to Disclose Yue Liu, Stockholm, Sweden (*Abstract Co-Author*) Nothing to Disclose Kevin Smith, Stockholm, Sweden (*Abstract Co-Author*) Nothing to Disclose Hossein Azizpour, Stockholm, Sweden (*Abstract Co-Author*) Nothing to Disclose Karin H. Dembrower, MD, Stockholm, Sweden (*Abstract Co-Author*) Nothing to Disclose Peter Lindholm, MD, PhD, Stockholm, Sweden (*Abstract Co-Author*) Nothing to Disclose

For information about this presentation, contact:

fredrik.strand@ki.se

PURPOSE

Almost half of breast cancer diagnoses among women attending mammographic screening are interval cancers or large screendetected cancers. To enable more effective individualized screening, accurate risk prediction is paramount. In this study, we examine how our trained deep learning network compares with mammographic density in risk prediction based on negative screening mammograms.

METHOD AND MATERIALS

The Swedish cohort of screen-age women (CSAW) contains over 500,000 women linked to the cancer registry and to an image database. Our deep learning network was trained on negative mammograms from incident cases from one uptake area 2008 to 2011. The test set consisted of cases from 2013 and 2014. In each set, we included a random sample of concurrent non-overlapping controls. The input was each negative mammogram downscaled as well as full-resolution central crops, age at mammography and selected DICOM parameters. The prediction output is called deep learning risk score (DLR). For comparison, mammographic density was calculated using the validated LIBRA software. Logistic regression models were fitted to examine odds ratios.

RESULTS

The training set consisted of 3167 negative mammograms from women with subsequent breast cancer and 125,683 mammograms from healthy women. The test set consisted of negative mammograms from 752 screening rounds of 326 women with subsequent breast cancer and 6728 rounds of 2065 healthy women. AUC was higher for DLR (0.63; 95%CI: 0.61 to 0.66) than for density (0.57; 95%CI: 0.54 to 0.60) and for age-adjusted density (0.58; 95%CI: 0.56 to 0.61). The proportion of cases were 10.1% in the top quintile and 2.5% in the bottom quintile of DLR. The top-to-bottom quintile odds ratio was 4.37 (95%CI: 3.01 to 6.45) and 1.69 (95%CI: 1.23 to 2.32) for DLR and age-adjusted density respectively.

CONCLUSION

We have demonstrated that it is possible to train a deep learning network on negative screening mammograms from subsequent breast cancer cases, and produce risk predictions with reasonable accuracy and ability to identify women at elevated risk.

CLINICAL RELEVANCE/APPLICATION

After external validation, our network may be used in individualizing breast cancer screening.

SSM02-04 Potential Role of Convolutional Neural Network based Algorithms in Patient Selection for DCIS Observation Trials

Wednesday, Nov. 28 3:30PM - 3:40PM Room: E350

Participants

Simukayi Mutasa, MD, New York, NY (*Presenter*) Nothing to Disclose Peter Chang, MD, San Francisco, CA (*Abstract Co-Author*) Nothing to Disclose Jenika Karcich, MD, New York, NY (*Abstract Co-Author*) Nothing to Disclose Eduardo Pascual Van Sant, BS, New York, NY (*Abstract Co-Author*) Nothing to Disclose Mary Q. Sun, MD, Manhasset, NY (*Abstract Co-Author*) Nothing to Disclose Michael Z. Liu, MS, New York, NY (*Abstract Co-Author*) Nothing to Disclose Sachin Jambawalikar, PhD, New York, NY (*Abstract Co-Author*) Nothing to Disclose Richard S. Ha, MD, New York, NY (*Abstract Co-Author*) Nothing to Disclose

For information about this presentation, contact:

s.mutasa@columbia.edu

PURPOSE

Minimizing over-diagnoses and treatment of Ductal Carcinoma in Situ (DCIS) has led to clinical trials of observing patients with DCIS instead of surgery. Despite careful selection for 'low risk' DCIS patients, there is evidence of occult invasive cancers in a significant number of these patients. We investigated the feasibility of utilizing convolutional neural networks (CNN) for predicting patients with pure DCIS versus DCIS with invasion using mammographic images.

METHOD AND MATERIALS

An IRB-approved retrospective study was performed. 246 unique images from 123 patients were used for our CNN algorithm. 164 images in 82 patients diagnosed with DCIS by stereotactic-guided biopsy of calcifications without any upgrade at the time of surgical excision (pure DCIS group). 82 images in 41 patients with mammographic calcifications yielding occult invasive carcinoma as the final upgraded diagnosis on surgery (occult invasive group). Two standard mammographic magnification views (CC and ML/LM) of the calcifications were used for analysis. Calcifications were segmented using an open source software platform 3D Slicer and resized to fit a 128x128 pixel bounding box. A 15 hidden layer topology based on residual convolutions was used to implement the

neural network. A class balanced holdout set with 40 patients was used for testing. 5-fold cross validation was utilized with cases randomly separated into a training set [80%] and validation set [20%].

RESULTS

The CNN algorithm for predicting patients with pure DCIS achieved an overall validation accuracy of 74.6% (95%CI, \pm 5) with area under the ROC curve of 0.71 (95% CI, \pm 0.04), specificity of 49.4% (95% CI, \pm 6%) and sensitivity of 91.6% (95% CI, \pm 5%).

CONCLUSION

It's feasible to apply a CNN to distinguish pure DCIS from DCIS with invasion using mammographic images. A larger dataset will likely improve our prediction model and could potentially be useful in appropriate patient selection for observation trials.

CLINICAL RELEVANCE/APPLICATION

Convolutional neural networks have demonstrated strong performance in various image classification tasks and may potentially be used in appropriate patient selection for DCIS observation trials.

SSM02-05 The Effect of Screening Modality and Race on BI-RADS Breast Density in a Large Urban Screening Cohort

Wednesday, Nov. 28 3:40PM - 3:50PM Room: E350

Participants

Aimilia Gastounioti, Philadelphia, PA (*Presenter*) Nothing to Disclose Anne Marie McCarthy, Boston, MA (*Abstract Co-Author*) Nothing to Disclose Lauren Pantalone, BS, Philadelphia, PA (*Abstract Co-Author*) Nothing to Disclose Marie Synnestvedt, Philadelphia, PA (*Abstract Co-Author*) Nothing to Disclose Despina Kontos, PhD, Philadelphia, PA (*Abstract Co-Author*) Nothing to Disclose Emily F. Conant, MD, Philadelphia, PA (*Abstract Co-Author*) Grant, Hologic, Inc; Consultant, Hologic, Inc; Grant, iCAD, Inc; Consultant, iCAD, Inc; Speaker, iiCME

For information about this presentation, contact:

aimilia.gastounioti@uphs.upenn.edu

PURPOSE

Increased breast density is an independent breast cancer risk factor and also limits the sensitivity and specificity of mammography. We investigated the effect of screening mammography modality and race on BI-RADS breast density assessments, accounting for age and body-mass index (BMI).

METHOD AND MATERIALS

We retrospectively analyzed data from 24,740 individual women (45% White, 55% Black) who underwent screening from September 2010 through February 2017 at our institution. 15,147 women (55%) had repeated screening studies (N = 60,774 studies). Over this time period, three screening modalities were used: digital mammography alone (DM; N = 8,936); digital breast tomosynthesis (DBT) with DM (DM/DBT, N = 30,786); and synthetic 2D with DBT (s2D/DBT, N = 21,052). BI-RADS density classifications ranging from lower (fatty or scattered) to higher (heterogeneous or extremely dense) density were extracted from screening reports. Random-effects ordered logistic regression (panel variable: individual woman) was performed to estimate the odds of being assigned to higher BI-RADS density by each modality, adjusted for race, age, BMI and radiologist. The interaction of modality and race on density was tested in the model, and analyses were stratified by race.

RESULTS

Women screened with DBT had significantly lower odds of high density compared to those screened with DM alone (DM/DBT vs. DM: OR = 0.62, p < .0001; s2D/DBT vs. DM: OR = 0.48, p < .0001). Lower odds of high density were also observed in s2D/DBT compared to DM/DBT (OR = 0.76, p < .0001). There was a significant interaction of modality and race on breast density (p = .0003). All differences by modality maintained statistical significance in analyses stratified by race, with lower ORs for black (DM/DBT vs. DM: OR = 0.61; s2D/DBT vs DM: OR = 0.40; s2D/DBT vs. DM/DBT: OR = 0.67) than for white women (DM/DBT vs. DM: OR = 0.65; s2D/DBT vs. DM: OR = 0.58; s2D/DBT vs. DM/DBT: OR = 0.89).

CONCLUSION

Screening mammography modality has a significant effect on BI-RADS density assessment with an overall trend of assigning lower density with DBT and s2D/DBT screening versus DM alone. Furthermore, this effect seems to be more prominent in black than in white women.

CLINICAL RELEVANCE/APPLICATION

Our findings have direct implications for personalized screening since breast density assignments, which often drive recommendations for supplemental screening, may vary greatly by modality and race.

SSM02-06 Breast Keynote Speaker: Risk Based Screening

Wednesday, Nov. 28 3:50PM - 4:00PM Room: E350

Participants

Daniel B. Kopans, MD, Waban, MA (*Presenter*) Royalties, Cook Group Incorporated; Research Consultant, Deep Health; Scientific Advisory Board, Dart, Inc



SSM03

Cardiac (Anatomy)

Wednesday, Nov. 28 3:00PM - 4:00PM Room: S102CD



AMA PRA Category 1 Credit ™: 1.00 ARRT Category A+ Credit: 1.00

Participants

Evan J. Zucker, MD, Stanford, CA (*Moderator*) Nothing to Disclose Karin E. Dill, MD, Worcester, MA (*Moderator*) Nothing to Disclose

Sub-Events

SSM03-01 The Automated Segmentation of the Left Ventricle Myocardium from Cardiac Computed Tomography using Deep Learning

Wednesday, Nov. 28 3:00PM - 3:10PM Room: S102CD

Participants

Hyun Jung Koo, MD, Seoul, Korea, Republic Of (*Presenter*) Nothing to Disclose Joon-Won Kang, MD, Seoul, Korea, Republic Of (*Abstract Co-Author*) Nothing to Disclose Ji-Yeon Ko, Seoul, Korea, Republic Of (*Abstract Co-Author*) Nothing to Disclose June-Goo Lee, PhD, Seoul, Korea, Republic Of (*Abstract Co-Author*) Nothing to Disclose Dong Hyun Yang, MD, Seoul, Korea, Republic Of (*Abstract Co-Author*) Nothing to Disclose

For information about this presentation, contact:

donghyun.yang@gmail.com

PURPOSE

Segmentation of the left ventricle myocardium of the heart is important to obtain information regarding myocardial wall thickening and functional analysis data. In this study, we performed deep learning analysis for the automated segmentation of the left ventricle of the heart in cardiac computed tomography (CT) data.

METHOD AND MATERIALS

To develop a fully automated deep learning algorithm using sementic segmentation methods based on fully convolution network, 50 subjects with coronary artery diseases were used as training set, and the approach is evaluated using a data set of 1000 subjects with coronary artery diseases present whole 3D volume images of the LV. Reference standard manual segmentation data generated by experienced cardiac radiologists. Cross validation was performed using randomly selected 5% cases from the training set. The comparison of quantitative measurement data between the manual and automatic segmentations was performed using dice similarity coefficient.

RESULTS

Overall, automated segmentation data were comparable to manual segmentation data. We obtained mean 88.3% (min 78.1% and max 96.5%) of dice similarity coefficient in whole LV myocardium. The sensitivity and specificity of automated segmentation in each segment (1-16 segments) were high (range: 85.5 - 99.9).

CONCLUSION

Using a large data set, we presented a deep learning based automatic segmentation of the left ventricle of the heart, and the results was comparable to manual segmentation data with high dice index.

CLINICAL RELEVANCE/APPLICATION

Automated LV segmentation can reduce time to obtain information regarding myocardial wall thickening and LV function, and might improve the reproducibility of clinical assessment.

SSM03-02 Microcirculation Dysfunction in Patients with End-Stage Renal Disease Undergoing Dialysis: Associated with Heart Failure in the Follow-Up

Wednesday, Nov. 28 3:10PM - 3:20PM Room: S102CD

Participants

Ying-Kun Guo, MD, Chengdu, China (*Presenter*) Nothing to Disclose Rong Xu, Chengdu, China (*Abstract Co-Author*) Nothing to Disclose Huayan Xu, Chengdu, China (*Abstract Co-Author*) Nothing to Disclose Zhigang Yang, MD, Chengdu, China (*Abstract Co-Author*) Nothing to Disclose

For information about this presentation, contact:

Xrongdoctor@163.com

PURPOSE

The dialysis treatment was used widely in the ESRD patients, but myocardial ischemia and the cardiovascular disease were the major cause of death in chronic kidney disease (CKD) patients. Our study aimed to quantitative evaluation of myocardial microcirculation dysfunction by rest CMR perfusion imaging in patients with ESRD undergoing dialysis, and to understand of the association between perfusion parameters and heart failure.

METHOD AND MATERIALS

In total, 67 ESRD patients with preserved EF (EF>=50%) and 22 healthy subjects underwent rest first-pass perfusion. The LV regional myocardial perfusion parameters were analyzed by a commercial soft included upslope, time to maximum signal intensity (TTM) and max signal intensity (Max SI). Continuous variables were compared using one-way analysis of variance (ANOVA). The association between perfusion parameters and the composite of CHF was assessed by Cox proportional hazards regression.

RESULTS

For the analysis, the Max SI of basal, mid- and apical segments were reduced in ESRD patients with preserved EF compared with normal controls (all P < 0.05). In contrast to the patients with preserved EF, the patients with impaired EF had lower upslope and longer TTM in the basal segment. Over a mean follow-up period of 12.5 months, 24 subjects developed heart failure. The TTM of Basal-, mid-, and apical- segments were inversely associated with risk of heart failure (per unit increment, HR:1.052, 95% CI: 1.010-1.095, HR:1.086, 95% CI: 1.033-1.143, and HR:1.084, 95% CI: 1.024-1.146, respectively) after multivariable adjustment by gender, age, BMI, dialysis time, hypertension, and diabetes.

CONCLUSION

In summary, the first-pass perfusion CMR parameters can early detect the regional myocardial microcirculation dysfunction in ESRD patients undergoing dialysis. The myocardial dysfunction can predictor the progression of heart failure.

CLINICAL RELEVANCE/APPLICATION

(dealing with first-pass perfusion CMR)CMR perfusion imaging with vasodilator can detect myocardial microcirculation dysfunction in ESRD patients undergoing dialysis.

SSM03-03 Differences in Cardiac MR-based Assessment of Myocardial 2D Strain between Subjects with Prediabetes, Diabetes, and Normal Controls in the General Population

Wednesday, Nov. 28 3:20PM - 3:30PM Room: S102CD

Participants

Tanja Zitzelsberger, MD, Tuebingen, Germany (*Presenter*) Nothing to Disclose Astrid Scholz, Tuebingen, Germany (*Abstract Co-Author*) Nothing to Disclose Susanne Rospleszcz, Munich, Germany (*Abstract Co-Author*) Nothing to Disclose Roberto Lorbeer, Greifswald, Germany (*Abstract Co-Author*) Nothing to Disclose Konstantin Nikolaou, MD, Tuebingen, Germany (*Abstract Co-Author*) Advisory Panel, Siemens AG; Speakers Bureau, Siemens AG; Speaker Bureau, Bayer AG Maximilian F. Reiser, MD, Munich, Germany (*Abstract Co-Author*) Nothing to Disclose Fabian Bamberg, MD, Tuebingen, Germany (*Abstract Co-Author*) Speakers Bureau, Bayer AG; Speakers Bureau, Siemens AG; Research Grant, Siemens AG

Christopher L. Schlett, MD, MPH, Heidelberg, Germany (Abstract Co-Author) Nothing to Disclose

PURPOSE

In the setting of diabetes mellitus, diabetic cardiomyopathy is associated with limited event-free survival but difficult to detect. However, cardiac MR based assessment of subtle alterations of left ventricular function using 2D cardiac strain analysis may represent an early marker of disease development. Thus, we determined differences in left ventricular strain between subjects with prediabetes, diabetes, and healthy controls in a sample from the general population.

METHOD AND MATERIALS

Subjects without prior history of stroke, coronary or peripheral artery disease were enrolled in a case-controlled study and underwent 3T whole body MRI. In all patients without history of hypertension, LGE and normal ejection fraction, radial, longitudinal and circumferential strain was measured on Cine SSFP imaging (TR: 29.97ms, TE: 1.46ms, ST: 8mm) using a semiautomatic segmentation algorithm (CVI42, Circle, Canada). Differences in strain rates were derived in multivariate linear regression analysis adjusting for age, gender, BMI, blood pressure, and smoking, HDL, LDL and TG.

RESULTS

Radial and circumferential strain analysis was performed in in total 347 subjects, of which 41 (11.8%) suffered from diabetes, 92 (26.5%) from pre-diabetes and 214 (61.7%) controls. Mean HbA1c of diabetic subjects was 6.5 ± 1 mmol/mol Hb. Pre-diabetic subjects showed a significantly higher systolic global and endocardial radial strain compared to controls (p=0.036 and p=0.011 respectively), whereas diabetic subjects didn't show any significant difference (p=1.00 and p=0.811). Similarly we detected significant lower systolic global and endocardial strain values in pre-diabetic subjects (p=0.044 and p=0.009), whereas diabetic subjects didn't show a significant difference (p=1.00 and p=0.580). Regarding diastolic radial and circumferential strain we didn't find any significant difference.

CONCLUSION

In our cohort of well-treated diabetic subjects we didn't find any changes in strain values whereas pre-diabetic subjects showed early changes. Therefore early and consequent treatment of diabetes seems to be cardioprotective.

CLINICAL RELEVANCE/APPLICATION

MR based Strain Imaging is able to detect early changes in cardic function in patients with prediabetes. As these changes are not seen in well treated diabetic patients consideration should be given to early antidiabetic therapy.

SSM03-04 Left Atrial Functional Impairment in Patients with Stroke: A Cardiovascular Magnetic Resonance

Study

Wednesday, Nov. 28 3:30PM - 3:40PM Room: S102CD

Participants

Wieland Staab, MD, Goettingen, Germany (*Presenter*) Nothing to Disclose Laura Wandelt, Goettingen, Germany (*Abstract Co-Author*) Nothing to Disclose Andreas Schuster, Goettingen, Germany (*Abstract Co-Author*) Nothing to Disclose Rolf Wachter, Goettingen, Germany (*Abstract Co-Author*) Nothing to Disclose Michael Steinmetz, Goettingen, Germany (*Abstract Co-Author*) Nothing to Disclose Christina Unterberg-Buchwald, Goettingen, Germany (*Abstract Co-Author*) Nothing to Disclose Joachim Lotz, MD, Gottingen, Germany (*Abstract Co-Author*) Nothing to Disclose Johannes T. Kowallick, Gottingen, Germany (*Abstract Co-Author*) Nothing to Disclose

For information about this presentation, contact:

wieland.staab@med.uni-goettingen.de

PURPOSE

In 25 % of patients with ischemic stroke, no etiologic factor can be identified. Asymptomatic paroxysmal atrial fibrillation (AF) is often suspected to be the cause of these cryptogenic strokes (CS). AF is frequently associated with left atrial (LA) structural and functional alterations. Accordingly, the aim of this study was to examine LA deformation in patients with CS using cardiovascular magnetic resonance myocardial feature tracking (CMR-FT).

METHOD AND MATERIALS

29 patients with the diagnosis of CS underwent CMR imaging. Based on the initial cranial computed tomography (cCT), the patient group was divided into patients with previous ischemic lesions (recurrent CS) and patients without (first-time CS). LA deformation was analyzed based on CMR-FT of standard cine 4- and 2-chamber views including LA reservoir function (peak total strain [s], peak positive SR [SRs]), LA conduit function (passive strain [e], peak early negative SR [SRe]) and LA booster pump function (active strain [a], late peak negative SR [SRa]). Moreover, the "time to s" and "time to SRs" were calculated and expressed as a percentage of the entire cardiac cycle.

RESULTS

Previous ischemic lesions were detected in 5 of 29 patients (17%). LA conduit strain was lower in patients with recurrent CS as compared to first-time CS (6.4 ± 1.1 % vs. 10.3 ± 3.3 %, respectively, p=0.005). Furthermore, "time to s" and "time to SRs" were prolonged in patients with recurrent CS (47 ± 6 % vs. 57 ± 8 %, p=0.007; and 19 ± 5 % vs. 30 ± 7 %, p=0.001, respectively). In multivariable regression models "time to s" and "time to SR" were independently associated with the presence of previous ischemic lesions (β =0.41, p=0.006 and β =0.51, p=0.015, respectively) after adjustment for traditional risk factors (age, gender, arterial hypertension, vascular disease and diabetes).

CONCLUSION

Prolonged time to peak LA reservoir strain and SR is associated with the presence of previous ischemic lesions in patients with CS. These findings propose advanced LA impairment as a distinct feature of CS which may be associated with unrecognized paroxysmal AF. Future research is warranted to confirm these findings alongside their prognostic implications in larger prospective clinical trials.

CLINICAL RELEVANCE/APPLICATION

Advanced LA impairment detected by cardiac magnetic resonance imaging may improve management of patients with or prior to CS.

SSM03-05 Machine Learning for Automated Image Quality Control and Segmentation of Large-Scale CMR Population Studies

Wednesday, Nov. 28 3:40PM - 3:50PM Room: S102CD

Participants

Wenjia Bai, DPhil, London, United Kingdom (*Abstract Co-Author*) Nothing to Disclose Giacomo Tarroni, London, United Kingdom (*Abstract Co-Author*) Nothing to Disclose Hideaki Suzuki, London, United Kingdom (*Abstract Co-Author*) Nothing to Disclose Ozan Oktay, PhD, London, United Kingdom (*Abstract Co-Author*) Nothing to Disclose Jo Schlemper, London, United Kingdom (*Abstract Co-Author*) Nothing to Disclose Paul M. Matthew, MD,DPhil, London, United Kingdom (*Abstract Co-Author*) Nothing to Disclose Daniel Rueckert, PhD, London, United Kingdom (*Presenter*) Nothing to Disclose

PURPOSE

UK Biobank is a large-scale prospective cohort study that follows the health of 500,000 subjects across the UK. Of all the subjects, 100,000 will undergo imaging scans including brain, heart and body scans. We propose a machine learning-based and automated pipeline for cardiac MR (CMR) image quality control and segmentation on this large-scale dataset.

METHOD AND MATERIALS

CMR images were obtained from the UK Biobank under Application Number *****. Short-axis and long-axis cine images were acquired using a Siemens 1.5T scanner with the balanced steady state free precession (bSSFP) sequence. For image quality control, hybrid random forests were trained to detect landmarks on long-axis images, specifically the apex and mitral valve, which were then compared to the space encompassed by short-axis image stacks for identifying incomplete heart coverage. For image segmentation, fully convolutional networks were trained to segment the left ventricle (LV) and right ventricle (RV) on short-axis images and the left atrium (LA) and right atrium (RA) on long-axis images. The segmentation accuracy was evaluated using the Dice metric and mean contour distance error.

RESULTS

The pipeline took ~1 second for image quality control and ~10 seconds for short-axis and long-axis image segmentation. Cases

with heart coverage deemed incomplete by visual examination were automatically identified with 88% sensitivity and 99% specificity on a random test set of 3,000 subjects. Regarding segmentation accuracy, the average Dice metric is 0.94 for LV cavity, 0.88 for LV myocardium, 0.90 for RV cavity, 0.93 for LA cavity (2-chamber view), 0.95 for LA cavity (4-chamber view) and 0.96 for RA cavity (4-chamber view), evaluated on a test set of 600 subjects. The average mean contour distance error is smaller than the in-plane pixel resolution of 1.8mm.

CONCLUSION

We have proposed a machine learning-based pipeline for CMR image quality control and segmentation, which is automated, fast and accurate.

CLINICAL RELEVANCE/APPLICATION

The pipeline will facilitate the analysis of large-scale CMR population studies such as the UK Biobank and enable automated extraction of clinically relevant phenotypes including the ventricular volumes and mass. Future work could evaluate its potential to add quantitative image-derived phenotypes as part of routine clinical practice.

SSM03-06 Cardiac Adaptation of Left Ventricular Volume and Mass during a Multistage Marathon Over 4486 Km

Wednesday, Nov. 28 3:50PM - 4:00PM Room: S102CD

Participants

Christopher Klenk, MD, Basel, Switzerland (*Presenter*) Nothing to Disclose Florian Sagmeister, MD, Ulm, Germany (*Abstract Co-Author*) Nothing to Disclose Thomas Nickel, Munich, Germany (*Abstract Co-Author*) Nothing to Disclose Meinrad J. Beer, MD, Ulm, Germany (*Abstract Co-Author*) Nothing to Disclose Arno Schmidt-Trucksass, Basel, Switzerland (*Abstract Co-Author*) Nothing to Disclose Uwe H. Schuetz, MD, Ulm, Germany (*Abstract Co-Author*) Nothing to Disclose

For information about this presentation, contact:

florian.sagmeister@uniklinik-ulm.de

PURPOSE

Long-term side effects of intense physical training and long-distance running has led to increasing concerns especially among athletes. However, the consequences on long-term endurance training on cardiac structure and function are not yet fully understood. The purpose of this study was to evaluate the effect of running a transcontinental, multistage ultramarathon of 4486km on 64 consecutive days on the heart.

METHOD AND MATERIALS

20 ultra-endurance athletes with a mean (standard deviation) age of 47.9 (10.4) years received a cardio MRI-scan at three time points (baseline, at ~2000km, ~3500km) during the multistage ultramarathon. Cardiovascular magnetic resonance (CMR) was performed on a portable 1.5 Tesla MRI unit (Magnetom Avanto[™] mobile MRI) which was installed on a specially hired truck. Left ventricular mass (LVM), end-diastolic volume (EDV), end-systolic volume (ESV) and myocardial strain was calculated from SSFP-cine gradient echo sequences using the commercially available software (Heart Deformation Analysis, HDA, Siemens, Erlangen, Germany). Cardiac MRI-parameters were indexed for body surface area (BSA). Ten runners were serially examined in follow-up scans eight months after the race.

RESULTS

Athletes ran at a mean running speed of 8.2 ± 1.2 km/h during the ultramarathon. Left ventricular mass increased significantly (p<0.001) over the course of the race while no significant changes were observed in end-diastolic volume, end-systolic volume as well as global radial, circumferential and longitudinal left ventricular strain. Results of follow-up scans showed a significant reduction in LVMi (p=0.004), left ventricular EDVi (p=0.015) and right ventricular EDVi (p=0.045). We did not observe any significant differences regarding myocardial strain during follow-up.

CONCLUSION

The observed structural cardiac alterations during a multistage ultra-endurance marathon indicates a physiological response to excessive cardiac volume load. The reduction in end-diastolic volumes during follow-up corresponds to the reduced endurance exercise volume within eight months after the multistage ultramarathon.

CLINICAL RELEVANCE/APPLICATION

Extreme long-distance running leads to physiological cardiac adaptations without any detectable adverse cardiovascular remodeling in non-contrast enhanced cardiovascular magnetic resonance imaging.



Cardiac (Arrhythmia and Electrophysiology)

Wednesday, Nov. 28 3:00PM - 4:00PM Room: S103AB



AMA PRA Category 1 Credit ™: 1.00 ARRT Category A+ Credit: 1.00

FDA Discussions may include off-label uses.

Participants

Susan K. Hobbs, MD, PhD, Pittsford, NY (*Moderator*) Nothing to Disclose Dharshan R. Vummidi, MD, FRCR, Sale, United Kingdom (*Moderator*) Consultant, Boehringer Ingelheim GmbH

Sub-Events

SSM04-01 Radiographic Features of Pulmonary Veins Morphology from Chest CT Predicts Risk of Post-Ablation Atrial Fibrillation

Wednesday, Nov. 28 3:00PM - 3:10PM Room: S103AB

Participants Michael LaBarbera, Cleveland, OH (*Presenter*) Nothing to Disclose Mina K. Chung, MD, Cleveland, OH (*Abstract Co-Author*) Nothing to Disclose Anant Madabhushi, PhD, Cleveland, OH (*Abstract Co-Author*) Research funded, Koninklijke Philips NV

For information about this presentation, contact:

labarbm@ccf.org

PURPOSE

Atrial fibrillation (AF) is the most common sustained arrhythmia, affecting 1-2% of the population. Although endovascular pulmonary vein isolation (PVI) may temporarily reduce symptoms in patients failing medical management, recurrence rates are high and identifying patients likely to have successful outcomes remains elusive. Pulmonary vein morphology and left atrial size have been previously identified as radiographic markers for AF, but have not been assessed for PVI outcome. We explore pulmonary vein and left atrial morphometry as a means of predicting response to PVI.

METHOD AND MATERIALS

A retrospective review of PVI procedures from 2014-2016 excluding prior PVI or valve surgery revealed 314 cases. 154 had pre-PVI CT imaging and clinician-assessed PVI outcome recorded in the EMR at follow-up, with 50 cases diagnosed with recurrent AF within 3 months to 1 year. 50 non-recurrent cases were randomly selected to produce a balanced dataset for analysis (n = 100). Radiographic features were obtained characterizing left atrium size, pulmonary vein morphology, and angle of vein entry into the left atrium using Syngo.Via (©Siemens Healthcare). The 5 most distinguishing features were selected by Wilcoxon rank-sum and used to train a support vector machine classifier in a 3-fold cross-validation setting. Ability to predict recurrence was assessed by area under the receiver operating characteristic curve (AUC) among all patients and the predictive ability including clinical features was investigated similarly.

RESULTS

Distinguishing radiographic features include angle between right pulmonary veins (p = 0.063) and angle of left inferior pulmonary vein entry into the left atrium (p = 0.060). Radiographic features effectively predicted recurrence of AF within 1 year of PVI (AUC = 0.65 ± 0.03) and inclusion of clinical features further improved performance (AUC = 0.77 ± 0.02). Distinguishing clinical features include age (p < 0.001), BMI (p = 0.005), left ventricular ejection fraction (p = 0.014), history of hypertension (p = 0.016), NYHA class of I or greater (p = 0.016), and use of apixaban (p = 0.016).

CONCLUSION

Pulmonary vein morphology in CT successfully predicts recurrence of AF after endovascular treatment.

CLINICAL RELEVANCE/APPLICATION

The ability to identify patients likely to have recurrent AF based on CT morphometric features may provide a pre-treatment indicator of response and anatomic features that may be targeted.

SSM04-02 Relationship Between Chronicity of Atrial Fibrillation and Left Atrial Remodeling Determined with Cardiac Magnetic Resonance Imaging in Patients with Atrial Fibrillation: Significance of Regional Left Atrial Late Gadolinium Enhancement

Wednesday, Nov. 28 3:10PM - 3:20PM Room: S103AB

Participants

Yu-Whan Oh, MD, Seoul, Korea, Republic Of (*Abstract Co-Author*) Nothing to Disclose Sung Ho Hwang, MD, Seoul, Korea, Republic Of (*Abstract Co-Author*) Nothing to Disclose

PURPOSE

Left atrial (LA) remodeling is associated with progression of atrial fibrillation (AF). Cardiac magnetic resonance (CMR) imaging can assess the LA remodeling with LA volume (LAV) and LA late gadolinium enhancement (LA-LGE). The distribution of LA-LGE by LAV is largely unknown. This study aimed to determine the relationship of LA-LGE distribution with LAV and progression of AF.

METHOD AND MATERIALS

195 patients (mean age: 55.7 \pm 10.7 years, 82.6% men) underwent LGE-CMR examinations before ablation of paroxysmal AF (PAF, n = 121) or persistent AF (PeAF, n = 74). The LAV and LA-LGE were assessed by three-dimension reconstruction of LGE-CMR images. In each of all 9 preselected LA regions, the presence of LA-LGE was evaluated. Additionally, the incidences (in %) of LA-LGE were calculated in every LA region.

RESULTS

Of all the preselected LA regions, the anterior wall and left inferior pulmonary vein (LIPV) region showed a significantly different incidence of LA-LGE (p < 0.05, respectively) depending on the LAV. In all 195 patients, the incidences of LA-LGE in the anterior wall and LIPV region were 15.4% and 15.9%. The patients with PeAF showed significantly higher LA-LGE incidence in the anterior wall (31.1% vs. 5.8%, p < 0.001) and LIPV region (29.7% vs. 7.4%, p < 0.001) than did those with PAF. After adjusting for LAV, the odd ratios for PeAF of the LA-LGE in anterior wall and LIPV region were 3.8 (95% CI = 1.40-10.41, p = 0.009) and 3.7 (95% CI = 1.46-9.75, p = 0.006), respectively.

CONCLUSION

In evaluation of LA remodeling using CMR imaging, the regional LA-LGE in anterior wall and LIPV region of LA may be associated with the presence of PeAF.

CLINICAL RELEVANCE/APPLICATION

Cardiac MRI can describe the LA remodeling related to the chronicity of AF. Furthermore, the LA remodling determined with cardiac MRI may help understanding the AF mechanism.

SSM04-03 Determination of Conducting Channels from LGE CMR in Patients with Myocardial Infarction-Direct Comparison with Electroanatomic Mapping for Ventricular Tachycardia Ablation

Wednesday, Nov. 28 3:20PM - 3:30PM Room: S103AB

Participants

Avanti Gulhane, Philadelphia, PA (*Abstract Co-Author*) Nothing to Disclose Saman Nazarian, MD, Baltimore, MD (*Abstract Co-Author*) Scientific Advisor, Johnson & Johnson Research funded, Johnson & Johnson Harold I. Litt, MD, PhD, Philadelphia, PA (*Presenter*) Research Grant, Siemens AG ; ; ;

For information about this presentation, contact:

avy.cutie@gmail.com

PURPOSE

LGE CMR is an excellent tool to evaluate scar in patients after myocardial infarction (MI). Electroanatomic mapping (EAM) is traditionally used to locate areas in scar tissue giving rise to ventricular tachycardia (VT) and guide ablation. However, new software using pixel signal intensity (PSI) algorithms has made it possible to locate conducting channels (CC) in scar tissue which form VT substrate using LGE CMR. We compared LGE derived CC with EAM findings in patients with VT post MI.

METHOD AND MATERIALS

We evaluated retrospectively 28 patients with previous MI and VT who underwent CMR prior to EAM and VT ablation. Short axis LGE CMR were evaluated using ADAS-VT (Galgo Medical SL, Barcelona) to identify CC within myocardial layers. A PSI-based algorithm was applied to characterize the LGE area as scar core or border zone, using 60% and 40% of the maximum LGE intensity as thresholds. CC were identified topologically by finding border zone coursing through scar core, representing corridors of viable tissue. CC on LGE-CMR were co-registered with EAM on Carto system. This data was evaluated according to AHA 17 segment model for targeted sites of VT ablation on a per patient and per channel basis

RESULTS

In 28 patients, 232 potential VT sites were identified on EAM-CMR merge, of which 129(55%) were targeted for ablation.138 sites of CC were identified. On a per patient basis, 4 CMR analyses were in total agreement with EAM, 24 had partial agreement. 87(67.4%) CC sites matched sites of ablation, 50(21%) CC sites were detected only on CMR. 53(23%) scar sites had neither CC on CMR nor ablation on EAM. 42(32.5%) sites of ablation on EAM did not show CC on LGE CMR. CC were also correlated with sites having late(64%), fractionated(65%) potentials, critical isthmus, entry points (60%), pacing sites(60%) and induced VT(48%). LGE CMR PSI-based analysis showed sensitivity of 67.4%(95%CI 58.6%-75.4%), specificity of 52%, positive predictive value of 64%(95%CI 58.% - 69.6%) and negative predicting value of 56% and overall diagnostic accuracy of 60% in identifying sites of EAM sites of ablation.

CONCLUSION

LGE CMR PSI-based analysis has good sensitivity and positive predictive value in identifying sites of VT on EAM.

CLINICAL RELEVANCE/APPLICATION

Target sites for VT ablations can predicted by LGE-CMR to aid preprocedural planning, potentially reducing the need for extensive EAM and additional CC on CMR can also identify cause of recurrent VT

SSM04-04 Comparison of Cardiac Venous Anomalies in Complete and Congenitally Corrected Transposition of

the Great Arteries: Implications for Cardiac Resynchronization Therapy

Wednesday, Nov. 28 3:30PM - 3:40PM Room: S103AB

Participants Hugo Vidal, MD, Toronto, ON (*Presenter*) Nothing to Disclose Kate Hanneman, MD, FRCPC, Toronto, ON (*Abstract Co-Author*) Nothing to Disclose Krishnakumar Nair, Toronto, ON (*Abstract Co-Author*) Nothing to Disclose Elsie Nguyen, MD, Toronto, ON (*Abstract Co-Author*) Nothing to Disclose

For information about this presentation, contact:

hugo.vidalalberdi@uhn.ca

PURPOSE

Cardiac resynchronization therapy (CRT) can help improve cardiac function of progressively failing subaortic morphologic right ventricles in both complete (c-TGA) and congenitally corrected (cc-TGA) transposition of the great arteries, but requires transvenous access to the subaortic morphologic right ventricle. We aim to compare the prevalence of cardiac venous anomalies and accessibility for CRT in c-TGA and cc-TGA using cardiac gated computed tomography angiography (CTA).

METHOD AND MATERIALS

With institutional review board approval, all CTA studies performed between 2007-2018 in patients with c-TGA and cc-TGA were retrospectively reviewed. CTAs were evaluated for cardiac venous anomalies and whether both subaortic and subpulmonic ventricles could be accessed via the subpulmonic atrium and coronary sinus. Statistical analysis included independent samples t-test for continuous variables and Fisher's exact test for categorical variables.

RESULTS

121 patients were included [mean age 36 years (range 18-69 yrs), 75 males (62%)] including 70 patients with c-TGA (44 atrial switch, 13 arterial switch, 13 Rastelli) and 51 with cc-TGA (48 no surgery, 3 double switch). Cardiac venous anomalies were more frequent in cc-TGA (30% vs. 6%; p<0.001). Accessibility was significantly higher in cc-TGA compared to c-TGA (86% vs 60%; p<0.002). Accessibility was lower among c-TGA patients who had undergone atrial switch compared to those with arterial switch or Rastelli procedures (39% vs. 96%, p<0.001). Accessibility was also significantly lower among cc-TGA patients who had undergone double switch compared to those who had not (33% vs. 89%, p=0.048).

CONCLUSION

Cardiac CTA identifies cardiac venous anomalies that impact eligibility for CRT. CRT eligibility is significantly lower among both c-TGA patients who have undergone atrial switch procedure and cc-TGA patients who have undergone double switch procedure compared to patients who have not.

CLINICAL RELEVANCE/APPLICATION

Cardiac-gated CTA is essential prior to CRT due to high prevalence of cardiac venous anomalies that may render the patient ineligible due to lack of access.

Honored Educators

Presenters or authors on this event have been recognized as RSNA Honored Educators for participating in multiple qualifying educational activities. Honored Educators are invested in furthering the profession of radiology by delivering high-quality educational content in their field of study. Learn how you can become an honored educator by visiting the website at: https://www.rsna.org/Honored-Educator-Award/ Kate Hanneman, MD, FRCPC - 2017 Honored EducatorKate Hanneman, MD, FRCPC - 2018 Honored Educator

SSM04-05 Anatomical Shape Differences of Left Atrium on CT Predicts Post-Ablation Recurrence of Atrial Fibrillation

Wednesday, Nov. 28 3:40PM - 3:50PM Room: S103AB

Participants Thomas Atta-Fosu, Cleveland, OH (*Abstract Co-Author*) Nothing to Disclose Michael LaBarbera, Cleveland, OH (*Presenter*) Nothing to Disclose Mina K. Chung, MD, Cleveland, OH (*Abstract Co-Author*) Nothing to Disclose Anant Madabhushi, PhD, Cleveland, OH (*Abstract Co-Author*) Research funded, Koninklijke Philips NV

For information about this presentation, contact:

thomas.atta-fosu@case.edu

PURPOSE

Approximately 30% of Atrial Fibrillation (AF) patients who undergo endovascular ablation experience recurring symptoms within the first year after ablation. Patients with long-standing AF demonstrate changes in left atrial morphology and the atrial appendage and pulmonary veins are known regions of interest in ablation, although the impact of morphology on ablation outcome remains unclear. In this study we employed image analysis and machine learning approaches to investigate whether the morphology of the left atrium (LA) was predictive of recurrence in patients undergoing ablation for AF.

METHOD AND MATERIALS

Pre-operative chest CT scans of 68 patients who underwent surgical ablation were acquired between July 2015 and November 2016, of which 31 had AF episodes between 3 and 12 months after ablation. LA masks were created for each patient using an inhouse segmentation toolbox and verified by a cardiologist. All patient LA were registered to a common atlas defined by the LA with median volume. Sites of interest (SOI) was then defined for each patient as the regions on the atrial surface with significant difference between recurrent (AF+) and non-recurrent (AF-) patients using a t-test based comparison of the registered atrial. First order statistics of the Gaussian curvature of the surface within the SOI and deformation from atlas to patient LA were extracted,

and a 5-fold cross-validation scheme across 100 runs was conducted to evaluate performance of the features in distinguishing between AF+ and AF- patients using area under the receiver operating characteristic curve (AUC).

RESULTS

The identified regions of maximum shape variation consisted of sites around the atrial appendage and pulmonary veins. Employing feature maps from these regions to classify recurrence performed better (AUC= 0.69 ± 0.049) than features from the remaining atrial sites (AUC= 0.58 ± 0.58). Combining the feature maps with clinical features (Age, Height, BMI and Weight) produced an AUC of 0.77 ± 0.09 , while Using Clinical variables alone produced AUC of 0.66 ± 0.11

CONCLUSION

We identified shape differences between AF+ and AF- patients as well as a set of features relating to local curvature within regions differing different between the two populations that was correlated with likelihood of recurrence.

CLINICAL RELEVANCE/APPLICATION

A systematic process for identifying patients at increased risk for post-ablation recurrence may lead to improved management.

SSM04-06 Detects Myocardial Dyssynchrony of Isolated Left Ventricular Noncompaction Patients with Preserved Ejection Fraction Using Cardiac Magnetic Resonance Feature Tracking

Wednesday, Nov. 28 3:50PM - 4:00PM Room: S103AB

Participants Rong Xu, Chengdu, China (*Presenter*) Nothing to Disclose Ying-Kun Guo, MD, Chengdu, China (*Abstract Co-Author*) Nothing to Disclose Zhigang Yang, MD, Chengdu, China (*Abstract Co-Author*) Nothing to Disclose Linjun Xie, Chengdu, China (*Abstract Co-Author*) Nothing to Disclose

For information about this presentation, contact:

Xrongdoctor@163.com

PURPOSE

Left ventricular non-compaction (LVNC) is a rare congenital cardiomyopathy, with or without LV dysfunction, and it may be asymptomatic or it may lead to severe HF, sudden death. The aim of our study is to early evaluate the myocardial dyssynchrony in isolated LVNC children with preserved EF by using cardiac magnetic resonance (CMR), and to explore the correlate factors of progress of LVNC.

METHOD AND MATERIALS

we investigated 17 isolated LVNC patients with preserved LVEF (EF>=50%), and 23 age- and gender-matched controls. The feature tracking parameters including peak strain (PS), peak displacement (PD) and strain rate in radial, circumferential, and longitudinal directions were measurement in all subjects.

RESULTS

In all patients, 14 patients were left ventricular apical (73.7%), two patients were left ventricular septum (10.5%), one patient were global left ventricular noncompaction (5.3%). The PS and PD in radial, circumferential, and longitudinal directions decreased significantly in the LVNC patients with preserved EF compared with the normal controls (all p<0.001), Furthermore, the PS in three directions were associated with the EF (r = 0.43; r = -0.41; r = -0.54); and PS in three directions were also significant correlates with age (r = -0.47; r = 0.46; and r = 0.47).

CONCLUSION

CMR feature tracking can be used for the detection of early myocardial deformation in the isolated LVNC children who are subclinical left ventricular dysfunctions, and early clinical intervention might be important for the decrease of LVEF function and myocardial deformation.

CLINICAL RELEVANCE/APPLICATION

(dealing with MRI feature tracking) CMR feature tracking can detect early myocardial deformation in the isolated LVNC children with subclinical dysfunctions.



Chest (Vascular/Interventional)

Wednesday, Nov. 28 3:00PM - 4:00PM Room: S404CD



AMA PRA Category 1 Credit ™: 1.00 ARRT Category A+ Credit: 1.00

FDA Discussions may include off-label uses.

Participants

Seth J. Kligerman, MD, Denver, CO (*Moderator*) Nothing to Disclose Matthew D. Cham, MD, New York, NY (*Moderator*) Nothing to Disclose

Sub-Events

SSM05-01 Image-guided Intratumoral Radiofrequency Hyperthermia-Enhanced HSV-TK Gene Therapy of Lung Cancer: The Underlying Molecular Mechanisms

Wednesday, Nov. 28 3:00PM - 3:10PM Room: S404CD

Participants

Peicheng Li, MD, Seattle, WA (*Presenter*) Nothing to Disclose Feng Zhang, MD, Seattle, WA (*Abstract Co-Author*) Nothing to Disclose Qiaoyou Weng, Seattle, WA (*Abstract Co-Author*) Nothing to Disclose Guangxin Jin, Seattle, WA (*Abstract Co-Author*) Nothing to Disclose Liangcai Zhao, Seattle, WA (*Abstract Co-Author*) Nothing to Disclose Minjiang Chen, Seattle, WA (*Abstract Co-Author*) Nothing to Disclose Qiang Li, Seattle, WA (*Abstract Co-Author*) Nothing to Disclose Yiming Zhou, Seattle, WA (*Abstract Co-Author*) Nothing to Disclose Kun Qian, Seattle, WA (*Abstract Co-Author*) Nothing to Disclose Kun Qian, Seattle, WA (*Abstract Co-Author*) Nothing to Disclose Caifang Ni, MD, PhD, Suzhou, China (*Abstract Co-Author*) Nothing to Disclose Xiaoming Yang, MD, PhD, Mercer Island, WA (*Abstract Co-Author*) Nothing to Disclose

For information about this presentation, contact:

lpccat@163.com

PURPOSE

To develop a new interventional oncologic technique, namely 'image-guided intratumoral radiofrequency hyperthermia (RFH)enhanced local HSV-TK/GCV-mediated suicide gene therapy of lung cancers' and investigate its associated bio-molecular mechanisms.

METHOD AND MATERIALS

Human lung cancer cells (A549) transduced with Luciferase/mCherry/lentivirus for in-vitro confirmation, and 24 nude rats with the same orthotopic lung cancers for in-vivo validation were divided into four study groups with different treatments of (i) combination therapy with intratumoral HSV-TK/GCV gene therapy followed by RFH at 41-42 °C for 30 minutes; (ii) HSV-TK/GCV gene therapy alone; (iii) RFH alone; (iv) PBS as a control. In in-vitro experiments, bioluminescence assay, confocal microscopy and flow cytometry were used to determine the viability and apoptosis of cells, while in the in-vivo experiments molecular optical/x-ray imaging was used to evaluate the changes of bioluminescent signals among different groups over 2 weeks. To investigate the potential mechanisms of apoptosis, IHC staining and WB were used for detecting the expression of Bcl-2/Bax, and Caspase-3. To determine mechanisms of immune-response, IHC and WB were used to exam the expression of HSP-70, IL-2 and CD94.

RESULTS

Of in-vitro experiments, compared with gene therapy alone, RFH alone or PBS, combination therapy induced the lowest cell viability (P<0.01), the highest cell apoptosis (P<0.001), and a significant decrease of relative bioluminescence signal (P<0.01). Of in-vivo experiments, optical imaging detected a significantly decreased bioluminescence signal of the tumor with combination therapy (P<0.05). Regarding to the mechanisms, both WB analysis and IHC staining displayed the significantly decreased expression of Bcl-2, as well as increased expression of Bax, Caspase-3, HSP-70, IL-2 and CD94 in cancer tissues of combination therapy, compare to other control treatments.

CONCLUSION

This study validated the feasibility of image-guided interventional RFH-enhanced direct suicide gene therapy of orthotopic lung cancers, which is activated through the mechanisms of augmenting Bax/Bcl-2/caspase-3-depended apoptosis and the HSP-70/IL-2 depended immune regulation pathway.

CLINICAL RELEVANCE/APPLICATION

This alternative technique may open new avenues for effective treatment of lung cancers via integrating image-guided interventional oncology, RF technology, and direct gene therapy.

SSM05-02 Impact of Availability of PET-CT Imaging on Diagnostic Accuracy and Biopsy Safety of CT-Guided Percutaneous Needle Biopsy (PNB) of Suspected Lung Cancer

Wednesday, Nov. 28 3:10PM - 3:20PM Room: S404CD

Participants

Konstantinos Stefanidis, MD, PhD, London, United Kingdom (*Presenter*) Nothing to Disclose Anouchka Goldman, MBBS, London, United Kingdom (*Abstract Co-Author*) Nothing to Disclose Sisa Grubnic, MD, London, United Kingdom (*Abstract Co-Author*) Nothing to Disclose Alaa K. Witwit, MD, FRCR, Oslo, Norway (*Abstract Co-Author*) Nothing to Disclose Teresa Jacob, MBBS, London, United Kingdom (*Abstract Co-Author*) Nothing to Disclose Joanna Moser, MBChB,FRCR, London, United Kingdom (*Abstract Co-Author*) Nothing to Disclose Ioannis Vlahos, MRCP,FRCR, London, United Kingdom (*Abstract Co-Author*) Research Consultant, Siemens AG Research Consultant, General Electric Company

For information about this presentation, contact:

kstefanidis@nhs.net

PURPOSE

To determine whether the availability of PET-CT improves diagnostic yield and safety in lung cancer PNB.

METHOD AND MATERIALS

PNB diagnostic rates over 3yrs for 3 thoracic radiologists (6-17yr practice) were retrospectively reviewed. Radiologists review PET-CT, if available, prior to PNB, to target the maximum activity tissue (PET-CT-MA). The availability of PET-CT pre or post PNB was recorded, and whether PNB was ultimately taken from the PET-CT-MA (whether PET-CT pre- or post PNB). The number of needle passes, complications and biopsy results were recorded. The influence of lesion morphology on results was assessed.

RESULTS

353 PNBs were performed in 350 patients (median lesion size 30mm, 7-120mm). 178 PNB (50.4%) had PET-CT pre-PNB, in 102 (28.9%) cases PET-CT was post-PNB. In 73 (20.7%) PET-CT was never performed.Overall PNB success was 83.9% (95.8% malignant). 88.8% of 178 PNB with PET-CT pre-PNB were diagnostic, versus 78.9% of 175 PNB without PET-CT upfront (p<0.01 Fisher exact test).Correct targeting to PET-CT-MA was present in 87.1% of 278 cases with PET-CT. 88.8% of 242 PNB targeting the PET-CT-MA were successful, but only 52.8% of 36 PNB not targeting PET-CT-MA (p<0.0001). PET-CT pre-PNB had higher rates of PET-CT-MA targeting compared to PET-CT post PNB (91.0% v 80.0%, p=0.01).More patients with PET-CT pre-PNB (n=162) and correct localization had diagnostic PNB than patients with PET-CT pre-PNB (n=16) but incorrect localization (90.1% v 75%). Similarly, more patients with no PET-CT pre-PNB (n=80) but ultimately correct localization had successful PNB compared to patients with no PET-CT pre-PNB (n=20) and ultimately incorrect localization (86.3% v 35%, p<=0.0001).Patients with a PET-CT pre-PNB underwent fewer PNB passes (mean 2.6 v 3.1, p<0.0001 Mann Whitney U). Serious complications were less common in PET-CT pre-PNB group (4.5% v 10.9%, p<0.05). Pre-PNB PET-CT performance improvement applied to all 3 radiologists and was greatest for masses and infiltrative abnormalities.

CONCLUSION

PNB localisation to the PET-CT-MA is associated with higher diagnostic biopsy rates and appears to account for improved performance, less needle passes and complications when available pre-biopsy.

CLINICAL RELEVANCE/APPLICATION

Prospective studies are required to confirm the results that suggest PET-CT should be available prior to biopsy particularly for larger masses or infiltrative lesions.

Honored Educators

Presenters or authors on this event have been recognized as RSNA Honored Educators for participating in multiple qualifying educational activities. Honored Educators are invested in furthering the profession of radiology by delivering high-quality educational content in their field of study. Learn how you can become an honored educator by visiting the website at: https://www.rsna.org/Honored-Educator-Award/ Ioannis Vlahos, MRCP, FRCR - 2015 Honored Educator

SSM05-03 Diagnostic Success and Complication Rate of Ultrasound-Guided Percutaneous Needle Biopsy of Thoracic Lesions: Study of 147 Cases

Wednesday, Nov. 28 3:20PM - 3:30PM Room: S404CD

Participants

Eduardo Portela de Oliveira, MD, Ottawa, ON (*Presenter*) Nothing to Disclose Carolina A. Souza, MD, Ottawa, ON (*Abstract Co-Author*) Consultant, Pfizer Inc; Consultant, Boehringer Ingelheim GmbH; Consultant, AstraZeneca PLC; Speaker, Pfizer Inc; Speaker, Boehringer Ingelheim GmbH; Speaker, F. Hoffmann-La Roche Ltd; Speaker, AstraZeneca PLC; Advisory Board, AstraZeneca PLC Fabricio D. Cyrineu, MD, Sao Paulo, Brazil (*Abstract Co-Author*) Nothing to Disclose Kawan S. Rakhra, MD, Ottawa, ON (*Abstract Co-Author*) Nothing to Disclose

For information about this presentation, contact:

eporteladeoliveira@toh.ca

PURPOSE

The goal of this study was to assess the diagnostic yield and safety profile of US-guided biopsy in the diagnosis of thoracic lesions, including lesions located in the chest wall, mediastinal and lung parenchyma.

METHOD AND MATERIALS

A total of 147 US-guided percutaneous needle biopsies of thoracic lesions performed in 146 consecutive patients (66±7y,83M,63F)

were analyzed, including lesions originating from the lung (67/147), chest wall (54/147), mediastinum (14/147) and pleura (12/147), obtained with FNA and/or CNB (FNA/CNB). Lesions varied in size from 1.5cm to 16cm. The overall diagnostic yield and complication rate of US-guided biopsy as well as the influence of lesion location and size, biopsy technique (FNA or CNB) and number of specimens on diagnostic yield and complication were calculate. Fisher's exact test, Chi-square test and logistic regression were used for statistical analysis. Results with p<0.05 were considered to be statistically significant and yield was summarized as proportion with 95% CI.

RESULTS

The overall diagnostic yield of US-guided needle biopsy was 88%. Biopsy of lesions located in the chest wall were diagnostic in 91% of cases, compared to 88% for lung lesions and 75% for pleural lesions and 93% for mediastinal lesions, although this was not statistically significant (p = 0.45). The diagnostic yield of FNA was similar to that of CNB (89% and 86% respectively) and the number of specimens obtained for either FNA or CNB did not affect yield (p = 0.10). Complications occurred in 4/147(3%) cases, including pneumothorax in two and mild hemoptysis in one patient. In all cases patients were treated conservatively with no cases requiring intervention. Complications were not statistically associated with any of the covariates analyzed.

CONCLUSION

US-guided biopsy has high yield for the diagnosis of thoracic lesions, including lesions located in the mediastinum and lung parenchyma. Tissue diagnosis sufficient to direct specific management is often obtained. The safety profile of US-guided thoracic biopsy is excellent with very low complication rates.

CLINICAL RELEVANCE/APPLICATION

Imaging-guided percutaneous biopsy is a safe minimally invasive technique used for the diagnosis of thoracic lesions and usually considered the initial modality to obtain tissue diagnosis.

SSM05-04 Artificial Intelligence Based Aortic Diameter Quantification on Routine Unenhanced Chest CT

Wednesday, Nov. 28 3:30PM - 3:40PM Room: S404CD

Awards

Student Travel Stipend Award

Participants

Cody R. Branch, MD, Charleston, SC (*Presenter*) Nothing to Disclose Saikaran Rapaka, Malvern, PA (*Abstract Co-Author*) Employee, Siemens AG Puneet Sharma, Princeton, NJ (*Abstract Co-Author*) Research Director, Siemens AG Pooyan Sahbaee, Malvern, PA (*Abstract Co-Author*) Employee, Siemens AG Razvan Ionasec, PhD, Princeton, NJ (*Abstract Co-Author*) Employee, Siemens AG U. Joseph Schoepf, MD, Charleston, SC (*Abstract Co-Author*) Research Grant, Astellas Group; Research Grant, Bayer AG; Research Grant, Siemens AG; Research support, Bayer AG; Consultant, Guerbet SA; Consultant, General Electric Company; Consultant, HeartFlow, Inc; Consultant, Bayer AG; Consultant, Siemens AG; ; ; John W. Nance JR, MD, Charleston, SC (*Abstract Co-Author*) Nothing to Disclose

For information about this presentation, contact:

nancej@musc.edu

PURPOSE

To validate a supervised machine learning algorithm to quantify thoracic aortic diameters on non-ECG synchronized, non-contrast material enhanced chest CT.

METHOD AND MATERIALS

A novel deep learning based radiology assistant was applied to a training dataset of manually annotated chest CTs. Aortic measurements were made by a single observer off of volumetric datasets utilizing double-oblique short axis measurements at 7 levels, as defined by the American Heart Association (sinuses of Valsalva, sino-tubular junction, mid ascending aorta, proximal aortic arch, mid aortic arch, proximal descending thoracic aorta, mid descending aorta). A deep convolutional image-to-image learning model was used to learn the mapping between the input CT volume and the ground truth aorta mask. The algorithm was then applied to a test set of 72 cases, and aortic diameters between manual measurements and the machine learning algorithm were compared.

RESULTS

The overall correlation between manual and machine learning measurements was r=0.86. The best correlation between manual and machine learning measurements was in the mid descending aorta (r=0.875). The model predictions resulted in an area under the curve of 0.877 when applying a threshold of 38 mm to detect an abnormally enlarged mid ascending aorta, with peak performance of the model set at cutoff 39 mm (indicating a small bias in the model) and resulting in sensitivity and specificity of 77% and 89%, respectively.

CONCLUSION

A machine learning algorithm may be able to automatically provide reliable quantitative measures of thoracic aortic diameters and flag abnormal values.

CLINICAL RELEVANCE/APPLICATION

Automated aortic measurements could enrich radiology reports for epidemiologic studies, save time for the interpreting clinician, and ensure that abnormally dilated aortas are not missed.

SSM05-05 Volume-Helical-Shuttle Mode with Low Contrast Dose and Low Tube Voltage in CT Pulmonary Angiography for Critically III Patients

Wednesday, Nov. 28 3:40PM - 3:50PM Room: S404CD

Participants

Xiaoxia Chen, MMed, Xianyang City, China (*Presenter*) Nothing to Disclose Yang Xiao, PhD,PhD, Xian, China (*Abstract Co-Author*) Nothing to Disclose Nan Yu, MD, Xian Yang, China (*Abstract Co-Author*) Nothing to Disclose Yongjun Jia, MMed, Xianyang City, China (*Abstract Co-Author*) Nothing to Disclose Dong Han, MD, Xianyang, China (*Abstract Co-Author*) Nothing to Disclose Ma Guangming, MMed, Xianyang City, China (*Abstract Co-Author*) Nothing to Disclose

For information about this presentation, contact:

1183729657@qq.com

PURPOSE

To explore the value of using volume-helical-shuttle (VHS) mode with low contrast dose and low kVp in CT pulmonary artery (CTPA) imaging for critically ill patients.

METHOD AND MATERIALS

38 critically ill patients for CTPA were in the study group (Group A), and other 38 cases of conventional CTPA served as the control group (Group B). Group A used the VHS mode: tube voltage 80kVp, smart mA, noise index (NI) 25HU, pitch 1.375:1, rotation speed 0.5s for 4 passes with scan started 6s after the contrast injection. Contrast dose of 25mL (350mgI/ml) at 4mL/s flow rate was used. Images were reconstructed using 60%ASiR and the best images were selected from the 4 passes for analysis. Group B used tube voltage 120kVp, smart mA for NI of 12HU, pitch 1.375:1, rotating speed 0.8s and contrast dose of 60ml, and images were reconstructed with 40%ASiR. The CT values and SD values of vessels and the vertical spinal muscles were measured to calculate SNR and CNR for vessels. Artifacts near superior vena cava was graded with 5 being the worst. The attenuation difference between the right inferior pulmonary artery and right inferior pulmonary vein was calculated. Two experienced physicians also evaluated image quality double blindly using a 5-point scoring system. Measurements in both groups were statistically compared.

RESULTS

The total radiation dose in VHS mode (Group A) was the same as the conventional CTPA (P>0.05), but the contrast dose in Group A was reduced by 58% compared with Group B. The target vessel CT and SD values in Group A were both higher than group B (P<0.05), resulting in similar SNR and CNR values in both groups (P>0.05), except that the CNR values of MPA and RPA in group B were higher (P<0.05); There was no difference in the subjective score of image quality between the two groups (P>0.05). However, Group A was better in both the attenuation difference and superior vena cava artifacts (P<0.05).

CONCLUSION

CTPA using VHS mode at low kVp works for critically ill patients who were unable to cooperate. Compared with the conventional CTPA, the proposed method provides more satisfactory image results with the same total radiation dose and 58% contrast dose reduction.

CLINICAL RELEVANCE/APPLICATION

For critically ill patients, this method can reduce contrast dose, make multi-phase diagnosis, overcome difficulties that patients cannot cooperate well and ensure the success rate of examination.

SSM05-06 Real-Time Patient Specific Scan Initiation for Pulmonary Embolism CTA: Impact on Image Quality

Wednesday, Nov. 28 3:50PM - 4:00PM Room: S404CD

Participants

Fides Schwartz, Durham, NC (*Presenter*) Grant, Siemens AG Juan Carlos Ramirez-Giraldo, PhD, St Louis, MO (*Abstract Co-Author*) Employee, Siemens AG Ralf Gutjahr, Forchheim, Germany (*Abstract Co-Author*) Employee, Siemens AG Daniel Boll, Basel, Switzerland (*Abstract Co-Author*) Nothing to Disclose Lynne M. Hurwitz Koweek, MD, Durham, NC (*Abstract Co-Author*) Departmental Research Grant, Siemens AG; Departmental Research Grant, Bayer AG

For information about this presentation, contact:

fides.schwartz@duke.edu

PURPOSE

Real-time modulation of scan initiation based on patient specific hemodynamics may allow for optimal timing of contrast enhancement in the pulmonary arteries in evaluation of pulmonary embolism (PE), reducing the number of non-diagnostic scans. The purpose of this study is to assess image quality for PE chest CTA using a modulated scan initiation delay based on patient specific hemodynamics.

METHOD AND MATERIALS

This was a HIPAA compliant, IRB approved quality improvement project. Fluoroscopic administration of contrast was used for all PE chest CTA exams. A new modulated scan initiation delay software was evaluated in 30 patients (cohort 1) scanned on a dual-source 192 detector CT (Siemens FORCE, Forchheim, Germany) from 01/2018-04/2018. 30 patients (cohort 2, matched to cohort 1 for BMI and age) with exams performed using a fixed scan initiation delay of 5 seconds (sec) were identified from 10/2016-12/2017. Subjective image quality was graded on a 4-point Likert-scale (1=excellent, 2=good, 3=fair and 4=inadequate). Objective image quality was determined by measuring the Hounsfield (HU) values in the main pulmonary artery, the bilateral lower lobe segmental and subsegmental arteries (150 arterial segments/cohort). HU values and standard deviations were compared for both cohorts.

RESULTS

Average patient age was 54.5 vs 54.3 years for cohorts 1 and 2 respectively. Average BMI was 32.9 kg/m2 for both cohorts. There was a statistically significant difference in scan initiation delay of 11 ± 3.6 sec (range 7.8 to 27.8 sec) for cohort 1 vs the set delay of 5 sec for cohort 2 (P<0.01). Subjective image quality for cohort 1 was graded as excellent or good in 22 patients, fair in 5 and inadequate in 3 patients; for cohort 2 it was graded as excellent or good in 20 patients, fair in 4 and inadequate in 6 patients. Average HU values were higher for cohort 1 vs cohort 2 in segmental (382 vs 349 HU right/387 vs 359 HU left) and subsegmental arteries (371 vs 327 HU right/382 vs 330 HU left). A total of 20/150 segments in cohort 1 and 31/150 segments in cohort 2 were non-diagnostic (HU<250; 7.4% reduction).

CONCLUSION

Real time, patient specific modulated scan initiation delay achieved higher image quality than a set delay for PE chest CTA.

CLINICAL RELEVANCE/APPLICATION

A real-time patient specific scan initiation can improve subjective image quality for PE chest CTA exams and reduce the total number of non-diagnostic pulmonary artery segments.



Chest (Diffuse Lung Disease)

Wednesday, Nov. 28 3:00PM - 4:00PM Room: S402AB



AMA PRA Category 1 Credit ™: 1.00 ARRT Category A+ Credit: 1.00

FDA Discussions may include off-label uses.

Participants

Jonathan H. Chung, MD, Chicago, IL (*Moderator*) Royalties, Reed Elsevier; Consultant, Boehringer Ingelheim GmbH; Consultant, F. Hoffmann-La Roche Ltd; Consultant, Applied Clinical Intelligence LLC; Consultant, Veracyte, Inc; Speakers Bureau, Boehringer Ingelheim GmbH; Speakers Bureau, F. Hoffmann-La Roche Ltd

John P. Lichtenberger III, MD, Bethesda, MD (Moderator) Nothing to Disclose

Sub-Events

SSM06-01 Imaging Manifestations of IgG4-Related Disease in the Thorax: Association Between CT Findings and IgG4 Antibody Levels

Wednesday, Nov. 28 3:00PM - 3:10PM Room: S402AB

Awards

Student Travel Stipend Award

Participants

Dania Daye, MD, PhD, Philadelphia, PA (*Presenter*) Nothing to Disclose Zachary S. Wallace, MD, Boston, MA (*Abstract Co-Author*) Nothing to Disclose Micheal McInnis, MD, Toronto, ON (*Abstract Co-Author*) Nothing to Disclose Lida Hariri, MD, Boston, MA (*Abstract Co-Author*) Nothing to Disclose Vikram Deshpande, Boston, MA (*Abstract Co-Author*) Nothing to Disclose John Stone, MD, MPH, Boston, MA (*Abstract Co-Author*) Nothing to Disclose Amita Sharma, MBBS, Boston, MA (*Abstract Co-Author*) Nothing to Disclose

For information about this presentation, contact:

dania.daye@gmail.com

PURPOSE

IgG4-related disease (RD) is an immune-mediated fibro-inflammatory disease that can affect the respiratory system. The goal of this study is to investigate the association between thoracic imaging manifestations of IgG4-RD, IgG4 antibody levels and pulmonary symptoms.

METHOD AND MATERIALS

In this IRB-approved retrospective study, 62 patients with a pathology-proven diagnosis of IgG4-RD and thoracic CT imaging were identified. Images were reviewed by two thoracic radiologists. IgG4 antibody levels, pulmonary symptoms and patient demographics were collected. Wilcoxon rank-sum test was used to assess for differences of the mean IgG4 levels between patients with and without thoracic imaging manifestations of disease. Fischer's exact test was performed to assess for independent association between IgG4 levels and the presence of imaging findings. Spearman correlation analysis was used to assess the correlation between the number of imaging findings and IgG4 levels. Univariate logistic regression analysis was performed to assess for independent contribution of IgG4 levels and pulmonary symptoms in predicting the presence of imaging manifestation on CT.

RESULTS

Of the 62 patients enrolled, 36 patients (58%) had imaging findings attributable to IgG4-RD. Patients with imaging findings had significantly higher IgG4 antibody levels ($897\pm218 \text{ mg/dL vs. } 87\pm17 \text{ mg/dL}$ in those without imaging findings) (p<0.01). Airway involvement was a common imaging finding, present in 19/36 (52.8%) patients. Patients with bronchial wall thickening (p<0.01), mosaic lung attenuation (p=0.01), and saber sheath trachea (p=0.03) had significantly higher serum IgG4 levels compared to those without airway involvement. IgG4 levels and pulmonary symptoms were independent predictors of presence of thoracic imaging manifestations on regression analysis (p=0.02 and 0.01 respectively). Overall, there was a positive correlation between the number of thoracic manifestations on CT and serum IgG4 levels (r=0.60, P<0.01).

CONCLUSION

Airway involvement is a common manifestation of IgG4-RD. High IgG4 levels and pulmonary symptoms are independently associated with presence of findings on chest CT in patients with IgG4-RD.

CLINICAL RELEVANCE/APPLICATION

Elevated IgG4 antibody levels and the presence of pulmonary symptoms should prompt thoracic imaging to identify lung involvement and direct management decisions in patients with IgG4-RD.

SSM06-02 Chest CT Analysis for Prediction of Treatment Response in Organizing Pneumonia: A 20-year Retrospective Cohort Study

Wednesday, Nov. 28 3:10PM - 3:20PM Room: S402AB

Participants

Younghoon Cho, MD, Seoul, Korea, Republic Of (*Presenter*) Nothing to Disclose Eun Jin Chae, MD, PhD, Seoul, Korea, Republic Of (*Abstract Co-Author*) Nothing to Disclose Jin Woo Song, Seoul, Korea, Republic Of (*Abstract Co-Author*) Nothing to Disclose Joon Seon Song, Seoul, Korea, Republic Of (*Abstract Co-Author*) Nothing to Disclose Kyung-Hyun Do, MD, Seoul, Korea, Republic Of (*Abstract Co-Author*) Nothing to Disclose Se Jin Jang, Seoul, Korea, Republic Of (*Abstract Co-Author*) Nothing to Disclose

For information about this presentation, contact:

ejinchae@gmail.com

PURPOSE

To investigate the CT imaging features associated with poor clinical outcome after steroid treatment (Tx) in patients diagnosed with organizing pneumonia (OP).

METHOD AND MATERIALS

The study retrospectively enrolled 166 patients (M:F=55:111; mean age, 57.2; mean FVC, 65.9; mean DLco, 58.5) with the pathologically proven OP, which included 131 cases of cryptogenic OP (COP) and 35 cases of connective tissue disease-related OP (CTD). Baseline chest CTs prior to Tx were semi-quantitatively analyzed by two thoracic radiologists in consensus. Lesion extent (consolidation, GGO, reticulation, and total), dominant lesion pattern, dominant distribution, and presence of bronchiectasis (BE), lymph nodes, pleural or pericardial effusions, and reverse halo were evaluated. Uni- and multivariate logistic regression analyses were performed to identify variables associated with poor clinical outcomes including failure to achieve complete response (non-CR) and relapse after Tx.

RESULTS

CR was achieved in 40 (24%) patients and relapse was detected in 53 (31%) patients. While BE was detected in 30% of patients with CR, 65% of patients with non-CR were found to have BE on baseline chest CT. Average extent of consolidation for CR and non-CR group was 14.1% and 15.2%, respectively. Presence of BE (hazard ratio (HR), 4.38) and extent of consolidation greater than 10% of the lung (con>10%) (HR, 2.46) were significantly associated with higher non-CR rate (all, p < 0.01). CTD-OP was also found to have higher non-CR rate (HR, 4.19) than COP. On multivariate logistic regression analysis adjusted for age and sex, BE, con>10%, and CTD-OP all remained as significant predictors. For the prediction of relapse, significant associations were found with con>10% (HR, 2.86), total extent > 25% (HR, 2.77), and CTD-OP (HR, 6.79). After adjusted for age and sex, con>10 % and CTD-OP were found be significant predictors of relapse.

CONCLUSION

In patients diagnosed with OP, patients with BE and greater extent of consolidation on baseline chest CT were less likely to achieve CR, and the latter was also associated with higher rate of relapse after treatment. Additionally, CTD-OP was found to have worse treatment outcome than COP.

CLINICAL RELEVANCE/APPLICATION

Patients with underlying CTD, bronchiectasis, and greater extent of consolidation at the time of diagnosis were found to have worse treatment outcome in OP, and therefore should be monitored with extra vigilance.

SSM06-03 Identification of CT Patterns for Disease Progression in CTs of Patients with Idiopathic Pulmonary Fibrosis - An Unsupervised Machine-Learning Approach

Wednesday, Nov. 28 3:20PM - 3:30PM Room: S402AB

Participants

Helmut Prosch, MD, Vienna, Austria (*Abstract Co-Author*) Nothing to Disclose Jeanny Pan, Vienna, Austria (*Abstract Co-Author*) Nothing to Disclose Johannes Hofmanninger, Vienna, Austria (*Abstract Co-Author*) Siemens AG; Boehringer Ingelheim GmbH Nicola Sverzellati, MD, Parma, Italy (*Abstract Co-Author*) Nothing to Disclose Venerino Poletti, Forli, Italy (*Abstract Co-Author*) Nothing to Disclose Florian Prayer, MD, Vienna, Austria (*Abstract Co-Author*) Nothing to Disclose Sebastian Roehrich, MD, Vienna, Austria (*Abstract Co-Author*) Nothing to Disclose Markus Holzer, Vienna, Austria (*Abstract Co-Author*) Founder, contextflow GmbH Georg Langs, Vienna, Austria (*Presenter*) Nothing to Disclose

PURPOSE

To identify CT patterns which can be used as markers of disease progression in patients with idiopathic pulmonary fibrosis (IPF) using an unsupervised machine-learning approach.

METHOD AND MATERIALS

695 CT scans from 106 IPF patients (1-4 per patient) were investigated in the study. All CT studies were automatically segmented into into super-voxels and gray-level co-occurrence features at the centroid positions were extracted. Twenty clusters of these super-voxels proved to be stable across the population in the feature space. The volume of each cluster relative to the entire lung was used as the signature of a lung. To identify prognostic markers in these signatures, we trained a random-forest classifier to predict for any pair of scans for one patient (scans A and B) if A was acquired prior to B or vice versa (overall 230 pairs). The classifier determined which features were most informative regarding the classification. To determine whether the signature was predictive and stable, a four-fold cross-validation was performed on the data set. The classifier was trained on 3/4 of the patients, and predicted an A/B sequence on the remaining 1/4 of these patients. To study the distribution of predictive information in the lung, we split the volume into upper-, middle-, and lower third, and performed the evaluation for each of them individually.

RESULTS

The random forest identified four distinct clusters as predictive for the temporal course. In the four-fold cross-validation experiment, using all lung data, the classifier correctly determined the sequence of scans for 80.35% of the cases. Using only cluster information in one of three parts of the lung reduces the accuracy, but reveals that the middle segment results in highest accuracy (76.52%) compared to upper (73.04%) and lower (72.61%) segments. Three clusters where among the top four most predictive clusters in all folds, and one cluster was in the top four for three of four folds.

CONCLUSION

The described approach identified four patterns that were markers of disease progression in lung CT data of IPF patients. The information contributed by individual clusters differs depending on their location in the lung.

CLINICAL RELEVANCE/APPLICATION

Data-driven identification of imaging markers enables the exploitation of complex patterns for the detection and quantification of progression.

SSM06-04 Interstitial Lung Abnormalities in Stage IV Non-Small Cell Lung Cancer Patients: A Validation Study for the Association with Poor Clinical Outcome

Wednesday, Nov. 28 3:30PM - 3:40PM Room: S402AB

Awards

Student Travel Stipend Award

Participants

Tetsuro Araki, MD, PhD, Boston, MA (*Presenter*) Nothing to Disclose Suzanne E. Dahlberg, Boston, MA (*Abstract Co-Author*) Consultant, AstraZeneca PLC Michael S. Rabin, MD, Boston, MA (*Abstract Co-Author*) Nothing to Disclose Hiroto Hatabu, MD, PhD, Boston, MA (*Abstract Co-Author*) Research Grant, Canon Medical Systems Corporation ; Research Grant, Konica Minolta, Inc Bruce E. Johnson, MD, Boston, MA (*Abstract Co-Author*) Research support, Toshiba Corporation; Research support, Novartis AG; Royalties, EGFR Mutation Testing; Researcher, Dana-Farber Cancer Institute Mizuki Nishino, MD, MPH, Newton, MA (*Abstract Co-Author*) Institutional Research Grant, Merck & Co, Inc; Institutional Research Grant, Canon Medical Systems Corporation; Institutional Research Grant, AstraZeneca PLC; Speaker, F. Hoffmann-La Roche Ltd; Consultant, DAIICHI SANKYO Group Tomoyuki Hida, Boston, MA (*Abstract Co-Author*) Research Grant, Konica Minolta, Inc

For information about this presentation, contact:

mizuki_nishino@dfci.harvard.edu

PURPOSE

The presence of interstitial lung abnormalities (ILA) at diagnosis of stage IV non-small cell lung cancer (NSCLC) patients have previously shown to be associated with shorter survival. The present study aimed to validate the association in a larger cohort of treatment-naïve stage IV NSCLC patients.

METHOD AND MATERIALS

This study included 484 patients (205 males and 279 females, median age: 62) with stage IV NSCLC. ILA was scored on the baseline chest CT scans at diagnosis prior to therapy using 3-point scale (0=no ILA, 1=equivocal for ILA, 2=ILA) using a sequential reading method by 3 readers as published previously. Clinical characteristics and overall survival (OS) were compared in patients with ILA (score 2) vs. those without ILA (score 0 or 1).

RESULTS

ILA was present (score 2) on baseline CT in 19 of the 484 patients (3.9%, 95%CI: 2.4 - 6.1%). Patients with baseline ILA were older (median age: 69 vs. 62 years, Wilcoxon p=0.0008) and were more commonly male (68.4% (13/19) vs. 41.3% (192/465); Fisher p=0.03) compared to those without ILA. Other variables including race, smoking history, and histology were not significantly associated with baseline ILA. Patients with baseline ILA had significantly shorter overall survival compared to those without (median OS: 9.95 months [95%CI: 5.88-15.5] vs. 16.95 months [95%CI: 14.65-18.7]; Log-rank p=0.002). In multivariable analyses, baseline ILA remained significant as a marker for shorter overall survival (HR=2.09; Cox p=0.004), after adjusting for age (>70 years using the 75th percentile; HR=1.48; Cox p=0.001), male gender (HR= 1.22; Cox p=0.055) and smoking (never vs. current/former smoker; HR=0.79; Cox p=0.051).

CONCLUSION

The presence of ILA at diagnosis of stage IV NSCLC was significantly associated with shorter survival, validating ILA as an independent marker for poor outcome.

CLINICAL RELEVANCE/APPLICATION

Recognition of ILA on chest CT at diagnosis of stage IV NSCLC is important, because ILA can serve as a marker for shorter survival and may contribute to patient monitoring and management.

SSM06-05 Juxta-Pleural and Acutely-Folded Bronchi: Differential CT Findings of IPF without Evidence Honeycombing From NSIP

Wednesday, Nov. 28 3:40PM - 3:50PM Room: S402AB

Participants

Heekyung Kim, Seoul, Korea, Republic Of (*Presenter*) Nothing to Disclose Soon Ho Yoon, MD, Seoul, Korea, Republic Of (*Abstract Co-Author*) Nothing to Disclose Hyun-Ju Lee, MD, PhD, Seoul, Korea, Republic Of (*Abstract Co-Author*) Nothing to Disclose Gong Yong Jin, MD, PhD, Jeonju, Korea, Republic Of (*Abstract Co-Author*) Nothing to Disclose Kwang Nam Jin, MD, PhD, Seoul, Korea, Republic Of (*Abstract Co-Author*) Nothing to Disclose Ki Yeol Lee, MD, PhD, Ansan, Korea, Republic Of (*Abstract Co-Author*) Nothing to Disclose Kum Ju Chae, MD, Jeonju, Korea, Republic Of (*Abstract Co-Author*) Nothing to Disclose

For information about this presentation, contact:

Heekyung0363@gmail.com

PURPOSE

To evaluate juxta-pleural and acutely-folded bronchi for the differentiation of IPF patients without honeycombing from idiopathic NSIP.

METHOD AND MATERIALS

The derivation cohort consisted of 80 consecutive patients (41 IPF and 39 NSIP; 17 probable, 10 indeterminate, 53 non-IPF CT patterns) who met following criteria in a single hospital: (a) multidisciplinary diagnosis of IPF or idiopathic NSIP with surgical biopsy from 2005 to 2017, (b) diagnostic thin-section chest CT, and (c) lack of honeycombing in case of IPF. For validation, 22 patients (14 IPF and 8 NSIP; 4 probable, 11 indeterminate, 7 non-IPF CT patterns) with the same condition were included from another institution. Two radiologists for derivation cohort independently assessed the presence of juxta-pleural and acutely-folded bronchi on axial, coronal, sagittal minimum intensity projection (MinIP) images (20mm overlap, 5mm increment; MEDIP software, MEDICALIP Co., Ltd. Seoul, South Korea). Juxta-pleural bronchus was defined as bronchiectasis attached perpendicular to the pleura 1.5cm or longer in length. Acutely-folded bronchus was defined if a single bronchus folded abruptly over 90 degrees and if bronchus branched at an angle of 135 degrees or larger. Logistic regression analysis was used to identify the association of the MinIP findings with IPF. For validation, we assessed the diagnostic accuracy and interobserver agreement of 4 radiologists blinded to any clinical information using a proportion of correct diagnosis of IPF and NSIP and ROC curve before and after reviewing MinIP images.

RESULTS

Non-juxta-pleural and juxta-pleural acutely-folded bronchi (OR, 3.5 95%CI, 1.37-8.66; p=.008 and OR, 6.22, 95%CI, 1.62-23.84; p=.008, respectively), and co-existence of non-juxta-pleural acutely-folded bronchus and juxta-pleural bronchus in same patient (OR, 5.67, 95%CI, 2.03-15.85; p=.001) were significant imaging features for IPF. After reviewing MinIP images, the readers' area under the curve mildly improved from 0.496-0.808 to 0.554-0.808 with increased proportion of correct diagnosis from 40.9-54.5% to 50.0-77.3%. Mean interobserver kappa values for juxta-pleural and acutely-folded bronchi were 0.373 and 0.475.

CONCLUSION

Juxta-pleural and acutely-folded bronchi were differential CT findings for IPF without honeycombing.

CLINICAL RELEVANCE/APPLICATION

Analysis of bronchial trajectory using MinIP images could increase an imaging confidence of IPF without honeycombing.

SSM06-06 Fibrotic Lung Disease on CT Predicts Adverse Outcomes in Patients Undergoing Transcatheter Aortic Valve Replacement

Wednesday, Nov. 28 3:50PM - 4:00PM Room: S402AB

Participants

Cheng Ting Lin, MD, Baltimore, MD (*Presenter*) Nothing to Disclose Matthew Czarny, Baltimore, MD (*Abstract Co-Author*) Nothing to Disclose Amira F. Hussien, MBBCh, Rochester, NY (*Abstract Co-Author*) Nothing to Disclose Rani K. Hasan, MD, Baltimore, MD (*Abstract Co-Author*) Nothing to Disclose Elliot K. Fishman, MD, Baltimore, MD (*Abstract Co-Author*) Institutional Grant support, Siemens AG; Institutional Grant support, General Electric Company; Co-founder, HipGraphics, Inc Jon Resar, Baltimore, MD (*Abstract Co-Author*) Nothing to Disclose Stefan L. Zimmerman, MD, Ellicott City, MD (*Abstract Co-Author*) Project consultant, Siemens Healthcare; Research grant, American Heart Association;

For information about this presentation, contact:

clin97@jhmi.edu

PURPOSE

To evaluate the relationship between CT findings of diffuse lung disease (fibrosis and emphysema) and outcomes in patients who underwent transcatheter aortic valve replacement (TAVR).

METHOD AND MATERIALS

Retrospective review of pre-operative CT scans obtained from 507 patients who underwent TAVR during 2012-2017. Lung images were divided into ten contiguous axial sections spaced equally apart. The extent of fibrotic lung disease - characterized by reticular abnormality and/or honeycombing - was graded by a thoracic radiologist using a five-point scale based on the percent of lung parenchyma involved. A similar approach was used to grade the extent of emphysema. Scores from all the axial slices for each patient were summed to determine fibrosis and emphysema scores. Demographic and clinical data, including pulmonary function tests, were extracted from institutional data submitted to the national Transcatheter Valve Therapy (TVT) Registry. Outcome analyses were performed according to the Kaplan-Meier method using a combined endpoint of death and readmission as the primary outcome.

RESULTS

Complete clinical parameters and outcome data were available in 335 patients. Fibrosis was present in 91 out of 507 (18%) patients with fibrosis scores ranging from 1-34. Emphysema was seen in 33 out of 507 (6.5%) patients. Fibrosis scores between patients with and without chronic lung disease - defined according to TVT registry as FEV1 below 60% - were not statistically different (p=0.59). The presence of fibrotic lung disease on CT was significantly associated with the primary outcome (HR 1.62; 95% CI

1.09-2.40; p=0.016) after adjustment for pre-specified covariates (including FEV1, smoking status, age, and LVEF). Emphysema scores were not associated with the primary outcome. FEV1 was also an independent predictor of worse outcome (HR 0.99; 95% CI 0.984-0.998; p<0.01).

CONCLUSION

The presence of fibrotic lung disease on pre-TAVR CT scans was a significant predictor of adverse events, independent of known risk factors for mortality. Radiologists should be aware that these pulmonary findings could help identify patients who are at higher risk among those referred for TAVR.

CLINICAL RELEVANCE/APPLICATION

Visual assessment of reticular abnormality and honeycombing on pre-operative CT scans can predict adverse events in patients undergoing transcatheter aortic valve replacement.

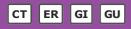
Honored Educators

Presenters or authors on this event have been recognized as RSNA Honored Educators for participating in multiple qualifying educational activities. Honored Educators are invested in furthering the profession of radiology by delivering high-quality educational content in their field of study. Learn how you can become an honored educator by visiting the website at: https://www.rsna.org/Honored-Educator-Award/ Stefan L. Zimmerman, MD - 2012 Honored EducatorStefan L. Zimmerman, MD - 2015 Honored EducatorElliot K. Fishman, MD - 2012 Honored EducatorElliot K. Fishman, MD - 2016 Honored EducatorElliot K. Fishman, MD - 2018 Honored Educator



Emergency Radiology (Abdomen and Pelvis Trauma)

Wednesday, Nov. 28 3:00PM - 4:00PM Room: S404AB



AMA PRA Category 1 Credit ™: 1.00 ARRT Category A+ Credit: 1.00

Participants

Michael N. Patlas, MD, FRCPC, Hamilton, ON (*Moderator*) Nothing to Disclose Karen S. Lee, MD, Boston, MA (*Moderator*) Nothing to Disclose

Sub-Events

SSM07-01 Can Contrast Enhanced Ultrasound Be an Alternative to CECT for Grading and Triaging Management of Blunt Traumatic Solid Abdominal Organ Injuries?

Wednesday, Nov. 28 3:00PM - 3:10PM Room: S404AB

Awards

Trainee Research Prize - Resident

Participants

Deepak Ravichandran, MD, New Delhi, India (*Presenter*) Nothing to Disclose Atin Kumar, MD, New Delhi, India (*Abstract Co-Author*) Nothing to Disclose Raju Sharma, MD, New Delhi, India (*Abstract Co-Author*) Nothing to Disclose Ashu S. Bhalla, MD, New Delhi, India (*Abstract Co-Author*) Nothing to Disclose Shivanand R. Gamanagatti, MBBS, MD, New Delhi, India (*Abstract Co-Author*) Nothing to Disclose

For information about this presentation, contact:

deepakindy2@gmail.com

PURPOSE

CECT is the gold standard for the detection and grading of hepatic and splenic injuries in BAT. Due to the high incidence of low energy trauma with negative CECT findings and the high doses of iodinated contrast used, contrast enhanced ultrasound(CEUS) is an alternative tool in the detection of solid organ injuries in the emergency setting. This study was done to assess the agreement between the grades of hepatic and splenic injuries assigned on CEUS and CECT

METHOD AND MATERIALS

In this ethically approved study consecutive hemodynamically stable patients with BAT with CECT showing solid abdominal organ injuries were recruited. These patients underwent CEUS by a radiologist who was blinded to the findings of CECT. The injuries were graded on both modalities using the American Association for the Surgery of Trauma (AAST) scales. The agreement between the grading of injuries on CECT and CEUS was analysed through kappa statistics. The injuries were further classified as high grade (AAST grades IV & above) and low grade (AAST grades I to III) and agreement between the grading on CECT and CEUS was compared

RESULTS

Among the 105 patients included as a part of a larger study, there were 66 hepatic and 43 splenic injuries detected on CECT. CEUS identified 63 out of the 66 liver injuries and these 63 injuries were graded and compared with CECT. There was significant agreement between their grading on CECT and CEUS with a kappa value of 0.95 (>0.75 is significant). On combining the grades as low grade and high grade injuries, there was significant agreement on both modalities with a kappa value of 1.00. Similarly, 40 splenic injuries were detected on CEUS out of the 43 detected on CECT and these were graded on both the modalities and compared. There was significant agreement between the grading with a kappa value of 0.87. On combining the grades as low grade and high grade injuries there was significant agreement between the grading of splenic injuries on both modalities with a kappa value of 0.91

CONCLUSION

CEUS is accurate in grading of hepatic and splenic injuries in case of blunt traumatic solid abdominal organ injuries

CLINICAL RELEVANCE/APPLICATION

CEUS can provide a radiation free alternative for accurately grading hepatic and splenic injuries and can suggest further management.

SSM07-02 Accuracy of Preoperative MDCT in Patients with Penetrating Abdominal and Pelvic Trauma

Wednesday, Nov. 28 3:10PM - 3:20PM Room: S404AB

Participants Zonia Ghumman, MD, Hamilton, ON (*Presenter*) Nothing to Disclose Vincent M. Mellnick, MD, Saint Louis, MO (*Abstract Co-Author*) Nothing to Disclose Angela Coates, MEd, Hamilton, ON (*Abstract Co-Author*) Nothing to Disclose Sandra Monteiro, PhD, Hamilton, ON (*Abstract Co-Author*) Nothing to Disclose Paul Engels, MD, Hamilton, ON (*Abstract Co-Author*) Nothing to Disclose Michael N. Patlas, MD, FRCPC, Hamilton, ON (*Abstract Co-Author*) Nothing to Disclose

For information about this presentation, contact:

patlas@hhsc.ca

PURPOSE

The role of imaging has become more important for preoperative assessment of traumatic penetrating injuries (PIs). This study aims to evaluate the overall diagnostic accuracy of preoperative MCDT in abdominal and pelvic PIs.

METHOD AND MATERIALS

We used our hospital's trauma registry to retrospectively identify patients with penetrating abdominal and pelvic injuries from 1/1/2006 to12/31/2016. Only patients who had a 64-MDCT scan at presentation and subsequently underwent laparotomy or laparoscopy were included in our study cohort. Each finding noted on MDCT was rated using a 5-point scale to indicate certainty of injury, with a score of 0 being definitive. Using surgical findings as the gold standard, the accuracy of radiology reports was analyzed in 2 ways. A kappa statistic was calculated to evaluate each pair of values for absolute agreement, and ratings for all organ systems were analyzed using a repeated measures ANOVA to determine if radiology and OR findings were similar enough to be clinically meaningful.

RESULTS

Of the 194 trauma patients identified from the trauma registry, 42 met our inclusion criteria - 14 of which sustained GSW, 25 sustained stab wounds, and 3 were miscellaneous penetrating injuries. Our cohort consisted of 38 males and 4 females with a median age of 29 years and a median injury severity score (ISS) of 15.6. For this study, 15 different organ groups were categorized and analysed. Of those organ groups, absolute agreement between MDCT and surgical findings was found only for liver, spleen, peritoneal space and retroperitoneum (kappa values ranging from 0.2 to 0.5). Additionally, the ANOVA revealed an interaction between finding type and organ system (F (1, 33) = 7.4, p <0.001). The most clinically significant discrepancies between MDCT and OR findings were for gallbladder (GB), bowel and mesenteric, and diaphragmatic injuries (DI). In particular, MDCT imaging showed a slight tendency towards false negatives for GB, mesenteric and DI.

CONCLUSION

The detection of clinically significant injuries to solid organs in trauma patients with penetrating abdominal and pelvic injuries on 64-MDCT is adequate. However, detection of injury to the remaining organ groups on MDCT - especially the GI tract, mesentery, and diaphragm - remains a challenge.

CLINICAL RELEVANCE/APPLICATION

The accurate preoperative detection of bowel, mesenteric and diaphragmatic injuries on preoperative MDCT remains a challenge.

Honored Educators

Presenters or authors on this event have been recognized as RSNA Honored Educators for participating in multiple qualifying educational activities. Honored Educators are invested in furthering the profession of radiology by delivering high-quality educational content in their field of study. Learn how you can become an honored educator by visiting the website at: https://www.rsna.org/Honored-Educator-Award/ Vincent M. Mellnick, MD - 2016 Honored EducatorVincent M. Mellnick, MD - 2018 Honored Educator

SSM07-03 Evaluation of CT and Clinical Features of Bowel and Mesenteric Injuries in Blunt Abdominal Trauma: A Case-Control Study

Wednesday, Nov. 28 3:20PM - 3:30PM Room: S404AB

Participants

Alexandre Lansier, Paris, France (Presenter) Nothing to Disclose

Camille Bourillon, Paris, France (Abstract Co-Author) Nothing to Disclose

Olivier G. Clement, MD, PhD, Paris, France (Abstract Co-Author) Consultant, Bracco Group Research Consultant, Bayer AG Research collaboration, Guerbet SA

Charles-Andre Cuenod, Paris, France (Abstract Co-Author) Research collaboration, Guerbet SA Speaker, Guerbet SA

PURPOSE

To evaluate accuracy of individual or associations of CT and clinical signs To determine signs that are implied in missed diagnosis on first CT

METHOD AND MATERIALS

This retrospective case-control study included 30 cases with surgically confirmed bowel and/or mesentery requiering surgical repair and 52 consecutive controls with blunt abdominal or chest trauma and no surgically important bowel and/or mesenteric injury. CT findings were screened by two radiologists: a 10-year-experimented in abdominal imaging radiologistand a second-year resident blinded to the patients' outcome. Clinical outcomes were analysed by consulting the medical file. Sensitivity and specificity were calculated for each sign and a kappa coefficient were used to establish the interobserver variability.

RESULTS

The CT signs with best positive likelihood ratio were extra luminal air, bowel wall defect and thickening, decreased bowel wall enhancement and mesenteric vessels abnormalities. The specificity of clinical seat belt sign associated with anterior abdominal wall injury on CT was 98%. The sensitivity of free intraperitoneal fluid was 100% and its density was higher in cases. More than 50% of patients with missed diagnosis on first CT had a visceral injury associated. Diagnosis of mesenteric and/or bowel injury depends on the experience of the radiologist (kappa = 0,6).

CONCLUSION

CT scan is accurate for the diagnosis of bowel and/or mesenteric injuries in blunt abdominal trauma depending on the experience of the radiologist. The association of clinical seat belt sign and anterior abdominal wall injury on CT is highly specific.

CLINICAL RELEVANCE/APPLICATION

The radiologist should know the relevant signs and have a stratified strategy for the diagnosis. Therefore we propose an algorithm for the diagnosis.

SSM07-04 Radiation Dose versus Injury Yield: A Study of CT Imaging Findings in Stabbing Related Injuries at an Urban Level 1 Trauma Center

Wednesday, Nov. 28 3:30PM - 3:40PM Room: S404AB

Participants

Oliver Duxbury, MBBCh, FRCR, London, United Kingdom (*Presenter*) Nothing to Disclose Gurinder Nandra, FRCR, MBChB, London, United Kingdom (*Abstract Co-Author*) Nothing to Disclose Ioannis Vlahos, MRCP, FRCR, London, United Kingdom (*Abstract Co-Author*) Research Consultant, Siemens AG Research Consultant, General Electric Company

PURPOSE

Clinical uncertainty over stab injury severity results in extensive CT use based solely on anatomic location often without consideration of injury depth or other clinical parameters. The study aim was to determine whether the diagnostic yield of emergency department (ED) requests justifies the CT radiation dose exposure.

METHOD AND MATERIALS

All ED CT examinations performed for stabbing in 2017 at an Urban Level 1 Trauma Center were retrospectively assessed. CT coverage/protocol phases were determined by ED referral based on injury anatomic location. CT evaluation (Definition,Siemens Medical Solutions,Forchheim,DE) was performed with autoKVp selection (80-140kVp, filtered back projection). Parameters recorded included: age, body parts imaged, phases per scan, identifiable site injuries and depth, organ injuries, presence of active bleeding and patient management. Effective radiation dose was calculated.

RESULTS

A total of 175 patients were scanned for 179 stabbing related injuries (median age 25, 87% male). A mean 1.6 phases of CT were performed per patient (range 1-3), imaging a mean 3.9 body part-phases/patient. Mean dose was 11.8mSv (1.5-43.9). A total of 79 organ injuries were identified in 61/179 patient episodes, imaged at a cost of 26.7mSv/organ injury. The injury site was identifiable in 95% of cases, but was limited to the subcutaneous layer in 38% and the muscular layer in 66% of patients. No injuries were fatal. 106/179 (59%) of studies had more than one phase, but only 17% of all patients demonstrated active bleeding, and only one third of these required surgery or interventional radiology. Excluding 15 patients with clinically overt injuries (knife in situ, evisceration, needing chest drain prior to CT), only 22% of 164 patients had CT detected injuries necessitating treatment. The dose in patients without injuries was only slightly lower than patients with treatable injuries(11.3mSv v. 13.1mSv, p<0.05, Mann-Whitney U).

CONCLUSION

Most stab injuries are superficial, or not necessitating treatment. A high radiation dose burden in young patients without significant injury dictates better CT use criteria are required to limit imaging to the minority with significant injuries.

CLINICAL RELEVANCE/APPLICATION

The high radiation dose in young patients dictates better clinical criteria are needed to limit CT in stabbing injuries to the patient minority likelier to have injuries requiring further management.

Honored Educators

Presenters or authors on this event have been recognized as RSNA Honored Educators for participating in multiple qualifying educational activities. Honored Educators are invested in furthering the profession of radiology by delivering high-quality educational content in their field of study. Learn how you can become an honored educator by visiting the website at: https://www.rsna.org/Honored-Educator-Award/ Ioannis Vlahos, MRCP, FRCR - 2015 Honored Educator

SSM07-05 Diagnostic Value of IV Contrast Extravasation (CE) at CT for Major Arterial Injury After Blunt Pelvic Ring Disruption: A Meta-Analysis of 3855 Patients

Wednesday, Nov. 28 3:40PM - 3:50PM Room: S404AB

Participants

David Dreizin, MD, Baltimore, MD (*Presenter*) Research Grant, Siemens AG; Yuanyuan Liang, PhD, Baltimore, MD (*Abstract Co-Author*) Nothing to Disclose James J. Dent, MD, Baltimore, MD (*Abstract Co-Author*) Nothing to Disclose Nabeel M. Akhter, MBBS, Baltimore, MD (*Abstract Co-Author*) Consultant, AngioDynamics, Inc Daniel C. Mascarenhas, BS, Cinnaminson, NJ (*Abstract Co-Author*) Nothing to Disclose Thomas M. Scalea, MD, Baltimore, MD (*Abstract Co-Author*) Nothing to Disclose

For information about this presentation, contact:

ddreizin@umm.edu

PURPOSE

The diagnostic performance of intravenous contrast extravasation on computed tomography for prediction of angiopositivity after pelvic ring disruption has not been previously assessed using meta-analysis, despite ongoing controversy and widely variable results

in the literature. We performed a meta-analysis to determine pooled accuracy of CE, and to assess the influence of CT scanner generation and multiphasic protocols.

METHOD AND MATERIALS

We conducted a systematic literature search to answer the following: 'What is the diagnostic accuracy of intravenous contrast extravasation (CE) at admission trauma CT for predicting angiopositivity and need for angioembolization in patients who have sustained blunt pelvic ring disruptions?'. MEDLINE, Embase, and Cochrane databases were queried using a combination of text words and MeSH terms. Of 206 potentially eligible studies, 23 studies that met criteria were assessed for methodologic quality using the QUADAS-2 tool. Sensitivity and specificity were synthesized using bivariate mixed-effects logistic regression. Heterogeneity was assessed using the I2 statistic. Publication bias was examined using Deeks' test. Subgroup analyses were conducted to explore the heterogeneity based on the use of 64-section CT, multiphasic versus single phase protocols, study sample size, and prevalence of arterial bleeding on angiography.

RESULTS

23 included studies provided 3855 patients for meta-analysis. There was no evidence of publication bias (p=0.62) Pooled sensitivity and specificity were 80% (95% CI: 66-90%, I2 = 92.65%) and 93% (CI: 90-96, I2 = 89.34%), respectively, with substantial heterogeneity. Subgroup analysis showed pooled sens and spec of 94% and 89% for 64-section CT compared to 69% and 95% with older generation scanners. With multiphasic protocols, CE had pooled sensitivity and specificity of 95% and 92%, compared to 74% and 94% with single phase protocols. Studies with lower disease prevalence and larger sample size also had better diagnostic performance.

CONCLUSION

Multiphasic protocols and improved scanner quality result in substantial gains in sensitivity of CE, potentially at the expense of specificity.

CLINICAL RELEVANCE/APPLICATION

Little further improvement in sensitivity can be expected beyond 64MDCT. Increased conspicuity of small foci of self-limiting CE could potentially reduce specificity for angioembolization need.

SSM07-06 Whole Body CT Using Biphasic Injection Protocol with Adaptive Statistical Iterative Reconstruction-V (Asir-V) in Multi-Trauma Patients: Impact on Dose Reduction and Image Quality

Wednesday, Nov. 28 3:50PM - 4:00PM Room: S404AB

Awards

Student Travel Stipend Award

Participants Ali H. Elmokadem, MD,PhD, Mansoura, Egypt (*Presenter*) Nothing to Disclose Enas A. Ibrahim, MD, Cairo, Egypt (*Abstract Co-Author*) Nothing to Disclose Walaa A. Gouda, MD, Shebeen El-Kom, Egypt (*Abstract Co-Author*) Nothing to Disclose Ahmed Abdel Razek, MD, Mansoura, Egypt (*Abstract Co-Author*) Nothing to Disclose

For information about this presentation, contact:

mokadem83@yahoo.com

PURPOSE

To evaluate potential dose savings and image quality after implementing adaptive statistical iterative reconstruction-V (ASIR-V) algorism on a revised protocol for whole-body computed tomography (WBCT) for multi-trauma patients and compare it to conventional protocols.

METHOD AND MATERIALS

One hundred multi-trauma patients were scanned using a 256-multidetector CT system (GE Healthcare Revolution system). They were randomized into two groups using two different scanning protocols. Group (A) (n=50, age 32.48±8.09) underwent conventional protocol including unenhanced WBCT scan, then contrast-enhanced arterial-phase of the thorax and abdomen followed by a portal and delayed scan of the abdomen and pelvis. Group (B) (n=50, age 35.94±13.57) underwent biphasic injection protocol including unenhanced WBCT scan, followed by a one-step acquisition of the thorax, abdomen, and pelvis following a biphasic injection, the examination was ended by delayed phase for the abdomen and pelvis. All examination were done under 50 % ASiR-V. Image count, radiation dose, total acquisition time, mediastinal artifacts were compared. Two radiologists independently graded image quality from 1 to 5. In addition, contrast enhancement was measured in the pulmonary artery, aorta, inferior vena cava, portal vein, liver, spleen, and kidneys.

RESULTS

The mean (\pm SD) dose length product value for group (A) was 2202.3 \pm 271.8 mGy*cm and higher when compared to group (B) (p < 0.001) which was 1485.8 \pm 489.2 mGy*cm. Protocol B gave a dose reduction of 32.5% and 7.7% acquisition time reduction. The Houndsfield unit values of the aorta, liver and spleen were significantly higher in group (A) while both kidneys values were higher in group (B). There was no statistically significant difference between the image quality scores for both groups however, group (A) scored higher grades (4.62 \pm 0.56 & 4.56 \pm 0.67).

CONCLUSION

Implementing ASiR-V algorism on biphasic injection WBCT protocol reduced radiation dose significantly with maintenance of diagnostic accuracy and image quality.

CLINICAL RELEVANCE/APPLICATION

Whole body computed tomography (WBCT) is an important diagnostic tool for initial clinical trauma management. Dose reduction with maintenance of image quality is still a concerning subject for emergency radiologists.



Gastrointestinal (Liver, Quantitative Imaging)

Wednesday, Nov. 28 3:00PM - 4:00PM Room: S502AB



AMA PRA Category 1 Credit ™: 1.00 ARRT Category A+ Credit: 1.00

Participants

Mustafa R. Bashir, MD, Cary, NC (*Moderator*) Research Grant, Siemens AG; Research Grant, General Electric Company; Research Grant, NGM Biopharmaceuticals, Inc; Research Grant, TaiwanJ Pharmaceuticals Co, Ltd; Research Grant, Madrigal Pharmaceuticals, Inc; Research Consultant, RadMD

Utaroh Motosugi, MD, Chuo, Japan (Moderator) Nothing to Disclose

Sub-Events

SSM08-01 Prediction of Overall Survival and Treatment Response in HCC Patients Using Baseline Imaging and Biochemical Biomarkers

Wednesday, Nov. 28 3:00PM - 3:10PM Room: S502AB

Participants

Mounes Aliyari Ghasabeh, MD, Baltimore, MD (*Presenter*) Nothing to Disclose Sanaz Ameli, MD, Baltimore, MD (*Abstract Co-Author*) Nothing to Disclose Pegah Khoshpouri, MD, Baltimore, MD (*Abstract Co-Author*) Nothing to Disclose Pallavi Pandey, MD, Baltimore, MD (*Abstract Co-Author*) Nothing to Disclose Bharath Ambale Venkatesh, PhD, Baltimore, MD (*Abstract Co-Author*) Nothing to Disclose Ankur Pandey, MD, Baltimore, MD (*Abstract Co-Author*) Nothing to Disclose Yan Luo, MD, Baltimore, MD (*Abstract Co-Author*) Nothing to Disclose Angela Jacob, Baltimore, MD (*Abstract Co-Author*) Nothing to Disclose Manijeh Zarghampour, MD, Baltimore, MD (*Abstract Co-Author*) Nothing to Disclose Inab R. Kamel, MD, PhD, Baltimore, MD (*Abstract Co-Author*) Nothing to Disclose

For information about this presentation, contact:

maliyar1@jhmi.edu

PURPOSE

To identify baseline imaging and biochemical factors that would determine prognosis, tumor response to treatment and overall survival in patients with HCC.

METHOD AND MATERIALS

This retrospective, IRB approve HIPAA compliant study included 220 HCC patients between March 2005 and November 2016. Diagnosis was confirmed either pathologically (n=105) or by typical imaging criteria (n = 115). All patients had baseline liver MRI before treatment. Baseline tumor variables were measured including tumor volume, volumetric ADC, and viable tumor volume. Baseline Child score, BCLC criteria, laboratory data, comorbidities and etiology of the liver disease were recorded. Patients were followed until death, or until December 2017. Cox regression models were utilized to identify the impact of clinical and imaging variables on patient survival. Additive value of imaging variables to the BCLC criteria and clinical variables was quantified. Classification and Regression Trees (CART) analysis was performed to predict patient overall survival based on the final model with independent predictive variables.

RESULTS

Among baseline variables BCLC criteria, tumor type (infiltrative vs well vs ill-defined tumors on MRI), tumor volume and viable tumor volume had significant impact on overall patient survival. Adding imaging variables to BCLC significantly increased the accuracy of overall patient survival prediction by 6% (p<=0.001); the number of treatments did not alter the predictive ability of the imaging variables. However, including liver transplantation status in the model with BCLC and imaging criteria significantly improved the accuracy of overall survival prediction by 7% (p<= 0.001), Figure 1. CART analysis showed that patients who received liver transplant had the highest survival. In patients who did not receive liver transplant, those with viable tumor volume <=800 ml3 had higher survival compared to those who had viable tumor volume >800 ml3, Figure 2.

CONCLUSION

In a relatively large sample size of HCC patients we were able to show that in patients who do not receive transplant, viable tumor volume and tumor type were the most important criteria in predicting survival.

CLINICAL RELEVANCE/APPLICATION

Baseline features in HCC patients stratified patients into those who would benefit from management with improved overall survival and those who would not.

Honored Educators

Presenters or authors on this event have been recognized as RSNA Honored Educators for participating in multiple qualifying educational activities. Honored Educators are invested in furthering the profession of radiology by delivering high-quality educational content in their field of study. Learn how you can become an honored educator by visiting the website at: https://www.rsna.org/Honored-Educator-Award/ Ihab R. Kamel, MD, PhD - 2015 Honored Educator

SSM08-02 Categorization of Indeterminate Nodules in Patients at High Risk of HCC by Quantitative CT-Scan Features

Wednesday, Nov. 28 3:10PM - 3:20PM Room: S502AB

Participants

Fatima-Zohra Mokrane, MD, Toulouse, France (*Presenter*) Nothing to Disclose
Lin Lu, New York, NY (*Abstract Co-Author*) Nothing to Disclose
Lawrence H. Schwartz, MD, New York, NY (*Abstract Co-Author*) Committee member, Celgene Corporation Committee member,
Novartis AG Committee member, ICON plc Committee member, BioClinica, Inc
Jean-Marie Peron, Toulouse, France (*Abstract Co-Author*) Nothing to Disclose
Adrien R. Vavasseur, Toulouse, France (*Abstract Co-Author*) Nothing to Disclose
Hao Yang, New York, NY (*Abstract Co-Author*) Nothing to Disclose
Philippe Otal, MD, Toulouse, France (*Abstract Co-Author*) Nothing to Disclose
Herve P. Rousseau, MD, Toulouse, France (*Abstract Co-Author*) Nothing to Disclose
Binsheng Zhao, DSc, New York, NY (*Abstract Co-Author*) License agreement, Varian Medical Systems, Inc; Royalties, Varian Medical
Systems, Inc; License agreement, Keosys SAS; License agreement, Hinacom Software and Technology, Ltd;
Laurent Dercle, MD, New York, NY (*Abstract Co-Author*) Nothing to Disclose

For information about this presentation, contact:

mokrane_fatimazohra@yahoo.fr

PURPOSE

Radiological categorization of liver nodules is standardized by the AASLD and LIRADS criteria. However, a significant proportion of nodules in cirrhotic livers remains classified as indeterminate. We aimed to improve categorization of indeterminate nodules recognized at CT, in patients at high risk of hepatocellular carcinoma (HCC) through machine-learning.

METHOD AND MATERIALS

We analyzed retrospectively and consecutively 106 pts with indeterminate liver nodules reaching predefined quality criteria: (i) biopsy-proven, (ii) follow-up at our institution, (iii) triphasic CT-scan (non contrast-enhanced 'NCP', arterial 'AP' and portal 'PVP' phases). The volume of HCC was contoured on CT-scans gathered from 2010 and 2015. Model building used Random Forest algorithm and 1.160 quantitative imaging features extracted from NCP, AP, PVP, deltaNCP-AP, deltaAP-PVP, and delta NCP-PVP, respectively. The performance of prediction model was evaluated by the area under the receiver operating characteristic curve (AUC) and ten-fold cross-validation. The Synthetic Minority Over-sampling Technique (SMOTE) was employed to alleviate the sample imbalance problem.

RESULTS

The proportion of HCC in indeterminate liver nodules biopsied was 81%: 86 pts in HCC group and 20 pts in non-HCC group. The model based on DeltaAP-PVP features achieved the highest AUC=0.85. As a comparison, model built on NCP, AP, PVP, DeltaAP-PVP, Delta DeltaNCP-PVP imaging features reached AUCs of 0.73, 0.73, 0.78, 0.71, and 0.72. The 5 most important features were features characterizing lesion contours and homogeneity (DWT1, Gabor, GLCM homogeneity, Laws and RSRE). Non-HCC nodules were composed of dysplastic (n=8), regenerative nodules (n=5), steatohepatitis (n=4), and others (n=3).

CONCLUSION

This study is a proof of concept that quantitative CT interpretation can categorize indeterminate nodules of cirrhotic patients as HCC or non-HCC, with a great precision. We demonstrated that the optimal imaging features characterized the change in lesion contours and homogeneity and allow to differenciate HCC from non HCC.

CLINICAL RELEVANCE/APPLICATION

Noninvasive categorization of indeterminate nodules in cirrhotic patients is feasible. Virtual biopsies using artificial intelligence will improve patients' management for earlier diagnosis of HCC.

SSM08-03 Exploring the Uncharted Realm of Laboratory Radiology: Quantification and Landmark-Based Normalization of Liver Volume

Wednesday, Nov. 28 3:20PM - 3:30PM Room: S502AB

Participants

Therese Lincke, Basel, Switzerland (*Presenter*) Nothing to Disclose Guillaume J. Chabin, MS, Princeton, NJ (*Abstract Co-Author*) Employee, Siemens AG Sasa Grbic, Princeton, NJ (*Abstract Co-Author*) Employee, Siemens AG Dorin Comaniciu, PhD, Princeton, NJ (*Abstract Co-Author*) Employee, Siemens AG Daniel Boll, Basel, Switzerland (*Abstract Co-Author*) Nothing to Disclose Bram Stieltjes, MD,PhD, Basel, Switzerland (*Abstract Co-Author*) Nothing to Disclose

PURPOSE

To become meaningful in a clinical context, quantitative imaging-based values, in this case liver volumes, may need to be normalized to reveal their relevance. Here, we evaluate variability of liver volumes and assess methods for normalization using automatically detected osseous and soft tissue body landmarks.

METHOD AND MATERIALS

4578 CT-datasets of 1812 woman and 2766 men were consecutively included. Liver volumes and body landmarks were fully automatically detected using Multi-scale Deep-Reinforcement Learning for 3D body markers detection and Adversarial Deep

Image2Image for 3D liver segmentation. The landmark detection library includes 17 landmarks e.g. th6, liver top and right lung top. Distances between landmark pairs were extracted and Pearson correlation was calculated for landmark-distances/liver volumes. As a measure of normalization effect, the quartile coefficient of dispersion before and after normalization was calculated.

RESULTS

A large spread of liver volumes was found (mean f:1496.4 \pm 486.1ml, m:1746.0 \pm 571.2ml, total 1647.2 \pm 552.7ml). Of all extracted landmark pairs, a high correlation was found between the distance vertebral body th6-I5 and I1-I5 (m/f: r=0.83/0.87) and liver volume. The high correlation between liver volume normalized by the th6-I5 distance and liver volume itself confirms that the normalization step preserves the information (r=0.97/0.95). In parallel, a 68% drop of the quartile coefficient of dispersion using this landmark pair illustrates the highest reduction of the variability within the normalized volume among all available landmarks

CONCLUSION

The large variance of non-normalized liver volumes illustrates the limited potential of liver volume as a measure of disease. The distance between th6 and I5 is a valid candidate for normalization since the thus normalized volume shows little loss of information while reducing substantially the variability

CLINICAL RELEVANCE/APPLICATION

Automatically derived imaging-based reference values, very much comparable to current laboratory medicine, may be helpful to classify an organ as normal or pathological. In future research, the pathological value of thus extracted normalized volumes will be further elucidated.

SSM08-04 Comparison of Magnetic Resonance Elastography and Ultrasound Shear Wave Elastography for Long-Term Monitoring of Direct Antiviral HCV-Treatment

Wednesday, Nov. 28 3:30PM - 3:40PM Room: S502AB

Awards

Student Travel Stipend Award

Participants

Stephan Marticorena Garcia, MD, Berlin, Germany (Presenter) Nothing to Disclose Jing Guo, MD, PhD, Berlin, Germany (Abstract Co-Author) Nothing to Disclose Heiko Tzschatzsch, Berlin, Germany (Abstract Co-Author) Nothing to Disclose Christian E. Althoff, MD, Berlin, Germany (Abstract Co-Author) Nothing to Disclose Christian Burkhardt, Berlin, Germany (Abstract Co-Author) Nothing to Disclose Michael Durr, Berlin, Germany (Abstract Co-Author) Nothing to Disclose Fabian Halleck, Berlin, Germany (Abstract Co-Author) Nothing to Disclose Klemens Budde, Berlin, Germany (Abstract Co-Author) Nothing to Disclose Korinna Johrens, Berlin, Germany (Abstract Co-Author) Nothing to Disclose Bernd K. Hamm III, MD, Berlin, Germany (Abstract Co-Author) Research Consultant, Canon Medical Systems Corporation; Stockholder, Siemens AG; Stockholder, General Electric Company; Research Grant, Canon Medical Systems Corporation; Research Grant, Koninklijke Philips NV; Research Grant, Siemens AG; Research Grant, General Electric Company; Research Grant, Elbit Imaging Ltd; Research Grant, Bayer AG; Research Grant, Guerbet SA; Research Grant, Bracco Group; Research Grant, B. Braun Melsungen AG; Research Grant, KRAUTH medical KG; Research Grant, Boston Scientific Corporation; Equipment support, Elbit Imaging Ltd; Investigator, CMC Contrast AB Jurgen Braun, PhD, Berlin, Germany (Abstract Co-Author) Nothing to Disclose Ingolf Sack, PhD, Berlin, Germany (Abstract Co-Author) Nothing to Disclose

Thomas Fischer, MD, Berlin, Germany (*Abstract Co-Author*) Speaker, Canon Medical Systems Corporation; Advisory Board, Canon Medical Systems Corporation

For information about this presentation, contact:

stephan.marticorena-garcia@charite.de

PURPOSE

Direct antiviral treatment of chronic hepatitis C virus (HCV) induced liver fibrosis is associated with viscoelastic tissue changes. The purpose of this prospective study is to non-invasively monitor treatment-related liver elasticity changes in HCV-patients over a period of 15 months using magnetic resonance elastography (MRE) and shear wave elastography (SWE).

METHOD AND MATERIALS

In this prospective study a total of 54 MRE/SWE examinations of the liver was performed in 15 patients with chronic HCV infection and biopsy proven liver fibrosis. Patients were treated daily over 3 months with direct-acting antivirals (Daclatasvir/Sofosbuvir). MRE/SWE and laboratory results were obtained at baseline and during a follow-up period after therapy at 3, 6 and 15 months. The results were compared to a healthy control group (CTR, n=7). Multifrequency MRE (1.5 T scanner, Siemens) with tomoelastography postprocessing was performed at 4 frequencies from 30 to 60 Hz. SWE (Aplio500, Canon Medical Systems) based on an ultrasonic burst captured by a 5 MHz convex broadband transducer was employed. Shear wave speed (SWS), reflecting tissue stiffness, was obtained from both MRE and SWE and compared to each other.

RESULTS

Mean time point to reach undetectable viral RNA was 22±13 days. Analysis of repeated measurements of MRE and SWE showed a significant decrease in liver SWS at 6 months ($1.56\pm0.27 \text{ m/s}$; $1.62\pm0.36 \text{ m/s}$; p<0.01) compared to baseline ($1.67\pm0.33 \text{ m/s}$; $2.09\pm0.68 \text{ m/s}$), being stable at 15 months ($1.55\pm0.26 \text{ m/s}$; $1.63\pm0.34 \text{ m/s}$; p<0.05). Compared to CTR (MRE, 1.36 m/s; SWE, $1.48\pm0.23 \text{ m/s}$), the patient group showed higher values at baseline and after 3 months (patients vs. CTR: baseline, p<0.01; 3 months, p<0.05). SWS values from MRE and SWE were highly correlated (r=0.8; p<0.000.1).

CONCLUSION

Changes in liver stiffness after viral clearance were related to reduction in the inflammatory response. Both, MRE and SWE are sensitive in detecting early changes in hepatic stiffness after direct antiviral treatment.

CLINICAL RELEVANCE/APPLICATION

Mechanical properties obtained from both techniques could be used as non-invasive biomarker for novel antiviral HCV-treatment.

SSM08-05 Individuals with NAFLD Show Stronger Improvements in Liver Function and Insulin Sensitivity Than Individuals without NAFLD upon Dietary Weight Loss

Wednesday, Nov. 28 3:40PM - 3:50PM Room: S502AB

Participants

Johanna Nattenmueller, MD, Heidelberg, Germany (*Presenter*) Nothing to Disclose Tilman Kuhn, Heidelberg, Germany (*Abstract Co-Author*) Nothing to Disclose Tobias Nonnenmacher, Heidelberg, Germany (*Abstract Co-Author*) Nothing to Disclose Christopher L. Schlett, MD, MPH, Heidelberg, Germany (*Abstract Co-Author*) Nothing to Disclose Cornelia Ulrich, PhD, Heidelberg, Germany (*Abstract Co-Author*) Nothing to Disclose Rudolf Kaaks, Heidelberg, Germany (*Abstract Co-Author*) Nothing to Disclose Hans-Ulrich Kauczor, MD, Heidelberg, Germany (*Abstract Co-Author*) Nothing to Disclose Speakers Bureau, Boehringer Ingelheim GmbH Speakers Bureau, Siemens AG Speakers Bureau, Koninklijke Philips NV Speakers Bureau, Bracco Group Speakers Bureau, AstraZeneca PLC Ruth Schubel, Heidelberg, Germany (*Abstract Co-Author*) Nothing to Disclose

For information about this presentation, contact:

Johanna.nattenmueller@med.uni-heidelberg.de

PURPOSE

Non-alcoholic fatty liver disease (NAFLD) is a driver of insulin resistance and metabolic diseases. The presence or absence of NAFLD in obesity may in part explain the phenomena of metabolically healthy vs. unhealthy obesity. Here, we tested whether individuals with NAFLD at baseline show stronger metabolic improvements upon dietary weight loss with regard to liver function and insulin sensitivity than individuals without NAFLD.

METHOD AND MATERIALS

We used data of the HELENA-Trial, an RCT among 143 non-smokers with BMIs between 25 and 40 kg/m2 at baseline (50 % female). The participants underwent a three-month dietary intervention that induced moderate weight loss (5.0±4.3% on average). MRIderived liver fat content before and after the intervention was evaluated on a post-processing software (OsiriX, Pixmeo SARL, Bernex, Switzerland) manually using the proton density fat fraction map, based on mean counts from three identical regions of interest. Liver fat values >5.56 % were classified as NAFLD.

RESULTS

Overall, 52.4% of the study participants had NAFLD at baseline; 73.3% of those with NAFLD and 47.1 % of those without NAFLD were obese (BMI values >30 kg/m2). Mean age was 50.0 ± 8.1 years among participants with NAFLD, and 50.1 ± 8.1 years among participants without NAFLD. The prevalence of NAFLD was higher among men (61.1%) then women (43.6%). Diet-induced weight loss was similar in both groups (NAFLD: $-5.0\pm0.6\%$, No NAFLD: $-5.3\pm0.5\%$), while the relative decrease in liver fat was significantly greater in the NAFLD group ($-50.1\pm5.7\%$ vs. $-11.9\pm4.2\%$). Relative decreases in liver function tests (GGT, ALT, AST) and HOMA-IR were also significantly stronger in the NAFLD group. Other metabolic parameters (blood lipids, adipokines, CRP) showed no significant differences between the groups.

CONCLUSION

Our data suggest that individuals with NAFLD show stronger improvements of liver function and insulin sensitivity with moderate diet-induced weight loss than individuals without NAFLD.

CLINICAL RELEVANCE/APPLICATION

With increasing incidence of obesity also NAFLD is increasing. NAFLD is an important entity as it can progress in NASH and advanced liver disease and therefore intervention to stop development of NAFLD and NASH is crucial.

SSM08-06 Association Between 3D Radiomic Features and Size of Hepatic Metastasis in Breast Cancer

Wednesday, Nov. 28 3:50PM - 4:00PM Room: S502AB

Participants

Yuri Velichko, PhD, Chicago, IL (*Presenter*) Nothing to Disclose Amirhossein Mozafarykhamseh, MD, Chicago, IL (*Abstract Co-Author*) Grant, Siemens AG Tugce Agirlar Trabzonlu, MD, Chicago, IL (*Abstract Co-Author*) Grant, Siemens AG Zhuoli Zhang, MD,PhD, Chicago, IL (*Abstract Co-Author*) Nothing to Disclose Vahid Yaghmai, MD, Chicago, IL (*Abstract Co-Author*) Nothing to Disclose

PURPOSE

To evaluate the effect of the size of the hepatic metastasis in patients with breast cancer on 3D radiomic imaging features.

METHOD AND MATERIALS

This HIPAA compliant retrospective study was IRB approved. CT scans of 81 liver metastases from 54 patients with breast cancer were evaluated. To exclude imaging variability, the same CT scanner and imaging protocol were used. 3D radiomic features from the histogram and gray level co-occurrence matrix (GLCM) categories were calculated for the normal liver and hepatic metastasis. The effect of size (tumor volume) was evaluated by using linear mixed-effects regression models with variable slopes and intercepts. The tumor size and the treatment period were considered as independent variables. If the slope of the regression was significantly (P < 0.05) different between the normal liver and hepatic metastasis, then the effect of the size was considered to be significant.

RESULTS

3D radiomic features from GLCM demonstrate tumor-size dependence. In particular, Homogeneity (log model, P < 0.001), Energy

(power model, P < 0.03), Contrast (power model, P < 0.001), Correlation (log model, P < 0.001), Entropy (log model, P < 0.024) and Dissimilarity (power model, P < 0.001) show statistically significant size dependence.

CONCLUSION

Radiomic imaging features from the major texture feature category demonstrate statistically significant size dependence in breast cancer hepatic metastasis. This finding demonstrates the complex behavior of imaging features and the need to include feature specific properties into radiomic models.

CLINICAL RELEVANCE/APPLICATION

Radiomic features of breast cancer hepatic metastasis may be affected by tumor size. Caution should be exercised when directly comparing radiomic features of different size tumors.

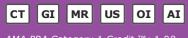
Honored Educators

Presenters or authors on this event have been recognized as RSNA Honored Educators for participating in multiple qualifying educational activities. Honored Educators are invested in furthering the profession of radiology by delivering high-quality educational content in their field of study. Learn how you can become an honored educator by visiting the website at: https://www.rsna.org/Honored-Educator-Award/ Vahid Yaghmai, MD - 2012 Honored EducatorVahid Yaghmai, MD - 2015 Honored Educator



Gastrointestinal (Gallbladder and Bile Ducts)

Wednesday, Nov. 28 3:00PM - 4:00PM Room: S503AB



AMA PRA Category 1 Credit ™: 1.00 ARRT Category A+ Credit: 1.00

Participants

Alice W. Fung, MD, Portland, OR (*Moderator*) Nothing to Disclose Benjamin Wildman-Tobriner, MD, Durham, NC (*Moderator*) Nothing to Disclose

Sub-Events

SSM09-01 Apparent Diffusion Coefficient as a Potential Marker for Tumor Differentiation, Staging, and Long-Term Clinical Outcomes in Gallbladder Cancer

Wednesday, Nov. 28 3:00PM - 3:10PM Room: S503AB

Participants

Ji Hye Min, MD, PhD, Daejeon, Korea, Republic Of (*Presenter*) Nothing to Disclose Tae Wook Kang, MD, Seoul, Korea, Republic Of (*Abstract Co-Author*) Nothing to Disclose Seo-Youn Choi, MD, Bucheon, Korea, Republic Of (*Abstract Co-Author*) Nothing to Disclose Jeong Eun Lee, Daejeon, Korea, Republic Of (*Abstract Co-Author*) Nothing to Disclose Kyung-Sook Shin, MD, Taejon, Korea, Republic Of (*Abstract Co-Author*) Nothing to Disclose

For information about this presentation, contact:

minjh1123@gmail.com

PURPOSE

To evaluate the correlation between tumor differentiation or stage of gallbladder cancer (GBC) and the apparent diffusion coefficient (ADC), as well as to assess whether ADC value can predict long-term disease-free survival (DFS) after surgery.

METHOD AND MATERIALS

This retrospective study was approved by the Institutional Review Board and the requirement for informed consent was waived. Between March 2008 and June 2016, 79 patients who underwent magnetic resonance (MR) imaging with diffusion-weighted image and subsequent surgery for GBC were included in this study. Correlations between quantitative ADC values, and tumor differentiation or stage based on the American Joint Committee on Cancer (AJCC) were assessed using Spearman's correlation analysis. Prognostic factors for DFS were identified with multivariate Cox regression analysis using imaging and clinical characteristics.

RESULTS

All patients were classified as having well- (n = 18), moderately- (n = 35), or poorly-differentiated GBCs (n = 26). The ADC value of GBCs was significantly correlated with tumor differentiation and AJCC stage (p < 0.001 and p < 0.001, respectively). Sixty nine patients were followed up for 2.0-92.4 months (median, 23.5 months). On multivariate analysis, the significant prognostic factor for DFS was not tumor differentiation or AJCC stage, but a binary tumor ADC value (hazard ratio, 4.29, p = 0.009).

CONCLUSION

The ADC value of GBCs was significantly correlated with tumor differentiation as well as AJCC stage. In addition, it predicted long-term outcomes after surgery in patients with GBC.

CLINICAL RELEVANCE/APPLICATION

Tumor recurrence after curative surgical resection in patients with GBC could be predicted by using ADC values on diffusionweighted images preoperatively.

SSM09-02 Is the MR Contrast Agent Gadoxetate Disodium Suitable for CT Cholangiography?

Wednesday, Nov. 28 3:10PM - 3:20PM Room: S503AB

Participants

Samantha Dilger, PhD, Rochester, MN (*Presenter*) Nothing to Disclose Noelle Nelson, Rochester, MN (*Abstract Co-Author*) Nothing to Disclose Lifeng Yu, PhD, Chicago, IL (*Abstract Co-Author*) Nothing to Disclose Thomas J. Vrieze, RT, Rochester, MN (*Abstract Co-Author*) Nothing to Disclose Tammy A. Drees, Rochester, MN (*Abstract Co-Author*) Nothing to Disclose Sudhakar K. Venkatesh, MD, FRCR, Rochester, MN (*Abstract Co-Author*) Nothing to Disclose Jeff L. Fidler, MD, Rochester, MN (*Abstract Co-Author*) Nothing to Disclose Joel G. Fletcher, MD, Rochester, MN (*Abstract Co-Author*) Grant, Siemens AG; Consultant, Medtronic plc; ; Cynthia H. McCollough, PhD, Rochester, MN (*Abstract Co-Author*) Research Grant, Siemens AG

For information about this presentation, contact:

yu.lifeng@mayo.edu

PURPOSE

Gadoxetate disodium (Eovist®), a Gadolinium-based contrast agent, is primarily used in MR, with an FDA approved dose limit of 0.1 mL/kg. The purpose of this work is to determine whether low doses of gadoxetate disodium can be visualized for CT cholangiography using a phantom setup.

METHOD AND MATERIALS

Vials containing four concentrations of gadoxetate disodium (9.6, 4.8, 3.4, and 1.9mgGd/ml) were placed in a 35x26cm2 water phantom and imaged on two CT scanners: Siemens Somatom Flash and Force (Siemens Healthcare, Erlangen, Germany). These concentrations correspond to the dose limit for a 200, 100, 70, 40kg patient, respectively. Single-energy (SE) scans were acquired at 70, 80, 90, 100, 120, and 140kVp. Dual-energy (DE) scans were acquired at 90/150Sn (Force) and 100/150 (Flash) for two dose levels (13 and 23 mGy). Virtual monoenergetic images at 50keV were created (Mono+, Siemens). The mean intensity and standard deviation for each concentration of gadoxetate disodium and the water background were extracted from each image set. To determine whether the signal provided by gadoxetate disodium was sufficient for clinical imaging, the contrast, noise, and contrast-to-noise ratio (CNR) were compared to measurements acquired from 12 clinical CT cholangiography exams performed with iodine-containing iodipamide meglumine.

RESULTS

From the retrospective clinical cohort, mean contrast (± standard deviation) of 239±107HU and CNR of 12.8±4.2 were found in the bile duct relative to the liver. Comparing these metrics to the gadoxetate disodium samples, the highest concentration (9.6mgGd/ml) surpassed these thresholds at all energy levels. The 4.8mgGd/ml had sufficient CNR in the Force, but not in the Flash. The 3.4mgGd/ml had clinically relevant CNR at low kV of SE (<100kVp) and 50 keV of DE in the Force but was insufficient in the Flash. Images acquired by the Force had a lower noise level and greater CNR compared to the Flash. Similar trends were seen at both dose levels.

CONCLUSION

Gadoxetate disodium shows promise as a viable contrast agent for CT cholangiography, with CNR similar to those seen clinically with an iodine-based contrast agent. DE CT or low kV SE CT is helpful to enhance the signal.

CLINICAL RELEVANCE/APPLICATION

Gadoxetate disodium, a Gadolinium-based hepatobiliary contrast agent, shows promise as a CT cholangiography contrast agent with contrast-to-noise ratios similar to iodine contrast-enhanced CT.

Honored Educators

Presenters or authors on this event have been recognized as RSNA Honored Educators for participating in multiple qualifying educational activities. Honored Educators are invested in furthering the profession of radiology by delivering high-quality educational content in their field of study. Learn how you can become an honored educator by visiting the website at: https://www.rsna.org/Honored-Educator-Award/ Sudhakar K. Venkatesh, MD, FRCR - 2017 Honored Educator

SSM09-03 CT and Ultrasound for the Diagnosis of Cholecystitis in the Adult Emergency Department: A Comparison of Accuracy and Incremental Value Offered By Each Modality Over the Other

Wednesday, Nov. 28 3:20PM - 3:30PM Room: S503AB

Awards

Student Travel Stipend Award

Participants Kevin D. Hiatt, MD, Winston-Salem, NC (*Presenter*) Nothing to Disclose Jao J. Ou, MD,PhD, Winston-Salem, NC (*Abstract Co-Author*) Nothing to Disclose James Lovato, Winston-Salem, NC (*Abstract Co-Author*) Nothing to Disclose David D. Childs, MD, Clemmons, NC (*Abstract Co-Author*) Nothing to Disclose

PURPOSE

To compare the diagnostic accuracy and relative value of CT and ultrasound (US) in the workup of cholecystitis in adult emergency department (ED) patients.

METHOD AND MATERIALS

A retrospective chart review conducted over a 5 year period identified adult ED encounters for right upper quadrant pain where patients were evaluated with CT and/or US. Those with prior cholecystectomy, current pregnancy, and acute trauma were excluded. Imaging studies were assessed for the reported presence of gallstones, gallbladder distension, wall thickening, and pericholecystic fluid/inflammation. A positive suspicion for cholecystitis required at least two findings, or a positive sonographic Murphy's sign with at least one additional finding. Sensitivity, specificity, positive predictive value (PPV), and negative predictive value (NPV) were calculated for each modality based on linked clinical, surgical, and pathology data. When both US and CT were performed, the second modality was determined to add value if it correctly identified cholecystitis when the first study was incorrect or provided a non-gallbladder alternative diagnosis for acute abdominal pain. The second study was determined to detract value if it was incorrectly positive or negative for cholecystitis when the first study was correct.

RESULTS

3495 ED encounters were reviewed, with 2859 meeting inclusion criteria. 91% of patients had one or more imaging studies performed, with US performed in 81%, CT performed in 30%, and both US and CT performed in 20%. 559 patients went on to cholecystectomy with pathology results available for 540. For US and CT, respectively: sensitivity 48% and 53%, specificity 93% and 93%, PPV 65% and 58%, and NPV 88% and 92%. Only NPV represented a statistically significant difference. When performed after CT, US added value in 8% and detracted value in 6% of cases. When performed after US, CT added value in 35% and detracted value in 2% of cases.

CONCLUSION

In this patient cohort, imaging diagnosis of cholecystitis by CT was non-inferior to the more commonly utilized gold standard of US. There was also little added value for use of US after already obtaining a CT.

CLINICAL RELEVANCE/APPLICATION

CT performance in the diagnosis of cholecystitis is essentially equivalent to ultrasound and has an advantage in supplying additional information for adult ED patients presenting with right upper quadrant pain.

SSM09-04 Development and Validation of Deep Learning Based Clinical Decision Supporting System for the Diagnosis of Neoplastic Gallbladder Polyps Using High Resolution Ultrasonography: Preliminary Results

Wednesday, Nov. 28 3:30PM - 3:40PM Room: S503AB

Awards

Student Travel Stipend Award

Participants

Younbeom Jeong, MD, Seoul, Korea, Republic Of (*Presenter*) Nothing to Disclose Jung Hoon Kim, MD, Seoul, Korea, Republic Of (*Abstract Co-Author*) Nothing to Disclose Hee-Dong Chae, MD, Seoul, Korea, Republic Of (*Abstract Co-Author*) Nothing to Disclose Ijin Joo, MD, Seoul, Korea, Republic Of (*Abstract Co-Author*) Nothing to Disclose Jae Seok Bae, MD, Seoul, Korea, Republic Of (*Abstract Co-Author*) Nothing to Disclose Joon Koo Han, MD, Seoul, Korea, Republic Of (*Abstract Co-Author*) Nothing to Disclose

For information about this presentation, contact:

jhkim2008@gmail.com

PURPOSE

To investigate the added value of the deep learning based clinical decision supporting system for the differential diagnosis of neoplastic gallbladder (GB) polyps using high resolution ultrasonography (HRUS)

METHOD AND MATERIALS

We retrospectively collected 337 patients with GB polyps (>4 mm) proved by cholecystectomy. They were divided into training set (239 patients) and test set (98 patients) according to the time period. Based on pathology, all images of polyps (neoplastic: 1822 images in 137 patients, non-neoplastic: 2058 images in 200 patients) were manually cropped into a square box containing the polyp and labeled as either neoplastic or non-neoplastic. The binary classification convolutional neural network model was constructed by transfer learning based on Inception-v3 architecture. Using test set, two radiologists with different experience level, retrospectively graded the possibility of neoplastic polyp using a 5-point confident scale. After providing model's probability value on the test set for each patient, reviewers requested to re-evaluate the grade. Diagnostic performances were measured by ROC analysis and sensitivity, specificity, and accuracy were calculated.

RESULTS

For the diagnosis of neoplastic polyp, model itself provided AUC 0.920, sensitivity 82.1%, specificity 88.1%, accuracy 85.4% with optimal cut off >0.503 in training set and AUC 0.903, sensitivity 80.5%, specificity 85.3%, accuracy 82.8% with optimal cut off >0.726 in test set. On the first review, highly and less experienced reviewers showed AUC 0.944 and 0.775; sensitivity 88.6% and 71.4%; specificity 85.7% and 68.2%; accuracy 86.7% and 69.4%, respectively. On the second review with the supporting system, less experienced reviewer's AUC was improved from 0.775 to 0.859 (p=0.0513), whereas, highly experienced reviewer's AUC showed no significant change (0.944 to 0.940).

CONCLUSION

Our preliminary results suggest that deep learning based clinical decision supporting system for differential diagnosis of neoplastic GB polyp is helpful for improving diagnostic performance, especially in less experienced readers.

CLINICAL RELEVANCE/APPLICATION

Differential diagnosis of neoplastic GB polyp is important as it has a malignant potential. Our decision supporting system can improve the diagnostic performance of radiologists using HRUS.

SSM09-05 Differentiation Between Gallbladder Premalignant or Malignant Polyps and Cholesterol Polyps Using Contrast-Enhanced Ultrasound: Preliminary Study

Wednesday, Nov. 28 3:40PM - 3:50PM Room: S503AB

Participants

Jae Seok Bae, MD, Seoul, Korea, Republic Of (*Presenter*) Nothing to Disclose Se Hyung Kim, MD, Seoul, Korea, Republic Of (*Abstract Co-Author*) Nothing to Disclose Hyo-Jin Kang, MD, Seoul, Korea, Republic Of (*Abstract Co-Author*) Nothing to Disclose Ji Kon Ryu, Seoul, Korea, Republic Of (*Abstract Co-Author*) Nothing to Disclose Jin-Young Jang, Seoul, Korea, Republic Of (*Abstract Co-Author*) Nothing to Disclose Sang Hyub Lee, Seoul, Korea, Republic Of (*Abstract Co-Author*) Nothing to Disclose Woo Hyun Paik, Seoul, Korea, Republic Of (*Abstract Co-Author*) Nothing to Disclose Wooil Kwon, Seoul, Korea, Republic Of (*Abstract Co-Author*) Nothing to Disclose Jae Young Lee, MD,PhD, Seoul, Korea, Republic Of (*Abstract Co-Author*) Nothing to Disclose Joon Koo Han, MD, Seoul, Korea, Republic Of (*Abstract Co-Author*) Nothing to Disclose

PURPOSE

To differentiate between gallbladder (GB) premalignant or malignant polyps and cholesterol polyps using contrast-enhanced

ultrasound (CEUS).

METHOD AND MATERIALS

From September 2017 to March 2018, 20 patients with large GB polyps (>= 1 cm) who were scheduled to undergo cholecystectomy were prospectively enrolled. All patients underwent conventional US including color Doppler and CEUS prior to surgery. CEUS was performed using a LOGIQ E9 US scanner (GE Healthcare) after an injection of 2.5 ml of SonoVue® for 1 minute. After CEUS, perfusion US parameters including peak enhancement, mean transit time, fall time (FT), wash-in rate (WiR), and wash-out rate (WoR) were obtained using VueBox® software. Patients were separately classified into the cholesterol polyp group (n = 6) and premalignant or malignant polyp group (n = 14) according to the final histopathology. All US features and quantitative CEUS parameters between the two groups were compared using the Mann-Whitney U test. Diagnostic performances of the parameters were assessed using receiver operating characteristic (ROC) analysis.

RESULTS

Among US imaging features, there were significant differences in lesion size (2.20 cm for adenomatous polyps and 1.18 cm for cholesterol polyps) and internal homogeneity between the two groups (P<0.05); internal homogeneity was more commonly found in cholesterol polyps (5/6, 83%) than in malignant polyps (4/14, 28%). On quantitative analysis of CEUS parameters, FT and WoR demonstrated significant differences between the two groups (P<0.05), i.e., premalignant or malignant polyps showed significantly longer FT (12.74 sec) and smaller WoR (183.3 arbitrary units [a.u]) than cholesterol polyps (5.37 sec and 1068.3 a.u). On ROC analysis, an area under the curve (AUC) of 1.00, 100% (14/14) sensitivity, and 100% (4/4) specificity were demonstrated when the cut-off value was set at 9.62 sec for FT; and WoR yielded an AUC of 0.89, sensitivity of 100% (14/14), and a specificity of 75% (3/4) using a cut-off value of 784.4 a.u.

CONCLUSION

CEUS can be useful for the differentiation of premalignant or malignant GB polyps from cholesterol polyps >= 1 cm.

CLINICAL RELEVANCE/APPLICATION

CEUS can help distinguish premalignant or malignant GB polyps from cholesterol polyps >= 1 cm, thereby aiding in the selection of an optimal management option for large GB polyps.

SSM09-06 Fully Automated Detection of Primary Sclerosing Cholangitis (PSC) in 3D-MRCP Images Using Deep Learning

Wednesday, Nov. 28 3:50PM - 4:00PM Room: S503AB

Participants

Hinrich B. Winther, MD, Hannover, Germany (*Presenter*) Nothing to Disclose Van Dai Vo Chieu, MD, Hannover, Germany (*Abstract Co-Author*) Nothing to Disclose Christian Hundt, DIPLPHYS,PhD, Mainz, Germany (*Abstract Co-Author*) Nothing to Disclose Bertil Schmidt, Mainz, Germany (*Abstract Co-Author*) Nothing to Disclose Jens Vogel-Claussen, MD, Hannover, Germany (*Abstract Co-Author*) Nothing to Disclose Frank K. Wacker, MD, Hannover, Germany (*Abstract Co-Author*) Nothing to Disclose Kristina I. Ringe, MD, Hannover, Germany (*Abstract Co-Author*) Nothing to Disclose

PURPOSE

To automatically detect PSC-typical cholangiographic changes in 3D-MRCP images.

METHOD AND MATERIALS

428 patients (m = 274 / w = 154, age 42.5 \pm 18.5 years) who underwent liver MRI including 3D MRCP were included in this retrospective study. The study population consisted of 206 patients with confirmed PSC (based on clinical, typical cholangiographic and confirmatory histologic findings) and 222 patients in whom this diagnosis was excluded. The patients were randomized into a training (n = 386) and validation group (n = 42). For each individual case, 20 uniformly distributed axial MRCP rotations, covering a total of 180°, were calculated, followed by a maximum intensity projection (MIP). This resulted in a training record of 7720 and a validation record of 840 2D images. An Inception ResNet (Inception-v4 arXiv: 1602.07261) was trained, which was initialized with weights previously learned from ImageNet. Finally, we fine-tuned the entire network with a small learning rate of 10-5.

RESULTS

The mean absolute error (MAE) on the validation record was 30% and therefore insufficient. This value could be improved to 7.1% (3/42) by applying an ensemble strategy. For this purpose, the 20 related MRCP projections of each patient were binned and a majority vote was conducted. With this approach, sensitivity, specificity, positive predictive and negative predictive value for the detection of PSC-typical cholangiographic changes were 95.0%, 90.9%, 90.5%, and 95.2% respectively.

CONCLUSION

The results of this study demonstrate the feasibility of transfer learning to detect PSC-typical cholangiographic changes in 3D MRCP images with an MAE of ~7%. Further validation with more and multicentric data should be made, as experience shows that neural networks tend to overfit the characteristics of the dataset.

CLINICAL RELEVANCE/APPLICATION

Automatic detection of PSC typical changes at MRCP may improve early detection and aid in follow-up imaging, especially of subtle changes.



Genitourinary (Pelvic Ultrasound: Male and Female)

Wednesday, Nov. 28 3:00PM - 4:00PM Room: E353A



AMA PRA Category 1 Credit ™: 1.00 ARRT Category A+ Credit: 1.00

FDA Discussions may include off-label uses.

Participants

Mary C. Frates, MD, Sharon, MA (*Moderator*) Nothing to Disclose Harris L. Cohen, MD, Memphis, TN (*Moderator*) Nothing to Disclose

Sub-Events

SSM10-01 Contrast Enhanced Ultrasound (CEUS) of Intra-Testicular Lesions: Inter-Observer Variation in the Assessment of Non-Neoplastic versus Neoplastic Abnormalities

Wednesday, Nov. 28 3:00PM - 3:10PM Room: E353A

Participants

Phillip Lung, Middlesex, United Kingdom (Abstract Co-Author) Advisory Board, Takeda Pharmaceutical Company Limited; Speaker, Siemens AG

Cheng Fang, MBBS, FRCR, London, United Kingdom (Presenter) Nothing to Disclose

Ounali Jaffer, MBBS, FRCR, London, United Kingdom (*Abstract Co-Author*) Nothing to Disclose

Annamaria Deganello, MD, London, United Kingdom (Abstract Co-Author) Speaker, Bracco Group

Aarti Shah, MBBCh, MRCP, London, United Kingdom (Abstract Co-Author) Nothing to Disclose

Venus Hedayati, MRCP, FRCR, London, United Kingdom (Abstract Co-Author) Nothing to Disclose

Anu Obaro, MBBS, London, United Kingdom (Abstract Co-Author) Nothing to Disclose

Gibran Yusuf, MBBS, London, United Kingdom (Abstract Co-Author) Speaker, Bracco Group; Speaker, Siemens AG

Dean Y. Huang, FRCR, London, United Kingdom (Abstract Co-Author) Nothing to Disclose

Maria E. Sellars, MD, FRCR, London, United Kingdom (Abstract Co-Author) Nothing to Disclose

Paul S. Sidhu, MRCP, FRCR, London, United Kingdom (*Abstract Co-Author*) Speaker, Koninklijke Philips NV; Speaker, Bracco Group; Speaker, Hitachi, Ltd; Speaker, Siemens AG; Speaker, Samsung Electronics Co, Ltd; Advisory Board, Samsung Electronics Co, Ltd; Advisory Board, Itreas Ltd

For information about this presentation, contact:

chengfang@nhs.net

PURPOSE

To assess the additional benefit of microbubble ultrasound contrast agents (UCA) over conventional ultrasonography (US) to differentiate between neoplastic and non-neoplastic intra-testicular abnormalities among observers with various levels of experience in contrast enhanced ultrasound (CEUS).

METHOD AND MATERIALS

Seven blinded observers divided into experienced (n=3, 7-9 years experience) and inexperienced groups (n=4, 2-3 years experience) retrospectively reviewed testicular B-mode/color Doppler images and repeated this one month later with the addition of CEUS images. Observers rated each testicular lesion on a 5-point scale: 1-definitely non-neoplastic; 2-likely non-neoplastic; 3-don't know; 4-likely neoplastic; 5-definitely neoplastic. Electronic medical records were reviewed for histological results (n=59) and follow up US (n=32). Inter-observer agreement was calculated using kappa statistics and AUROC/Sensitivity/Specificity compared using McNemar test.

RESULTS

Ninety patients with 91 lesions, neoplastic (n=46) and non-neoplastic (n=45), were accessed from a database from 2008-2013. Overall, specificity (73.7% vs 54.9%, p<0.001), PPV (77.6% vs 67.8%, p=0.001), accuracy (81.6% vs 74.1%, p<0.001) were better with the addition of UCA, at the expense of slightly reduced sensitivity (89.4% vs 92.3%, p=0.04). Subgroup analysis showed that the addition of CEUS images significantly improved diagnostic specificity and accuracy for both experienced (Specificity: 71.1% vs 59.3%, P=0.005; Accuracy: 83.5% vs 76.9%, P=0.003) and inexperienced reader groups (Specificity: 75.6% vs 51.7%, p=0.005; Accuracy: 80.2% vs 72.0%, P<0.001). Significant inter-observer variability between experienced and inexperienced observer groups were observed for conventional US (Kappa 0.51 vs 0.68 respectively; p=0.03), but this was not detected with the additional of CEUS (Kappa 0.60 vs 0.69 respectively; p=0.24).

CONCLUSION

The addition of CEUS not only significantly improves the accuracy of subjective interpretation for both experienced and inexperienced blinded observers, but also eliminates variability between the two observer groups with different experiences.

CLINICAL RELEVANCE/APPLICATION

The use of CEUS in addition to conventional US improves diagnostic accuracy of differentiating neoplastic and non-neoplastic

intratesticular lesion, potentially reducing unnecessary orchidectomies.

SSM10-02 Cause of Avascular Hypoechoic Testicular Lesions Detected at Scrotal Color Doppler Ultrasound: Can They Be Considered Benign? Correlation with Histological, Clinical and Contrast-Enhanced Ultrasound (CEUS) Imaging Findings

Wednesday, Nov. 28 3:10PM - 3:20PM Room: E353A

Participants

Dean Y. Huang, FRCR, London, United Kingdom (*Presenter*) Nothing to Disclose Majed R. Alsadiq, MD,FRCR, London, United Kingdom (*Abstract Co-Author*) Nothing to Disclose Maria E. Sellars, MD, FRCR, London, United Kingdom (*Abstract Co-Author*) Nothing to Disclose Kirsten M. Christensen-Jeffries, PhD, London, United Kingdom (*Abstract Co-Author*) Nothing to Disclose Robert J. Eckersley, PhD, London, United Kingdom (*Abstract Co-Author*) Nothing to Disclose Paul S. Sidhu, MRCP, FRCR, London, United Kingdom (*Abstract Co-Author*) Speaker, Koninklijke Philips NV; Speaker, Bracco Group; Speaker, Hitachi, Ltd; Speaker, Siemens AG; Speaker, Samsung Electronics Co, Ltd; Advisory Board, Samsung Electronics Co, Ltd; Advisory Board, Itreas Ltd

For information about this presentation, contact:

dean.huang@nhs.net

PURPOSE

The purposes of this study were to determine the cause of avascular lesions detected at scrotal color Doppler ultrasound (CDUS) with histological and clinical correlations and to assess the added value of contrast-enhanced ultrasound (CEUS) in identifying benign testicular lesions.

METHOD AND MATERIALS

This retrospective study included 113 focal testicular lesions detected with CDUS and further assessed with CEUS. The sonographic features recorded were lesion size, the presence of focal calcification, and presence or absence of vascularity on CEUS. Also recorded were patient age, symptoms, and levels of serum tumor markers. The reference standard was histopathologic results or at least at least 6 months documented stability with serial follow-ups. Sonographic and clinical features associated with malignant, including 'burnt-out' tumors, and benign lesions were examined.

RESULTS

Of the 113 avascular lesions on CDUS, 6 (5.3%) were malignant and 107 (94.6%) were benign. 2 of the 6 patients (33.3%) with malignant lesions had elevated serum tumor marker levels. Histologically, malignant lesions include mixed germ cell tumors and 'burnt-out' tumors with metastatic lymphadenopathy. The size of a lesion or presence of calcification were not significantly associated with either the benign or the malignant nature of a lesion. 18 lesions (17.6%) showed enhancement on CEUS despite lack of signal on CDUS. Enhancement was demonstrated on CEUS in all 6 of the 6 malignant lesions (100%). The remaining lesions which demonstrated enhancement on CEUS include pathologies such as sarcoidosis, post-biopsy change, intra-testicular adenomatoid tumour, focal scarring with history of previous orchiopexy, and focal atrophy in a patient with Klinefelter syndrome. All 95 of 95 lesions with no enhancement on CEUS were of benign nature.

CONCLUSION

Although most avascular testicular lesions on CDUS are benign, our experience suggests that caution should be made in assuming benignity when a testicular lesion demonstrates no vascularity on CDUS. A proportion of these lesions are malignant and demonstrate vascularity with CEUS, which could improve diagnostic confidence for the benign nature of testicular pathologies.

CLINICAL RELEVANCE/APPLICATION

Caution should be made in assuming benignity lesions demonstrate no vascularity on CDUS. CEUS improves detection of vascularity and adds value to conventional CDUS in assessing testicular lesions.

SSM10-03 The Audiovisual Sexual Stimulation during Penile Duplex-Doppler Ultrasound: Is it a Tool to Avoid False-Positive Diagnostic of Venous Leak?

Wednesday, Nov. 28 3:20PM - 3:30PM Room: E353A

Participants Felipe Carneiro, MD, Sao Paulo, Brazil (*Presenter*) Nothing to Disclose Jose Cury, Sao Paulo, Brazil (*Abstract Co-Author*) Nothing to Disclose Maria Cristina Chammas, MD,PhD, Sao Paulo, Brazil (*Abstract Co-Author*) Nothing to Disclose Peter C. Francolin, Sao Paulo, Brazil (*Abstract Co-Author*) Nothing to Disclose

For information about this presentation, contact:

drcarneiro91@gmail.com

PURPOSE

Erection is a neurovascular phenomenon under hormonal control. It involves arterial dilatation, trabecular smooth muscle relaxation and activation of the corporeal veno-occlusive mechanism. Penile Duplex-Doppler ultrasound (PDDU) with intracavernous injection (ICI) is the first-line diagnostic modality used to determine the subtype of vasculogenic erectile dysfunction (ED). Unfortunately, anxiety and other psychological inhibitions may hinder the optimal response of cavernous arteries relaxation imparing the venoocclusive mechanism leading to possible false venous leak diagnostic. Several methods to assist PDDU in order to avoid falsepositive results have been suggested, including audiovisual sexual stimulation (AVSS). The purpose of the present study is to assess the use of AVSS in combination with PDDU in vasculogenic ED.

METHOD AND MATERIALS

Prospective study on adult patients with ED that were referred to PDDU by Urology Department. Twenty seven men (mean age =

62.7 years, range 26 to 80 years) were enrolled in the study. Each patient underwent 2 PDDU sessions. During session 1, patients were injected with ICI (20 μ g of alprostadil) and after 5 minutes submitted to PDDU. During session 2, after the ICI injection, patients watched a 4 minute erotic movie before PDDU. The interval between the 2 sessions was 7 days. Cavernous artery flow was considered normal when peak systolic velocity (PSV) was >30 cm/s, while the corporeal veno-occlusive function was considered normal when ending diastolic velocity (EDV) was <5 cm/s) and resistant index (IR) >0.9. Penile vascular parameters were monitored and recorded before ICI administration, and 5, 10, 15 and 20 min after ICI.

RESULTS

The mean cavernous artery diameter was higher in session 2 (p = 0.003). The mean cavernous artery systolic velocity was higher in session 2 in the moment 15 and 20 minute (p=0.022 and p=0.026). The mean artery resistant index was higher in session 2 in the moment 15 minute (p = 0.043).

CONCLUSION

The AVSS improves smooth muscle relaxation of cavernous arteries and penile blood flow. Therefore, it is a good tool to avoid false-positive diagnostic of venous leak.

CLINICAL RELEVANCE/APPLICATION

AVSS during PDDU with ICI can improve penile blood flow and is recommended in all cases manly on anxious patients. The real venous leak has bad prognosis but the psicogenic ED (false venous leak) can be treated clinically. Diferenciate both is mandatory.

SSM10-04 Can Shear Wave Elastography of Endometrial and Subendometrial Lesions Provide Additive Information: Initial Experience

Wednesday, Nov. 28 3:30PM - 3:40PM Room: E353A

Participants

Zainab A. Vora, MBBS, New Delhi, India (*Presenter*) Nothing to Disclose Smita Manchanda, MD, Delhi, India (*Abstract Co-Author*) Nothing to Disclose Raju Sharma, MD, New Delhi, India (*Abstract Co-Author*) Nothing to Disclose Smriti Hari, New Delhi, India (*Abstract Co-Author*) Nothing to Disclose Sandeep Mathur, MBBS, MD, New Delhi, India (*Abstract Co-Author*) Nothing to Disclose Garima Kachhawa, New Delhi, India (*Abstract Co-Author*) Nothing to Disclose

For information about this presentation, contact:

zainab8@gmail.com

PURPOSE

-Evaluate the normal sono-elastographic characteristics of endometrium and its variability with menstrual phase-Investigate the role of Shear Wave Elastography (SWE) in distinguishing benign and malignant endometrial and subendometrial masses.

METHOD AND MATERIALS

A total of 110 women were enrolled in this ethically approved prospective study, and they were divided into two groups:Group I-55 women with pathologically proven endometrial masses, including 27 cases of endometrial carcinoma, and 28 cases of benign lesions (9-endometrial hyperplasia, 5-endometrial polyp and 5-focal adenomyoma, 9-submucosal fibroid)Group II- 56 women with normal endometrium (14 women each in menstrual, proliferative, secretory and post-menopausal phase)All patients underwent transvaginal ultrasound including B-mode and real time SWE (SuperSonic Aixplorer ultrasound system). The variability of mean elasticity value (in kPa) of endometrium in different menstrual phases and the difference in elasticity value of normal endometrium and various pathological sub-groups in Group I was analysed.

RESULTS

Normal endometrium (n=56) showed a mean elasticity value of 25.54 ± 8.56 kPa. There was no significant difference (p-0.227) in the mean elasticity value in women in different menstrual phases. In the evaluation of endometrial and subendometrial pathologies, the mean elasticity values of submucosal fibroid, focal adenomyoma and polyp were significantly (p<0.01) different from normal endometrium. However, there was no significant difference in the elasticity value of normal endometrium versus carcinoma (p-0.276), and carcinoma versus hyperplasia (p-0.191).

CONCLUSION

SWE is not useful to distinguish normal endometrium from hyperplasia or carcinoma. However, significantly different elasticity values obtained in case of submucosal fibroid, endometrial polyp and focal adenomyoma can be useful in confidently diagnosing these pathologies.

CLINICAL RELEVANCE/APPLICATION

This study shows that SWE, as an adjunct to ultrasound may play a role to increase the specificity of diagnosis of certain endometrial pathologies like submucosal fibroid and endometrial polyp and help to appropriately triage patients for more invasive testing. However, it is not a reliable tool to distinguish normal endometrium from carcinoma or hyperplasia.

SSM10-05 Diagnostic Pitfall for Early Complete Hydatidiform Mole by Transvaginal Ultrasound: A Large Cohort Study

Wednesday, Nov. 28 3:40PM - 3:50PM Room: E353A

Participants

Jiale Qin, MD, PhD, Hangzhou, China (*Presenter*) Nothing to Disclose Xiaodong Wu, Hangzhou, China (*Abstract Co-Author*) Nothing to Disclose Jiamin Luo, Hangzhou, China (*Abstract Co-Author*) Nothing to Disclose Junmei Wang, Hangzhou, China (*Abstract Co-Author*) Nothing to Disclose Xing Xie, Hangzhou, China (*Abstract Co-Author*) Nothing to Disclose

Weiguo Lu, Hangzhou, China (Abstract Co-Author) Nothing to Disclose

For information about this presentation, contact:

qinjiale@zju.edu.cn

PURPOSE

With the availability of hCG and transvaginal ultrasound, CHM diagnosis is typically made in the first trimester, rather than in the second trimester over the past two decades, which makes the difficulty of correct diagnose due to the lack of understanding about early features. In our study, we revealed sonographic features of early CHM in large cohort study, to improve the diagnose accuracy.

METHOD AND MATERIALS

This study included 337 retrospective and 182 prospective cases of histologically proven CHM in the first trimester in our institute 2003 to 2017. In additional, 519 missed abortion patients were matched with CHM cases on ultrasound scan date. The data were recorded: age, gestational age, the serum hCG level before evacuation, the sonographic features (the length, width and anteroposterior diameter of uterus and cavity mass, the extent of vesicular area, lutein ovarian cyst). The volume was calculated using the prolate ellipsoid formula. The software used for statistical analysis was SPSS 19.0 for Mac.

RESULTS

Among all CHM cases (mean gestational age 64.2 \pm 7.2 days), 335 cases (64.5%) were correctly diagnosed on the basis of the initial sonographic examination, but almost (94.6%, 105/112) cases of gestational age <42 days could not be made a definitive diagnose. Compared with missed abortion, the higher serum hCG level, the larger volume of uterus and cavity mass, the more severe extent of vesicular area were the significant index for CHM (all p<0.05). However, on the time scale of gestational age, the 95% confidence interval of four index in CHM overlapped with missed abortion group at the certain time points (such as before 42 days). Thus, it was hard to distinguish two entities in very early pregnancy by initial ultrasound exam. Among the 184 suspicious cases, 104 cases made a second scan 7 days later, the volume of cavity mass in CHM (42 cases) increased 2.3 \pm 0.9 fold, significantly higher than 1.6 \pm 1.0 fold in the missed abortion group (62 cases) (p<0.05)

CONCLUSION

The ultrasound diagnostic pitfall exists in early CHM, especially in the gestational age <42 days. For the case with suspicious findings in the initial ultrasound, the second scan after 7 days could help to improve the diagnose power for early CHM.

CLINICAL RELEVANCE/APPLICATION

The second ultrasound scan after 7 days is an easy method to improve the diagnose power for early CHM on the cases with suspicious findings in the initial exam.

SSM10-06 Sonographic Detection of Ovarian Cancer in Adnexal Cysts: Comparing IOTA Simple Rules, SRU Guidelines, and Original Radiologists' Interpretation

Wednesday, Nov. 28 3:50PM - 4:00PM Room: E353A

Participants

Krupa K. Patel-Lippmann, MD, Durham, NC (*Abstract Co-Author*) Nothing to Disclose
Katherine E. Maturen, MD, Ann Arbor, MI (*Abstract Co-Author*) Royalties, Reed Elsevier; Royalties, Wolters Kluwer nv; Consultant, Allena Pharmaceuticals, Inc;
Elizabeth A. Sadowski, MD, Madison, WI (*Presenter*) Nothing to Disclose
Jessica B. Robbins, MD, Madison, WI (*Abstract Co-Author*) Nothing to Disclose
Viktoriya Paroder, MD,PhD, Bronx, NY (*Abstract Co-Author*) Nothing to Disclose
Elizabeth B. Maddox, Madison, WI (*Abstract Co-Author*) Nothing to Disclose
Lisa Barroilhet, MD, Madison, WI (*Abstract Co-Author*) Nothing to Disclose
Timothy McMahon, New York, NY (*Abstract Co-Author*) Nothing to Disclose
Ashish P. Wasnik, MD, Ann Arbor, MI (*Abstract Co-Author*) Nothing to Disclose

Alexander D. Blaty, BS, Ann Arbor, MI (Abstract Co-Author) Nothing to Disclose

For information about this presentation, contact:

esadowski@uwhealth.org

PURPOSE

To evaluate the performance of the IOTA group simple rules, the SRU consensus statement guideline criteria and the original radiologist's report for detecting ovarian malignancy in women with adnexal cystic lesions presenting to academic radiology departments.

METHOD AND MATERIALS

An IRB-approved retrospective multicenter cohort study of ultrasound-detected adnexal cystic lesions with appropriate follow up was conducted. Lesions were classified into benign, indeterminate, or malignant categories according to criteria based on the IOTA simple rules, SRU guidelines and the original radiologist's report. The prevalence of non-neoplastic cysts, neoplasms, and malignant tumors was calculated. Sensitivity, specificity, positive predictive values (PPV), negative predictive values (NPV), accuracy and ROC analysis for the diagnosis of malignancy were performed.

RESULTS

697 women with 764 cystic lesions were included: 85.2% (651/764) were non-neoplastic, 12.2% (93/764) were benign neoplasms and 2.6% (20/764) were malignant. Nearly all malignancies were classified by imaging into indeterminate (7-10/20) or malignant (10-13/20) categories. The sensitivity/specificity/PPV/NPV/accuracy for malignancy were: IOTA = 90%/96.5%/29%/99.8%/96.4%, SRU = 100%/89.6%/14.9%/100%/89.8% and radiologist's report = 100%/82%/7.6%/100%/82.3%. From the ROC analysis, the performance of both the IOTA simple rules and SRU guidelines was superior to the original radiologist's report (p<0.0001).

All imaging classification methods evaluated were sensitive for identifying potential ovarian malignancies on ultrasound. Nearly all malignancies were classified into the malignant or indeterminate imaging categories. The PPV was low in a general population of women presenting to academic radiology departments and the appropriate management of indeterminate cystic lesions remains an open question warranting further investigation.

CLINICAL RELEVANCE/APPLICATION

Image-based classification systems are sensitive in detecting ovarian cancer; the PPV is low in our patient cohort and considering other clinical/imaging data may improve the PPV.

Honored Educators

Presenters or authors on this event have been recognized as RSNA Honored Educators for participating in multiple qualifying educational activities. Honored Educators are invested in furthering the profession of radiology by delivering high-quality educational content in their field of study. Learn how you can become an honored educator by visiting the website at: https://www.rsna.org/Honored-Educator-Award/ Katherine E. Maturen, MD - 2014 Honored Educator



Science Session with Keynote: Health Service, Policy and Research (Patient and Family-Centered Care)

Wednesday, Nov. 28 3:00PM - 4:00PM Room: S403B

HP

AMA PRA Category 1 Credit ™: 1.00 ARRT Category A+ Credit: 0

Participants

Martha G. Menchaca, MD, PhD, Brookfield, IL (*Moderator*) Nothing to Disclose Keith D. Herr, MD, Atlanta, GA (*Moderator*) Nothing to Disclose

Sub-Events

SSM11-01 Health Service, Policy and Practice Keynote Speaker: Patient and Family Centered Care

Wednesday, Nov. 28 3:00PM - 3:10PM Room: S403B

Participants

Jason N. Itri, MD, PhD, Winston-Salem, NC (Presenter) Nothing to Disclose

SSM11-02 The Value of Real Time Thoracic Radiology Consulting in an Integrated Lung Center Clinic: Bringing the Radiologist to the Center of Multidisciplinary Health Care

Wednesday, Nov. 28 3:10PM - 3:20PM Room: S403B

Participants

Eduardo J. Mortani Barbosa JR, MD, Philadelphia, PA (*Presenter*) Nothing to Disclose Sean Novak, MD, Philadelphia, PA (*Abstract Co-Author*) Nothing to Disclose

PURPOSE

We have established an integrated thoracic radiology reading room within a multidisciplinary Lung Center clinic (LC). While our subjective experience has been positive, we sought to quantify how this model affects radiology workflow and whether the referring practitioners perceive value in having real time access to a radiologist consultant

METHOD AND MATERIALS

One attending thoracic radiologist and one trainee continuously staffed the LC on regular work hours on a daily schedule. We assessed the impact on workflow by recording over six months the number, duration and type of face-to-face radiology consultations to LC practitioners. We also conducted an anonymous survey to assess how LC practitioners felt regarding the utility and value of our service.

RESULTS

Face-to-face consultations account for an average of 10% of total time spent by radiologists in the LC, though on busy clinical days this can reach 25-30%. Our survey response rate was very high (86.4%, n=51), with overwhelming positive response by referring practitioners, who unanimously rate the usefulness of this service as high (9.8%) or extremely high (90.2%). Not a single respondent had a negative or even neutral view of this service. Moreover, 90.2% thought that radiology consultations directly add clinical value in greater than 60% of episodes, whereas 86.2% responded that these alter management in greater than 40% of episodes.

CONCLUSION

Face-to-face radiology consultations in an integrated LC are numerous and comprise a sizable share of radiologist workload, but are not compensated under the current fee for service payment model. More importantly, the radiologist is highly praised as a consultant and this service is considered valuable and impactful for patient care.

CLINICAL RELEVANCE/APPLICATION

The integrated radiology practice setup we proposed can be implemented in most facilities across the country, however it will be crucial to steer the payment model away from emphasizing volume to emphasizing quality, effectiveness and clinical impact. The radiologist as a consultant is at the same time the future of our specialty and also a return to a past in which the interaction of radiologists and referring practitioners was the foundation of diagnosis and medical decision-making.

SSM11-03 Online-Results in Mammography: Do Patients Really Want to Wait?

Wednesday, Nov. 28 3:20PM - 3:30PM Room: S403B

Participants

Kerri Vincenti, MD, Philadelphia, PA (*Presenter*) Nothing to Disclose Dayna Levin, MD, Philadelphia, PA (*Abstract Co-Author*) Nothing to Disclose Junjian Huang, MD, Philadelphia, PA (*Abstract Co-Author*) Nothing to Disclose Brian S. Englander, MD, Philadelphia, PA (*Abstract Co-Author*) Nothing to Disclose

For information about this presentation, contact:

kerri.vincenti@uphs.upenn.edu

PURPOSE

According to the American College of Radiology, all women, beginning at the age of 40 years old, should undergo yearly screening mammograms to aid in the detection of clinically occult breast cancers. Most women are contacted with the results of their examinations by postal service or by viewing their electronic medical record. Timing of results varies by institution from same day to several days following exam. Additionally, if an abnormality is detected, patients typically have to schedule additional workup for a later date. At our institution, all patients who undergo a screening mammogram receive online-results (patients wait for a radiologist to provide in-person results prior to leaving the breast center). Additionally, for women who need to undergo additional workup, our practice contacts referring physicians for additional imaging authorizations (if not conditionally ordered) for follow up imaging (diagnostic mammography with or without ultrasound). We aimed to query screening patients in the breast center to determine if the use of same-day and in-person results reduces their reported anxiety level. Additionally, we wanted to increase our understanding of patient preferences with regards to timing of results and who provides the results accounting for various demographic factors such as age, income level and ethnicity.

RESULTS

There were a total of 919 respondents to the survey during the study period. 680 patients completed the survey in its entirety (74%). Of the 680 patients with complete responses, most patients reported that they preferred to wait for results 64% (n = 437). 25% reported that it depended on wait time (n = 168)and only 8% preferred not to wait (n = 51). Most (65%) respondents did not have a preference with who provided results (n =441). For the remaining 239 patients who indicated a preference, the majority (90%) preferred to receive results from an attending or resident physician (n = 214) as opposed to a technologist or nurse. When queried about the prospect of a same-day biopsy, slightly more than half of patients stated that they would prefer a same day procedure (n = 364). Approximately one third of patients indicated that they would not want a biopsy performed on the same day (n = 197). The remaining patients indicated no preference. Most (68%) respondents indicated that their level of anxiety was decreased as a result of receiving same day results (n = 461). Responses did not vary significantly by age, income level, or ethnicity. The majority of patients indicated they preferred yearly mamnographic screening (n = 542). Patients ranged in age from 31 to 86, with a median age of 56. The majority of patients were white 70% (n = 475), followed by African American 23% (n = 158), Asian 4% (n = 24), Hispanic 3% (n = 19) and other 1% (n = 4).

CONCLUSION

There are approximately 325,000 new cases of breast cancer diagnosed each year. The use of screening mammography aids in the detection of cancers before they become clinically evident and has been proven to decrease breast cancer mortality by over 30%. The United States Preventative Taskforce (USPTF) has criticized the use of yearly mammograms based on the 'harms of screening' including excess anxiety from false positive results, which includes the need for additional diagnostic imaging to further assess suspected abnormalities. As radiologists, we should aim to improve our practice patterns and workflow to reduce this anxiety when possible. Offering online-results and the opportunity to perform additional tests/interventions has the potential to decrease the degree of anxiety for patients. While this may require additional time on the part of the radiologist to provide results to waiting patients, this model allows patients to engage in face-to-face interactions with radiologists and offers opportunities for patients ask questions and gain a better understanding of their results. For our practice, the use of online-results has allowed radiologists in our breast center provide a service that we believe adds value to the patient care experience.

METHODS

The study was conducted following IRB Waiver for Human Subjects research. Questionnaires were given to all screening patients entering the breast center over a 2 week time period. Closed-ended questions were given related to preferences of wait time and regading who delivered test results. Patients were also asked about whether they preferred a same day biopsy option. Patients were also asked if received same day results reduced their level of anxiety. One question focused on patient preferences regarding how often to be screened with mammography. For demographic information, patients were given a closed-ended question regarding income and open-ended questions for age and ethnicity (sample survey included in PDF). Results were organized in an Excel spreadsheet and responses were coded into ordinal data. Any patients who did not answer all questions on the survey were excluded from analysis.

PDF UPLOAD

http://abstract.rsna.org/uploads/2018/18011727/18011727_bzb2.pdf

SSM11-04 A Contemporary Survey of Patient and Referring Physician Preferences for Direct Radiologic Reporting of Results

Wednesday, Nov. 28 3:30PM - 3:40PM Room: S403B

Participants

Janice Thai, MD, Staten Island, NY (*Presenter*) Nothing to Disclose Raina Josemon, BS, Staten Island, NY (*Abstract Co-Author*) Nothing to Disclose Shrita Smith, MD, New York, NY (*Abstract Co-Author*) Nothing to Disclose Jose Morey, MD, Philadelphia, PA (*Abstract Co-Author*) Nothing to Disclose Arnold Brenner, DO, Staten Island, NY (*Abstract Co-Author*) Nothing to Disclose

PURPOSE

To identify contemporary preferences of patients and referring physicians for direct patient communication and notification of results by the radiologist.

RESULTS

368 patients completed the survey (39.9% male and 60.1% female). 168 referring physician surveys were completed [surgery (16.7%), pediatrics (18.6%), internal medicine (38.5%), emergency medicine (4.3%), obstetrics and gynecology (7.4%), and other (14.3%)]. Patient preference: 81.5% of patient responders preferred all results communicated from the radiologist within the same day. 65.9% of patients preferred same day results - if normal vs 65.8% if abnormal. 34.5% preferred to wait and review normal results with the referring physician. 41.5% preferred to wait and review abnormal results with the referring physician. It was found

that patients were more likely to strongly agree with waiting to review results with the referring physician if the results were abnormal, as opposed to normal (18.5% vs 11.9%, respectively; P < 0.0141). Physician preference: 36% of referring physicians preferred same day communication by the radiologist to the patient along with a report sent to their office. 12.4% preferred radiology reports to be sent to their office with a summary report sent to the patient. 59% preferred traditional communication with reports sent to their office. Conversely, 64% of physicians did not want results reviewed with their patients; 87.6% did not want a report sent to their office.

CONCLUSION

58-82% of patients preferred same day radiologist communication of their results while 55-87.6% of physicians did not prefer same day radiologist communication of results directly with their patients. Our study examined and identified contemporary preferences of patients and their referring physicians regarding direct radiologic reporting of results. This could potentially impact the current movement in radiology towards a patient-centered care model by providing direct access to radiologic reports and direct communication of results by the radiologist.

METHODS

An anonymous survey was conducted between July 2017 and February 2018 of all patients undergoing radiologic imaging studies and their referring physicians. Two survey questionnaires were designed to examine patient and physician preferences for reporting of radiologic results. The surveys consisted of questions related to real time communication of results by the radiologist to the patient. The surveys elicited responses regarding preferences on a 5-point likert scale (Strongly disagree, disagree, neutral, agree and strongly agree), as well as indicated by responding yes or no to specific questions. All categorical variables were summarized using frequency counts and percentages. Comparisons between groups (Gender, age, medical specialty) with respect to responses to questions were analyzed using either the chi-square test or Fisher's exact test. Kappa statistics and Bowker's test of symmetry were used to determine if there was agreement in response within a patient, when examination results were assumed to be 'normal' or 'abnormal'. All statistical tests were two-sided at the alpha=0.05 level of significance.

PDF UPLOAD

http://abstract.rsna.org/uploads/2018/18018812/18018812_ywd7.pdf

SSM11-05 A Pilot Trial of a Decentralized General Ultrasound Imaging Consultation Service

Wednesday, Nov. 28 3:40PM - 3:50PM Room: S403B

Participants Jason C. Birnholz, MD, Delray Beach, FL (*Presenter*) Consultant, Sonoscanner SARL

For information about this presentation, contact:

jbirnholz@gmail.com

PURPOSE

This study concerns the feasibility and utilization of an interactive consultation service provided by a Radiologist equipped with high performance portable ultrasound equipment at selected medical care facilities.

METHOD AND MATERIALS

Facilities selected for 'field testing of a portable ultrasound device with reporting in one or two visits' were a suburban family practice clinic (FPC) providing care for the indigent, a suburban OB/GYN practice (GYN) adjacent to a community hospital, a private Urology clinic (UROL) with associated facilities. A limited number of ultrasound exams performed at patient designated locations (HOME). Limited exams were performed as part of feasibility assessment at a free standing Mammography center and at 3, level III NICU's. Facilities were not informed that full services would be continued on request. Patients were selected by the attending physician; the Radiologist confirmed that ultrasound was appropriate and performed an interactive examination, deciding the extent and content of each session, reporting findingswhile the patient was in the facility. All examinations were performed with a high performance, adjustable, touch screen tablet sized, dynamic beam former instrument with 6 interchangeable, broadband, array transducers. Variable aperture settings enabled 180 degree field of view with the endocavitary probe and transfontanelle imaging with a linear array.

RESULTS

There were 150 patients with 4206 archived static images in the utilization group, characterized by frequency of 12 exam components for each venue. Every requested was able to be performed for all indications. Findings were reported in a context of individual patient management. One or more secondary findings occurred in 52% for GYN, 48% for FPC, 38% for HOME, and 74% for UROL. Each location requested that the service be continued. As the trial progressed, GYN broadened their study indications; UROL did not.

CONCLUSION

Feasibility of high level remote operation was noted in limited but clinically typical, prospective exam conditions. This on-site consultative model had wide diagnostic yield., but utilization of secondary findings varied.

CLINICAL RELEVANCE/APPLICATION

A consultative model warrants further evaluation for planning expanded diagnostic ultrasound coverage for selected patient and practice cohorts.

SSM11-06 Care Integration in Radiology: Screening Mammography Encounters as Opportunities to Improve Lung Cancer Screening Engagement

Wednesday, Nov. 28 3:50PM - 4:00PM Room: S403B

Diego Lopez, Boston, MA (*Abstract Co-Author*) Nothing to Disclose Jo-Anne O. Shepard, MD, Boston, MA (*Abstract Co-Author*) Nothing to Disclose Constance D. Lehman, MD,PhD, Boston, MA (*Abstract Co-Author*) Research Grant, General Electric Company; Medical Advisory Board, General Electric Company Efren J. Flores, MD, Boston, MA (*Abstract Co-Author*) Nothing to Disclose

For information about this presentation, contact:

gxwang@partners.org

PURPOSE

A main barrier to uptake of lung cancer screening (LCS) for primary care providers (PCPs) is difficulty in identifying eligible patients, in part due to incomplete electronic medical record (EMR) data. Screening mammography (SM) is a common point of contact with the healthcare system for women within LCS age criteria. At our institution, detailed smoking history data is collected as a routine part of SM, but is not communicated to PCPs or integrated with the EMR in a way that facilitates its clinical use. We studied whether SM encounters at a community health center can be used to assist PCPs in identifying eligible patients for LCS.

METHOD AND MATERIALS

This IRB approved, HIPAA-compliant, retrospective study was performed at a community health center affiliated with a quaternary care academic medical center. Medical record review was performed of all consecutive SM patent encounters from 1/2018-3/2018 to extract patient demographic data, date of most recent LCS chest CT, and smoking history available prior to SM encounter and history obtained at SM. Determination of LCS eligibility was based on institutional criteria: age 55-77, smoked at least 30 pack-years, and either currently smoking or quit within 15 years.

RESULTS

There were 733 unique patient encounters during the study period. Smoking history was obtained at SM for 611 (83%): there were 75 (12%) current and 169 (28%) former smokers. Among current smokers, 14/75 (19%) met LCS eligibility criteria: 7 (50%) were not enrolled in LCS and 3 (21%) were overdue. 12/169 (7%) former smokers met LCS eligibility criteria: 8 (67%) were not enrolled, none overdue. Smoking status from SM was concordant with EMR data for 353/362 (98%) never smokers, 69/75 (92%) current smokers, and 132/169 (78%) former smokers. Among smokers with concordant smoking status, sufficient data to determine LCS eligibility was only available from SM data and not from EMR for 37/69 (54%) current and 87/132 (66%) former smokers.

CONCLUSION

Smoking history data in the EMR is often insufficient to allow determination of LCS eligibility, and can be supplemented with data obtained at SM. Furthermore, at the time of SM, most eligible patients are either not enrolled or are overdue for LCS.

CLINICAL RELEVANCE/APPLICATION

SM encounters can serve as opportunities to integrate radiology care, provide added value to PCPs, and decrease barriers to LCS participation by identifying eligible smokers for screening engagement.



Informatics (Quantitative Imaging)

Wednesday, Nov. 28 3:00PM - 4:00PM Room: E353B



AMA PRA Category 1 Credit ™: 1.00 ARRT Category A+ Credit: 1.00

FDA Discussions may include off-label uses.

Participants

Gary J. Wendt, MD, Middleton, WI (*Moderator*) Medical Advisory Board, McKesson Corporation; Medical Advisory Board, HealthMyne, Inc; Stockholder, HealthMyne, Inc; Co-founder, ImageMoverMD; Christopher R. Deible, MD, PhD, Allison Park, PA (*Moderator*) Nothing to Disclose

Pamela T. Johnson, MD, Baltimore, MD (Moderator) Consultant, Oliver Wyman

Sub-Events

SSM12-01 Quantitative DCE-MRI Features Can Complement Molecular Markers for Predicting Tumor Infiltrating Lymphocytes in Breast Cancer: Model Discovery and Independent Validation

Wednesday, Nov. 28 3:00PM - 3:10PM Room: E353B

Participants

Jia Wu, PhD, Stanford, CA (*Presenter*) Nothing to Disclose Xuejie Li, Hangzhou, China (*Abstract Co-Author*) Nothing to Disclose Xiaodong Teng, Hangzhou, China (*Abstract Co-Author*) Nothing to Disclose Daniel L. Rubin, MD, MS, Stanford, CA (*Abstract Co-Author*) Nothing to Disclose Sandy Napel, PhD, Stanford, CA (*Abstract Co-Author*) Medical Advisory Board, Fovia, Inc; Consultant, Carestream Health, Inc; Scientific Advisor, EchoPixel, Inc; Scientific Advisor, RADLogics, Inc Bruce L. Daniel, MD, Stanford, CA (*Abstract Co-Author*) Nothing to Disclose Ruijiang Li, PHD, Palo Alto, CA (*Abstract Co-Author*) Nothing to Disclose

For information about this presentation, contact:

jiawu@stanford.edu

PURPOSE

To investigate the association between DCE MRI features and tumor infiltrating lymphocytes (TILs) in breast cancer.

METHOD AND MATERIALS

We retrospectively analyzed two breast cancer cohorts, with 126 patients from the cancer genome atlas (TCGA) as discovery cohort and 106 patients from ACRIN 6657/I-SPY 1 TRIAL as validation cohort. 17 computational features were extracted from DCE MRI to characterize functional tumor volume, tumor morphology and texture as well as parenchymal enhancement patterns. The percentage of stromal TILs was evaluated on hematoxylin and eosin stained histologic whole-tumor sections by two experienced pathologists. From tumor molecular data, we computed two markers as surrogates for TILs, including the non-synonymous somatic mutational burden and cytolytic activity score. First, we evaluated the associations between individual DCE-MRI features and TILs read by pathologists. Multiple hypotheses testing was corrected by the Benjamini-Hochberg method using false discovery rate (FDR). Next, we built a composite prediction model for TILs by combining DCE-MRI features with molecular surrogates. Finally, we independently validated the prognostic significance of the built TILs model in the I-SPY cohort.

RESULTS

Four image features were significantly associated with TILs (P<0.05 and FDR<0.2). Among molecular and clinicopathologic factors, only cytolytic score showed significant correlation with TILs (p=0.51, 95% confidence interval [CI]: 0.36-0.63). A composite model combining an imaging signature and cytolytic score improved correlation with TILs (p=0.62, 95% CI: 0.50-0.72). Compared with molecular surrogates as baseline, the composite model showed significant improvement in distinguishing intermediate vs high and low vs high TILs groups, with area under the curve or AUC=0.76 and 0.94, as shown in Fig. 1A and B. In the validation cohort, the predicted TILs separated patients into two groups with distinct recurrence-free survival (log-rank P=0.0008) among triple negative breast cancer (Fig. 1C and D).

CONCLUSION

Specific DCE-MRI features of tumor and parenchyma are associated with TILs in breast cancer, and integrating imaging and molecular features may allow better prediction for TILs.

CLINICAL RELEVANCE/APPLICATION

Imaging may play an important role in the evaluation of TILs, by providing key complementary information in equivocal cases or situations that are prone to sampling bias (e.g., in core biopsy).

Honored Educators

Presenters or authors on this event have been recognized as RSNA Honored Educators for participating in multiple qualifying educational activities. Honored Educators are invested in furthering the profession of radiology by delivering high-quality educational content in their field of study. Learn how you can become an honored educator by visiting the website at: https://www.rsna.org/Honored-Educator-Award/ Daniel L. Rubin, MD, MS - 2012 Honored EducatorDaniel L. Rubin, MD, MS - 2013 Honored Educator

SSM12-02 Development and Validation of a Radiomics Nomogram for Identifying Invasiveness of Pulmonary Adenocarcinomas Appearing as Subcentimeter Ground-Glass Opacity Nodules

Wednesday, Nov. 28 3:10PM - 3:20PM Room: E353B

Participants

Wei Zhao, MD, Shanghai, China (*Presenter*) Nothing to Disclose Ming Li, MD, Shanghai, China (*Abstract Co-Author*) Nothing to Disclose Yingli Sun Jr, Shanghai, China (*Abstract Co-Author*) Nothing to Disclose Cheng Li, Shanghai, China (*Abstract Co-Author*) Nothing to Disclose Liang Jin, MD, Shanghai, China (*Abstract Co-Author*) Nothing to Disclose Pan Gao, Shanghai, China (*Abstract Co-Author*) Nothing to Disclose

For information about this presentation, contact:

zbsasd@163.com

PURPOSE

This study aimed to develop and validate a radiomics-based nomogram for differentiation of pre-invasive lesions from invasive lesions that manifest as ground-glass nodules (GGNs) <=10 mm (sub-centimeter) in diameter at CT.

METHOD AND MATERIALS

542 consecutive patients with 626 pathologically confirmed pulmonary subcentimeter GGNs were retrospectively studied from October 2011 to September 2017, which were divided into a training-set (n=334) and a validation-set (n=292). Researchers extracted 475 radiomics features from the plain CT images and a radiomics signature was constructed with the least absolute shrinkage and selection operator (LASSO) based on multivariable regression in the training-set. Based on the multivariable logistic regression model, a radiomics nomogram was developed in the training-set. The performance of the nomogram was evaluated with respect to its calibration, discrimination, and clinical-utility and this was assessed in the validation-set.

RESULTS

The constructed radiomics signature, which consisted of 15 radiomics features, was significantly associated with the invasiveness of subcentimeter GGNs (P < 0.0001 for both training-set and validation-set). To build the nomogram model Radiomics signature and mean CT value were used. The nomogram model demonstrated good discrimination and calibration in both training-set (C-index, 0.716 [95% CI, 0.632 to 0.801]) and validation-set (C-index, 0.707 [95% CI, 0.625 to 0.788]). Decision curve analysis indicated that radiomics-based nomogram was clinically useful.

CONCLUSION

A radiomics-based nomogram that incorporates both radiomics signature and mean CT value is constructed in the study, which can be conveniently used to facilitate the preoperative individualized prediction of the invasiveness in patients with subcentimeter GGNs.

CLINICAL RELEVANCE/APPLICATION

Using the radiomics nomogram in the current study to predict the invasiveness of subcentimeter GGNs adds more benefit especially with respect to the treat-all scenario or the treat-none scenario, which in meanwhile indicated that this tool could aid in clinical decision making and facilitate the individualized precision medical treatment.

SSM12-03 18F FDG Positron Emission Tomography (PET) Tumor Penumbra Texture Predicts Recurrence in Non-Small Cell Lung Cancer

Wednesday, Nov. 28 3:20PM - 3:30PM Room: E353B

Participants

Sarah Mattonen, PhD, Stanford, CA (*Presenter*) Nothing to Disclose Guido A. Davidzon, MD, Stanford, CA (*Abstract Co-Author*) Nothing to Disclose Shaimaa Bakr, Stanford, CA (*Abstract Co-Author*) Nothing to Disclose Sebastian Echegaray, MS, Mt. View, CA (*Abstract Co-Author*) Nothing to Disclose Ann N. Leung, MD, Stanford, CA (*Abstract Co-Author*) Nothing to Disclose Minal Vasanawala, Palo Alto, CA (*Abstract Co-Author*) Nothing to Disclose George Horng, San Francisco, CA (*Abstract Co-Author*) Nothing to Disclose Viswam S. Nair, MD, Stanford, CA (*Abstract Co-Author*) Nothing to Disclose Sandy Napel, PhD, Stanford, CA (*Abstract Co-Author*) Medical Advisory Board, Fovia, Inc; Consultant, Carestream Health, Inc; Scientific Advisor, EchoPixel, Inc; Scientific Advisor, RADLogics, Inc

For information about this presentation, contact:

smattonen@stanford.edu

PURPOSE

To identify computational imaging features (radiomics) in the tumor and surrounding area on Fluorodeoxyglucose (FDG) Positron Emission Tomography (PET) that predict time to recurrence in non-small cell lung cancer (NSCLC). We hypothesize that radiomic features can augment traditional metrics of stage and maximum standardized uptake value (SUVmax) to predict recurrence.

METHOD AND MATERIALS

We identified 300 patients with NSCLC from two cohorts acquired between 2008-2016 (training. n=145: validation. n=155). Two

observers used commercial software to contour the Metabolic Tumor Volume (MTV) on pre-treatment PET images and added a 3dimensional penumbra region that extended outward 1cm from the tumor surface. We generated 512 radiomics features from these volumes of interest. We selected features based on robustness to contour variations, and then applied randomized sparse regression (LASSO) to identify features that predicted recurrence in the training cohort. We built a Cox proportional hazards model in the training cohort and independently evaluated the model in the validation cohort.

RESULTS

SUVmax was a significant predictor of recurrence in the training (concordance=0.67, log-rank p<0.001) and validation cohorts (concordance=0.67, Noether's p<0.001). Stage was also a significant predictor in both cohorts (training: concordance=0.68, log-rank p<0.001; validation: concordance=0.70, Noether's p<0.001). The top radiomic feature selected by LASSO was the grey-level co-occurrence matrix maximum probability feature in the union of the MTV and penumbra regions. This texture feature was a significant predictor in the training (concordance=0.66, log-rank p=0.002) and validation cohorts (concordance=0.66, Noether's p<0.001). The radiomic feature integrated with stage and SUVmax significantly improved performance in both cohorts (training: concordance=0.73, log-rank p<0.001; validation: concordance=0.76, Noether's p<0.001), with both stage and texture being significant predictors in the multivariate model. Adding additional radiomic features to the model did not significantly improve performance.

CONCLUSION

A radiomics texture feature in the MTV plus surrounding penumbra improved upon staging and SUVmax for NSCLC recurrence prediction.

CLINICAL RELEVANCE/APPLICATION

PET radiomics may assist clinicians in stratifying patients at a higher risk of recurrence and could be used to recommend more aggressive personalized treatments options.

SSM12-04 Direct Validation of Quantitative MRI Cerebral Perfusion at Rest, Stress and Ischemia

Wednesday, Nov. 28 3:30PM - 3:40PM Room: E353B

Participants Niloufar S. Saadat, MD, Chicago, IL (*Presenter*) Nothing to Disclose Yong I. Jeong, Chicago, IL (*Abstract Co-Author*) Nothing to Disclose Timothy J. Carroll, PhD, Chicago, IL (*Abstract Co-Author*) Nothing to Disclose Steven Roth, MD, Chicago, IL (*Abstract Co-Author*) Nothing to Disclose Keigo Kawaji, PhD, Chicago, IL (*Abstract Co-Author*) Nothing to Disclose Gregory A. Christoforidis, MD, Columbus, OH (*Abstract Co-Author*) Nothing to Disclose

For information about this presentation, contact:

nsaadat@uchicago.edu

PURPOSE

This study sought to assess the accuracy of a quantitative MRI-based (qMRI) measure of cerebral blood flow (qCBF) against reference stable isotope neutron capture microsphere-based cerebral blood flow quantification in an experimental model during normocapnia, hypercapnia and middle cerebral artery (MCAO)

METHOD AND MATERIALS

Five female, mongrel dogs (20-30 kg) each studied over two days. On day 1, qCBF images acquired during normocapnia (target PaCO2 30-40 mmHg) and hypercapnia (target PaCO2 > 60 mmHg) induced by CO2 gas inhalation (5% CO2/95% O2). On day 2 animals underwent angiographically verified permanent endovascular occlusion of the M1 segment while in a normocapnic state. Anesthesia selected to minimize the influence on cerebrovascular reactivity. Physiologic parameters kept within normal range except for PCO2 for hypercapnia. Microspheres injected at the time of qMRI acquisition to obtain reference-standard CBF values. qMRI acquired on a 3 Tesla unit using a 15-channel receive-only head coil a 'bookend dynamic susceptibility (DSC)' approach, which uses pre- and post-contrast T1 maps bookended to a DSC MRI sequence to calculate parenchymal T1 changes and calibrate the DSC scan for quantitative perfusion in ml/100 g/min. Quantitative T1 maps created using a standard inversion recovery Look-Locker imaging, co-localized to the DSC perfusion scan using a previously reported approach

RESULTS

MRI correlated strongly with microsphere perfusion (qCBFMRI = 0.93*qCBFSPHERES + 3.85 ml/100g/min; r2 = 0.96; p < 0.001), for individual CVR (CVRMRI = 1.17*CVRSPHERES - 0.95 %;CBF/mmHg CO2; r2 = 0.84; p < 0.001), and for post-occlusion CBF (qCBFMRI = 0.80*qCBFSPHERES + 12.9 ml/100g/min; r2 = 0.82; p = 0.002). Correction for delay and dispersion resulted in a significant improvement in the correlation between MRI and microsphere deposition in the ischemic state (qCBFMRI = 0.97*qCBFSPHERES + 2.58 ml/100g/min; r2 = 0.96; p < 0.001).

CONCLUSION

MRI derived values of CBF are strongly correlated with reference value microsphere deposition in normocapnia, hypercapnia, and MCAO ischemic stroke. Correction for delay and dispersion significantly improved the accuracy of this quantification during MCAO, underscoring the importance of this correction under focal ischemic condition

CLINICAL RELEVANCE/APPLICATION

Quantitative CBF by MRI perfusion accurately measures CBF, improving our ability to triage patients with acute ischemic stroke for treatment

SSM12-05 Utility of Radiomics Features to Detect Pancreatic Adenocarinoma

Wednesday, Nov. 28 3:40PM - 3:50PM Room: E353B

Linda C. Chu, MD, Baltimore, MD (*Abstract Co-Author*) Nothing to Disclose Seyoun Park, Baltimore, MD (*Presenter*) Nothing to Disclose Satomi Kawamoto, MD, Laurel, MD (*Abstract Co-Author*) Nothing to Disclose Daniel Fadaei Fouladi, MD, Baltimore, MD (*Abstract Co-Author*) Nothing to Disclose Shahab Shayesteh, MD, Baltimore, MD (*Abstract Co-Author*) Nothing to Disclose Karen M. Horton, MD, Baltimore, MD (*Abstract Co-Author*) Nothing to Disclose Elliot K. Fishman, MD, Baltimore, MD (*Abstract Co-Author*) Nothing to Disclose Elliot K. Fishman, MD, Baltimore, MD (*Abstract Co-Author*) Institutional Grant support, Siemens AG; Institutional Grant support, General Electric Company; Co-founder, HipGraphics, Inc Alan Yuille, Baltimore, MD (*Abstract Co-Author*) Nothing to Disclose

For information about this presentation, contact:

lindachu@jhmi.edu

PURPOSE

Pancreatic adenocarcinoma is one of the leading causes of cancer related death. Recent advances in computer analytics offer the potential of computer aided detection of pancreatic adenocarcinoma. The purpose of this study is to determine if quantitative radiomics features can be used to differentiate pancreatic adenocarcinoma from normal controls.

METHOD AND MATERIALS

As an IRB-approved matched case-control study, 190 cases of pathologically proven pancreatic adenocarcinoma (PDAC) and 190 normal controls were retrospectively selected from the radiology and pathology databases. The whole pancreas boundary (including tumor region) were manually segmented from preoperative pancreatic protocol CT using dedicated software, VelocityAI (Varian Medical Systems, USA). The phenotype of pancreas on CT images was expressed with 478 radiomics features, which include the first order statistics, shape, texture, and texture features from wavelet and Laplacian of Gaussian filtering. The studies were randomly split into a training set (251 cases) and a testing set (129 cases). Feature reduction was performed by the minimum-redundancy maximum-relevance selection approach and random forest was applied for the PDAC classification.

RESULTS

The mean and standard deviation of PDAC masses were 4.4±2.0cm. The overall classification accuracy of the testing set was 0.992 (128 among 129 cases were correctly classified) with 0.999 of the area under the curve. The sensitivity was 0.98, only 1 among 62 PDAC cases were incorrectly classified, and specificity and PPV showed all 1.00. Most relevant features to differentiate PDAC include intensity uniformity, shape compactness, and texture features of gray level non-uniformity, skewness, fractal dimension from the original images and filtered images.

CONCLUSION

Radiomics features can differentiate pancreatic adenocarcinoma from normal pancreas with 3D segmented pancreas.

CLINICAL RELEVANCE/APPLICATION

Radiomics features can be used to differentiate pancreatic adenocarcinoma from normal pancreas, which can serve as one of the tools towards automatic detection of pancreatic adenocarcinoma.

Honored Educators

Presenters or authors on this event have been recognized as RSNA Honored Educators for participating in multiple qualifying educational activities. Honored Educators are invested in furthering the profession of radiology by delivering high-quality educational content in their field of study. Learn how you can become an honored educator by visiting the website at: https://www.rsna.org/Honored-Educator-Award/ Elliot K. Fishman, MD - 2012 Honored EducatorElliot K. Fishman, MD - 2014 Honored EducatorElliot K. Fishman, MD - 2016 Honored EducatorElliot K. Fishman, MD - 2018 Honored Educator

SSM12-06 Chaos-Based Fractal Radiomic Features of Nodule Vasculature Distinguish Granulomas from Adenocarcinomas on Non-Contrast Lung CT

Wednesday, Nov. 28 3:50PM - 4:00PM Room: E353B

Participants

Mehdi Alilou, PhD, Cleveland, OH (*Presenter*) Nothing to Disclose Marjan Firouznia, Cleveland, OH (*Abstract Co-Author*) Nothing to Disclose Prateek Prasanna, Cleveland, OH (*Abstract Co-Author*) Nothing to Disclose Robert C. Gilkeson, MD, Cleveland, OH (*Abstract Co-Author*) Research Consultant, Riverain Technologies, LLC; Research support, Koninklijke Philips NV; Research support, Siemens AG; Research support, General Electric Company Prabhakar Rajiah, MD, FRCR, Dallas, TX (*Abstract Co-Author*) Nothing to Disclose Vamsidhar Velcheti, MD, Saint Louis, MO (*Abstract Co-Author*) Nothing to Disclose Anant Madabhushi, PhD, Cleveland, OH (*Abstract Co-Author*) Research funded, Koninklijke Philips NV

For information about this presentation, contact:

me.alilou@gmail.com

PURPOSE

A wide variety of fungal processes can cause a chronic granulomatous reaction in the lungs manifesting as benign pulmonary nodules on CT. Visually to a radiologist, granulomas can appear similar to a malignant adenocarcinoma making them difficult to distinguish. However, these nodules differ in terms of the morphology of the nodule vasculature. The purpose is to model the distinct vessel tortuosity patterns and find associated deterministic dynamics. We sought to evaluate if fractal features of nodule vasculature on non-contrast CT are significantly different between granulomas and adenocarcinomas. We present a set of chaosbased fractal radiomic features of the vasculature (VFR) which transform the nodule vasculature to a low-dimensional discriminative feature space.

METHOD AND MATERIALS

Our study comprised non-contrast CT scans of 100 patients, including 50 adenocarcinomas and 50 granulomas, with pixel size

ranging from 0.42×0.42 mm to 0.97×0.97 mm. All patients had previously undergone resection for suspicious nodules. From nodule annotations provided by a trained radiologist, a region-growing algorithm was used to segment the surrounding vasculature (Fig 1ad). A set of 6 chaotic features pertaining to the fractal analysis and the state space reconstruction of tumor vasculature were extracted from each nodule vasculature. The extracted features include fractal dimensions 1-dimension (D), 2D, and 3D, the mutual information, and the optimal delay of the state space reconstruction from each nodule vasculature. A linear discriminant analysis classifier was then used, in a 3-fold cross-validation setting, to identify adenocarcinomas.

RESULTS

VFR features (Fig 1 e-f, i-j) were capable identifying malignant nodules with AUC=0.70. Statistically significant difference was observed for one of the VFR features between adenocarcinomas and granulomas (p=0.009).

CONCLUSION

Adenocarcinomas can be distinguished from granulomas using VFR radiomics extracted from nodule vasculature.

CLINICAL RELEVANCE/APPLICATION

VFR radiomic markers could allow for improved discrimination of benign from malignant nodules, and could help reduce unnecessary surgical interventions for pathologic confirmation of nodule diagnosis.

Honored Educators

Presenters or authors on this event have been recognized as RSNA Honored Educators for participating in multiple qualifying educational activities. Honored Educators are invested in furthering the profession of radiology by delivering high-quality educational content in their field of study. Learn how you can become an honored educator by visiting the website at: https://www.rsna.org/Honored-Educator-Award/ Prabhakar Rajiah, MD, FRCR - 2014 Honored Educator



Informatics (3D Printing and Alt Realities - AR/VR)

Wednesday, Nov. 28 3:00PM - 4:00PM Room: E353C

IN

AMA PRA Category 1 Credit ™: 1.00 ARRT Category A+ Credit: 1.00

FDA Discussions may include off-label uses.

Participants

Ciprian N. Ionita, PhD, Buffalo, NY (*Moderator*) Grant, Canon Medical Systems Corporation; Grant, Stratasys, Ltd; Grant, Medtronic plc;

Kenneth C. Wang, MD, PhD, Ellicott City, MD (Moderator) Co-founder, DexNote, LLC; Software support, 3D Systems, Inc

Sub-Events

SSM13-01 Evaluation of the Accuracy of 3D Printed Patient-Specific Coronary Tree Phantoms Using 320-Detector Row Aquilion ONE

Wednesday, Nov. 28 3:00PM - 3:10PM Room: E353C

Participants

Lauren Shepard, Buffalo, NY (*Presenter*) Nothing to Disclose Kelsey N. Sommer, Buffalo, NY (*Abstract Co-Author*) Nothing to Disclose Erin Angel, PhD, Tustin, CA (*Abstract Co-Author*) Employee, Canon Medical Systems Corporation Vijay Iyer, Buffalo, NY (*Abstract Co-Author*) Nothing to Disclose Michael F. Wilson, Buffalo, NY (*Abstract Co-Author*) Nothing to Disclose Frank J. Rybicki III, MD, PhD, Ottawa, ON (*Abstract Co-Author*) Medical Director, Imagia Cybernetics Inc Dimitris Mitsouras, PhD, Boston, MA (*Abstract Co-Author*) Research Grant, Canon Medical Systems Corporation; Sabee Y. Molloi, PhD, Irvine, CA (*Abstract Co-Author*) Research Grant, Canon Medical Systems Corporation Ciprian N. Ionita, PhD, Buffalo, NY (*Abstract Co-Author*) Grant, Canon Medical Systems Corporation; Grant, Stratasys, Ltd; Grant, Medtronic plc;

For information about this presentation, contact:

lmshepar@buffalo.edu

PURPOSE

3D printing of cardiovascular anatomy can be used for radiology applications such as diagnostic software validation and image guided surgical training. We developed coronary tree phantoms from materials that are capable of sustaining physiological flow and pressure conditions while maintaining the stress and strain characteristics of human coronary arteries. The purpose of this research is to assess the accuracy of 3D printed patient-specific phantoms with coronary artery disease.

METHOD AND MATERIALS

Five patients underwent 320-detector row coronary CT angiography (CCTA) (Aquilion ONE, Canon Medical Systems). Reconstructed voxel size was 0.63 mm. The aortic root and three main coronary arteries were segmented (Vitrea, Vital Images) and 3D printed (Eden 260V, Stratasys). The patient-specific phantoms were connected into a pulsatile flow loop which replicated physiological flow and pressure gradients. Contrast was introduced and the phantoms were scanned using the same CT scanner model and same CCTA protocol as used for the patients. Patient and phantom CCTA images were segmented using Mimics Research (Materialise). The minimum vessel diameter and tortuosity (defined as shortest distance / vessel length) were measured for all three vessels at 20, 40, 60, 80, and 100 mm distances from the ostium for both patients and phantoms. Results were compared to assess the accuracy of the 3D printed patient-specific phantoms.

RESULTS

The average absolute difference between all minimum diameter measurements of the coronaries for the patient and phantom images was 0.73 ± 0.58 mm (~ 1 ± 1 voxels), and in vessels with known stenosis (n = 5), the average absolute difference was 0.58 ± 0.20 mm (~ 1 voxel), range of 0.04 - 2.48 mm. The average absolute difference in tortuosity for the patients and phantoms was 0.06 ± 0.05 , and in stenosed vessels was 0.05 ± 0.008 , range of 0 - 0.17.

CONCLUSION

The phantoms showed high accuracy in maintaining the inner vessel lumen geometry and on average were within the scanner resolution, 1-2 voxels (630 μ m each) of the patient images. Overall, the 3D printed patient-specific phantom accuracy has been evaluated and shown to replicate the patient images.

CLINICAL RELEVANCE/APPLICATION

Accurate 3D printing of patient-specific coronary phantoms allows for the replication of physiological blood flow conditions to allow precise evaluation of image-based diagnostic software.

Presenters or authors on this event have been recognized as RSNA Honored Educators for participating in multiple qualifying educational activities. Honored Educators are invested in furthering the profession of radiology by delivering high-quality educational content in their field of study. Learn how you can become an honored educator by visiting the website at: https://www.rsna.org/Honored-Educator-Award/ Frank J. Rybicki III, MD, PhD - 2016 Honored Educator

SSM13-02 Reducing Operating Room Time by Using In-House 3D-Printed Models of Inferior Orbital Wall Fractures for Pre-contouring Osteosynthesis Implants

Wednesday, Nov. 28 3:10PM - 3:20PM Room: E353C

Participants

Philipp Brantner, MD, Basel, Switzerland (*Presenter*) Nothing to Disclose Marina Barba, Basel, Switzerland (*Abstract Co-Author*) Nothing to Disclose Bilal Msallem, Basel, Switzerland (*Abstract Co-Author*) Nothing to Disclose Florian Thieringer, Basel, Switzerland (*Abstract Co-Author*) Nothing to Disclose

For information about this presentation, contact:

Philipp.Brantner@usb.ch

PURPOSE

To investigate if the use of CT data based 3D printed models for pre-contouring implants in inferior orbital wall fracture surgery is able to shorten operating room time.

METHOD AND MATERIALS

22 patients (11 m, 11 f, age: $52,38 \pm 21,59$ years) received an inferior orbital wall reconstruction with a titanium implant due to trauma (14 pts) or physical altercation (8 pts). For 12 patients a 3D mesh-model was created by segmenting the bone on the initial CT scan. The model was printed in 1:1 scale using either fused filament fabrication, stereolithography or polyjetting techniques. The 3D printed model was preoperatively used as a scaffold for pre-contouring a dedicated titanium mesh, which was implanted after sterilization using a mid-eyelid approach. Operating room times (incision to suture time points) were analyzed for both groups.

RESULTS

Overall the use of a 3D model to precontour the orbital floor implant shortened the mean operating room time significantly (p<0.05) from 96 min to 64 min (- 32 min). The model creation time including DICOM-export, segmentation and post-processing with precontouring of the implant took approx. 30 min. Printing time took between 2 to 4 hours, depending on the printer used.

CONCLUSION

A preoperative 3D printed model of orbital wall fractures significantly reduces operating room time while also supposedly improving patient care through shorter operating times. Since model creation and printing is less cost- and staff-intensive this workload shift from operating room to the 3D print lab represents a considerable cost reduction while at the same time offering an opportunity to expand the radiologic service through 3D printing.

CLINICAL RELEVANCE/APPLICATION

3D models in orbital wall surgery reduce costs and improve patient care by significantly reducing operating time.

SSM13-03 Utilizing Semantic Segmentation Method with Convolutional Neural Net to Model a Partial Nephrectomy Simulator for 3D Printing

Wednesday, Nov. 28 3:20PM - 3:30PM Room: E353C

Participants

Taehun Kim, Seoul, Korea, Republic Of (*Presenter*) Nothing to Disclose Beomhee Park, Seoul, Korea, Republic Of (*Abstract Co-Author*) Nothing to Disclose Namkug Kim, PhD, Seoul, Korea, Republic Of (*Abstract Co-Author*) Stockholder, Coreline Soft, Co Ltd Sangwook Lee, BS, Seoul, Korea, Republic Of (*Abstract Co-Author*) Nothing to Disclose Dayeong Hong, Seoul, Korea, Republic Of (*Abstract Co-Author*) Nothing to Disclose Min Je Lim, Seoul, Korea, Republic Of (*Abstract Co-Author*) Nothing to Disclose Eunseo Gwon, Seoul, Korea, Republic Of (*Abstract Co-Author*) Nothing to Disclose Chuanbing Wang, Nanjing, China (*Abstract Co-Author*) Nothing to Disclose Jinhee Kwon, Seoul, Korea, Republic Of (*Abstract Co-Author*) Nothing to Disclose Guk Bae Kim, Seoul, Korea, Republic Of (*Abstract Co-Author*) Nothing to Disclose Yoon Soo Kyung, Seoul, Korea, Republic Of (*Abstract Co-Author*) Nothing to Disclose Choung-Soo Kim, Seoul, Korea, Republic Of (*Abstract Co-Author*) Nothing to Disclose

For information about this presentation, contact:

namkugkim@gmail.com

CONCLUSION

We have developed a semantic segmentation method with CNN for modeling a partial nephrectomy simulator for 3DP. The parenchyma showed robust performance, but segmenting the relatively complex vessels was still challenging. However, this segmentation application could dramatically reduce the time for 3DP.

Background

The image segmentation is necessary for modeling a simulator for 3D printing (3DP). However, segmenting process is very tedious and labor intensive. Therefore, we proposed and evaluated a deep-learning-based segmentation method to model kidney surgical simulators and fabricate them by using 3DP.

Evaluation

 Thirty-six patients with renal cell carcinoma (RCC) and normal kidney were enrolled. For 50 kidneys in this dataset, the artery, ureter, vein, and RCC connected to the kidney parenchyma were manually delineated for ground truth. Because the kidneys are symmetrically located on the left and right sides, a right kidney was flipped as left kidney to augment data. A certain margin was set based on the segmented kidney coordinates to extract the region of interest including the vessels connected to the kidney. The segmentation was performed using a 3D U-Net architecture of deep convolutional neural networks (CNN), with 80% and 20% for training and test, respectively. The segmentation performance on each class was evaluated using the Dice similarity coefficient (DSC). The mean and SD of DSC were 51.7 ± 21.0 , 48.9 ± 12.7 , 67.5 ± 15.8 , 32.6 ± 34.8 , 95.0 ± 3.6 % for artery, ureter, vein, RCC and parenchyma, respectively.

Discussion

The performance for parenchyma segmentation was the highest, while that of RCC was the lowest with large SD. Among the artery, ureter, and vein, vein accuracy was the highest. Using this method the time on modeling procedure for 3DP has been drastically reduced. The less complex parenchyma and ureter have been useful, but the blood vessels inside the parenchyma seem to be still challenging. The boundaries between parenchyma and RCC were not distinguished clearly, so more data is required.

SSM13-04 3D Printed and Augmented Reality Urologic Oncology Models: Impact in Patient Education

Wednesday, Nov. 28 3:30PM - 3:40PM Room: E353C

Participants

Nicole Wake, PhD, New York, NY (*Presenter*) In-kind support, Stratasys, Ltd Andrew B. Rosenkrantz, MD, New York, NY (*Abstract Co-Author*) Nothing to Disclose Katalina U. Park, MS, New York, NY (*Abstract Co-Author*) Nothing to Disclose William C. Huang, MD, New York, NY (*Abstract Co-Author*) Nothing to Disclose Samir S. Taneja, MD, New York, NY (*Abstract Co-Author*) Royalties, Reed Elsevier; Consultant, Reed Elsevier James Wysock, New York, NY (*Abstract Co-Author*) Nothing to Disclose Richard Huang, New York, NY (*Abstract Co-Author*) Nothing to Disclose Daniel Sodickson, MD, PhD, New York, NY (*Abstract Co-Author*) Nothing to Disclose Electric Company Royalties, Bruker Corporation License agreement, Bruker Corporation Research collaboration, Siemens AG Hersh Chandarana, MD, New York, NY (*Abstract Co-Author*) Equipment support, Siemens AG; Software support, Siemens AG; Advisory Board, Siemens AG; Speaker, Bayer AG;

For information about this presentation, contact:

nicole.wake@med.nyu.edu

PURPOSE

To investigate the impact of using 3D printed and augmented reality (AR) urologic cancer models for patient education.

METHOD AND MATERIALS

Patients with renal cancer (nephrometry score >= 7, diameter >= 4cm, or polar lesions) or MRI visible prostate cancer (PI-RADS v2 score >= 3) scheduled to undergo partial nephrectomy, radical prostatectomy, or focal therapy for prostate cancer were enrolled in our ongoing prospective study. Upon enrollment, patients were randomized to receive a pre-operative, patient-specific 3D printed or AR cancer model. A Likert-scale questionnaire was administered to assess patient understanding of disease, cancer size, cancer location, and treatment plan before and after reviewing the patient-specific 3D printed or AR model. Survey responses were compared using a paired t-test. For a subset of patients, additional questions were included asking patients to rate from 1-10 to what extent the 3D model helped them learn about their anatomy, disease, procedure, and potential complications; and results for the 3D printed and AR models were compared with an unpaired t-test.

RESULTS

73 patients completed the questionnaire twice, once before and once after reviewing the 3D printed model (n=31) or AR model (n=42). Both the 3D printed and AR kidney and prostate cancer models outperformed conventional imaging. Patient understanding of disease, cancer size, cancer location, and treatment plan improved with the 3D printed models compared to imaging alone (range = 4.56-4.84/5 for 3D printed model vs. 4.20-4.36/5 for imaging; all p<0.03). For the AR models, only understanding of cancer size improved (4.31 ± 0.87 for AR model vs. 3.90 ± 0.91 for imaging, p =0.03). Seventeen patients with 3D printed models and 25 patients with AR models completed the additional questions. For the question regarding how much the model helped improve understanding of disease, ratings were 9.6 ± 0.8 for 3D printed model and 8.5 ± 2.4 for the AR models, p = 0.05.

CONCLUSION

Overall, the 3D printed models performed better than both conventional imaging and AR models at helping patients to understand their disease and treatment plan.

CLINICAL RELEVANCE/APPLICATION

Patients frequently do not fully understand their disease or surgical plan using conventional imaging methods. By providing enhanced visualization and tactile feedback, 3D printed models may help to overcome this limitation.

SSM13-05 Implementation of Multiparametric Magnetic Resonance Imaging into Robotic - Assisted Radical Prostatectomy Using Virtual Reality

Wednesday, Nov. 28 3:40PM - 3:50PM Room: E353C

Participants

Sherif Mehralivand, MD, Bethesda, MD (*Presenter*) Nothing to Disclose Abhishek Kolagunda, Newark, DE (*Abstract Co-Author*) Nothing to Disclose Chandra Kambhamettu, Newark, CT (*Abstract Co-Author*) Nothing to Disclose Kai Hammerich, Bristol, CT (*Abstract Co-Author*) Nothing to Disclose Kaitlan Cobb, Washington, DC (*Abstract Co-Author*) Nothing to Disclose Vladimir Valera Romero, Bethesda, MD (*Abstract Co-Author*) Nothing to Disclose Jonathan Bloom, Bethesda, MD (*Abstract Co-Author*) Nothing to Disclose Gustavo Pena Lagrave, Bethesda, MD (*Abstract Co-Author*) Nothing to Disclose Vikram Sabarwal, Bethesda, MD (*Abstract Co-Author*) Nothing to Disclose
Samuel Gold, Bethesda, MD (*Abstract Co-Author*) Nothing to Disclose
Graham R. Hale, Bethesda, MD (*Abstract Co-Author*) Nothing to Disclose
Kareem Rayn, Bethesda, MD (*Abstract Co-Author*) Nothing to Disclose
Stephanie A. Harmon, PhD, Bethesda, MD (*Abstract Co-Author*) Nothing to Disclose
Stephanie A. Harmon, PhD, Bethesda, MD (*Abstract Co-Author*) Nothing to Disclose
Marcin Czamiecki, MD, Bethesda, MD (*Abstract Co-Author*) Nothing to Disclose
Bradford J. Wood, MD, Bethesda, MD (*Abstract Co-Author*) Researcher, Koninklijke Philips NV; Researcher, Celsion Corporation;
Researcher, BTG International Ltd; Researcher, Siemens AG; Researcher, XAct Robotics; Researcher, NVIDIA Corporation;
Intellectual property, Koninklijke Philips NV; Intellectual property, BTG International Ltd; Royalties, Invivo Corporation; Royalties,
Koninklijke Philips NV; ;
Peter L. Choyke, MD, Rockville, MD (*Abstract Co-Author*) Nothing to Disclose

Peter L. Choyke, MD, Rockville, MD (*Abstract Co-Author*) Nothing to Disclose Baris Turkbey, MD, Bethesda, MD (*Abstract Co-Author*) Nothing to Disclose Peter Pinto, Bethesda, MD (*Abstract Co-Author*) Nothing to Disclose

For information about this presentation, contact:

N/A

sherif.mehralivand@nih.gov

CONCLUSION

Realtime use of in-vivo mpMRI derived 3D prostate and periprostatic anatomy information during laparoscopic RARP procedure via the da Vinci® surgical system can be advantageous to better tailor the surgery procedure and can improve spatial awareness. Future goals include use of the robot's stereo image viewer instead of HMD and advancement of the MRI-stereo image alignment for direct intraoperative use of mpMRI.

Background

Robotic-assisted radical prostatectomy (RARP) has become a more popular approach for prostate cancer (PCa) recently. Its 3D stereo-laparoscopic view allows for optimal spatial awareness. Recently, multiparametric magnetic resonance imaging (mpMRI) is more commonly used pre- and intraoperatively. Currently, surgeons can only utilize mpMRI data cognitively to guide surgery. In this study, we present use of mpMRI data and intraoperative stereo captures of RARP to create 3D virtual reality (VR) models which can guide surgeons during RARP to optimize spatial awareness.

Evaluation

Axial T2W MRI was utilized to create 3D models of the prostate, bladder, rectum, NVBs, seminal vesicles, urethra and PCa lesions by a manual contouring process. These contours were then used to create 3D mesh models for a commercially available VR platform with head mounted display (HMD) and touch controls (Oculus Rift®). During RARP, stereo images of the laparoscopic views were extracted using the da Vinci´s DVI outputs. Both models were then aligned to each other using an in-house algorithm and provided to urologists during RARP. When needed surgeons withdrew from the console and interacted with the 3D models using the HMD.

Discussion

VR system was used during 9 RARPs. All models were successfully generated and integrated into the VR system. The time between the stereo image capture to full applicability of the model was approximately 3 minutes. The VR system was utilized at 4 steps: General check before the surgery, prior to bladder neck separation, apical dissection and during separation of nerves from the prostate capsule in lesions with proximity to the NVB. The system was used for one minute during each step and did not interfere with routine workflow.

SSM13-06 Head Mounted Display Augmented Reality for Image Guided Procedures of the Spine

Wednesday, Nov. 28 3:50PM - 4:00PM Room: E353C

Participants

Jacob Gibby, BS, Washington, DC (*Presenter*) Nothing to Disclose Samuel Swenson, Arlington, VA (*Abstract Co-Author*) Nothing to Disclose Steve T. Cvetko, PhD, American Fork, UT (*Abstract Co-Author*) Vice President, Novarad Corporation Ramin Javan, MD, Washington, DC (*Abstract Co-Author*) Nothing to Disclose Wendell A. Gibby, MD, Provo, UT (*Abstract Co-Author*) CEO, Novarad Corporation

For information about this presentation, contact:

jakegibby@hotmail.com

CONCLUSION

We demonstrated feasibility of using HMD-AR in facet and sacroiliac joint injections, and percutaneous discectomy. To the authors' knowledge, this is the first reported use of HMD-AR guidance in live surgery.

Background

Head Mounted Display Augmented Reality (HMD-AR) is a recent technological advancement that can be used to superimpose CT or MRI images on a patient in real space to visualize inner anatomical structures in three dimensions, as well as axial, sagittal, and coronal views. We used HMD-AR to perform three common image-guided spine procedures, facet and sacroiliac (SI) joint injections as well as percutaneous discectomy, with no real time fluoroscopic guidance on a 3D printed lumbar model. Finally, we successfully demonstrated the utility of HMD-AR by performing these procedures on live patients using HMD-AR guidance.

Evaluation

CT images were performed of a 3D printed lumbar phantom made of radiodense gypsum-based material encased in silicone. Suggested trajectories for instrumentation were embedded in the images, which were uploaded to the Microsoft Hololens using Novarad Open Sight system. Images were superimposed on the phantom, and localization of the facet joint, sacroiliac joint, and nucleus pulposus was performed by placing 18-gauge cannulated needles along holographic trajectories. Repeat CT images confirmed accurate placement of the needles. Registration accuracy was determined by measuring deviation of model to hologram and was found to be roughly spherical with radius of 2.5 mm (STD 0.44 mm). Finally, a certified neuro-radiologist used the same method to localize the facet joint, sacroiliac joint and nucleus pulposus during three separate live procedures, all of which were confirmed with fluoroscopy.

Discussion

HMD-AR can be used to project holographic guidance trajectories within vital anatomic structures, allowing accurate interventional and surgical instrumentation, potentially decreasing operating and fluoroscopy time and reducing error for select procedures. HMD-AR can also utilize existing images, potentially reducing radiation exposure by minimizing need of fluoroscopy use intraoperatively.



Molecular Imaging (Oncology Therapy)

Wednesday, Nov. 28 3:00PM - 4:00PM Room: S505AB



AMA PRA Category 1 Credit ™: 1.00 ARRT Category A+ Credit: 1.00

FDA Discussions may include off-label uses.

Participants

Pedram Heidari, MD, Boston, MA (*Moderator*) Nothing to Disclose Gabriel C. Fine, MD, Salt Lake City, UT (*Moderator*) Stockholder, Apple Inc

Sub-Events

SSM14-02 Furin-Targeted Nanotheranostics for CEST MR Imaging and Cancer Therapy

Wednesday, Nov. 28 3:10PM - 3:20PM Room: S505AB

Participants

Yue Yuan, PhD, Baltimore, MD (*Abstract Co-Author*) Nothing to Disclose Jia Zhang, Baltimore, MD (*Abstract Co-Author*) Nothing to Disclose Guanshu Liu, PhD, Baltimore, MD (*Abstract Co-Author*) Nothing to Disclose Xiaolei Song, Baltimore, MD (*Abstract Co-Author*) Nothing to Disclose Michael T. McMahon, PhD, Baltimore, MD (*Abstract Co-Author*) Nothing to Disclose Jeff W. Bulte, PhD, Baltimore, MD (*Presenter*) Research Grant, Koninklijke Philips NV; Research Grant, Weinberg Physics, LLC

For information about this presentation, contact:

jwmbulte@mri.jhu.edu

PURPOSE

Furin is a membrane-bound proprotein convertase that is overexpressed in many types of tumors. It activates certain specific proteins associated with tumor progression, with the degree of expression correlating to 5-year survival rates. We have adapted the compound olsalazine, an anti-cancer agent that also exhibits chemical exchange saturation transfer (CEST) MRI contrast, with a synthetic peptide (RVRR) that is cleaved by furin. Our aim was to assess the imaging and therapeutic effects of the furin-catalyzed condensation reaction and subsequent formation of intracellular OLSA nanoparticles.

METHOD AND MATERIALS

NU/J immunodeficient mice (n=20) were subcutaneously injected with 1×106 HCT116 (furin-overexpressing) human tumor cells in the left flank and 1×106 LoVo (low furin-expressing) human tumor cells in the right flank. Animals received 0.14 mmol/kg furin-targeted RVRR-OLSA or 0.14 mmol/kg OLSA as non-targeted control injected i.v. In vivo CEST MRI was performed at different time points using a 11.7 T horizontal scanner. In three separate cohorts (n=4 each), animals received 0.07 mmol/kg RVRR-OLSA, 0.07 mmol/kg OLSA, or PBS only (as control) injected i.v. 8 times with 3-day intervals.

RESULTS

After i.v. injection of RVRR-OLSA, furin-overexpressing HCT116 tumors and low furin-expressing LoVo tumors could be clearly distinguished from each other in vivo on CEST MRI (Fig. 1a, shown at 2h post injection). No such differences were observed for OLSA without RVRR. Mice injected with RVRR-OLSA showed significantly reduced tumor sizes compared to those injected with OLSA alone for the HCT 116 tumor (p<0.05) but not the LoVo tumor (Fig. 1b). At day 33, average tumor volumes of HCT116 tumors and LoVo tumors for the RVRR-OLSA treated group were reduced to 38% and 61%, respectively, as compared to the control group.

CONCLUSION

Furin-induced intracellular formation of OLSA-NPs following administration of RVRR-OLSA enhances CEST contrast and reduces tumor size in vivo.

CLINICAL RELEVANCE/APPLICATION

The new nanotheranostic probe RVVR-OLSA may be further developed for imaging tumor aggressiveness and tumor response to furin-targeted therapy.

SSM14-03 Orthotopic Pancreatic Cancers: Molecular Imaging-Guided Radiofrequency Hyperthermia-Enhanced Immuno/Oncolytic Therapy

Wednesday, Nov. 28 3:20PM - 3:30PM Room: S505AB

Awards Trainee Research Prize - Fellow

Participants

Qiang Li SR, MD, PhD, Ningbo, China (*Presenter*) Nothing to Disclose Yiming Zhou, MD, Beijing, China (*Abstract Co-Author*) Nothing to Disclose Feng Zhang, MD, Seattle, WA (*Abstract Co-Author*) Nothing to Disclose JianSong Ji, MD, Hangzhou, China (*Abstract Co-Author*) Nothing to Disclose Peicheng Li, MD, Seattle, WA (*Abstract Co-Author*) Nothing to Disclose Jingjing Song Jr, Seattle, WA (*Abstract Co-Author*) Nothing to Disclose Minjiang Chen, Seattle, WA (*Abstract Co-Author*) Nothing to Disclose Yaying Li, Seattle, WA (*Abstract Co-Author*) Nothing to Disclose Kun Qian, Seattle, WA (*Abstract Co-Author*) Nothing to Disclose Xiaoming Yang, MD, PhD, Mercer Island, WA (*Abstract Co-Author*) Nothing to Disclose

For information about this presentation, contact:

captaindavis@163.com

PURPOSE

To validate the feasibility of using interventional molecular imaging to guide radiofrequency hyperthermia (RFH)-enhanced local immune/oncolytic therapy of rat orthotopic pancreatic cancers.

METHOD AND MATERIALS

Luciferase-labeled rat pancreatic cancer cells and 24 Lewis rats with orthotopic pancreatic cancers in four groups (n = 6/group) were treated by (i) combination therapy of oncolytic virus (T-VEC, 10×106 pfu) plus RFH at 42? for 30 mins; (ii) oncolytic virotherapy-only; (iii) RFH-only; and (iv) saline. MTS and flow cytometry were used to analyze cell proliferation and apoptosis. Optical/x-ray imaging and ultrasound imaging were used to follow up and compare the therapeutic effects among various groups, correlated with subsequent pathologic examinations.

RESULTS

Both confocal microscopy and MTS assay demonstrated diminished number of viable cells with combination therapy (RHF+T-VEC) compared with other three treatments (Fig. A&B), as well as significant increase of cell apoptosis in flow cytometry (Fig. C). Optical/x-ray imaging demonstrated decreased tumor bioluminescent signal (Fig. D) and ultrasound imaging showed the smallest tumor volume of combination therapy, in comparison to other treatments (Fig. E). Imaging findings were well correlated with pathologic examinations, shown as (1) the smallest tumor size (Fig. F&G); (2) increased apoptosis with TUNEL staining (Fig. F&H); and (3) significantly decreased cell proliferation with Ki-67 stain (Figs. F&I) in the combination therapy group, compared to other treatment groups.

CONCLUSION

We validated the feasibility of using molecular imaging-guided interventional RFH to enhance immune/oncolytic therapy of pancreatic cancer, which may open the new avenues for effective management of pancreatic cancer, one of the deadliest malignancies worldwide.

CLINICAL RELEVANCE/APPLICATION

Molecular imaging-guided interventional RFH can enhance immune/oncolytic therapy of pancreatic cancer.

SSM14-04 Molecular Imaging-Monitored Radiofrequency Hyperthermia-Enhanced Intratumoral Herpes Simplex Virus-Thymidine Kinase/Ganciclovir Gene Therapy for Rat Hepatic Cancers

Wednesday, Nov. 28 3:30PM - 3:40PM Room: S505AB

Participants Fu Xiong, PhD, MD, Seattle, WA (*Presenter*) Nothing to Disclose Feng Zhang, MD, Seattle, WA (*Abstract Co-Author*) Nothing to Disclose Yin Jin, MD, Seattle, WA (*Abstract Co-Author*) Nothing to Disclose Qiaoyou Weng, Seattle, WA (*Abstract Co-Author*) Nothing to Disclose Jingjing Song Jr, Seattle, WA (*Abstract Co-Author*) Nothing to Disclose Chuansheng Zheng, Wuhan, China (*Abstract Co-Author*) Nothing to Disclose Xiaoming Yang, MD, PhD, Mercer Island, WA (*Abstract Co-Author*) Nothing to Disclose

For information about this presentation, contact:

xiongfumd@hust.edu.cn

PURPOSE

To explore a new method using optical/ultrasound imaging to monitor RF hyperthermia(RFH)-enhanced herpes simplex virusthymidine kinase/Ganciclovir(HSV-TK/GCV)suicide gene therapy of rat hepatocellular carcinoma(HCC).

METHOD AND MATERIALS

Rat liver cancer cells(MCA-RH-7777)were transduced with lentivirus/luciferase gene. Serial in-vitro experiments with luciferase-cells and in-vivo experiments of rat orthotopic HCC were divided into four groups :(i) HSV-TK/GCV combined with RFH; (ii) HSV-TK/GCV; (iii) RFH; and (iv) PBS. HSV-tk gene expression was qualified by western blotting, while cell viability was evaluated by confocal microscopy and MTS. Bioluminescence optical imaging and ultrasound imaging were used to monitor the photon signal and size changes of tumors in each groups at different time points. The imaging findings were correlated with histologic analysis.

RESULTS

Of in-vitro experiments, MTS assay demonstrated the lowest cell proliferation in the group of combination therapy, compared with other three groups ($26.1\pm3.2\%$ vs $50.4\pm4.6\%$ vs $82.9\pm6.3\%$ vs 100%, p<0.01), which was corresponding to the lowest number of survived cells with confocal microscopy and the lowest bioluminescence signal with the optical imaging. Of in-vivo experiments, ultrasound imaging showed the smallest tumor volumes in the combination therapy group, compared to other control groups (0.28 ± 0.11 , 1.28 ± 0.23 vs 4.64 ± 0.35 vs 6.37 ± 0.36 , p<0.05). Bioluminescent optical imaging further demonstrated a significantly decreased bioluminescence signal intensities in the combination group, compared with three control groups (0.57 ± 0.09 , 1.06 ± 0.10

vs 3.43 ± 0.27 vs 3.85 ± 0.12 , p<0.05). These imaging findings were further confirmed by significantly increased apoptotic cells in the combination therapy group.

CONCLUSION

It is feasibility using optical imaging and ultrasound imaging to monitor intratumoral RFH-enhanced HSV-TK/GCV gene therapy of rat HCC, which may provide a new image-guided interventional oncology technique for efficient management of liver malignancies by simultaneous integration of radiofrequency technology, interventional oncology, and direct intratumoral gene therapy.

CLINICAL RELEVANCE/APPLICATION

Optical imaging is a useful tool for monitoring intratumoral RFH-enhanced HSV-TK/GCV gene therapy of rat hepatic cancers, which may provide a new opportunity for effectively managing liver cancers

SSM14-05 2D Magnetic Titanium Carbide (Ti3C2 MXene) for Cancer Theranostics

Wednesday, Nov. 28 3:40PM - 3:50PM Room: S505AB

Participants

Zhuang Liu, PhD,MD, Shanghai, China (*Presenter*) Nothing to Disclose Shengjian Zhang, Shanghai, China (*Abstract Co-Author*) Nothing to Disclose Weijun Peng, MD, Shanghai, China (*Abstract Co-Author*) Nothing to Disclose

For information about this presentation, contact:

liuzhuang201010@126.com

PURPOSE

The aim of this part was to construct superparamagnetic 2D Ti3C2 MXenes for enhance MR molecular imaging and photothermal therapy (PTT).

METHOD AND MATERIALS

The fabrication of ultrathin Ti3C2 MXene nanosheets was based on an exfoliation strategy and the construction of superparamagnetic 2D Ti3C2 MXenes is based on the specific MXenes' surface chemistry for the in-situ growth of superparamagnetic Fe3O4 nanocrystals onto the surface of Ti3C2 MXenes. The magnetic Ti3C2-IONPs composite MXenes were modified with soybean phospholipid (SP) to guarantee high stability in physiological conditions. These MXenes were characterized via transmission electron microscopy (TEM), scanning electron microscopy (SEM), energy dispersive X-ray spectroscopy (EDS), electron energy loss spectroscopy (EELS), dynamic light scattering (DLS), zeta-potential, X-ray photoelectron spectroscopy (XPS) and UV-Vis-NIR spectra. The photothermal therapy, T2-weighted magnetic resonance imaging and the high biocompatibility of these composite nanosheets have also been evaluated in vitro and in vivo.

RESULTS

These magnetic Ti3C2-IONPs composite MXenes exhibit high T2 relaxivity of 394.2 mM-1s-1 and efficient contrast-enhanced magnetic resonance imaging of tumor, providing the potential for the therapeutic guidance. Importantly, these superparamagnetic MXenes have shown high photothermal-conversion efficiency (48.6%) to guarantee their efficient photothermal killing of cancer cells and ablation of tumor tissues, which has been systematically demonstrated both in vitro and in vivo.

CONCLUSION

For the first time, we have successfully illustrated that the superparamagnetic MXenes nanosheets feature the high intrinsic photothermal-conversion capability for PTT against tumor, which are also the first paradigm of integrated superparamagnetic IONPs acted as the contrast agents for T2-weighted MR imaging. The high biocompatibility of these elaborately designed magnetic Ti3C2-based composite MXenes guarantees their further potential clinical translation. This report paves a new way for the functionalization of MXene-based 2D nanosheets for broadening their novel applications based on the unique surface chemistry of MXenes, especially in theranostic nanomedicine.

CLINICAL RELEVANCE/APPLICATION

These superparamagnetic MXenes nanosheets feature the high intrinsic photothermal-conversion capability to against tumor and acted as the contrast agents for T2-weighted MR imaging.

SSM14-06 Gene Therapy Targeting of GDPD5/6 in Choline Metabolism of Breast Cancer

Wednesday, Nov. 28 3:50PM - 4:00PM Room: S505AB

Awards

Student Travel Stipend Award

Participants Marina Stukova, BS, Denver, CO (*Presenter*) Nothing to Disclose Kanchan Sonkar, PhD, Baltimore, MD (*Abstract Co-Author*) Nothing to Disclose Caitlin Tressler, PhD, Baltimore, MD (*Abstract Co-Author*) Nothing to Disclose Balaji Krishnamachary, PhD, Baltimore, MD (*Abstract Co-Author*) Nothing to Disclose Zaver M. Bhujwalla, PhD, Baltimore, MD (*Abstract Co-Author*) Nothing to Disclose Kristine Glunde, PhD, Baltimore, MD (*Abstract Co-Author*) Nothing to Disclose

For information about this presentation, contact:

marinas@sanjuanbautista.edu

PURPOSE

Glycerophosphocholine (GPC) is an important 1H MRS-detected metabolite in choline metabolism1. The GDPD52,4/GDPD63 enzymes, which convert GPC to free choline, are overexpressed in breast cancer. Previously we have shown that GDPD5/GDPD6 silencing

increased cellular GPC5 levels and reduced migration and proliferation of breast cancer cells4. We are continuing our studies *in-vivo* to evaluate if lentiviral vector based silencing of GDPD5/GDPD6 will reduce tumor growth in breast cancer xenograft models. The metabolic effects of silencing were studied for identifying novel biomarkers and therapeutic targets for anti-cancer therapy.

METHOD AND MATERIALS

GDPD5 and GDPD6 were silenced in nude mice growing human breast cancer xenografts. In these mice, we injected lentiviral vectors expressing GDPD5-shRNA, or GDPD6-shRNA along with control vector expressing luc-shRNA. Once tumor sizes reached 150mm3, mice were treated with viral suspension. Upon necropsy, tumors were harvested and subjected to 1H MRS analysis.

RESULTS

Initially, tumors showed a gradual increase in size. Upon treatment, tumor growth was significantly reduced in the GDPD6-shRNA treated group compared to other groups. 1H MR spectra of tumor extracts showed significant differences in various metabolites (Fig 1A-B). A heatmap demonstrated % changes among the three treated groups (Fig 1C).Significant changes were observed in metabolites from metabolic pathways including amino acid and protein synthetic pathways and glycolysis, which are in accordance with the literature. Choline was decreased while GPC was increased in the GDPD6-shRNA treated group (Fig 1D). The PC/GPC ratio was lower in the GDPD6-shRNA treated group (Fig 1E), which was consistent with our previous findings4.

CONCLUSION

These data in breast tumor xenografts suggest that GDPD5 and GDPD6 silencing could be an effective molecular treatment strategy. Additional studies are continuing in our lab to corroborate these initial findings. Ref.: Glunde et al, Nat Rev Cancer 2011 Cao, et al, NMR Biomed 2012 Cao, et al, NMR Biomed 2016 4. Wijnen et al, NMR Biomed 2014 5. Krishnamachary et al, Can Res 2009

CLINICAL RELEVANCE/APPLICATION

Lentiviral gene silencing is emerging as efficient technique for suppressing genes of interest for cancer treatment. We are assessing effects of gene silencing by means of 1H MRS based metabolomics following silencing of two glycerophosphodiesterases GDPD5 and GDPD6.



Musculoskeletal (Novel Signs and Patterns)

Wednesday, Nov. 28 3:00PM - 4:00PM Room: E450B



AMA PRA Category 1 Credit ™: 1.00 ARRT Category A+ Credit: 1.00

Participants

Ogonna K. Nwawka, MD, New York, NY (*Moderator*) Research Grant, General Electric Company Donna G. Blankenbaker, MD, Fitchburg, WI (*Moderator*) Consultant, Reed Elsevier; Royalties, Reed Elsevier

Sub-Events

SSM15-01 Expert Consensus on Determination of Acuity/Chronicity of Neuropathic Arthropathy on MRI: Results of a Delphi Survey

Wednesday, Nov. 28 3:00PM - 3:10PM Room: E450B

Awards

Student Travel Stipend Award

Participants

Erik Lawrence, BS, Manhasset, NY (*Presenter*) Nothing to Disclose James J. Kang, BA, Stony Brook, NY (*Abstract Co-Author*) Nothing to Disclose Jenny T. Bencardino, MD, Lake Success, NY (*Abstract Co-Author*) Nothing to Disclose Elaine S. Gould, MD, Stony Brook, NY (*Abstract Co-Author*) Consultant, Endo International plc William B. Morrison, MD, Philadelphia, PA (*Abstract Co-Author*) Consultant, AprioMed AB; Patent agreement, AprioMed AB; Consultant, Zimmer Biomet Holdings, Inc; Consultant, Samsung Electronics Co, Ltd; Consultant, Medical Metrics, Inc William E. Palmer, MD, Boston, MA (*Abstract Co-Author*) Nothing to Disclose Nogah Shabshin, MD, MBA, Afula, Israel (*Abstract Co-Author*) Consultant, Active Implants Corporation Lynne S. Steinbach, MD, Tiburon, CA (*Abstract Co-Author*) Nothing to Disclose Mark E. Schweitzer, MD, Stony Brook, NY (*Abstract Co-Author*) Consultant, MMI Munich Medical International GmbH; Data Safety Monitoring Board, Histogenics Corporation

For information about this presentation, contact:

erik.lawrence@stonybrookmedicine.edu

PURPOSE

As diabetes becomes more commonplace, neuropathic arthropathy (NA) is a mushrooming problem in clinical interpretation. Although radiographic classification schema was well established, many of these patients come to MR for potential superimposed infections. Thus, it behooves us to develop MR imaging staging criteria for various temporal points of NA.

METHOD AND MATERIALS

An international expert panel of 6 musculoskeletal radiologists was formed and participated in a two-round Delphi survey. A total of 30 qualitative radiologic features associated with various NA stages were compiled after a comprehensive literature search of 9 papers. For round 1, experts were asked to rate the relevance of selected criteria for identifying NA at acute, intermediate, and chronic stages on a scale of 1-10, with 1 as not relevant at all and 10 as extremely important. For round 2, panelists resubmitted answers to the same questionnaire after distributing the group median, interquartile range, and range results from round 1. A Cronbach's a score was calculated to determine consistency of signs.

RESULTS

The median scores for each sign ranged from 2-9. The highest medians for diagnostic relevance of acute presentations were marrow edema with visible fracture, inhomogeneous marrow edema, and diffuse bone marrow edema with medians of 9, 9, and 8.5 respectively. The lowest medians were irregular bone shape on T2, ligament damage, and cartilage damage with medians of 4, 3, and 2 respectively. For chronic presentations of NA, the highest medians were subchondral sclerosis, new bone formation, and fibrosis with medians of 8.5, 8, and 6.5 respectively. The lowest medians were the ghost sign, T1 tapering of distal second and third metatarsals, and sinus tracts with medians of 4, 4, and 2.5 respectively. For intermediate presentations of NA, subchondral cysts scored a higher median of 6 than the 4.5 median for intra-articular bodies. Cronbach's a score of the first and second round of questionnaires were 0.69 and 0.79 respectively.

CONCLUSION

Results of the delphi survey suggest consensus of several qualitative MRI features of neuropathic arthropathy that are indicative of disease acuity/chronicity and show good consistency.

CLINICAL RELEVANCE/APPLICATION

Staging criteria for the acuity/chronicity of neuropathic arthropathy was established such that radiologists may interpret MR images at a similar level to current standards for radiographic images.

Honored Educators

Presenters or authors on this event have been recognized as RSNA Honored Educators for participating in multiple qualifying educational activities. Honored Educators are invested in furthering the profession of radiology by delivering high-quality educational content in their field of study. Learn how you can become an honored educator by visiting the website at: https://www.rsna.org/Honored-Educator-Award/ Jenny T. Bencardino, MD - 2014 Honored Educator

SSM15-02 The Metaphyseal Flare Sign: A Secondary Sign on MRI of Subchondral Insufficiency Fracture of the Knee

Wednesday, Nov. 28 3:10PM - 3:20PM Room: E450B

Participants

Alessandro Vidoni, MD, Cardiff, United Kingdom (*Presenter*) Nothing to Disclose Rachit Shah, MBBS, Birmingham, United Kingdom (*Abstract Co-Author*) Nothing to Disclose Davina Mak, MBBS, BSC, Middlesex, United Kingdom (*Abstract Co-Author*) Nothing to Disclose David Beale, birmingham, United Kingdom (*Abstract Co-Author*) Nothing to Disclose Steven L. James, Birmingham, United Kingdom (*Abstract Co-Author*) Nothing to Disclose Rajesh Botchu, MBBS, Kettering, United Kingdom (*Abstract Co-Author*) Nothing to Disclose

For information about this presentation, contact:

alessandrovidoni@icloud.com

PURPOSE

To describe a novel secondary sign of subchondral insufficiency fracture of the knee, the metaphyseal flare sign.

METHOD AND MATERIALS

A retrospective research of 7926 knee MRI examinations was performed. 48 scans were included in the study. The diagnosis of subchondral insufficiency fracture (SIF) was confirmed in a consensus review by one fellowship trained MSK radiologist and one radiology registrar. The presence of metaphyseal flare sign (soft tissue oedema in the meta-epiphyseal region of the affected condyle) was evaluated in the cohort.

RESULTS

41 patients were included in the study (21 male, 20 female). The mean age was 61.5 years (range 41 to 80 years). The anatomical location of the SIF were the medial femoral condyle (n=28), the lateral femoral condyle in (n=5) and medial tibial condyle (n=8). The metaphyseal flare sign was present in 45 of the 48 scans reviewed. The average craniocaudal length of the soft tissue oedema defined as metaphyseal flare sign was 7 cm (range 10.5 to 4.5).

CONCLUSION

The metaphyseal flare sign is an early, indirect sign of subchondral insufficiency fracture (SIF).

CLINICAL RELEVANCE/APPLICATION

The metaphyseal flare sign is an early, indirect sign of subchondral insufficiency fracture (SIF) particularly useful if the diagnosis is unclear to promptly begin the treatment and prevent the progression of the pathology.

SSM15-03 Uncovered Medial Meniscus Sign on Knee Magnetic Resonance Imaging: Evidence of Lost Brake Stop Mechanism of Posterior Horn Medial Meniscus

Wednesday, Nov. 28 3:20PM - 3:30PM Room: E450B

Participants

Youngjune Kim, Seongnam, Korea, Republic Of (*Presenter*) Nothing to Disclose Joong Mo Ahn, MD, PhD, Pittsburgh, PA (*Abstract Co-Author*) Nothing to Disclose Yusuhn Kang, MD, Seoul, Korea, Republic Of (*Abstract Co-Author*) Nothing to Disclose Eugene Lee, Seongnam-Si, Korea, Republic Of (*Abstract Co-Author*) Nothing to Disclose Joon Woo Lee, MD, PhD, Sungnamsi, Korea, Republic Of (*Abstract Co-Author*) Nothing to Disclose Heung Sik Kang, Gyeonggi-Do, Korea, Republic Of (*Abstract Co-Author*) Nothing to Disclose

PURPOSE

To evaluate the association between anterior tibial translation and injuries on the posterior horn medial meniscus (PHMM) and the integrity of brake stop mechanism of the PHMM in anterior cruciate ligament (ACL) deficient knee.

METHOD AND MATERIALS

This retrospective study included 85 consecutive patients with arthroscopically confirmed complete ACL tear. Anterior tibial translation was quantitatively measured using sagittal MRI at the midpoint of the lateral femoral condyle. Uncovered medial meniscus sign was considered positive if a vertical line tangent to the posterior most margin of the medial tibial plateau intersected the PHMM at the midpoint of the medial femoral condyle on sagittal MRI. Concomitant injury on the structures of the posteromedial and posterolateral corners of the knee, including PHMM tear and meniscal ramp lesion, was recorded. Stratified subgroup analysis and multivariable regression analysis were performed to identify factors associated with anterior tibial translation.

RESULTS

The uncovered medial meniscus sign was positive in 21.2% (18/85) of patients and was significantly associated with anterior tibial translation. In the stratified subgroup analysis and multivariable regression analysis, positive uncovered medial meniscus sign consistently demonstrated a significant association with anterior tibial translation and generated an additional 3.5 mm of anterior tibial translation. Other injuries, including PHMM tear and meniscal ramp lesion, were not associated with anterior tibial translation.

CONCLUSION

The uncovered medial maniceus sign demonstrated a statistically significant correlation with anterior tibial translation and could be

The uncovered medial meniscus sign demonstrated a statistically significant correlation with anterior tiblal translation and could be a useful marker for the lost brake stop mechanism of PHMM in the ACL deficient knee.

CLINICAL RELEVANCE/APPLICATION

1. An uncovered medial meniscus sign proved to have a statistically significant correlation with anterior translation of the tibia in patients with complete tear of the anterior cruciate ligament. 2. The uncovered medial meniscus sign could be a useful magnetic resonance imaging marker for a lost brake stop mechanism of the posterior horn medial meniscus in the knee. 3. A tear at the PHMM or meniscal ramp lesion itself should not be interpreted as an evidence of lost brake stop function of the PHMM.

SSM15-04 T2 Relaxation Times of the Anterolateral Femoral Cartilage in Patients After ACL-Repair with and Without a Deep Lateral Femoral Notch Sign

Wednesday, Nov. 28 3:30PM - 3:40PM Room: E450B

Participants

Cyrus Behzadi, Hamburg, Germany (*Presenter*) Nothing to Disclose Goetz H. Welsch, MD, Hamburg, Germany (*Abstract Co-Author*) Nothing to Disclose Jan Philipp Petersen, Hamburg, Germany (*Abstract Co-Author*) Nothing to Disclose Bjoern Schoennagel, MD, Hamburg, Germany (*Abstract Co-Author*) Nothing to Disclose Peter Bannas, MD, Hamburg, Germany (*Abstract Co-Author*) Nothing to Disclose Michael G. Kaul, Hamburg, Germany (*Abstract Co-Author*) Nothing to Disclose Gerhard Schon, Hamburg, Germany (*Abstract Co-Author*) Nothing to Disclose Josephine Berger-Groch, Hamburg, Germany (*Abstract Co-Author*) Nothing to Disclose Gerhard B. Adam, MD, Hamburg, Germany (*Abstract Co-Author*) Nothing to Disclose Marc Regier, Hamburg, Germany (*Abstract Co-Author*) Nothing to Disclose

For information about this presentation, contact:

C.Behzadi@uke.de

PURPOSE

To assess T2 relaxation times of the anterolateral femoral cartilage following anterior cruciate ligament (ACL)-repair with and without a positive deep lateral femoral notch sign (DLNS) at post-traumatic MRI.

METHOD AND MATERIALS

In 52 patients post-traumatic MRI as well as 12 months after ACL-rupture (ACLR) and surgical treatment were analysed. In 28 patients a positive DLNS was present at post-traumatic MRI. For quantitative analysis, T2 relaxation time measurements (7 TE: 10-70 ms) were performed at time of re-evaluation. Polygonal ROIs encompassing the full cartilage layer were placed in the anterolateral as well as adjacent femoral cartilage. Clinical assessment included Lysholm-Tegner-Activity-Score, Rasmussen's clinical score and modified Cincinnati-Rating-System-Questionnaire. Description and differences were calculations as means and confidence intervals of means, controlled for the cluster effect of person, if appropriate.

RESULTS

In patients with a positive DLNS after ACLR, relaxation times in the notch region were significantly prolonged compared to patients without a positive DLNS (Δ 7.4 ms, CI: 5.6 - 9.2; p-value <0.001) as well as to the adjacent anterior (Δ 5.7 ms, CI: 4.7 - 6.7; p-value <0.001) and central femoral cartilage (Δ 6.6 ms, CI: 5.7 - 7.6; p-value <0.001). No significant differences in the performed clinical scores between the two groups were noticed (p>0.05).

CONCLUSION

Significantly prolonged T2 relaxation times of the anterolateral femoral cartilage were found in patients with a positive DLNS following ACL-repair compared to patients without a DLNS. Based on these results, it has to be assumed that a positive DLNS is associated with higher cartilage degradation.

CLINICAL RELEVANCE/APPLICATION

The presented results implicate an impact on relaxation times in patients with a femoral notch sign after ACL-rupture. T2 analysis might help identifying patients at risk for earlier onset of Osteoarthritis, which might benefit from precocious surgical treatment.

SSM15-05 Decreased Vertebral Enhancement in Patients with Infectious Spondylitis, Presenting 'Black Vertebrae' as an Atypical Enhancement Pattern

Wednesday, Nov. 28 3:40PM - 3:50PM Room: E450B

Awards

Student Travel Stipend Award

Participants Sungeun Park, MD, Seoul, Korea, Republic Of (*Presenter*) Nothing to Disclose Hye Jin Yoo, MD, Seoul, Korea, Republic Of (*Abstract Co-Author*) Nothing to Disclose Sung Hwan Hong, MD, Seoul, Korea, Republic Of (*Abstract Co-Author*) Nothing to Disclose Ja-Young Choi, MD, Seoul, Korea, Republic Of (*Abstract Co-Author*) Nothing to Disclose Hee-Dong Chae, MD, Seoul, Korea, Republic Of (*Abstract Co-Author*) Nothing to Disclose

PURPOSE

To investigate the characteristics of patients with infectious spondylitis who show decreased vertebral enhancement.

METHOD AND MATERIALS

From January 2010 to November 2017, 767 patients with reports containing terms about infectious spondylitis was collected for this retrospective study. After reviewing images and medical record, we included 456 patients suspicious for infectious spondylitis with 706 post-contrast MR exams. When affected vertebra showed markedly lower degree of enhancement than that of normal bone

marrow(BM) and when the area showing decreased enhancement was greater than 50% of the area of the vertebral body, the vertebra was recognized as 'black vertebra'. Finally 10 patients(M:F=5:5, mean age=66.4 years) with 10 MRI were identified as showing 'black vertebra'. In those patients, imaging findings of MRI and CT within 2 weeks interval from MRI were evaluated. Clinical characteristics including comorbidities, causative organism and treatment course were reviewed.

RESULTS

10 patients with black vertebra showed atypical findings as for infectious spondylitis. There was little BM signal alteration on T1weighted image(n=9), or absence of fluid-equivalent discal signal intensity(SI) on T2-weighted image(n=5). However, 6 patients showed T2 signal voids in or around the vertebral body and 8 patients showed air burbles on CT images(average interval : -1.1days from MR), suggesting emphysematous infection. On follow-up MRI(average interval: 7.2weeks from initial MR), available in 5 patients, those atypical findings almost disappeared but marked progression of infection was evident: increased range of affected segments (n = 3); low T1 SI of affected vertebra(n = 5); and increased contrast enhancement(n = 3). 9 patients had underlying disease such as Diabetes mellitus(n =5) or connective tissue disease(n=2) or etc. Causative organisms were identified as Klebsiella pneumonia(n=3), Staphylococcus aureus(n=3), Escherichia coli(n=2) and etc. Finally, 5 patients underwent surgery due to uncontrolled infection despite antibiotic treatment.

CONCLUSION

'Black vertebra' on contrast enhanced image seems to be associated with early finding of emphysematous infection.

CLINICAL RELEVANCE/APPLICATION

Recognition of decreased enhancement of affected spine, 'black vertebra', would be important to diagnose early emphysematous infection, known to have worse course than typical infectious spondylitis.

SSM15-06 Leopard Spot Edema: An Osseous Stress, Healing and Reinjury Phenomenon in Professional Ballet Dancers Seen on MR

Wednesday, Nov. 28 3:50PM - 4:00PM Room: E450B

Participants

Felix Gonzalez, MD, atlanta, GA (*Presenter*) Nothing to Disclose Bethany U. Casagranda, DO, Pittsburgh, PA (*Abstract Co-Author*) Nothing to Disclose William B. Morrison, MD, Philadelphia, PA (*Abstract Co-Author*) Consultant, AprioMed AB; Patent agreement, AprioMed AB; Consultant, Zimmer Biomet Holdings, Inc; Consultant, Samsung Electronics Co, Ltd; Consultant, Medical Metrics, Inc Samia K. Sayyid, Atlanta, GA (*Abstract Co-Author*) Nothing to Disclose Adam D. Singer, MD, Atlanta, GA (*Abstract Co-Author*) Nothing to Disclose Monica B. Umpierrez, MD, Atlanta, GA (*Abstract Co-Author*) Nothing to Disclose Adam C. Zoga, MD, Philadelphia, PA (*Abstract Co-Author*) Nothing to Disclose

For information about this presentation, contact:

felix.m.gonzalez@emory.edu

PURPOSE

Professional ballet dancers are subject to numerous overuse syndromes about the ankle and foot. Anecdotally, we observed a patchy bone marrow pattern on MR in the hindfeet of skeletally mature dancers, similar to the "starry night" pattern described as normal in children. We sought to describe this pattern of "leopard spot marrow edema" (LSME) at MR and explore its potential etiology and significance using clinical correlation and follow-up imaging.

METHOD AND MATERIALS

28 MR exams of the ankle/hindfoot in 19 professional ballet dancers were reviewed by 2 MSK radiologists. The presence of LSME was recorded along with age, gender, clinical indication and primary MR findings potentially related to symptoms. Follow-up MRs were reviewed and edema was graded as improved or progressive. Correlation with clinical findings was made.

RESULTS

LSME was observed in 14/18 subjects (78%) and 22/28 MRs (78.5%). 8/22 with LSME had repeat MR (interval 3-71, mean 33 months). 5/8 showed improvement of LSME including 2 with complete resolution, both of whom were not dancing at follow-up. 1 subject showed improvement at 5 months but progression at 24 months. 3/8 had progressive LSME, and all 3 were dancing in an active production at follow-up. For subjects with LSME, the age range was 22-35, mean 25 years. There was little gender difference as 9/11 females and 5/7 males had LSME. As for other MR findings, 9/18(50%) had focal osseous stress response or stress fracture, 7/18(39%) had findings of posterior impingement, 2 had lateral ligament injury, 2 had posterior tibial tendon injury, and 1 each had Achilles tendinopathy, Lisfranc sprain and peroneal tendinopathy. 2 subjects with LSME at 1st MR had stress fractures at follow-up.

CONCLUSION

"Leopard spot marrow edema" is a common but previously unreported finding at MR of the hindfoot in ballet dancers, and our series suggests progression with active dancing such that it may reflect a syndrome of microtrabecular injury, healing response, and reinjury distinct from the pediatric marrow pattern reported as normal.

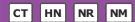
CLINICAL RELEVANCE/APPLICATION

The observation of this bone marrow pattern in an active ballet dancer should raise concern for evolving osseous stress response and a period of limited activity should be considered. Worsening bone marrow edema suggests that a process of microtrabecular injury with a healing response and re-injury is present explaining the observed MR findings.



Nuclear Medicine (Thyroid/Parathyroid Imaging and Therapy)

Wednesday, Nov. 28 3:00PM - 4:00PM Room: S504CD



AMA PRA Category 1 Credit ™: 1.00 ARRT Category A+ Credit: 1.00

FDA Discussions may include off-label uses.

Participants

Don C. Yoo, MD, E Greenwich, RI (*Moderator*) Consultant, Endocyte, Inc Brian M. Rodgers, MD, New Orleans, LA (*Moderator*) Nothing to Disclose

Sub-Events

SSM16-01 Complementary Gadoxetic Acid-Enhanced MRI in Addition to 18F-DOPA-PET/CT Improves Liver Staging in Patients with Medullary Thyroid Carcinoma

Wednesday, Nov. 28 3:00PM - 3:10PM Room: S504CD

Participants

Daniel Puhr-Westerheide, MD, Munich, Germany (*Presenter*) Nothing to Disclose Philipp M. Kazmierczak, MD, Munich, Germany (*Abstract Co-Author*) Nothing to Disclose Axel Rominger, Munich, Germany (*Abstract Co-Author*) Nothing to Disclose Matthias Brendel, Munich, Germany (*Abstract Co-Author*) Nothing to Disclose Wolfgang G. Kunz, MD, Munich, Germany (*Abstract Co-Author*) Research Grant, Medtronic plc Clemens C. Cyran, MD, Munich, Germany (*Abstract Co-Author*) Research Grant, Thera Medical GmbH Speakers Bureau, Siemens AG Robert Stahl, MD, Munich, Germany (*Abstract Co-Author*) Nothing to Disclose Josef Sargsyan-Bergmann, Munich, Germany (*Abstract Co-Author*) Nothing to Disclose Christine Spitzweg, Munich, Germany (*Abstract Co-Author*) Nothing to Disclose Christine Spitzweg, Munich, Germany (*Abstract Co-Author*) Nothing to Disclose Sargsyan-Bergmann, Keisai Co, Ltd; Advisory Board, AstraZeneca PLC; Speaker, Swedish Orphan Biovitrum AB; Advisory Board, Bayer AG; Advisory Board, Eisai Co, Ltd; Speaker, AstraZeneca PLC Maximilian F. Reiser, MD, Munich, Germany (*Abstract Co-Author*) Nothing to Disclose Jens Ricke, MD,PhD, Munich, Germany (*Abstract Co-Author*) Nothing to Disclose

For information about this presentation, contact:

daniel.puhr-westerheide@med.lmu.de

PURPOSE

To investigate the additional diagnostic value of gadoxetic acid-enhanced MRI to 18F-DOPA-PET/CT for liver staging in patients with medullary thyroid carcinoma (MTC).

METHOD AND MATERIALS

41 consecutive patients with histologically confirmed MTC who underwent gadoxetic acid-enhanced MRI and 18F-DOPA-PET/CT within one month between 2010 and 2015 were selected for this retrospective study. The 18F-DOPA-PET/CT and multiparametric gadoxetic acid-enhanced MRI data sets were analyzed by two blinded radiologists. A 5-point Likert scale (based on the LI-RADS criteria: 1-definitely benign, 2-probably benign, 3-intermediate risk for metastasis, 4-probably metastasis, 5-definitely metastasis) was used for lesion categorization in both modalities. The additional value of MRI was defined as detection of 18F-DOPA-PET/CT-occult category 5 lesions or a definitive categorization (category 1 or 5) of lesions remaining inconclusive on the 18F-DOPA-PET/CT scan.

RESULTS

We categorized a total of 212 liver lesions (166 lesions on 18F-DOPA-PET/CT, 212 lesions on MRI; 165 metastases, 37 cysts, 18 hemangiomas). Out of 165 category 5 lesions on MRI, only 94 were classified as category 5 lesions on 18F-DOPA-PET/CT. In 65 % (30/46) of inconclusively categorized lesions on 18F-DOPA-PET/CT (category 2-4), a definitive lesion classification was possible with MRI (change in categorization to categories 1 or 5, respectively). A change in lesion classification by MRI was made in 12 patients (lesions with a change in category from 2 to 1: n=10; from 3 to 1: n=3; from 4 to 5: n=12; from 3 to 5: n=5).

CONCLUSION

Complementary liver-specific MRI allows for the detection of 18F-DOPA-PET/CT-occult metastases and optimizes liver lesion classification in MTC patients.

CLINICAL RELEVANCE/APPLICATION

The definitive categorization of detected liver lesions and timely identification of liver metastases in MTC patients is essential in guiding treatment decisions on early surgical or interventional management.

SSM16-02 Radiotheranostics for Regionally Advanced and Metastatic Differentiated Thyroid Cancer: Outcomes Following Initial Treatment Strategy Informed By Diagnostic 131-I Scintigraphy with SPECT/CT

Participants

Anca Avram, MD, Ann Arbor, MI (*Presenter*) Nothing to Disclose Natalja Rosculet, BS, Ann Arbor, MI (*Abstract Co-Author*) Nothing to Disclose Nazanene H. Esfandiari, MD, Ann Arbor, MI (*Abstract Co-Author*) Nothing to Disclose Paul G. Gauger, MD, Ann Arbor, MI (*Abstract Co-Author*) Nothing to Disclose Barbra S. Miller, MD, Ann Arbor, MI (*Abstract Co-Author*) Nothing to Disclose Mark Cohen, MD, Ann Arbor, MI (*Abstract Co-Author*) Nothing to Disclose Kirk A. Frey, MD, PhD, Ann Arbor, MI (*Abstract Co-Author*) Nothing to Disclose Kirk A. Frey, MD, PhD, Ann Arbor, MI (*Abstract Co-Author*) Nothing to Disclose Kirk A. Frey, MD, PhD, Ann Arbor, MI (*Abstract Co-Author*) Consultant, MIM Software Inc; Stockholder, General Electric Company; Stockholder, Johnson & Johnson; Stockholder, Novo Nordisk AS; Stockholder, Bristol-Myers Squibb Company; Stockholder, Merck & Co, Inc;

David T. Hughes, MD, Ann Arbor, MI (Abstract Co-Author) Nothing to Disclose

For information about this presentation, contact:

ancaa@umich.edu

PURPOSE

Diagnostic staging 131-I scans with SPECT/CT (Dx scan) guide patient-individualized 131-I therapy for differentiated thyroid cancer (DTC). The objective of this study was to determine dynamic risk stratification outcomes after surgery and activity-adjusted 131-I therapy informed by diagnostic 131-I scintigraphy with SPECT/CT.

METHOD AND MATERIALS

Single-institution retrospective cohort study analysis of clinical outcomes in 350 patients with DTC associated with histopathologic risk factors, nodal metastases, and/or distant metastases treated at University of Michigan. Post-operatively all patients underwent Dx 131-I SPECT/CT scans for completion of staging and risk stratification. 131-I therapy was based on integration of information from histopathology, stimulated thyroglobulin (Tg) and scintigraphy. The patients were followed for 1-5 years (mean 39.6 ±23.4 months)

RESULTS

23 patients (6.6%) underwent re-operative neck dissection for removal of unsuspected residual nodal metastases identified on Dx scans. Dynamic risk stratification outcomes were: 84.3% complete response; 1.4% biochemical incomplete response; 2.3% indeterminate response and 12% structural incomplete response. Of the entire cohort only 8 patients (2.3%) had persistent iodine-avid metastatic disease which required repeated 131-I therapy. Of 31 patients with iodine-avid distant metastases identified on Dx scans, 13 patients (42%) achieved complete response with a single 131-I treatment.

CONCLUSION

Detection of regional and distant metastases on postoperative Dx scans permits adjustment of prescribed 131-I activity for targeted treatment, as compared to fixed-activity ablation. This approach resulted in complete response after a single 131-I treatment in 88% patients with histopathologic risk factors and regional metastases, and 42% patients with distant metastases. Most patients (81%) with structural incomplete response had negative follow-up 131-I scans and positive PET/CT and/or CT scans consistent with altered tumor biology (non-iodine avid disease).

CLINICAL RELEVANCE/APPLICATION

Postoperative Diagnostic 131-I scans with SPECT/CT are useful for identification of regional and distant metastases in thyroid cancer, informing 131-I therapy decisions. Elimination of iodine-avid regional and distant metastases with complete therapeutic response is achieved in the majority of patients after a single 131-I treatment based on radiotheranostics principles.

SSM16-03 I-131 Thyroid Dosimetry in Patients with Lung Metastases

Wednesday, Nov. 28 3:20PM - 3:30PM Room: S504CD

Participants

Kenneth Nichols, PhD, New Hyde Park, NY (*Presenter*) Royalties, Syntermed, Inc; Maria B. Tomas, MD, New Hyde Park, NY (*Abstract Co-Author*) Nothing to Disclose Gene G. Tronco, MD, New Hyde Park, NY (*Abstract Co-Author*) Nothing to Disclose Sagine A. Berry-Tony, MD, New Hyde Park, NY (*Abstract Co-Author*) Nothing to Disclose Kuldeep K. Bhargava, PhD, New Hyde Park, NY (*Abstract Co-Author*) Nothing to Disclose Christopher J. Palestro, MD, New Hyde Park, NY (*Abstract Co-Author*) Nothing to Disclose

For information about this presentation, contact:

knichols@northwell.edu

PURPOSE

To protect bone marrow from excessive radiation, maximum permissible activity (MPA) of I-131 to treat thyroid cancer is the value that limits absorbed dose to blood (as a surrogate of marrow) to < 200 cGy. Pts with thyroid carcinoma pulmonary metastases potentially are a unique subgroup because I-131 uptake in the lungs could result in apparently accelerated blood clearance, which in turn could lead to an overestimation of MPA. The objective of this investigation was to test the hypothesis that in pts with diffuse lung metastases from thyroid carcinoma, MPA based on blood measurements alone is not affected by the presence of diffuse lung metastases.

METHOD AND MATERIALS

Data were analyzed retrospectively for 87 thyroid cancer pts (60 ± 15 yrs; 45 female; 42 male) referred for determination of MPA prior to I-131 treatment. Method1 for determining MPA computed total absorbed dose to blood (DTotal) as the sum of mean wholebody γ ray dose component (D γ) from un-collimated gamma-camera measurements, along with dose due to β emissions (D β) from blood samples. Method2 estimated DTotal from D β alone, using linear regression to associate in-vitro blood sample measurements

alone to conventional Method1 DTotal. MPA was computed as 200 cGy/DTotal for each DTotal estimate for Method1 & Method2. All pts also underwent whole body imaging 48 hrs after I-131 administration.

RESULTS

Six pts had iodine avid diffuse lung metastases. MPA values were similar for Method1 & Method2 for all pts (14.3 \pm 8.9 versus 14.1 \pm 8.7 GBq, p = 0.34), pts with lung metastases (12.4 \pm 6.9 versus 11.7 \pm 6.4 GBq, p = 0.06) & for pts without lung metastases (14.4 \pm 9.0 versus 14.3 \pm 8.8 GBq, p = 0.52). MPA values were similar for pts with lung metastases & pts without lung metastases (12.4 \pm 6.9 versus 14.4 \pm 9.0 GBq, p = 0.52). Correlations between Method1 & Method2 MPA values were similar for all pts (r = 0.990, p < 0.0001), those with lung metastases (r = 0.999, p < 0.0001), & those without lung metastases (0.989, p < 0.0001).

CONCLUSION

Our data suggest that in pts with iodine avid diffuse lung metastases from thyroid carcinoma, MPA can be accurately estimated by measuring I-131 blood clearance alone without the need to perform un-collimated gamma camera whole body counting.

CLINICAL RELEVANCE/APPLICATION

MPA can be estimated by I-131 blood clearance alone in pts with lung metastases from thyroid carcinoma.

SSM16-04 Influence of Age on Multivariate Analysis of Disease Specific Survival in Differentiated Thyroid Cancer

Wednesday, Nov. 28 3:30PM - 3:40PM Room: S504CD

Participants

Jasna Mihailovic, MD, 21204 Sremska Kamenica, Serbia (*Presenter*) Nothing to Disclose Emil Matovina, MD, Sremska Kamenica, Serbia (*Abstract Co-Author*) Nothing to Disclose Jelena Roganovic, MD, Sremska Kamenica, Serbia (*Abstract Co-Author*) Nothing to Disclose Veljko Crnobrnja, MD, Novi Sad, Serbia (*Abstract Co-Author*) Nothing to Disclose

For information about this presentation, contact:

jasnam61@gmail.com

PURPOSE

The aim of the study was to analyze the influence of age (<45 years versus >=45 years) on disease-specific survival (DSS) and its prognostic factors in patients with differentiated thyroid cancer (DTC).

METHOD AND MATERIALS

569 DTC patients were treated with I-131 (RAI) in our institution from 2001 to 2010. We analyzed DSS and its predicting factors in all 569 patients as well as in different age groups (Group I<45 years, 237 patients and Group II: >=45 years, 332 patients) by Kaplan-Meier's method. Statistical significance of differences was tested by Log rank test.

RESULTS

There were 185 (32.51%) high risk and 378 (66.43%) low-risk patients, while T was not defined in 5 (0.88%) patients; 132 (23.2%) males, 437 (76.8%) females; 57 (10%) follicular and 465 (81.7%) papillary carcinomas, while histology was not defined in 3 (0.53%) patients. Initial regional metastases were present in 202 (35.5%) patients. DSS was 96.5%; 93.5%; 87%, and 69.6% after 5,10,15 and 17 years, respectively. Prognostic factors that significantly influenced DSS were: gender (p=0.003), age (p=0.0001), T stage (p=0.02), initial metastases (p=0.0001), histology (p=0.039), type of initial treatment (p=0.01), while number of RAI course did not influence the survival (p=0.087). In Group I, DSS after 5, 10 and 15 years was 99.1%. Prognostic factors that significantly influenced DSS in this group were: initial metastases (p=0.015) and histology (p=0.007), while gender, type of initial therapy, T stage, and number of RAI courses had no significant influence (p=0.89; p=0.143; p=0.969; p=0.504, respectively). In Group II, DSS after 5 years was 94%, after 10 years = 89.3% and after 15 years = 78%. Strong predicting factors were: gender (p=0.0001), initial metastases (p=0.0001), type of initial therapy (p=0.028), and number of RAI courses (p=0.031), while histology and T stage had no influence to DSS (p=0.275; p=0.101, respectively).

CONCLUSION

DSS prognostic factors differ among age groups. Young patients show longer DSS significantly influenced by the presence of initial metastases and histology. In contrast, elderly patients have shorter DSS with significant influence of gender, type of initial therapy, presence of initial metastases and number of RAI courses.

CLINICAL RELEVANCE/APPLICATION

In comparison to elderly, young DTC patients have longer DSS that is influenced by different prognostic factors.

SSM16-05 Feasibility of Parathyroid Adenoma Localization with Fluciclovine (18F) PET-CT

Wednesday, Nov. 28 3:40PM - 3:50PM Room: S504CD

Awards

Student Travel Stipend Award

Participants

Akinyemi A. Akintayo, MD, Atlanta, GA (*Presenter*) Nothing to Disclose Olayinka A. Abiodun-Ojo, MD,MPH, Atlanta, GA (*Abstract Co-Author*) Nothing to Disclose Collin Weber, MD, Atlanta, GA (*Abstract Co-Author*) Nothing to Disclose Joe Sharma, MD, Atlanta, GA (*Abstract Co-Author*) Nothing to Disclose Cynthia Cohen, Atlanta, GA (*Abstract Co-Author*) Nothing to Disclose Raghuveer K. Halkar, MD, Atlanta, GA (*Abstract Co-Author*) Nothing to Disclose Raghuveer K. Halkar, MD, Atlanta, GA (*Abstract Co-Author*) Research Grant, General Electric Company Research Grant, Gilead Sciences, Inc Royalties, General Electric Company Mark M. Goodman, PhD, Atlanta, GA (*Abstract Co-Author*) Royalties, Nihon Medi-Physics Co, Ltd David M. Schuster, MD, Decatur, GA (*Abstract Co-Author*) Institutional Research Grant, Nihon Medi-Physics Co, Ltd; Institutional Research Grant, Blue Earth Diagnostics Ltd; Institutional Research Grant, Advanced Accelerator Applications SA; Consultant,

Syncona Ltd; ; ;

For information about this presentation, contact:

dschust@emory.edu

PURPOSE

Localization of parathyroid adenomas is essential for surgical planning. Uptake of fluciclovine (18F) by parathyroid cells has been reported in-vitro. We conducted a feasibility pilot study to evaluate the ability of fluciclovine PET-CT in comparison to 99m Tc sestamibi SPECT-CT for localization of parathyroid adenomas in patients with hyperparathyroidism.

METHOD AND MATERIALS

Four patients with hyperparathyroidism underwent PET-CT of the neck and upper mediastinum for 60 mins after IV injection of fluciclovine (351.5±28MBq). SUVmax of the adenomas, and target-to-background ratios (TBR) (SUVmax/SUVmean) utilizing blood pool (aortic arch), muscle (pectoralis) or thyroid gland as the background were compared with TBRs of the 45-minute sestamibi (798.3±26.8MBq)SPECT-CT in the same patient. Surgical confirmation was reference standard for truth.

RESULTS

Both modalities had 100% concordance in the localization of the adenomas at surgery (n=4). Mean SUVmax (\pm SD) of the adenomas were 3.5 \pm 1.67, 2.6 \pm 1.17, 2.1 \pm 0.81, 2.1 \pm 0.95, and 2.2 \pm 1.03 at 5, 10, 20, 35 and 50 minutes, respectively. The highest fluciclovine SUVs and TBRs were at the 5 min time-point with rapid washout. Sestamibi had significantly higher TBRs compared with fluciclovine (5 min) for blood pool (10.9 \pm 4.70 vs 1.3 \pm 0.57; p<0.01) and pectoralis muscle (5.8 \pm 3.01 vs 1.7 \pm 0.55; p<0.01) with a non-significant trend for thyroid gland (1.3 \pm 0.48 vs 1.1 \pm 0.45; p=0.73), respectively. After surgical resection of the adenomas, the post-operative parathyroid hormone levels decreased to normal. A 2x2 mm adenoma at surgery was not detected by either modality.

CONCLUSION

In this small series we found that parathyroid adenomas can be detected on fluciclovine PET-CT at early imaging but with rapid washout. In addition, adenoma conspicuity (TBR) was better with sestamibi compared with fluciclovine. Fluciclovine PET-CT does not seem promising in the detection and localization of parathyroid adenomas compared with sestamibi SPECT-CT. Studies in patients with negative sestamibi scans are encouraged.

CLINICAL RELEVANCE/APPLICATION

Parathyroid adenomas can be detected on fluciclovine PET-CT at early imaging; however, adenoma conspicuity (TBR) seems better with sestamibi compared with fluciclovine.

SSM16-06 Evaluating the Role of Tc99m Sestamibi Scan in Parathyroid Surgery: A 10-Year Institutional Experience

Wednesday, Nov. 28 3:50PM - 4:00PM Room: S504CD

Participants

Parul Mohan, MBBS, MD, New Delhi, India (*Abstract Co-Author*) Nothing to Disclose Harsh Mahajan, MD, MBBS, New Delhi, India (*Presenter*) Nothing to Disclose S Bal SR, MBBS, MS, New Delhi, India (*Abstract Co-Author*) Nothing to Disclose

For information about this presentation, contact:

drparulmohan@gmail.com

PURPOSE

In this study we aim to evaluate the (99mTc) sestamibi parathyroid scan as a single localizing modality, and we also assess its relation to the weight of the gland and to the preoperative parathyroid hormone (PTH) levels.

METHOD AND MATERIALS

We reviewed 744 patients from our hospital from 2007 to 2017, with a mean age of 56.6 years and a female to male ratio of 3.3:1. With primary hyperparathyroidism, all of them had (99mTc) sestamibi parathyroid scan for the localization of the parathyroid adenoma. Preoperative and postoperative PTH levels were recorded. The histopathology reports confirmed the diagnosis and weight of the diseased gland, which were recorded every time. The results were analyzed and correlated with the sestamibi results, to evaluate its accuracy.

RESULTS

506 patients (68%) of the 744 had an exact match (EM) sestamibi results, 227 (30.5%) had a partial match, and only 11 patients were reported as mismatch. Analyzing the mean weight of the gland in each group between matching (EM, PM) versus mismatch resulted in a mean difference of 0.823 g (1.05 and 0.247 g, respectively) P = 0.045. Hyperplasia to adenoma ratio was more in the partial matching group (18.5%) versus the exact matching group (7.6%). Finally the mean PTH level was higher in the EM group (36.8 pmol/L) compared to the mismatch group (10.1 pmol/L) P = 0.02. Overall sensitivity and specificity for the (99 mTc) sestamibi in our data was 98.1 and 97%, respectively.

CONCLUSION

(99mTc) sestamibi is a highly accurate test that can be employed as a single localizing modality for identifying a hypersecreting parathyroid, a parathyroid adenoma, or a parathyroidectomy. The weight of the gland plays an important role in the accuracy of the test, as also the preoperative PTH levels.

CLINICAL RELEVANCE/APPLICATION

(99mTc) sestamibi is a highly accurate test that can be employed as a single localizing modality for identifying a parathyroid adenoma.



Neuroradiology/Head and Neck (Dual-Energy CT in Head and Neck Imaging)

Wednesday, Nov. 28 3:00PM - 4:00PM Room: N228



AMA PRA Category 1 Credit ™: 1.00 ARRT Category A+ Credit: 1.00

Participants

Reza Forghani, MD,PhD, Cote-saint-Luc, QC (*Moderator*) Stockholder, Real-Time Medical, Inc; Founder, 4 Intel Inc; Stockholder, 4 Intel Inc; Consultant, General Electric Company; Speaker, General Electric Company Salman Qureshi, MBChB, BSc, Sale, United Kingdom (*Moderator*) Nothing to Disclose

Sub-Events

SSM17-01 Differentiation of Benign and Malignant Neck Lymph Nodes on Dual-Energy CT

Wednesday, Nov. 28 3:00PM - 3:10PM Room: N228

Awards Student Travel Stipend Award

Participants Jeanne Kochkodan, BS, Ann Arbor, MI (*Presenter*) Nothing to Disclose Remy R. Lobo, MD, Ann Arbor, MI (*Abstract Co-Author*) Nothing to Disclose Ashok Srinivasan, MD, Canton, MI (*Abstract Co-Author*) Nothing to Disclose

For information about this presentation, contact:

jeankoch@med.umich.edu

PURPOSE

Differentiation of benign versus malignant metastatic lymph nodes in the head and neck currently relies on size, morphology and functional status, such as abnormal FDG metabolism. Dual energy CT (DECT) has shown potential in differentiating benign and malignant head and neck lesions in prior studies. Our aim was to evaluate the utility of DECT derived parameters in differentiating benign and metastatic lymph nodes in head and neck squamous cell carcinoma (HNSCC).

METHOD AND MATERIALS

This retrospective IRB approved study included 14 patients with HNSCC who underwent head/neck DECT and PET/CT within 60 days of each other. One reader placed regions of interest within multiple lymph nodes deemed metastatic (on PET/CT, histopathology or both), normal nodes and skeletal muscle in the same patients (32 metastatic, 49 normal nodes). Independent sample t-tests were used to compare differences in DECT parameters between the two groups, including node HU at 40keV, 50keV, 70keV, 140keV, HU40keV-HU140 keV, effective Z and iodine concentration after normalizing the values by creating node to muscle ratios. When gross necrosis was present in the nodes, ROIs including entire node and those that excluded the necrotic portion were separately studied.

RESULTS

Significant differences in node HU40keV and RATIO-HU40keV were seen between normal and metastatic nodes (207 vs 177 HU, p=0.048; 2.29 vs 1.91, p=0.027) when necrosis was excluded. Similarly, significant differences were seen in node HU140keV and RATIO-HU140keV between normal and metastatic nodes (30.4 vs 38.2 HU, p=0.003; 0.75 vs 0.62, p=0.012), as well as RATIO-HU40-140keV (p=0.047). The other DECT parameters studied did not reveal any differences between the two groups.

CONCLUSION

DECT derived lymph node HU at monochromatic 40keV and 140 keV and ratio of node to muscle HU at monochromatic 40keV and 140 keV are significantly different between normal and metastatic nodes in patients with HNSCC, implying that DECT could have utility, in addition to size and morphology of nodes, in distinguishing these groups. We plan to further study the thresholds that can be used for employing this in clinical practice.

CLINICAL RELEVANCE/APPLICATION

Since most patients with HNSCC undergo CT examination for disease workup, utilizing DECT based metrics for improving the differentiation of normal from metastatic nodes in patients with HNSCC without any additional radiation can help better stage disease.

SSM17-02 Diagnostic Value of Dual-energy Spectral Computed Tomography in Differentiating Parotid Gland Tumors

Wednesday, Nov. 28 3:10PM - 3:20PM Room: N228

For information about this presentation, contact:

linlin77216@sina.com

PURPOSE

To quantitatively evaluate the value of single-source dual-energy spectral computed tomography in differentiating parotid gland tumors.

METHOD AND MATERIALS

43 patients underwent enhanced neck dual-energy spectral CT scan before operation. The spectral CT scan protocol included tube current of 260mA, helical pitch of 0.984 and rotation speed of 0.7s/r. The material decomposition images and monochromatic images were reconstructed and transferred to a GEAW4.6 workstation for spectral analysis using the Gemstone Spectral Imaging (GSI) Viewer software. Tumors were divided into pleomorphic adenomas (PAs), Warthin tumors (WTs) and malignant tumors (MTs) types. The CT number as function of photon energy, iodine concentration (IC) and water concentration (WC) of tumors were measured. The slope value (λ HU) of the spectral HU curve and normalized iodine concentration (to common carotid artery, NICA) were calculated and compared among the three types of tumors. The statistical analysis was performed with SPSS 13.0 software. ROC analysis was performed to evaluate the efficiency of these multiple parameters for the differential diagnosis.

RESULTS

52 tumors were confirmed by pathology and were included in our study, including 12 pleomorphic adenomas, 24 Warthin tumors (15 patients), and 16 malignant tumors. The IC, NICA and λ HU values of WTs (2.45±0.82mg/ml, 0.33±0.08 and 2.76±0.08, respectively) were significantly higher than those of MTs (1.48±0.90mg/ml) which were in turn higher than those of PAs (0.59±0.28mg/ml) (all P<0.05). The optimal IC, NICA and λ HU threshold was 0.91mg/ml, 0.15 and 1.09, respectively for differentiating PAs from MTs, achieving sensitivity of 91.7%, 91.7% and 91.7%, specificity of 95.0%, 85.0% and 95.0%, and accuracy of 94.2%, 86.5% and 94.2%, respectively for distinguishing PAs from MTs. The optimal IC, NICA and λ HU threshold was1.46mg/ml, 0.20 and 1.72, achieving 91.7%, 95.8% and 91.7% sensitivity, 89.3%, 85.7% and 89.3% specificity, respectively. The accuracy was 90.4%, 90.4% and 90.4%, respectively for distinguishing WTs from MTs.

CONCLUSION

The single-source dual-energy spectral CT-related measurements such as iodine concentration in parotid tumors in the enhanced CT scans are useful in the differential diagnosis of parotid tumors.

CLINICAL RELEVANCE/APPLICATION

The single-source dual-energy spectral CT imaging is helpful to differentiate various pathological types of parotid gland tumors.

SSM17-03 Comparison of Dual and Single Source Dual Energy CT in Head and Neck Imaging

Wednesday, Nov. 28 3:20PM - 3:30PM Room: N228

Participants

Matthias S. May, MD, Erlangen, Germany (*Presenter*) Speakers Bureau, Siemens AG Rafael Heiss, Erlangen, Germany (*Abstract Co-Author*) Speakers Bureau, Siemens AG Michael Uder, MD, Erlangen, Germany (*Abstract Co-Author*) Speakers Bureau, Bracco Group Speakers Bureau, Siemens AG Speakers Bureau, Bayer AG Research Grant, Siemens AG Wolfgang Wust, MD, Erlangen, Germany (*Abstract Co-Author*) Speakers Bureau, Siemens AG

For information about this presentation, contact:

matthias.may@uk-erlangen.de

PURPOSE

Aim of this study was to compare image quality of Single-Source Dual-Energy CT (SS-DECT) with third-generation Dual-Source dual energy CT (DS-DECT) in head and neck cancer.

METHOD AND MATERIALS

102 patients with histologically proven head and neck cancer were prospectively randomized to undergo radiation dose matched SS-DECT (n=51, 120 kV, split filter technique, 384 ref. mAs) or DS-DECT (n=51, 80/Sn150 kV, tube A 100/ tube B 67 ref. mAs). Inline default images (DI) and virtual monoenergetic images (VMI) for two different low energies (40 and 60 keV) were reconstructed. Objective image quality was evaluated as dose normalized contrast to noise ratio (CNRD) and subjective image quality was rated on a 5-point Likert-scale.

RESULTS

In both groups highest CNRD values for vessel and tumor attenuation were obtained at 40 keV. DS-DECT was significantly better than SS-DECT regarding vessel and tumor attenuation. Overall subjective image quality in the SS-DECT group was highest on the DI followed by 40 keV and 60 keV. In the DS-DECT group subjective image quality was highest at 40 keV followed by 60 keV and the DI. 40 keV and 60 keV were significantly better in the DS-DECT compared to the SS-DECT group (both p<0.01).

CONCLUSION

In split filter SS-DECT as well as DS-DECT highest overall image quality in head and neck imaging can be obtained with a combination of DI and low keV reconstructions. DS-DECT is superior to split filter SS-DECT in terms of subjective image quality, vessel and tumor attenuation.

CLINICAL RELEVANCE/APPLICATION

This is the first study comparing image quality of two different dual energy techniques of the same vendor in a radiation dosematched setting for head and neck imaging.

SSM17-05 Iodine Quantification in Patients with Initially Diagnosed Head and Neck Cancer Using Dual-Layer

Detector Spectral CT: Which Factor Could Significantly Affect the Tumoral Iodine Concentration?

Wednesday, Nov. 28 3:40PM - 3:50PM Room: N228

Participants

Younghen Lee, MD, Ansan, Korea, Republic Of (*Presenter*) Nothing to Disclose Hyung Suk Seo, Ansan-si, Korea, Republic Of (*Abstract Co-Author*) Nothing to Disclose Soon Young Kwon, Ansan, Korea, Republic Of (*Abstract Co-Author*) Nothing to Disclose Kyung Ho Oh, Ansan, Korea, Republic Of (*Abstract Co-Author*) Nothing to Disclose

For information about this presentation, contact:

younghen@korea.ac.kr

PURPOSE

We aimed to investigate of impacts of patient- & tumor-related factors on the dual-layer detector spectral CT-derived iodine concentration(IC) in the patients initially diagnosed with head and neck squamous cell carcinoma(HNSCC).

METHOD AND MATERIALS

From July 2016 to March 2018, a total of 46 patients (M:F=41:5, mean age: 62.8years) initially diagnosed with HNSCC which were identified by contrast-enhanced neck CT examination using a double-layer detector spectral CT (IQon CT, Philips healthcare) were retrospectively enrolled. To obtain the IC of the primary tumors, an experienced neuroradiologist draw the region of interest (ROI) on the representative axial images after reviewing the corresponding MRI images, and then copied the same ROI on the additional iodine density map. In addition, other ROIs were drawn on the aortic arch and ipsilateral neck muscle for normalization. We statistically determined the variables which significantly influenced the IC and normalized IC (nIC) of primary HNSCC using a multivariate linear regression: age, gender, iodine concentration, body surface area, T stage, histologic grading and location of tumor.

RESULTS

According to our quantitative analysis obtained from contrast-enhanced neck CT examination with fixed scan delay (50-sec), only histologic grading significantly influenced the mean IC of primary HNSCC (p<0.05). The mean IC (mg/ml) was significantly highest in well differentiated ($n=11;2.2\pm0.84$), followed by those of moderately-($n=27;2.0\pm0.65$), poorly differentiated ($n=4;1.8\pm0.49$) and that of non-keratizing type were lowest ($n=4;1.40\pm0.18$).

CONCLUSION

Dual-layer detector spectral CT-derived mean IC could be used as useful predictor of histologic grading in patients initially diagnosed HNSCC.

CLINICAL RELEVANCE/APPLICATION

Dual-layer detector spectral CT-derived mean IC could be used as useful predictor of histologic grading in patients initially diagnosed HNSCC. Iodine quantification using dual-layer detector spectral CT might potentially improve the role of contrast-enhanced CT examination in the HNSCC.

SSM17-06 Preliminary Study on Spectral CT in the Diagnostic Value of Papillary Thyroid Microcarcinoma

Wednesday, Nov. 28 3:50PM - 4:00PM Room: N228

Participants

Lin Li, MD, Beijing, China (Presenter) Nothing to Disclose

PURPOSE

The aim of the current study was to retrospectively analyze spectral CT images of papillary thyroid microcarcinoma (PTMC) and evaluate the detection and diagnostic value for PTMC.

METHOD AND MATERIALS

33 cases (35 lesions) of PTMC which were confirmed by surgical pathology from January 2015 to January 2016 were included in this retrospective study. All the patients underwent Spectral CT scan using Discovery CT750 HD scanner. All the spectral CT images were divided into 3 groups: polychromatic image (group A), optimal monochromatic image (group B), and the fused image which blended optimal monochromatic image with iodine-based material decomposition image together (group C). The image qualities of group A and B were evaluated objectively, and the detection abilities of the 3 groups were evaluated subjectively.

RESULTS

The optimal CNR level is (65.96 ± 4.01) keV (range from 62 to 75keV). The CNR of optimal monochromatic image of spectral CT was higher than that of polychromatic image(t=-5.626,P=0.000), and the noise of optimal monochromatic image was lower than that of polychromatic image(t=12.00,P=0.000), and the differences were significant(P<0.05). The detection rate of the 3 groups of images for microcarcinoma lesions were 91.4%(32/35),97.1%(34/35), and 100%(35/35) respectively, while the subjective scores of the 3 groups of images were $2.54\pm1.15,3.31\pm0.93$, and 3.46 ± 0.74 respectively. The detection ability of fused image was better than that of polychromatic image and similar to that of optimal monochromatic image. The characteristics of microcarcinoma were irregular shape (19 cases, 54.3%), indistinct margin (24 cases, 68.6%), heterogeneous density (24 cases, 68.6%), detection of microcalcification (16 cases, 45.7%), and lymph node metastasis (20 cases, 57.1%). The lesions' average iodine concentration, normalized iodine concentration, and the average spectral HU curve slope values were (25.0 ± 10.3)×100µg/ml (range from ($9\sim43$)×100µg/ml), $0.33\pm0.14(0.14\sim0.61)$, and $2.99\pm1.59(-0.83\sim5.38)$, respectively.

CONCLUSION

Spectral CT could provide more detailed information for PTMC diagnosis, and the fused image which blended optimal monochromatic image with iodine-based material decomposition image may be useful for PTMC detection and diagnosis in the clinics.

CLINICAL RELEVANCE/APPLICATION

 $\label{eq:spectral CT} \mbox{ imaging is helpful to detect and diagnosis papillary thyroid microcarcinomas.}$



Neuroradiology (Advances in Neuro MRI)

Wednesday, Nov. 28 3:00PM - 4:00PM Room: N226



AMA PRA Category 1 Credit ™: 1.00 ARRT Category A+ Credit: 1.00

FDA Discussions may include off-label uses.

Participants

Sugoto Mukherjee, MD, Charlottesville, VA (*Moderator*) Nothing to Disclose David M. Wilson, MD, PhD, San Francisco, CA (*Moderator*) Nothing to Disclose

Sub-Events

SSM18-01 Quantitative Assessment of the Effect of Endovascular Treatment for Cerebral Venous Sinus Thrombosis by Using Magnetic Resonance Black-Blood Thrombus Imaging (MRBTI)

Wednesday, Nov. 28 3:00PM - 3:10PM Room: N226

Participants Xiaoxu Yang, Beijing, China (*Presenter*) Nothing to Disclose Qi Yang, MD, Los Angeles, CA (*Abstract Co-Author*) Nothing to Disclose Fang Wu, Beijing, China (*Abstract Co-Author*) Nothing to Disclose Xunming Ji, Beijing, China (*Abstract Co-Author*) Nothing to Disclose

For information about this presentation, contact:

cehuijuyxx--7@163.coom

PURPOSE

Our study aims to quantitatively evaluate the treatment effect of endovascular treatment for patients with acute cerebral venous sinus thrombosis(CVST) by Magnetic Resonance Black-Blood Thrombus Imaging(MRBTI) for the first time.

METHOD AND MATERIALS

From 2014 to 2018, 34 patients diagnosed with acute CVST were included in this study, of whom 19 patients received endovascular treatment(experimental group) while 15 patients received anticoagulant therapy(control group). Initial MRBTI and MRV, follow-up MRBTI and MRV were performed on all these enrolled patients. Thrombus Volume (TV) of each person was measured between endovascular group and anticoagulant group on BTI images. Thrombosed segments, venous colleterals, degree of recanalization and modified Rankin Scale(mRS) were noted between these two groups.

RESULTS

In endovascular and anticoagulant groups, the volume of thrombus(VT) was $9538\pm5343 \text{ mm}^3$ and $6424\pm3633 \text{ mm}^3(P>0.05, P=0.77)$ before treatment, the volume of thrombus was $2028\pm3836 \text{ mm}^3$ and $2642\pm2234 \text{ mm}^3(P>0.05, P=0.604)$ respectively. The decreased volume after treatment were $7509\pm4660 \text{ mm}^3$ and $3782\pm2269 \text{ mm}^3(P<0.01, P=0.009)$. Before treatment, the thrombosed segments in experimental group and control group were 6.3 ± 2.8 and $5.9\pm2.5(P>0.05, P=0.692)$ and were 2.9 ± 2.5 and $4.5\pm2.7(P>0.05, P=0.109)$ after treatment, and the decreased segments were 3.3 ± 1.8 and $1.4\pm1.3(P<0.01, P=0.002)$, respectively. And the degree of recanalization in endovascular group is better than anticoagulant group (P < 0.01, P=0.000), which predict a satisfied prognosis. While as for venous collaterals, the venous collateral in anticoagulant group(control group) is more than endovascular group(experimental group).

CONCLUSION

MRBTI can quantitatively assess the effect of endovascular treatment for patients with CVST. Furthermore this technique should be the best imaging technique to follow up patients with CVST after treatment, which may help to judge prognosis of patients with CVST.

CLINICAL RELEVANCE/APPLICATION

The novel imaging technique-MRBTI to quantitatively assess the effect of endovascular therapy for the first time. It may help to predict the prognosis of patients with CVST.

SSM18-02 Amine Protons Were Increased in the Demented Patients: Evaluation of the Chemical Exchange Dependent Saturation Transfer MRI

Wednesday, Nov. 28 3:10PM - 3:20PM Room: N226

Participants Na Young Choi, Seoul, Korea, Republic Of (*Presenter*) Nothing to Disclose Yeji Shin, Seoul, Korea, Republic Of (*Abstract Co-Author*) Nothing to Disclose Young Hoon An, Seoul, Korea, Republic Of (*Abstract Co-Author*) Nothing to Disclose Bo Guem Choi, Seoul, Korea, Republic Of (*Abstract Co-Author*) Nothing to Disclose Hak Young Rhee, Seoul, Korea, Republic Of (*Abstract Co-Author*) Nothing to Disclose Chang-Woo Ryu, MD, Seoul, Korea, Republic Of (*Abstract Co-Author*) Nothing to Disclose Geon-Ho Jahng, PhD, Seoul, Korea, Republic Of (*Abstract Co-Author*) Nothing to Disclose

PURPOSE

Chemical exchange dependent saturation transfer (CEST) MRI is sensitive to solid-like proteins and may detect mobile proteins and peptides in tissues. There is no study for investigating various substances such as amine, hydroxyl protons with a full Z spectrum. Therefore, the purpose of our study is to evaluate the characteristics of chemical exchange proton pools using a CEST MRI technique in dementia patients.

METHOD AND MATERIALS

Nineteen demented (mean=77.9 years, range=55-92 years) and 22 non-demented (mean=66.7 years, range=51-83 years) subjects were included in this study. Using two 3.0 Tesla MRI systems, the full Z spectrum data by total 38 dynamics from -5.00 ppm to 5.00 ppm frequency offset ranges were acquired with using a 3D turbo-spin-echo (TSE) sequence in the brain using alternative increased frequency interval of 0.25 ppm. To map the voxel-based exchangeable signals with the special frequency offsets of protons and the magnetization transfer ratio (MTR) asymmetry (MTRasym), we quantified exchangeable protons with the Lorentzian fitting method using the six-pool model consisted of amide, amine, hydroxyl, direct water saturation (DWS), nuclear overhauser effect (NOE) and magnetization transfer (MT). The voxel-based MTRasym maps were calculated at the frequency offsets of 1.00 ppm, 3.00 ppm, 3.50 ppm. The two sample t-test was used for comparison between two groups.

RESULTS

Based on the Lorentzian fitting, the amide was not significantly different between the two groups and the amine was significantly different between the two groups at the anterior cingulate, hippocampus, parahippocampal gyrus, and pons. MTRasym values were significantly different between the two groups at the anterior cingulate, hippocampus, and putamen for both 3 ppm and 3.5 ppm.

CONCLUSION

In the demented subjects, the amine and the MTR asymmetry values were increased, probably related with increased proteins, neurotransmitters, or metabolites. CEST MRI has several advantages compared with amyloid PET. Therefore, CEST MRI may be useful to investigate brain changes in demented patients without radiation exposure and with high resolution.

CLINICAL RELEVANCE/APPLICATION

CEST MRI technique in dementia patients can be effective for the evaluation of brain changes in demented patients without radiation exposure and with high resolution.

SSM18-03 Assessing Histologic and Genetic Subtypes in Glioma Patients Using CEST MRI at 7T

Wednesday, Nov. 28 3:20PM - 3:30PM Room: N226

Participants

Daniel Paech, MD, Heidelberg, Germany (Presenter) Nothing to Disclose Johannes Windschuh, New York, NY (Abstract Co-Author) Nothing to Disclose Johanna Oberhollenzer, Heidelberg, Germany (Abstract Co-Author) Nothing to Disclose Constantin Dreher, Heidelberg, Germany (Abstract Co-Author) Nothing to Disclose Felix Sahm, Heidelberg, Germany (Abstract Co-Author) Nothing to Disclose Jan-Eric Meissner, Heidelberg, Germany (Abstract Co-Author) Nothing to Disclose Steffen Goerke, Heidelberg, Germany (Abstract Co-Author) Nothing to Disclose Patrick Schuenke, Heidelberg, Germany (Abstract Co-Author) Nothing to Disclose Moritz Zaiss, Tuebingen, Germany (Abstract Co-Author) Nothing to Disclose Sebastian Regnery, Heidelberg, Germany (Abstract Co-Author) Nothing to Disclose Sebastian Bickelhaupt, Heidelberg, Germany (Abstract Co-Author) Nothing to Disclose Philipp Baeumer, Heidelberg, Germany (Abstract Co-Author) Nothing to Disclose Martin Bendszus, Heidelberg, Germany (Abstract Co-Author) Nothing to Disclose Wolfgang Wick, Heidelberg, Germany (Abstract Co-Author) Nothing to Disclose Andreas Unterberg, Heidelberg, Germany (Abstract Co-Author) Nothing to Disclose Peter Bachert, PhD, Heidelberg, Germany (Abstract Co-Author) Nothing to Disclose Mark E. Ladd, PhD, Heidelberg, Germany (Abstract Co-Author) Nothing to Disclose Heinz-Peter W. Schlemmer, MD, Heidelberg, Germany (Abstract Co-Author) Nothing to Disclose Alexander Radbruch, MD, Heidelberg, Germany (Abstract Co-Author) Consultant, Guerbet SA Consultant, Bayer AG Support, Guerbet SA Support, Bayer AG Advisory Board, Guerbet SA Advisory Board, Bayer AG Advisory Board, Bracco Group Advisory Board, AbbVie Inc Speaker, Guerbet SA Speaker, Bayer AG Speaker, Siemens AG Speaker, prIME Oncology Advisory Board, General Electric Company

For information about this presentation, contact:

d.paech@dkfz.de

PURPOSE

The study purpose was to investigate the non-invasive predictability of IDH-mutation status, MGMT promotor methylation, and differentiation of lower versus higher grade glioma (LGG vs. HGG) in newly-diagnosed WHO grade I-IV glioma patients employing Chemical Exchange Saturation Transfer (CEST) magnetic resonance imaging (MRI) at 7.0 Tesla (7T).

METHOD AND MATERIALS

Thirty-four newly-diagnosed glioma patients were included in this prospective study (WHO grade I-II: 7/34=20.6%=LGG; WHO grade III-IV: 27/34=79.4%=HGG; IDH1-R132H status: 9/33=27.3% IDH-mutant; 24/33=72.7% IDH-wildtype, 1 patient not assessed; MGMT promotor methylation status 13/28=46.4% methylated, 11/28=39.3% unmethylated, 4/28=14.3% indeterminate, 2 patients not assessed). CEST MRI was performed at a 7T whole-body scanner followed by a multi-Lorentzian fit analysis. Nuclear Overhauser Effect (NOE) and amide proton transfer (APT) CEST signals were quantitatively investigated in the whole tumor area with regard to predictability of IDH-mutation, MGMT status, and differentiation of LGG vs. HGG. Statistics were performed using

receiver operating characteristic (ROC) and area under the curve (AUC) analysis.

RESULTS

The APT CEST contrasts yielded highest AUCs in IDH-mutation status prediction (dns-APT=0.92, p<0.01; sensitivity=81%, specificity=100%). NOE mediated CEST imaging yielded inferior performance in IDH status prediction (AUC=0.78, p=0.02; sensitivity=61%, specificity=83%). Furthermore, dns-APT metrics enabled significant differentiation of LGG vs. HGG (AUC: dns-APT=0.78, p<0.05; sensitivity=71%, specificity=100%). There was no significant difference regarding MGMT status at any CEST contrast (p>0.05).

CONCLUSION

CEST MRI at 7T, particularly APT imaging, enabled prediction of IDH-mutation status and differentiation of LGG vs. HGG and should therefore be considered as non-invasive MR biomarker to assess histologic and genetic subtypes in glioma patients in the diagnostic workup.

CLINICAL RELEVANCE/APPLICATION

Early identification of prognostic superior characteristics in glioma patients such as IDH-mutation and MGMT status is of great clinical importance. Our study demonstrates that CEST MRI at 7.0T enables non-invasive prediction of IDH mutation status and differentiation of LGG vs. HGG tumors. Consequently, CEST MRI may add valuable information as a non-invasive imaging biomarker in the preoperative diagnostic work-up of glioma patients.

SSM18-04 NODDI: A Promising Method for Assessing Glioma Grade and Cellular Proliferation

Wednesday, Nov. 28 3:30PM - 3:40PM Room: N226

Participants

Shihui Li, Wuhan, China (*Presenter*) Nothing to Disclose Changliang Su, Wuhan, China (*Abstract Co-Author*) Nothing to Disclose Xiaowei Chen, Wuhan, China (*Abstract Co-Author*) Nothing to Disclose Ju Zhang, Wuhan, China (*Abstract Co-Author*) Nothing to Disclose Wenzhen Zhu, MD, PhD, Wuhan, China (*Abstract Co-Author*) Nothing to Disclose

For information about this presentation, contact:

lishihui9376@sohu.com

PURPOSE

To explore the diagnostic performance of neurite orientation dispersion and density imaging (NODDI) in grading gliomas and to evaluate the cellular proliferation.

METHOD AND MATERIALS

NODDI and diffusion-weighed imaging were performed on 80 patients with histopathologically proven glioma. Parameter maps of intra-cellular volume fraction (ficvf), isotropic volume fraction (fiso) and orientation dispersion index (odi) were calculated. Regions of interest were placed in the most solid parts of the tumor. These metrics were normalized to the contralateral normal-appearing white matter and correlated with Ki-67 expression.

RESULTS

Significant differences in normalized ficvf, odi and fiso were observed between low-grade gliomas and high-grade gliomas (ficvf: $0.213 \pm 0.107 \text{ vs}$. 0.718 ± 0.234 ; odi: $0.962 \pm 0.426 \text{ vs}$. 1.767 ± 0.636 ; fiso: $2.482 \pm 2.040 \text{ vs}$. 0.109 ± 0.140 ; p < 0.001 for all) and between grade II and grade III (ficvf: $0.208 \pm 0.104 \text{ vs}$. 0.603 ± 0.253 ; odi: $0.952 \pm 0.428 \text{ vs}$. 1.762 ± 0.542 ; fiso: $2.550 \pm 2.031 \text{ vs}$. 0.115 ± 0.133 , p < 0.001 for all). Only normalized ficvf was significant different between grade III and grade IV ($0.603 \pm 0.253 \text{ vs}$. 0.803 ± 0.182 , p = 0.004). Ki-67 labeling index was positively correlated with ficvf and odi (r = 0.758 and 0.616), and negatively correlated with fiso and ADC (r = -0.523 and -0.703).

CONCLUSION

NODDI can effectively grade gliomas, and also showed great potential in predicting Ki-67 expression.

CLINICAL RELEVANCE/APPLICATION

NODDI offers a novel and non-invasive method in grading gliomas and to evaluate the cellular proliferation in gliomas.

SSM18-05 T2 Nerve Imaging of the Brachial Plexus Using Compressed-SENSE Effect on Image Quality and Acquisition Time

Wednesday, Nov. 28 3:40PM - 3:50PM Room: N226

Participants

Rupsa Bhattacharjee, MENG, Gurgaon, India (*Abstract Co-Author*) Nothing to Disclose Shikha Panwar, MBBS, New Delhi, India (*Presenter*) Nothing to Disclose Vasanthakumar Venugopal, MD, New Delhi, India (*Abstract Co-Author*) Nothing to Disclose Vidur Mahajan, MBBS, New Delhi, India (*Abstract Co-Author*) Nothing to Disclose Harsh Mahajan, MD, MBBS, New Delhi, India (*Abstract Co-Author*) Nothing to Disclose Indrajit Saha, PhD, Gurgaon, India (*Abstract Co-Author*) Employee, Koninklijke Philips NV

For information about this presentation, contact:

drvasanth@mahajanimaging.com

PURPOSE

In this study, compressed sensing is combined with the parallel-imaging or SENSE infrastructure, i.e., Compressed-SENSE (CSENSE),

for accelerating anatomical MR data acquisition by exploiting the multi-element receiver coil sensitivity variation and sparsity constraining. We quantitatively evaluate the dual role of CSENSE imaging in reducing scan time without loss in resolution and in improving resolution with minimal increase in scan time.

METHOD AND MATERIALS

Ten healthy volunteers were scanned on a 3.0T MRI (Ingenia, Philips) using a proprietary "3D NerveView Sequence" (NVS), a T2W TSE isotropic sequence (TR 2200, TE 170, 2 mm slice thickness). Three versions of NVS were developed, SEQ1 (no CSENSE), SEQ2 (CSENSE factor = 9) and SEQ3 (CSENSE factor = 9) with acquisition times 6:16, 3:22 and 8:19 minutes respectively. SEQ1 and SEQ2 had the same acquisition and recon matrix of 252X325 and 640X640 while SEQ3 had a higher resolution having acquisition and recon matrix of 316X414 and 720X720 respectively. Contrast-to-Noise Ratio (CNR) was measured in all at the levels of the nerve roots (C5 to T1 levels), trunks and cords using Shinkei's formula of CNR = (SI-Nerve - SI-Muscle)/ (SI-Nerve + SI-Muscle) where SI is average Signal Intensity in the region.

RESULTS

There was no significant difference in CNR for roots in all three sequences, i.e. SEQ1 - 0.7102±0.102, SEQ2 - 0.7040±0.044 and SEQ3 - 0.7253±0.035. In the trunks, SEQ3 performed as well as SEQ1 with a CNR of 0.567±0.10 against 0.5497±0.09. SEQ2 had a lower CNR of 0.4843±0.11. At the level of cords, SEQ1 outperformed both SEQ2 and SEQ3 with a CNR of 0.4248±0.17 against 0.3079±0.11 and 0.3505±0.19 respectively. We note that CSENSE performs better in areas where average CNR is on the higher side.

CONCLUSION

While CSENSE gives radiologists flexibility of reducing time or increasing resolution, the decision of when and how to use CSENSE depends on the clinical context. It can be used to reduce scan time when root lesions are suspected and improve resolution when lesions of the trunks and cords are suspected.

CLINICAL RELEVANCE/APPLICATION

Compressed Sensing for nerve imaging should be part of every radiologist and technologists' arsenal to conduct patient-specific personalised scanning. Lower scan time leads to improved patient comfort and hence less motion artefacts, and higher resolution improves diagnostic accuracy of the scan.

SSM18-06 Visualization of the Peripheral Branches of the Mandibular Nerve Using a Micro Surface Coil and Three-Dimensional Double-Echo Steady-State with Water Excitation Sequence

Wednesday, Nov. 28 3:50PM - 4:00PM Room: N226

Participants

Guixun Hong, MD, Guangzhou, China (*Presenter*) Nothing to Disclose Zhiyun Yang, Guangzhou, China (*Abstract Co-Author*) Nothing to Disclose

PURPOSE

To investigated the detectability of the branches of the mandibular nerve on a three-dimensional double-echo steady-state with water excitation sequence using a small surface coil.

METHOD AND MATERIALS

The maxillofacial regions of 52 volunteers were scanned unilaterally by a small surface coil combined with 3D-DESS-WE sequence. According to the Gray's anatomy atlas, MPR and CPR was done according to the anatomic position of mandibular nerve and the branches, the signal characteristics of the nerves and neighboring structures were analyzed, the displaying rate of the mandibular nerves and their branches were evaluated, the image quality and display of the nerve were subjectively scored, the signal intensity(SI) of the nerve and adjacent lateral pterygoid muscle were measured, the signal intensity ratio(SIR) of mandibular nerve/lateral pterygoid muscle (SIRN/M) was calculated.

RESULTS

Compared with the muscles, the nerve showed iso signal intensity. The subjective scores for all small coil 3D-DESS-WE images were 3.02±0.82. The displaying rates of the mandibular nerve trunk, anterior trunk, buccal nerve, posterior trunk, inferior alveolar nerve and lingual nerve were all 100%. The posterior trunk, inferior alveolar nerve and lingual nerve showed the best quality scores, which were all about 3 points, and the SIRN/M were about 1. The displaying rates of the auricular temporal nerve and masseter muscle nerve were also satisfied. The displaying rate of mylohyoid muscle nerve, medial pterygoid nerve and lateral pterygoid nerve was low.

CONCLUSION

The small surface coil combine with 3D-DESS-WE sequence demonstrated excellent visualization of the extracranial branches of the mandibular nerves in most volunteers, which has the potential for diagnosing mandibular nerve pathologies and preoperatively identifying peripheral cranial nerves to prevent surgical complications.

CLINICAL RELEVANCE/APPLICATION

Small surface coil combine with 3D-DESS-WE sequence performed high-quality in mandibular nerves imaging using MPR, CPR postprocessing technology, which are suitable for clinical application.



Neuroradiology (Contrast Issues in Neuroimaging)

Wednesday, Nov. 28 3:00PM - 4:00PM Room: N227B



AMA PRA Category 1 Credit ™: 1.00 ARRT Category A+ Credit: 1.00

FDA Discussions may include off-label uses.

Participants

Alberto Bizzi, MD, Milan, Italy (*Moderator*) Nothing to Disclose Takashi Yoshiura, MD, PhD, Kagoshima, Japan (*Moderator*) Nothing to Disclose

Sub-Events

SSM19-01 The Gadolinium Deposition Debate Revisited Using a Fully Automated Big Data Approach

Wednesday, Nov. 28 3:00PM - 3:10PM Room: N227B

Participants

Julian Gehweiler, Basel, Switzerland (*Presenter*) Nothing to Disclose Thomas J. Re, MD, Princeton, NJ (*Abstract Co-Author*) Consultant, Siemens AG Michael Amann, Basel, Switzerland (*Abstract Co-Author*) Nothing to Disclose Sabine Schadelin, MSc, Basel, Switzerland (*Abstract Co-Author*) Nothing to Disclose Ruben Cabezon, Basel, Switzerland (*Abstract Co-Author*) Nothing to Disclose Bram Stieltjes, MD, PhD, Basel, Switzerland (*Abstract Co-Author*) Nothing to Disclose

For information about this presentation, contact:

julian.gehweiler@usb.ch

PURPOSE

Numerous independent studies reported increasing T1w signal intensity (SI) of the dentate nucleus (DN) and the globus pallidus (GP) after repetitive administrations of linear Gadolinium-based contrast agents (LGBCA). Also, a recent study indicates that a high number of macrocyclic GBCA (MGBCA) administrations may also lead to an increase of SI. However, most previous studies were performed at small scale and predominantly by using manual ROI-based methods. In this study, we present results from a large-scale study that uses a completely automated high performance computing pipeline.

METHOD AND MATERIALS

In-house developed PACS/RIS mining software was used to locate and retrieve all native T1W MPRAGE datasets performed on patients that received at least 2 exams with GBCA. Datasets were histogram-normalized and segmented utilizing FSL and a cerebellum atlas. Calculations were performed overnight on a high performance computing cluster. SI increase was analyzed in a mixed effects model.

RESULTS

3021 consecutive patients receiving 11,922 MRI brain scans were included. Repeated administration of GBCA was associated with increased overall SI for both LGBCA (Estimate 0.23, 95% CI 0.07-0.39, p=.006) and MGBCA (Estimate 0.06, 95% CI 0.02-0.09, p<.001). Stratified among brain nuclei, significant SI increase was found only after LGBCA application in the DN (Estimate 0.6, 95% CI 0.077-1.12, p=.027) and the GP (Estimate 0.38, 95% CI 0.03-0.72, p=.033) but not for MGBCA. On the other hand, significant SI increase was found only after MGBCA in the thalamus, putamen, amygdala, caudate, hippocampus, and accumbens (Estimates up to 0.29, p<.001) but not for LGBCA.

CONCLUSION

Our findings confirm previous reports on increased SI after LGBCA application in the DN and GP, but not after MGBCA. However, we found increase in SI for other brain nuclei only for MGBCA. Based on our findings, Gadolinium accumulation in the brain may be more widespread than assumed and could occur with the use of both L- and MGBCA.

CLINICAL RELEVANCE/APPLICATION

Gadolinium accumulation in the brain may be more widespread than assumed and could occur with the use of both L- and MGBCA.

SSM19-02 The Correlation of GD Deposition with Administration of GBCAs and the Elimination Rates in Human Brain, Bone, and Skin

Wednesday, Nov. 28 3:10PM - 3:20PM Room: N227B

Participants Nozomu Murata, MD, PhD, Tokyo, Japan (*Presenter*) Nothing to Disclose Kiyoko Murata, MD,PhD, Tokyo, Japan (*Abstract Co-Author*) Nothing to Disclose Luis F Gonzalez-Cuyar, MD, Seattle, WA (*Abstract Co-Author*) Nothing to Disclose Desiree Marshall, MD, Seattle, WA (*Abstract Co-Author*) Nothing to Disclose Daniel S. Hippe, MS, Seattle, WA (*Abstract Co-Author*) Research Grant, Koninklijke Philips NV; Research Grant, General Electric Company; Research Grant, Canon Medical Systems Corporation; Research Grant, Siemens AG Russell Dills, PhD, Seattle, WA (*Abstract Co-Author*) Nothing to Disclose Kenneth R. Maravilla, MD, Seattle, WA (*Abstract Co-Author*) Consultant, Bracco Group; Research Grant, Guerbet SA; Consultant, Guerbet SA; Advisory Board, Guerbet SA; Research Grant, Koninklijke Philips NV

For information about this presentation, contact:

b-n-murata@med.toho-u.ac.jp

PURPOSE

The purpose of this study was to determine the correlation of Gadolinium (Gd) deposition between Brain tissue ,white matter (WM),Globus Paliidus (GP),Dentate nuclueus (DN) ,and Bone,Skin in human with administration of gadolinium-based contrast agents (GBCAs) and to determine the elimination rates.

METHOD AND MATERIALS

Under the IRB approved study , medical records of decedents coming to autopsy were reviewed, 35 cases were identified that received GBCAs including 13 who received only macrocyclic agents(gadoteridol, gadobutrol) and 8 decedents only linear type of agents (gadodiamide,gadobenate, gadoxetic acid, gadoversetamide and gadopentate) and 3 with mix type of agents.(gadoteridol and gadoversetamide, gadoteridol with gadopentate and gadobenate, gadoteridol and gadobenate). All cases are with normal renal function (eGFR>60) and have more than a week from last injection to death.11 cases not exposed to a GBCA during life are included as control. Tissue from WM, GP, DN along with bone and skin were collected. Inductively coupled plasma mass spectrometry (ICP-MS) analysis was used to quantify levels of Gd in tissue. The time from last injection of GBCA to death was determined for each case. Gd levels for each subject were plotted versus time interval from last contrast administration for each agent to compare elimination rates.

RESULTS

Median Gd concentrations significantly higher in GBCA cases than controls in WM, GP and bone. (<0.001).Macrocyclic agents group showed significantly lower deposition than Linear agent groups in WM, GP, DN, Bone.(P<0.001).Gd deposition in all tissues ,WM, GP, DN, Bone, Skin were correlated with each other (rho ranging from 0.71to.86). And Bone had significantly higher deposition than all other tissues (P<0.001),whereas WM had significantly lower deposition (P<0.001).Graphical results of tissue concentration versus time from last administration showed the Macrocyclic subjects had more rapid decline and plateaued at a lower level than the linear subjects.

CONCLUSION

Gd deposition in each human tissues were correlated significantly and deposition in bone was much higher than other organs. Gd deposition with Macrocyclis agents showed more rapid elimination that appeared to plateau at a lower level of retained Gd concentration than linear agents.

CLINICAL RELEVANCE/APPLICATION

This study shows correlation of Gd deposition in human tissues with the administration of GBCAs and elimination rates.

SSM19-03 Gd Deposition in Rat and Human Cerebral Cortex After Systemic Administration of Gd-Containing Contrast Agents

Wednesday, Nov. 28 3:20PM - 3:30PM Room: N227B

Participants

Lee Goldstein, MD, PhD, Boston, MA (Presenter) Research funded, General Electric Company Stephan W. Anderson, MD, Cambridge, MA (Abstract Co-Author) Nothing to Disclose Olga Minaeva, Boston, MA (Abstract Co-Author) Nothing to Disclose Ning Hua, PhD, Boston, MA (Abstract Co-Author) Nothing to Disclose Nicola Lupoli, Boston, MA (Abstract Co-Author) Nothing to Disclose Erich Franz, BS, Boston, MA (Abstract Co-Author) Nothing to Disclose Mark Wojnarowicz, PhD, Boston, MA (Abstract Co-Author) Nothing to Disclose Allison Griffin, Washington, DC (Abstract Co-Author) Nothing to Disclose Victor Alvarez, Bedford, MA (Abstract Co-Author) Nothing to Disclose Sarah Rind, Boston, MA (Abstract Co-Author) Nothing to Disclose Audrey Hildebrandt, Boston, MA (Abstract Co-Author) Nothing to Disclose Chad W. Farris, MD, PhD, Boston, MA (Abstract Co-Author) Nothing to Disclose Juliet Moncaster, PhD, Boston, MA (Abstract Co-Author) Nothing to Disclose Hernan Jara, PhD, Boston, MA (Abstract Co-Author) Inventor, Boston University Ali Guermazi, MD, PhD, Boston, MA (Abstract Co-Author) Shareholder, Boston Imaging Core Lab, LLC; Research Consultant, Merck KGaA; Research Consultant, sanofi-aventis Group; Research Consultant, TissueGene, Inc; Research Consultant, OrthoTrophix, Inc; Research Consultant, AstraZeneca PLC ; Research Consultant, General Electric Company ; Research Consultant, Pfizer Inc Asim Z. Mian, MD, Cambridge, MA (Abstract Co-Author) Stockholder, Boston Imaging Core Lab, LLC; Consultant, Median Technologies Bertrand Huber, MD, PhD, Boston, MA (Abstract Co-Author) Nothing to Disclose Ann McKee, Boston, MA (Abstract Co-Author) Nothing to Disclose Lawrence L. Latour, PhD, Bethesda, MD (Abstract Co-Author) Nothing to Disclose Jorge A. Soto, MD, Boston, MA (Abstract Co-Author) Royalties, Reed Elsevier

For information about this presentation, contact:

huaning@bu.edu

PURPOSE

While Gd accumulation in the deep cerebellar nuclei (DCN) and globus pallidus (GP), has received considerable attention, Gd accumulation in the cerebral cortex remains poorly characterized and of potential clinical concern given the central role of the

cortex in cognition, affect, and behavior. The purpose of this study was to analyze the degree and distribution of Gd deposition in the cortex. The study utilized high-resolution metallomic imaging mass spectrometry (MIMS) to anatomically localize and analytically quantify Gd in postmortem brains from rats and humans.

METHOD AND MATERIALS

IACUC/IRB protocols approved at our institute. Sprague-Dawley rats received Magnevist (dose: 2.4mmol/Kg x 3 times, IV) or volume-matched saline(control). Harvested brains fixed with 4% PFA. Human brain specimens (n=3) were analyzed, two specimens from subjects with antemortem Gd exposure and a third from a control subject without Gd exposure. MIMS was performed using a quadrupole ICP-MS (Thermo Scientific) custom hyphenated to a Nd-YAG laser ablation system. Calibration was performed with matrix-matched standards and NIST reference standard (SRM 612).

RESULTS

We detected non-homogeneous Gd retention in rat brain after Gd exposure. Cortical Gd accumulation was far greater in gray matter than adjacent white matter. We detected variation in Gd accumulation by cortical subregion (cingulate=medial prefrontal>piriform>insular>motor) and cortical layer (layers II-III>>layerI>layers V,VIa,sVib) and subcortical structures (caudateputamen, GP, DCN>olfactory tubercle>nucleus accumbens). Gd accumulation also varied by cortex type: agranular>dysgranular. We confirmed Gd accumulation with long post-exposure retention in human cortex.

CONCLUSION

Gd is retained in cerebral cortex after systemic Gd administration. Cortical Gd deposition is non-uniform and demonstrates regional, laminar, type variation. Gd accumulation in human cerebral cortex and persists long after Gdexposure and washout. These results raise concern about possible long-term functional effects of Gd accumulation in the brain.

CLINICAL RELEVANCE/APPLICATION

Our results suggest that Gd deposits not only in deep gray matter, but also in specific regions in cerebral cortex. As the cerebral cortex exerts a large influence on brain function and behavior, our study suggests that additional clinical/pre-clinical studies should be conducted and focused on the cortex.

Honored Educators

Presenters or authors on this event have been recognized as RSNA Honored Educators for participating in multiple qualifying educational activities. Honored Educators are invested in furthering the profession of radiology by delivering high-quality educational content in their field of study. Learn how you can become an honored educator by visiting the website at: https://www.rsna.org/Honored-Educator-Award/ Stephan W. Anderson, MD - 2018 Honored EducatorJorge A. Soto, MD - 2013 Honored EducatorJorge A. Soto, MD - 2014 Honored EducatorJorge A. Soto, MD - 2017 Honored EducatorJorge A. Soto, MD - 2018 Honored EducatorJorge A. Soto, MD - 2017 Honored EducatorJorge A. Soto, MD - 2018 Honored EducatorHernan Jara, PhD - 2014 Honored EducatorAli Guermazi, MD, PhD - 2012 Honored Educator

SSM19-04 Evaluation of Chelating Agent Administration Following Exposure to Gadolinium-Based Contrast Agents in Rats

Wednesday, Nov. 28 3:30PM - 3:40PM Room: N227B

Participants

Janina Boyken, Berlin, Germany (*Abstract Co-Author*) Nothing to Disclose Thomas Frenzel, PhD, Berlin, Germany (*Abstract Co-Author*) Employee, Bayer AG Gregor Jost, PhD, Berlin, Germany (*Abstract Co-Author*) Employee, Bayer AG Gunnar Schuetz, Berlin, Germany (*Abstract Co-Author*) Employee, Bayer AG Hubertus Pietsch, PhD, Berlin, Germany (*Presenter*) Employee, Bayer AG

PURPOSE

This study investigates the efficacy of the chelating agent calcium trisodium pentetate (Ca-DTPA) on the urinary excretion and presence of gadolinium (Gd) in the brain after single administration of gadodiamide and gadobutrol in rats.

METHOD AND MATERIALS

Rats received either a single injection of gadodiamide, gadobutrol (1.8 mmol/kg, n=18 per group) or saline. 7 weeks after GBCA injection, 6 animals of each group were sacrificed prior to chelation treatment. The remaining 12 animals received either 3 infusions of Ca-DTPA (180 μ mol/kg, once weekly) or saline. Urine was collected daily for 3 days following each infusion. Gd measurements by ICP-MS were performed in urine and tissue samples obtained prior and post treatment.

RESULTS

After a Gd-free period of 7 weeks, urinary excretion of Gd under physiological conditions (saline infusion) was still observed for gadobutrol (sum of Gd in all urine samples: 33 ± 12 nmol Gd, p <= 0.0005) but not gadodiamide (10 ± 4 nmol Gd, p=0.68) when compared to animals which initially received a saline injection instead of GBCA (5 ± 5 nmol Gd). Ca-DTPA increased the urinary excretion of Gd originating from gadodiamide (114 ± 21 nmol Gd), but not from gadobutrol (30 ± 11 nmol Gd). The highest Gd brain concentration in nmol/g tissue was present in the cerebellum after injection of gadodiamide (0.55 ± 0.07), which was partially reduced by Ca-DTPA (0.47 ± 0.08 , p=0.015). The cerebellar Gd concentration from gadobutrol was 20-fold lower (0.024 ± 0.006) and unaffected by Ca-DTPA (0.027 ± 0.017).

CONCLUSION

Administration of a chelating agent increased the urinary excretion and partial elimination of the residual Gd in brain tissue originating from gadodiamide but not from gadobutrol. This indicates a pool among the chemical Gd forms present in the rat brain and other organs that can be mobilized and excreted by Ca-DTPA after the use of linear gadodiamide. The lower Gd tissue concentrations found for macrocyclic gadobutrol were associated with a continuous physiological urinary excretion which was not influenced by Ca-DTPA, indicating that this Gd represents the intact gadobutrol.

CLINICAL RELEVANCE/APPLICATION

 $\label{eq:chelation} \mbox{Chelation treatment efficacy is dependent on the administered GBCA class.}$

SSM19-05 Experimental Sepsis Increases Brain Deposition of Gadolinium in the Rat

Wednesday, Nov. 28 3:40PM - 3:50PM Room: N227B

Participants Nik Damme, MD, Salt Lake City, UT (*Presenter*) Nothing to Disclose Rheal A. Towner, PhD, Oklahoma City, OK (*Abstract Co-Author*) Nothing to Disclose John M. Hoffman, MD, Salt Lake City, UT (*Abstract Co-Author*) Research Grant, General Electric Company; Research Grant, Blue Earth Diagnostics Ltd Kathryn A. Morton, MD, Salt Lake City, UT (*Abstract Co-Author*) Nothing to Disclose

For information about this presentation, contact:

kathryn.morton@hsc.utah.edu

PURPOSE

There is emerging concern that gadolinium based contrast agents (GBCA) may undergo dechelation, leading to deposition of potentially neurotoxic Gd3+ in the brain. Because GBCA do not cross an intact BBB, disruption of the BBB may result in enhanced deposition of Gd in the brain. We have previously reported that a lipopolysaccharide (LPS) endotoxemia sepsis model in rats results in secondary neuroinflammation, increased cerebral blood flow and blood brain barrier permeability. Septic patients often have neurocognitive compromise and frequently undergo CEMR. The purpose of this study was to determine whether experimental sepsis results in increased Gd deposition in the brain.

METHOD AND MATERIALS

Male Sprague Dawley rats (250 g) were injected intraperioneally with 10 mg/kg LPS. Control animals received no injection. 24h later, 100 ul of gadobenate dimeglumine (MultiHance®) MRI contrast was injected intravenously. The brains were harvested at 1 h, 24 h, 1 week, 3 weeks and 6 weeks post GBCA administration. Gd content in the brain was measured by inductively coupled plasma mass spectroscopy.

RESULTS

At 1 h post injection of GBCA, there was 56% greater content of Gd in the brain of LPS animals than controls. At 1 week, 3 weeks and 6 weeks post GBCA administration, further decreases in Gd content in the brains of both LPS-treated and control rats occurred, but at a much slower rate than between 1 h and 24 h. The percent of initial (1 h) Gd in the brain of LPS treated rats was 3.2% at 24 h, 2.7% at 1 week, 2.3% at 3 weeks and 2.3% at 6 weeks. At all time points beyond 1 h, there were statistically significant increases in the content of Gd in the brains of LPS-treated animals when compared to controls. LPS:control ratios of brain Gd were 3.2 at 24 h, 1.9 at 1 week, 2.4 at 3 weeks and 2.4 at 6 weeks.

CONCLUSION

When GBCA is administered to septic rats, there is a significantly higher deposition of Gd in the brain compared to control rats. In both LPS and control rats, the brain retains substantial Gd even at 6 weeks post GBCA injection.

CLINICAL RELEVANCE/APPLICATION

Consideration should be given to avoidance of GBCA in vulnerable patients who may have an increase in blood brain barrier permeability.

SSM19-06 Screening for Gadolinium Brain Retention in Patients Receiving Multiple Doses of Gadobutrol in a University Medical Center Over 10 Years

Wednesday, Nov. 28 3:50PM - 4:00PM Room: N227B

Participants

Tobias Baeuerle, MD, Erlangen, Germany (*Presenter*) Research Grant, Bayer AG Alexandra Schmidle, Erlangen, Germany (*Abstract Co-Author*) Nothing to Disclose Markus Kopp, Erlangen, Germany (*Abstract Co-Author*) Nothing to Disclose Jannis Hanspach, Erlangen, Germany (*Abstract Co-Author*) Nothing to Disclose Tobias Hepp, Erlangen, Germany (*Abstract Co-Author*) Nothing to Disclose Arnd R. Doerfler, MD, Erlangen, Germany (*Abstract Co-Author*) Nothing to Disclose Frederik B. Laun, Erlangen, Germany (*Abstract Co-Author*) Nothing to Disclose Frederik B. Laun, Erlangen, Germany (*Abstract Co-Author*) Nothing to Disclose Bureau, Bayer AG Research Grant, Siemens AG Marc Saake, Erlangen, Germany (*Abstract Co-Author*) Nothing to Disclose

For information about this presentation, contact:

tobias.baeuerle@uk-erlangen.de

PURPOSE

Purpose was to screen a large MRI population for the frequency of applied doses of gadobutrol in patients with normal and impaired kidney function and to recall selected individuals for assessment of gadolinium brain retention.

METHOD AND MATERIALS

The database of the University Hospital Erlangen, Germany was searched for patients receiving gadobutrol between 2007 and 2017 and not any other intravenous MRI contrast agent in the patients' history. Patients with at least 5 (range 5-20) contrast-enhanced MRI scans and normal kidney function (group 1) and at least 1 (range 1-9) contrast-enhanced MRI scans and impaired kidney function (group 2) were matched with control patients receiving no MRI contrast agent before (groups 3 and 4). The aim was to recall all individuals from groups 1-4 performing the following brain MRI protocol: T1w morphology, T1/T2 mapping and quantitative susceptibility mapping (QSM).

Between 2007 and 2017, more than 35.000 patients at our institution received up to 26 single doses of gadobutrol only. Of these, 701, 1239, 94 and 409 patients matched the criteria of groups 1-4, respectively. After recalling 2.444 individuals, we were able to perform brain MRI in 220 individuals (groups 1-4: 76, 84, 25, 35, respectively). In the study population, no significant differences in T1w signal intensity ratios, T1/T2 mapping and QSM were found in the dentate nucleus and globus pallidus between patients of groups 1 and 2 and the matched controls.

CONCLUSION

In this recall study, we found no statistical evidence for gadolinium brain retention after administration of multiple doses of gadobutrol in patients with normal and impaired kidney function.

CLINICAL RELEVANCE/APPLICATION

To the best of our knowledge, here we present the first recall study on gadolinium brain retention in a large cohort of patients receiving multiple doses of gadobutrol and no other MRI contrast agent.



Pediatrics (Interventional Radiology)

Wednesday, Nov. 28 3:00PM - 4:00PM Room: E260



AMA PRA Category 1 Credit ™: 1.00 ARRT Category A+ Credit: 1.00

FDA Discussions may include off-label uses.

Participants

Kamlesh U. Kukreja, MD, Bellaire, TX (*Moderator*) Nothing to Disclose Anne Marie Cahill, MBBCh, Philadelphia, PA (*Moderator*) Nothing to Disclose

Sub-Events

SSM20-01 A Single Center Experience of Gastrojejunosomy Tube Interventions: Comparison of Manufacturers and Complications

Wednesday, Nov. 28 3:00PM - 3:10PM Room: E260

Participants

Daniel J. Ashton, MD, Houston, TX (*Abstract Co-Author*) Nothing to Disclose Shireen Hayatghaibi, MA, MPH, Houston, TX (*Presenter*) Nothing to Disclose Varshana Gurusamy, MD, Houston, TX (*Abstract Co-Author*) Nothing to Disclose Joanna Slover, The Woodlands, TX (*Abstract Co-Author*) Nothing to Disclose Kristin Lingle, The Woodlands, TX (*Abstract Co-Author*) Nothing to Disclose

PURPOSE

Report single insititution experience of interventions related to gastrojejunostomy tubes, their complications, and comparison of complication rates between gastrojejunostomy tube types and manufacturers.

METHOD AND MATERIALS

379 patients with a gastrojejunostomy tube (GJ tube) were retrospecitively reviewed from January 2016 through February 2018. PACS and electronic medical records were reviewed for GJ tube exchanges or conversions. Date of procedure, indication for procedure, complications associated with the GJ tube, GJ tube specifics, and patient demographics were entered into a HIPAA compliant database. Complications were defined as GJ tube condition that necessitated urgent exchange or conversion. Comparisons of complications were made using chi-square test between GJ tube length and manufacturer.

RESULTS

There were 1,792 interventions during the study period, with 641 conversions (35.8%) and 1151 (64.2%) exchanges performed in 379 patients. There were 810 GJ tubes from Applied Medical Technology, Inc (Brecksville, Oh), and 834 from Halyard (Alpharetta, Ga). Patients presented as outpatients (65.3%) through the emergency center (9.2%) or as inpatients (25.5%). There were 595 (53.5%) GJ tubes exchanged as routine, and there were 176 (27.9%) initial conversions, comprising 43% of interventions. 57% exchanges and conversions were performed due to complication. There was no difference between manufacturers and overall complications (p=0.243 for exchanges; p=0.821 for conversions). There was a significant difference between complication and tube length (p=0.000054), with 15 cm length tubes having a complication rate of 52%, 22 cm of 40%, 30 cm of 44%, and 45 cm of 63%.

CONCLUSION

Gastrojejunostomy tubes are frequently replaced urgently do to tube malfunction or malposition, with increased rates seen in 15 cm and 45 cm length tubes. There is no difference between manufacturers for overall complications.

CLINICAL RELEVANCE/APPLICATION

GJ tubes have a high frequncey of complication, highlighting an area for significant quality improvement.

SSM20-02 Early Experience on the Impact of Contrast-Enhanced Ultrasound in Drainage Catheter Placement and Management

Wednesday, Nov. 28 3:10PM - 3:20PM Room: E260

Awards

Student Travel Stipend Award

Participants

Aditi S. Hendi, MD, Philadelphia, PA (*Presenter*) Nothing to Disclose Sphoorti Shellikeri, Philadelphia, PA (*Abstract Co-Author*) Nothing to Disclose Fernando A. Escobar, MD, Pittsburgh, PA (*Abstract Co-Author*) Nothing to Disclose Seth Vatsky, DO, Phoenix, AZ (*Abstract Co-Author*) Nothing to Disclose Susan J. Back, MD, Philadelphia, PA (*Abstract Co-Author*) Consultant, Bracco Group; Grant, Bracco Group Sudha A. Anupindi, MD, Philadelphia, PA (*Abstract Co-Author*) Nothing to Disclose Kassa Darge, MD, PhD, Philadelphia, PA (*Abstract Co-Author*) Nothing to Disclose Michael R. Acord, MD, Boston, MA (*Abstract Co-Author*) Nothing to Disclose Abhay S. Srinivasan, MD, Houston, TX (*Abstract Co-Author*) Nothing to Disclose Anne Marie Cahill, MBBCh, Philadelphia, PA (*Abstract Co-Author*) Nothing to Disclose

For information about this presentation, contact:

hendia@email.chop.edu

PURPOSE

To describe use of contrast-enhanced ultrasound (CEUS) in aiding drainage catheter management in children.

METHOD AND MATERIALS

An IRB-approved retrospective review identified13 drainage catheter procedures in which contrast-enhanced ultrasound (CEUS) prompted changes in management by illuminating the need for additional treatment or cessation thereof.

RESULTS

13 patients underwent drainage catheter placement with concurrent intracavitary contrast-enhanced ultrasound (CEUS). 6 abscess catheters were injected, revealing: noncommunicating locules in 2 of 6 cases (one inaccessible and one requiring an additional drain), safe accessibility in 3 of 6 cases with communicating locules without need for additional catheter, and confirmation of fistula to small bowel in a Crohn's patient in 1 of 6 cases. Simultaneous CEUS cholangiogram though a cholecystostomy tube and percutaneous biliary drain in a presumed case of Mirizzi syndrome showed patency of both the common bile and cystic ducts leading to catheter removal. CEUS injection in 1 chest tube showed multiseptated pleural effusion requiring t-PA via the drain, later shown at bedside with CEUS to have achieved complete lysis of septations. Injection of a catheter in a large renal cyst showed no connection to the collecting system where there was concern for urinoma and calyceal rupture, leading to drain removal. Injection of a sinus tract and cecostomy tube in a patient with peristomal leak showed an enterocutaneous fistula, requiring catheter placement through the fistula to promote diversion and healing. CEUS in 3 sclerotherapy cases showed adequate distribution of sclerosant in one lymphatic malformation and an inaccessible small, noncommunicating moiety of a second lymphatic malformation left untreated. In a third case, no connection was seen between a renal cyst and the renal collecting system, allowing for safe sclerotherapy. No adverse reaction to the agent occured.

CONCLUSION

CEUS is an adjunctive imaging modality allowing real-time catheter-directed provision of additional or cessation of medical treatment while reducing radiation dose to the patient.

CLINICAL RELEVANCE/APPLICATION

Intracavitary CEUS administration via drainage catheters can help in identifying clinical situations in the IR suite and at bedside where addition or cessation of treatment will improve patient outcome and shorten the time to drainage catheter removal while reducing radiation dose to the patient.

Honored Educators

Presenters or authors on this event have been recognized as RSNA Honored Educators for participating in multiple qualifying educational activities. Honored Educators are invested in furthering the profession of radiology by delivering high-quality educational content in their field of study. Learn how you can become an honored educator by visiting the website at: https://www.rsna.org/Honored-Educator-Award/ Kassa Darge, MD,PhD - 2016 Honored Educator

SSM20-03 Early Experience: Periprocedural Contrast-Enhanced Ultrasound Guidance in Targeted Soft Tissue and Organ Biopsy

Wednesday, Nov. 28 3:20PM - 3:30PM Room: E260

Participants

Aditi S. Hendi, MD, Philadelphia, PA (*Presenter*) Nothing to Disclose Sphoorti Shellikeri, Philadelphia, PA (*Abstract Co-Author*) Nothing to Disclose Seth Vatsky, DO, Phoenix, AZ (*Abstract Co-Author*) Nothing to Disclose Fernando A. Escobar, MD, Pittsburgh, PA (*Abstract Co-Author*) Nothing to Disclose Susan J. Back, MD, Philadelphia, PA (*Abstract Co-Author*) Nothing to Disclose Sudha A. Anupindi, MD, Philadelphia, PA (*Abstract Co-Author*) Nothing to Disclose Kassa Darge, MD,PhD, Philadelphia, PA (*Abstract Co-Author*) Nothing to Disclose Michael R. Acord, MD, Boston, MA (*Abstract Co-Author*) Nothing to Disclose Abhay S. Srinivasan, MD, Houston, TX (*Abstract Co-Author*) Nothing to Disclose Anne Marie Cahill, MBBCh, Philadelphia, PA (*Abstract Co-Author*) Nothing to Disclose

For information about this presentation, contact:

hendia@email.chop.edu

PURPOSE

To show that contrast-enhanced ultrasound (CEUS) may be leveraged during targeted soft tissue and organ biopsy to improve pathologic yield and differentiate benign from malignant lesions.

METHOD AND MATERIALS

An IRB-approved retrospective review identified 19 lesions biopsied with CEUS guidance in patients aged 2 mo to 19 years with median weight 30 kg (range 3.6-107 kg). Outcomes included concordance of CEUS enhancement with pathology and ability to differentiate benign from malignant lesions equal to or better than MRI. Concordance was defined as agreement between enhancement pattern and pathology diagnosis.

RESULTS

10 coft ticcus and organ based losions bionsid with CEUS guidance were reviewed. Bionsy or CEUS avaluation was recommended

If solit tissue and organ-based lesions biopsied with CEOS guidance were reviewed. Diopsy of CEOS evaluation was recommended on pre-biopsy MRI in 18 cases. One patient with known lymphoma had a new hypermetabolic lesion on PET/CT requiring biopsy. Hyperenhancing areas of biopsy targets on CEUS correlated with hypermetabolic areas on PET, aiding accurate needle placement in high yield parts of lesions. There was concordance of CEUS enhancement pattern with pathologic diagnosis in 18 lesions (11 malignant and 7 benign). In the only discordant CEUS case, enhancement on both MRI and CEUS was concerning for malignancy showing brisk arterial enhancement with early washout, however pathology showed benign hepatic fibrosis. MRI enhancement patterns were discordant with pathology results in 3 of 18 lesions. Of those, 2 showed enhancement on CEUS which was concordant with pathology. Diagnostic specimens were obtained in all 19 cases. No adverse reactions to the contrast agent occurred.

CONCLUSION

Peri-procedural CEUS can further differentiate benign from malignant soft tissue and organ-based lesions and aids in their biopsy. In the future, this modality could reduce cost in the work-up of focal lesions requiring tissue diagnosis. Additional studies need to be performed to validate use of CEUS in pediatric biopsies.

CLINICAL RELEVANCE/APPLICATION

CEUS has equal or better lesion characterization compared to MRI and early experience shows it can be a powerful tool in biopsy guidance.

Honored Educators

Presenters or authors on this event have been recognized as RSNA Honored Educators for participating in multiple qualifying educational activities. Honored Educators are invested in furthering the profession of radiology by delivering high-quality educational content in their field of study. Learn how you can become an honored educator by visiting the website at: https://www.rsna.org/Honored-Educator-Award/ Kassa Darge, MD,PhD - 2016 Honored Educator

SSM20-04 Image Guided Sacroiliac Steroid Joint Injections in Children

Wednesday, Nov. 28 3:30PM - 3:40PM Room: E260

Participants

Racha Chamlati, Toronto, ON (*Presenter*) Nothing to Disclose Bairbre L. Connolly, MD, Toronto, ON (*Abstract Co-Author*) Nothing to Disclose Ronald Laxer, MD, Toronto, ON (*Abstract Co-Author*) Nothing to Disclose Jennifer Stimec, MD, Toronto, ON (*Abstract Co-Author*) Nothing to Disclose Shirley M. Tse Sr, MD, Toronto, ON (*Abstract Co-Author*) Nothing to Disclose Dimitri A. Parra, MD, Toronto, ON (*Abstract Co-Author*) Nothing to Disclose

PURPOSE

Image guided sacroiliac (SI) joint injections are frequently requested in pediatric patients with sacroilitis, which is characterized by the inflammation of SI joints (+/- adjacent tissues) and it is commonly seen in enthesitis-related arthritis (ERA), a subtype of juvenile idiopathic arthritis (JIA). The treatment involves systemic therapy with or without corticosteroid joint injections. The aim of this study is to evaluate our experience performing SI joint injections in children in terms of indications, technique and efficacy.

METHOD AND MATERIALS

This is a retrospective study of all patients that were referred to the department of Image Guided Therapy for SI joint steroid injections (Jan 2004 - Jan 2018). Patient demographis and clinical histories were collected from Electronic Patient Charts (EPC) and procedural details from our Picture Archiving and Communication System (PACS).

RESULTS

51 patients underwent SI joint injections during the time of the study, 35 were boys (68.6%). Mean age was 13.8 y/o (8-18 y/o). The most common etiology was JIA (82.4%) followed by inflammatory bowel disease (13.7%). 78% had bilateral injections and 22% unilateral (45.5% Left; 54.5% Right). All procedures were technically successful. 78% of patients received general anesthetics and 22% sedation, The steroid of choice was triamcinolone hexacetonide (20 mg most common dose). Needle guidance and confirmation was done with CT fluroscopy in 55% and Cone Beam CT in 45%. Ultrasound was used in the initial needle guidance in 33.3%. 40 patients had long term follow up. 21 (52.5%) documented clinical improvement. 26 patients had a pre and post-procedure MRI, with 81% showing improvement based on imaging findings. No complications were encountered.

CONCLUSION

Image guided SI joint injections is a safe and technically feasible procedure in children. In our cohort, the majority of patients showed clincal and imaging improvement post procedure. Cone beam CT is our current imaging modality of choice for this intervention.

CLINICAL RELEVANCE/APPLICATION

This study will provide evidence and guidance to (pediatric) interventional radiologist performing SI joint injections in children.

SSM20-05 Recurrent Pediatric Thyroid Cancer: Diagnosis and Treatment Dilemma

Wednesday, Nov. 28 3:40PM - 3:50PM Room: E260

Awards

Student Travel Stipend Award

Participants

Zachary S. Jeng, MD, Houston, TX (*Presenter*) Nothing to Disclose Alberto J. Hernandez, MD, Galveston, TX (*Abstract Co-Author*) Nothing to Disclose Kevin J. Chiou, Houston, TX (*Abstract Co-Author*) Nothing to Disclose Jessica A. Brown, MS, Houston, TX (*Abstract Co-Author*) Nothing to Disclose Katelyn Burch, Houston, TX (*Abstract Co-Author*) Nothing to Disclose Raphael J. Yoo, MD,MS, Houston, TX (*Abstract Co-Author*) Nothing to Disclose

For information about this presentation, contact:

jeng@bcm.edu

PURPOSE

Analyze the experience of a tertiary pediatric referral center with biopsy for recurrent thyroid cancer in children for a planned, future prospective trial using other minimally invasive techniques for treatment.

METHOD AND MATERIALS

278 thyroid biopsies were performed from 2004 to 2018. 25 biopsies were performed specifically for recurrent thyroid cancer in 18 patients (5 males, 13 females) with a total of 38 lesions sampled. 3 patients underwent 2 biopsies with 1 patient undergoing 5 biopsies. Age and weight at time of biopsy ranged from 13 y, 3 mo to 19 y 11, mo (median 17 yr) and from 33 kg to 124 kg (median 69.2 kg). 17 patients had a prior diagnosis of papillary thyroid cancer while 1 patient had a diagnosis of medullary thyroid cancer.

RESULTS

The technical success rate and diagnostic yield were both 100%. There were no complications. 25/38 (66%) of sampled lesions were malignant while 13/38 (34%) were benign. 20/25 (80%) of biopsies were malignant while 5/25 (20%) were benign. Benign and malignant lesions were evaluated based on size and TIRADS imaging criteria (composition, echogenicity, borders, calcifications, vascularity, shape, and punctate echogenic foci). Size was assessed using the Wilcoxon rank test and imaging characteristics were assessed using the Fisher's exact test with no significant difference between malignant and benign lesions. 7 patients have since undergone repeat surgery with the rest remaining on surveillance with suppressive thyroid hormone therapy.

CONCLUSION

Children who have had thyroidectomy and lateral neck dissection represent a surgical dilemma with early recurrence due to the difficulty of reoperation in an already treated field. No specific imaging criteria (including TIRADS) can easily distinguish between benign and malignant nodules in the surgical bed. FNA reliably provides accurate diagnosis of early recurrent thyroid carcinoma. When small lesions are confidently confirmed as recurrent disease, percutaneous treatments such as High Intensity Focused Ultrasound (HIFU) and Radiofrequency Ablation (RFA) may be a feasible alternative to a more complicated surgical approach.

CLINICAL RELEVANCE/APPLICATION

Recurrent pediatric thyroid cancer presents a surgical dilemma. FNA provides an accurate diagnosis of recurrence. Alternative minimally invasive methods for treatment (HIFU, RFA) should be considered

SSM20-06 Minimally Invasive CT- and US-Guided Biopsies of Mediastinal Masses in Pediatric Patients in a Large Pediatric Hospital

Wednesday, Nov. 28 3:50PM - 4:00PM Room: E260

Awards

Student Travel Stipend Award

Participants

Thomas Shum, PhD, Houston, TX (*Presenter*) Patent holder, Immunotherapy Heather Cleveland, BS, Houston, TX (*Abstract Co-Author*) Nothing to Disclose Alex Chau, MD, New Hyde Park, NY (*Abstract Co-Author*) Nothing to Disclose Alberto J. Hernandez, MD, Galveston, TX (*Abstract Co-Author*) Nothing to Disclose Norma Quintanilla, Houston, TX (*Abstract Co-Author*) Nothing to Disclose Hao Wu, Houston, TX (*Abstract Co-Author*) Nothing to Disclose Darryl Kinnear, Houston, TX (*Abstract Co-Author*) Nothing to Disclose

PURPOSE

Tissue diagnosis of mediastinal masses remains essential for directing subsequent medical or surgical management of patients. Minimally invasive procedures utilizing CT and ultrasound guidance are an alternative method to obtain biopsies, in comparison to open surgical approaches. However, analysis of procedural correlates associated with minimally invasive mediastinal biopsies such as sampling adequacy, patient risk level, and complications remain largely anecdotal.

METHOD AND MATERIALS

We therefore reviewed 25 mediastinal biopsy cases performed at the Texas Children's Hospital in which the procedure was performed before surgical intervention.

RESULTS

Risk characterization in patients: A number of patients demonstrated pre-existing compression of mediastinal structures that are known to increase risk for surgery and anesthesia, including airway (10/25), superior vena cava (8/25), pulmonary vessel (4/25), heart (2/5), and aorta (1/25). Pericardial effusions were found in 2/25 patients and pleural effusions were found in 5/25 patients. Atelectasis was detected in 7/25 patients. Results: The majority of the cases were located in the anterior mediastinum (80%), whereas 4% were in the middle mediastinum, and 16% in the posterior mediastinum. In 22/25 patients, biopsy samples had adequate tissue content for pathological diagnosis using histology and/or flow cytometry. In the three patients with inadequate biopsies, 2/3 patients required subsequent surgeries to gain additional tissue for definitive diagnosis, of which only 1/2 generated a different pathological diagnosis. Four patients had pre-existing airway compression. Minor complications were found in 3 patients post-procedure, which consisted of trace pneumothorax detected in 2 patients and minimal hemorrhage at the biopsy site in 1 patient, all of which resolved without need for further intervention.

CONCLUSION

Our data with CT- and US-guided mediastinal biopsies in a large quaternary pediatric treatment center show that it is a feasible method as a first-line for obtaining biopsies for definitive pathological diagnosis with minimal complications, even in patients with pre-existing risk factors for surgical intervention

This will increase feasibility and speed of clinical diagnosis.



SSM21

Physics (Photon-Counting CT)

Wednesday, Nov. 28 3:00PM - 4:00PM Room: S104B

СТ РН

AMA PRA Category 1 Credit ™: 1.00 ARRT Category A+ Credit: 1.00

FDA Discussions may include off-label uses.

Participants

Guang-Hong Chen, PhD, Madison, WI (*Moderator*) Research funded, General Electric Company Research funded, Siemens AG Katsuyuki Taguchi, PhD, Baltimore, MD (*Moderator*) Research Grant, Siemens AG; Consultant, JOB Corporation

Sub-Events

SSM21-01 Improving Iodine Contrast to Noise Ratio on a Whole-Body Photon-Counting-Detector CT System using Virtual Mono-Energetic Imaging and Spectral Prior Image Constrained Compressed Sensing

Wednesday, Nov. 28 3:00PM - 3:10PM Room: S104B

Participants

Shengzhen Tao, Rochester, MN (*Presenter*) Nothing to Disclose Kishore Rajendran, PhD, Rochester, MN (*Abstract Co-Author*) Nothing to Disclose Wei Zhou, PhD, Rochester, MN (*Abstract Co-Author*) Nothing to Disclose Cynthia H. McCollough, PhD, Rochester, MN (*Abstract Co-Author*) Research Grant, Siemens AG Shuai Leng, PHD, Rochester, MN (*Abstract Co-Author*) License agreement, Bayer AG

For information about this presentation, contact:

leng.shuai@mayo.edu

PURPOSE

Virtual mono-energetic images (VMIs) at lower keV can improve iodine contrast but have increased noise. For photon-countingdetector (PCD)-CT, spatio-spectral data redundancy exists between VMIs and the low-energy threshold (TL) images, which are reconstructed using all available photons and have the lowest noise. Here, we develop a denoising technique named spectral image constrained compressed sensing (SPICCS) that exploits this data redundancy to denoise VMIs and improve iodine contrast-to-noise ratio (CNR).

METHOD AND MATERIALS

A multi-energy CT phantom (Sun Nuclear) and iodine inserts of different concentrations (2, 5, 10, 15 mg/mL) were scanned on a whole-body PCD-CT using a routine abdomen protocol (140 kV, 100 mAs, energy thresholds = 25/75keV). VMIs at 40-70keV were generated using vendor-supplied software (Mono+, Siemens). The images were then denoised using the SPICCS algorithm which is applied in the image domain by minimizing an objective function consisting of a data fidelity term and a regularization term. The regularization term penalizes total variation (TV) of the VMIs and TV of the difference between VMIs and TL images. A uniform water phantom and a thin wire phantom were scanned to assess noise texture and spatial resolution, respectively. With IRB approval, patient images were acquired on the same PCD-CT (140 kV, 100 mAs, energy thresholds = 25/75keV). The iodine CNR was calculated from VMIs before/after SPICCS.

RESULTS

VMIs processed with SPICCS preserved iodine contrast and reduced noise compared to the original VMIs (129±51 vs. 128±27 HU before/after SPICCS, measured from 5mg/mL iodine insert at 50keV), which improved iodine CNR especially at lower keV (5.65 vs 10.3 at 50keV). Compared with TL images, SPICCS-processed VMIs had improved CNR at lower keV (e.g., 50keV). MTF and NPS data showed that SPICCS preserved resolution and noise texture compared to TL images and original VMIs. The 50 keV VMI from patient data demonstrated similar improvement in iodine CNR (1.8 fold increase in iodine CNR at 50 keV).

CONCLUSION

We developed a denoising framework to improve iodine CNR in VMIs acquired on PCD-CT using SPICCS, while preserving spatial resolution and noise texture.

CLINICAL RELEVANCE/APPLICATION

The proposed denoising scheme improved iodine CNR for VMIs acquired on a whole-body PCD-CT system while preserving spatial resolution and noise texture, which may improve clinical diagnosis.

SSM21-02 Multi-Energy (ME) CT Imaging for Large Patients Using Photon-Counting-Detector (PCD) Technology

Wednesday, Nov. 28 3:10PM - 3:20PM Room: S104B

Ashley Tao, PhD, Rochester, MN (*Abstract Co-Author*) Nothing to Disclose Gregory J. Michalak, PhD, Rochester, MN (*Abstract Co-Author*) Nothing to Disclose Kishore Rajendran, PhD, Rochester, MN (*Abstract Co-Author*) Nothing to Disclose Richard Huang, Rochester, MN (*Abstract Co-Author*) Nothing to Disclose Cynthia H. McCollough, PhD, Rochester, MN (*Abstract Co-Author*) Research Grant, Siemens AG Shuai Leng, PHD, Rochester, MN (*Abstract Co-Author*) License agreement, Bayer AG

For information about this presentation, contact:

leng.shuai@mayo.edu

PURPOSE

Imaging large patients with conventional dual-source dual-energy (DSDE) CT using energy-integrating-detectors (EIDs) is challenging due to artifacts in lower kV (80-100) images caused by photon starvation and electronic noise. Although the use of higher kV (e.g. 120) can reduce this effect, the energy separation is insufficient for multi-energy CT (MECT) imaging, even with the addition of a tin filter in the high kV beam. Photon-counting-detector (PCD) CT is more resistant to electronic noise and can provide spectral information with a single tube potential, which may be more suitable for MECT imaging on large patients. This work aims to evaluate the feasibility of MECT imaging on large patients assuming a dual-PCD acquisition system.

METHOD AND MATERIALS

An anthropomorphic CT phantom was padded with an additional 5 cm tissue-mimicking layer to simulate a large patient, and scanned on a conventional DSDE EID-CT system with 100 kV and Sn140 kV (i.e., 140 kV with additional tin filter) tube potentials. In addition, iodine inserts of known concentrations (2, 5, 10, 15 mg/mL) were attached to the phantom. The same phantom was then scanned on a whole-body PCD-CT system. This system was built based on a conventional DSDE CT platform, with the second EID replaced with a PCD. A dual-source, dual-PCD acquisition was emulated by scanning the object separately with tube potentials of 100 kV and Sn140 kV. Tube current for PCD scans was matched to that of EID scans. Material decomposition was then performed to generate iodine and water maps.

RESULTS

The low-energy image (100 kV) acquired on the conventional DSDE EID-CT system showed noticeable shading, which limited its use for clinical diagnosis. These artifacts were largely eliminated in images acquired on the PCD system. The iodine quantification root-mean-square-errors (RMSE) measured from iodine inserts was 2.3 mg/mL for EID and 2.1 mg/mL for PCD.

CONCLUSION

This work demonstrated the feasibility of MECT imaging for large patient assuming a dual-source PCD acquisition. The DS-PCD system out-performs conventional DS-EID CT system by reducing image artifacts and yet providing reasonable energy separation.

CLINICAL RELEVANCE/APPLICATION

Imaging large patients using DECT is known to be challenging. This work demonstrated the feasibility of MECT imaging for large patients using PCD, which allows all patients to benefit from MECT.

SSM21-03 Photon-Counting CT: Dependence of Noise Power Spectra, Task-Transfer Function, and Detectability Index (d') on Patient Size, Imaging Mode, and Reconstruction Kernel

Wednesday, Nov. 28 3:20PM - 3:30PM Room: S104B

Participants

Jayasai R. Rajagopal, BA, Durham, NC (*Presenter*) Nothing to Disclose

Pooyan Sahbaee, Malvern, PA (Abstract Co-Author) Employee, Siemens AG

Bradford J. Wood, MD, Bethesda, MD (*Abstract Co-Author*) Researcher, Koninklijke Philips NV; Researcher, Celsion Corporation; Researcher, BTG International Ltd; Researcher, Siemens AG; Researcher, XAct Robotics; Researcher, NVIDIA Corporation; Intellectual property, Koninklijke Philips NV; Intellectual property, BTG International Ltd; Royalties, Invivo Corporation; Royalties, Koninklijke Philips NV; ; ;

Elizabeth C. Jones, MD, Bethesda, MD (Abstract Co-Author) Nothing to Disclose

Ehsan Samei, PhD, Durham, NC (*Abstract Co-Author*) Research Grant, General Electric Company; Research Grant, Siemens AG; Advisory Board, medInt Holdings, LLC; License agreement, 12 Sigma Technologies; License agreement, Gammex, Inc

For information about this presentation, contact:

jayasai.rajagopal@duke.edu

PURPOSE

To evaluate image quality in photon-counting CT due to change in patient size, imaging mode, and reconstruction kernel as measured by a tiered phantom

METHOD AND MATERIALS

The study utilized a five-tiered size variant phantom (Mercury Phantom, Gammex/Duke University). Images were acquired on a prototype photon-counting CT system (Siemens, Germany) using two imaging modes: Macro and Ultra High-Resolution (UHR) with effective voxel sizes of 0.5 and 0.25 mm, respectively, at a clinically-relevant dose (CTDIvol = 16 mGy). UHR scans were also done at maximum allowable mAs. Images were reconstructed with three kernels of increasing sharpness with 5 mm slice thickness. A task-based assessment was performed including calculation of noise power spectra, task-transfer function, and detectability index (d') of an iodine insert using the standard methodology of AAPM TG 233.

RESULTS

UHR had a higher d' of 8-88% across all reconstruction kernels and phantom sizes when compared to Macro mode. For softer kernels, TTFs were comparable between the two modes. The magnitude and shape of the noise power spectrum was different influencing d'. Sharp kernel showed edge enhancement with increased noise magnitude for UHR mode and different TTFs for different imaging modes. For ultra-sharp kernels, UHR mode showed a significant reduction of noise magnitude while preserving the shape of the spectra and the TTF. As expected, increasing dose led to a reduction in noise magnitude without affecting the task

transfer function.

CONCLUSION

UHR mode showed reduced noise and superior detectability for an iodinated task when controlling for patient size and reconstruction kernel. Task performance was dependent on selected reconstruction kernel and imaging mode.

CLINICAL RELEVANCE/APPLICATION

Ultra high-resolution mode in photon-counting CT offers improved spatial resolution and superior detectability compared to macro mode, and superior to conventional energy-integrating CT.

SSM21-04 Deep Inpainting for Photon-Counting Cone-Beam CT

Wednesday, Nov. 28 3:30PM - 3:40PM Room: S104B

Participants

Elias Eulig, BSC, Heidelberg, Germany (*Presenter*) Nothing to Disclose Joscha Maier, Heidelberg, Germany (*Abstract Co-Author*) Nothing to Disclose Andreas Hahn, Heidelberg, Germany (*Abstract Co-Author*) Nothing to Disclose Marc Kachelriess, PhD, Heidelberg, Germany (*Abstract Co-Author*) Nothing to Disclose

For information about this presentation, contact:

elias.eulig@dkfz.de

PURPOSE

To provide an efficient method to close the gaps of large area photon counting detectors in x-ray imaging and cone-beam CT (CBCT).

METHOD AND MATERIALS

Photon counting detector technology promises improved CT image quality at reduced patient dose. Moreover, the new detectors have the potential to provide diagnostic image quality in cone-beam CT systems that, today, still suffer from inferior image quality. However, the limited size of the ASICs (typically about 3x3 cm) requires tiling of many detector modules in order to assemble detectors large enough for almost any medical application. Inevitably, one or more pixel wide gaps between the modules may occur. Prior to reading the x-ray images or to reconstructing the CBCT data, the gaps or dead pixels need to be closed by inpainting. Therefore, we developed a deep adversarial architecture based on a generator and discriminator network that trains itself to fill the dead pixels. Training was performed using uncorrupted CBCT thoracic and abdominal patient data with artificially induced pixel gaps. Since the adversarial approach is unsupervised the same architecture can be applied to photon-counting flat dectector data in the same way. The performance was compared to a linear inpainting, to a diffusion-based inpainting and to an exemplar-based inpainting algorithm. Our novel approach was implemented using the PyTorch Deep Learning framework and trained on 6400 samples for 20 epochs on a GeForce GTX 1080 Ti GPU.

RESULTS

The visual impression of the correction was best with the deep inpainting approach and the exemplar-based algorithm, second best with the linear interpolation and worst with the diffusion-based algorithm where the location of the gaps was clearly visible after inpainting. The computation time per 1024×768 projection was 83 ms, 52 s, 29 ms and 2 s, respectively. The network was running on the GPU while all the other algorithms were running on the CPU.

CONCLUSION

Deep inpainting has the potential to remove pixel defects or gaps between detector modules at least as good as exemplar-based inpainting while reducing computation times drastically.

CLINICAL RELEVANCE/APPLICATION

Photon counting detector technology has the potential to improve CT and CBCT imaging in the near future. An efficient inpainting approach, such as the deep inpainting algorithm presented here, brings the new detector technology one step closer to clinical routine.

SSM21-05 Can a Universal Protocol for Photon-Counting-Detector CT Provide Equivalent Iodine Detectability as Optimal kV Energy-Integrating-Detector CT: A Feasibility Study

Wednesday, Nov. 28 3:40PM - 3:50PM Room: S104B

Participants

Wei Zhou, PhD, Rochester, MN (*Presenter*) Nothing to Disclose Gregory J. Michalak, PhD, Rochester, MN (*Abstract Co-Author*) Nothing to Disclose Jayse Weaver, Rochester, MN (*Abstract Co-Author*) Nothing to Disclose Hao Gong, PhD, Rochester, MN (*Abstract Co-Author*) Nothing to Disclose Kenneth A. Fetterly, PhD, Rochester, MN (*Abstract Co-Author*) Nothing to Disclose Cynthia H. McCollough, PhD, Rochester, MN (*Abstract Co-Author*) Research Grant, Siemens AG Shuai Leng, PHD, Rochester, MN (*Abstract Co-Author*) License agreement, Bayer AG

For information about this presentation, contact:

zhou.wei1@mayo.edu

PURPOSE

To determine iodine detectability using a single-kV universal protocol on a photon-counting-detector (PCD) CT for different phantom sizes, and to compare with optimized-kV single-energy (SE) and dual-source, dual-energy (DSDE) CT using an energy-integrating-detector (EID).

METHOD AND MATERIALS

A 4-mm diameter hole in a water-equivalent cylinder was filled with iodine solutions at one of 4 concentrations (0.2, 0.5, 1.0 and 2.0 mgI/cc) and the cylinder was inserted into one of 3 abdomen phantoms (QRM, lateral widths of 30, 35 and 40 cm). The whole phantom was scanned on a 2nd generation DSDE CT with SE and DE protocols using a kV or kV pair adjusted for phantom size. The phantom was also scanned on a whole body PCD CT using a single-kV universal protocol for all phantom sizes: 140 kV, 25 and 75 keV energy thresholds. EID-SE tube current was automatically adjusted (CareDose4D, 120 kV, 200 QRM), resulting in CTDIvol of 6.9 to 17.7 mGy for different size phantoms. EID-DE and PCD tube current was adjusted to match the CTDIvol of the EID-SE scans. Scans were repeated 200 times for each of 24 conditions: 4 concentrations, 3 phantom sizes and 3 protocols. All images were reconstructed with a quantitative kernel (D30) and 5 mm thickness. Virtual monoenergetic images (VMI) at 50 keV were generated from PCD and EID-DE images. CNR and AUC of the ROC from a calibrated channelized hoteling observer (CHO) model were calculated as figures of merit for quantifying iodine detection for PCD VMI@50 keV, EID-SE, and EID-DE VMI@50keV.

RESULTS

VMI@50 keV from PCD and EID-DE showed higher iodine CNR than the EID-SE images for all phantom sizes. For 0.5 mg/cc iodine, VMI@50 keV from PCD (0.93) and EID-DE (0.94) showed comparable AUC for iodine detection on a 30cm phantom and superior AUC for 35 cm (PCD: 0.93; EID-DE: 0.90) and 40 cm (PCD: 0.81; EID-DE: 0.88) phantoms compared to that of EID-SE (30 cm: 0.95; 35cm: 0.83; 40 cm: 0.77). A similar trend showing preference for VMI from PCD and EID-DE was observed for other iodine concentrations.

CONCLUSION

VMI images from a single kV PCD acquisition demonstrated comparable or improved iodine detectability and CNR compared to SE images where kV was selected based on patient size.

CLINICAL RELEVANCE/APPLICATION

A universal PCD CT protocol can maintain iodine sensitivity, simplify protocol selection and avoid sub-optimal images from inappropriate kV (or kV pair) selection with EID CT.

SSM21-06 A Method of Calculating Lesion Detectability in Photon-Counting Spectral CT

Wednesday, Nov. 28 3:50PM - 4:00PM Room: S104B

Participants

Mats Persson, Stanford, CA (*Presenter*) Stockholder, Prismatic Sensors AB; Consultant, Prismatic Sensors AB Paurakh L. Rajbhandary, BS, Palo Alto, CA (*Abstract Co-Author*) Nothing to Disclose

Norbert J. Pelc, DSc, Stanford, CA (*Abstract Co-Author*) Research support, General Electric Company; Consultant, General Electric Company; Consultant, NanoX; Scientific Advisory Board, RefleXion Medical Inc; Scientific Advisory Board, Prismatic Sensors AB; Scientific Advisory Board, Theranos, Inc; Stockholder, Theranos, Inc; Medical Advisory Board, OurCrowd, LP; Scientific Advisory Board, Izotropic, Inc; Stockholder, Inc

For information about this presentation, contact:

matspers@stanford.edu

PURPOSE

To develop a method of calculating the lesion detectability attainable in photon-counting spectral CT and demonstrate it for a cadmium telluride detector in a simulation study.

METHOD AND MATERIALS

Using a Monte Carlo simulation of an X-ray beam incident on a 3 mm thick cadmium telluride detector with 0.5x0.5 mm2 pixels and five energy bins, the energy-dependent point-spread function and autocorrelation function were calculated. Correlation between pixels due to fluorescence and charge diffusion was included in the simulation model. A recently developed linear-systems methodology was used to calculate the optimal-linear-observer detectability, i. e. the maximal detectability that can be obtained through optimal weighting of the data from the five energy bins. This detectability was computed for nonenhancing (soft tissue) and enhancing (10 mg/ml iodine) spherical lesions of different sizes in a 250 mm soft tissue cylinder, for a system with detector-limited resolution and a 120 kVp spectrum with 2.5 mm Al filtration. The results were compared to an ideal detector with perfect spatial and energy resolution and to an energy-integrating detector with 1x1 mm2 pixels but otherwise ideal.

RESULTS

The ideal-linear-observer detectability, relative to the ideal detector, was 67%, 83% and 91% for nonenhancing lesions with 1 mm, 2 mm and 10 mm diameter. For enhancing lesions the corresponding values were 48%, 58% and 62%, respectively. This is an improvement of 6-98 % (nonenhancing) and 58-203% (enhancing) compared to the energy-integrating detector.

CONCLUSION

Whereas large-area image quality metrics such as CNR have been used to characterize photon-counting CT scanners in previous work, so far there has not been a method of calculating the attainable detectability for smaller objects with energy-resolving photon-counting detectors. This simulation study demonstrates for the first time how the detectability of lesions in a photon-counting CT scanner can be simulated, taking energy resolution, pixel size and cross-talk between pixels into account. The results show that the detector performance is closer to ideal for nonenhancing lesions than for enhancing lesions.

CLINICAL RELEVANCE/APPLICATION

With photon-counting CT scanners expected to become clinically available in a few years, the proposed method will enable comprehensive comparison of systems and optimization of imaging protocols.



SSM22

Radiation Oncology (Genitourinary)

Wednesday, Nov. 28 3:00PM - 4:00PM Room: E261



AMA PRA Category 1 Credit ™: 1.00 ARRT Category A+ Credit: 1.00

Participants

Martin Colman, MD, Houston, TX (*Moderator*) Stockholder, Steward Health Care Edward Y. Kim, MD, Seattle, WA (*Moderator*) Nothing to Disclose

Sub-Events

SSM22-01 Deep Decision Forests of Radiomic Features for Automatic Contouring of Pelvic Anatomy for Prostate Radiotherapy

Wednesday, Nov. 28 3:00PM - 3:10PM Room: E261

Participants

Meghan W. Macomber, MD, Seattle, WA (*Abstract Co-Author*) Nothing to Disclose Mark H. Phillips, PhD, Seattle, WA (*Abstract Co-Author*) Nothing to Disclose Ivan Tarapov, MSc, Redmond, WA (*Abstract Co-Author*) Nothing to Disclose Rajesh Jena, MD, FRCR, Cambridge, United Kingdom (*Abstract Co-Author*) Royalties, Microsoft Corporation; Antonio Criminisi, PhD, Cambridge, United Kingdom (*Abstract Co-Author*) Employee, Microsoft Corporation Matthew J. Nyflot, PhD, Seattle, WA (*Presenter*) Nothing to Disclose

PURPOSE

Machine learning for image segmentation is a potentially innovative approach to improve efficiency and promote standardization for radiotherapy treatment planning. We evaluated a new model that uses deep decision forests of image features to contour pelvic anatomy on treatment planning CTs.

METHOD AND MATERIALS

We anonymized 193 prostate treatment planning CTs (acquired 2012-2016 at 1 UK and 2 US sites, GE and Toshiba scanners, 512x512 pixels inplane, 1.25 or 2.5 mm between slices). A deep decision forest (DF) was trained to contour prostate, bladder, rectum, femurs, and seminal vesicles on 94 images from Site 1. Testing was done on 99 separate scans (n=35, 34, and 25 from Site 1, 2, and 3). Similarity between DF contours and clinical (ground truth) contours was measured with Dice score (DSC) in the validation datasets. DF performance was compared to four commercial tools on a random subset of images (n=20). Additionally, interobserver variability (IOV) between three physicians' contours and ground truth was evaluated on 10 random images and compared to DF performance with Student's t-test.

RESULTS

Across all sites, DF agreement with ground truth was: bladder, DSC 0.94-0.97 [interquartile range (IQR) 0.92-0.98], prostate, DSC 0.75-0.76 [IQR 0.67-0.82], rectum: DSC 0.71-0.82 [IQR 0.63-0.87], femurs: DSC 0.96-0.97 [IQR 0.94-0.97], seminal vesicles: DSC 0.49-0.70 [IQR 0.31-0.79]. The results were similar across the three sites (e.g. median prostate DSC for each site was 0.76, 0.76, 0.75). In the commercial model comparison, DF had highest DSC for all organs, followed by the two model-based systems, with atlas-based systems having worst performance. For IOV data, variability between DF and ground truth was smaller than variability between raters for prostate (median DSC 0.87 vs 0.77, p=0.006) and femurs (median DSC 0.973 vs 0.968, p=0.002), and not significantly different for other contours (p>0.3).

CONCLUSION

Deep decision forests are effective at contouring pelvic anatomy for radiotherapy planning, with good performance relative to commercial programs, and agreement with ground truth was as similar as can be expected between human experts.

CLINICAL RELEVANCE/APPLICATION

Machine learning methods for automated treatment planning would be useful to improve clinical efficiency and increase standardization in radiation oncology.

SSM22-02 Nationwide Prostate Cancer Outcome Prediction Study of Permanent Iodine-125 Seed Implantation: Outcome Prediction Using Machine Learning Techniques with Cohort 1

Wednesday, Nov. 28 3:10PM - 3:20PM Room: E261

Participants

Taiki Magome, Tokyo, Japan (*Presenter*) Nothing to Disclose Katsumasa Nakamura, MD, PhD, Hamamatsu, Japan (*Abstract Co-Author*) Nothing to Disclose Takashi Kikuchi, Kobe, Japan (*Abstract Co-Author*) Nothing to Disclose Shinsuke Kojima, Kobe, Japan (*Abstract Co-Author*) Nothing to Disclose Kazuto Ito, Maebashi, Japan (*Abstract Co-Author*) Nothing to Disclose Atsunori Yorozu, MD, Tokyo, Japan (*Abstract Co-Author*) Nothing to Disclose Shiro Saito, Tokyo, Japan (*Abstract Co-Author*) Nothing to Disclose Masanori Fukushima, Kobe, Japan (*Abstract Co-Author*) Nothing to Disclose

PURPOSE

The nationwide Japanese Prostate Cancer Outcome Study of Permanent Iodine-125 Seed Implantation (J-POPS) is a big novel data with the fundamental aim of collecting clinical data as a prospective cohort study. The purpose of this study is to predict prostate cancer outcome after brachytherapy based on machine learning techniques using J-POPS big data.

METHOD AND MATERIALS

Among 72 hospitals performing brachytherapy in Japan, 46 (64 %) hospitals provided 2,339 cases of the J-POPS cohort 1. Patient/family background, TNM classification, serum PSA level, Gleason score, brachytherapy and external radiotherapy parameters, adverse event and outcome information, etc. were included in the survey items. Two types of dataset were used for the prediction; i.e., the large dataset including the majority of survey items, and limited dataset including only the survey items which are considered as relevant items with the outcome by radiation oncologists. In this study, four machine learning algorithms, i.e., logistic regression (LR), support vector machine (SVM), random forest (RF), and deep neural network (DNN) were tested. Outcome information including biochemical failure and rectal/urinary toxicity were predicted by the machine learning techniques. The prediction accuracy, defined as (true positive + true negative cases) / all cases, was evaluated by 10-fold cross-validation test.

RESULTS

The prediction accuracy with the large dataset was higher than that with the limited dataset in each machine learning algorithm. Although 5.2 percent of cases showed the biochemical failure, the highest accuracy of biochemical failure prediction with a large dataset and limited dataset was 0.938 and 0.892, respectively, for test data. The prediction model using RF had the highest accuracy.

CONCLUSION

Our results showed a potential to predict the outcome of prostate cancer patients with the big nationwide data including many survey items.

CLINICAL RELEVANCE/APPLICATION

Prostate cancer outcome after brachytherapy could be accurately predicted with big nationwide data.

SSM22-03 Dose to the Bladder Neck in MRI-guided High Dose-Rate Prostate Brachytherapy

Wednesday, Nov. 28 3:20PM - 3:30PM Room: E261

Participants

Noelia Sanmamed, MD, Toronto, ON (*Presenter*) Nothing to Disclose Peter Chung, Toronto, ON (*Abstract Co-Author*) Nothing to Disclose Sangeet Ghai, MD, Toronto, ON (*Abstract Co-Author*) Grant, InSightec Ltd Grant, Exact Imaging Inc Alejandro Berlin, Toronto, ON (*Abstract Co-Author*) Nothing to Disclose Jette Borg, PhD, Toronto, ON (*Abstract Co-Author*) Nothing to Disclose Bernadeth Lao, BSC, Toronto, ON (*Abstract Co-Author*) Nothing to Disclose Robert Weersink, Toronto, ON (*Abstract Co-Author*) Nothing to Disclose Anna Simeonov, Toronto, ON (*Abstract Co-Author*) Nothing to Disclose Alexandra Rink, PhD, Toronto, ON (*Abstract Co-Author*) Nothing to Disclose Cynthia Menard, MD, Montreal, QC (*Abstract Co-Author*) Nothing to Disclose Joelle Helou, Toronto, ON (*Abstract Co-Author*) Nothing to Disclose

PURPOSE

We aim to assess the impact of the dose to the bladder neck (BN) on physician and patient-reported GU toxicity after MRI-guided high dose-rate brachytherapy (HDR-BT) boost.

METHOD AND MATERIALS

Sixty-three patients were treated with a single 15-Gy MRI-guided HDR-BT implant followed by external beam radiotherapy. MRIbased treatment planning was used. The clinical target volume (CTV) was defined as the prostate and planning target volume was CTV + 2mm craniocaudal margin. BN was delineated in retrospect on T2-weighted images by a radiation oncologist (RO) and reviewed by an independent RO and a radiologist. Dosimetric parameters, acute (<=3 months) toxicity using CTCAE v.4 and healthrelated quality of life (HRQoL)using the expanded prostate index composite (EPIC) were collected prospectively. A minimally important difference (MID) was defined as a deterioration of HRQoL scores at 3 months compared to baseline >= 0.5 standard deviation of baseline score. Linear and logistic regression models were used to assess the impact of BN dose on GU toxicity and HRQoL. A p-value <=0.05 was considered statistically significant.

RESULTS

The median BN volume was 0.6 cc [interquartile range (IQR): 0.4-0.7]. Median maximum dose to the BN (BNDmax) and urethra (UDmax) was 24.9 Gy (IQR 18.8- 26.4) and 17 Gy (IQR 16.7- 17.7) respectively. Median dose to 2cc of the urethra was 52 Gy (IQR: 36-62). BNDmax was significantly associated with UDmax (p=0.027) and 7.7% of the total amount of variation in BNDmax was explained by the UDmax (R2=0.059, p=0.028). Grade 2+ GU toxicity was observed in 31% of patients. Among those, 4 patients had an acute urinary retention. No grade 4+ toxicity was reported. Furthermore 46% of patients reported a MID in EPIC urinary domain score at 3 months. None of the dosimetric parameters including BNDmax was associated with acute grade 2+ urinary toxicity or MID. However, 3 out of 4 patients with acute urinary retention had a BND max in the highest quartile; 26.4, 28.3 and 52.7 Gy (>175% of prescription dose).

CONCLUSION

MRI-based planning offers a unique opportunity to delineate and assess the dose to the BN. Although the predictive value of this parameter is yet to be determined in a larger population, it is worthwhile including BN contours and constraints into HDR-BT

treatment planning if an MRI-planning is available.

CLINICAL RELEVANCE/APPLICATION

Uncertainties exist regarding bladder neck definition.

SSM22-04 Machine Leaning Based Prediction of Prostate Cancer Recurrence After Radiotherapy with Radiosensitivity Related Proteins

Wednesday, Nov. 28 3:30PM - 3:40PM Room: E261

Participants

Takuya Mizutani, Tokyo, Japan (*Presenter*) Nothing to Disclose Taiki Magome, Tokyo, Japan (*Abstract Co-Author*) Nothing to Disclose Masanori Someya, MD,PhD, Hokkaido, Japan (*Abstract Co-Author*) Nothing to Disclose Tomokazu Hasegawa, Sapporo, Japan (*Abstract Co-Author*) Nothing to Disclose Koichi Sakata, Sapporo, Japan (*Abstract Co-Author*) Nothing to Disclose

For information about this presentation, contact:

mizutaku17@gmail.com

PURPOSE

There are several reports that the expression of proteins in tumors related to radiosensitivity could be used as biomarkers for the outcome prediction after radiotherapy. The purpose of this study was to predict local relapse of prostate cancer after radiotherapy using a machine learning methodology with the combination of conventional factors and the protein information related to radiosensitivity.

METHOD AND MATERIALS

A total of 100 patients with localized adenocarcinoma of the prostate who were treated from 2001 to 2010 were included in this study. Support vector machine (SVM) was used as a machine learning methodology to predict local relapse of prostate cancer. Candidate input features for the prediction included 16 clinical features (age, Gleason score, PSA level, etc.), 16 radiation dose features (mean dose, dose per fraction, etc.) and 3 protein information related to radiosensitivity (Ku70, Ku86, XRCC4). Effective features for prediction were determined by a sequential forward selection using Akaike's information criterion. The prediction performance of the models with or without protein information were compared by a leave-one-out cross-validation test. Accuracy, sensitivity, specificity and Matthew's correlation coefficient (MCC) were used as prediction performance metrics.

RESULTS

The prediction performance was improved by considering the radiosensitivity related protein information, e.g., accuracy of the models with and without the protein information was 0.78 and 0.69, respectively. Ku70 was the most selected feature in the proteins related to radiosensitivity.

CONCLUSION

Our result showed the potential to predict local relapse of prostate cancer with the combination of conventional factors and the protein information related to radiosensitivity. Accurate outcome prediction after radiotherapy could be useful for personalized optimal selection of treatment modalities of cancer.

CLINICAL RELEVANCE/APPLICATION

Accuracy of the machine learning model for outcome prediction after radiotherapy could be improved with the radiosensitivity related protein information.

SSM22-05 Prostate Cancer: Assessment of Toxicity of Focal Dose Escalation of Radiotherapy Guided by Multiparametric Magnetic Resonance Imaging

Wednesday, Nov. 28 3:40PM - 3:50PM Room: E261

Participants

Michael W. Schmuecking, Hamburg, Germany (*Presenter*) Nothing to Disclose Volker Brandes, Hamburg, Germany (*Abstract Co-Author*) Nothing to Disclose Arne Blechschmidt, MS, Hamburg, Germany (*Abstract Co-Author*) Nothing to Disclose Sarah Lomp, MS, Hamburg, Germany (*Abstract Co-Author*) Nothing to Disclose Imke Luetjens, MS, Hamburg, Germany (*Abstract Co-Author*) Nothing to Disclose Matthias Roethke, MD, Heidelberg, Germany (*Abstract Co-Author*) Nothing to Disclose

For information about this presentation, contact:

schmuecking@strahlentherapie-veritaskai.com

PURPOSE

To evaluate acute and late toxicity after moderately hypofractionated radiotherapy of prostate cancer with focal dose escalation guided by multiparametric magnetic resonance imaging (mpMRI) using intensity-modulated treatment planning and image-guided treatment (IGRT) delivery.

METHOD AND MATERIALS

58 patients (age 55-82y, cT2/cT3, initial PSA 3.3-16.4ng/ml, Gleason Score >3+4) were included into the study. Before implantation of three gold markers, each patient underwent mpMRI (T2-TSE, DCE, DWI) that detected a suspicious focal lesion (PIRADS 4+5) followed by image fusion with the radiation treatment planning CT. In total, a dose of 79.2Gy in 33 fractions (single dose 2.4Gy) were prescribed to PIRADS 4 and 5 intraprostatic lesions with a margin of 3mm (gross target volume + 3mm = planning target volume) delivered with a simultaneous integrated boost (SIB) by static field intensity-modulated radiotherapy (IMRT) or volumetric modulated arc therapy (VMAT). Further dose levels were 76.23Gy and 60.06Gy prescribed to the prostate and the

seminal vesicles, respectively. Patients with high risk prostate cancer received 46Gy to the pelvic lymphatics, lymph node metastases 60Gy in 25 fractions with SIB. Daily IGRT by cone-beam computed tomography (CBCT) in addition to gold markers. Acute and late gastrointestinal (GI) and genitourinary (GU) toxicity was evaluated using CTCAE v4.03.

RESULTS

Treatment was completed according to the treatment plan in all included patients. Acute GI and GU toxicity grade >=2 was observed in 13.8% and 39.6% of the patients, respectively, with 6.8% suffering from GU toxicity grade 3. Six weeks after treatment, the incidence of acute toxicity grade >=2 had decreased to 15.5%. With a median follow-up of 28 months, late GI and GU toxicity grade >=2 was seen in 1.7% and 8.6% of the patients, respectively. Three patients developed late toxicity grade 3 (GI n=2; GU n=1).

CONCLUSION

Moderately hypofractionated high-dose radiotherapy with further dose-escalation to mpMRI PIRADS 4 and 5 lesions resulted in acceptable rates of acute and late toxicity according to the current literature. Conformal IMRT / VMAT planning and accurate daily IGRT treatment delivery using goldmarker and CBCT may have contributed to these results.

CLINICAL RELEVANCE/APPLICATION

The use of mpMRI for focal dose escalation in patients with prostate cancer may enhance post-radiotherapeutic local control.

SSM22-06 Weekly Magnetic Resonance Imaging Using a Linear Accelerator Equipped with a 1.5 Tesla MRI (MR-Linac) Reveals Intra-Treatment Signal Variance in Regional Organs at Risk (OAR), An Exploratory Analysis

Wednesday, Nov. 28 3:50PM - 4:00PM Room: E261

Participants

Joshua Lorenz, Milwaukee, WI (*Presenter*) Nothing to Disclose Diane Schott, PhD, Milwaukee, WI (*Abstract Co-Author*) Nothing to Disclose Farshad Mostafaei, PhD, Milwaukee, WI (*Abstract Co-Author*) Nothing to Disclose Colleen A. Lawton, MD, Milwaukee, WI (*Abstract Co-Author*) Nothing to Disclose Manpreet Bedi, MD, Milwaukee, WI (*Abstract Co-Author*) Nothing to Disclose X. Allen Li, Milwaukee, WI (*Abstract Co-Author*) Nothing to Disclose Christopher J. Schultz, MD, Milwaukee, WI (*Abstract Co-Author*) Medical Advisory Board, Prism Clinical Imaging, Inc Eric Paulson, PHD, Milwaukee, WI (*Abstract Co-Author*) Nothing to Disclose William A. Hall, MD, Milwaukee, WI (*Abstract Co-Author*) Departmental research support, Elekta AB

PURPOSE

To investigate changes in quantitative signal variables of organs at risk (OAR) in serially obtained T2-weighted MR images, acquired on an MR-Linac, in patients being treated for prostate cancer.

METHOD AND MATERIALS

Four patients with prostate cancer undergoing treatment with radiation therapy (RT) were compiled from an ongoing prospective observational imaging trial using MR-Linac. All patients provided informed consent for weekly imaging; images were obtained between November 2017 and March 2018. Contiguous sections of rectal and bladder wall adjacent to the prostate were contoured and normalized to temporally corresponding regions of rectum and bladder removed from the planning target volume. Similarly, contiguous axial slices of Sartorius muscle outside of the regions of high dose RT exposure were also contoured as a normal control. The quantitative features considered included: max-to-mean ratio, kurtosis, mean, median, skewness, and standard deviation. A student's t-test was used to evaluate for statistically significant variance week-to-week.

RESULTS

Between weeks 1 and 2, significant variance in the mean and median signal values were seen in sections of rectal wall adjacent to the prostate (p=0.05, p=0.04). Bladder wall near the prostate also exhibited significant variance in the mean and median signal values between weeks 1 and 4 (p=0.05, p=0.04). No significant variance in signal values for the variables considered was observed in the Sartorius muscle control.

CONCLUSION

This is one of the earliest analyses examining quantitative signal value changes in regional organs (bladder and rectum), using an MR-Linac in patients being actively treated with RT for prostate cancer. Significant changes occurred after only 1 week of therapy in regional organs at risk during treatment with RT. Expanded data sets are needed to evaluate if these early changes correlate with clinical outcomes such as acute or late toxicity.

CLINICAL RELEVANCE/APPLICATION

Radiotherapy (RT) response assessment with a 1.5 Tesla MRI may allow for intra-treatment modification of RT plans to increase oncologic control and reduce toxicity. Increased understand of radiomic changes in OAR's will improve RT response assessment.



SSM23

Vascular Interventional (Neurovascular Interventions)

Wednesday, Nov. 28 3:00PM - 4:00PM Room: E263



AMA PRA Category 1 Credit ™: 1.00 ARRT Category A+ Credit: 1.00

FDA Discussions may include off-label uses.

Participants

Gordon McLennan, MD, Chagrin Falls, OH (*Moderator*) Grant, Siemens AG; Grant, Surefire Medical, Inc; Speakers Bureau, Medtronic plc; Speakers Bureau, General Electric Company; Speakers Bureau, Stryker Corporation; Advisory Board, Siemens AG; Advisory Board, Surefire Medical, Inc; Advisory Board, Stealth Medical; Advisory Board, Rene Medical, Inc; Advisory Board, F. Hoffmann-La Roche Ltd; Advisory Board, Bristol-Myers Squibb Company; Advisory Board, B. Braun Melsungen AG; Advisory Board, General Electric Company;

Dimitrios Filippiadis, MD, PhD, Athens, Greece (Moderator) Nothing to Disclose

Sub-Events

SSM23-01 Experimental Study of the Self-Expandable Partial-Covered Stent Insertion for the Treatment of Side-Wall Aneurysms in a Canine Model

Wednesday, Nov. 28 3:00PM - 3:10PM Room: E263

Participants

Yueqi Zhu, MD, Shanghai, China (*Presenter*) Nothing to Disclose Yingsheng Cheng, MD, Shanghai, China (*Abstract Co-Author*) Nothing to Disclose

PURPOSE

to test the safety and efficacy of a newly designed self-expandable partial-covered stents insertion for the treatment of side-wall aneurysms with a comparation to bared stents in a canine model

METHOD AND MATERIALS

Thirty-six saccular side-wall aneurysms were created in 18 dogs and were randomly divided into a partial-covered stent group (PSG; receive partial-covered stent insertion, n=9) to and a bared stent group (BSG; receive bared stent insertion, n=9) as control. Angiography was performed post implantation and at 1, 3 and 6 months follow-up to investigate aneurysm isolation, endoleak, stent angulation, parent-artery (PA) patency, and restenosis. Light and scanning electron (SEM) microscopy was used at each follow-up to identify aneurysmal sac thrombi, intima hyperplasia, and endothelial progress

RESULTS

Immediate angiography demonstrated complete isolation of 6 (33.3%) aneurysms, mild endoleak in 9 (50%) and obvious endoleak in 3 (16.7%) in the PSG, with a comparison to that were 0 (0%), 5 (27.8%) and 13 (72.2%) in the BSG. Follow-up angiography at 6 months revealed 17 (94.4%) aneurysms were completely occluded and mild endoleak in 1 (5.6%) aneurysm in the PSG and complete occlusion in 3 (16.7%), mild endoleak in 6 (33.3%) and obvious endoleak in 9 (50%) in the BSG. Mild stenosis (<30%) and occlusion was revealed in 2 and 1 PAs in the PSG. Light microscopy revealed that all aneurysm sacs were filled with thrombi and small residual sac was found in the aneurysm with endoleak filling in the PSG. Endothelial progress was almost complete at 6 months after partial-covered stent insertion and endothelial cell coverage was closely correlated with the occurrence of endoleak

CONCLUSION

this new kind of partial-covered stent was technically feasible and effective to occlude aneurysm sac in canine models

CLINICAL RELEVANCE/APPLICATION

The self-expandable partial-covered stent insertion is safe and leads to satisfied occlusion to aneurysm sac in canine models, thus this device may further be applied for the treatment of brain aneurysms in clinical.

SSM23-02 Placement Of Laser-Cut Stents Within Flow Diverters Enhances Anatomic Results Of Flow Diverters

Wednesday, Nov. 28 3:10PM - 3:20PM Room: E263

Participants Osman Ocal, MD, Ankara, Turkey (*Presenter*) Nothing to Disclose Ahmet Peker, MD, Ankara, Turkey (*Abstract Co-Author*) Nothing to Disclose Anil Arat, MD, Madison, WI (*Abstract Co-Author*) Nothing to Disclose

For information about this presentation, contact:

drosmanocal@hotmail.com

PURPOSE

To evaluate the effect of better wall apposition of flow diverters by placement of laser-cut stents with higher radial force within the flow diverters during the same treatment session.

METHOD AND MATERIALS

Patients treated using a Surpass flow diverter (SFD) in a single institution with and without placement of a laser-cut stent were retrospectively evaluated. Patients with flow diverter placement inside a scaffolding stent, adjunctive use of another flow diverter, intrasaccular treatment and previously placed stents were excluded from study. Patient and aneurysm characteristics and clinical and imaging follow-up results were compared.

RESULTS

Of the 68 patients (mean age 50.4 ± 14), 35 patients (41 aneurysms) were treated with SFD only ("SFD-only group") and in 33 patients (35 aneurysms) a stent was placed within SFD for better apposition ("apposed group"). No statistical difference was noted between two groups in age, body weight, gender, history of thromboembolic events, smoking, hypertension, hyperlipidemia, diabetes mellitus and malignancy or rate of procedure-related complications. Aneurysms of apposed group were significantly larger than SFD-only group (14.8 vs 9.1 mm, P<0.001). There was no difference between two groups with respect to aneurysm location in anterior versus posterior circulation (P=0.326) or proximal versus distal location with regard to the circle of Willis (P=0.281). In spite of a trend for earlier aneurysm occlusion in the apposed group, complete aneurysm occlusion rates were similar at 0-3 and 3-6 months imaging follow-up (73.3% vs. 61.3%, P=0.466 and 83.9% vs. 72.9%, P=0.432). On 9-12 months follow-up, a significantly higher proportion of aneurysms in the apposed group achieved complete occlusion compared to SFD-only group (93.8% vs. 73.2%, P=0.049). There was no significant difference in complete aneurysm obliteration rates after one year (93.3% vs. 78.0%, P=0.154).

CONCLUSION

Enhancement of flow diverter wall apposition increases rate of aneurysm occlusion. We propose that placement of laser-cut stents with higher radial force within flow diverters is a safe method for improved wall apposition.

CLINICAL RELEVANCE/APPLICATION

Enhanced wall apposition of FD with higher radial force laser-cut stents increases flow diverter efficiency with safety profile.

SSM23-03 Perioperative Result of Carotid Artery Stenting in Patients with Atherosclerotic Extracranial Internal Carotid Artery near Occlusion

Wednesday, Nov. 28 3:20PM - 3:30PM Room: E263

Participants Ferdi Cay, MD, Ankara, Turkey (*Presenter*) Nothing to Disclose Ethem M. Arsava, Ankara, Turkey (*Abstract Co-Author*) Nothing to Disclose Barbaros E. Cil, MD, Ankara, Turkey (*Abstract Co-Author*) Nothing to Disclose Mehmet A. Topcuoglu, MD, Ankara, Turkey (*Abstract Co-Author*) Nothing to Disclose Anil Arat, MD, Madison, WI (*Abstract Co-Author*) Nothing to Disclose

For information about this presentation, contact:

ferdicay@hotmail.com

PURPOSE

'Near occlusion' of the carotid artery (NOCA) is not a well-defined entity. Recently, NOCA has been subclassified into two forms: 1) NOCA with collapse of the carotid artery, 2) NOCA without collapse. We aimed to compare the technical success and perioperative complication rates of these two sub-types to see whether there is a clinical correlate of this classification.

METHOD AND MATERIALS

We retrospectively evaluated all patients with atherosclerotic extracranial carotid stenosis treated by carotid artery stenting (CAS) in a single medical institution between January 2014 and January 2018. Patients with NOCA were identified based on cerebral DSA findings. Patient demographics, presence of vessel collapse distal to the stenosis, technical success rate and perioperative (<=30 day) complication rate were analyzed.

RESULTS

We identified 59 NOCAs in 58 (46 male, 12 women) patients; one patient had bilateral NOCA. The mean age of patients was 67.4 (range 46 to 86) years. Twelve cases (20.3%) had NOCA with collapse and 47 cases (79.6%) had NOCA without collapse. The NOCAs were symptomatic in 42 cases (71.1%) and asymptomatic in 17 cases (28.8%). Fifty-eight of the 59 CAS procedures were successful. In one case of NOCA, we were not able to pass through the stenosis because of significant patient motion; the patient was advised to undergo stenting under general anesthesia but refused this procedure. The overall perioperative complications included hyperperfusion (HP; 8.6%) and minor stroke (1.7%). Compared to patients with NOCA but no collapse (4.2% of 47 cases), those with NOCA resulting in vascular collapse (27.2% of 11 cases stented) had significantly higher rates of post-intervention HP (Fisher's exact test, p=0.042). Permanent morbidity and mortality rate was 1.7% and 1.7%, respectively.

CONCLUSION

CAS is feasible in the setting of NOCAs with and without collapse. Care should be taken for HP risk, especially in the subgroup of patients with collapse.

CLINICAL RELEVANCE/APPLICATION

Special care should be taken for HP in the treatment of NOCA by CAS

SSM23-04 Intraaneurysmal Air After Flow Diverter Treatment of Intracranial Aneurysms: Incidence, Characteristics, and Clinical Significance

Wednesday, Nov. 28 3:30PM - 3:40PM Room: E263

Participants Osman Ocal, MD, Ankara, Turkey (*Presenter*) Nothing to Disclose Anil Arat, MD, Madison, WI (*Abstract Co-Author*) Nothing to Disclose

For information about this presentation, contact:

drosmanocal@hotmail.com

PURPOSE

To describe the rate and characteristics of air bubble retention within cerebral aneurysms treated by flow diverters.

METHOD AND MATERIALS

Patients with cerebral aneurysms treated by flow diversion in a single institution over 30 months were identified. Patients were excluded if selective intrasaccular treatment was also attempted or performed in the same session. Among the remaining patients, those with immediate postprocedure flat detector CT (FDCT) images were identified. FDCT studies were included unless there were surgical or endovascular materials previously used to treat the target aneurysm or other aneurysms interfering with image interpretation. 66 FDCT studies in 66 patients were identified and were scrutinized for presence of air in the aneurysm. Clinical outcome, aneurysm characteristics and imaging features of air within the aneurysm were evaluated.

RESULTS

Intraaneurysmal air bubbles were noted in eleven aneurysms (16.9%). Six aneurysms were saccular and remaining five were fusiform/dissecting. Seven were located in the anterior circulation. All of these aneurysms except one were large or giant and were significantly larger than aneurysms without air bubbles (mean diameter 16 mm versus 9.7 mm in 55 aneurysms, P=0.0277). Air bubbles were more frequently encountered when multiple devices/stents were used for flow diversion as compared to a single flow diverter (P=0.0275). There was a single air bubble in 6 patients, two bubbles in three patients and three bubbles in one patient. All of the bubbles were in the rostral portion of the aneurysm sac, were smaller than 5 mm in maximum diameter (mean diameter 2.6 mm). None of the patients had postprocedural change in neurological status. Air had spontaneously disappeared on all postprocedure follow-up CT images (available in 9 patients) at a mean CT follow-up duration of 2 days.

CONCLUSION

Intravascular microbubble formation probably occurs in all endovascular procedures despite rigorous attention to technique. Flow diverters probably result in the intraaneurysmal entrapment of these microbubbles. In this study this finding was common, incidental, self-limited and without clinical consequences.

CLINICAL RELEVANCE/APPLICATION

The finding of intraaneurysmal microbubble within cerebral aneurysms treated by flow diverters is clinical inconsequential and selflimited.

SSM23-06 Initial Experience and One Year Follow-Up with Neuroform Atlas™ Stent System for the Treatment of Brain Aneurysms

Wednesday, Nov. 28 3:50PM - 4:00PM Room: E263

Participants Paola A. Rueda Mejia, MD, Oviedo, Spain (*Presenter*) Nothing to Disclose Eduardo Murias, Oviedo, Spain (*Abstract Co-Author*) Nothing to Disclose Pedro V. Valdes, Oviedo, Spain (*Abstract Co-Author*) Nothing to Disclose Edison Morales, MD, Oviedo, Spain (*Abstract Co-Author*) Nothing to Disclose Jose Maria Jimenez, MD, Madrid, Spain (*Abstract Co-Author*) Nothing to Disclose

For information about this presentation, contact:

palolarueda84@gmail.com

PURPOSE

The Neuroform Atlas Stent System is a recently introduced modification of the classical Neuroform stent consisting of a hybrid design with open and closed cells. Initial experience, technical considerations, treatment outcomes and one year follow up using the Atlas stent in combination with coil embolization are reported.

METHOD AND MATERIALS

Thirty unruptured aneurysms (from 30 patients) were treated with stent reconstruction. Control angiography and clinical assessment were performed inmediately, at four-month and at twelve-month after treatment.

RESULTS

The stents were delivered and positioned without difficulty in 29 cases. There were technical complications in one case, related to the displacement of the stent during its delivery. Only in one case occurred procedure-related clinical complications, with no permanent neurological deficit. We aimed for intial complete aneurysm occlusion with coils whenever technically feasible. The control angiography shortly after procedure showed class 1 or 2 occlusion (Raymond Roy classification) in 29 of 30 aneurysms. At one year angiographic follow-up, all 30 patients were clinically stable, 18 of 30 aneurysms were total occluded and two presented recanalizations. The objective ATLAS implantation was treatment stability. The treatment stability remained in 93% of our patients at four mounts and one year follow-up. In aneurysms with initial complete occlusion, this was maintained by the ATLAS system, while aneurysms with neck remnants showed no progression of the degree of closure. Our series of patients treated with ATLAS stents showed a very low rate of technical incidents (during the implantation and release of the stent) with permanent clinical complications (0%), compared with a review of series treated with other devices (1.4% to 4.3%).

CONCLUSION

The ATLAS stent is technically simple to implant and has a low thrombogenic potential. There are fewer problems associated with implantation, thromboembolic complications and hemorrhagic events compared with other types of stent, including braided stents. On the other hand, because of its low thrombogenic potential, partially occluded aneurysms or those with aneurysm remnants do not progress to complete occlusion.

CLINICAL RELEVANCE/APPLICATION

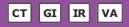
ATLAS stent implantation is useful to remaind the treatment stability of wide-neck auneurysms with complete initial occlusion with out or minimal procedure-related complications.



SSM24

Vascular Interventional (Portal Interventions)

Wednesday, Nov. 28 3:00PM - 4:00PM Room: E264



AMA PRA Category 1 Credit ™: 1.00 ARRT Category A+ Credit: 1.00

Participants

Naganathan B. Mani, MD, Chesterfield, MO (*Moderator*) Nothing to Disclose Nael E. Saad, MBBCh, ROCHESTER, NY (*Moderator*) Nothing to Disclose

Sub-Events

SSM24-01 Effect of Portal Decompression on Pulmonary Gas Exchange in Patients with Budd-Chiari Syndrome and Hepatopulmonary Syndrome

Wednesday, Nov. 28 3:00PM - 3:10PM Room: E264

Participants

Jiaywei Tsauo, Beijing, China (*Presenter*) Nothing to Disclose Xiaowu Zhang, Beijing, China (*Abstract Co-Author*) Nothing to Disclose He Zhao, Beijing, China (*Abstract Co-Author*) Nothing to Disclose Tao Gong, Beijing, China (*Abstract Co-Author*) Nothing to Disclose Jingui Li, Beijing, China (*Abstract Co-Author*) Nothing to Disclose Xiao Li, PhD, Chengdu, China (*Abstract Co-Author*) Nothing to Disclose

For information about this presentation, contact:

jiayweitsauo@qq.com

PURPOSE

To evaluate the effect of portal decompression on pulmonary gas exchange in patients with Budd-Chiari syndrome (BCS) and hepatopulmonary syndrome (HPS).

METHOD AND MATERIALS

From June 2014 to June 2015, all patients with BCS undergoing balloon angioplasty and transjugular intrahepatic portosystemic shunt creation at our institution were eligible for inclusion in this study. The primary endpoint was the changes in alveolar-arterial oxygen gradient (A-aO2) before and over 3 months after portal decompression.

RESULTS

Eleven patients with HPS (mean age, 51.7 years; six males) and 14 patients without HPS (mean age, 47.2 years; nine males) were included. Of the 11 patients with HPS, dyspnea was found in three (27.3%), all of which (100%) reported improvement in dyspnea after portal decompression. However, this improvement was not maintained at 3-month follow-up in two (33.7%) patients. For patients with HPS, the mean change in A-aO2 was statistically significant before and at 1 month (-11.7 \pm 6.4 mmHg; P < .001) but not at 2-3 days (-3.2 \pm 11.9 mmHg; P = .412) and 3 months (-1.3 \pm 12.5 mmHg; P = .757) after portal decompression. For patients without HPS, the mean change in A-aO2 was not statistically significant before and at 2-3 days (+1.4 \pm 8.3; P = .543) and 1 (+3.5 \pm 8.1 mmHg; P = .137) and 3 months (+1.3 \pm 8.2 mmHg; P = .565) after portal decompression. The overall mean changes in A-aO2 before and over 3 months after portal decompression was statistically significant for patients with HPS (-5.4 \pm 6.9 mmHg; P = .035) but not for patients without HPS (+2.0 \pm 7.6 mmHg; P = .333).

CONCLUSION

Portal decompression can improve pulmonary gas exchange in patients with BCS and HPS, but this effect is not sustainable at 3 months.

CLINICAL RELEVANCE/APPLICATION

1. Hepatopulmonary syndrome are common in patients with Budd-Chiari syndrome. 2. Portal decompression via balloon angioplasty and transjugular intrahepatic portosystemic shunt creation is effective and safe for the treatment of hepatopulmonary syndrome in patients with Budd-Chiari syndrome. 3. The treatment effect of balloon angioplasty and transjugular intrahepatic portosystemic shunt creation on hepatopulmonary syndrome is not sustainable at 3 months in patients with Budd-Chiari syndrome

SSM24-02 Outcomes in Cirrhotic Patients with Recurrent Ascites Who Received TIPS (Transjugular Intrahepatic Portosystemic Shunt) and/or Paracentesis

Wednesday, Nov. 28 3:10PM - 3:20PM Room: E264

Participants Kenneth J. Fearn, MD, Kansas City, KS (*Presenter*) Nothing to Disclose Steven M. Lemons, MD, Kansas City, KS (*Abstract Co-Author*) Nothing to Disclose Jacqueline Hill, PhD,MPH, Kansas City, KS (*Abstract Co-Author*) Nothing to Disclose Carissa Walter, Kansas City, KS (*Abstract Co-Author*) Nothing to Disclose Charles B. Davis, BS, Kansas City, KS (*Abstract Co-Author*) Nothing to Disclose Travis Everett, Kansas City, KS (*Abstract Co-Author*) Nothing to Disclose Trevor L. Everett, MD, Kansas City, KS (*Abstract Co-Author*) Nothing to Disclose

For information about this presentation, contact:

kjfearn@gmail.com

PURPOSE

Many cirrhotic patients who cannot undergo liver transplantation are symptomatically treated for recurrent ascites with paracenteses and/or transjugular intrahepatic portosystemic shunts (TIPS). Placing TIPS earlier in the cirrhotic disease process can potentially decrease the cost and inconvenience of repeated paracenteses. This study aimed to determine if there were differences in paracenteses and hospital admissions from bacterial peritonitis, variceal bleeds, and hepatic encephalopathy between cirrhotic patients who did and did not receive TIPS.

METHOD AND MATERIALS

A retrospective analysis was performed on all cirrhotic patients, age 18 and older, with refractory ascites between January 1, 2008 and December 31, 2016 at our institution. Demographics, cirrhosis etiology, lab values, paracentesis, TIPS, and hospitalization information were documented. A shared frailty model with TIPS placement as a time-varying covariate was used to calculate the association of time between paracentesis with TIPS placement, while chi-square tests examined the association between hospitalization rates for each outcome with TIPS placement.

RESULTS

A total of 344 patients with refractory ascites and a median age of 57 (IQR=50-62) were included. Of these, 92 (26.8%) received TIPS. Median MELD score at refractory date was higher among patients without TIPS compared to patients with TIPS (18 and 13, respectively; p<0.01). TIPS and the risk of paracentesis for ascites were highly associated (p<0.01). A 60% reduction in the risk of a paracentesis post-TIPS was observed regardless of MELD score, age, or gender (HR=0.40, 95%CI=0.33, 0.49). There was no significant difference in hospitalizations for bacterial peritonitis (p=0.13), variceal bleeding (p=0.23), or hepatic encephalopathy (p=0.46) between patients with and without TIPS.

CONCLUSION

This study found that cirrhotic patients with refractory ascites have a 60% reduction in the risk of receiving a paracentesis for symptomatic ascites after TIPS is placed with no change in hospitalizations for TIPS-associated outcomes. This suggests that TIPS placement should be considered earlier in the cirrhosis disease process to improve symptomatic control and decrease the need and associated costs of frequent paracenteses.

CLINICAL RELEVANCE/APPLICATION

Early placement of TIPS in cirrhotic patients reduces risk of repeat paracenteses without effecting hospitalization rates for common complications of ESLD.

SSM24-03 Optimal Energy Level in Assessment of TIPS Stent Luman in Dual-Energy CT Portal Venography in Liver Cirrhosis: A Prospective Study

Wednesday, Nov. 28 3:20PM - 3:30PM Room: E264

Participants Jian Dong, PhD, Beijing, China (*Presenter*) Nothing to Disclose Fuliang He, Beijing, China (*Abstract Co-Author*) Nothing to Disclose ChunYan Zhang, Beijing, China (*Abstract Co-Author*) Nothing to Disclose

For information about this presentation, contact:

dongjianradiology@163.com

PURPOSE

To investigate the optimal energy level in monochromatic imaging of portal vein for the assessment of transjugular intrahepatic portosystemic shunt stent (TIPSS) lumen using 16-cm wide-detector spectral CT.

METHOD AND MATERIALS

Thirty-seven patients with TIPSS for portal hypertension performed spectral CT (Revolution, GE Healthcare) portal venography (CTPV) in our study. 120 kVp-like images as well as 4 groups of monochromatic images from 55 to 85 keV with an interval of 10 keV were collected. CTPV images at main portal vein, proximal, middle and distant level of stent were evaluated. Objective image quality indexes for portal vein and stent lumen included CT attenuations, noise, signal-to-noise ratio (SNR) and contrast-to-noise ratio (CNR) were measured. Two experienced radiologists subjectively evaluated image quality independently with a 5-point scale on image quality and diagnostic confidence was obtained.

RESULTS

Within 37 patients with TIPS, 3 were classified into grade A, 24 were classified as grade B while 10 were graded C according to Child - Pugh staging. In portal vein and stent lumen, CT attenuations, SNR and CNR decreased with the increase of keV (all P<0.01). CT attenuations were higher than 200 HU in 55 keV (287.6 \pm 36.9 HU) and 65 keV (223.1 \pm 42.7 HU) in portal vein and stent lumen. Images at 55 keV demonstrated the highest objective indexes (CT attenuations, SNR and CNR). However, the subject score was the lowest (2.1 \pm 0.7), with 9 (24.3%) of undiagnosed rate. Images at 65 keV exhibited highest subjective image quality score (3.6 \pm 0.8) and diagnostic confidence (3.3 \pm 0.6) while the second best CT attenuations, noise, SNR and CNR (all P<0.01). Subjective as well as objective indexes at 75 keV showed no statistical difference from 120 kVp-like group (all P>0.05), and these 75 keV indexes were inferior to 65 keV group, and superior to 85 keV group.

CONCLUSION

In manachromatic impains of nortal vain for the accommant of transitional intrahanatic nortaevetamic chunt stant (TIDCC) luman

using 16-cm wide-detector spectral CT, images at 55 keV manifested best objective image quality (CT attenuation, SNR and CNR), while 65 keV images demonstrated best subjective image quality and diagnostic confidence.

CLINICAL RELEVANCE/APPLICATION

It is recommended to conduct CT portal venography using 16-cm wide-detector spectral CT for the visualization of TIPS stent lumen in liver cirrhosis patients at 65 keV.

SSM24-04 Metal Artifact Reductions with Monochromatic Imaging in Spectral CT Portal Venography after Gastric Coronary Vein Embolization (GCVE) in Portal Hypertension: A Comparative Study

Wednesday, Nov. 28 3:30PM - 3:40PM Room: E264

Participants

Jian Dong, PhD, Beijing, China (*Presenter*) Nothing to Disclose Fuliang He, Beijing, China (*Abstract Co-Author*) Nothing to Disclose

For information about this presentation, contact:

dongjianradiology@163.com

PURPOSE

To investigate the clinical value of metal artifact reductions (MARs) combined with monochromatic imaging in spectral CT portal venography (CTPV) after gastric coronary vein embolization (GCVE) by comparison with 120 kVp-like imaging.

METHOD AND MATERIALS

Thirty-one patients with GCVE artifacts were performed CTPV with spectral CT in our study. All raw data were reconstructed as 120 kVp-like imaging without MARs (group A), and monochromatic imaging with MARs at 65 keV (group B) and 74 keV (group C), respectively. Three slices of CTPV images were evaluated, including main portal vein, heaviest artifacts and no artifacts level from all groups. Objective indexes for portal vein included signal intensity (SI), standard deviation (SD), signal-to-noise ratio (SNR), contrast-to-noise ratio (CNR) and artifact index (AI). Subjective indexes were assessed by two radiologists separately with 5-point scale. Statistical analyses were analyzed.

RESULTS

With the use of MARs, AI in group B (29.1 ± 3.6)and C (35.6 ± 4.4) are much lower than group A (87.2 ± 11.3)(P<0.01). As for the quantitative indices of main portal vein, group B demonstrates the highest SI (243 ± 20.6), SNR (22.1 ± 3.7) and CNR (11.5 ± 2.6) than the other two groups (all P<0.01), while there is no statistical differences in SI (184 ± 19.7 Versus 179 ± 21.6), SNR (20.4 ± 3.1 Versus 21.6 ± 3.7) and CNR (9.2 ± 2.4 Versus 9.6 ± 2.9) between group A and C (all P>0.05). For subjective assessment, group B (3.8 ± 1.6) is superior to group A (2.1 ± 1.4)and (3.1 ± 1.1) (P<0.01).

CONCLUSION

Combination of MARs with monochromatic imaging decreased metal artifacts, and improved image quality in spectral CT portal venography with GCVE, with 65 keV as the optimal energy level.

CLINICAL RELEVANCE/APPLICATION

It is recommended that 65 keV with MARs as the optimal CTPV protocol for liver cirrhosis patients with GCVE.

SSM24-05 Role of Preoperative MSCT and MRI for Endovascular Procedures in Budd-Chiari Syndrome with Inferior Vena Cava (IVC) Obstruction: A Retrospective Study of 112 Cases

Wednesday, Nov. 28 3:40PM - 3:50PM Room: E264

Participants Xiangwen Xia, Wuhan, China (*Presenter*) Nothing to Disclose Dehan Liu, Wuhan, China (*Abstract Co-Author*) Nothing to Disclose Tianhe Ye, Wuhan, China (*Abstract Co-Author*) Nothing to Disclose Chuansheng Zheng, Wuhan, China (*Abstract Co-Author*) Nothing to Disclose

For information about this presentation, contact:

xinwu0401@163.com

PURPOSE

This article focuses specifically on the obstructive characteristics, collateral vessels and floating thrombus demonstrated on preoperative imaging, to determine the role of preoperative MSCT and/or MRI for endovascular procedures.

METHOD AND MATERIALS

This retrospective analysis included 112 patients who underwent endovascular procedures for BCS between October 2009 and Jun 2017 in our institution. All patients had preoperative MSCT and/or MRI imaging. Two radiologists independently assessed (on a 5-point scale) the imaging data to evaluate diagnostic accuracy, inter-reader agreement, and association between imaging presentation and interventional procedures.

RESULTS

Eighty-two patients had preoperative MSCT data and corresponding sensitivities were 83.33%, 86.96%, 88%, and 81.25% for reader 1, and 83.33%, 91.30%, 92.00%, and 81.25% for reader 2. Thirty two patients had preoperative MRI data and corresponding sensitivities were 88.89%, 100%, 100%, and 83.33% for reader 1, and 100%, 100%, 100% and 100% for reader 2. Areas under the receiver operating characteristic curves (AUCs) for judging IVC secondary thrombus were 0.88 for reader 1, 0.87 for reader 2 in group MSCT, and 0.975 for reader 1, 0.933 for reader 2 in group MRI. Inter-reader agreement was substantial or excellent for diagnostic accuracy (κ =0.745-0.927).

CONCLUSION

In patients with BCS, it is important to focus preoperatively on the degree and extent of the obstruction, collateral vessels and floating thrombus, to optimize interventional procedures and minimize complications.

CLINICAL RELEVANCE/APPLICATION

Interventional therapy is the preferred microinvasive therapeutic for patients with BCS, however, varying degree of procedurerelated complications still exist. If we properly estimate obstructive characteristics preoperatively and detect risk factors, such as dangerous collateral vessels and IVC secondary thrombosis, we can design a reasonable interventional program and minimize complications.

SSM24-06 The Feasibility and Utility of the Overlay Technique Under Cone-Beam Computed Tomography Guidance for Portal Vein Puncture During Transjugular Intrahepatic Portosystemic Shunt

Wednesday, Nov. 28 3:50PM - 4:00PM Room: E264

Participants

Cheng Sun, Tianjin, China (*Presenter*) Nothing to Disclose Changlu Yu, Tianjin, China (*Abstract Co-Author*) Nothing to Disclose Kefeng Jia, Tianjin, China (*Abstract Co-Author*) Nothing to Disclose

PURPOSE

The purpose of this study was to investigate the feasibility and utility of the overlay technique under cone-beam computed tomography (CBCT) which was used as a navigation method for portal vein puncture during transjugular intrahepatic portosystemic shunt (TIPS).

METHOD AND MATERIALS

From February 2016 to April 2017, 15 consecutive cirrhotic patients (12 males and 3 females; mean age 58 years, range from 44 to 68 years) received TIPS treatment and prospectively enrolled in this study. An initial CBCT image acquisition was performed before TIPS and we applied the overlay technique by register the preoperative contrast enhanced CT or MRI portal venous phase images with the newly acquired CBCT images. According to the overlaid images, a planned needle path was made and displayed simultaneously on the axial, sagittal and coronal plane. The angle from hepatic vein to portal vein was calculated manually on three planes and intended for the interventional radiologists' reference. The contrast material consumption, number of needle puncture attempts, radiation dose and fluoroscopic time were recorded from hepatic vein catheterization to portal vein entry.

RESULTS

The overlay technique was technically feasible in 14 of 15 patients (93%). The only failure was due to the overlay misregistration caused by progress of ascites. No complications were observed postoperative monitoring. The mean (\pm SD) contrast material consumption was 38 \pm 9.2ml, number of needle attempts was 1.9 \pm 1.1 punctures(range 1 to 4), dose area product (DAP) was 138 \pm 55.8 Gy·cm3 ,fluoroscopic time was 19 \pm 5.5min.

CONCLUSION

The overlay technique under CBCT guidance is a feasible and safe method for TIPS portal vein puncture. It contributes to the creation of TIPS and facilitate the portal vein pressure reduction.

CLINICAL RELEVANCE/APPLICATION

The overlay techique under cone-beam computed tomography for portal vein puncture during TIPS is feasible, safe and helps portal puncture vein pressure reduction.



MSCT42

Case-based Review of Thoracic Radiology (Interactive Session)

Wednesday, Nov. 28 3:30PM - 5:00PM Room: S406A



AMA PRA Category 1 Credits ™: 1.50 ARRT Category A+ Credit: 1.75

Participants

Diana Litmanovich, MD, Haifa, Israel (Director) Nothing to Disclose

Sub-Events

MSCT42A Thoracic Emergencies

Participants Sanjeev Bhalla, MD, Saint Louis, MO (*Presenter*) Nothing to Disclose

For information about this presentation, contact:

sanjeevbhalla@wustl.edu

LEARNING OBJECTIVES

1) To use cases to highlight an approach to embolic disease. 2) To use cases to discuss the acute aortic syndromes. 3) To review other conditions which may manifest with acute chest pain.

Honored Educators

Presenters or authors on this event have been recognized as RSNA Honored Educators for participating in multiple qualifying educational activities. Honored Educators are invested in furthering the profession of radiology by delivering high-quality educational content in their field of study. Learn how you can become an honored educator by visiting the website at: https://www.rsna.org/Honored-Educator-Award/ Sanjeev Bhalla, MD - 2014 Honored EducatorSanjeev Bhalla, MD - 2016 Honored EducatorSanjeev Bhalla, MD - 2017 Honored EducatorSanjeev Bhalla, MD - 2018 Honored Educator

MSCT42B Large Airway Disorders

Participants Phillip M. Boiselle, MD, Boca Raton, FL (*Presenter*) Nothing to Disclose

For information about this presentation, contact:

pboiselle@health.fau.edu

LEARNING OBJECTIVES

1) Apply a pattern-based approach to enhance accurate detection, characterization and diagnosis of a variety of benign and malignant large airway disorders. 2) Recognize normal variants which may mimic large airways diseases. 3) Understand the importance of carefully inspecting the large airways on CT scans.

Honored Educators

Presenters or authors on this event have been recognized as RSNA Honored Educators for participating in multiple qualifying educational activities. Honored Educators are invested in furthering the profession of radiology by delivering high-quality educational content in their field of study. Learn how you can become an honored educator by visiting the website at: https://www.rsna.org/Honored-Educator-Award/ Phillip M. Boiselle, MD - 2012 Honored Educator

MSCT42C Cystic Lung Disease

Participants Theresa C. McLoud, MD, Boston, MA (*Presenter*) Nothing to Disclose

LEARNING OBJECTIVES

1) Learn to distinguish cystic lung disease from bronchiectasis and emphysema. 2) Recognize specific features of different cystic disease entities. 3) Understand the common complications, other systemic findings and prognosis of each of the entities discussed.

MSCT42D Adult Manifestations of Congenital Lung Disease

Participants

Diane C. Strollo, MD, Gibsonia, PA (Presenter) Nothing to Disclose

LEARNING OBJECTIVES

1) Recognize the spectrum of congenital lung abnormalities that may manifest in adulthood. 2) Understand developmental abnormalities of tracheobronchial tree, to include anomalous branching, such as bronchial atresia, and airway malformations such as

congenital lobar emphysema and congenital pulmonary airway malformation. 3) Review etiologies of intra- and extra-lobar sequestration and partial anomalous pulmonary venous return. 4) Discuss characteristic imaging findings and clinical management.



MSES44

Essentials of Genitourinary Imaging

Wednesday, Nov. 28 3:30PM - 5:00PM Room: E450A

GU

AMA PRA Category 1 Credits ™: 1.50 ARRT Category A+ Credit: 1.75

Sub-Events

MSES44A Management of Incidental Renal Findings

Participants

Brian R. Herts, MD, Cleveland, OH (Presenter) Grant, Siemens AG

For information about this presentation, contact:

hertsb@ccf.org

LEARNING OBJECTIVES

1) Define an incidental renal mass. 2) Understand the features of a renal mass that should be evaluated before recommending further evaluation or management. 3) Describe the best options for further evaluation on an incompletely characterized incidental renal mass.

ABSTRACT

Renal masses are common and often detected as an incidental finding on cross-sectional imaging studies. While most incidental renal masses are benign cysts, the majority of renal cell carcinomas are also incidental findings; therefore it is important to correctly identify potential renal cell carcinomas, but not unnecessarily image benign lesions. The management of the incidental renal lesion is based on the features of a fully characterized mass, indentification of reliably benign features, or of indeterminate features that need further evaluation before management can be recommended. This presentation will review the features that allow us to make these determinations, based on the type of imaging available at the time of the detection of the incidental renal mass. The utility of MR, active surveillance and percutaneous biopsy in the management of incidental renal masses will also be discussed.

MSES44B Management of Incidental Adrenal Findings

Participants William W. Mayo-Smith, MD, Boston, MA (*Presenter*) Nothing to Disclose

For information about this presentation, contact:

wmayo-smith@bwh.harvard.edu

LEARNING OBJECTIVES

1) Describe frequency of adrenal incidentalomas. 2) Explain advances in imaging techniques to differentiate benign from malignant adrenal tumors. 3) Describe 2017 American College of Radiology Adrenal Incidentaloma Algorithm.

ABSTRACT

Review the ACR Adrenal Incidental Findings Algorithm

MSES44C Management of Incidental Adnexal Findings

Participants Susan M. Ascher, MD, Washington, DC (*Presenter*) Nothing to Disclose

For information about this presentation, contact:

aschers@gunet.georgetown.edu

LEARNING OBJECTIVES

1) Comprehend the importance of Adnexal Incidentalomas and the rationale for having a vetted approach to manage them. 2) Apply accepted algorithms for the management of Adnexal Incidentalomas. 3) Analyze the data for adherence to published recommendations to include methods for improvement.

MSES44D First Trimester Emergencies: Where is the Baby?

Participants Katherine M. Richman, MD, La Jolla, CA (*Presenter*) Nothing to Disclose

For information about this presentation, contact:

kmrichman@ucsd.edu

LEARNING OBJECTIVES

1) Know the criteria to call a nonviable pregnancy. 2) Know the algorithm for pregnancy of unknown location. 3) Know the appearance of a variety of ectopic pregnancies.

ABSTRACT

The course discusses the types of first trimester emergencies a radiologist may encounter including ectopic pregnancies, molar pregnancies, completed and in progress spontaneous abortions, fetal demise, and pregnancy of unknown location.



MSSR44

RSNA/ESR Sports Imaging Symposium: Postoperative Imaging of Sports Injuries (Interactive Session)

Wednesday, Nov. 28 3:30PM - 5:00PM Room: E352



AMA PRA Category 1 Credits ™: 1.50 ARRT Category A+ Credit: 1.75

FDA Discussions may include off-label uses.

Participants

Laura W. Bancroft, MD, Orlando, FL (*Moderator*) Author with royalties, Wolters Kluwer nv; Speaker, World Class CME; Editor, Thieme Medical Publishers, Inc; Travel support, Thieme Medical Publishers, Inc; ;

Andrew J. Grainger, MRCP, FRCR, Leeds, United Kingdom (Moderator) Consultant, Levicept Ltd; Director, The LivingCare Group;

For information about this presentation, contact:

andrewgrainger@nhs.net

Sub-Events

MSSR44A Postoperative Shoulder MRI after Instability Surgery

Participants

Laura W. Bancroft, MD, Orlando, FL (*Presenter*) Author with royalties, Wolters Kluwer nv; Speaker, World Class CME; Editor, Thieme Medical Publishers, Inc; Travel support, Thieme Medical Publishers, Inc; ;

For information about this presentation, contact:

laura.bancroft.md@flhosp.org

LEARNING OBJECTIVES

1) To become familiar with the expected and abnormal MR imaging findings after labral repair. 2) To learn about the postoperative imaging features after capsular shift/capsulorrhaphy. 3) To appreciate normal imaging and complications after remplissage and Laterjet/Bristow procedures.

MSSR44B ACL Reconstruction and Cartilage Repair

Participants

Claudia Weidekamm, MD, Napier, New Zealand (Presenter) Nothing to Disclose

LEARNING OBJECTIVES

1) To review the common and uncommon ACL reconstruction techniques. 2) To appreciate the expected and abnormal MR imaging findings after ACL reconstruction. 3) To understand common cartilage repair techniques, and corresponding normal and abnormal postoperative MRIs.

ABSTRACT

The aim of ACL reconstruction is to stabilize the knee and prevent chondral and meniscal injuries, which are sequelae of anteroposterior translation and are associated with early osteoarthritis. The idea of the double-bundle ACL graft was to restore normal joint kinematics by anatomic reconstruction of the anteromedial and the posterolateral bundle of the original ACL. This was expected to improve clinical outcomes and restore anterior and rotational knee stability. The single-bundle technique, however, causes less osseous defects and is still a popular technique. Complications, such as ACL graft failure, impingement, cyclops lesion, arthrofibrosis, and patellar inferior syndrome, are discussed. The second part of this presentation will illustrate cartilage repair techniques and imaging findings. The radiologist must be familiar with the different cartilage repair procedures and characteristics in cartilage imaging to evaluate long-term progression or failure. Abnormal postoperative findings include hypertrophic filling, incomplete integration of the transplant into the surrounding cartilage, or subchondral defects, osteophytes, cysts, and persistent bone marrow edema and joint effusion.

MSSR44C Interactive Case Discussion

Participants

Laura W. Bancroft, MD, Orlando, FL (*Presenter*) Author with royalties, Wolters Kluwer nv; Speaker, World Class CME; Editor, Thieme Medical Publishers, Inc; Travel support, Thieme Medical Publishers, Inc; ; Claudia Weidekamm, MD, Napier, New Zealand (*Presenter*) Nothing to Disclose

For information about this presentation, contact:

laura.bancroft.md@flhosp.org

claudia.schueller-weidekamm@meduniwien.ac.at

4) To be a set of the set of the

LEARNING OBJECTIVES

1) To become raminar with the diagnostic reatures of railed ACL reconstructions. 2) To understand the imaging reatures of intact and failed cartilage repair.

ABSTRACT

Postoperative imaging after ACL or cartilage repair is indicated in patients with ongoing pain/instability or repetitive injury. Radiography remains the initial imaging modality; however, further assessment with CT or MRI is recommended. With a clear emphasis on MRI, we will review normal postoperative findings and complications after ACL reconstructions and cartilage repair. The case discussion will cover the most significant pathologies and pitfalls, and normal postoperative findings will be illustrated.



MSRT46

ASRT@RSNA 2018: Toward True Professionalism - Becoming Your 'True Self'

Wednesday, Nov. 28 3:40PM - 4:40PM Room: N230B

PR

AMA PRA Category 1 Credit ™: 1.00 ARRT Category A+ Credit: 1.00

Participants

Philip P. Kennedy, Saint John, NB (Presenter) Nothing to Disclose

For information about this presentation, contact:

philip.kennedy@horizonnb.ca

LEARNING OBJECTIVES

1) Identify factors contributing to the current accelerating decline in professionalism in health care professions across North America. 2) Compare professionalism traits and characteristics with traits and characteristics of self-actualizing individuals. 3) Define ego as the 'false-self'. 4) Explain how the false-self arises and why egotism is the single most important inhibiting factor to self-actualization and the development of true professionalism traits and characteristics. 5) Define the 'true-self' as consciousness and the sense of beingness that accompanies it. 6) Apply personal growth strategies toward self-actualization and the development of true professionalism traits and characteristics.

ABSTRACT

Health care is in the midst of a professionalism crisis. Professionalism is on an accelerating decline across all professions in North America, indicating that current efforts toward teaching and promoting professionalism simply are not working. Therefore new strategies for understanding, teaching, and promoting professionalism in educational institutions as well as in the workplace are needed. This presentation proposes new strategies for defining and understanding professionalism, and suggests ways of effectively facilitating the development of true and enduring professionalism traits and characteristics in individuals.



MSRO49

BOOST: eContouring (Spinal SBRT)

Wednesday, Nov. 28 4:30PM - 5:30PM Room: S104B



AMA PRA Category 1 Credit ™: 1.00 ARRT Category A+ Credit: 1.00

Participants

Simon S. Lo, MD, Seattle, WA (Presenter) Editor, Springer Nature;

Kristin J. Redmond, MD, MPH, Baltimore, MD (*Presenter*) Research support, Elekta AB; Research support, Accuray Incorporated; Speaker, Accuray Incorporated; Travel support, Accuray Incorporated; Consultant, Medtronic plc William T. Yuh, MD, Seattle, WA (*Presenter*) Nothing to Disclose

For information about this presentation, contact:

simonsmlo@gmail.com

LEARNING OBJECTIVES

1) Describe consensus CTV delineation for spine metastases in intact vertebra based on the extent of gross disease. 2) Describe consensus CTV delineation for post-operative spine SBRT including the imaging series most valuable in the contouring process. 3) Describe optimal spinal cord delineation. 4) Explain when CT myelogram may be important in treatment planning for SBRT for spinal metastases.

ABSTRACT

To perform stereotactic body radiotherapy for spinal metastases safely and effectively, proper target delineation based on patterns of failure and practice guidelines and proper spinal cord contouring are paramount. This session will provide guidance for contouring.



RCA45

Creating Patient-Specific Anatomical Models for 3D Printing and AR/VR (Hands-on)

Wednesday, Nov. 28 4:30PM - 6:00PM Room: S401AB

IN

AMA PRA Category 1 Credits ™: 1.50 ARRT Category A+ Credit: 0

Participants

Nicole Wake, PhD, New York, NY (*Presenter*) In-kind support, Stratasys, Ltd Amy E. Alexander, MSc, Rochester, MN (*Presenter*) Nothing to Disclose Andy Christensen, BS, Littleton, CO (*Presenter*) Consultant, Integrum AB; Board Member, Integrum AB; Stockholder, Somaden LLC Peter C. Liacouras, PhD, Bethesda, MD (*Presenter*) Nothing to Disclose Jane S. Matsumoto, MD, Rochester, MN (*Presenter*) Nothing to Disclose Todd Pietila, MBA, Plymouth, MI (*Presenter*) Employee, Materialise NV

For information about this presentation, contact:

nicole.wake@med.nyu.edu

LEARNING OBJECTIVES

1) Classify various image post-processing and 3D modeling software programs for enabling 3D printing or AR/VR applications. 2) Explain the workflow to create patient-specific 3D anatomical models from medical images. 3) Identify and apply image segmentation techniques used to create 3D anatomical models, including thresholding, region growing, and manual editing. 4) Describe and apply image post-processing techniques and 3D design principles required to save models in appropriate file formats (i.e. STL or OBJ). 5) Interface with 3D printing software or AR/VR devices.

ABSTRACT

Advanced image data visualization in the form of 3D printing and AR/VR continues to expand in clinical settings. In order to generate patient-specific models for 3D printing or AR/VR, image data must first be segmented and converted to virtual 3D models which represent the intended anatomy of interest. The RSNA 3D Printing Special Interest Group has adopted a position statement reflecting the FDA recommendation that FDA-cleared software is used when 3D models are created for clinical applications. This course covers the use of industry-standard FDA-cleared software (Mimics InPrint, Materialise, NV) for the design and fabrication of patient-specific 3D models. Cranio-maxillofacial and renal case examples will be shown. Once the virtual 3D models have been created, users will learn how to prepare these files for 3D printing and AR/VR. In order to aid with the hands-on course, an extensive training manual will be provided before the meeting. It is highly recommended that participants review the training manual to optimize the experience at the workstation.

Active Handout:Nicole Wake

http://abstract.rsna.org/uploads/2018/18020329/Handouts_RC-45 RCA45.pdf



RCC45

Informatics Strategic Planning and Execution: How-To's and Lessons Learned

Wednesday, Nov. 28 4:30PM - 6:00PM Room: S501ABC



AMA PRA Category 1 Credits ™: 1.50 ARRT Category A+ Credit: 1.75

Participants

Christopher J. Roth, MD, Raleigh, NC (Moderator) Nothing to Disclose

LEARNING OBJECTIVES

1) Learn how to create an effective imaging IT and informatics strategic plan that will align practice and health system operations, infrastructure, capabilities, human resources, and provider governance around future direction. 2) Understand how your strategic plan can incorporate cross cutting themes like revenue, care quality, branding, and innovation in areas such as EHR image enablement, image exchange, clinical decision support, procurement, and IT security.

ABSTRACT

Since almost all of radiology based in IT and informatics today, having a broad and multifaceted imaging informatics strategic plan is necessary. An imaging IT and informatics strategic plan requires alignment between the goals of your practice - private or academic - and your health system, and your department and health system IT teams. Strategic plan creation is however complex and time consuming work. This session will provide time saving how-tos and lessons learned from private practice and academic radiology departments who have successfully deployed an imaging informatics strategy.

Sub-Events

RCC45A Private Practice Informatics Strategy Development

Participants

Syed Furqan Zaidi, MD, El Segundo, CA (*Presenter*) Nothing to Disclose

For information about this presentation, contact:

syed.zaidi@radpartners.com

LEARNING OBJECTIVES

1) Discuss data analytic tools to measure clinical quality and outcomes. 2) Identify data mining strategies to build the radiology department's quality platform. 3) Describe the use of data mining to engage in population health management.

ABSTRACT

The purpose of this session is to educate radiologists about data analytics tools available for use, along with data mining strategies. The application of data mining to demonstrate the value and impact of radiology on downstream quality and utilization in healthcare will be discussed. Private practice strategies to use analytics as a strategic differentiator as well as defining the role of radiology in population health management, will be discussed.

RCC45B Radiology Department Informatics Strategy Development

Participants

Cree M. Gaskin, MD, Charlottesville, VA (*Presenter*) Author with royalties, Oxford University Press; Author with royalties, Thieme Medical Publishers, Inc; Research Grant, Carestream Health, Inc;

For information about this presentation, contact:

cree@virginia.edu

LEARNING OBJECTIVES

1) Identify major radiology informatics issues that may warrant a strategic plan. 2) Apply radiology departmental informatics strategies which have been successful at other institutions.

RCC45C Enterprise Imaging Informatics Strategy Development

Participants

Christopher J. Roth, MD, Raleigh, NC (Presenter) Nothing to Disclose

LEARNING OBJECTIVES

1) Understand methods for gathering and aligning individual and department imaging informatics needs with enterprise wide Goals, Strategies, Key Initiatives, Outcomes, Future States, Dependencies and Risks. 2) Review some strategic planning frameworks applicable to health systems wishing to pursue image capture, storage, indexing, EHR distribution, viewing, exchange, analytics, and governance for the spectrum of enterprise imaging content they own.



SPDL41

Neuro and MSK (Case-based Competition)

Wednesday, Nov. 28 4:30PM - 6:00PM Room: E451B



AMA PRA Category 1 Credits ™: 1.50 ARRT Category A+ Credit: 1.75

Participants

Paul J. Chang, MD, Chicago, IL (*Presenter*) Co-founder, Koninklijke Philips NV; Researcher, Koninklijke Philips NV; Researcher, Bayer AG; Advisory Board, Aidoc Ltd; Advisory Board, EnvoyAI; Advisory Board, Inference Analytics Omer A. Awan, MD, Philadelphia, PA (*Presenter*) Nothing to Disclose Gregory L. Katzman, MD, Chicago, IL (*Presenter*) Nothing to Disclose Neety Panu, MD, FRCPC, Ottawa, ON (*Presenter*) Nothing to Disclose

LEARNING OBJECTIVES

1) Be introduced to a series of neuroradiology and musculoskeletal radiology case studies via an interactive team game approach designed to encourage 'active' consumption of educational content. 2) Use their mobile wireless device (tablet, phone, laptop) to electronically respond to various imaging case challenges; participants will be able to monitor their individual and team performance in real time. 3) Receive a personalized self-assessment report via email that will review the case material presented during the session, along with individual and team performance. *This interactive session will use RSNA Diagnosis Live™*. Please bring your charged mobile wireless device (phone, tablet or laptop) to participate.

ABSTRACT

The extremely popular audience participation educational experience, Diagnosis Live!, is an expert-moderated session featuring a series of interactive case studies that will challenge radiologists' diagnostic skills and knowledge. The session features a lively, fast-paced game format: participants will be automatically assigned to teams who will then use their personal mobile devices to test their knowledge in a fast-paced session that will be both educational and entertaining. After the session, attendees will receive a personalized self-assessment report via email that will review the case material presented during the session, along with individual and team performance.



Controversy Session: Marginally Operable Stage I Non-small Cell Lung Cancer: Cut or Shoot (Surgery vs Radiation)?

Wednesday, Nov. 28 4:30PM - 6:00PM Room: E353C

CH RO

AMA PRA Category 1 Credits ™: 1.50 ARRT Category A+ Credit: 1.75

Participants

Candice A. Johnstone, MD, Milwaukee, WI (Moderator) Nothing to Disclose

For information about this presentation, contact:

cjohnstone@mcw.edu

Sub-Events

SPSC41A Evaluation of Suspicious Lung Nodule: Can Diagnostic Imaging Confidently Diagnose Non-small Cell Lung Cancer?

Participants

Michelle S. Ginsberg, MD, New York, NY (Presenter) Nothing to Disclose

LEARNING OBJECTIVES

1) To discuss imaging features of lung cancer and ability to accurately diagnose lung cancer. 2) To describe CT features of lepidic predominant adenocarcinoma that correlate with invasiveness on pathology.

SPSC41B Case for Surgical Resection

Participants

David W. Johnstone, Milwaukee, WI (Presenter) Nothing to Disclose

For information about this presentation, contact:

djohnstone@mcw.edu

LEARNING OBJECTIVES

1) Appraise the current data supporting surgical resection for early stage non-small cell carcinoma of the lung. 2) Understand the definitions of sublobar resection and lobectomy. 3) Compare outcomes between surgical resection and radiation therapy for early stage non-small cell carcinoma. 4) Appraise ongoing clinical trials comparing radiation to surgical resection for early stage lung cancer.

SPSC41C Case of Stereotactic Body Radiotherapy

Participants Gregory Videtic, MD, FRCPC, Cleveland, OH (*Presenter*) Nothing to Disclose

For information about this presentation, contact:

videtig@ccf.org

LEARNING OBJECTIVES

1) To discuss the approach to the radiographically suspicious lung nodule. 2) To discuss the management options including surgery and radiotherapy to address the suspicious nodule. 3) To discuss the evidence to support radiotherapy in the form of SBRT for the suspicious nodule.

ABSTRACT

TO discuss the clinically controversial question: 'Marginally operable stage I NSCLC:cut or shoot (surgery vs. radiation)?' A diagnostic radiologist will discuss the management approach for the radiographically suspicous lung nodule. A thoracic surgeon will discuss the role of surgery. A thoracic radiation oncologist will discuss the role for lung stereotactic body radiotherapy (SBRT).



Controversy Session: CT or MRI after Equivocal Appendix Visualization on Pediatric Ultrasound?

Wednesday, Nov. 28 4:30PM - 6:00PM Room: N226



AMA PRA Category 1 Credits ™: 1.50 ARRT Category A+ Credit: 1.75

Participants

Geetika Khanna, MD, MS, Iowa City, IA (Moderator) Nothing to Disclose

Sub-Events

SPSC43A CT for Appendicitis

Participants

Andrew T. Trout, MD, Cincinnati, OH (*Presenter*) Author, Reed Elsevier; Research Grant, Siemens AG; Research Grant, Canon America Medical Systems Corporation; Board Member, Joint Review Committee on Educational Programs in Nuclear Medicine Technology; Travel support, Koninklijke Philips NV; Consultant, Guerbet SA

For information about this presentation, contact:

andrew.trout@cchmc.org

LEARNING OBJECTIVES

1) Examine the evidence for CT for acute appendicitis in children. 2) Debate the role of CT versus other modalities for imaging of appendicitis in children. 3) Define the optimal imaging strategy for appendicitis in their practice.

SPSC43B MRI for Appendicitis

Participants

Michael S. Gee, MD, PhD, Boston, MA (Presenter) Nothing to Disclose

For information about this presentation, contact:

msgee@mgh.harvard.edu

LEARNING OBJECTIVES

1) To learn indications for MRI in pediatric appendicitis evaluation. 2) To apply knowledge of current literature on MRI performance for pediatric appendicitis diagnosis. 3) To analyze technical and patient-related considerations for performance of MRI in children for appendicitis evaluation.



Controversy Session: Gadolinium for MR Examination: To Give or Not to Give

Wednesday, Nov. 28 4:30PM - 6:00PM Room: N228



AMA PRA Category 1 Credits ™: 1.50 ARRT Category A+ Credit: 1.75

FDA Discussions may include off-label uses.

Participants

Yoshimi Anzai, MD, Salt Lake City, UT (Moderator) Nothing to Disclose

Max Wintermark, MD, Lausanne, Switzerland (*Moderator*) Advisory Board, General Electric Company; Consultant, More Health; Consultant, Magnetic Insight; Consultant, Icometrix; Consultant, Nines;

LEARNING OBJECTIVES

1) To learn the biological mechanism of GBCAs deposition in brain. 2) To understand implications of GBCAs deposition in patients. 3) To review the consensus recommendation for the clinical and research use of GBCAs. 4) To discuss how radiologists communicate with referring physicians and patients.

ABSTRACT

There has been emerging evidence of brain deposition of Gadolinium-based contrast agents (GBCAs) in patients who had received multiple doses of GBCAs in a dose-dependent manner. It has raised safety concern among imaging community, particularly for patients who regularly receive GBCAs. It is yet to be known if there are clinically significant manifestations or symptoms caused by brain deposition of GBCAs. Use of GBCAs on MRI help diagnose, evaluate, and differentiate various diseases. In this controversy session, we have four distinguished experts in this field to discuss i) the biological mechanism and of GBCAs deposition, ii) the current practice within and outside of the United States, and iii) how practicing radiologists should communicate the issue with referring physicians and patients.

Sub-Events

SPSC44A Gadolinium Deposition: Mechanism and Bio-distribution

Participants

Robert J. McDonald, MD, PhD, Rochester, MN (*Presenter*) Consultant, General Electric Company; Research Grant, General Electric Company; Consultant, Bracco Group

SPSC44B How Does Gadolinium Get to the Other Side of the Blood Brain Barrier

Participants

Emanuel Kanal, MD, Pittsburgh, PA (*Presenter*) Consultant, Medtronic plc; Investigator, Bracco Group; Royalties, Guerbet SA; Consultant, Koninklijke Philips NV

For information about this presentation, contact:

ekanal@pitt.edu

LEARNING OBJECTIVES

1) Identify the structure of the blood brain barrier and the blood CSF barrier and the major anatomical and functional differences between them. 2) Describe possible pathways for gadolinium to get to the other side of the blood brain barrier, which is supposedly a functional barrier that it does not cross. 3) Identify similarities and differences among the available GBCA in clinical neuroradiologic use today in neurologic bio-distribution and toxicity.

ABSTRACT

In the past few years there has been much attention focused on the fact that minute amounts of gadolinium remain, and can be found, within the brain, bones, and other tissues of patients who receive gadolinium based contrast agents (GBCA), even years after their last administration. Many questions have been raised concerning such residual gadolinium, including whether or not there are toxic effects of such retention, the molecular form(s) in which the residual gadolinium is found, and possible similarities or differences that might exist between the various GBCA. Among the unresolved questions associated with gadolinium retention in the brain concerns the seemingly paradoxical observation that these neuroradiologic GBCA do not cross an intact blood brain barrier (BBB.) However, several histologic studies have now found residual gadolinium in the brain parenchyma, which of course is on the other side of the BBB. If intravenously administered GBCA do not cross an intact BBB, then how, on these autopsy studies, did they get to the brain parenchyma in which they have been detected? This presentation will attempt to address this issue and provide possible explanations that might simultaneously shed light on the normal physiologic pathways GBCA traverse even in patients with normal renal function - and of which many may have been heretofore unaware.

SPSC44C Gadolinium Deposition in the Brain: Use Caution, But Don't Panic

Participants

Vikas Gulani, MD, PhD, Cleveland, OH (*Presenter*) Research support, Siemens AG; Licensed Technology, Siemens Healthineers - both myself and my spouse. MR Fingerprinting, on which we are both inventors, has been licensed by Siemens.

LEARNING OBJECTIVES

1) To understand the similarities and differences between Nephrogenic Systemic Fibrosis (NSF) and the Gadolinium deposition phenomenon. 2) To understand the clinical implications of the deposition of Gadolinium in tissues.

ABSTRACT

Gadolinium deposition in the brain after use of gadolinium based contrast agents has been documented extensively in the literature. Class based differences in the deposition phenomenon have also been discussed. However, to date, no harm from the deposition has been documented. There are parallels and differences between the controversies surrounding this phenomenon and the radiological community's prior experience with Nephrogenic Systemic Fibrosis (NSF). In this brief talk, I will try to put the deposition phenomonen in this broader context.

SPSC44D Gadolinium Deposition in the Brain: What Radiologists Can Do to Help Patients and Referrals?

Participants

Max Wintermark, MD, Lausanne, Switzerland (*Presenter*) Advisory Board, General Electric Company; Consultant, More Health; Consultant, Magnetic Insight; Consultant, Icometrix; Consultant, Nines;

For information about this presentation, contact:

max.wintermark@gmail.com

LEARNING OBJECTIVES

1) To review practical tips on protocoling MRI studies with or wihtout gadolinium. 2) To discuss how to address patients' questions about gadolinium. 3) To review how to collaborate efficiently with referring physicians around MRI studies involving gadolinium.

Honored Educators

Presenters or authors on this event have been recognized as RSNA Honored Educators for participating in multiple qualifying educational activities. Honored Educators are invested in furthering the profession of radiology by delivering high-quality educational content in their field of study. Learn how you can become an honored educator by visiting the website at: https://www.rsna.org/Honored-Educator-Award/ Max Wintermark, MD - 2018 Honored Educator

SPSC44E Panel Discussion



Controversy Session: CTA or MRA?

Wednesday, Nov. 28 4:30PM - 6:00PM Room: E353A



AMA PRA Category 1 Credits ™: 1.50 ARRT Category A+ Credit: 0

FDA Discussions may include off-label uses.

Participants

Vincent B. Ho, MD,MBA, Bethesda, MD (*Moderator*) Institution, In-kind support, General Electric Company Martin R. Prince, MD,PhD, New York, NY (*Moderator*) Patent agreement, General Electric Company; Patent agreement, Hitachi, Ltd; Patent agreement, Siemens AG; Patent agreement, Canon Medical Systems Corporation; Patent agreement, Koninklijke Philips NV; Patent agreement, Nemoto Kyorindo Co, Ltd; Patent agreement, Bayer AG; Patent agreement, Lantheus Medical Imaging, Inc; Patent agreement, Bracco Group; Patent agreement, Mallinckrodt plc; Patent agreement, Guerbet SA;

LEARNING OBJECTIVES

1) Discuss CTA and MRA methods and techniques for optimized vascular imaging in clinical practice. 2) Debate the advantages and disadvantages of CTA and MRA in clinical practice. 3) Recommend the application of CTA or MRA for common challenging clinical scenarios.

Sub-Events

SPSC45A MRA

Participants

Scott B. Reeder, MD, PhD, Madison, WI (*Presenter*) Institutional research support, General Electric Company; Institutional research support, Bracco Group; Founder, Calimetrix, LLC; Shareholder, Elucent Medical; Consultant, ArTara Robert R. Edelman, MD, Evanston, IL (*Presenter*) Nothing to Disclose

J. Paul Finn, MD, Los Angeles, CA (Presenter) Speakers Bureau, Bayer AG; Scientific Advisory Board, AMAG Pharmaceuticals, Inc

For information about this presentation, contact:

redelman999@gmail.com

SPSC45B CTA

Participants

Elliot K. Fishman, MD, Baltimore, MD (*Presenter*) Institutional Grant support, Siemens AG; Institutional Grant support, General Electric Company; Co-founder, HipGraphics, Inc

W. Dennis Foley, MD, Milwaukee, WI (Presenter) Research Consultant, General Electric Company

Geoffrey D. Rubin, MD, Durham, NC (*Presenter*) Consultant, Fovia, Inc; Consultant, HeartFlow, Inc; Consultant, General Electric Company;

For information about this presentation, contact:

dfoley@mcw.edu

Honored Educators

Presenters or authors on this event have been recognized as RSNA Honored Educators for participating in multiple qualifying educational activities. Honored Educators are invested in furthering the profession of radiology by delivering high-quality educational content in their field of study. Learn how you can become an honored educator by visiting the website at: https://www.rsna.org/Honored-Educator-Award/ Elliot K. Fishman, MD - 2012 Honored EducatorElliot K. Fishman, MD - 2014 Honored EducatorElliot K. Fishman, MD - 2016 Honored EducatorElliot K. Fishman, MD - 2018 Honored Educator